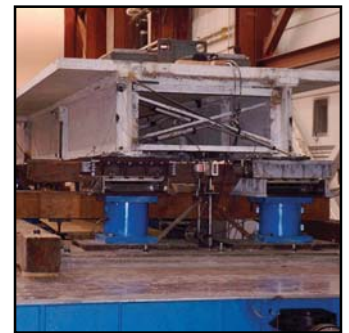
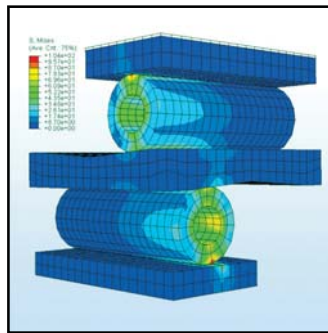


Principles and Performance of Roller Seismic Isolation Bearings for Highway Bridges

by
George C. Lee, Yu-Chen Ou, Zach Liang, Tiecheng Niu and
Jianwei Song



Technical Report MCEER-07-0019

December 10, 2007

NOTICE

This report was prepared by the University at Buffalo, State University of New York, as a result of research sponsored by MCEER through a contract from the Federal Highway Administration. Neither MCEER, associates of MCEER, its sponsors, the University at Buffalo, State University of New York, nor any person acting on their behalf:

- a. makes any warranty, express or implied, with respect to the use of any information, apparatus, method, or process disclosed in this report or that such use may not infringe upon privately owned rights; or
- b. assumes any liabilities of whatsoever kind with respect to the use of, or the damage resulting from the use of, any information, apparatus, method, or process disclosed in this report.

Any opinions, findings, and conclusions or recommendations expressed in this publication are those of the author(s) and do not necessarily reflect the views of MCEER or the Federal Highway Administration.

Principles and Performance of Roller Seismic Isolation Bearings for Highway Bridges

by

George C. Lee,¹ Yu-Chen Ou,² Zach Liang,³ Tiecheng Niu⁴ and Jianwei Song⁴

Publication Date: December 10, 2007

Submittal Date: July 27, 2007

Technical Report MCEER-07-0019

Task Number 094-D-2.2

FHWA Contract Number DTFH61-98-C-00094

Contract Officer's Technical Representative: W. Phillip Yen, Ph.D., P.E. HRDI-7
Senior Research Structural Engineer/Seismic Research Program Manager
Federal Highway Administration

- 1 Special Tasks Director, MCEER, Samuel P. Capen Professor of Engineering, Department of Civil, Structural and Environmental Engineering, University at Buffalo, State University of New York
- 2 Postdoctoral Associate, Department of Civil, Structural and Environmental Engineering, University at Buffalo, State University of New York
- 3 Research Associate, Department of Civil, Structural and Environmental Engineering, University at Buffalo, State University of New York
- 4 Research Scientist, Department of Civil, Structural and Environmental Engineering, University at Buffalo, State University of New York

MCEER

University at Buffalo, The State University of New York
Red Jacket Quadrangle, Buffalo, NY 14261

Phone: (716) 645-3391; Fax (716) 645-3399

E-mail: mceer@buffalo.edu; WWW Site: <http://mceer.buffalo.edu>

NTIS DISCLAIMER



This document has been reproduced from the best copy furnished by the sponsoring agency.

Preface

The Multidisciplinary Center for Earthquake Engineering Research (MCEER) is a national center of excellence in advanced technology applications that is dedicated to the reduction of earthquake losses nationwide. Headquartered at the University at Buffalo, State University of New York, the Center was originally established by the National Science Foundation in 1986, as the National Center for Earthquake Engineering Research (NCEER).

Comprising a consortium of researchers from numerous disciplines and institutions throughout the United States, the Center's mission is to reduce earthquake losses through research and the application of advanced technologies that improve engineering, pre-earthquake planning and post-earthquake recovery strategies. Toward this end, the Center coordinates a nationwide program of multidisciplinary team research, education and outreach activities.

MCEER's research is conducted under the sponsorship of two major federal agencies, the National Science Foundation (NSF) and the Federal Highway Administration (FHWA), and the State of New York. Significant support is also derived from the Federal Emergency Management Agency (FEMA), other state governments, academic institutions, foreign governments and private industry.

The Center's Highway Project develops improved seismic design, evaluation, and retrofit methodologies and strategies for new and existing bridges and other highway structures, and for assessing the seismic performance of highway systems. The FHWA has sponsored three major contracts with MCEER under the Highway Project, two of which were initiated in 1992 and the third in 1998.

Of the two 1992 studies, one performed a series of tasks intended to improve seismic design practices for new highway bridges, tunnels, and retaining structures (MCEER Project 112). The other study focused on methodologies and approaches for assessing and improving the seismic performance of existing "typical" highway bridges and other highway system components including tunnels, retaining structures, slopes, culverts, and pavements (MCEER Project 106). These studies were conducted to:

- assess the seismic vulnerability of highway systems, structures, and components;
- develop concepts for retrofitting vulnerable highway structures and components;
- develop improved design and analysis methodologies for bridges, tunnels, and retaining structures, which include consideration of soil-structure interaction mechanisms and their influence on structural response; and
- develop, update, and recommend improved seismic design and performance criteria for new highway systems and structures.

The 1998 study, “Seismic Vulnerability of the Highway System” (FHWA Contract DTFH61-98-C-00094; known as MCEER Project 094), was initiated with the objective of performing studies to improve the seismic performance of bridge types not covered under Projects 106 or 112, and to provide extensions to system performance assessments for highway systems. Specific subjects covered under Project 094 include:

- development of formal loss estimation technologies and methodologies for highway systems;
- analysis, design, detailing, and retrofitting technologies for special bridges, including those with flexible superstructures (e.g., trusses), those supported by steel tower substructures, and cable-supported bridges (e.g., suspension and cable-stayed bridges);
- seismic response modification device technologies (e.g., hysteretic dampers, isolation bearings); and
- soil behavior, foundation behavior, and ground motion studies for large bridges.

In addition, Project 094 includes a series of special studies, addressing topics that range from non-destructive assessment of retrofitted bridge components to supporting studies intended to assist in educating the bridge engineering profession on the implementation of new seismic design and retrofitting strategies.

This report presents a new roller seismic isolation bearing for use in highway bridges. The bearing uses rolling motions of cylindrical rollers between sloping surfaces to achieve seismic isolation. The bearing is characterized by a constant spectral acceleration under horizontal ground motions and by a self-centering capability, which are two desirable properties for seismic applications. The former ensures that resonance between the bearing and horizontal earthquakes will not occur while the latter guarantees that the bridge superstructure can self-center to its original position after an earthquake. Principles of the bearing under vertical loading and earthquake excitation are analytically and experimentally investigated. Two prototype roller isolation bearings have been developed, one with and the other without a built-in friction device for supplemental energy dissipation. A design example of the bearing for use in a bridge in a region of high seismicity is presented.

ABSTRACT

This report presents a new roller seismic isolation bearing for use in highway bridges. This new bearing uses rolling motions of cylindrical rollers between sloping surfaces to achieve seismic isolation. The bearing is characterized by a constant spectral acceleration under horizontal ground motions and by a self-centering capability, which are two desirable properties for seismic applications. The former ensures that resonance between the bearing and horizontal earthquakes will not occur while the latter guarantees the bridge superstructure can self-center to its original position after an earthquake.

Analytical models for the bearings under vertical loading and horizontal and vertical ground motions are derived and validated with results from finite element analyses and experimental studies. To decrease the displacement responses of the bearing and to maintain a constant spectral acceleration response while keeping the cost of the bearing low, sliding friction devices are integrated into a roller bearing. The seismic behavior of this new seismic isolation bearing with different design parameters under various ground motions is analytically studied. The parameters include the sloping angle, the sliding friction force and the PGA levels.

Two prototype roller seismic isolation bearings have been developed and their design details are presented in this report. The first prototype bearing does not have any built-in friction devices while the second prototype bearing has a unique built-in feature to achieve supplemental energy dissipation through sliding friction.

The last part of the report presents a design example of the second prototype roller seismic isolation bearing to be used in a bridge in a region of high seismicity.

ACKNOWLEDGEMENTS

The authors gratefully acknowledge the Federal Highway Administration for funding in support of the study reported herein (FHWA 094 Project No. DTFH61-98-C00094). They wish to express their sincere appreciation to Dr. Philip Yen, Mr. Ian Friedland and the late Mr. James Cooper for their support, advice and encouragement.

Several experimental programs have been carried out in different laboratories between 2000 and 2005. These laboratories include the University at Buffalo, University of Nevada at Reno, University of California at San Diego, National Center of Research on Earthquake Engineering, Taipei, Taiwan, Institute of Engineering Mechanics, Harbin, China. The authors would like to express their appreciation to Dr. Ian Buckle, Dr. Frieder Seible, Dr. Jianmario Benzoni, Dr. K. C. Chang, Dr. J. S. Hwang, Prof. Xiaozhai Qi and Dr. Xun Kou for their assistance and cooperation in the experimental studies.

Through the years, the authors have benefited greatly from the technical discussions with Dr. Joseph Penzien, Dr. Roy Imbsen, Dr. Michael Constantinou and Dr. Andrew Whittaker. Their advice is sincerely appreciated.

Several graduate students at the University at Buffalo have been involved in different aspects of the study described in this report. Dr. Tong Yang, Dr. Jun Wang, Mr. Alan Chu and Mr. Jongmin Seo are sincerely acknowledged for their contributions.

Experimental studies carried out at the University at Buffalo have been assisted by Mark Pitman, Dan Walsh and the late Dick Cizdziel. This report has been carefully edited by Ms. Jane Stoyale. To all of them, the authors express their sincere gratitude.

TABLE OF CONTENTS

CHAPTER		PAGE
1	INTRODUCTION	1
1.1	Motivation.....	1
1.2	Brief History of Rolling Type Seismic Isolation.....	3
1.3	Proposed Roller Seismic Isolation Bearing.....	4
2	PRINCIPLES OF ROLLER SEISMIC ISOLATION BEARINGS	7
2.1	Key Components of Roller Bearings.....	7
2.2	Forces due to Base Excitation.....	8
	2.2.1 Static Friction and Rolling Friction Forces.....	8
	2.2.2 Forces on the Components of a Roller Bearing.....	9
2.3	Governing Equations of Motion	16
2.4	Conditions for Rolling without Sliding	19
2.5	Uplift of Superstructure	20
2.6	Vertical Load Carrying Capacity.....	21
	2.6.1 Derivation	21
	2.6.2 Finite Element Analysis.....	22
2.7	Experimental Validation	30
	2.7.1 Description of the Bridge Model	30
	2.7.2 Test Results.....	32
	2.7.3 Comparison between Experiment and Analytical Study	32
3	ROLLER SEISMIC ISOLATION BEARINGS WITH SUPPLEMENTAL FRICTION ENERGY DISSIPATION	37
3.1	Governing Equations of Motion	37
3.2	Seismic Behavior under Horizontal Ground Motions	39
	3.2.1 Governing Equations of Motion	39
	3.2.2 Ground Motions for Parametric Study.....	40
	3.2.3 Parameters for Parametric Study	45
	3.2.4 Results and Discussions.....	45
3.3	Seismic Behavior under Combined Horizontal and Vertical Ground Motions	57
	3.3.1 Governing Equations of Motion	57
	3.3.2 Ground Motions for Parametric Study.....	57
	3.3.3 Parameters for Parametric Study	59
	3.3.4 Results and Discussion	59
3.4	Equivalent Linear Methods.....	67
	3.4.1 Secant Stiffness Method	67
	3.4.1.1 Rigid base	67
	3.4.1.2 Flexible base	68
	3.4.2 Proposed Equivalent Linear Method	70

TABLE OF CONTENTS (CONT'D)

CHAPTER	PAGE
3.4.2.1	Rigid base70
3.4.2.2	Flexible base72
3.4.3	Comparison with Results from Nonlinear Response History Analyses72
4	PROTOTYPE ROLLER SEISMIC ISOLATION BEARINGS 83
4.1	The First Prototype Roller Seismic Isolation Bearing83
4.1.1	Mechanical Properties83
4.1.2	Components85
4.2	The Second Prototype Roller Seismic Isolation Bearing88
4.2.1	Mechanical Properties88
4.2.2	Components91
4.2.3	Testing of the Bearing97
5	CASE STUDY 103
5.1	Description of the Bridge103
5.2	Design Procedures104
5.2.1	Vertical Load Carrying Capacity104
5.2.1.1	Vertical factor loads and seismic weight.104
5.2.1.2	Diameter of rollers and thickness of bearing plates105
5.2.2	Sloping Angle and Characteristic Strength105
5.2.3	Maximum Relative Displacement Demand under the Design Earthquake106
5.2.3.1	Equivalent linear system106
5.2.3.2	Elastic seismic response coefficient.107
5.2.3.3	Maximum relative displacement demand108
5.2.4	Displacement Capacity of the Bearings109
5.2.5	Fasteners for Normal forces on the Friction Interfaces109
5.2.6	Serviceability Limit State109
5.2.7	Column Base Shear110
5.2.8	Uplift of the Superstructure110
5.3	Schematic View of the Bearing111
6	SUMMARIES AND CONCLUSIONS 113
6.1	Summaries and Conclusions113
6.2	Future Research114
7	REFERENCES 115
APPENDIX A 117
APPENDIX B 119

LIST OF FIGURES

FIGURE		PAGE
1-1	Electrometric bearing	2
1-2	Lead-rubber bearing	2
1-3	Friction Pendulum bearing	2
1-4	EradiQuake bearing	2
1-5	The American River Bridge, City of Folsom, California (courtesy of Earthquake Protection Systems).....	3
1-6	Double concave rolling ball bearing	4
1-7	Rolling cylindrical rods between flat surfaces	4
1-8	Ball-in-cone seismic isolation bearing	4
1-9	Roller seismic isolation bearing	5
2-1	Variations of roller bearings.....	8
2-2	Key components of a roller bearing	8
2-3	Contact forces between a roller and a plate in pure rolling motion	9
2-4	Principal directions of the bearing.	10
2-5	Positions of the roller relative to the center of the lower plate.....	10
2-6	Free body diagram of a roller bearing under base excitation: roller on the left.....	12
2-7	Free body diagram of a roller bearing under base excitation: roller on the right	14
2-8	Relationship between displacements of the roller and superstructure	17
2-9	Base shear versus relative displacements of the superstructure	18
2-10	Top view of the bearing under base excitation along a direction 45 degrees away from the principal direction	19
2-11	A solid cylindrical roller in contact with a flat surface under a load per unit length p	22
2-12	Schematic view of the roller bearing.....	23
2-13	Stress-strain relationship of the steel.....	24
2-14	Positions of the rollers.....	25
2-15	Initial design: initial position.....	25
2-16	Initial design: 2.5-in from the initial position	26
2-17	Use of longer rollers	27
2-18	Revised design.....	28
2-19	Revised design: initial position	29
2-20	Revised design: 2.5-in from the initial position	29
2-21	Side view of the bridge model on the north shake table	31
2-22	Test setup.....	31
2-23	Side view of the bridge model.....	32
2-24	Measured shake table output under 50% of the El Centro earthquake	34
2-25	5% damped elastic absolute acceleration spectrum of the measured 50% of the El Centro earthquake	34

LIST OF FIGURES (CONT'D)

FIGURE		PAGE
2-26	Comparison of the South-East bearing responses between analytical and experiment under 50% of the El Centro earthquake	35
2-27	Measured shake table responses under 100% of the Kobe earthquake	35
2-28	5% damped elastic absolute acceleration spectrum of the measured 100% of the Kobe earthquake	36
2-29	Comparison of the North-East bearing responses between analytical and experiment under 100% of the Kobe earthquake	36
3-1	Lateral force-displacement behavior of roller seismic isolation bearings with supplemental friction energy dissipation	38
3-2	5% damped absolute acceleration spectra for the 28 ground motions	42
3-3	5% damped relative displacement spectra for the 28 ground motions	43
3-4	Acceleration history of ground motion No. 1 with PGA= 0.5g	46
3-5	Acceleration history of ground motion No. 17 with PGA= 0.5g	46
3-6	Acceleration history of ground motion No. 21 with PGA= 0.5g	46
3-7	Acceleration and displacement responses of bearings with $\theta = 2$ and 8 and with $Q_{dr} = 0$ to ground motion No. 1 with PGA= 0.5g	47
3-8	Hysteretic responses of bearings with $\theta = 2$ and 8 and with $Q_{dr} = 0$ to ground motion No. 1 with PGA= 0.5g	47
3-9	Acceleration and displacement responses of bearings with $\theta = 2$ and 8 and with $Q_{dr} = 0$ to ground motion No. 17 with PGA= 0.5g	48
3-10	Hysteretic responses of bearings with $\theta = 2$ and 8 and with $Q_{dr} = 0$ to ground motion No. 17 with PGA= 0.5g	48
3-11	Acceleration and displacement responses of bearings with $\theta = 2$ and 8 and with $Q_{dr} = 0$ to ground motion No. 21 with PGA= 0.5g	49
3-12	Hysteretic responses of bearings with $\theta = 2$ and 8 and with $Q_{dr} = 0$ to ground motion No. 21 with PGA= 0.5g	49
3-13	Acceleration and displacement responses of bearings with $\theta = 2$ and 8 and with $Q_{dr} = 1$ to ground motion No. 1 with PGA= 0.5g	51
3-14	Hysteretic responses of bearings with $\theta = 2$ and 8 and with $Q_{dr} = 1$ to ground motion No. 1 with PGA= 0.5g	51
3-15	Acceleration and displacement responses of bearings with $\theta = 2$ and 8 and with $Q_{dr} = 1$ to ground motion No. 17 with PGA= 0.5g	52
3-16	Hysteretic responses of bearings with $\theta = 2$ and 8 and with $Q_{dr} = 1$ to ground motion No. 17 with PGA= 0.5g	52
3-17	Acceleration and displacement responses of bearings with $\theta = 2$ and 8 and with $Q_{dr} = 1$ to ground motion No. 21 with PGA= 0.5g	53
3-18	Hysteretic responses of bearings with $\theta = 2$ and 8 and with $Q_{dr} = 1$ to ground motion No. 21 with PGA= 0.5g	53
3-19	Mean maximum relative displacement and absolute acceleration responses under PGA=0.2g	54

LIST OF FIGURES (CONT'D)

FIGURE	PAGE
3-20	Mean maximum relative displacement and absolute acceleration responses under PGA=0.3g.....55
3-21	Mean maximum relative displacement and absolute acceleration responses under PGA=0.4g.....55
3-22	Mean maximum relative displacement and absolute acceleration responses under PGA=0.5g.....55
3-23	Mean maximum relative displacement and absolute acceleration responses under PGA=0.6g.....56
3-24	Mean maximum relative displacement and absolute acceleration responses under PGA=0.7g.....56
3-25	Mean maximum relative displacement and absolute acceleration responses under PGA=0.8g.....56
3-26	Acceleration and displacement responses of a bearing with $\theta = 4$ and $Q_{dr} = 0$ to ground motion pair No. 2 with and without the vertical component.....60
3-27	Hysteretic responses of a bearing with $\theta = 4$ and $Q_{dr} = 0$ to ground motion pair No. 2 with and without the vertical component.....60
3-28	Acceleration and displacement responses of a bearing with $\theta = 4$ and $Q_{dr} = 0$ to ground motion pair No. 4 with and without the vertical component.....61
3-29	Hysteretic responses of a bearing with $\theta = 4$ and $Q_{dr} = 0$ to ground motion pair No. 4 with and without the vertical component.....61
3-30	Acceleration and displacement responses of a bearing with $\theta = 4$ and $Q_{dr} = 1$ to ground motion pair No. 2 with and without the vertical component.....62
3-31	Hysteretic responses of a bearing with $\theta = 4$ and $Q_{dr} = 1$ to ground motion pair No. 2 with and without the vertical component.....62
3-32	Acceleration and displacement responses of a bearing with $\theta = 4$ and $Q_{dr} = 1$ to ground motion pair No. 4 with and without the vertical component.....63
3-33	Hysteretic responses of a bearing with $\theta = 4$ and $Q_{dr} = 1$ to ground motion pair No. 4 with and without the vertical component.....63
3-34	Effects of vertical ground motions on the mean maximum relative displacement response.....64
3-35	Effects of vertical components of the ground motions on the mean maximum absolute acceleration response.....65
3-36	Secant stiffness method.....68
3-37	Displacements of the superstructure due to flexibility of the isolation bearings, column and surrounding soils (adapted from Constantinou et al. 2007).....69
3-38	Proposed method for computing effective stiffness.....71

LIST OF FIGURES (CONT'D)

FIGURE		PAGE
3-39	Mean absolute acceleration spectra for the 28 ground motions normalized by PGA	72
3-40	Mean relative velocity spectra for the 28 ground motions normalized by PGA	73
3-41	Mean relative displacement spectra for the 28 ground motions normalized by PGA	73
3-42	Errors of prediction by the proposed method and secant stiffness method under PGA=0.2g.....	75
3-43	Errors of prediction by the proposed method and secant stiffness method under PGA=0.3g.....	75
3-44	Errors of prediction by the proposed method and secant stiffness method under PGA=0.4g.....	75
3-45	Errors of prediction by the proposed method and secant stiffness method under PGA=0.5g.....	76
3-46	Errors of prediction by the proposed method and secant stiffness method under PGA=0.6g.....	76
3-47	Errors of prediction by the proposed method and secant stiffness method under PGA=0.7g.....	76
3-48	Errors of prediction by the proposed method and secant stiffness method under PGA=0.8g.....	77
3-49	Errors of prediction by the proposed method and secant stiffness method for all the bearings	77
3-50	Effective periods and damping ratios for a sloping angle of 2 degrees	79
3-51	Effective periods and damping ratios for a sloping angle of 3 degrees	79
3-52	Effective periods and damping ratios for a sloping angle of 4 degrees	79
3-53	Effective periods and damping ratios for a sloping angle of 5 degrees	80
3-54	Effective periods and damping ratios for a sloping angle of 6 degrees	80
3-55	Effective periods and damping ratios for a sloping angle of 7 degrees	80
3-56	Effective periods and damping ratios for a sloping angle of 8 degrees	81
4-1	Schematic view of the first prototype roller bearing.....	84
4-2	Design details of the first prototype roller bearing.....	86
4-3	Photos of the first prototype roller bearing	87
4-4	Schematic view of the second prototype roller bearing	90
4-5	Design details of the second prototype roller bearing.....	93
4-6	Photos of the second prototype roller bearing.....	96
4-7	Test setup.....	97
4-8	Bearing at a displacement of 3 in	98
4-9	Force-displacement responses to vertical loading.....	98
4-10	Change in the vertical displacement under sustained vertical loading.....	99
4-11	Force-displacement responses to lateral cyclic loading	101
5-1	Bridge location	103
5-2	A typical continuous unit of the bridge.....	104
5-3	Schematic view of the bearing	111
B-1	El Centro Array #6, horizontal: 230 degrees.....	119

LIST OF FIGURES (CONT'D)

FIGURE		PAGE
B-2	El Centro Array #6, horizontal: 140 degrees.....	119
B-3	Hollister, horizontal: 90 degrees	120
B-4	Hollister, horizontal: 0 degrees	120
B-5	Lexington Dam, horizontal: 90 degrees	121
B-6	Lexington Dam, horizontal: 0 degrees	121
B-7	Petrolia, horizontal: 90 degrees	122
B-8	Petrolia, horizontal: 0 degrees	122
B-9	Lucerne Valley, horizontal: L	123
B-10	Lucerne Valley, horizontal: T	123
B-11	Yermo, horizontal: 360 degrees	124
B-12	Yermo, horizontal: 270 degrees	124
B-13	Sylmar, horizontal: 90 degrees.....	125
B-14	Sylmar, horizontal: 360 degrees.....	125
B-15	Newhall Fire, horizontal: 90 degrees	126
B-16	Newhall Fire, horizontal: 360 degrees	126
B-17	Corralitos, horizontal: 90 degrees	127
B-18	Corralitos, horizontal: 0 degrees	127
B-19	Santa Monica City Hall Grounds, horizontal: 90 degrees.....	128
B-20	Santa Monica City Hall Grounds, horizontal: 360 degrees.....	128
B-21	Oakland Outer Harbor Wharf, horizontal: 305 degrees	129
B-22	Oakland Outer Harbor Wharf, horizontal: 35 degrees	129
B-23	Pomona, horizontal: 90 degrees	130
B-24	Pomona, horizontal: 0 degrees	130
B-25	Altadena, horizontal: 90 degrees.....	131
B-26	Altadena, horizontal: 0 degrees.....	131
B-27	Century City, horizontal: 90 degrees.....	132
B-28	Century City, horizontal: 360 degrees.....	132
B-29	Hollister, vertical.....	133
B-30	Lexington Dam, vertical.....	133
B-31	Petrolia, vertical	134
B-32	Lucerne Valley, vertical	134
B-33	Yermo, vertical.....	135
B-34	Sylmar, vertical	135
B-35	Newhall Fire, vertical.....	136
B-36	Corralitos, vertical.....	136
B-37	Santa Monica City Hall Grounds, vertical	137
B-38	Oakland Outer Harbor Wharf, vertical.....	137
B-39	Pomona, vertical.....	138
B-40	Altadena, vertical	138
B-41	Century City, vertical	139

LISTS OF TABLES

TABLE		PAGE
2-1	Scale factors for the bridge model.....	30
3-1	Ground motions.....	41
3-2	Parameters for the parametric study.....	45
3-3	Ground motion pairs.....	58
3-4	C_v for earthquakes with a magnitude 7.0 or less (MCEER/ATC 2003)	66
3-5	C_v for earthquakes with a magnitude greater than 7.0 (MCEER/ATC 2003).....	66
3-6	Damping coefficient B (AASHTO 2000).....	74
4-1	Design parameters of the first prototype roller bearing	84
4-2	Design parameters of the second prototype roller bearing.....	89
5-1	Site soil coefficient S_i (AASHTO 2000).....	108

CHAPTER 1

INTRODUCTION

1.1 Motivation

A major challenge in seismic resistant design of highway bridges is to minimize the damage to bridge columns to ensure structural integrity and low repairing/replacement cost. Depending on the type and configuration of bridges, the approach in general is to increase the load resisting capacity of the column or to decrease the demand or both. Our approach to decrease the seismic demand of the bridge column is to utilize isolation bearings, a technology developed and applied in recent years.

Seismic isolation bearings reduce the seismic forces that act on a bridge by lengthening its period through the flexibility of the bearings. Most of the bridge displacements induced by earthquakes are then concentrated over the height of the bearings, which are designed to accommodate these displacements with little damage. The use of seismic isolation bearings allows for elastic yet economical design of bridge substructures, which means that the bridge can remain fully functional after an earthquake.

Currently in the United States, there are two common types of seismic isolation bearings for bridge applications, elastomeric bearings and sliding bearings. Typical elastomeric bearings are low damping rubber bearings (see Figure 1-1), high damping rubber bearings and lead-rubber bearings (see Figure 1-2). Seismic isolation is achieved by the low shear stiffness of the elastomers. By using elastomers with special compound, high damping rubber bearings can achieve much higher energy dissipation than low damping rubber bearings. In lead-rubber bearings, energy dissipation is realized by yielding of the lead core. Typical sliding bearings are concave sliding bearings (e.g. the Friction Pendulum bearing, EPS 2007, see Figure 1-3) and flat sliding bearings (e.g. the EradiQuake bearing, R. J. Watson, Inc 2007, see Figure 1-4). In sliding bearings, seismic isolation is achieved by sliding actions. Energy dissipation is provided by sliding friction between contact surfaces. Constantinou et al. (2007) presents detailed information on these bearings. Figure 1-5 shows a bridge that was seismically isolated with concave sliding bearings (the Friction Pendulum bearing).

The seismic isolation bearings described above typically have a certain amount of post-elastic stiffness to ensure low permanent displacements after a design earthquake occurs. In this report, a new type of bearing, called a roller seismic isolation bearing, is proposed for use in highway bridges. This new bearing utilizes a rolling mechanism to achieve seismic isolation. Such a bearing can achieve zero post-elastic stiffness under a horizontal earthquake. This means that the spectral acceleration response of the bearing is independent of the magnitude and frequency content of the horizontal earthquake. Meanwhile, the bearing is able to self-center to its initial position after the earthquake.

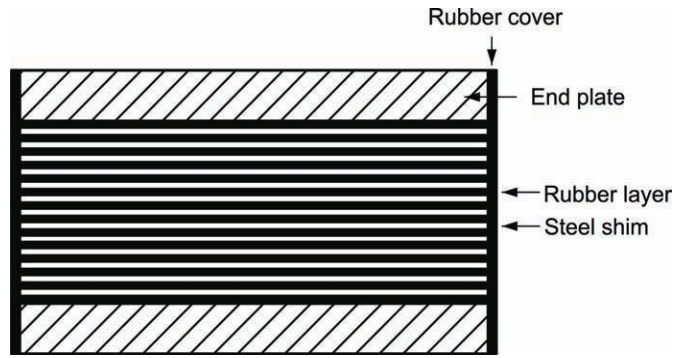


Figure 1-1 Electrometric bearing

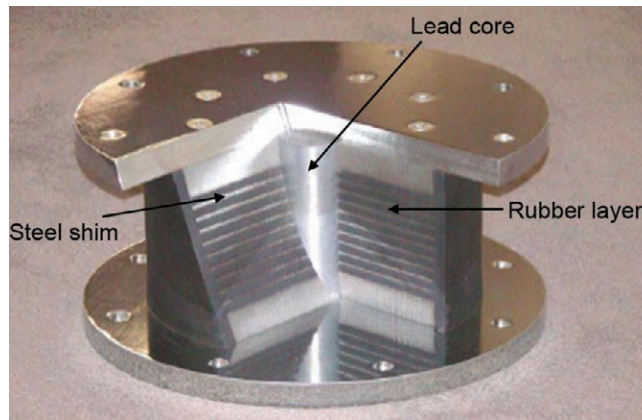


Figure 1-2 Lead-rubber bearing

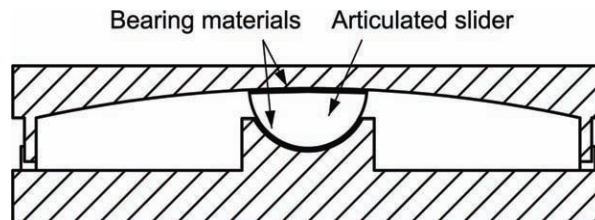


Figure 1-3 Friction Pendulum bearing

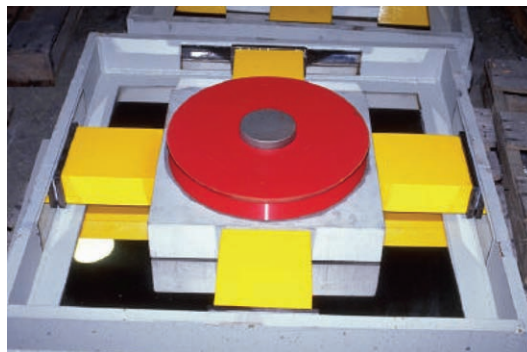


Figure 1-4 EradiQuake bearing



**Figure 1-5 The American River Bridge, City of Folsom, California
(courtesy of Earthquake Protection Systems)**

1.2 Brief History of Rolling Type Seismic Isolation

Use of a rolling mechanism for seismic isolation can be traced back to the late 19th century. Touaillon (1870) was granted a US patent on a double concave rolling ball bearing for use in buildings. This bearing consisted of a ball in two facing concave surfaces as shown in Figure 1-6. Similar to existing elastomeric bearings and sliding bearings, the bearing has a certain amount of post-elastic stiffness depending on the radius of the concave surfaces.

Lin and Hone (1993) used rolling cylindrical rods between two flat surfaces under a building for seismic isolation as shown in Figure 1-7. The maximum roof acceleration of the building was found to remain constant regardless of the frequency content of the base excitation when the rolling friction was smaller than 0.01. Lin's study demonstrated that zero post-elastic stiffness can be achieved by using rolling between flat (straight) surfaces. However, no restoring force was provided in the proposed bearing, which is unacceptable according to current building codes or bridge specifications for seismic isolation design (CBC 2001 and AASHTO 2000).

Kemeny (1997) invented a ball-in-cone seismic isolation bearing. In this type of rolling bearing, seismic isolation is achieved by a ball rolling between two facing conical surfaces as shown in Figure 1-8. Such a bearing achieves zero post-elastic stiffness if the sloping angle of the conical surfaces is small. Furthermore, due to the sloping surface, the bearing is self-centered by gravity as an earthquake ceases. Such a rolling bearing has been successfully used to protect critical equipment from earthquake-induced damage (WorkSafeTechnologies 2007). However, due to the point contact nature, the load carrying capacity of such a bearing is much smaller than typical bridge bearings, which limits its use in highway bridges.

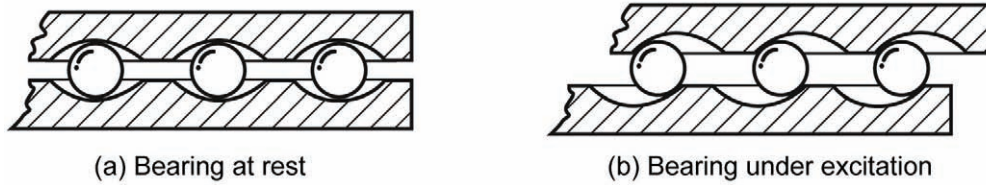


Figure 1-6 Double concave rolling ball bearing

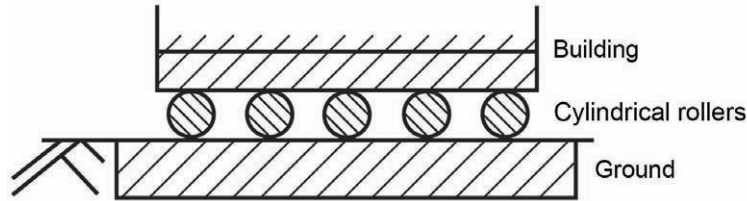


Figure 1-7 Rolling cylindrical rods between flat surfaces

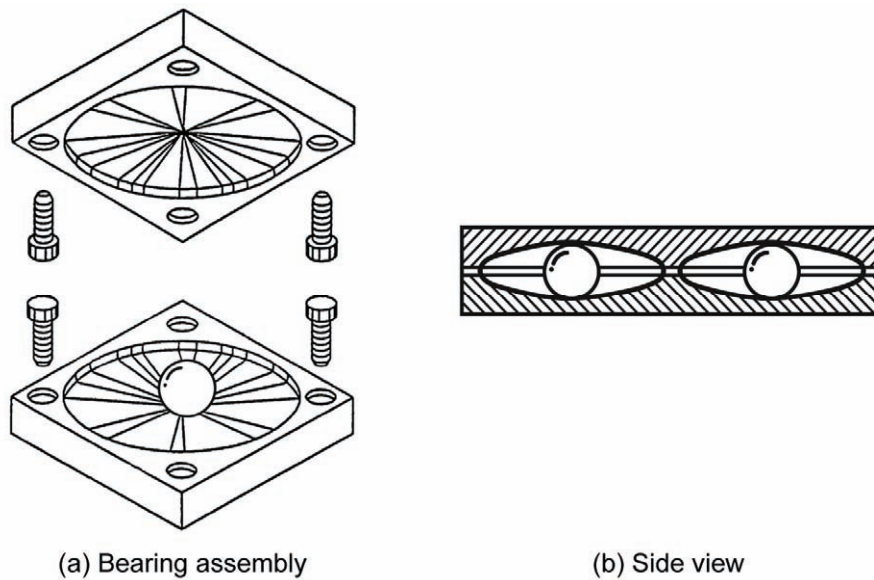


Figure 1-8 Ball-in-cone seismic isolation bearing

1.3 Proposed Roller Seismic Isolation Bearing

The proposed roller seismic isolation bearing utilizes a cylindrical roller rolling between two bearing plates with one contact surface machined to a V-shaped sloping surface and the other machined to a flat surface to achieve zero post-elastic stiffness under horizontal ground motions. The sloping surface allows gravity to act as a restoring force to self-center the bridge superstructure after the earthquake. Figure 1-9 shows the schematic view of the bearing. The bearing has a significantly larger load carrying capacity than the ball-in-cone rolling bearing due to a much larger contact area provided by using a cylinder instead of a ball.

The concept and principles of the roller seismic isolation bearing were first presented in 2000 (Lee et al. 2000) and subsequently at the 19th US-Japan Bridge Engineering Workshop (Lee and Liang 2003). Details are given in Lee et al. (2005).

The principles of the roller bearings are discussed in Chapter 2. Analytical models for the bearings under vertical loading and base excitation are derived and compared to results of finite element studies and experimental studies. Chapter 3 presents a new roller seismic isolation bearing for highway bridges that combines the roller bearing and friction energy dissipation devices. The seismic behavior of the bearing with different design parameters under various ground excitation is studied. Suggestions for selecting the design parameters are made. The last part of the chapter presents two equivalent linear methods, including a code-compliant method and a proposed method, for estimating the maximum displacement demand of the bearing. Both methods are compared to results from nonlinear response history analyses. Chapter 4 presents two prototype roller seismic isolation bearings. The second prototype bearing has built-in friction devices for supplemental energy dissipation. Properties and design details of the bearings are discussed. The experimental evaluation of the second prototype bearing is given at the end of the chapter. Chapter 5 presents the design procedures of the second prototype roller bearings to be used for bridges in areas of high seismicity. Finally, the summary and conclusions of this report are given in Chapter 6.

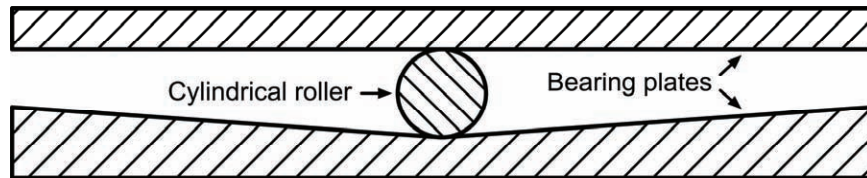


Figure 1-9 Roller seismic isolation bearing

CHAPTER 2

PRINCIPLES OF ROLLER SEISMIC ISOLATION BEARINGS

The principles of the proposed roller bearing under base excitation and vertical loading are presented in this chapter. First, the key elements of the roller bearing are introduced. Then, forces acting on the components of the bearing under base excitation are derived based on dynamic equilibrium. Next, the governing equations of motion of the bearing are derived. Conditions for rolling without sliding and uplift of the bearing are analytically investigated. Then the vertical load-carrying capacity of the bearing is discussed. Lastly, an experimental study using shake tables is briefly presented and used to validate the analytical models previously derived.

2.1 Key Components of Roller Bearings

The key elements of the proposed roller seismic isolation bearing are cylindrical rollers and bearing plates. Each roller bearing consists of two rollers for seismic isolation along two orthogonal directions. Each roller is sandwiched between two bearing plates. At least one of the bearing plates has a V-shaped sloping surface in contact with the roller. The contact surface of the other plate can be either V-shaped sloping or flat.

Figure 2-1 shows two variations of the roller bearings. As shown in the figure, a type A bearing has a V-shaped sloping surface at the top plate or at the bottom plate whereas a type B bearing has V-shaped sloping surfaces at both the plates. It can be proved that a type B bearing exhibits similar isolation performance to a type A bearing if the sum of the sloping angles of the two V-shaped sloping surfaces is equal to the sloping angle of the type A bearing, that is,

$$\theta_1 + \theta_2 = \theta \quad (2-1)$$

where θ_1 , θ_2 and θ are the sloping angles and are illustrated in Figure 2-1.

However, the cost of a type B bearing is higher than that of a type A bearing due to twice the number of the sloping surfaces and hence the cost associated with machining these sloping surfaces. Thus, this report focuses on type A bearings.

Figure 2-2 shows three-dimensional views of the keys components of a bi-directional type A roller bearing. The intermediate plate has V-shaped sloping surfaces both at the top and at the bottom of the plate. The upper plate and the lower plate have flat surfaces in contact with the roller. The upper plate is secured to the bridge superstructure and the lower plate mounted on the pier cap or abutment. To achieve stability, at least four bearings are needed to support a bridge superstructure unit.

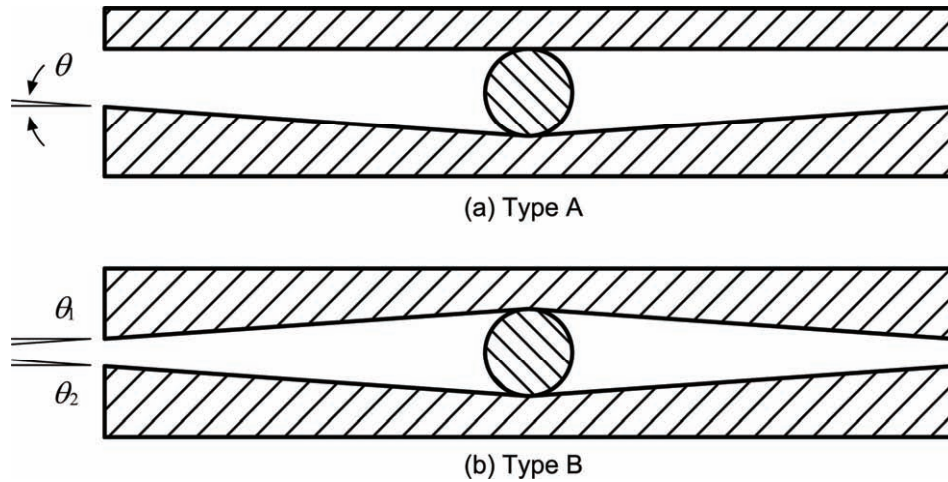


Figure 2-1 Variations of roller bearings

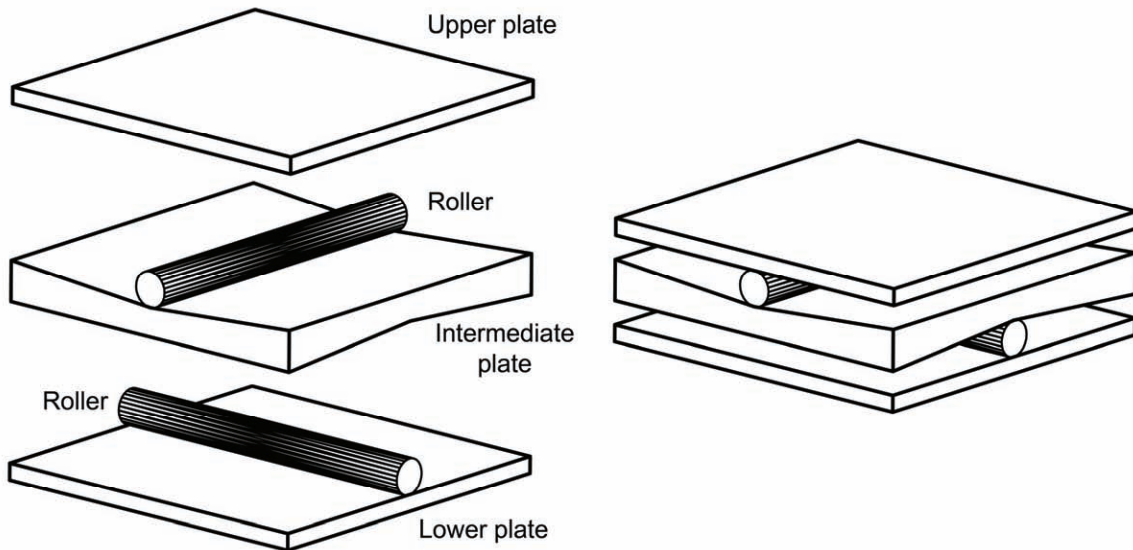


Figure 2-2 Key components of a roller bearing

2.2 Forces due to Base Excitation

2.2.1 Static Friction and Rolling Friction Forces

When a cylindrical roller rolls with an angular acceleration α due to an imposed horizontal base acceleration \ddot{x}_b , a static friction force f and a rolling friction moment M_r arise between the roller and the base shown in Figure 2-3. The force f acts along the opposite direction of the rolling direction so that the roller maintains a rolling motion. The value of f increases as the angular acceleration of the roller increases. Once it exceeds the maximum static friction force that can be provided by the contact interface, the roller starts sliding. On the other hand, the

rolling friction moment M_r resists the rolling motion. It arises mainly due to the deformation of the contact surfaces. M_r is defined as

$$M_r = \mu_r NR \quad (2-2)$$

where N is the normal force between the contact surfaces; δ is the horizontal distance between force N and the centroid of the cylinder, O ; R is the radius of the roller; and μ_r is the coefficient of rolling friction and is defined as

$$\mu_r = \frac{\delta}{R} \quad (2-3)$$

where the values of δ vary for different materials. For steel on steel, δ is 0.002 in (0.05 mm), and for hard polished steel on hard polished steel, δ ranges from 0.0002 in (0.005 mm) to 0.0004 in (0.01 mm) (Avallone and Baumeister 1996).

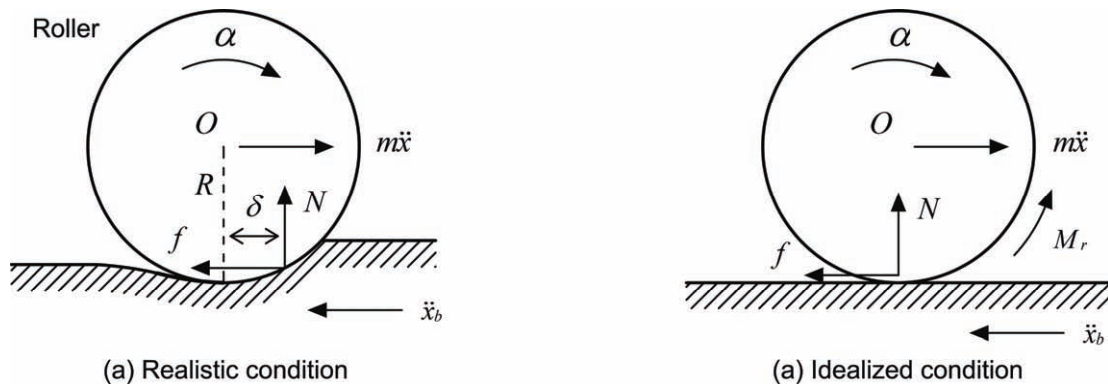


Figure 2-3 Contact forces between a roller and a plate in pure rolling motion

2.2.2 Forces on the Components of a Roller Bearing

In this section, forces acting on the components of a roller bearing under base excitation along the principal directions (see Figure 2-4) are derived. The principal directions are the rolling directions of the rollers. Only one roller is mobilized when rolling motion occurs along any of the two principal directions. As a result, only one roller and two bearing plates that sandwich the roller are considered in the derivation (see Figure 2-5). The upper and lower bearing plates are assumed to be directly fixed to a superstructure and a rigid base, respectively. The derivation is made first based on a condition when the roller is on the left side of the center of the lower bearing plate as shown in Figure 2-5a. Next, it is made for the condition when the roller is on the right side as shown in Figure 2-5b. Finally, a complete solution is derived to include both conditions. Note that the sloping angle is exaggerated in the figure for ease of presentation. In this research, the upper roller and the lower roller are identical. Thus, the bearing has identical behavior along the two principal directions.

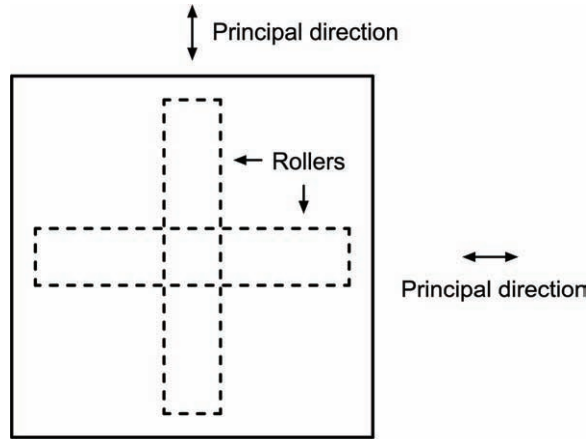


Figure 2-4 Principal directions of the bearing.

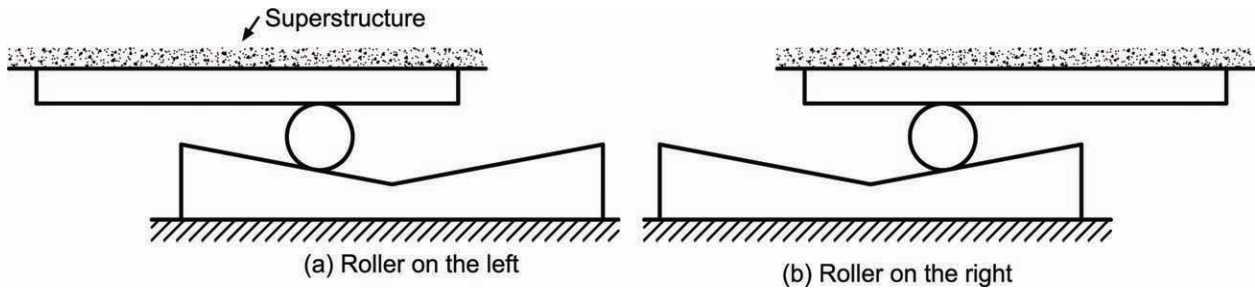


Figure 2-5 Positions of the roller relative to the center of the lower plate.

Figure 2-6 shows the free body diagram of the bearing subjected to base excitation when the roller is on the left side of the lower bearing plate. The bearing is assumed to be subjected to a horizontal acceleration excitation \ddot{x}_3 and a vertical acceleration excitation \ddot{z}_3 . The upper bearing plate is fixed to a bridge superstructure.

For the superstructure, the dynamic equilibrium along the horizontal direction gives

$$m_1(\ddot{x}_1 + \ddot{x}_3) + f_1 = 0 \quad (2-4)$$

where m_1 represents the tributary mass from the superstructure (including the upper bearing plate); \ddot{x}_1 is the horizontal acceleration response of the superstructure relative to the origin O ; f_1 is the static friction force between the roller and the upper bearing plate; and $\text{sgn}(\dot{x}_2)$ is 1 if \dot{x}_2 is positive and -1 if \dot{x}_2 is negative. For the vertical direction, we have

$$m_1(\ddot{z}_1 + \ddot{z}_3) - N_1 + m_1g = 0 \quad (2-5)$$

where \ddot{z}_1 is the vertical acceleration response of the superstructure relative to O ; N_1 is the normal force between the roller and the upper plate; and g is the acceleration of gravity. The equation of dynamic equilibrium for the roller along the horizontal direction is

$$m_2(\ddot{x}_2 + \ddot{x}_3) - f_1 + f_2 \cos \theta - N_2 \sin \theta = 0 \quad (2-6)$$

where m_2 and \ddot{x}_2 are the mass and horizontal acceleration response of the roller relative to O , respectively; f_2 and N_2 are the static friction force and normal force between the roller and the lower bearing plate, respectively; and θ is the sloping angle. For the vertical direction, we have

$$m_2(\ddot{z}_2 - \ddot{z}_3) - N_1 + f_2 \sin \theta + N_2 \cos \theta - m_2 g = 0 \quad (2-7)$$

where \ddot{z}_2 is the vertical acceleration response of the roller relative to O . Note that the value of \ddot{z}_2 is set as positive downward. The rotational dynamic equilibrium of the roller gives

$$I\alpha - [f_1 - \mu_r N_1 \operatorname{sgn}(\dot{x}_2)]R - [f_2 - \mu_r N_2 \operatorname{sgn}(\dot{x}_2)]R = 0 \quad (2-8)$$

where α , I_2 and R are the angular acceleration, moment of inertia and radius of the roller, respectively. If the roller is in a pure rolling motion, compatibility requirements lead to

$$\ddot{x}_2 = R \cos \theta \cdot \alpha \quad (2-9)$$

$$\ddot{z}_2 = R \sin \theta \cdot \alpha \quad (2-10)$$

$$\dot{x}_1 = \dot{x}_2 + R\alpha \quad (2-11)$$

$$\ddot{z}_1 = -\ddot{z}_2 \quad (2-12)$$

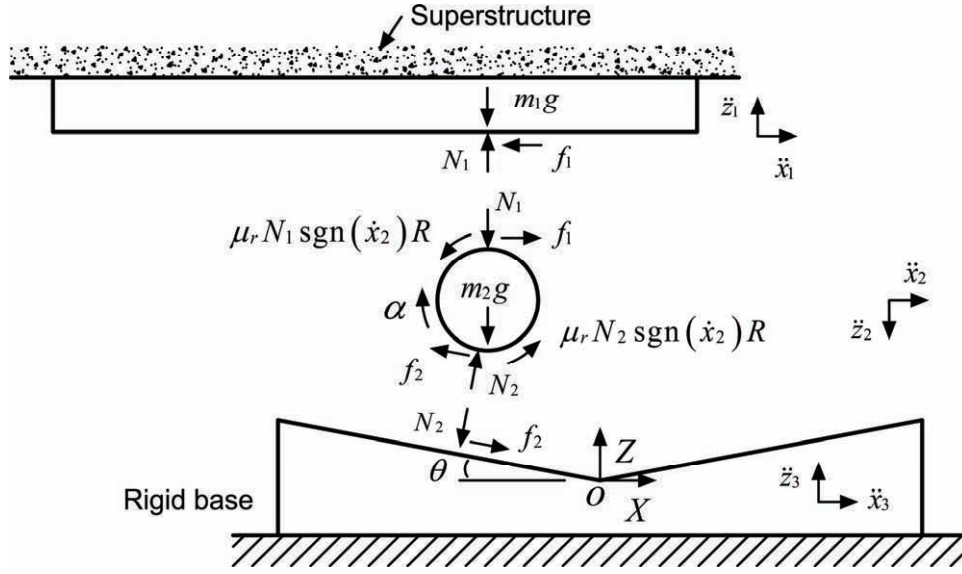


Figure 2-6 Free body diagram of a roller bearing under base excitation: roller on the left

Rearrange equations (2-4) to (2-12) in a matrix form gives

$$\begin{pmatrix}
 m_1 & 0 & 0 & 0 & 0 & 1 & 0 & 0 & 0 & 0 \\
 0 & m_1 & 0 & 0 & 0 & 0 & 0 & -1 & 0 & 0 \\
 0 & 0 & m_2 & 0 & 0 & -1 & \cos \theta & 0 & -\sin \theta & 0 \\
 0 & 0 & 0 & m_2 & 0 & 0 & \sin \theta & -1 & \cos \theta & 0 \\
 0 & 0 & 0 & 0 & I & -R & -R & \mu_r \operatorname{sgn}(\dot{x}_2) R & \mu_r \operatorname{sgn}(\dot{x}_2) R & 0 \\
 0 & 0 & 1 & 0 & -R \cos \theta & 0 & 0 & 0 & 0 & 0 \\
 0 & 0 & 0 & 1 & -R \sin \theta & 0 & 0 & 0 & 0 & 0 \\
 1 & 0 & -1 & 0 & -R & 0 & 0 & 0 & 0 & 0 \\
 0 & 1 & 0 & 1 & 0 & 0 & 0 & 0 & 0 & 0
 \end{pmatrix}
 \begin{pmatrix}
 \ddot{x}_1 \\
 \ddot{z}_1 \\
 \ddot{x}_2 \\
 \ddot{z}_2 \\
 \alpha \\
 f_1 \\
 f_2 \\
 N_1 \\
 N_2
 \end{pmatrix}
 =
 \begin{pmatrix}
 -m_1 \ddot{x}_3 \\
 -m_1 (g + \ddot{z}_3) \\
 -m_2 \ddot{x}_3 \\
 m_1 (g + \ddot{z}_3) \\
 0 \\
 0 \\
 0 \\
 0 \\
 0
 \end{pmatrix}$$

By solving the system of linear equations, we have, for example, the acceleration response of the superstructure

$$\ddot{x}_1 = \frac{2R^2 \cos^2 \frac{\theta}{2}}{I + (2m_1 + m_2)R^2 + 2m_1R^2 \cos \theta} \left\{ -[m_1 + (m_1 + m_2) \cos \theta] [\ddot{x}_3 + (\ddot{z}_3 + g) \mu_r \operatorname{sgn}(\dot{x}_2)] \right. \\
 \left. + [m_1 + m_2] \sin \theta [\ddot{z}_3 + g - \ddot{x}_3 \mu_r \operatorname{sgn}(\dot{x}_2)] \right\}$$

Since the mass of the superstructure m_1 is much larger than the mass of the roller m_2 , dividing both the denominator and numerator by m_1 and ignoring m_2 / m_1 leads to

$$\ddot{x}_1 = \frac{-\cos^2 \frac{\theta}{2} \{ [1 + \cos \theta] [\ddot{x}_3 + (\ddot{z}_3 + g) \mu_r \operatorname{sgn}(\dot{x}_2)] - \sin \theta [\ddot{z}_3 + g - \ddot{x}_3 \mu_r \operatorname{sgn}(\dot{x}_2)] \}}{1 + \cos \theta}$$

further simplification leads to

$$\ddot{x}_1 = -\cos^2 \frac{\theta}{2} [\ddot{x}_3 + (\ddot{z}_3 + g) \mu_r \operatorname{sgn}(\dot{x}_2)] + \frac{1}{2} \sin \theta [\ddot{z}_3 + g - \ddot{x}_3 \mu_r \operatorname{sgn}(\dot{x}_2)]$$

In a similar manner, the solutions for all the variables are

$$\begin{pmatrix} \ddot{x}_1 \\ \ddot{z}_1 \\ \ddot{x}_2 \\ \ddot{z}_2 \\ \alpha \\ f_1 \\ f_2 \\ N_1 \\ N_2 \end{pmatrix} \approx \begin{pmatrix} -\cos^2 \frac{\theta}{2} [\ddot{x}_3 + (\ddot{z}_3 + g) \mu_r \operatorname{sgn}(\dot{x}_2)] + \frac{1}{2} \sin \theta [\ddot{z}_3 + g - \ddot{x}_3 \mu_r \operatorname{sgn}(\dot{x}_2)] \\ \frac{1}{2} \sin \theta [\ddot{x}_3 + (\ddot{z}_3 + g) \mu_r \operatorname{sgn}(\dot{x}_2)] - \sin^2 \frac{\theta}{2} [\ddot{z}_3 + g - \ddot{x}_3 \mu_r \operatorname{sgn}(\dot{x}_2)] \\ \frac{1}{2} \cos \theta \left\{ -[\ddot{x}_3 + (\ddot{z}_3 + g) \mu_r \operatorname{sgn}(\dot{x}_2)] + \tan \frac{\theta}{2} [\ddot{z}_3 + g - \ddot{x}_3 \mu_r \operatorname{sgn}(\dot{x}_2)] \right\} \\ \frac{1}{2} \sin \theta \left\{ -[\ddot{x}_3 + (\ddot{z}_3 + g) \mu_r \operatorname{sgn}(\dot{x}_2)] + \tan \frac{\theta}{2} [\ddot{z}_3 + g - \ddot{x}_3 \mu_r \operatorname{sgn}(\dot{x}_2)] \right\} \\ \frac{1}{2R} \left\{ -[\ddot{x}_3 + (\ddot{z}_3 + g) \mu_r \operatorname{sgn}(\dot{x}_2)] + \tan \frac{\theta}{2} [\ddot{z}_3 + g - \ddot{x}_3 \mu_r \operatorname{sgn}(\dot{x}_2)] \right\} \\ m_1 \left[-\sin \frac{\theta}{2} + \cos \frac{\theta}{2} \mu_r \operatorname{sgn}(\dot{x}_2) \right] \left[\sin \frac{\theta}{2} \ddot{x}_3 + \cos \frac{\theta}{2} (\ddot{z}_3 + g) \right] \\ m_1 \left[\sin \frac{\theta}{2} + \cos \frac{\theta}{2} \mu_r \operatorname{sgn}(\dot{x}_2) \right] \left[\sin \frac{\theta}{2} \ddot{x}_3 + \cos \frac{\theta}{2} (\ddot{z}_3 + g) \right] \\ m_1 \left[\cos \frac{\theta}{2} + \sin \frac{\theta}{2} \mu_r \operatorname{sgn}(\dot{x}_2) \right] \left[\sin \frac{\theta}{2} \ddot{x}_3 + \cos \frac{\theta}{2} (\ddot{z}_3 + g) \right] \\ m_1 \left[\cos \frac{\theta}{2} - \sin \frac{\theta}{2} \mu_r \operatorname{sgn}(\dot{x}_2) \right] \left[\sin \frac{\theta}{2} \ddot{x}_3 + \cos \frac{\theta}{2} (\ddot{z}_3 + g) \right] \end{pmatrix}$$

When the roller is on the right side of the center of the lower bearing plate, the free body diagram is shown in Figure 2-7.

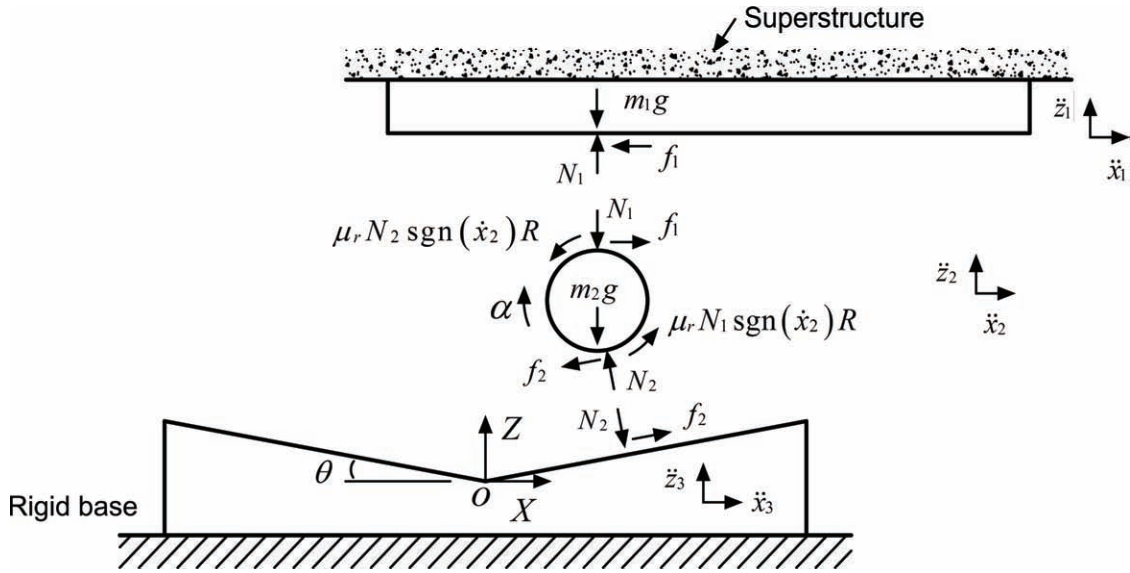


Figure 2-7 Free body diagram of a roller bearing under base excitation: roller on the right

The matrix form for the equations of dynamic equilibrium is

$$\begin{pmatrix}
 m_1 & 0 & 0 & 0 & 0 & 1 & 0 & 0 & 0 \\
 0 & m_1 & 0 & 0 & 0 & 0 & 0 & -1 & 0 \\
 0 & 0 & m_2 & 0 & 0 & -1 & \cos \theta & 0 & \sin \theta \\
 0 & 0 & 0 & -m_2 & 0 & 0 & -\sin \theta & -1 & \cos \theta \\
 0 & 0 & 0 & 0 & I & -R & -R & \mu_r \operatorname{sgn}(\dot{x}_2) R & \mu_r \operatorname{sgn}(\dot{x}_2) R \\
 0 & 0 & 1 & 0 & -R \cos \theta & 0 & 0 & 0 & 0 \\
 0 & 0 & 0 & 1 & -R \sin \theta & 0 & 0 & 0 & 0 \\
 1 & 0 & -1 & 0 & -R & 0 & 0 & 0 & 0 \\
 0 & 1 & 0 & -1 & 0 & 0 & 0 & 0 & 0
 \end{pmatrix}
 \begin{pmatrix}
 \ddot{x}_1 \\
 \ddot{z}_1 \\
 \ddot{x}_2 \\
 \ddot{z}_2 \\
 \alpha \\
 f_1 \\
 f_2 \\
 N_1 \\
 N_2
 \end{pmatrix}
 =
 \begin{pmatrix}
 -m_1 \ddot{x}_3 \\
 -m_1 (g + \ddot{z}_3) \\
 -m_2 \ddot{x}_3 \\
 m_1 (g + \ddot{z}_3) \\
 0 \\
 0 \\
 0 \\
 0 \\
 0
 \end{pmatrix}$$

The solutions are

$$\begin{pmatrix} \ddot{x}_1 \\ \ddot{z}_1 \\ \ddot{x}_2 \\ \ddot{z}_2 \\ \alpha \\ f_1 \\ f_2 \\ N_1 \\ N_2 \end{pmatrix} \approx \begin{pmatrix} -\cos^2 \frac{\theta}{2} [\ddot{x}_3 + (\ddot{z}_3 + g) \mu_r \operatorname{sgn}(\dot{x}_2)] - \frac{1}{2} \sin \theta [\ddot{z}_3 + g - \ddot{x}_3 \mu_r \operatorname{sgn}(\dot{x}_2)] \\ -\frac{1}{2} \sin \theta [\ddot{x}_3 + (\ddot{z}_3 + g) \mu_r \operatorname{sgn}(\dot{x}_2)] - \sin^2 \frac{\theta}{2} [\ddot{z}_3 + g - \ddot{x}_3 \mu_r \operatorname{sgn}(\dot{x}_2)] \\ \frac{1}{2} \cos \theta \left\{ -[\ddot{x}_3 + (\ddot{z}_3 + g) \mu_r \operatorname{sgn}(\dot{x}_2)] - \tan \frac{\theta}{2} [\ddot{z}_3 + g - \ddot{x}_3 \mu_r \operatorname{sgn}(\dot{x}_2)] \right\} \\ \frac{1}{2} \sin \theta \left\{ -[\ddot{x}_3 + (\ddot{z}_3 + g) \mu_r \operatorname{sgn}(\dot{x}_2)] - \tan \frac{\theta}{2} [\ddot{z}_3 + g - \ddot{x}_3 \mu_r \operatorname{sgn}(\dot{x}_2)] \right\} \\ \frac{1}{2R} \left\{ -[\ddot{x}_3 + (\ddot{z}_3 + g) \mu_r \operatorname{sgn}(\dot{x}_2)] - \tan \frac{\theta}{2} [\ddot{z}_3 + g - \ddot{x}_3 \mu_r \operatorname{sgn}(\dot{x}_2)] \right\} \\ m_1 \left[\sin \frac{\theta}{2} + \cos \frac{\theta}{2} \mu_r \operatorname{sgn}(\dot{x}_2) \right] \left[-\sin \frac{\theta}{2} \ddot{x}_3 + \cos \frac{\theta}{2} (\ddot{z}_3 + g) \right] \\ m_1 \left[-\sin \frac{\theta}{2} + \cos \frac{\theta}{2} \mu_r \operatorname{sgn}(\dot{x}_2) \right] \left[-\sin \frac{\theta}{2} \ddot{x}_3 + \cos \frac{\theta}{2} (\ddot{z}_3 + g) \right] \\ m_1 \left[\cos \frac{\theta}{2} - \sin \frac{\theta}{2} \mu_r \operatorname{sgn}(\dot{x}_2) \right] \left[-\sin \frac{\theta}{2} \ddot{x}_3 + \cos \frac{\theta}{2} (\ddot{z}_3 + g) \right] \\ m_1 \left[\cos \frac{\theta}{2} + \sin \frac{\theta}{2} \mu_r \operatorname{sgn}(\dot{x}_2) \right] \left[-\sin \frac{\theta}{2} \ddot{x}_3 + \cos \frac{\theta}{2} (\ddot{z}_3 + g) \right] \end{pmatrix}$$

Complete solutions that includes both conditions when the roller is on the left and right sides of the lower bearing plate are

$$\ddot{x}_1 = -\cos^2 \frac{\theta}{2} [\ddot{x}_3 + (\ddot{z}_3 + g) \mu_r \operatorname{sgn}(\dot{x}_2)] - \frac{1}{2} \sin \theta [\ddot{z}_3 + g - \ddot{x}_3 \mu_r \operatorname{sgn}(\dot{x}_2)] \operatorname{sgn}(x_2) \quad (2-13)$$

$$\ddot{z}_1 = -\frac{1}{2} \sin \theta [\ddot{x}_3 + (\ddot{z}_3 + g) \mu_r \operatorname{sgn}(\dot{x}_2)] \operatorname{sgn}(x_2) - \sin^2 \frac{\theta}{2} [\ddot{z}_3 + g - \ddot{x}_3 \mu_r \operatorname{sgn}(\dot{x}_2)] \quad (2-14)$$

$$\ddot{x}_2 = \frac{1}{2} \cos \theta \left\{ -[\ddot{x}_3 + (\ddot{z}_3 + g) \mu_r \operatorname{sgn}(\dot{x}_2)] - \tan \frac{\theta}{2} [\ddot{z}_3 + g - \ddot{x}_3 \mu_r \operatorname{sgn}(\dot{x}_2)] \operatorname{sgn}(x_2) \right\} \quad (2-15)$$

$$\ddot{z}_2 = \frac{1}{2} \sin \theta \left\{ -[\ddot{x}_3 + (\ddot{z}_3 + g) \mu_r \operatorname{sgn}(\dot{x}_2)] - \tan \frac{\theta}{2} [\ddot{z}_3 + g - \ddot{x}_3 \mu_r \operatorname{sgn}(\dot{x}_2)] \operatorname{sgn}(x_2) \right\} \quad (2-16)$$

$$\alpha = \frac{1}{2R} \left\{ -[\ddot{x}_3 + (\ddot{z}_3 + g) \mu_r \operatorname{sgn}(\dot{x}_2)] - \tan \frac{\theta}{2} [\ddot{z}_3 + g - \ddot{x}_3 \mu_r \operatorname{sgn}(\dot{x}_2)] \operatorname{sgn}(x_2) \right\} \quad (2-17)$$

$$f_1 = m_1 \left[\sin \frac{\theta}{2} \operatorname{sgn}(x_2) + \cos \frac{\theta}{2} \mu_r \operatorname{sgn}(\dot{x}_2) \right] \left[-\sin \frac{\theta}{2} \ddot{x}_3 \operatorname{sgn}(x_2) + \cos \frac{\theta}{2} (\ddot{z}_3 + g) \right] \quad (2-18)$$

$$f_2 = m_1 \left[-\sin \frac{\theta}{2} \operatorname{sgn}(x_2) + \cos \frac{\theta}{2} \mu_r \operatorname{sgn}(\dot{x}_2) \right] \left[-\sin \frac{\theta}{2} \ddot{x}_3 \operatorname{sgn}(x_2) + \cos \frac{\theta}{2} (\ddot{z}_3 + g) \right] \quad (2-19)$$

$$N_1 = m_1 \left[\cos \frac{\theta}{2} - \sin \frac{\theta}{2} \mu_r \operatorname{sgn}(\dot{x}_2) \operatorname{sgn}(x_2) \right] \left[-\sin \frac{\theta}{2} \ddot{x}_3 \operatorname{sgn}(x_2) + \cos \frac{\theta}{2} (\ddot{z}_3 + g) \right] \quad (2-20)$$

$$N_2 = m_1 \left[\cos \frac{\theta}{2} + \sin \frac{\theta}{2} \mu_r \operatorname{sgn}(\dot{x}_2) \operatorname{sgn}(x_2) \right] \left[-\sin \frac{\theta}{2} \ddot{x}_3 \operatorname{sgn}(x_2) + \cos \frac{\theta}{2} (\ddot{z}_3 + g) \right] \quad (2-21)$$

where $\operatorname{sgn}(x_2)$ is 1 if x_2 is positive (on the right side of the center of the lower bearing plate) and -1 if x_2 is negative (on the left side of the center of the lower bearing plate).

2.3 Governing Equations of Motion

Equation (2-13) represents the governing equation of motion for the horizontal movement the superstructure along the principal directions. In this report, steel rollers and steel bearing plates are used. The coefficient of rolling friction μ_r for a steel roller rolling on a steel plate is $0.002/R$ (in) (equation (2-3)). The value of μ_r can be further reduced for hard polished steel surfaces. The radius of the roller R in our applications is typically larger than 1 in, which means μ_r is smaller than 0.002. In addition, a small sloping angle θ is used. As a result, $\cos^2 \theta / 2 \approx 1$ and $\mu_r \cdot \sin(\theta / 2) \approx 0$. Simplifying and re-arranging equation (2-13) leads to

$$m_1 \ddot{x}_1 + \frac{1}{2} m_1 \sin \theta (\ddot{z}_3 + g) \operatorname{sgn}(x_2) + \mu_r m_1 (\ddot{z}_3 + g) \operatorname{sgn}(\dot{x}_2) = -m_1 \ddot{x}_3 \quad (2-22)$$

For a pure rolling motion, the relative displacement of the superstructure x_1 is twice that of the roller x_2 , that is,

$$2x_2 = x_1 \quad (2-23)$$

This means the displacement capacity of a bridge superstructure seating on a roller bearing is twice the available travel that can be provided by the bearing plate.

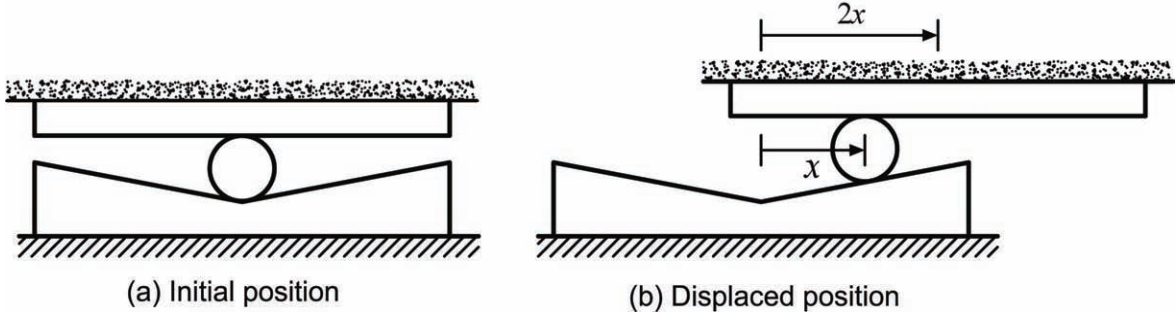


Figure 2-8 Relationship between displacements of the roller and superstructure

Thus, equation (2-22) can also be expressed as

$$m_1 \ddot{x}_1 + \frac{1}{2} m_1 \sin \theta (\ddot{z}_3 + g) \operatorname{sgn}(x_1) + \mu_r m_1 (\ddot{z}_3 + g) \operatorname{sgn}(\dot{x}_1) = -m_1 \ddot{x}_3 \quad (2-24)$$

The second term of equations (2-24) represents the restoring forces f_s of the bearing. The third term represents the rolling friction force f_{Dr} . Thus, equation (2-24) can also be expressed as

$$m_1 \ddot{x}_1 + f_s \operatorname{sgn}(x_1) + f_{Dr} \operatorname{sgn}(\dot{x}_1) = -m_1 \ddot{x}_3 \quad (2-25)$$

where

$$f_s = \frac{1}{2} m_1 (\ddot{z}_3 + g) \sin \theta \quad (2-26)$$

$$f_{Dr} = \mu_r m_1 (\ddot{z}_3 + g) \quad (2-27)$$

If the vertical base acceleration \ddot{z}_3 is not considered, equations (2-26) and (2-27) become

$$f_s = \frac{1}{2} m_1 g \sin \theta \quad (2-28)$$

$$f_{Dr} = \mu_r m_1 g \quad (2-29)$$

The base shear of the bearing is

$$V = f_s + f_{Dr} \quad (2-30)$$

Figure 2-9 shows the relationship between the base shear V and the relative displacement of the superstructure x_1 without the consideration of vertical base excitation. A constant “post-elastic” force can be observed.

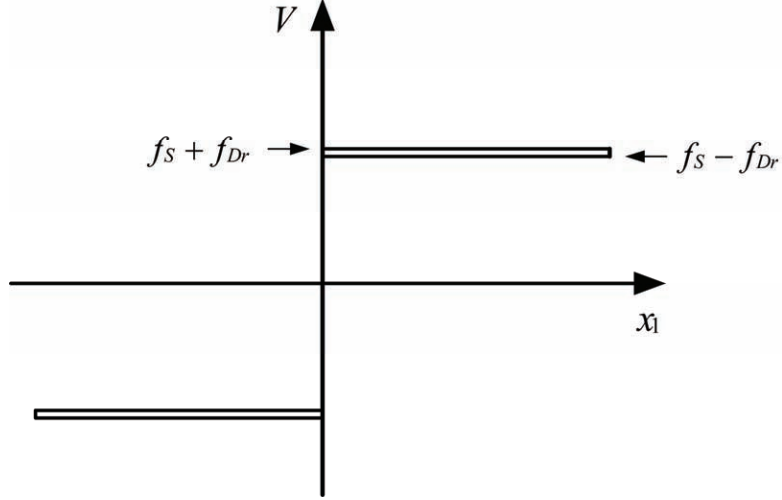


Figure 2-9 Base shear versus relative displacements of the superstructure

If the base excitation acts along directions 45 degrees away from the principal directions (see Figure 2-10), both the upper roller and the lower roller will be mobilized. As a result, the bearing will have the maximum magnitude of the restoring force and the rolling friction force. Under such a condition, the restoring force and the rolling friction force are

$$f_s = \frac{\sqrt{2}}{2} m_1 (\ddot{z}_3 + g) \sin \theta \quad (2-31)$$

$$f_{Dr} = \sqrt{2} \mu_r m_1 (\ddot{z}_3 + g) \quad (2-32)$$

If the vertical base acceleration \ddot{z}_3 is not considered, equations (2-31) and (2-32) become

$$f_s = \frac{\sqrt{2}}{2} m_1 g \sin \theta \quad (2-33)$$

$$f_{Dr} = \sqrt{2} \mu_r m_1 g \quad (2-34)$$

It can be seen from equations (2-26) to (2-34) that the values of V are independent of the magnitude and frequency content of the horizontal base acceleration \ddot{x}_3 , which eliminates the possibility of resonance between the bearing and base excitation. Note that the sloping angle θ needs to be small as previously stated to achieve this. On the other hand, a certain sloping angle is needed to provide a necessary restoring force to overcome the rolling friction force and hence to re-center the bearing. When the bearing is used in combination with sliding friction devices, the restoring force needs to be larger than the sliding friction force of the devices as well as the rolling friction force. This is discussed in detail in the next chapter. Note that equations (2-26) to (2-34) also show that vertical ground motions could have an effect on the responses of the

bearing. This is also investigated in the next chapter. Furthermore, it is demonstrated in the following section that there is an upper limit for the sloping angle θ to prevent sliding of the roller.

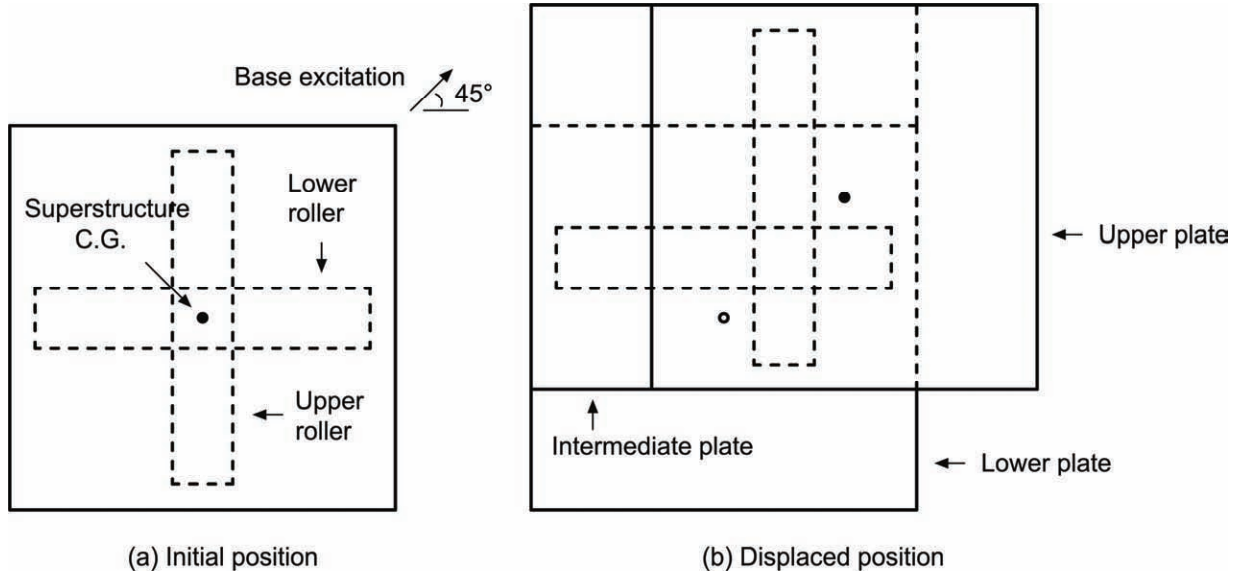


Figure 2-10 Top view of the bearing under base excitation along a direction 45 degrees away from the principal direction

2.4 Conditions for Rolling without Sliding

As mentioned in Section 2.2.1, once the static friction force between the roller and the bearing plate f developed by an angular acceleration of the roller exceeds the maximum static friction force f_{st} that can be provided by the contact interface, the roller starts sliding. Once the roller slides, the principles of a roller bearing as presented in this chapter no longer hold true. Furthermore, the bearing may exhibit significant permanent displacements after earthquakes. Thus, sliding of the roller needs to be prevented.

The maximum static friction force f_{st} is defined by

$$f_{st} = \mu_s N \quad (2-35)$$

where μ_s is the coefficient of static friction and N is the normal force between the surfaces in contact. To ensure rolling without sliding, the following equation must be satisfied.

$$f_{st} = \mu_s N \geq |f|_{\max} \quad (2-36)$$

Substituting N_1 and f_1 from equations (2-20) and (2-18) into equation (2-36) for N and f , respectively, leads to

$$\mu_s \geq \frac{m_1 \left[\sin \frac{\theta}{2} \operatorname{sgn}(x_2) + \cos \frac{\theta}{2} \mu_r \operatorname{sgn}(\dot{x}_2) \right] \left[-\sin \frac{\theta}{2} \ddot{x}_3 \operatorname{sgn}(x_2) + \cos \frac{\theta}{2} (\ddot{z}_3 + g) \right]}{m_1 \left[\cos \frac{\theta}{2} - \sin \frac{\theta}{2} \mu_r \operatorname{sgn}(\dot{x}_2) \operatorname{sgn}(x_2) \right] \left[-\sin \frac{\theta}{2} \ddot{x}_3 \operatorname{sgn}(x_2) + \cos \frac{\theta}{2} (\ddot{z}_3 + g) \right]} \quad (2-37)$$

As previously stated, the term $\mu_r \sin \theta / 2$ is small and hence can be ignored. Further simplification leads to

$$\mu_s \geq \mu_r + \tan \frac{\theta}{2} \quad (2-38)$$

In a similar manner, substituting N_2 and f_2 from equations (2-21) and (2-19) into equation (2-36) for N and f , respectively, also leads to equation (2-38). In other words, the sloping angle θ has to satisfy

$$\theta \leq 2 \tan^{-1}(\mu_s - \mu_r) \quad (2-39)$$

This equation shows the upper limit of the sloping angle θ for rolling without sliding increases as the value of the coefficient of static friction μ_s increases and decreases as the value of the coefficient of rolling friction increases. The values of μ_s for steel on steel range from 0.74 for dry condition to approximately 0.1 for greasy condition (Avallone and Baumeister 1996). For a conservative result, the value of μ_s is taken as 0.1. The value of μ_r can be taken as 0.002 as previously stated. The condition for rolling without sliding is

$$\theta \leq 11^\circ \quad (2-40)$$

2.5 Uplift of Superstructure

Another premise of the derivation previously presented is that the normal forces N_1 and N_2 have to be positive as shown by equations (2-41) and (2-42), respectively.

$$N_1 = m_1 \left[\cos \frac{\theta}{2} - \sin \frac{\theta}{2} \mu_r \operatorname{sgn}(\dot{x}_2) \operatorname{sgn}(x_2) \right] \left[-\sin \frac{\theta}{2} \ddot{x}_3 \operatorname{sgn}(x_2) + \cos \frac{\theta}{2} (\ddot{z}_3 + g) \right] > 0 \quad (2-41)$$

$$N_2 = m_1 \left[\cos \frac{\theta}{2} + \sin \frac{\theta}{2} \mu_r \operatorname{sgn}(\dot{x}_2) \operatorname{sgn}(x_2) \right] \left[-\sin \frac{\theta}{2} \ddot{x}_3 \operatorname{sgn}(x_2) + \cos \frac{\theta}{2} (\ddot{z}_3 + g) \right] > 0 \quad (2-42)$$

In other words, the superstructure has to remain in contact with the roller. If uplift of the superstructure takes places, the behavior of the bearing is complicated and unpredictable and

large permanent displacements of the bearing may occur after earthquakes. In the two equations shown above, when θ is small, $\sin \theta / 2 \cdot \ddot{x}_3$ becomes negligible compared to $\cos \theta / 2 (\ddot{z}_3 + g)$. Moreover, $\cos^2 \theta / 2 \approx 1$ and $\mu_r \sin \theta / 2 \approx 0$. Thus, equations (2-41) and (2-42) can be simplified and rearranged to equation (2-43), which shows that if the magnitude of downward vertical base acceleration \ddot{z}_{3-} is smaller than g , uplift of the superstructure will not occur.

$$|\ddot{z}_{3-}| < g \quad (2-43)$$

One can increase the level of force needed to uplift the superstructure by introducing sliding friction forces to the bearing. Under such a condition, the allowable downward vertical base acceleration is increased as shown in equation (2-44).

$$|\ddot{z}_{3-}| < g + \sum f_{Ds} / m_1 \quad (2-44)$$

where $\sum f_{Ds}$ is the total sliding friction force of the friction devices. Section 4.2 presents design details to integrate friction devices into the bearing.

2.6 Vertical Load Carrying Capacity

2.6.1 Derivation

The vertical load carrying capacity of a roller bearing can be determined using Hertz theory (Young and Budynas 2002). Although Hertz theory is based on the static condition of two contact bodies, it can be applied to rolling conditions if rolling without sliding holds true (Young and Budynas 2002). For a solid, elastic cylindrical roller of radius R rolling on a flat bearing plate as shown in Figure 2-11, the maximum contact stress $\sigma_{c(\max)}$ is given by

$$\sigma_{c(\max)} = 0.564 \sqrt{\frac{p}{RC_E}} \quad (2-45)$$

$$C_E = \frac{1-\nu_1^2}{E_1} + \frac{1-\nu_2^2}{E_2} \quad (2-46)$$

where p is the vertical load per unit length of the roller; and E_1 and E_2 , and ν_1 and ν_2 are the moduli of elasticity and Poisson's ratios, respectively, of the materials used in the two components in contact. The width of the contact area between the roller and plate, b , can be calculated by

$$b = 2.263 \sqrt{pRC_E} \quad (2-47)$$

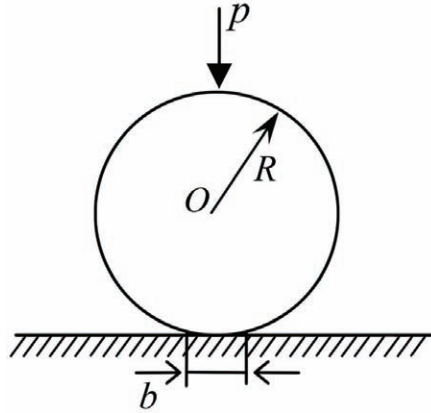


Figure 2-11 A solid cylindrical roller in contact with a flat surface under a load per unit length p

If both the roller and bearing plate are made of steel, then $E_1 = E_2 = E_s$ and $\nu_1 = \nu_2 = 0.3$. Equation (2-45) can then be specialized to

$$\sigma_{c(\max)} = 0.418 \sqrt{\frac{pE_s}{R}} \quad (2-48)$$

AASHTO (2004) Section 14.7.1.4 limits the maximum contact stress $\sigma_{c(\max)}$ in the contact regions at the service limit state to be $1.65 \sigma_y$.

$$\sigma_{c(\max)} \leq 1.65 \sigma_y \quad (2-49)$$

Substituting equation (2-49) into equation (2-48), the vertical load carried by the roller should be limited to

$$DL \geq \frac{PE_s}{8 \sigma_y^2} \quad (2-50)$$

where D and L are the diameter and the length of the roller; and P is the total factored vertical load applied to the roller.

2.6.2 Finite Element Analysis

Equation (2-50) was derived for a solid cylindrical roller on a flat, infinite thick body. However, a roller bearing would have one roller with a finite length on the top of a finite thick plate, which is supported by the other roller that is perpendicular to the roller above it. In addition, hollow rollers rather than solid rollers would be used to reduce the weight and cost of the rollers. This section presents a three-dimensional finite element study to evaluate the use of equation (2-50) in the design of the rollers for a roller bearing.

As shown in Figure 2-12, the roller bearing investigated had flat upper and lower plates. The bearing had two V-shaped sloping surfaces: one was located at the top and the other at the bottom of the intermediate plate.

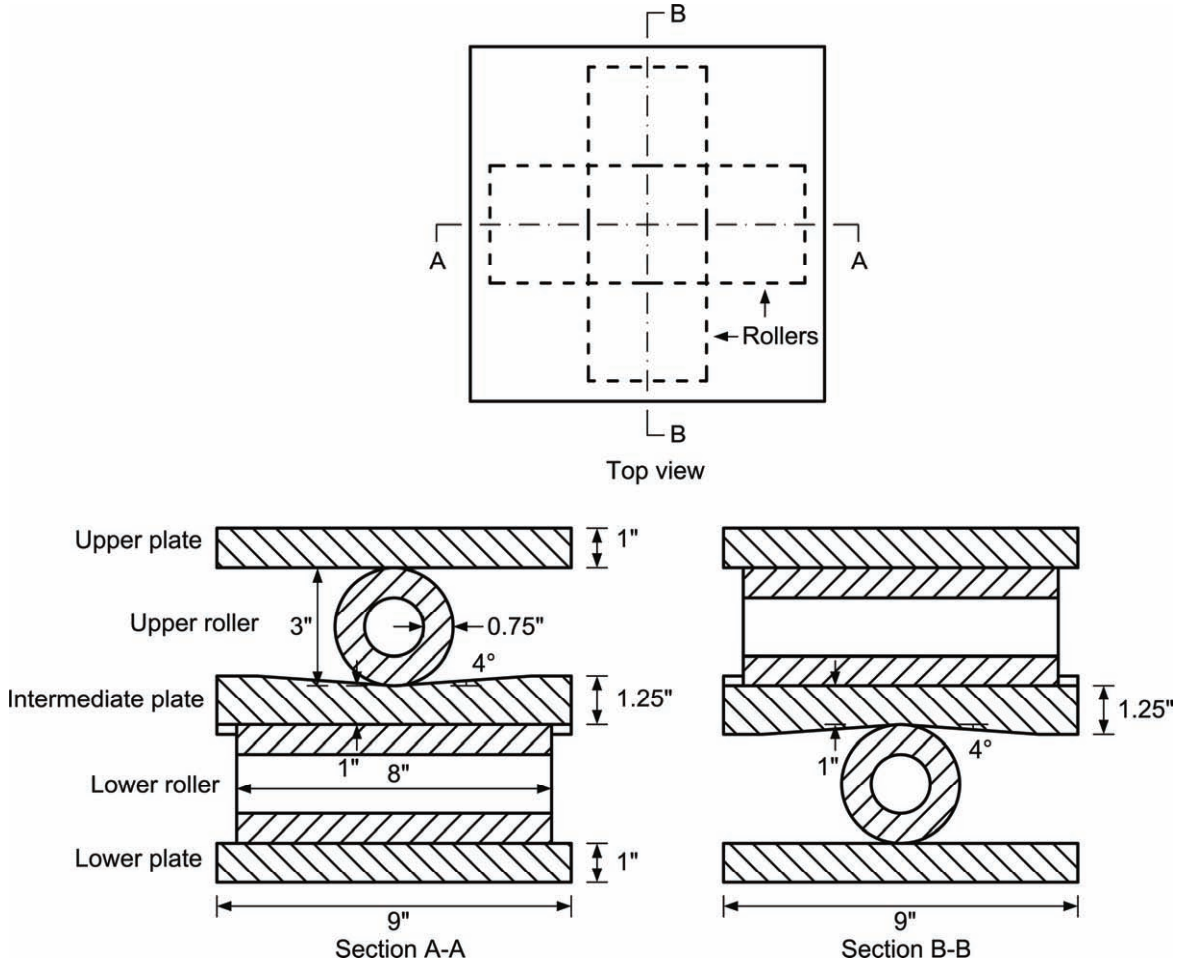


Figure 2-12 Schematic view of the roller bearing

The bearing was made of steel with a modulus of elasticity E_s of 29500 ksi (204000 MPa) and a yield strength σ_y of 100 ksi (689 MPa) and carried a factored vertical load of 65 kips (289 kN). According to equation (2-50), the product of the diameter D and length L of the roller should satisfy

$$DL \geq \frac{PE_s}{8 \sigma_y^2} = \frac{65 \times 29500}{8(100)^2} = 24 \text{ (in}^2\text{)} (= 15484 \text{ mm}^2)$$

Two identical rollers with a diameter D of 3 in (76 mm) and a length L of 8 in (20 mm) were selected. The wall thickness of the rollers was selected as 0.25 times the diameter, that is, 0.75 in

(19 mm). The intermediate plate should be designed with a thickness at least larger than the wall thickness of the roller. A thickness of 1 in (25 mm) was used in the center of the plate, that is, the position at the intersection of section lines A-A and B-B shown in Figure 2-12. The sloping angle of each of the two V-shaped sloping surfaces was selected as 4 degrees. The upper and lower plates were designed with a thickness of 1 in (25 mm).

A three-dimensional finite element model for this roller bearing was constructed using ABAQUS (HKS 2002). The model was formed with eight-node solid linear elements (C3D8). The top of the upper plate was constrained to prevent any horizontal movements and rotations. A 65 kip (289 kN) load was uniformly applied on the top of the upper plate. The bottom face of the lower plate was fixed to the ground. Contact elements were used between each roller and the plates with an assumed coefficient of static friction of 0.15. The material model for the steel is shown in Figure 2-13. The modulus of elasticity was assumed to be 29500 ksi (204000 MPa). The strain hardening curve was defined with a straight line connecting the yield point and the point with a stress and a strain of 138 ksi (951 MPa) and 0.157, respectively.

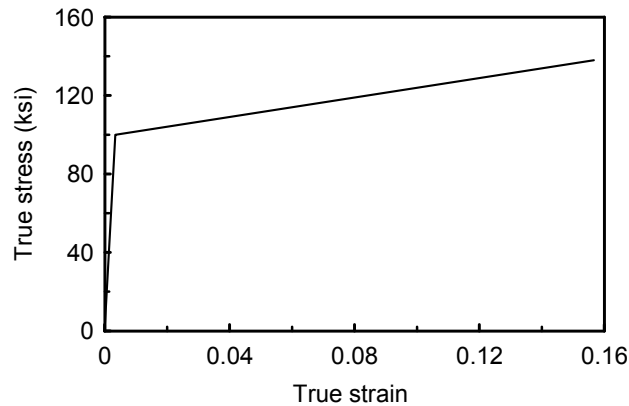


Figure 2-13 Stress-strain relationship of the steel

Two cases were investigated in terms of the position of the rollers shown in Figure 2-14. In the first case, the rollers were in their initial positions shown in Figure 2-14(a). In the second case, the rollers were placed in a position 2.5 in (51 mm) away from the center shown in Figure 2-14(b). It can be seen that at this position the effective contact areas between the rollers and plates are greatly reduced as compared to those at the initial position.

Results of the analyses of the two cases in terms of the Mises stress are shown in Figures 2-15 and 2-16. For the first case, the stress in the middle portion of the rollers was larger than at the two sides. This is expected since the two rollers are perpendicular to each other, which limits the contact area that is effective for carrying the load. The maximum Mises stress was found to be 70 ksi (483 MPa), which is $0.7 \sigma_y$, and located in the center region of the intermediate plate. The maximum stress in the rollers was found to be 49 ksi (338 MPa) and located in the top, middle region of the lower roller.

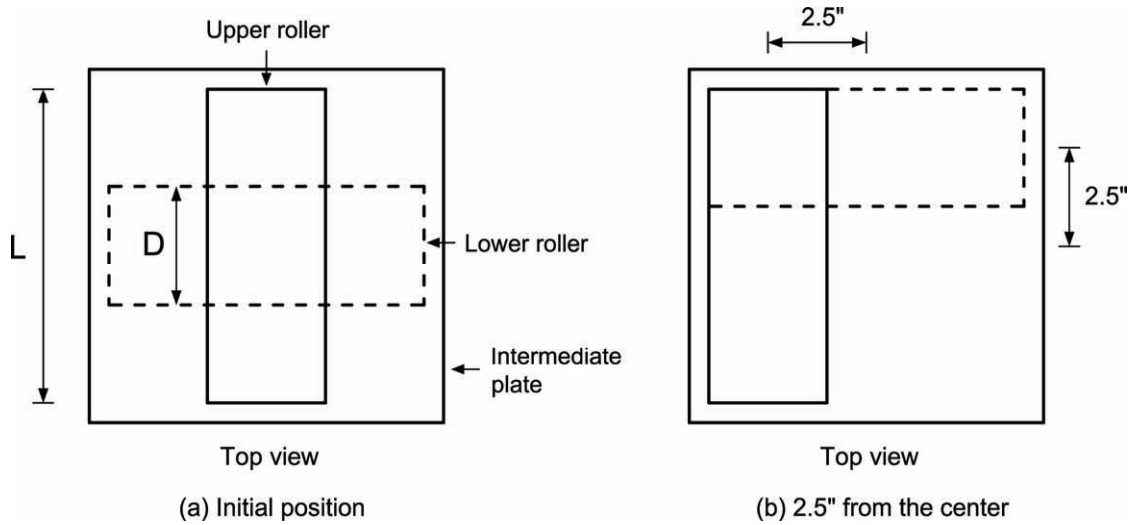


Figure 2-14 Positions of the rollers

For the second case, the maximum Mises stress was 121 ksi (834 MPa), which exceeded the yield strength. The yielding regions concentrated at the ends of both rollers. Upon unloading, permanent deformations resulted, causing small dents at the ends of the rollers. This would reduce the effective length of the roller for carrying the vertical load.

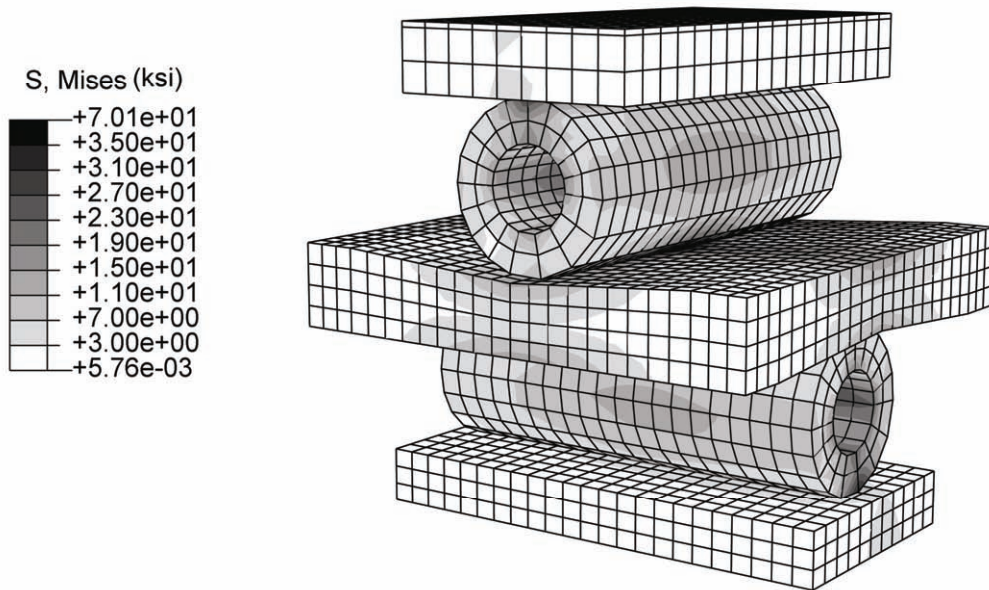


Figure 2-15 Initial design: initial position

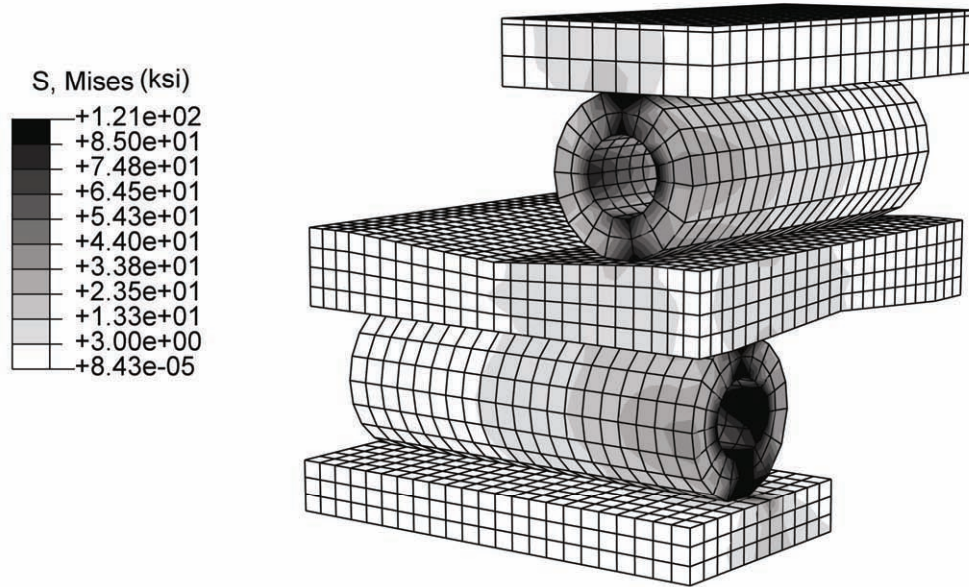


Figure 2-16 Initial design: 2.5-in from the initial position

To address this issue, we increased the length of the rollers by an amount that is equal to the required displacement capacity. The final length of the roller is

$$L' = L + 2D_r \quad (2-51)$$

where L' is the final length of the roller; L is length used in equation (2-50) and is referred to as the initial length hereafter; and D_r is the required displacement capacity of the roller. Note that the required displacement capacity of the bearing (or superstructure) is $2D_r$. Equation (2-51) ensures that the effective contact areas between the rollers and the plates when the rollers are in the positions corresponding to the displacement capacity of the bearing are not less than calculated using equation (2-50). This is illustrated in Figure 2-17.

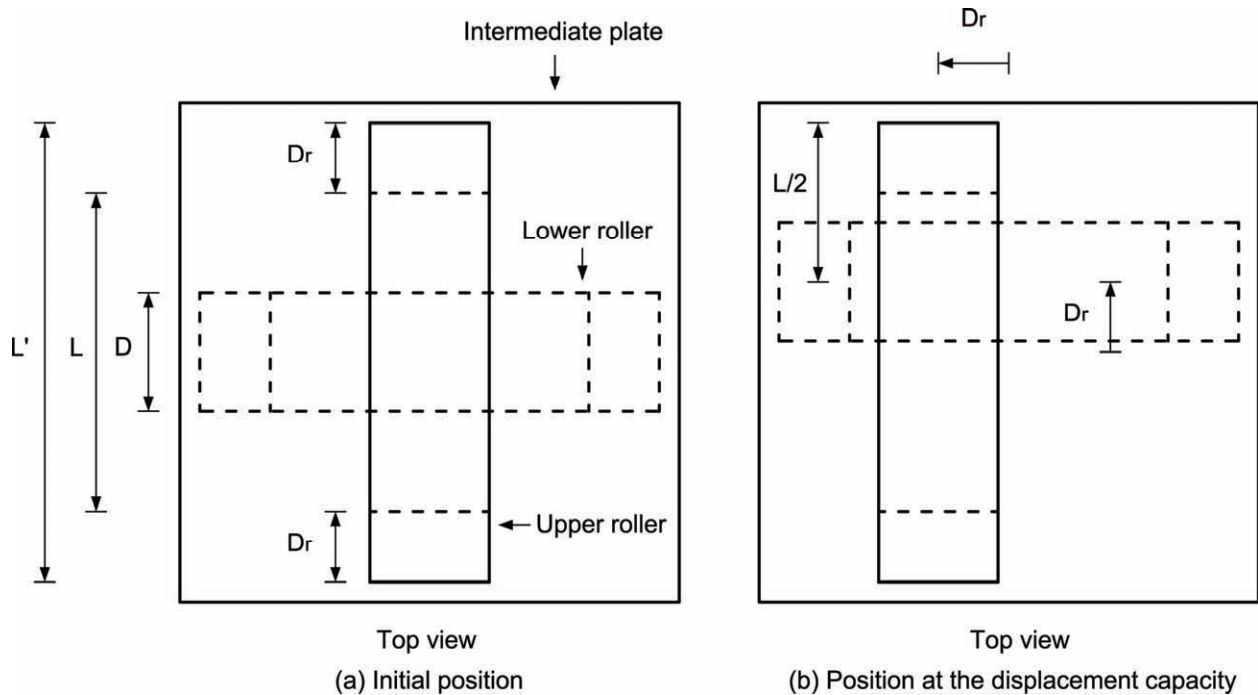


Figure 2-17 Use of longer rollers

Assume the required displacement capacity of the bearing previously investigated to be 2.5 in (64 mm). Thus, D_r is equal to 1.25 in (32 mm). That means the final length of the roller L' is

$$L' = 8 + 2 \cdot 1.25 = 10.5 \text{ (in)} (= 267 \text{ mm})$$

The final design of the bearing is shown in Figure 2-18. Figures 2-19 and 2-20 show the analysis results. At the initial position and at the position corresponding to the displacement capacity, the maximum Mises stresses were 30 ksi (207 MPa) and 25 ksi (172 MPa), respectively, both of which were lower than the yield strength. Furthermore, in the former case, the maximum stress occurred in the center region of the intermediate plate. The maximum stress in the rollers was 23ksi (159 MPa). At the position corresponding to the displacement capacity, since the rollers were displaced away from the center region of the intermediate plate, which has the smallest thickness of the plate, the maximum stress shifted to the rollers.

Note that the rollers investigated herein have a ratio of the wall thickness to diameter of 0.25. A ratio smaller than 0.25 would cause higher stresses in the rollers. A finite element analysis must be conducted before a smaller ratio can be used. A ratio that is larger than 0.25 will provide a more conservative design.

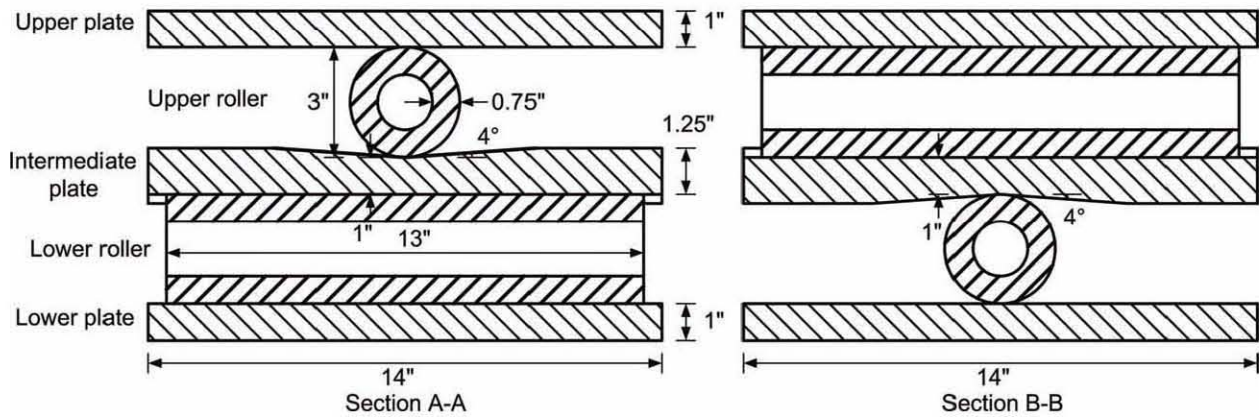
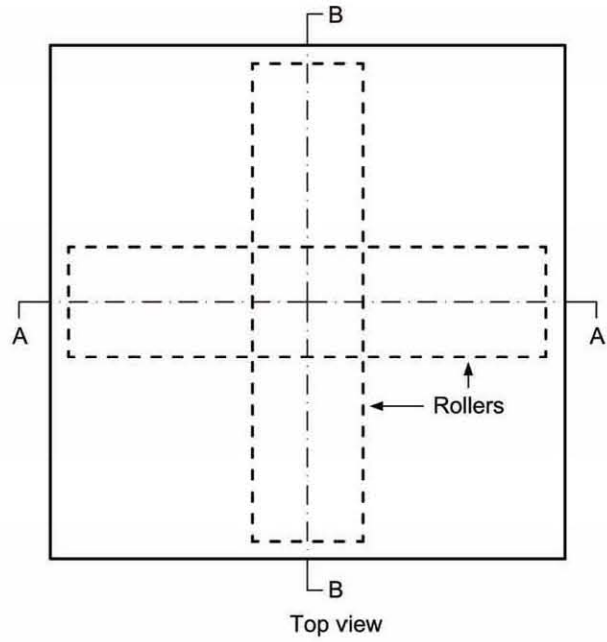


Figure 2-18 Revised design

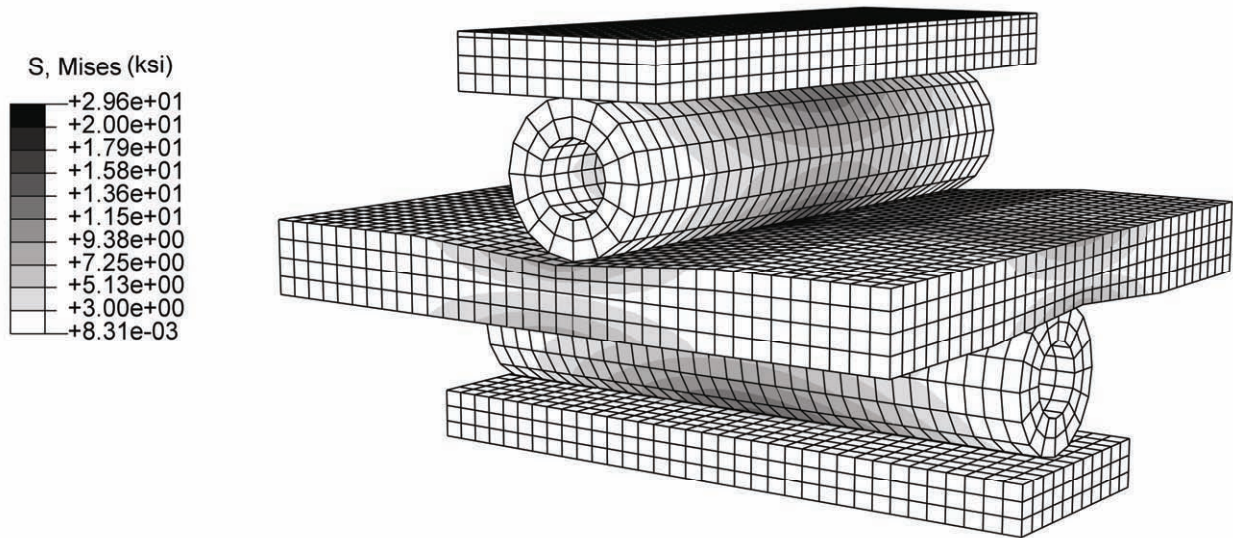


Figure 2-19 Revised design: initial position

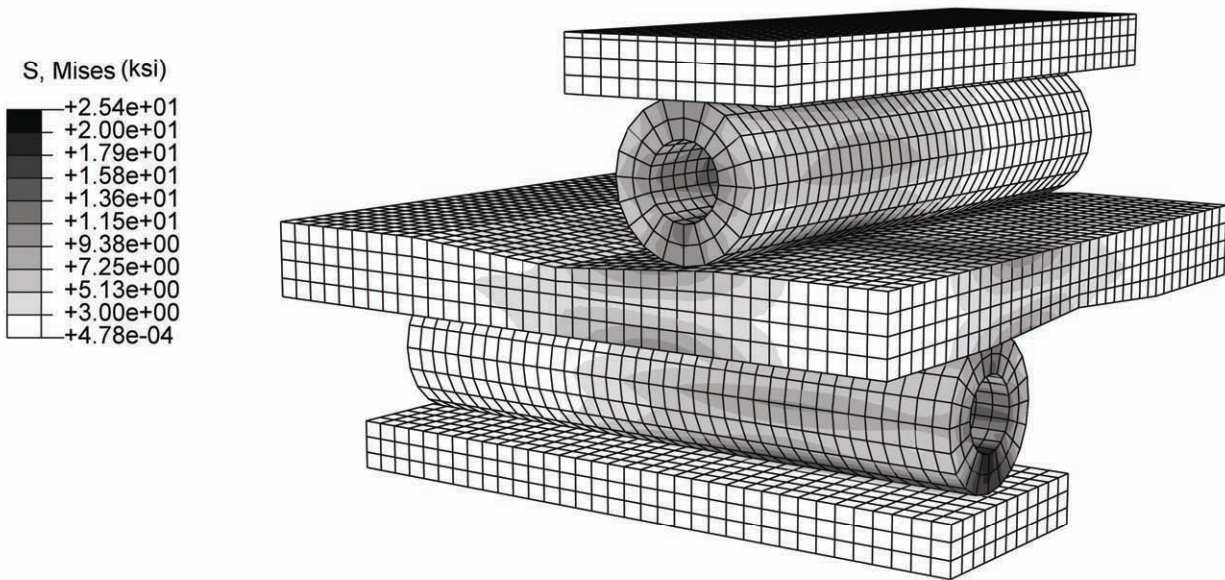


Figure 2-20 Revised design: 2.5-in from the initial position

2.7 Experimental Validation

To validate the analytical models for the proposed roller bearings under ground excitation, several experimental studies were carried out and are presented in Appendix A. Select results are shown in this section and compared to the analytical prediction.

2.7.1 Description of the Bridge Model

A scaled bridge superstructure was placed on four roller seismic isolation bearings mounted on two earthquake simulators (shake tables) in the NEES equipment site at the University of Nevada, Reno. Figure 2-21 illustrates the side view of the bridge model on the north shake table. The shear force in each bearing was measured by a load cell placed between the bearing and the shake table. The test step is shown in Figures 2-22 and 2-23. The superstructure consisted of a concrete deck composite with two steel girders. The length and width of the superstructure was 60 ft (18.3 m) and 8.25 ft (2.5 m), respectively. The total weight of the superstructure was 76.7 kips (341.2 kN). The principal directions of the roller bearings coincided with the transverse and longitudinal directions of the superstructure. The sloping angle of the bearing was 2 degrees. Detailed design information of the roller bearings is presented in Section 4.1.

The bridge model is a 0.4 scale to the prototype bridge. A summary of the scale factors in the model is presented in Table 2-1. Ground motions used were time-scaled by a factor of 0.632 ($=\sqrt{0.4}$).

Table 2-1 Scale factors for the bridge model

Quantity	Dimension	Scale factor
Length	L	0.4
Modulus of elasticity	$ML^{-1} T^{-2}$	1.0
Acceleration	LT^{-2}	1.0
Mass	M	0.16
Time	T	0.632
Displacement	L	0.4
Force	MLT^{-2}	0.16
Stiffness	MT^{-2}	0.4

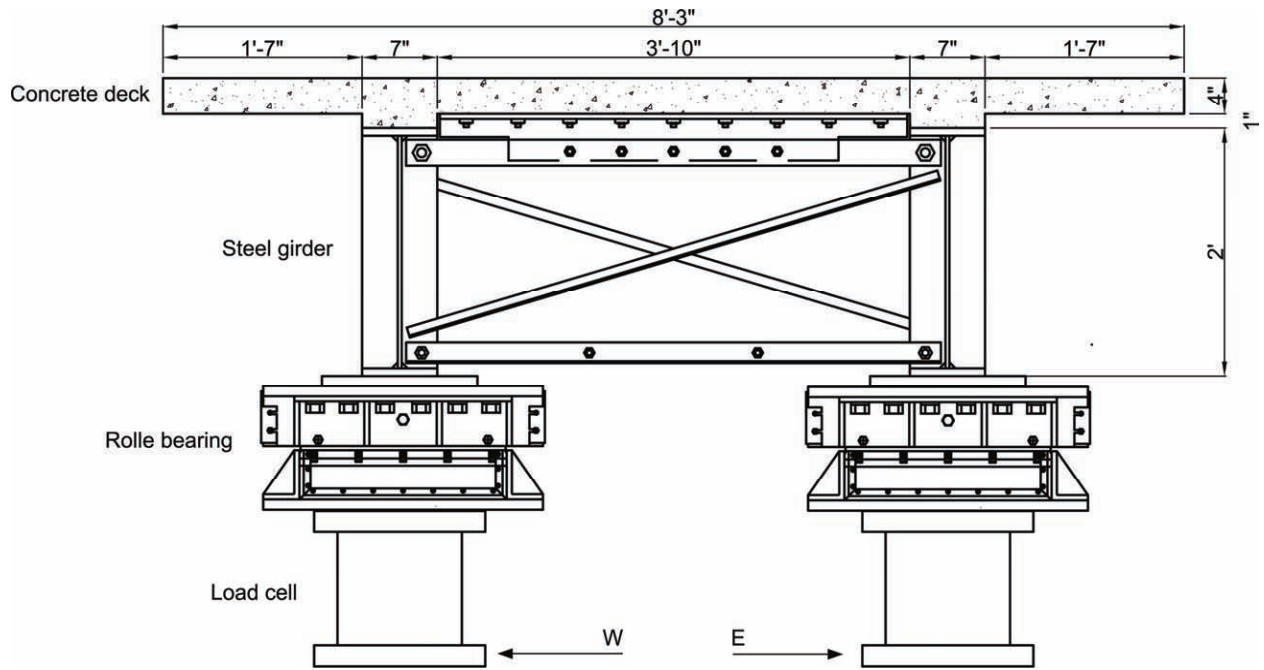


Figure 2-21 Side view of the bridge model on the north shake table

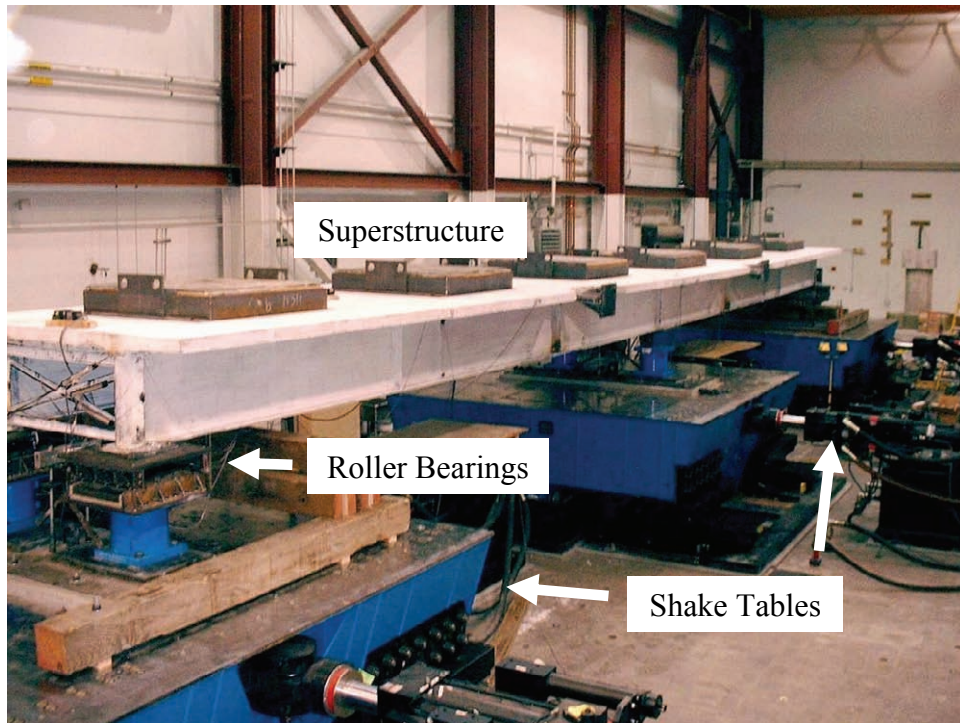


Figure 2-22 Test setup

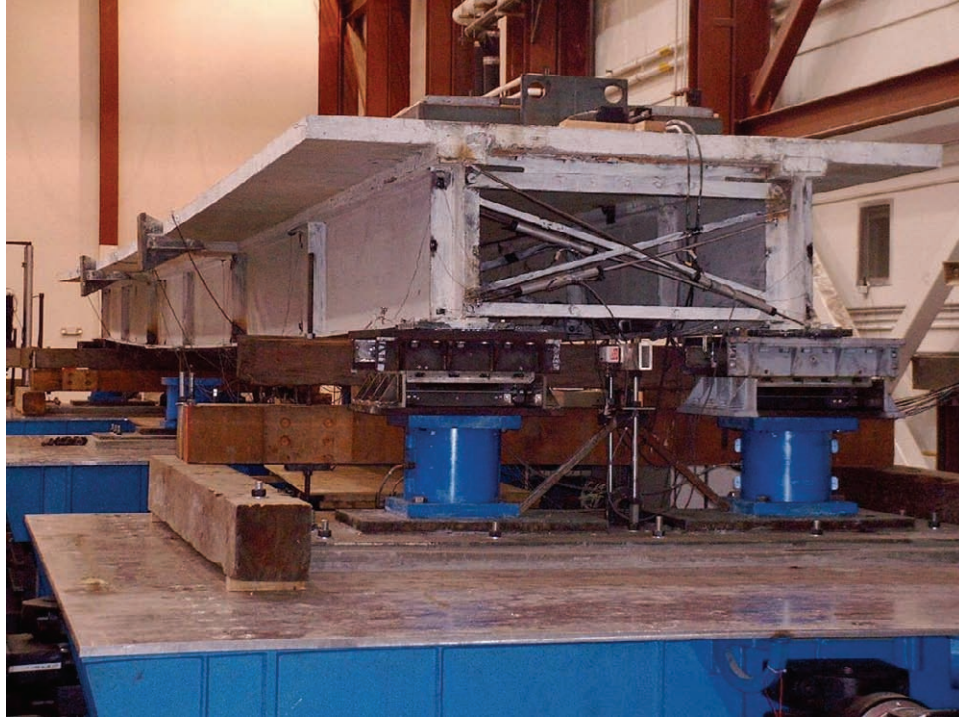


Figure 2-23 Side view of the bridge model

2.7.2 Test Results

Sample experimental results under 50% of the 1994 El Centro earthquake and 100% of the 1995 Kobe earthquake are presented here. The acceleration histories of the ground motions are shown in Figures 2-24 and 2-27, respectively, which were obtained from the accelerometers installed on the shake tables. Both the ground motions were applied in the longitudinal direction of the bridge. Figures 2-25 and 2-28 show the 5% damped elastic absolute acceleration response spectra for both ground motions. Figures 2-26 and 2-29 show the responses of the bearings under 50% El Centro and 100% Kobe, respectively. From Figures 2-26a and 2-29a, it can be seen that the peak acceleration responses of the bearings were limited to approximately 0.02 g and independent of the magnitude and frequency content of the horizontal ground motions. Jagged spikes in acceleration responses with amplitudes larger than 0.02 g can be observed in the figures. This may be attributed to the impacts of components of the bridge and vertical acceleration of the shake tables. The latter could increase the horizontal acceleration responses as explained by equation (2-24). The effects of vertical ground accelerations on the bearing performance are investigated later in Section 3.3. From Figures 2-26b and 2-29b, it is seen that the bearings had no permanent displacements after testing.

2.7.3 Comparison between Experiment and Analytical Study

According to equations (2-28), (2-29) and (2-30), the maximum base shear of the bridge model V under horizontal base excitation along the principal directions of the bearing is

$$V = \frac{1}{2} mg \sin \theta + \mu_r mg = \frac{1}{2} \cdot 76.7 \cdot \sin 2^\circ + 0.00089 \cdot 76.7$$

$$= 1.34 + 0.07 = 1.41 \text{ (kips)} (= 6.27 \text{ kN})$$

where mg is the weight of the superstructure; and μ_r was calculated by equation (2-3):

$$\mu_r = \frac{0.002}{R} = \frac{0.002}{2.25} = 0.00089$$

Four roller bearings were used in the bridge model. The maximum base shear for each bearing V_1 along the principal directions of the bearing is

$$V_1 = \frac{V}{4} = \frac{1.41}{4} = 0.35 \text{ (kips)} (= 1.57 \text{ kN})$$

The maximum absolute acceleration response A is

$$A = \frac{V_1}{mg/4} g = \frac{0.35}{76.7/4} g = 0.018 g$$

This value agrees well with the maximum acceleration responses of the bearings to both the ground motions as shown in Figures 2-26a and 2-29a.

For response-history analysis, the bridge model was simplified as a SDOF system. Equation (2-52) shows the governing equation of motion of the system (from equations (2-25), (2-28) and (2-29)):

$$\ddot{x} + \frac{1}{2} g \sin \theta \operatorname{sgn}(x) + \mu_r g \operatorname{sgn}(\dot{x}) = -\ddot{x}_g \quad (2-52)$$

where x , \dot{x} and \ddot{x} are the relative displacement, velocity and acceleration of the superstructure; and \ddot{x}_g is the shake table acceleration. Figures 2-26 and 2-29 show the comparisons of responses between experimental and analytical results under 50% El Centro and 100% Kobe, respectively. Acceleration responses from both results agree well except for responses near the end of the shaking when the bearing stopped rolling. Under such a condition, the effects of the flexibility of the bridge superstructure and connections between the superstructures and the shake tables became significant. These effects were not accounted for in equation (2-52). A similar trend can be observed for the displacement responses of the bearings.

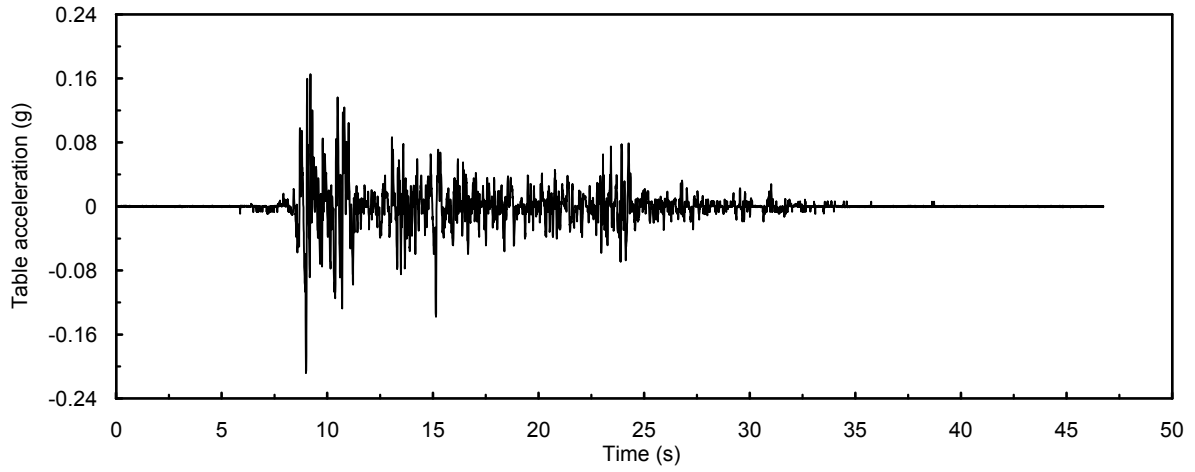


Figure 2-24 Measured shake table output under 50% El Centro

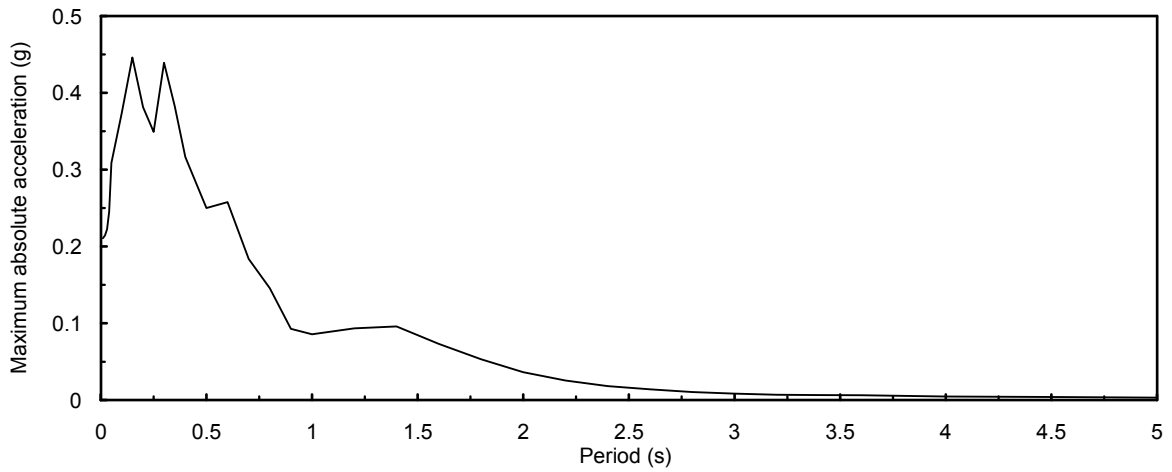
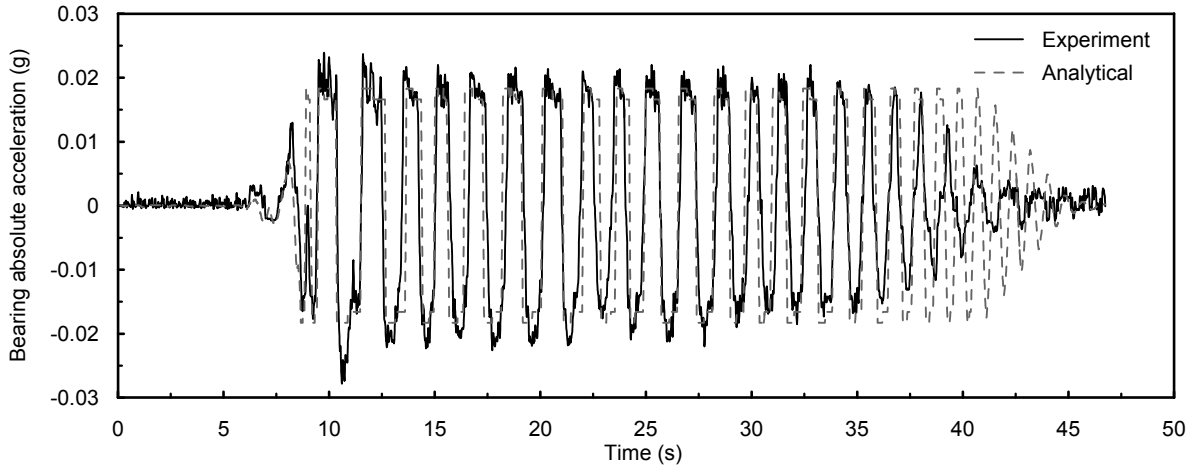
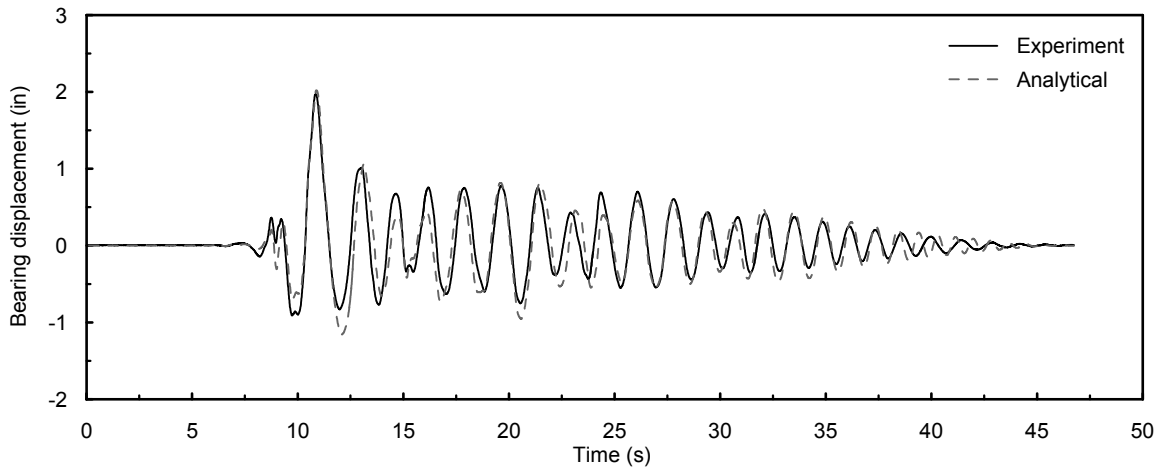


Figure 2-25 5% damped elastic absolute acceleration spectrum of the measured 50% El Centro



(a) Bearing absolute acceleration history



(b) Bearing displacement history

Figure 2-26 Comparison of the South-East bearing responses between analytical and experiment under 50% El Centro

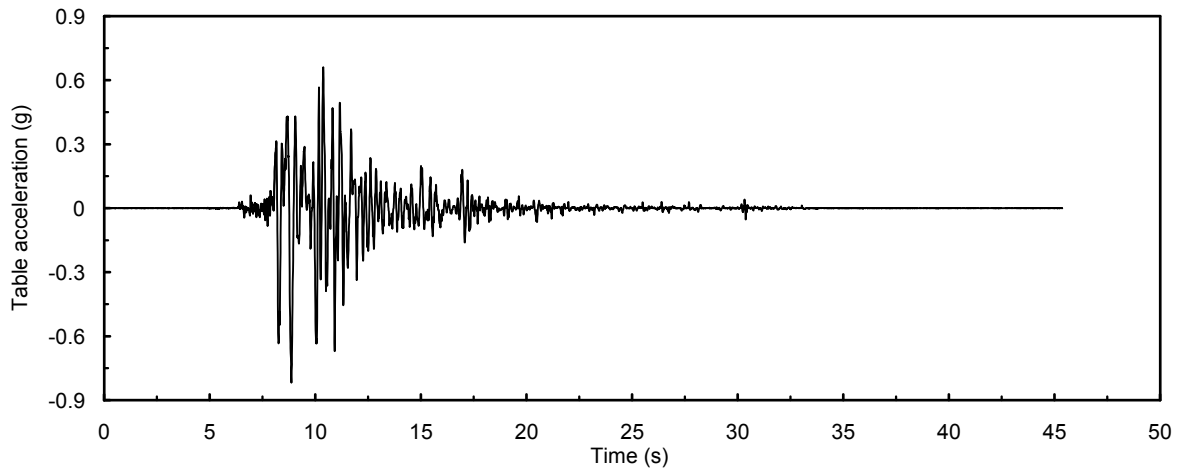


Figure 2-27 Measured shake table output under 100% Kobe

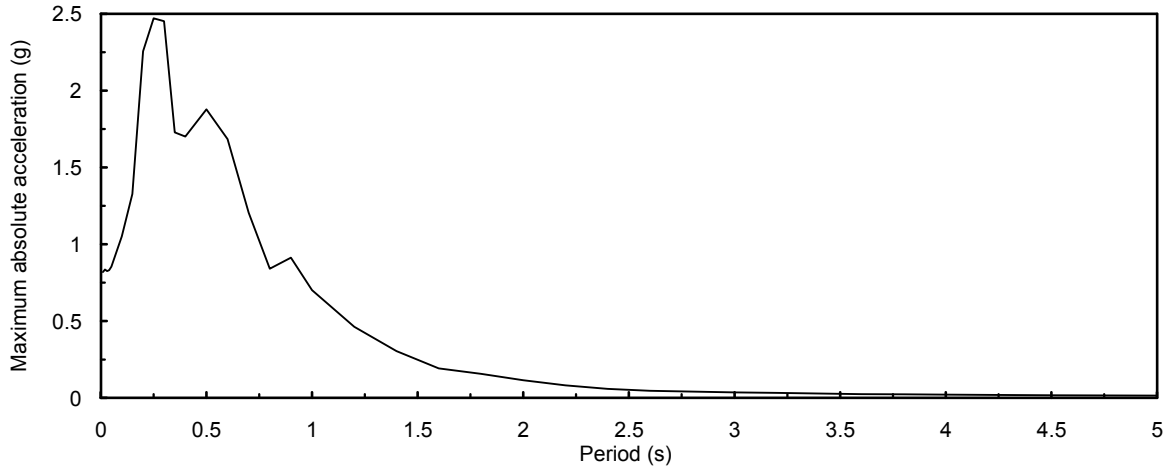


Figure 2-28 5% damped elastic absolute acceleration spectrum of the measured 100% Kobe

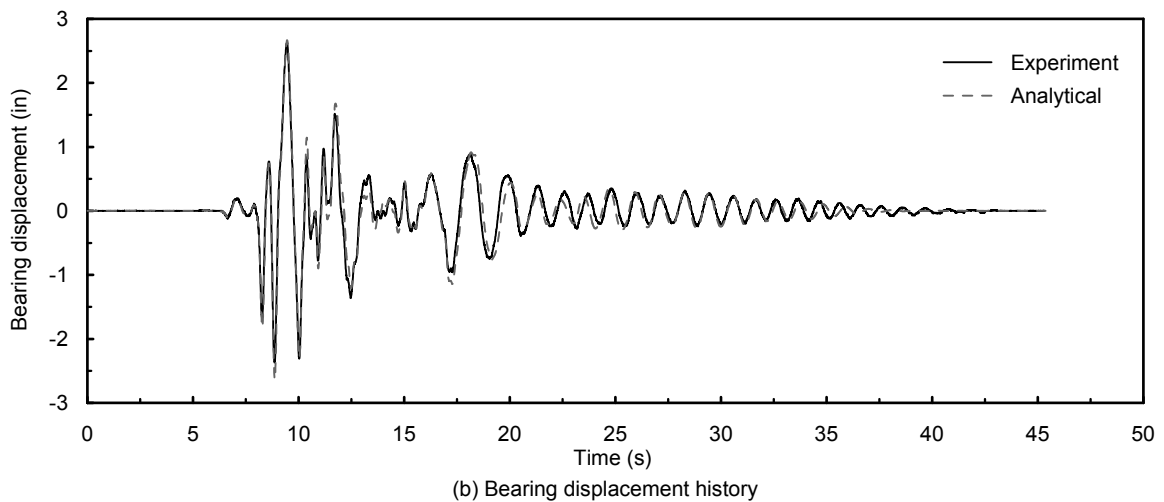
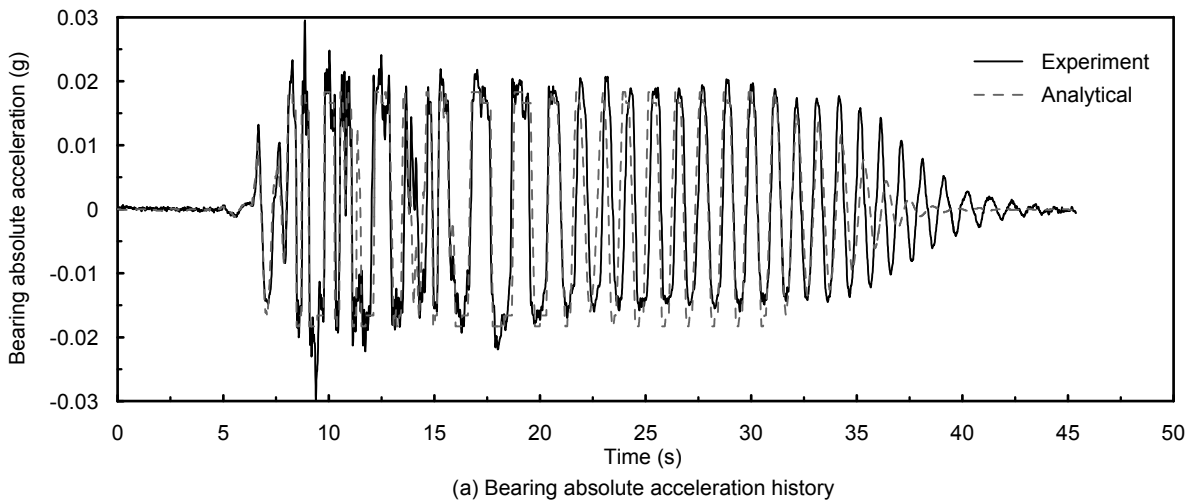


Figure 2-29 Comparison of the North-East bearing responses between analytical and experiment under 100% Kobe

CHAPTER 3

ROLLER SEISMIC ISOLATION BEARINGS WITH SUPPLEMENTAL FRICTION ENERGY DISSIPATION

Sliding friction devices are integrated into a roller bearing for supplemental energy dissipation to reduce the displacement demand. The governing equation of motion of this new roller seismic isolation bearing under ground excitation is presented first. Next, the seismic behavior of the bearing is investigated under only horizontal ground motions. The effect of vertical ground motions is evaluated next. The last section of this chapter presents two equivalent linear methods, a conventional secant stiffness method and a proposed method, to estimate the maximum relative displacement response of the bearing based on elastic response spectra. To validate the methods, predictions from both methods are compared to results of nonlinear response history analyses.

3.1 Governing Equations of Motion

To reduce the displacement responses of a roller bearing and to maintain a zero post-elastic stiffness under horizontal ground motions while keeping the cost of the bearing low, we propose to integrate sliding friction devices into a roller bearing. The design details of this new roller seismic isolation bearing are presented later in Section 4.2. In this chapter, we focus on the theoretical behavior of the bearing under ground motions.

If we assume a rigid substructure, the governing equation of motion of the bearing under ground motions can be expressed as

$$m\ddot{x} + f_s \operatorname{sgn}(x) + f_{Dr} \operatorname{sgn}(\dot{x}) + f_{Ds} \operatorname{sgn}(\dot{x}) = -m\ddot{x}_g \quad (3-1)$$

where m is the tributary mass carried by the bearing; x , \dot{x} and \ddot{x} are the relative displacement, velocity and acceleration of the bearing relative to the ground; \ddot{x}_g is the ground acceleration excitation; f_s is the restoring force defined by equations (2-26), (2-28), (2-31) or (2-33); f_{Dr} is the rolling friction force defined by equations (2-27), (2-29), (2-32) or (2-34); and f_{Ds} is the sliding friction force of the bearing. One friction device is integrated into each of the two principal directions. The two friction devices for the two principal directions are set to produce the same magnitude of sliding friction force. The sliding friction force along the principal directions is

$$f_{Ds} = \mu_s N \quad (3-2)$$

where μ_s is the coefficient of sliding friction; and N is the normal force applied to the sliding interface. For directions 45 degrees away from the principal directions, the sliding friction force is

$$f_{Ds} = \sqrt{2}\mu_s N \quad (3-3)$$

The maximum base shear of the bearing V is

$$V = f_S + f_{Dr} + f_{Ds} \quad (3-4)$$

AASHTO (2000) requires that the restoring force be greater than or equal to 1.05 times the characteristic strength of the bearing to ensure self-centering capability of the bearing. This means

$$f_S \geq 1.05(f_{Dr} + f_{Ds}) \quad (3-5)$$

and, the maximum allowable value of f_{Ds} is

$$f_{Dsa} = \frac{f_S}{1.05} - f_{Dr} \quad (3-6)$$

where f_{Dsa} is the maximum allowable sliding friction force.

Figure 3-1 shows the lateral force-displacement relationship of this new roller seismic isolation bearing under horizontal ground motions.

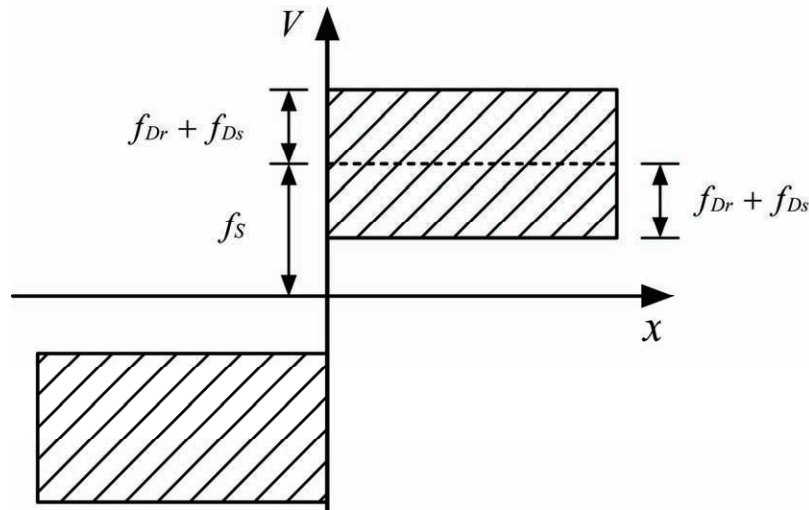


Figure 3-1 Lateral force-displacement behavior of roller seismic isolation bearings with supplemental friction energy dissipation

3.2 Seismic Behavior under Horizontal Ground Motions

3.2.1 Governing Equations of Motion

The roller seismic isolation bearing has the minimum and maximum strengths (restoring force, rolling friction force and sliding friction force) along the principal directions and directions 45 degrees away from the principal directions, respectively, as stated in Sections 2.3 and 3.1. Under horizontal ground motions, if a rigid substructure is assumed, the governing equation of motion for the principal directions, equation (3-7), can be obtained by substituting equations (2-28), (2-29) and (3-2) for f_s , f_{Dr} and f_{Ds} in equation (3-1):

$$m\ddot{x} + \frac{1}{2}mg \sin \theta \operatorname{sgn}(x) + \mu_r mg \operatorname{sgn}(\dot{x}) + \mu_s N \operatorname{sgn}(\dot{x}) = -m\ddot{x}_g \quad (3-7)$$

For responses along directions 45 degrees away from the principal directions, the governing equation of motion, equation (3-8), can be obtained by substituting equations (2-33), (2-34) and (3-3) for f_s , f_{Dr} and f_{Ds} in equation (3-1):

$$m\ddot{x} + \frac{\sqrt{2}}{2}mg \sin \theta \operatorname{sgn}(x) + \sqrt{2}\mu_r mg \operatorname{sgn}(\dot{x}) + \sqrt{2}\mu_s N \operatorname{sgn}(\dot{x}) = -m\ddot{x}_g \quad (3-8)$$

The lateral strength and energy dissipation of the bearing per loading cycle along directions 45 degrees are $\sqrt{2}$ larger than those along the principal directions. As a result, in estimating the maximum displacement response of the bearing, the properties of the bearing along the principal directions are used for a conservative result. On the other hand, the properties of the bearing along directions 45 degrees away from the principal directions are used in estimating the maximum base shear for substructure design.

This section presents a parametric study on the seismic behavior of the roller seismic isolation bearings along the principal directions. For the purpose of the parametric study, a variable denoted as a sliding friction force ratio Q_{dr} is introduced and defined as

$$Q_{dr} = \frac{f_{Ds}}{f_{Dsa}} \quad (3-9)$$

where f_{Ds} is equal to $\mu_s N$; and f_{Dsa} is defined by equation (3-6). The governing equation of motion defined by equation (3-7) can be re-written as

$$m\ddot{x} + \frac{1}{2}mg \sin \theta \operatorname{sgn}(x) + \mu_r mg \operatorname{sgn}(\dot{x}) + Q_{dr} f_{Dsa} \operatorname{sgn}(\dot{x}) = -m\ddot{x}_g \quad (3-10)$$

The diameter of the roller was assumed to be 2 in (51 mm). Thus, the coefficient of rolling friction μ_r was 0.001 according to equation (2-3).

3.2.2 Ground Motions for Parametric Study

Ground motions used in the parametric study were the 28 ground motions records from Naeim and Kelly (1999). Information on the original ground motions are listed in Table 3.1 including the locations, orientation, peak ground acceleration (PGA), peak ground velocity (PGV) and peak ground displacement (PGD). Acceleration, velocity and displacement histories of the ground motions are shown in Figures B-1 to B-28 of Appendix B. The ground motions are classified into three groups. The first group represents near-fault effects and large ground velocities (Ground motions No. 1 to 16). The second group (Ground motions No. 17 to 20) is characterized by high-frequency, large ground accelerations. The third group represents moderate ground shaking (Ground motions No. 21 to 28). These ground motions are intended to represent a wide range of ground motion characteristics that may be encountered by a seismically isolated structure. Figures 3-2 and 3-3 show the 5% damped elastic absolute acceleration and relative displacement response spectra for the 28 ground motions, respectively. In Figure 3-3, it can be seen that spectral displacements for long-period structures under the first group of ground motions are significantly larger than those under the other two groups.

Table 3-1 Ground motions

No.	Earthquake	Station	Orientation (degree)	PGA (g)	PGV (in/s ²)	PGD (in)
1	1979 Imperial Valley	El Centro Array #6	230	0.436	42.80	21.73
2			140	0.376	24.84	10.59
3	1989 Loma Prieta	Hollister	90	0.178	12.17	8.03
4			0	0.369	24.72	11.89
5		Lexington Dam	90	0.409	37.40	10.16
6			0	0.442	33.23	5.79
7	1992 Petrolia	Petrolia	90	0.662	35.24	12.05
8			0	0.589	19.02	5.98
9	1992 Landers	Lucerne Valley	L	0.703	10.12	3.46
10			T	0.665	26.93	11.10
11		Yermo	360	0.151	11.42	8.98
12			270	0.245	20.00	16.26
13	1994 Northridge	Sylmar	90	0.604	30.28	5.98
14			360	0.843	50.75	12.83
15		Newhall Fire	90	0.583	29.45	6.93
16			360	0.589	37.28	12.01
17	1989 Loma Prieta	Corralitos	90	0.478	18.70	4.53
18			0	0.630	21.73	3.74
19	1994 Northridge	Santa Monica City Hall Grounds	90	0.883	16.46	5.63
20			360	0.370	9.80	2.56
21	1989 Loma Prieta	Oakland Outer Harbor Wharf	305	0.271	16.65	3.62
22			35	0.287	16.06	3.90
23	1990 Upland	Pomona	90	0.207	3.15	0.51
24			0	0.186	4.09	0.43
25	1991 Sierra Madre	Altadena	90	0.179	3.07	0.35
26			0	0.447	10.71	1.10
27	1994 Northridge	Century City	90	0.256	8.43	2.36
28			360	0.222	9.88	2.36

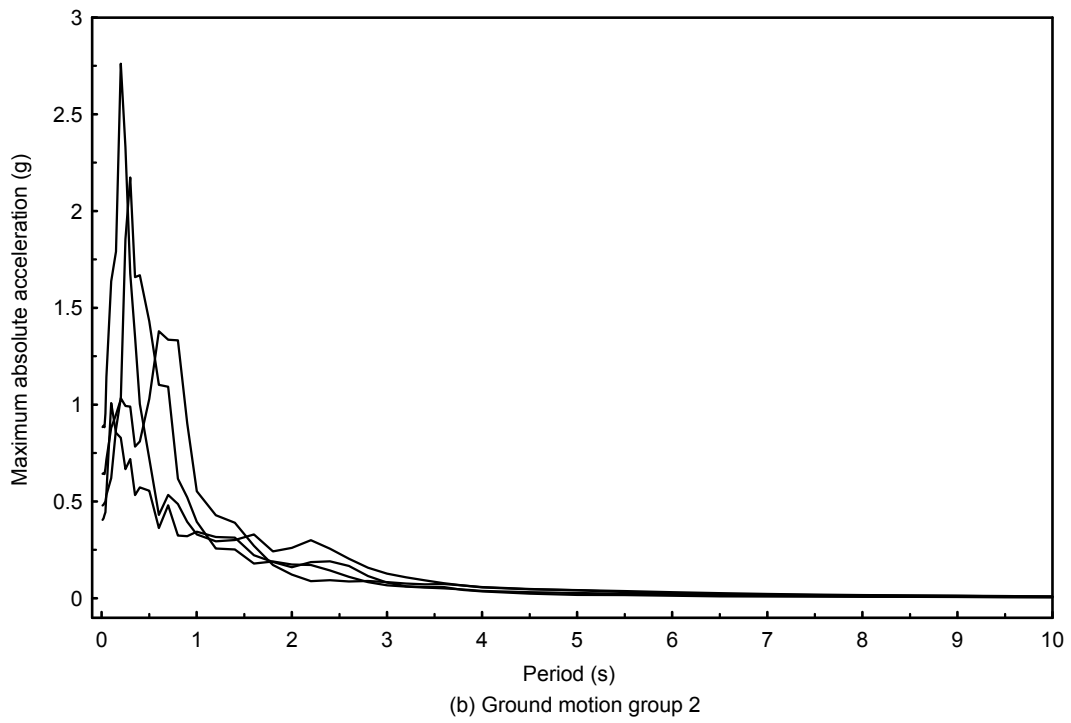
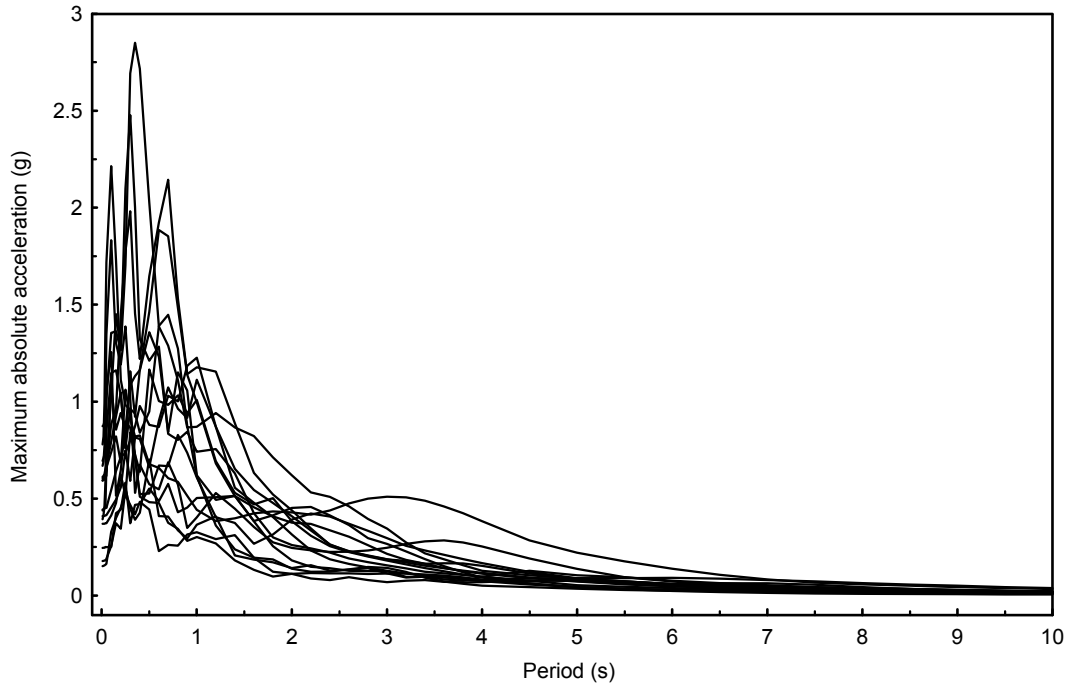


Figure 3-2 5% damped absolute acceleration spectra for the 28 ground motions

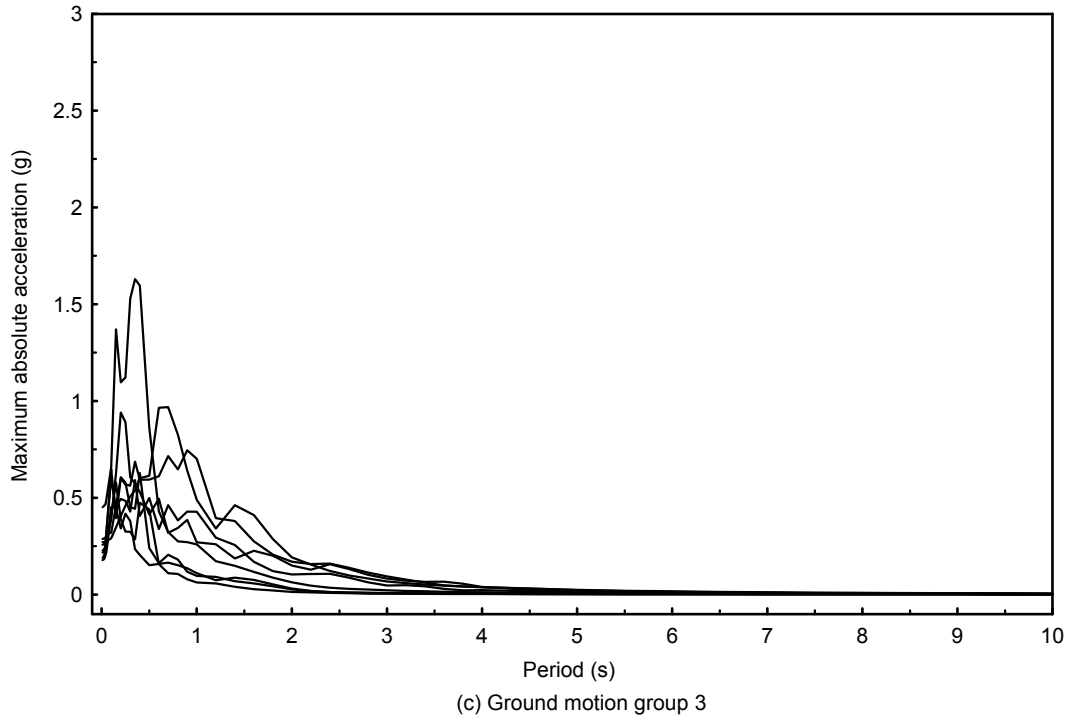


Figure 3-2 5% damped absolute acceleration spectra for the 28 ground motions (cont'd)

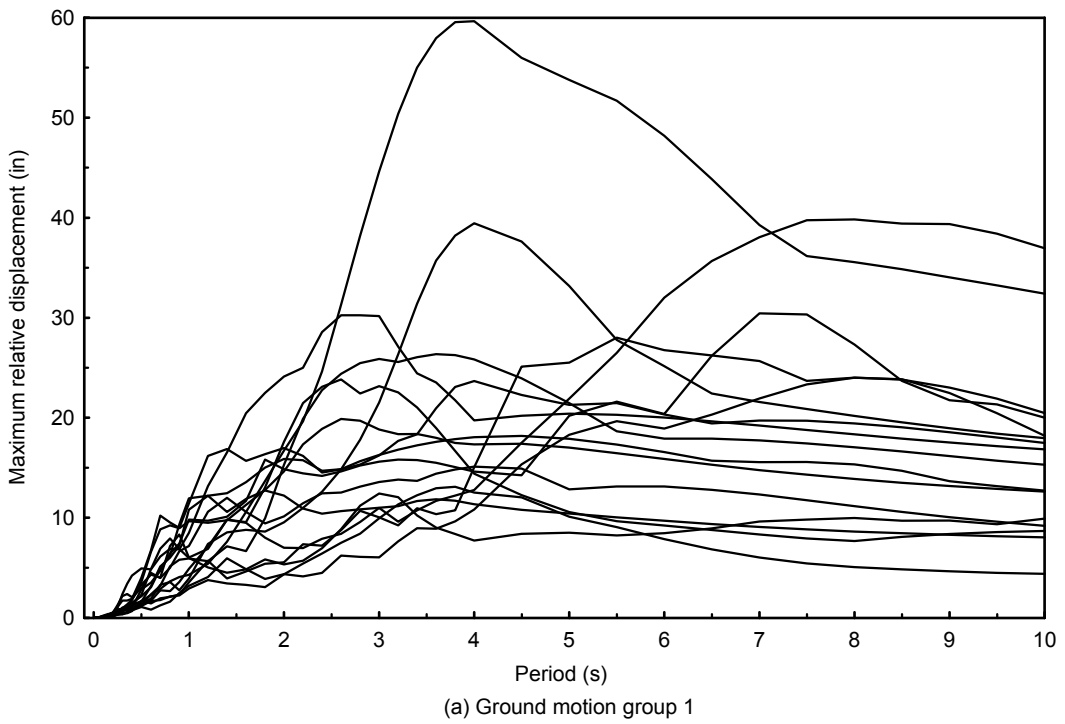
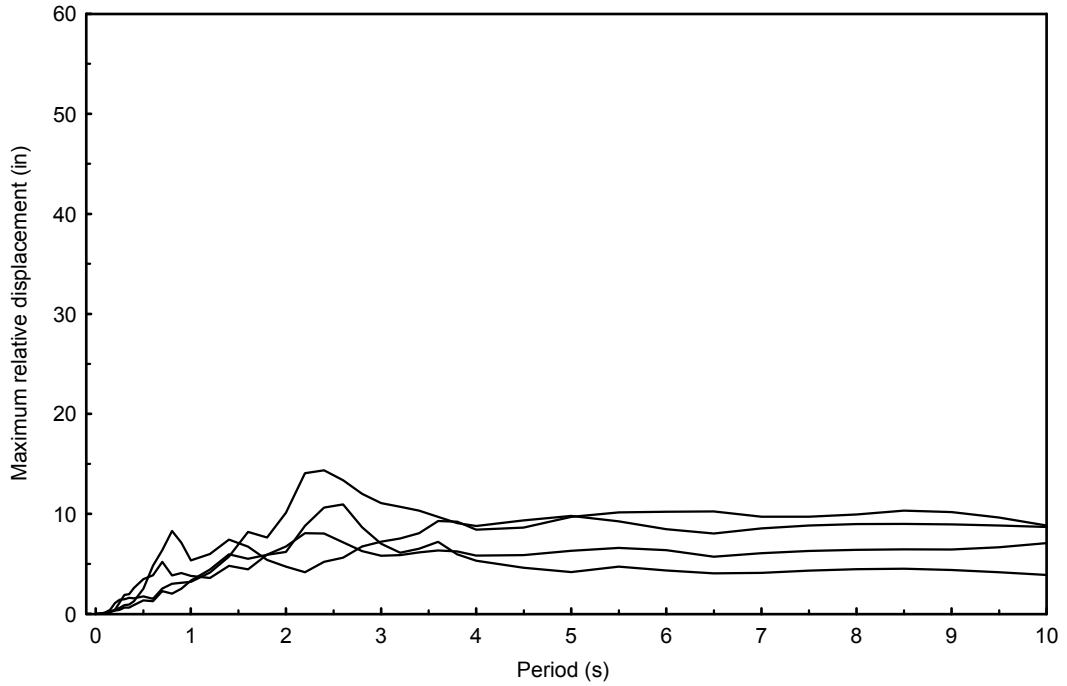
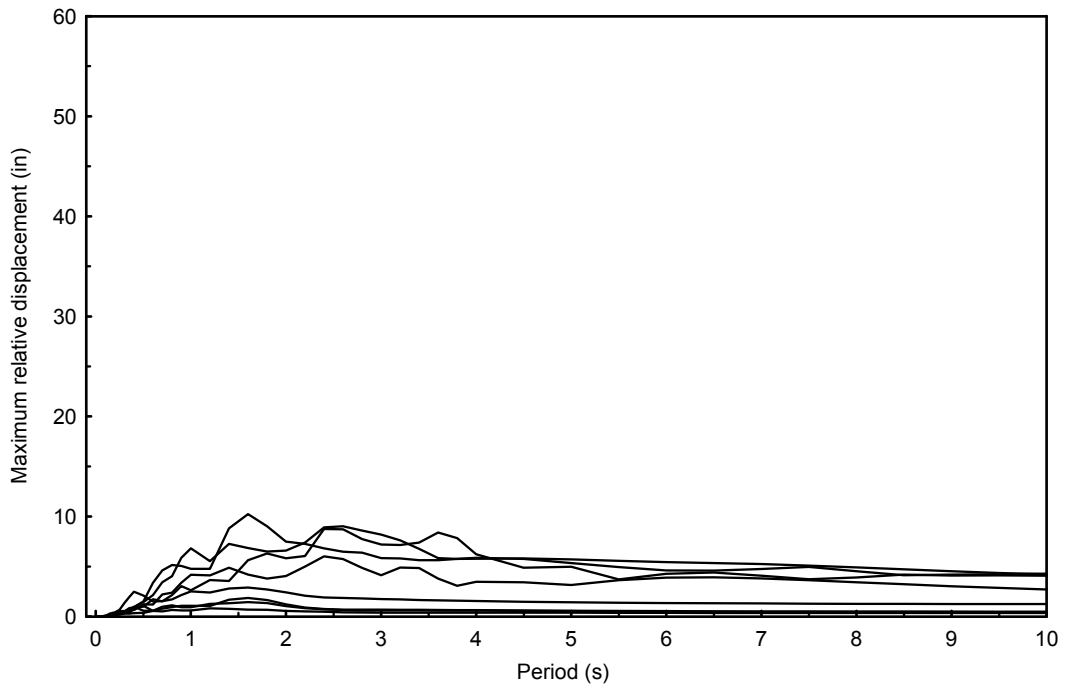


Figure 3-3 5% damped relative displacement spectra for the 28 ground motions



(b) Ground motion group 2



(c) Ground motion group 3

Figure 3-3 5% damped relative displacement spectra for the 28 ground motions (cont'd)

3.2.3 Parameters for Parametric Study

Parameters examined in the parametric study were the sloping angle θ , sliding friction force ratio Q_{dr} and PGA levels. The ranges of these parameters are listed in Table 3-2. The smallest sloping angle examined was 2 degrees. A sloping angle smaller than 2 degrees is not recommended because with such a small sloping angle, a small error in leveling the bearings during on-site installation could reduce a significant portion of the restoring capability of the bearing. The maximum sloping angle was 8 degrees. This was to ensure that no sliding of the rollers would occur (see Section 2.4) and that θ was small enough so that responses of the bearing would be independent of horizontal ground motions (see Section 2.3). The values of Q_{dr} examined ranged from 0, which means no friction devices, to 1, which means the sliding friction force is equal to the maximum allowable value f_{Dsa} . For each combination of θ and Q_{dr} , the bearing was subjected to the 28 ground motions scaled to various PGA levels as listed in Table 3-2.

Table 3-2 Parameters for the parametric study

Sloping angle θ (degree)	Sliding friction force ratio Q_{dr}	PGA (g)
2	0	0.2
3	0.25	0.3
4	0.5	0.4
5	0.75	0.5
6	1	0.6
7		0.7
8		0.8

3.2.4 Results and Discussions

Sample responses of four bearings ($\theta = 2$ or $\theta = 8$ with $Q_{dr} = 0$ or $Q_{dr} = 1$) are presented under ground motions Nos. 1 (see Figure 3-4), 17 (see Figure 3-5) and 21 (see Figure 3-6), respectively, with a PGA of 0.5g. Each of the three ground motions belongs to one of the three categories of the ground motions used. Figures 3-7 to 3-12 show responses of the bearings with no friction device ($Q_{dr} = 0$) under the three ground motions. Under all the three ground motions, the bearing with a larger sloping angle showed a higher maximum absolute acceleration response (see Figures 3-8, 3-10 and 3-12). This is expected since a larger sloping angle would lead to a higher restoring force and hence a larger maximum acceleration response. For the maximum displacement response, it is surprisingly to see that the bearing with a sloping angle of 8 degrees showed a higher peak displacement response than the bearing with a sloping angle of 2 degrees

under ground motion No. 1 (see Figure 3-7). Note that the former had a restoring force four times larger than the latter. This demonstrates the uncertainty in predicting the maximum displacement response due to the randomness of a ground motion. Under ground motions No. 17 and No. 21, the bearing with a sloping angle of 8 degrees showed a smaller maximum displacement response as expected (see Figures 3-9 and 3-11).

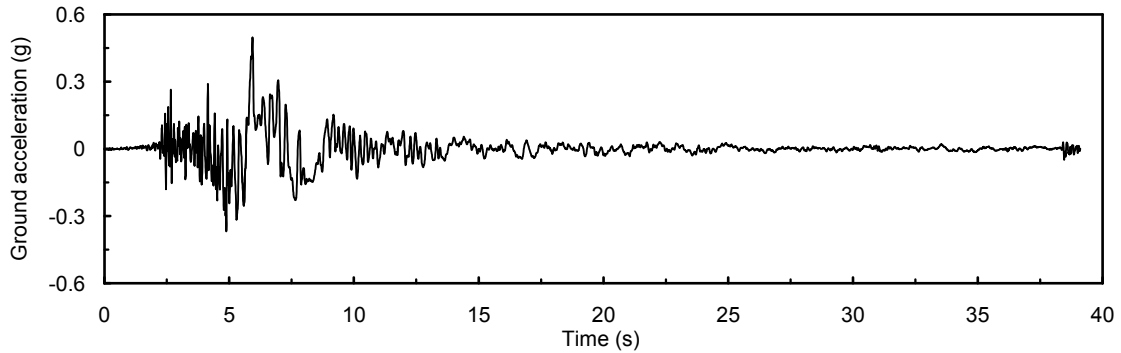


Figure 3-4 Acceleration history of ground motion No. 1 with PGA= 0.5g

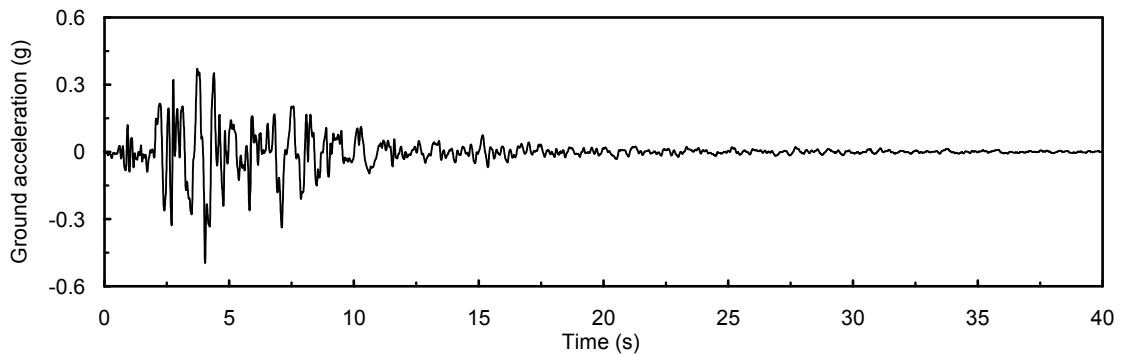


Figure 3-5 Acceleration history of ground motion No. 17 with PGA= 0.5g

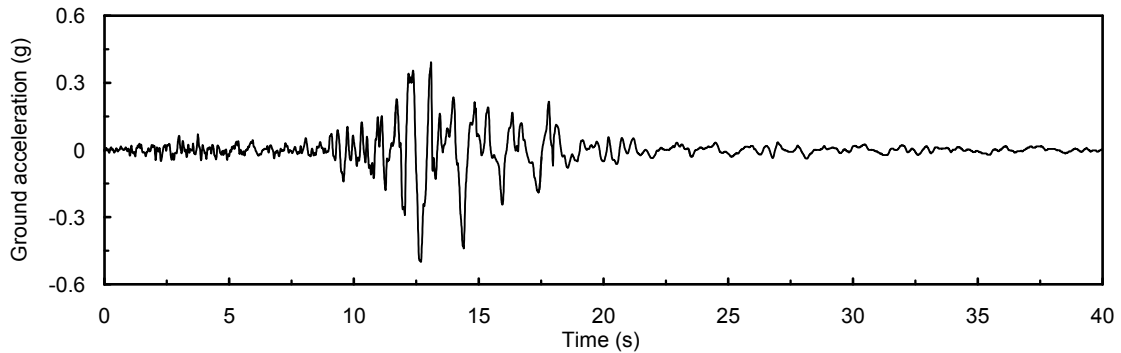


Figure 3-6 Acceleration history of ground motion No. 21 with PGA= 0.5g

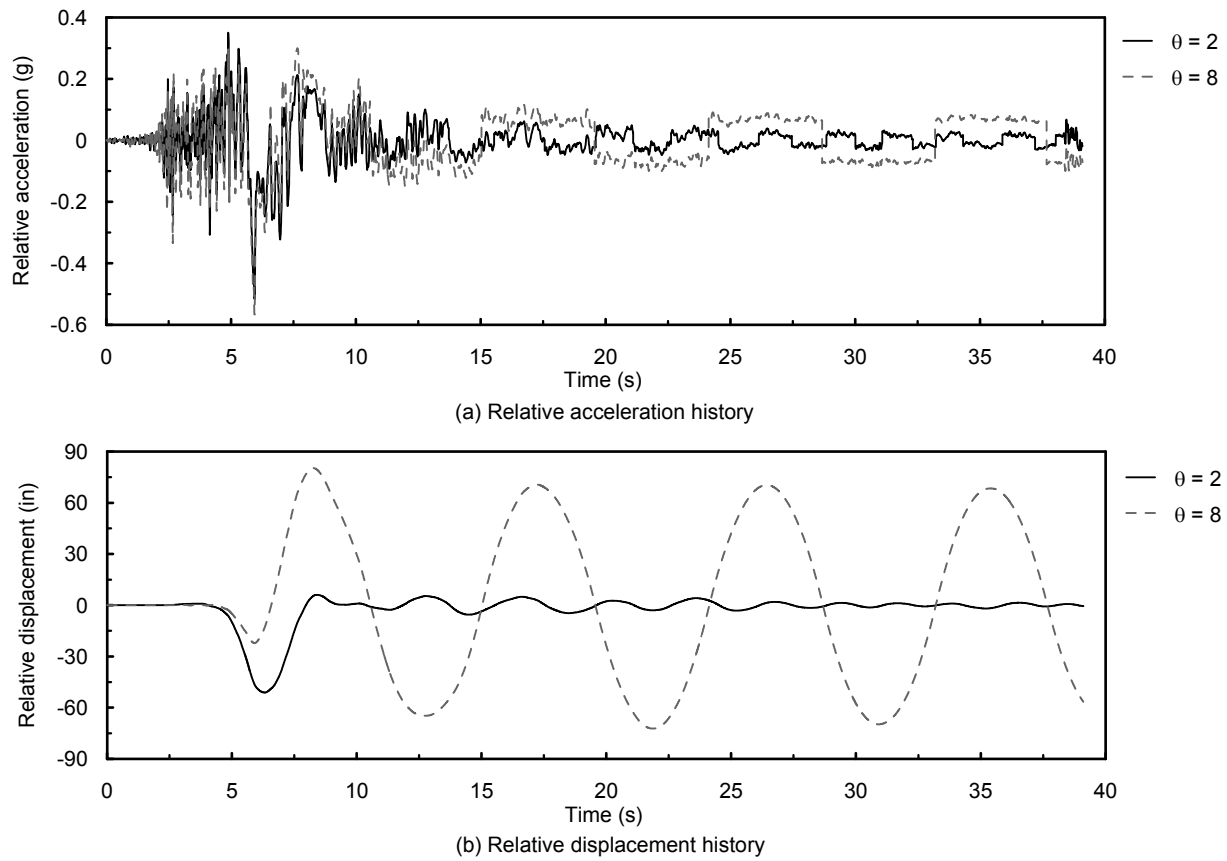


Figure 3-7 Acceleration and displacement responses of bearings with $\theta = 2$ and 8 and with $Q_{dr} = 0$ to ground motion No. 1 with PGA= 0.5g

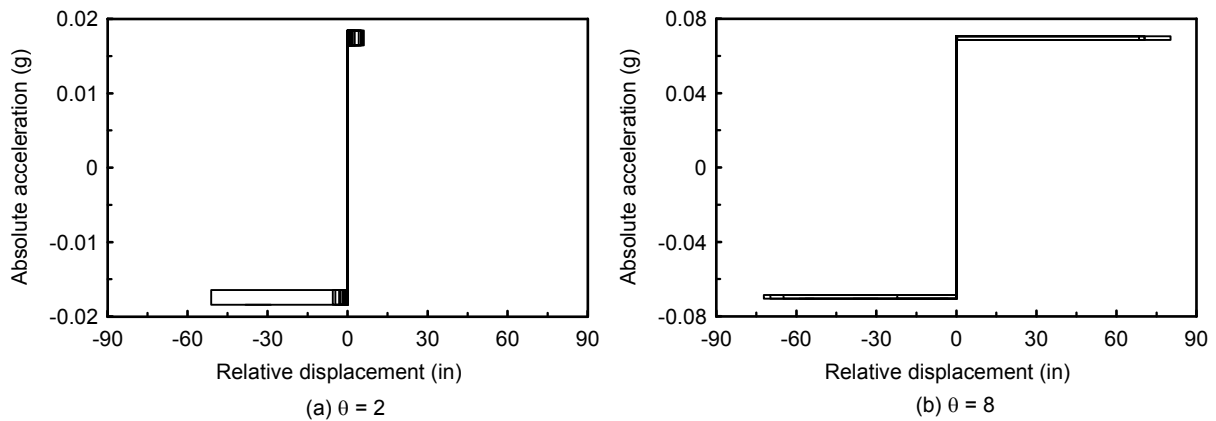
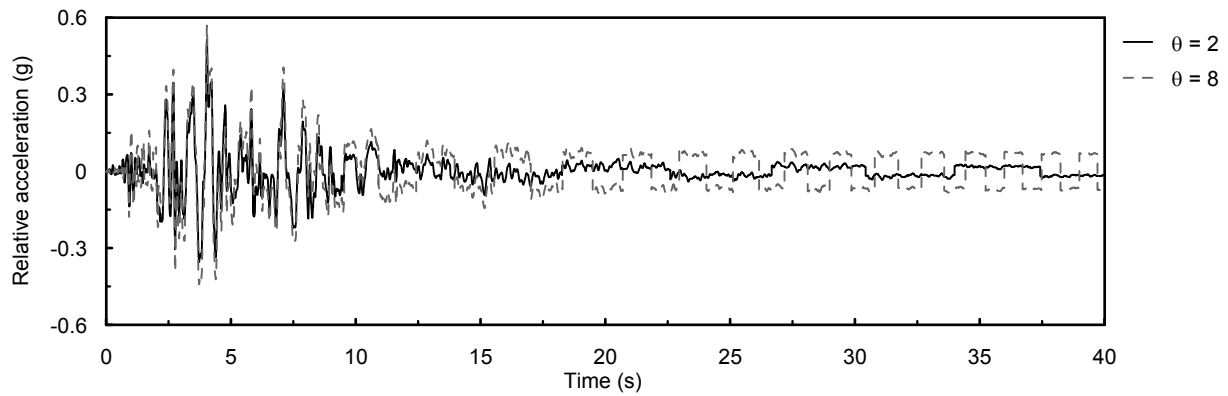
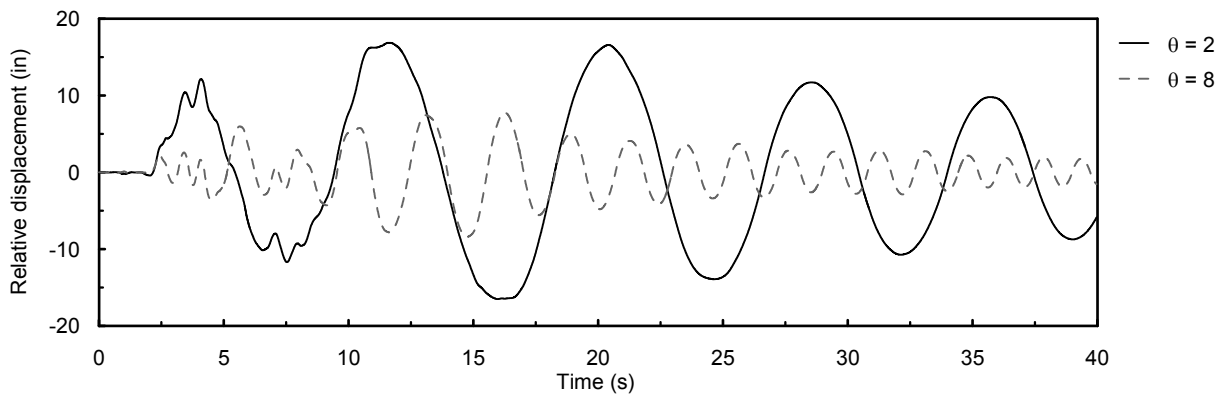


Figure 3-8 Hysteretic responses of bearings with $\theta = 2$ and 8 and with $Q_{dr} = 0$ to ground motion No. 1 with PGA= 0.5g



(a) Relative acceleration history



(b) Relative displacement history

Figure 3-9 Acceleration and displacement responses of bearings with $\theta = 2$ and 8 and with $Q_{dr} = 0$ to ground motion No. 17 with PGA= 0.5g

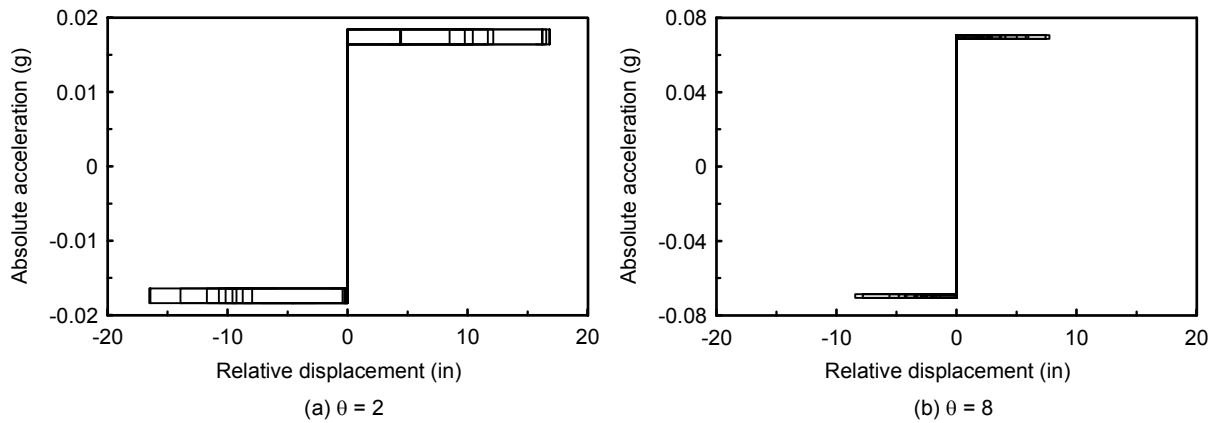
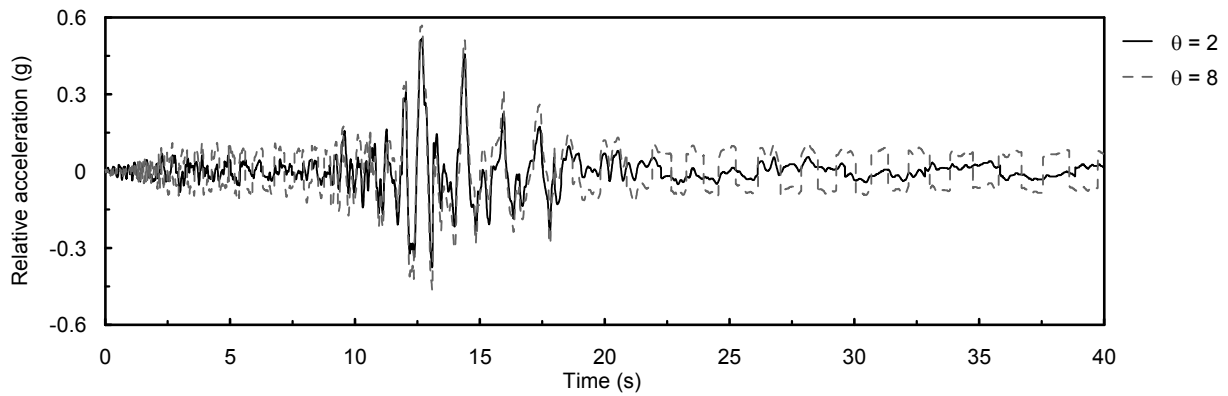
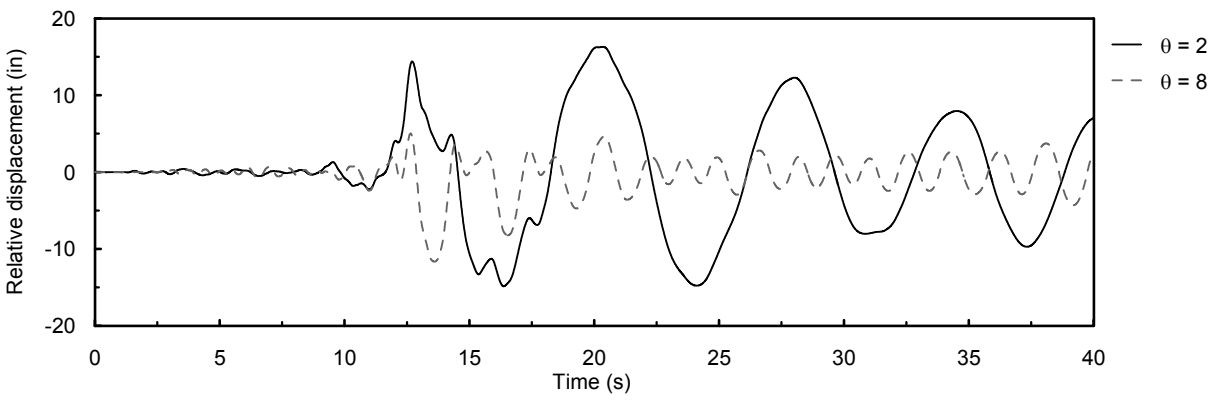


Figure 3-10 Hysteretic responses of bearings with $\theta = 2$ and 8 and with $Q_{dr} = 0$ to ground motion No. 17 with PGA= 0.5g



(a) Relative acceleration history



(b) Relative displacement history

Figure 3-11 Acceleration and displacement responses of bearings with $\theta = 2$ and 8 and with $Q_{dr} = 0$ to ground motion No. 21 with PGA= 0.5g

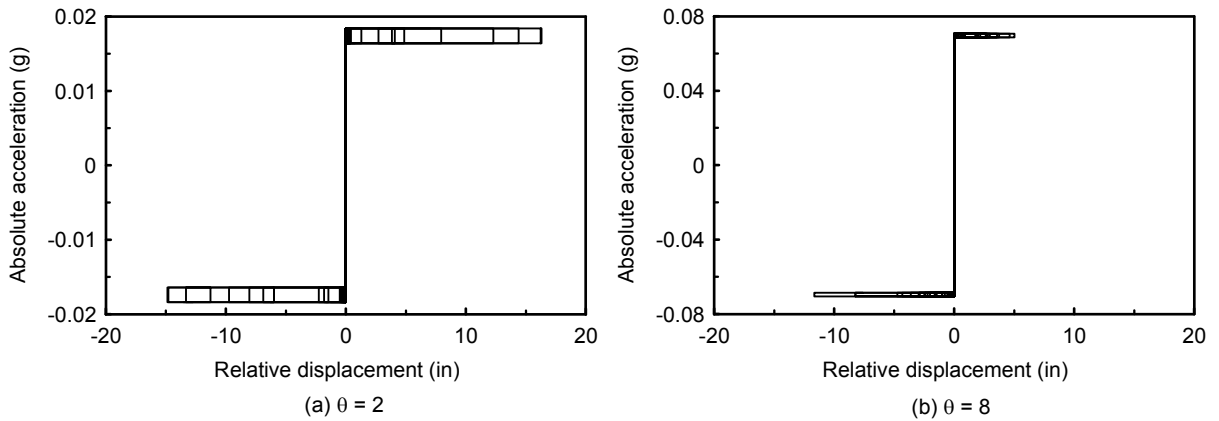
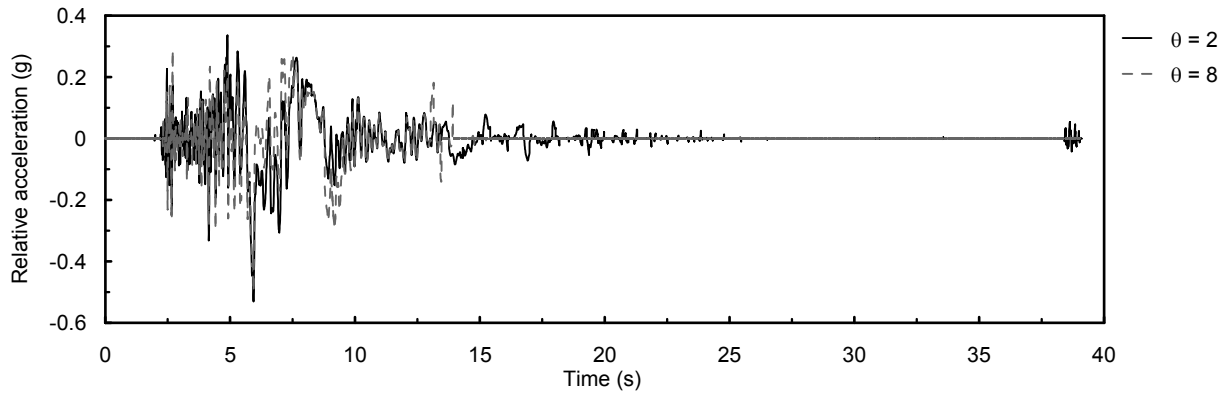
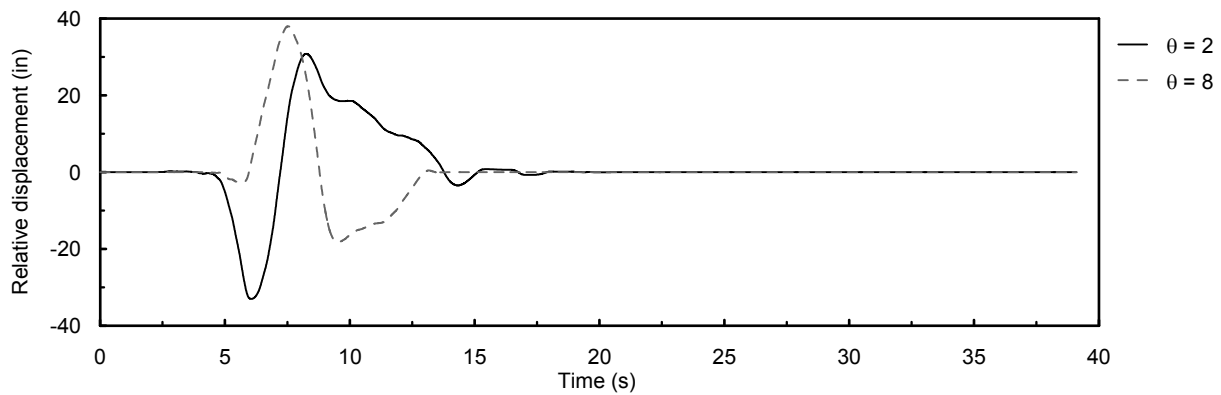


Figure 3-12 Hysteretic responses of bearings with $\theta = 2$ and 8 and with $Q_{dr} = 0$ to ground motion No. 21 with PGA= 0.5g

Figures 3-13 to 3-18 show responses of the bearings with the maximum allowable sliding friction force under the three ground motions. By comparing these responses with the responses from the bearings with no friction device, the use of a friction device significantly decreased the displacement responses. This is expected since the lateral strength and energy dissipation were increased. Under ground motion No. 1, although the bearing with a sloping angle of 8 degrees has both a higher lateral strength and higher energy dissipation than that with a sloping angle of 2 degrees, it showed a higher maximum displacement response (see Figure 3-13). This again shows the uncertainty in estimating the maximum displacement response. Under ground motions No. 17 and No. 21 (see Figures 3-15 and 3-17), the bearing with a sloping angle of 8 degrees exhibited a smaller maximum displacement response than the bearing with a sloping angle of 2 degrees as expected.



(a) Relative acceleration history



(b) Relative displacement history

Figure 3-13 Acceleration and displacement responses of bearings with $\theta = 2$ and 8 and with $Q_{dr} = 1$ to ground motion No. 1 with PGA= 0.5g

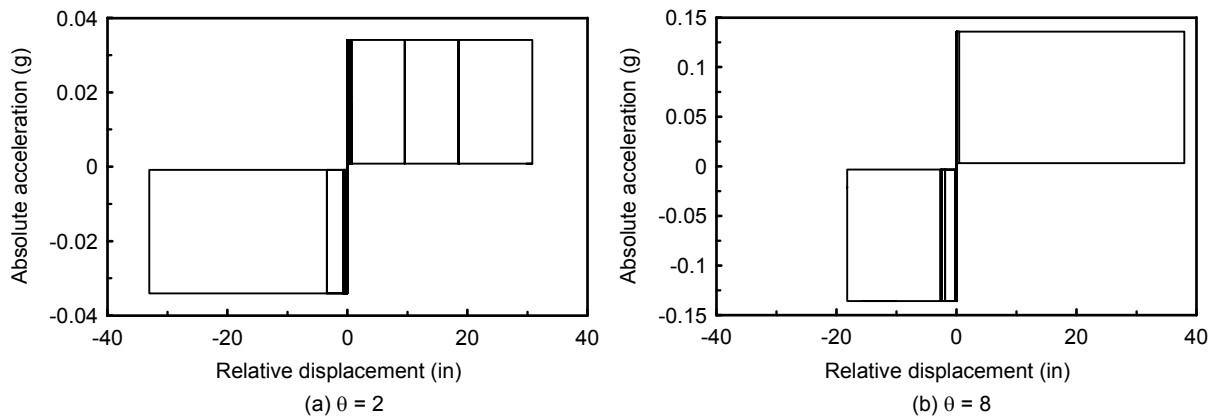
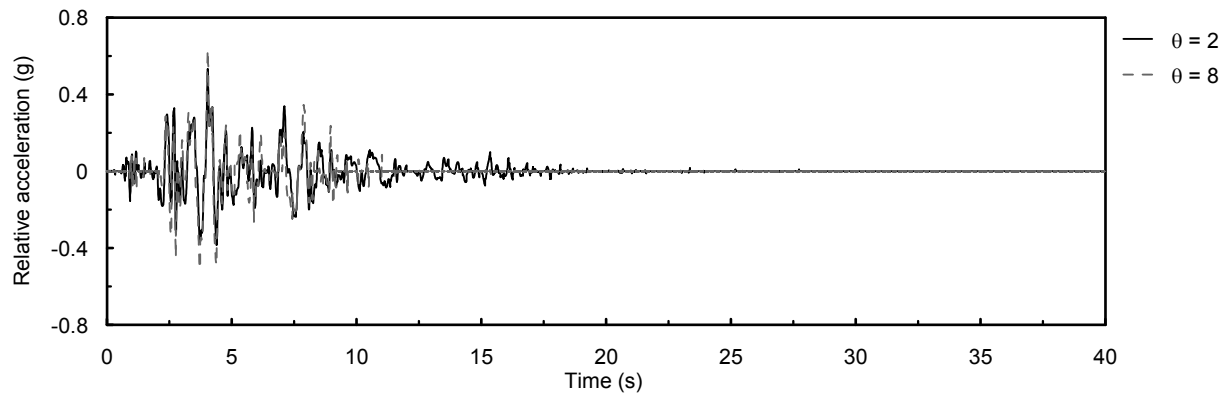
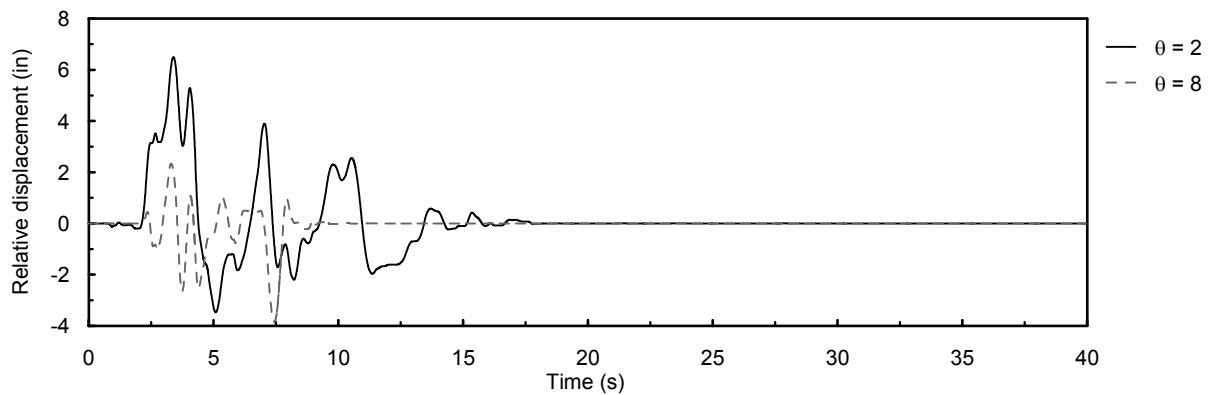


Figure 3-14 Hysteretic responses of bearings with $\theta = 2$ and 8 and with $Q_{dr} = 1$ to ground motion No. 1 with PGA= 0.5g



(a) Relative acceleration history



(b) Relative displacement history

Figure 3-15 Acceleration and displacement responses of bearings with $\theta = 2$ and 8 and with $Q_{dr} = 1$ to ground motion No. 17 with PGA= 0.5g

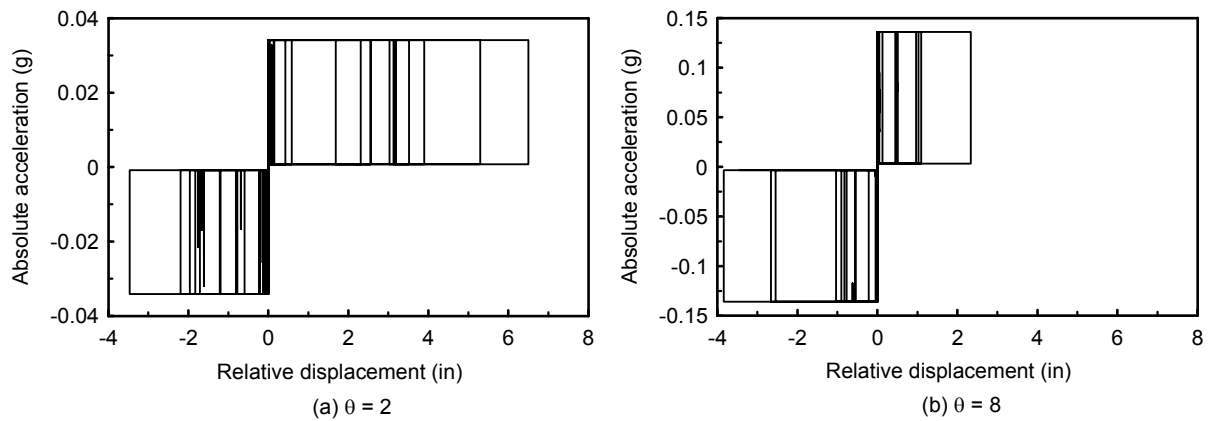
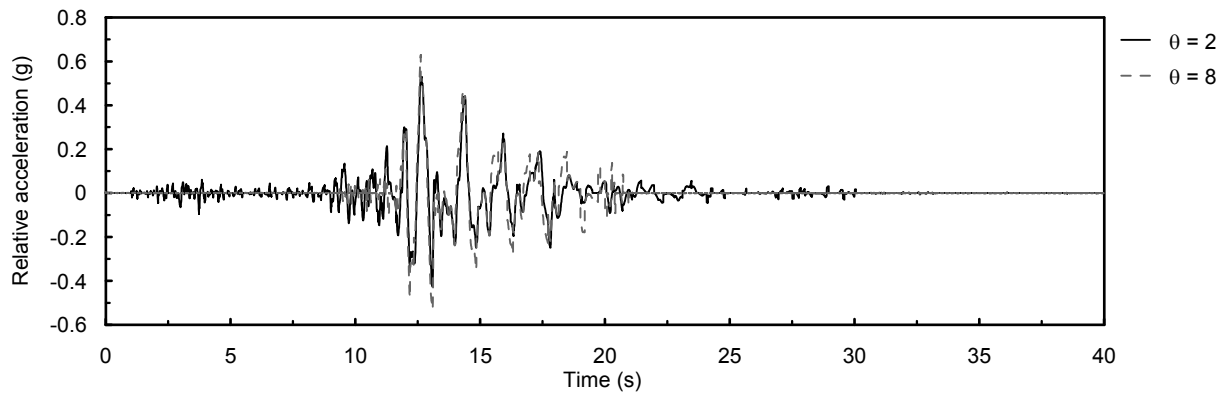
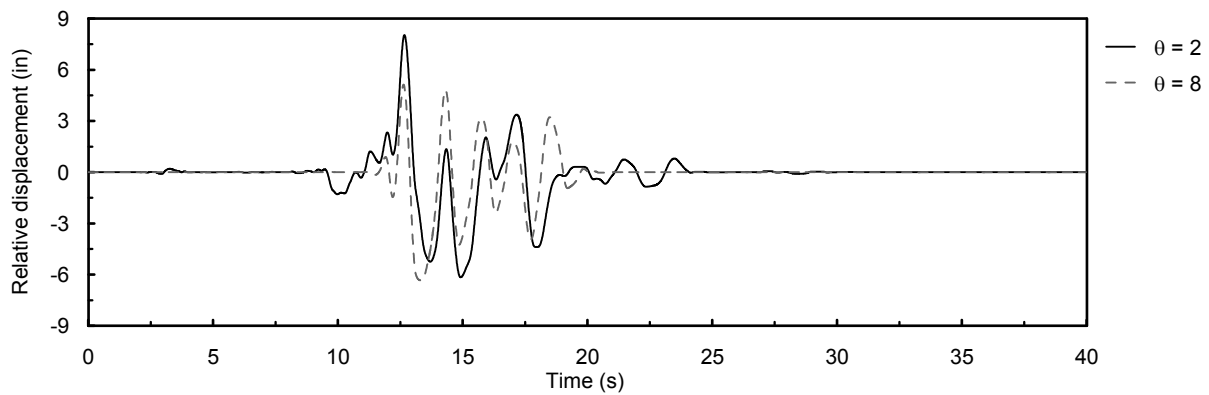


Figure 3-16 Hysteretic responses of bearings with $\theta = 2$ and 8 and with $Q_{dr} = 1$ to ground motion No. 17 with PGA= 0.5g



(a) Relative acceleration history



(b) Relative displacement history

Figure 3-17 Acceleration and displacement responses of bearings with $\theta = 2$ and 8 and with $Q_{dr} = 1$ to ground motion No. 21 with PGA= 0.5g

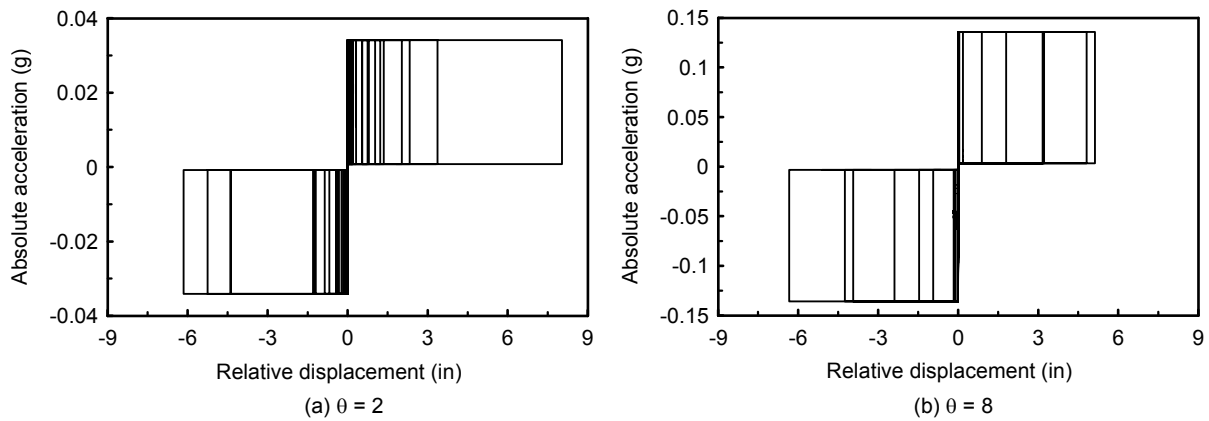


Figure 3-18 Hysteretic responses of bearings with $\theta = 2$ and 8 and with $Q_{dr} = 1$ to ground motion No. 21 with PGA= 0.5g

For each parametric combination, the arithmetic mean of the maximum relative displacement responses and that of the maximum absolute acceleration responses to the 28 ground motions scaled to various PGA levels were calculated. Results for all the parametric combinations are shown in Figures 3-19 to 3-25. In Figures 3-19a to 3-25a, it can be seen that for a given PGA level, the mean maximum displacement responses of bearings without friction devices tended to decrease as the sloping angle increased for smaller PGA levels (0.2 to 0.3 g). This is expected as a larger sloping angle means a higher restoring force. However, when the PGA level increased, the mean maximum displacement responses tended to increase as the sloping angle increases under a given PGA level. This means although a larger sloping angle gives a larger restoring force; it tends to cause a larger maximum relative displacement response. When a friction device was used, for a given sloping angle, the mean maximum displacement response decreased as the sliding friction force ratio Q_{dr} increased. This is expected as a higher Q_{dr} results in higher strength and energy dissipation capacity of the bearing. For a given Q_{dr} , the mean maximum displacement responses tended to decrease as the sloping angle increases. This is because a larger sloping angle means a higher sliding friction force for a given Q_{dr} and hence a lower maximum displacement response. This tendency became stronger when Q_{dr} was higher. This study shows that in terms of reducing the maximum displacement response, a higher sloping angle is desirable not because it can produce a higher lateral strength by increasing the restoring force, but because it allows for the use of a friction device with a higher force, which also means higher energy dissipation. The best performance of the bearing in terms of smaller relative displacement responses can be achieved by having the maximum allowable sliding friction force, that is,

$$V = f_S + f_{Dr} + f_{Dsa} \quad (3-11)$$

Figures 3-19b to 3-25b show the arithmetic mean values of the maximum absolute acceleration responses. These values were independent of the PGA levels and the ground motion used, and increased as the sloping angle and the sliding friction force increased as expected.

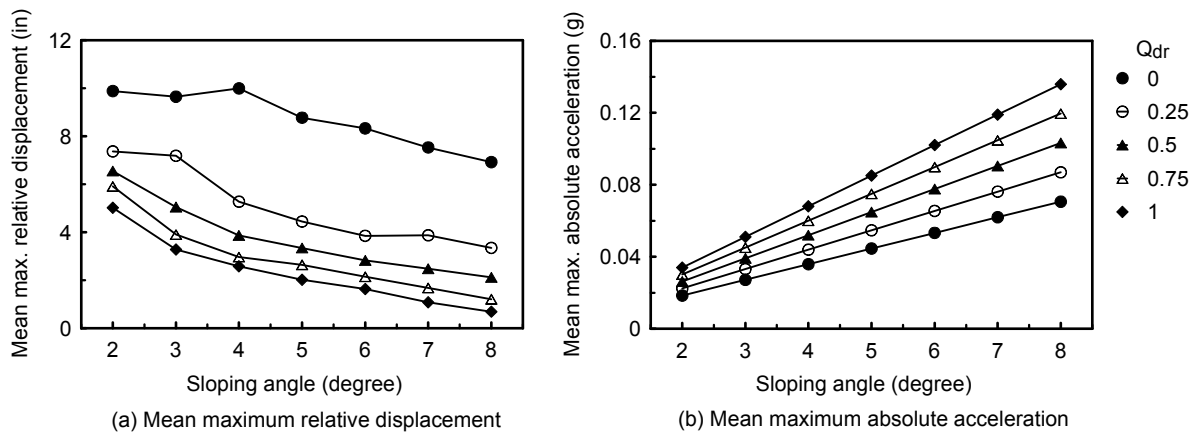


Figure 3-19 Mean maximum relative displacement and absolute acceleration responses under PGA=0.2g

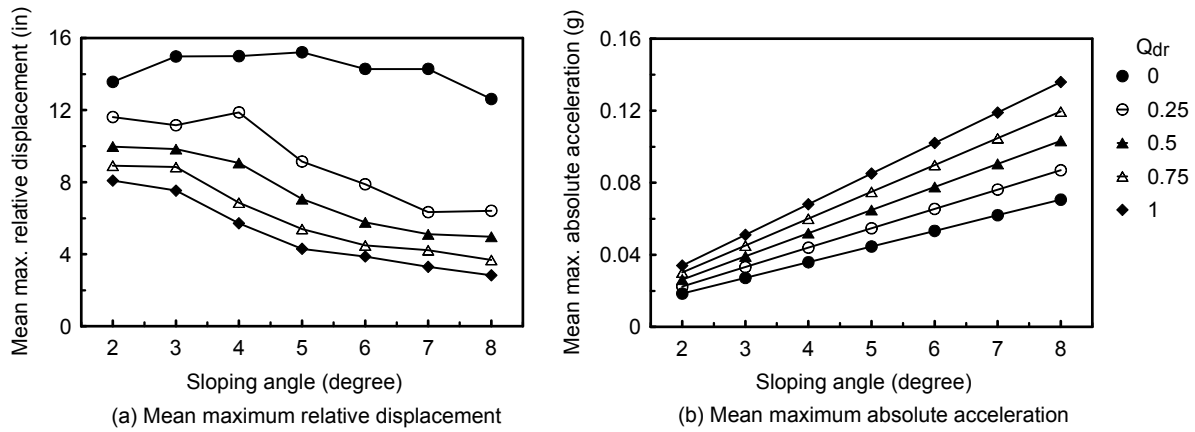


Figure 3-20 Mean maximum relative displacement and absolute acceleration responses under PGA=0.3g

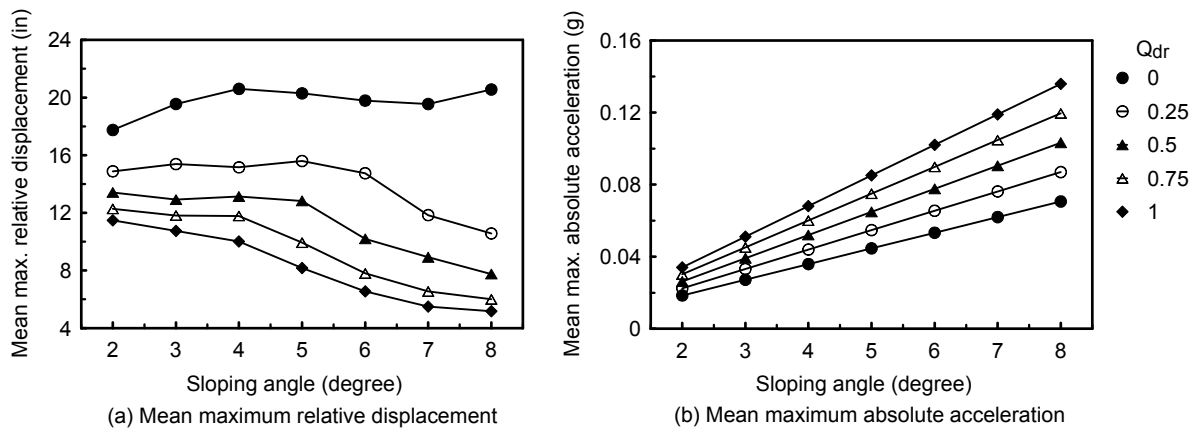


Figure 3-21 Mean maximum relative displacement and absolute acceleration responses under PGA=0.4g

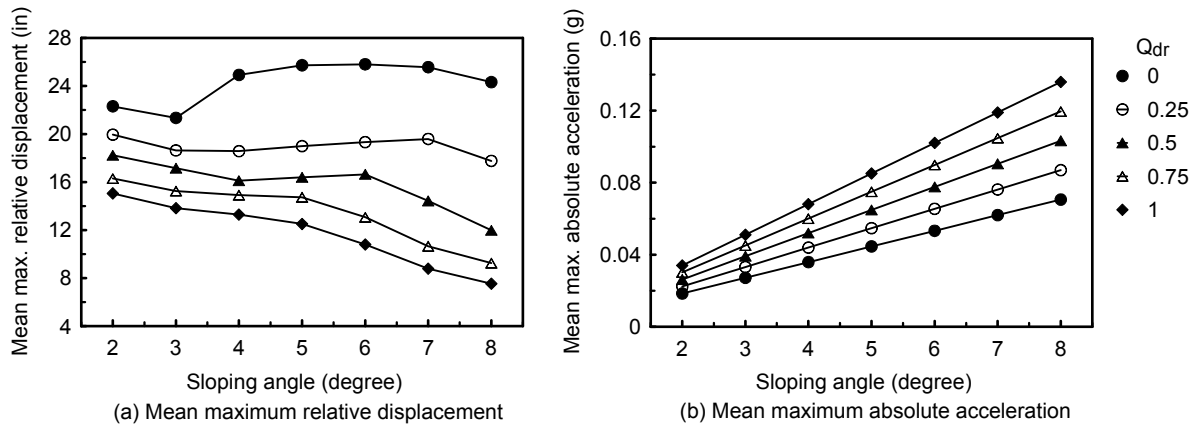


Figure 3-22 Mean maximum relative displacement and absolute acceleration responses under PGA=0.5g

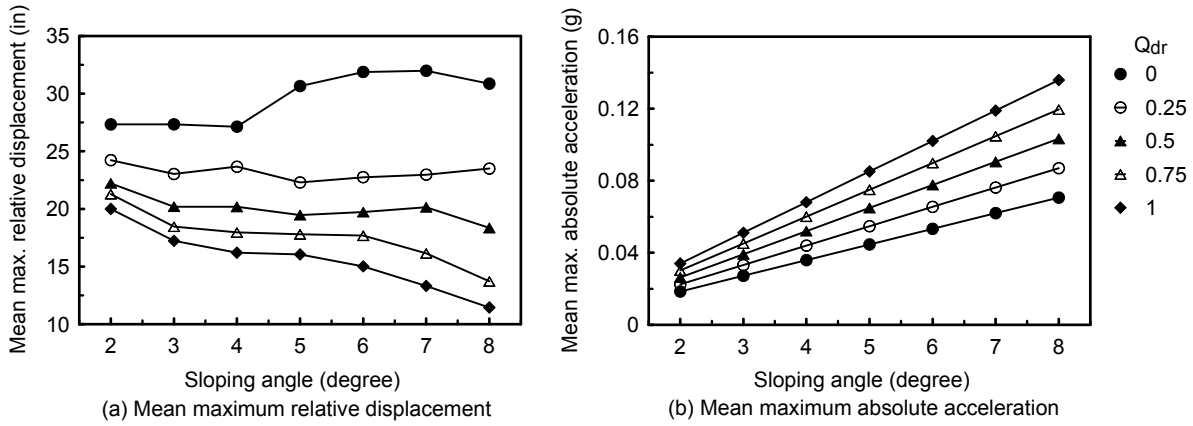


Figure 3-23 Mean maximum relative displacement and absolute acceleration responses under PGA=0.6g

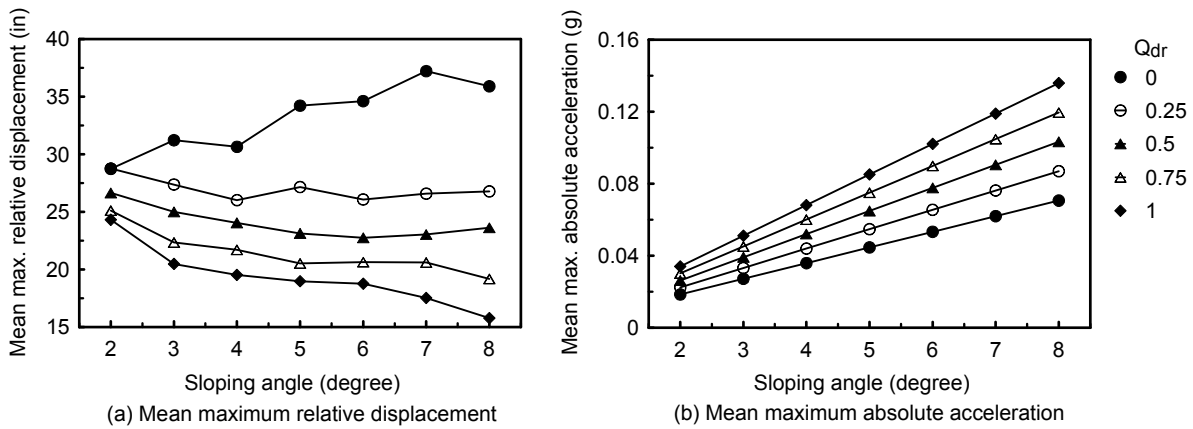


Figure 3-24 Mean maximum relative displacement and absolute acceleration responses under PGA=0.7g

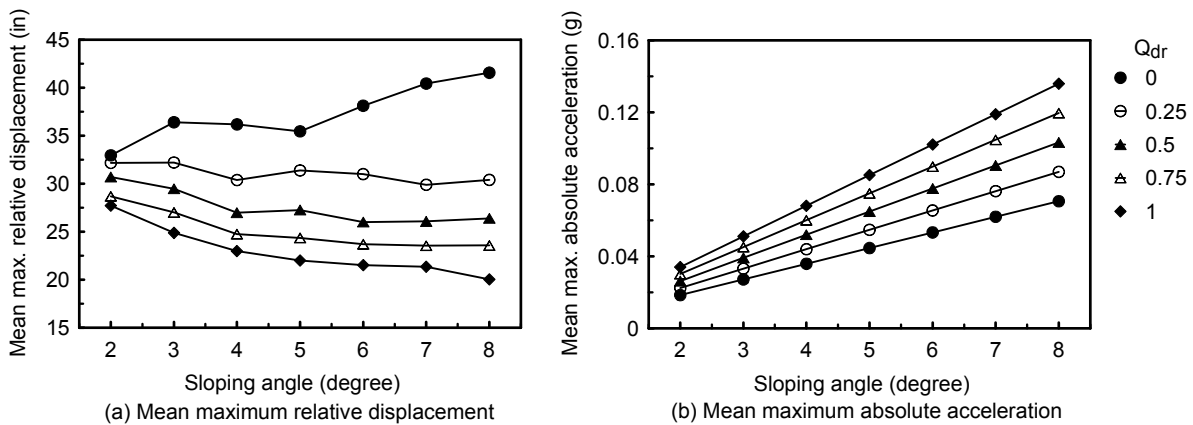


Figure 3-25 Mean maximum relative displacement and absolute acceleration responses under PGA=0.8g

3.3 Seismic Behavior under Combined Horizontal and Vertical Ground Motions

3.3.1 Governing Equations of Motion

Under combined horizontal and vertical ground motions and assuming a rigid substructure, the governing equation of motion for the principal directions, equation (3-12), can be obtained by substituting equations (2-26), (2-27) and (3-2) for f_s , f_{Dr} and f_{Ds} in equation (3-1):

$$m\ddot{x} + \frac{1}{2}m(\ddot{z}_g + g)\sin\theta\text{sgn}(x) + \mu_r m(\ddot{z}_g + g)\text{sgn}(\dot{x}) + \mu_s N \text{sgn}(\dot{x}) = -m\ddot{x}_g \quad (3-12)$$

where \ddot{z}_g is the vertical ground accelerations. It can be observed that vertical ground motions affect the seismic behavior of the bearing by changing the restoring force and rolling friction force of the bearing. For responses along directions 45 degrees away from the principal directions, the governing equation of motion, equation (3-13), can be obtained by substituting equations (2-31), (2-32) and (3-3) for f_s , f_{Dr} and f_{Ds} in equation (3-1):

$$m\ddot{x} + \frac{\sqrt{2}}{2}m(\ddot{z}_g + g)\sin\theta\text{sgn}(x) + \sqrt{2}\mu_r m(\ddot{z}_g + g)\text{sgn}(\dot{x}) + \sqrt{2}\mu_s N \text{sgn}(\dot{x}) = -m\ddot{x}_g \quad (3-13)$$

In this section, the seismic behavior of the bearing along the principal directions is examined using a parametric study. For the purpose of the parametric study, equation (3-12) can also be expressed as

$$m\ddot{x} + \frac{1}{2}m(\ddot{z}_g + g)\sin\theta\text{sgn}(x) + \mu_r m(\ddot{z}_g + g)\text{sgn}(\dot{x}) + Q_{dr}f_{Dsa} \text{sgn}(\dot{x}) = -m\ddot{x}_g \quad (3-14)$$

where the parameters have been defined in the previous section.

3.3.2 Ground Motions for Parametric Study

Thirteen ground motion pairs were selected for the parametric study and are summarized in Table 3-3 (Naeim and Kelly 1999). Each ground motion pair contains a horizontal component and a vertical component. The horizontal components have been used previously in Section 3.2. Acceleration, velocity and displacement histories of the vertical components are shown in Figures B-29 to B-41 in Appendix B. The ground motions pairs can be classified into three groups as described in Section 3.2.2. Ground motion pairs No. 1 to No 7, No. 8 to No. 9 and No. 10 to No. 13 are the first, second and third groups, respectively.

Table 3-3 Ground motion pairs

No.	Earthquake	Station	Orientation	PGA (g)	PGV (in/s ²)	PGD (in)
1	1989 Loma Prieta	Hollister	90°	0.178	12.17	8.03
			Vertical	0.197	6.06	2.91
2		Lexington Dam	90°	0.409	37.40	10.16
			Vertical	0.134	10.04	5.16
3	1992 Petrolia	Petrolia	90°	0.662	35.24	12.05
			Vertical	0.163	8.23	5.43
4	1992 Landers	Lucerne Valley	L	0.703	10.12	3.46
			Vertical	0.681	14.29	3.11
5		Yermo	360°	0.151	11.42	8.98
			Vertical	0.136	5.00	1.81
6	1994 Northridge	Sylmar	90°	0.604	30.28	5.98
			Vertical	0.535	7.32	2.99
7		Newhall Fire	90°	0.583	29.45	6.93
			Vertical	0.548	12.09	5.04
8	1989 Loma Prieta	Corralitos	90°	0.478	18.70	4.53
			Vertical	0.439	7.32	3.07
9	1994 Northridge	Santa Monica City Hall Grounds	90°	0.883	16.46	5.63
			Vertical	0.232	5.51	1.50
10	1989 Loma Prieta	Oakland Outer Harbor Wharf	305°	0.271	16.65	3.62
			Vertical	0.066	4.13	0.71
11	1990 Upland	Pomona	90°	0.207	3.15	0.51
			Vertical	0.097	1.89	0.20
12	1991 Sierra Madre	Altadena	90°	0.179	3.07	0.35
			Vertical	0.154	1.69	0.16
13	1994 Northridge	Century City	90°	0.256	8.43	2.36
			Vertical	0.115	3.43	1.26

3.3.3 Parameters for Parametric Study

Parameters investigated in the parametric study were the sloping angle θ and sliding friction force ratio Q_{dr} . The ranges of the parameters were the same as used in the previous section (see Table 3-2). For each combination of θ and Q_{dr} , the bearing was evaluated under the 13 pairs of ground motions.

3.3.4 Results and Discussion

Responses of one of the bearings with $\theta = 4$ and $Q_{dr} = 0$ under ground motion pairs No. 2 and No. 4 are shown in Figures 3-26 to 3-27 and Figures 3-28 to 3-29, respectively. As shown in these figures, the vertical components of these ground motion pairs could significantly affect the maximum absolute acceleration responses. The increase in the maximum absolute acceleration response under ground motion pair No. 4 was significant as shown in Figure 3-29a. This is because the PGA of the vertical component of ground motion pair No. 4 is large with a PGA of approximately 0.68 g compared to the acceleration of gravity g (see equation (3-14)). Figure 3-27a shows that the vertical component of ground motion pair No. 2 had less influence on the maximum absolute acceleration response. This is because the PGA of this vertical component is only 0.13 g compared to the acceleration of gravity g. Figure 3-26b shows that the vertical component of ground motion pair No. 2 had almost no effect on the relative displacement responses. However, the vertical component of ground motion pair No. 4 caused a significant increase in the maximum displacement response shown in Figure 3-28b.

Responses of the bearing with $\theta = 4$ and $Q_{dr} = 1$ under ground motion pairs No. 2 and No. 4 are shown in Figures 3-30 to 3-31 and Figures 3-32 to 3-33, respectively. For the maximum absolute acceleration response, similar trends to the bearing mentioned previously can be observed. However, the vertical components of both ground motions pairs have little influence on the maximum displacement response.

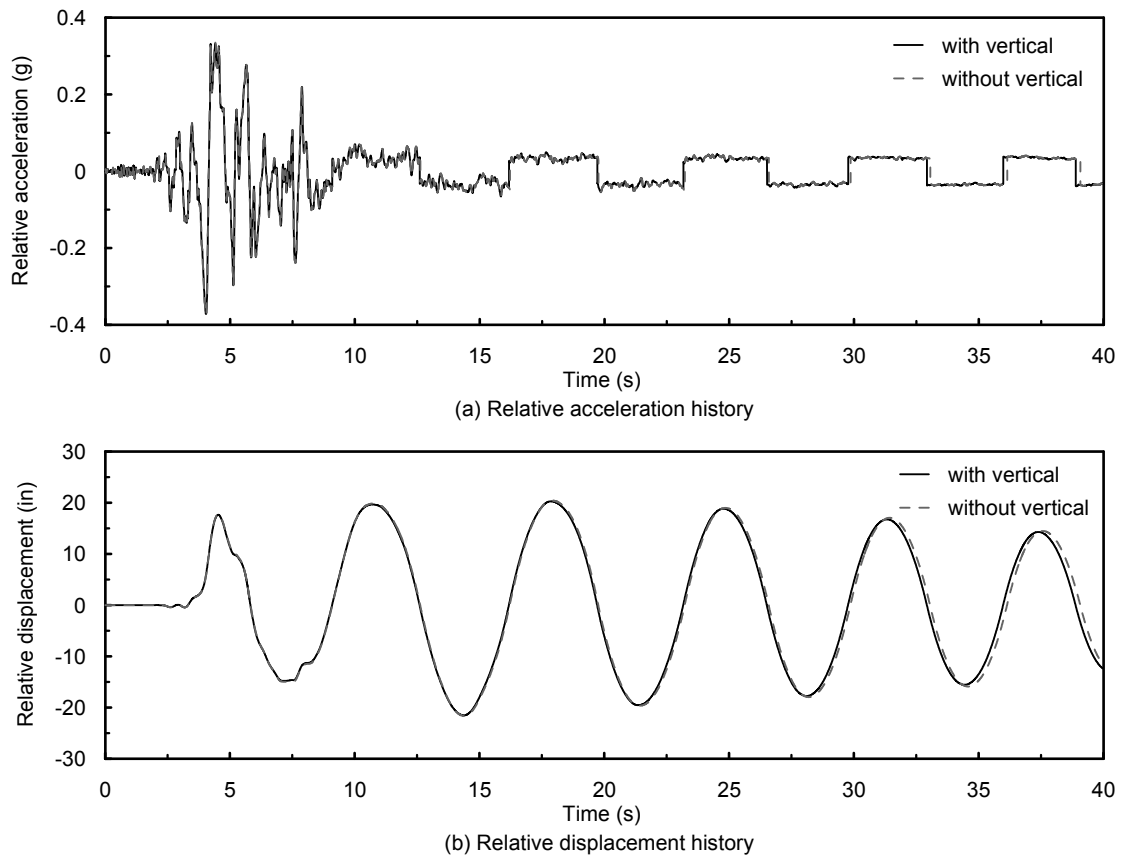


Figure 3-26 Acceleration and displacement responses of a bearing with $\theta = 4$ and $Q_{dr} = 0$ to ground motion pair No. 2 with and without the vertical component

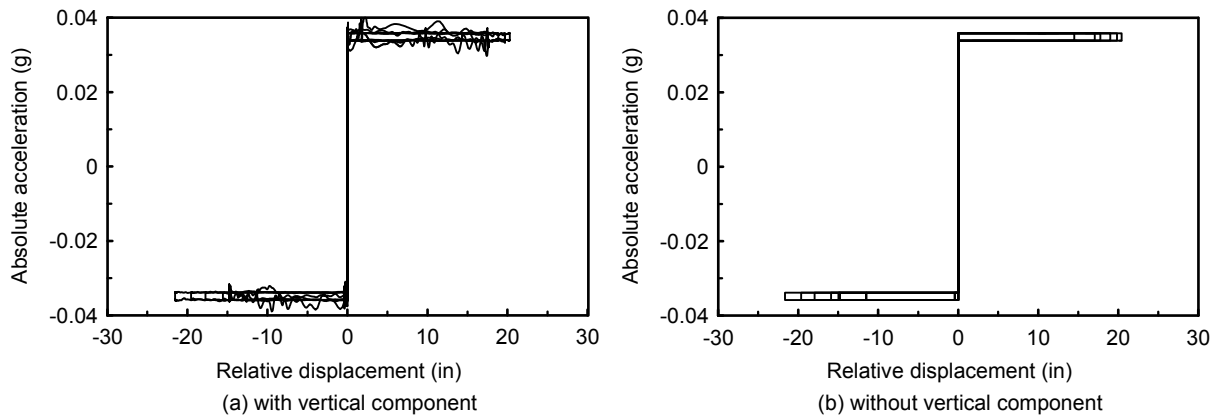
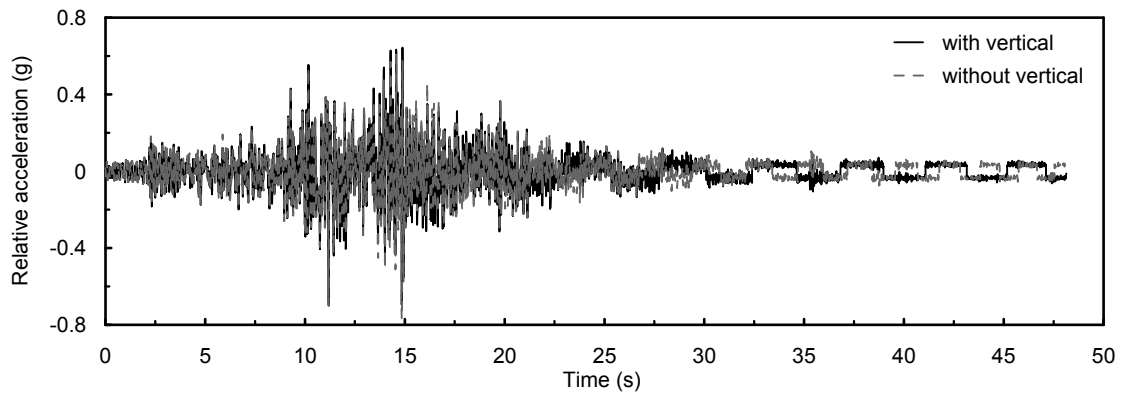
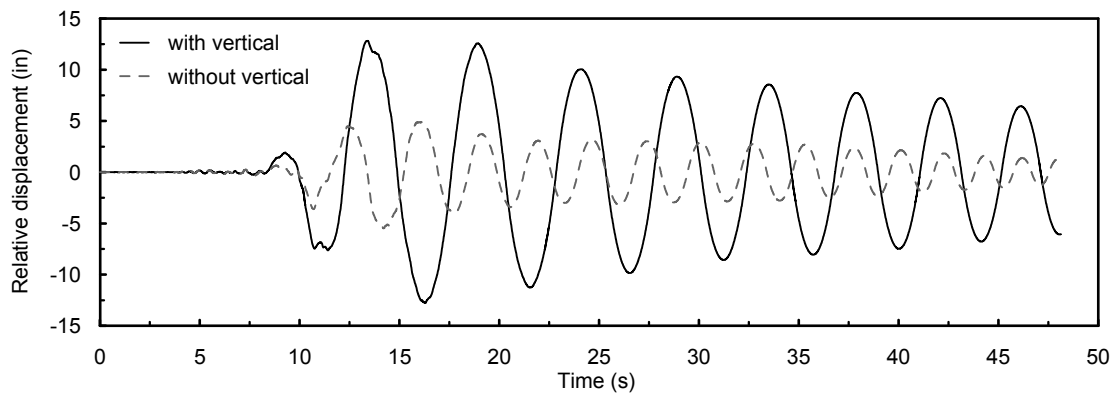


Figure 3-27 Hysteretic responses of a bearing with $\theta = 4$ and $Q_{dr} = 0$ to ground motion pair No. 2 with and without the vertical component



(a) Relative acceleration history



(b) Relative displacement history

Figure 3-28 Acceleration and displacement responses of a bearing with $\theta = 4$ and $Q_{dr} = 0$ to ground motion pair No. 4 with and without the vertical component

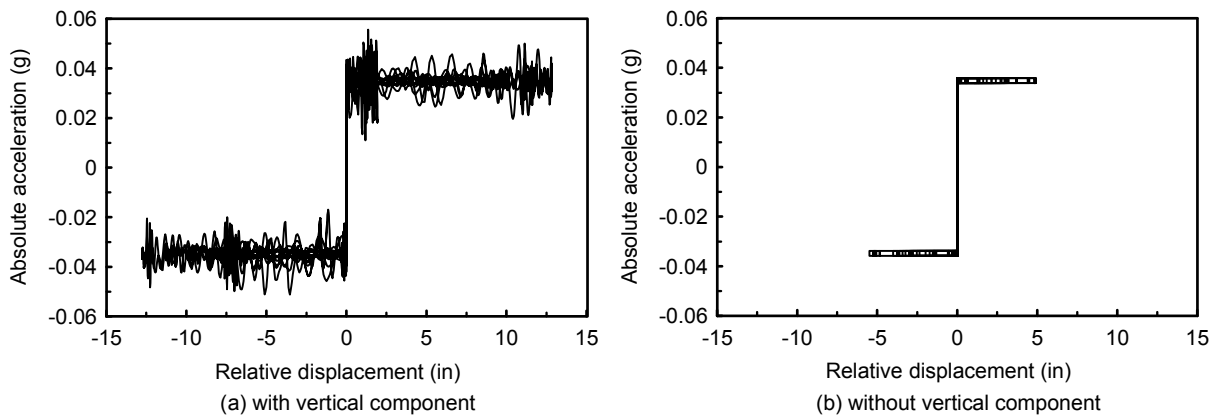
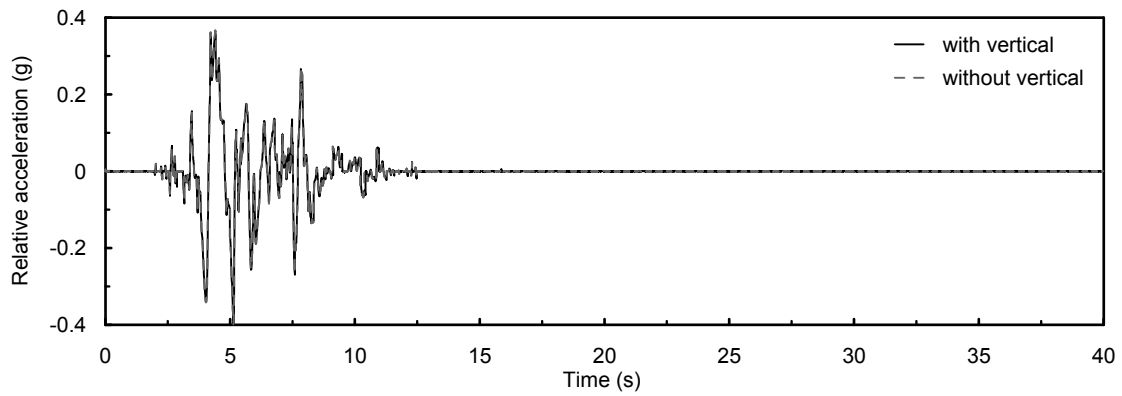
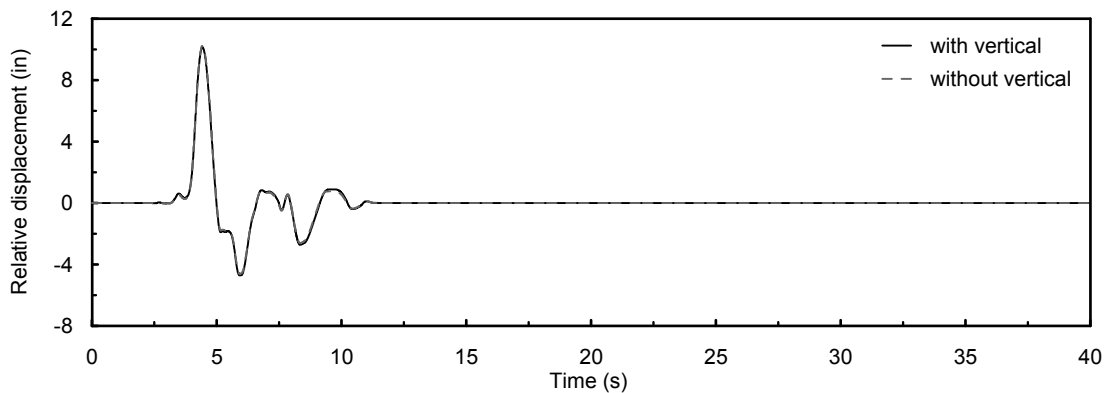


Figure 3-29 Hysteretic responses of a bearing with $\theta = 4$ and $Q_{dr} = 0$ to ground motion pair No. 4 with and without the vertical component



(a) Relative acceleration history



(b) Relative displacement history

Figure 3-30 Acceleration and displacement responses of a bearing with $\theta = 4$ and $Q_{dr} = 1$ to ground motion pair No. 2 with and without the vertical component

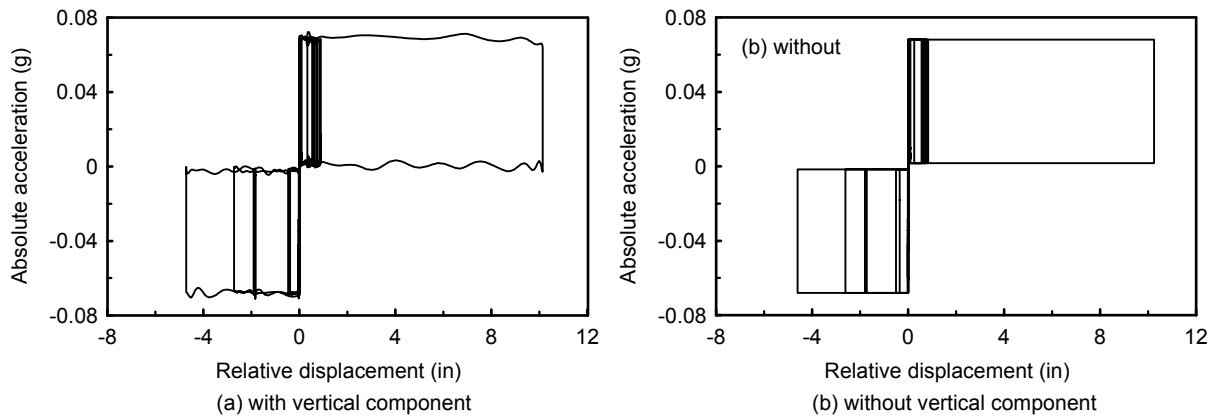
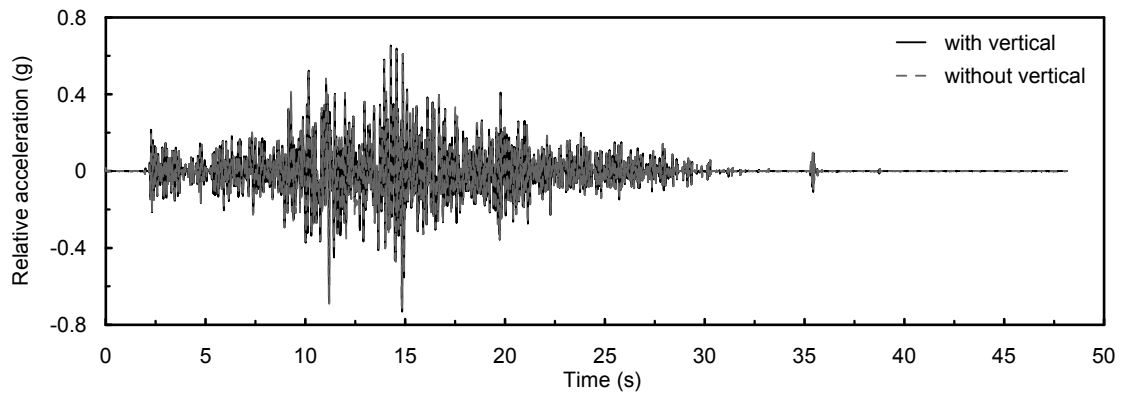
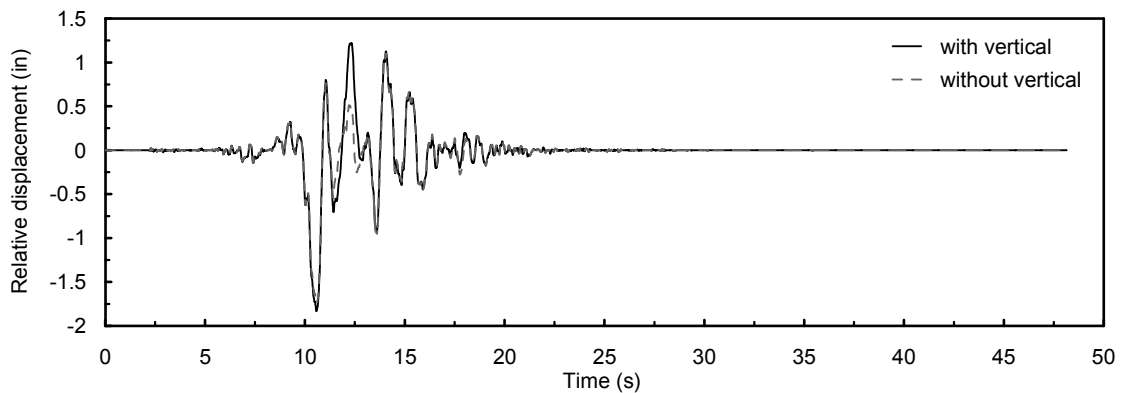


Figure 3-31 Hysteretic responses of a bearing with $\theta = 4$ and $Q_{dr} = 1$ to ground motion pair No. 2 with and without the vertical component



(a) Relative acceleration history



(b) Relative displacement history

Figure 3-32 Acceleration and displacement responses of a bearing with $\theta = 4$ and $Q_{dr} = 1$ to ground motion pair No. 4 with and without the vertical component

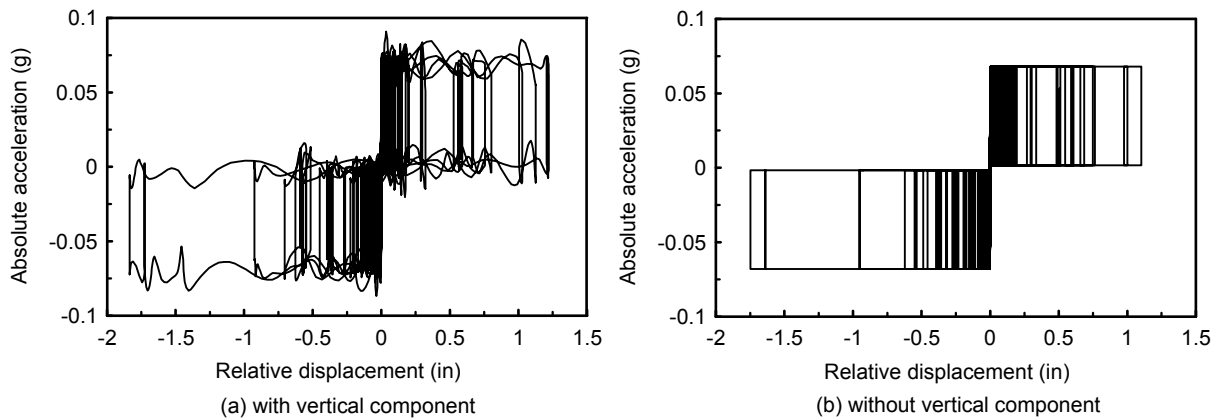


Figure 3-33 Hysteretic responses of a bearing with $\theta = 4$ and $Q_{dr} = 1$ to ground motion pair No. 4 with and without the vertical component

Analysis results of all the parametric combinations are shown in Figures 3-34 and 3-35. The vertical axis of these two figures represents errors caused by not considering the vertical components of the ground motions, which is defined as

$$error = \left| \frac{x_0 - x_v}{x_v} \right| \quad (3-15)$$

where x_v and x_0 represent the mean values of the maximum responses with and without considering the vertical ground motions, respectively. Figure 3-34 shows that errors for the mean maximum relative displacement responses were within 4% for bearings with friction devices. The errors reduced as the ratio Q_{dr} increased. This is because vertical ground motions have an influence on the restoring force f_s and the rolling friction force f_{Dr} , but have no effect on the sliding friction force f_{Ds} (see equation (3-14)). For bearings with the maximum allowable sliding friction force, f_{Dsa} , the errors reduced to be within 2%, which may be ignored in the design of the bearings.

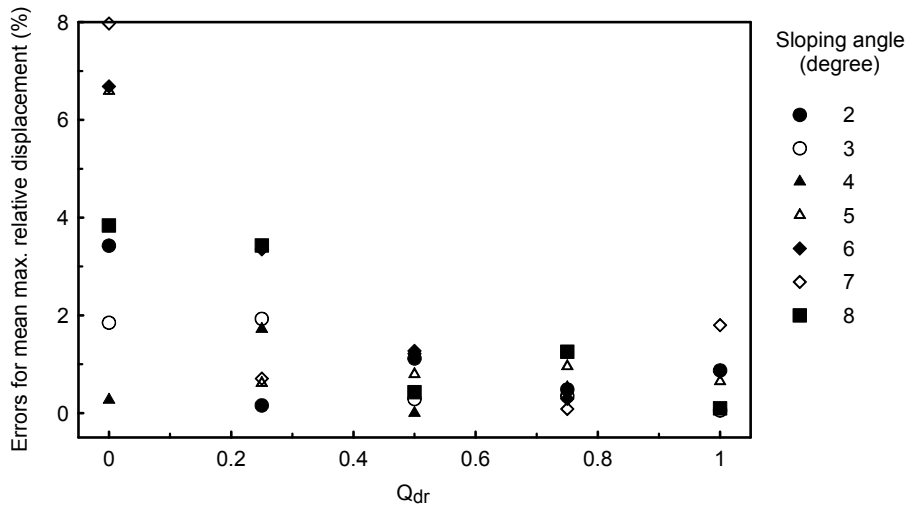


Figure 3-34 Effects of vertical ground motions on the mean maximum relative displacement response

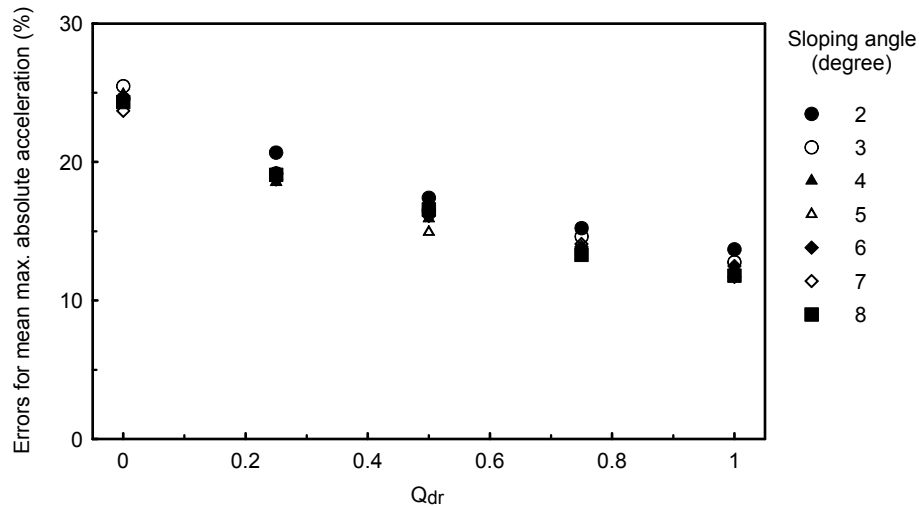


Figure 3-35 Effects of vertical components of the ground motions on the mean maximum absolute acceleration response

For the mean maximum absolute acceleration responses, errors ranged from approximately 25% for bearings with no friction device to 14% for bearings with the maximum allowable sliding friction force (see Figure 3-35). The errors decreased approximately linearly as the value of Q_{dr} increased. As previously mentioned, this is because vertical ground motions have no effect on the portion of the maximum acceleration response contributed from the friction device. Errors were significant even when a friction device with the maximum allowable friction forces was used. Therefore, the increase in maximum acceleration response and hence the increase in the base shear acting on the column where the bearings seat due to vertical ground motions need to be considered in design.

The maximum vertical acceleration demand to the bearing \ddot{Z}_m considering the flexibility of the substructure and soil may be estimated by

$$\ddot{Z}_m = C_v g \quad (3-16)$$

where the coefficient C_v is used in MCEER/ATC (2003) to account for the increase in pier axial force due to vertical ground motions. The values of C_v with respect to the distance from the site to the fault and the magnitude of the earthquake are given in Tables 3-4 and 3-5. It is stated in MCEER/ATC (2003) that the impact of vertical ground motions may be ignored for bridges that are located greater than 31 mi (50 km) from an active fault and may be ignored for bridges in the Central and Eastern U.S. as well as those areas impacted by subduction earthquakes in the Pacific Northwest.

The maximum base shear of the bearing occurs when the response of the bearing is along directions 45 degrees away from the principal directions. The maximum base shear including the effect of vertical ground motions may be estimated by

$$V = f_s + f_{Dr} + f_{Ds} = \frac{\sqrt{2}}{2} mg(1 + C_v) \sin \theta + \sqrt{2} \mu_r mg(1 + C_v) + \sqrt{2} \mu_s N \quad (3-17)$$

Under vertical ground motions, the seismic weight of the bearings may be increased to

$$W_{sv} = (1 + C_v) mg \quad (3-18)$$

where W_{sv} is the seismic weight of the bearing including the effect of vertical ground motions. This load should be considered in the design of the roller size.

Table 3-4 C_v for earthquakes with a magnitude 7.0 or less (MCEER/ATC 2003)

Fault Distance Zones (mi)	0-6	6-12	12-19	19-25	25-31
C_v	0.7	0.3	0.2	0.1	0.1

Table 3-5 C_v for earthquakes with a magnitude greater than 7.0 (MCEER/ATC 2003)

Fault Distance Zones (mi)	0-6	6-12	12-19	19-25	25-31
C_v	0.9	0.4	0.2	0.2	0.1

3.4 Equivalent Linear Methods

3.4.1 Secant Stiffness Method

The uniform load method and the single mode spectral method of AASHTO (2000) use an equivalent linear method, which is referred to as the secant stiffness method herein, to obtain the effective period and equivalent damping of a seismic isolation system. The maximum displacement response of the system is then estimated from a 5% damped elastic displacement response spectrum based on the period and damping of the equivalent linear system. Here, the secant stiffness method for the roller seismic isolation bearing is examined. Note that as stated in Section 3.2.1, properties of the bearing along the principal directions are used to estimate the maximum displacement demand for a conservative result.

3.4.1.1 Rigid base

For the secant stiffness method, the effective period T_{eff} of n_i roller seismic isolation bearings working in parallel on a rigid base is

$$T_{eff} = 2\pi\sqrt{\frac{k_{eff}}{M}} \quad (3-19)$$

where M is the tributary mass carried by n_i bearings; and k_{eff} is the effective stiffness of the bearings, which is defined as

$$k_{eff} = \frac{F_{max}}{x_i} = \frac{n_i (f_s + f_{Dr} + f_{Ds})}{x_i} \quad (3-20)$$

where F_{max} and x_i are the maximum force and the maximum relative displacement of a lateral force-displacement loop of the bearings, respectively, as illustrated in Figure 3-36; and f_s , f_{Dr} and f_{Ds} are defined by equations (2-28), (2-29) and (3-2). The relative displacement between the roller and plate is half the value of x_i (see Figure 2-8). Also note that the effects of vertical ground motion are not considered in the equation because it was shown in Section 3.3 that vertical ground motions have little influence on the maximum relative displacement response of the bearing with friction energy dissipation devices. The equivalent damping β of the bearings is defined as

$$\beta = \frac{EDC}{2\pi k_{eff} x_i^2} = \frac{2(f_{Dr} + f_{Ds})}{\pi (f_s + f_{Dr} + f_{Ds})} \quad (3-21)$$

where EDC is the energy dissipation of a lateral force-displacement loop of the bearings. The equation shows the roller equivalent damping β is a constant independent of the maximum relative displacement of the roller bearings.

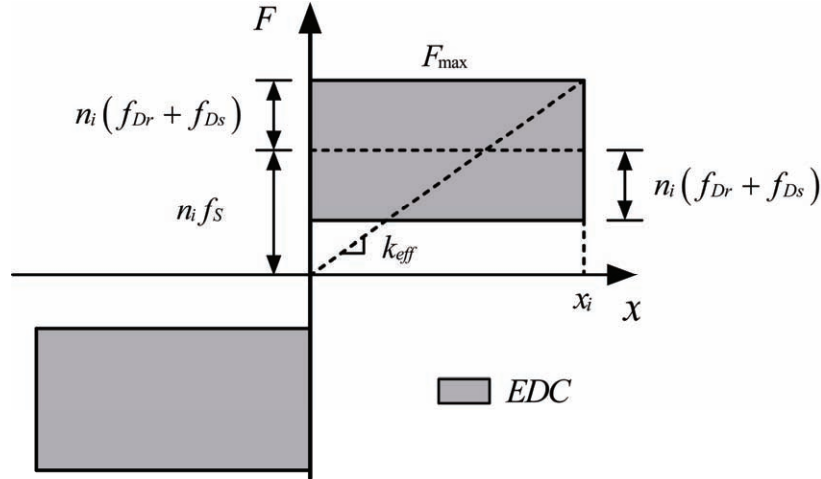


Figure 3-36 Secant stiffness method

3.4.1.2 Flexible base

The contribution to the maximum displacement of the superstructure from the flexibility of the substructure and the surrounding soil is considered next. The effective stiffness K_{eff} of the combined system, which consists of the bearings, a single column or a multiple-column bent and soils surrounding the column foundation, is

$$K_{eff} = \left(\frac{1}{k_{st}} + \frac{hL}{k_{sr}} + \frac{1}{k_c} + \frac{1}{n_i k_i} \right)^{-1} \quad (3-22)$$

where L is the distance from the base of the column to the centroid of the superstructure; h is the column height (see Figure 3-37); and k_{st} , k_{sr} , k_c and k_i are defined as follows.

$$k_{st} = \frac{n_i (f_s + f_{Dr} + f_{Ds})}{x_{st}}; \quad k_{sr} = \frac{n_i (f_s + f_{Dr} + f_{Ds}) h}{\theta_{sr}};$$

$$k_c = \frac{n_i (f_s + f_{Dr} + f_{Ds})}{x_c}; \quad k_i = \frac{f_s + f_{Dr} + f_{Ds}}{x_i} \quad (3-23)$$

where n_i is the number of the bearings; and x_{st} , $L\theta_{sr}$, x_c and x_i are relative displacements of the center of mass of the tributary superstructure due to horizontal movements of the soils, rotation of the soils, deformations of the column and flexibility of the bearings, respectively. Note that x_{st} , $L\theta_{sr}$ and x_c are typically designed to be much smaller than x_i for the bearings to function properly. Their magnitudes are exaggerated in Figure 3-37 for ease of presentation.

Substituting equation (3-23) to equation (3-22) gives

$$K_{eff} = \frac{n_i(f_S + f_{Dr} + f_{Ds})}{x_i + x_c + x_{st} + L\theta_{sr}} = \frac{n_i(f_S + f_{Dr} + f_{Ds})}{x_{max}} \quad (3-24)$$

The effective period of the combined system T_{eff} is

$$T_{eff} = 2\pi\sqrt{\frac{K_{eff}}{M}} \quad (3-25)$$

The equivalent damping β_c of the combined system is

$$\beta_c = \frac{EDC}{2\pi K_{eff} x_{max}^2} = \frac{2(f_{Dr} + f_{Ds})x_i}{\pi(f_S + f_{Dr} + f_{Ds})x_{max}} \quad (3-26)$$

Note that damping of the soil and the substructure is neglected in the above analysis.

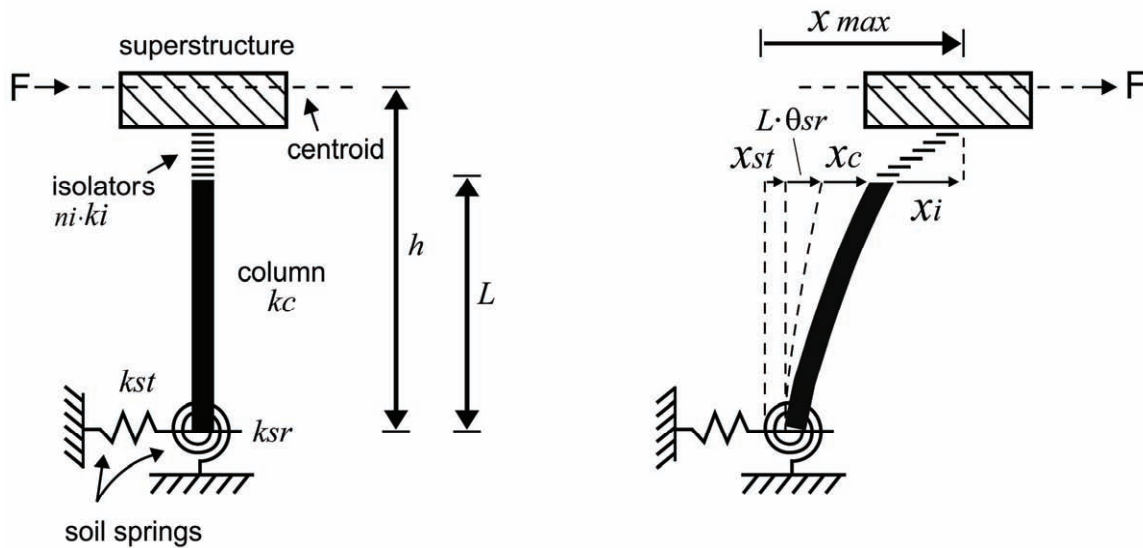


Figure 3-37 Displacements of the superstructure due to flexibility of the isolation bearings, column and surrounding soils (adapted from Constantinou et al. 2007)

3.4.2 Proposed Equivalent Linear Method

A new equivalent linear method is proposed to predict the maximum relative displacement response of the roller seismic isolation bearing. This method is based on relative displacement, relative velocity and absolute acceleration spectra.

3.4.2.1 Rigid base

For a given relative displacement of n_i roller seismic isolation bearings working in parallel on a rigid base, x_i , the potential energy W_p stored in the bearings due to the work done by the restoring force of the bearings f_s is

$$W_p = n_i f_s x_i = n_i \frac{1}{2} Mg \sin \theta x_i \quad (3-27)$$

Here, we assume that this potential energy is equal to the strain energy of the bearings. As a result, the potential energy can also be expressed as

$$W_p = \frac{1}{2} k_{eff} x_i^2 \quad (3-28)$$

This is illustrated in Figure 3-38. Substituting W_p from equation (3-27) into equation (3-28) and solving k_{eff} leads to

$$k_{eff} = \frac{2n_i f_s}{x_i} = \frac{n_i Mg \sin \theta}{x_i} \quad (3-29)$$

Comparing equations (3-29) and (3-20), it is seen that the effective stiffness from the proposed method is independent of the characteristic strength while that from the secant stiffness increases as the characteristic strength increases. This is because only the force related to potential energy is considered in the proposed method. Both the force related to potential energy and the force related to hysteretic energy are considered in the secant stiffness method. Substituting equation (3-29) for k_{eff} in equation (3-19) leads to the effective period of the bearings.

The damping of the bearings β is determined in a way such that the inertia force, damping force and amount of hysteretic energy dissipation of the equivalent linear system can approach those of the bearings. This is accomplished by seeking the smallest value of a goal parameter λ defined as

$$\lambda = \sqrt{\lambda_I^2 + \lambda_D^2 + \lambda_{EDC}^2} \quad (3-30)$$

where λ_I , λ_D and λ_{EDC} are parameters associated with inertia force, damping force and energy dissipation per cycle of the bearings. The inertial force parameter λ_I is defined as

$$\lambda_I = \frac{F_{\max} - MA}{F_{\max}} \quad (3-31)$$

where F_{\max} is $n_i(f_S + f_{Dr} + f_{Ds})$; and A is the absolute acceleration spectral response.

The damping force parameter λ_D is defined as

$$\lambda_D = \frac{n_i(f_{Dr} + f_{Ds}) - 2\beta M \omega_{\text{eff}} V}{n_i(f_{Dr} + f_{Ds})} \quad (3-32)$$

$$\omega_{\text{eff}} = \sqrt{\frac{k_{\text{eff}}}{M}} \quad (3-33)$$

where V is the relative velocity spectral response. The energy dissipation parameter λ_{EDC} is defined as

$$\lambda_{EDC} = \frac{EDC - 2\pi\beta M \omega_{\text{eff}}^2 x_i^2}{EDC} \quad (3-34)$$

$$EDC = n_i 4(f_{Dr} + f_{Ds}) x_i \quad (3-35)$$

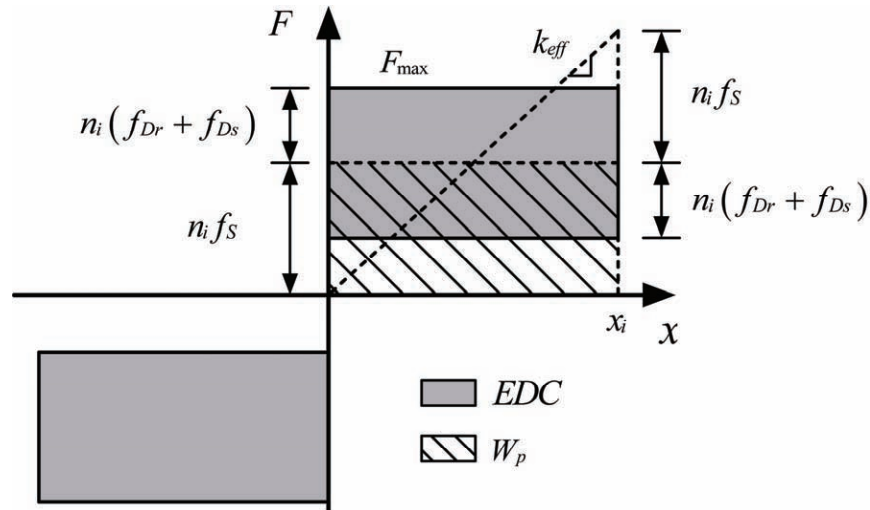


Figure 3-38 Proposed method for computing effective stiffness

3.4.2.2 Flexible base

The effective stiffness K_{eff} of the combined system, which consists of the bearings, a single column or a multiple-column bent and soils surrounding the foundation, is defined by equation (3-22) with k_{st} , k_{sr} and k_c defined by equation (3-23) and k_i defined by equation (3-29). The effective period of the combined system is calculated by equation (3-25). The equivalent damping of the combined system β_c is chosen with the same method as described by equations (3-30) to (3-35).

3.4.3 Comparison with Results from Nonlinear Response History Analyses

The secant stiffness method and the proposed equivalent linear method were used to predict the mean maximum relative displacement responses of the roller seismic isolation bearings under the 28 ground motions presented in Section 3.2. The design parameters of the bearings and the PGA levels of the ground motions examined were the same as listed in Table 3-2.

The proposed equivalent linear method used the mean absolute acceleration, mean relative velocity and mean relative displacement response spectra that were constructed with a range of equivalent damping ratios as shown in Figures 3-39, 3-40 and 3-41, respectively.

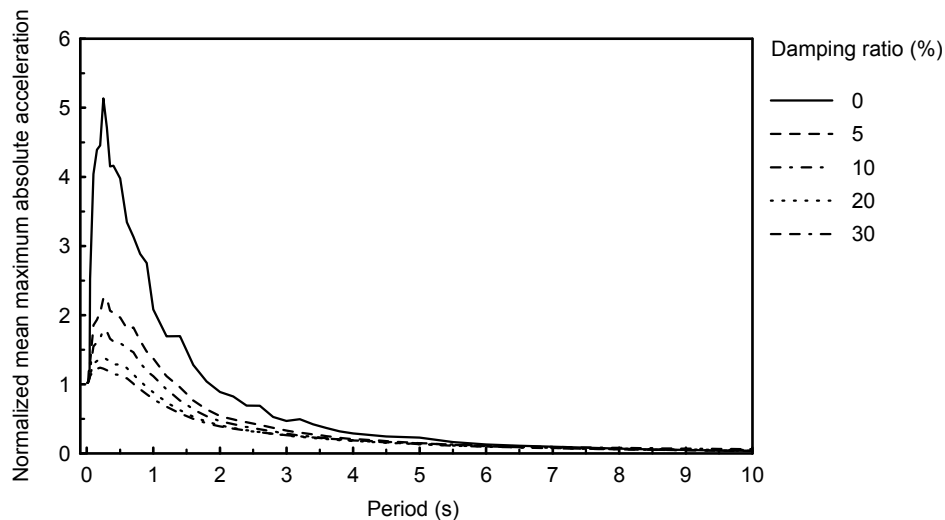


Figure 3-39 Mean absolute acceleration spectra for the 28 ground motions normalized by PGA

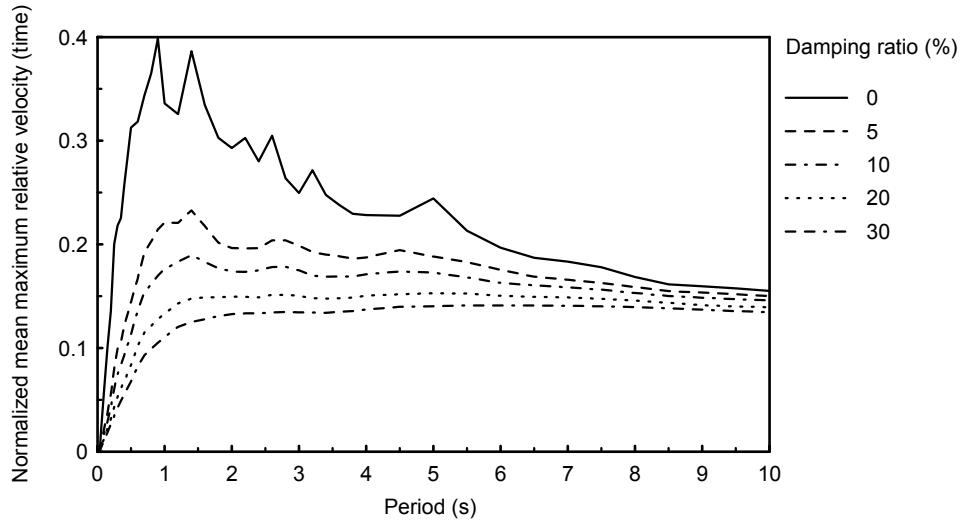


Figure 3-40 Mean relative velocity spectra for the 28 ground motions normalized by PGA

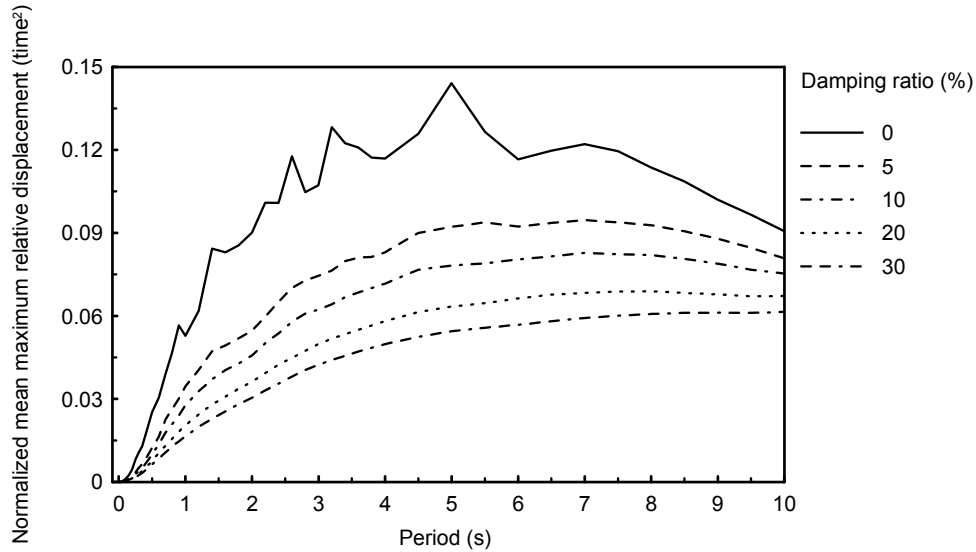


Figure 3-41 Mean relative displacement spectra for the 28 ground motions normalized by PGA

In the secant stiffness method, the 5% damped elastic mean relative displacement spectrum of the 28 ground motions as shown in Figure 3-41 was used. For a given effective period, the corresponding spectral value $S_{d,5\%}$ was obtained from Figure 3-41 and multiplied by the PGA level. For bearings with an equivalent damping ratio other than 5%, the mean spectral displacement value S_d was obtained by modifying the value of $S_{d,5\%}$ with the damping coefficient B (AASHTO 2000).

$$S_d = \frac{S_{d,5\%}}{B} \quad (3-36)$$

where B is the damping coefficient defined in Table 3-6. If damping exceeded 30%, B of 1.7 was used (AASHTO 2000). Chapter 5 of this report presents a case study where the secant stiffness method is used to predict the maximum displacement response of the bearings.

Table 3-6 Damping coefficient B (AASHTO 2000)

Damping (percentage to critical)	≤ 2	5	10	20	30
B	0.8	1.0	1.2	1.5	1.7

The mean relative displacement predicted by the equivalent linear methods for each combination of sloping angle θ , sliding friction force ratio Q_{dr} and PGA level are compared to that predicted by the corresponding nonlinear responses history analysis that has been presented in Section 3.2. The error of the response predicted by the equivalent linear methods to that calculated by nonlinear response history analyses is defined as

$$error = \frac{x_{eq} - x_{exact}}{x_{exact}} \quad (3-37)$$

where x_{eq} and x_{exact} represent responses predicted by the equivalent linear methods and nonlinear response history analyses, respectively.

Figures 3-42 to 3-48 show errors of mean maximum relative displacement responses predicted by the two equivalent linear methods for all the parametric combinations. From these figures, it is seen that the error tended to decrease when the PGA level increased or damping decreased. This implied that the error might be strongly correlated to the mean maximum displacement response. All the errors were plotted together in Figure 3-49 versus the corresponding mean maximum relative displacement from nonlinear response history analyses.

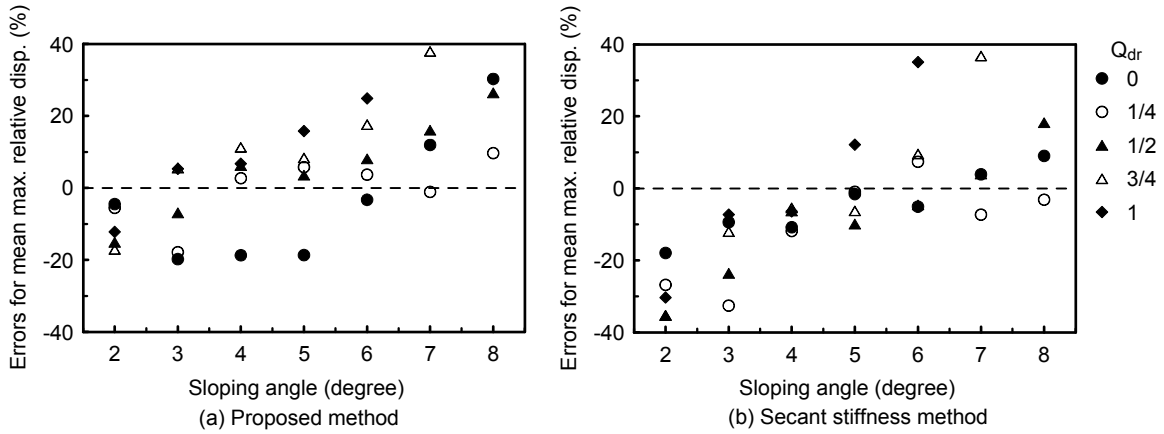


Figure 3-42 Errors of prediction by the proposed method and secant stiffness method under PGA=0.2g

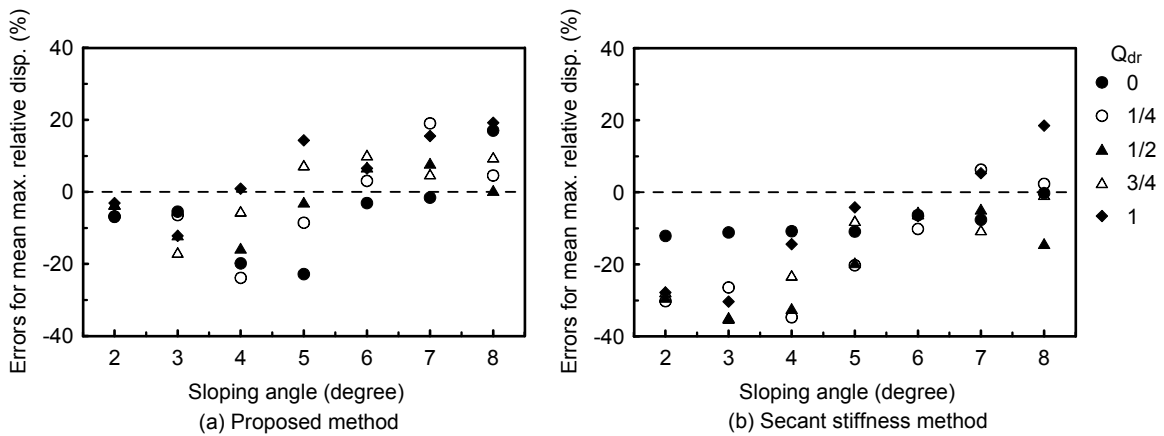


Figure 3-43 Errors of prediction by the proposed method and secant stiffness method under PGA=0.3g

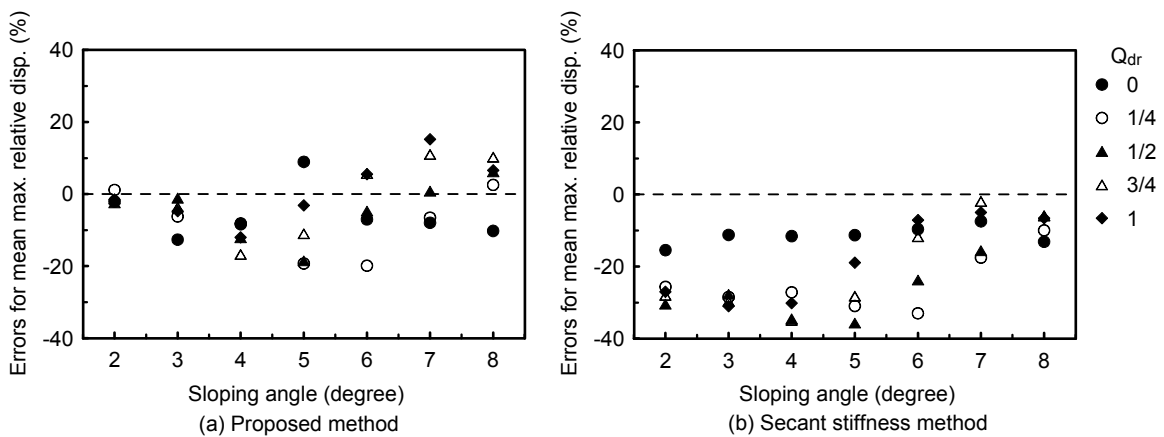


Figure 3-44 Errors of prediction by the proposed method and secant stiffness method under PGA=0.4g

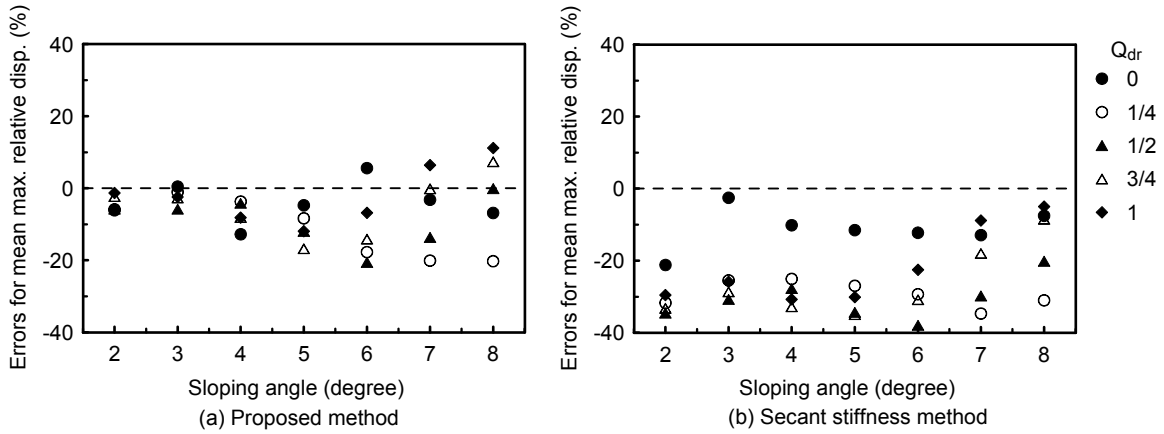


Figure 3-45 Errors of prediction by the proposed method and secant stiffness method under PGA=0.5g

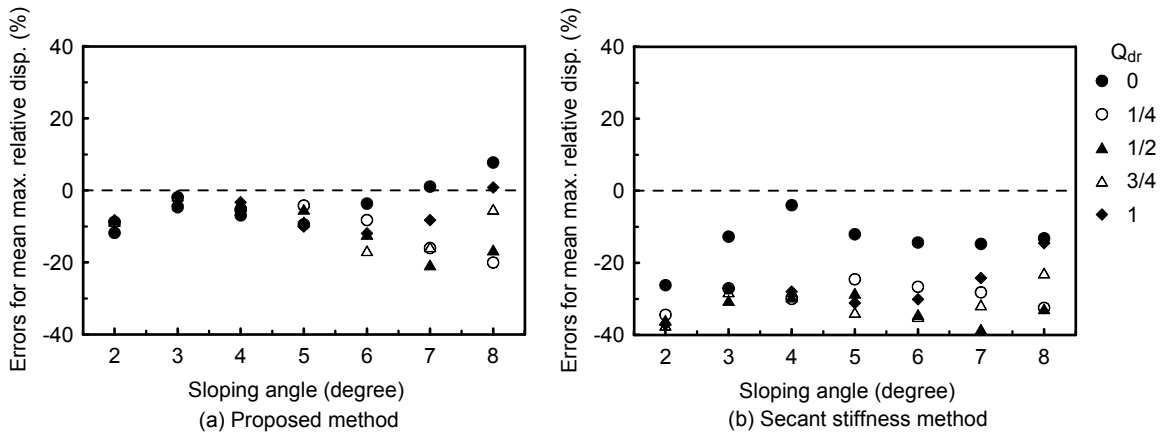


Figure 3-46 Errors of prediction by the proposed method and secant stiffness method under PGA=0.6g

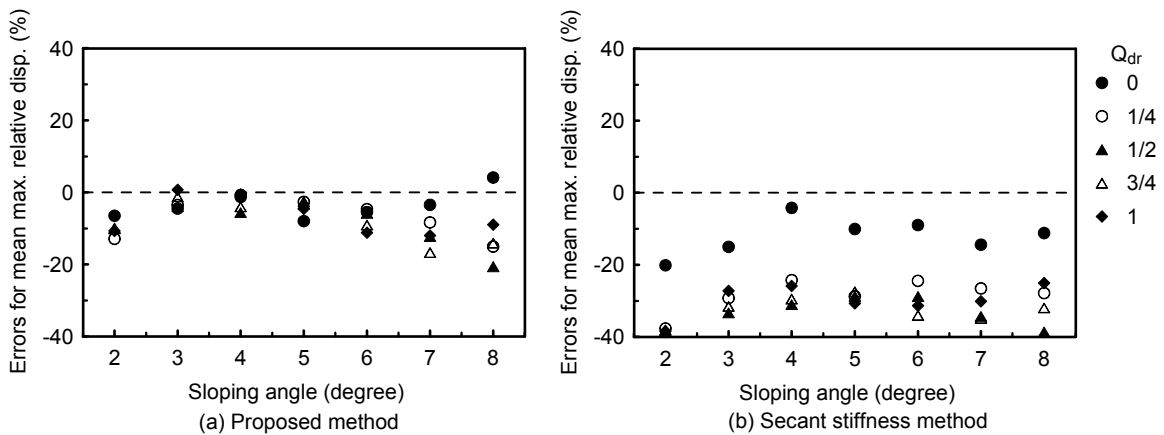


Figure 3-47 Errors of prediction by the proposed method and secant stiffness method under PGA=0.7g

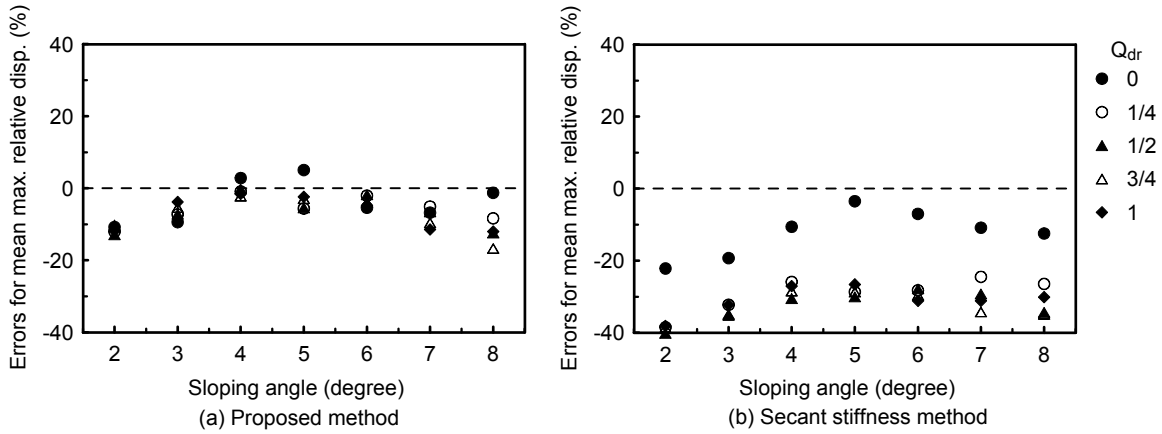


Figure 3-48 Errors of prediction by the proposed method and secant stiffness method under PGA=0.8g

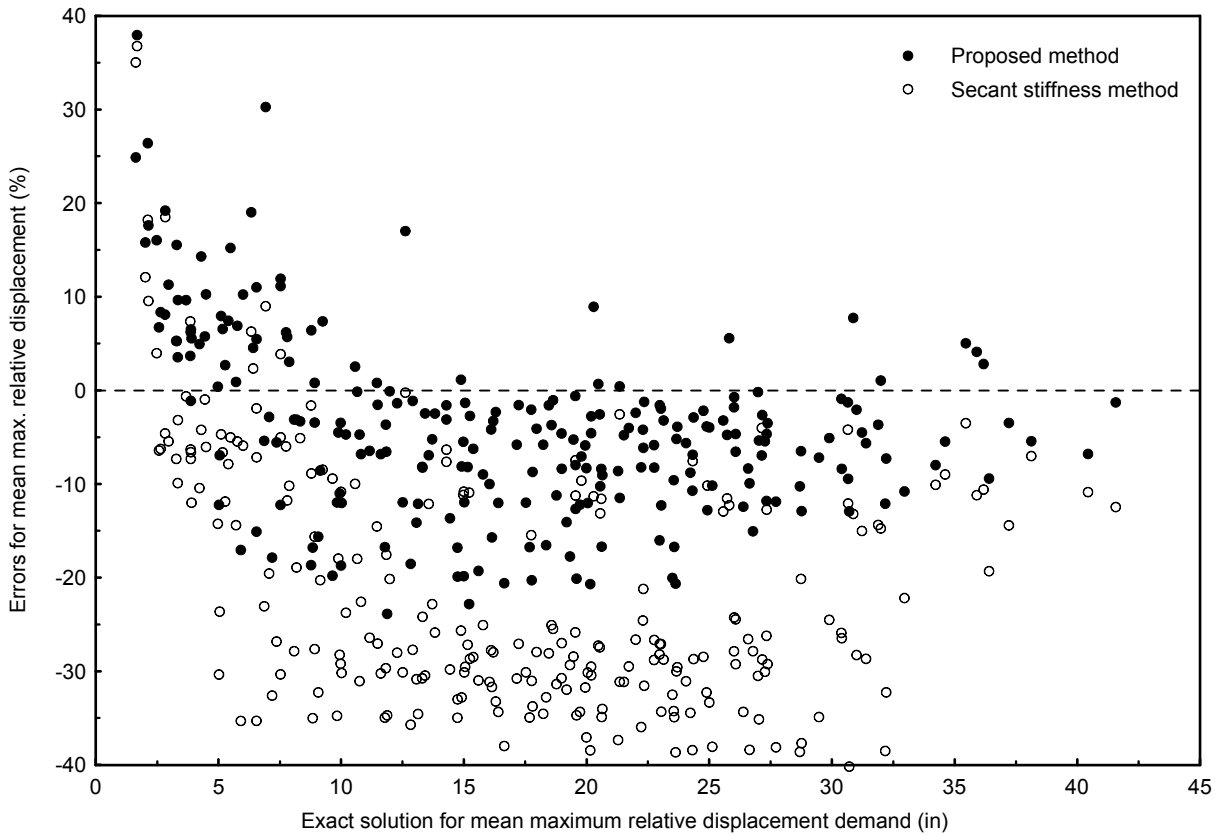


Figure 3-49 Errors of prediction by the proposed method and secant stiffness method for all the bearings

It was found that both methods produced a similar trend of results. When the maximum displacements were small, both methods tended to overestimate the responses, thus leading to conservative results. Since the maximum displacements were small, this did not cause excessive

displacement demand to the bearings. On the other hand, they tended to underestimate the responses when the maximum displacements were moderate or large. From these figures, it is clear that the proposed method provided better prediction of the maximum relative displacement responses. The errors generally fell within positive 10% to negative 20% for the proposed method while positive 10% to negative 40% for the secant stiffness method. To be conservative, the maximum displacement demand for the roller seismic isolation bearings may be increased by 20% and 40% for the proposed equivalent linear method and secant stiffness method, respectively.

$$S'_d = \begin{cases} 1.2S_d & \text{Proposed Method} \\ 1.4S_d & \text{Secant Stiffness Method} \end{cases} \quad (3-38)$$

where S'_d is the design displacement demand for the roller seismic isolation bearings; and S_d is the displacement spectral values.

The effective periods and damping of the bearings predicted by the proposed method and the secant stiffness method are shown in Figures 3-50 to 3-56. In Figures 3-50a to 3-56a, it can be seen that the effective periods predicted by both methods increased as the maximum displacement increased. This is expected as the effective stiffness is defined to be inversely proportional to the maximum displacement (see equations (3-20) and (3-29)). Moreover, it can be observed that the secant stiffness resulted in a larger effective period than the proposed method. This is expected since the denominator of equation (3-20) is smaller than that of equation (3-29) for the values of Q_{dr} investigated. Note that although the secant stiffness method led to a larger effective period, Figure 3-41 shows that it did not necessarily mean a larger displacement response for a given damping for periods examined.

Figures 3-50b to 3-56b show that the equivalent damping from the secant stiffness method remained constant for a given value of Q_{dr} . This was previously explained when equation (3-21) was introduced. For bearings with no friction device, both methods produced zero equivalent damping for most of the cases. For bearings with a friction device, the equivalent damping from the proposed method tended to decrease as the maximum displacement demand increased. It was also found that the equivalent damping from the proposed method was lower than that from the secant stiffness method. This in part explains why the proposed method was more likely to predict a higher maximum displacement demand than the secant stiffness method.

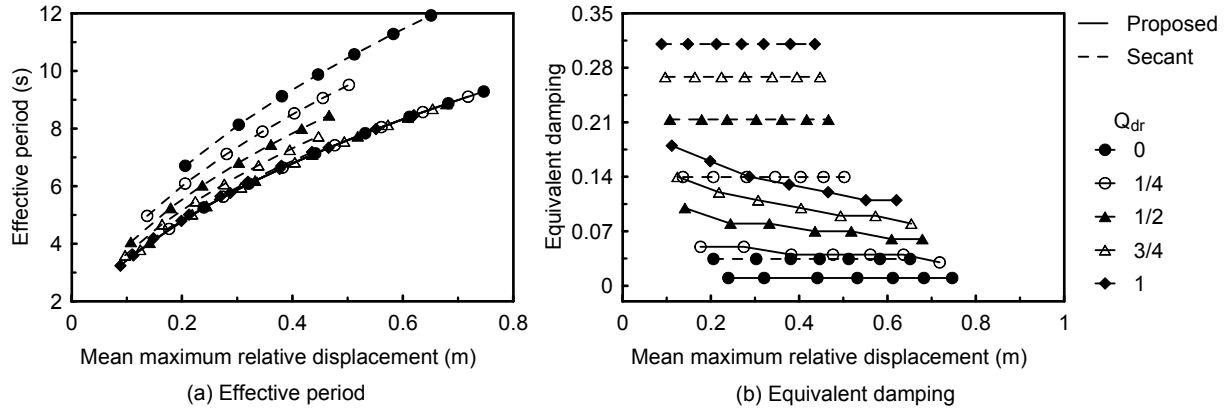


Figure 3-50 Effective periods and damping ratios for a sloping angle of 2 degrees

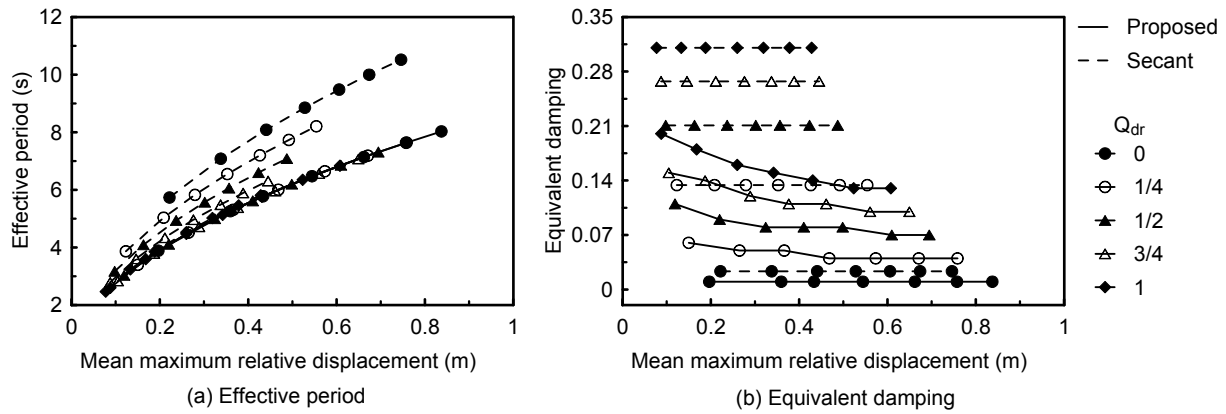


Figure 3-51 Effective periods and damping ratios for a sloping angle of 3 degrees

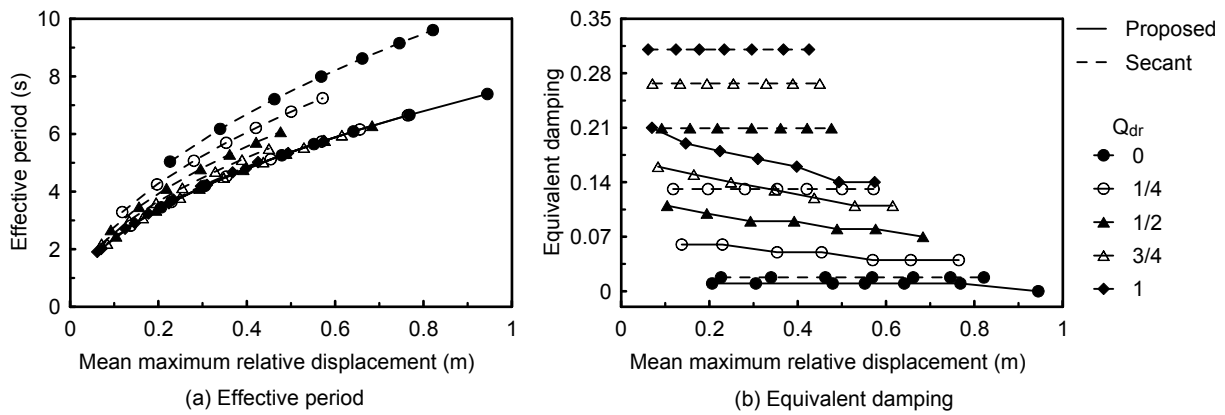


Figure 3-52 Effective periods and damping ratios for a sloping angle of 4 degrees

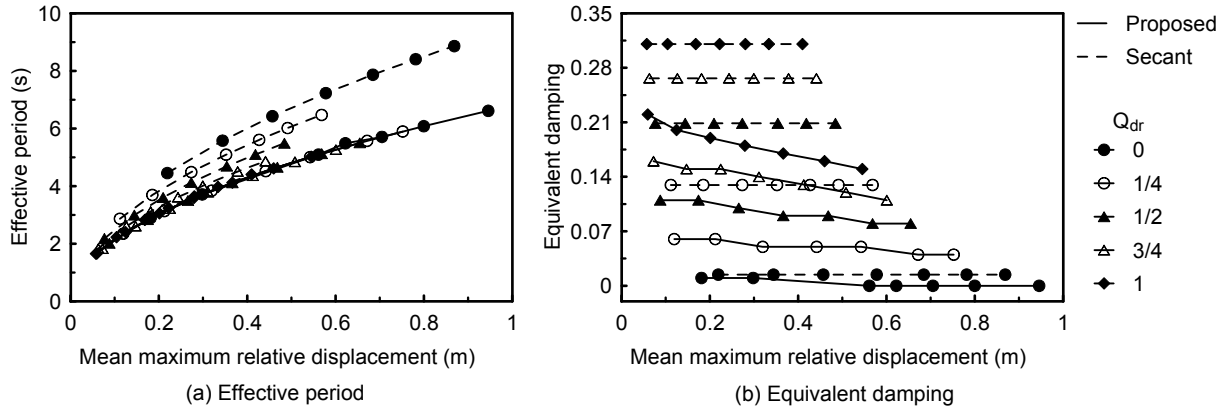


Figure 3-53 Effective periods and damping ratios for a sloping angle of 5 degrees

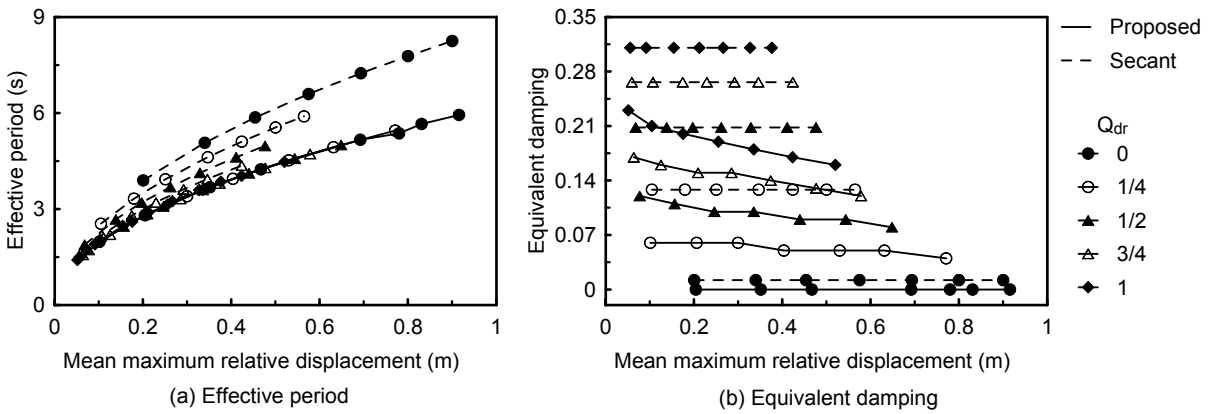


Figure 3-54 Effective periods and damping ratios for a sloping angle of 6 degrees

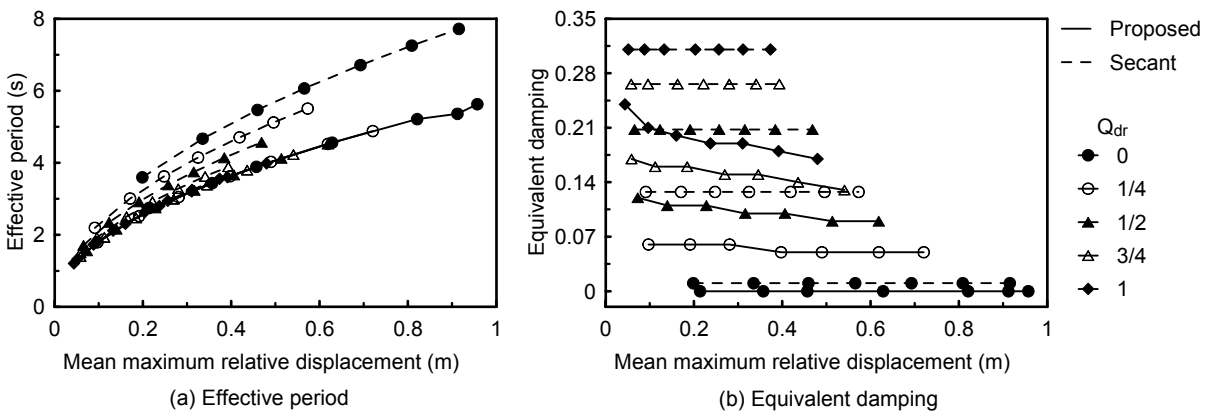


Figure 3-55 Effective periods and damping ratios for a sloping angle of 7 degrees

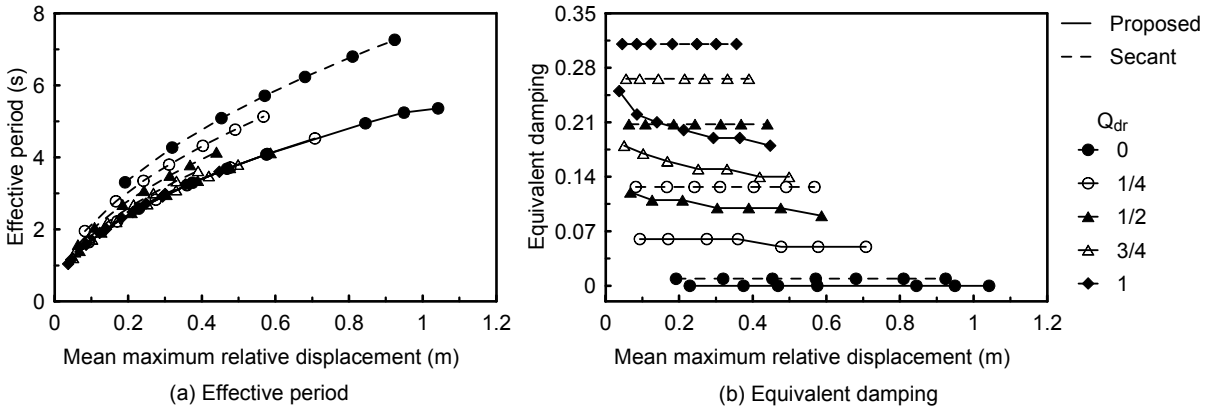


Figure 3-56 Effective periods and damping ratios for a sloping angle of 8 degrees

CHAPTER 4

PROTOTYPE ROLLER SEISMIC ISOLATION BEARINGS

In this chapter, two prototype roller seismic isolation bearings are presented. The first prototype bearing does not have any built-in friction devices. The second prototype roller bearing has several improvements over the first prototype bearing, including unique built-in friction mechanisms for supplemental energy dissipation.

4.1 The First Prototype Roller Seismic Isolation Bearing

4.1.1 Mechanical Properties

A schematic view of the first prototype bearing is shown in Figure 4-1. Both the upper and lower rollers of the bearing have a diameter D of 4.5 in (114.3 mm), a wall thickness t of 0.75 in (19.05 mm) and a final length L of 17 in (431.8 mm). The design displacement capacity of the bearing $2D_r$ is 8 in (203 mm). The rollers and plates are made of AISI 1045 hot rolled steel with a yield strength σ_y of 75 ksi (517 MPa). The vertical force capacity P of the bearing is listed in Table 4-1 and was calculated by equations (2-50) and (2-51).

The two sloping surfaces are designed at the intermediate plate: one at the top face and the other one at the bottom face. The sloping angle θ is 2 degrees. The restoring forces f_s for responses along the principal directions and along directions 45 degrees from the principal directions under horizontal ground motions were computed by equations (2-28) and (2-33), respectively. And, the rolling friction forces f_{Dr} were calculated by equations (2-29) and (2-34), respectively. Results are listed in Table 4-1. The coefficient of rolling friction μ_r was calculated by equation (2-3) with δ equal to 0.002 in (0.05 mm).

The thickness of the intermediate plate at the intersection of section lines A-A and B-B as shown in Figure 4-1 is 1 in (25 mm), which is linearly changed to 1.32 in (34 mm) at the edges of the plate along section line A-A for the top face of the plate and along section line B-B for the bottom face of the plate. The upper and lower plates have a thickness of 1 in (25 mm). The bearing is free to rotate until the upper plate touches the intermediate plate or until the intermediate plate touches the lower plate. The rotation under such conditions is 0.42 rad. The experimental studies on this prototype roller bearing are presented in Section 2.7 and Appendix A.

Table 4-1 Design parameters of the first prototype roller bearing

Vertical force capacity P (kips)		60
Restoring force f_s (mg^*)	Principal	0.017
	45°	0.025
Rolling friction force f_{Dr} (mg)	Principal	0.0009
	45°	0.0013
Displacement capacity (in)		8
Rotational capacity (rad)		0.42

* seismic weight carried by the bearing

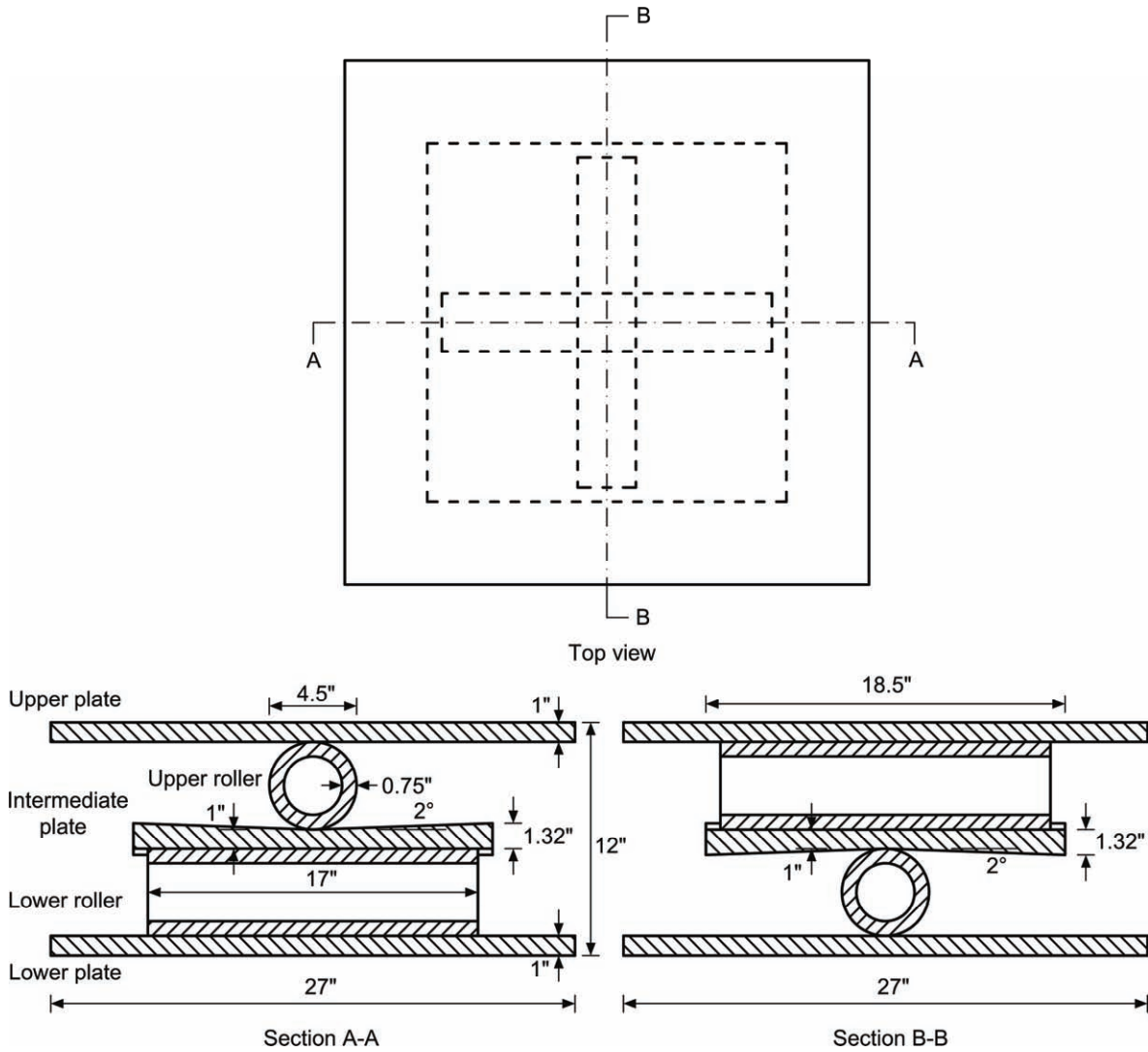


Figure 4-1 Schematic view of the first prototype roller bearing

4.1.2 Components

The design details of the first prototype roller bearing are illustrated in Figure 4-2. Figure 4-3 shows the photos of various components of the bearing. The materials and functions of each component shown in the figure are presented as follows.

1. **Lower plate:** a flat steel plate. The lower roller is designed to roll between this plate and the intermediate plate. This plate is secured to the top of a pier cap or abutment.
2. **Guide wall:** a steel angle with the exterior face strengthened by welded stiffeners. A stainless steel plate is welded to the interior face of the wall that was in contact with the side of the roller guide (see item 8). The function of the wall is to guide the movement of the roller.
3. **Lower protection wall:** a wall consisting of a steel plate and rubber sheets. It is used to seal the room formed by the intermediate plate, lower roller and lower plate to prevent entry of outside substances that might cause corrosion or interfere with the rolling motion of the roller.
4. **Upper protection wall:** a wall protecting the room formed by the upper plate, the upper roller and the intermediate plate. The wall will fall off automatically, if the displacement of the upper roller relative to the intermediate plate is large enough for this wall to hit the ends of the intermediate plate.
5. **Upper plate:** a flat steel plate. The upper roller is sandwiched between this plate and the intermediate plate. It would be secured to the bottom of the superstructure.
6. **Intermediate plate:** a steel plate with welded steel walls along its perimeter. The walls are used to stop the roller from rolling out of the plate. Each of the top and bottom faces of the plate is machined into a V-shaped sloping surface.
7. **Upper roller:** a seamless steel tube.
8. **Roller guide:** a steel block attached to the ends of the shaft (see item 13). One face of the block is in contact with the guide wall so that the roller moves only in parallel with the direction of the guide wall. The interface between the roller guide and guide wall has a lubricated layer of DU material (see item 12) to reduce interface friction.
9. **Sweeper device:** a device consisting of a steel plate with brooms attached to it. The device is located close to each side of the roller. Its function is to sweep debris, if any, away from the course of the rolling rollers.
10. **Lower roller:** a seamless steel tube.
11. **Sleeve:** a tubular piece made of aluminum alloy attached to the inner face of the roller body. It rotates together with the roller body relative to the shaft (see item 13). The interface between the sleeve and shaft is filled with a lubricated layer of DU material (see item 12).

- 12. **DU bearing material:** a self-lubricating bearing material consisting of a steel backing, porous bronze inner-structure and PTFE-lead overlay that provide the contact interface with low friction.
- 13. **Shaft:** consisting of several aluminum alloy pieces. It connects the roller body to the roller guide. When the roller body rolls relative to the shaft, it moves the shaft along the rolling direction. Consequently, the roller is guided by the roller guides located at two ends of the shaft.

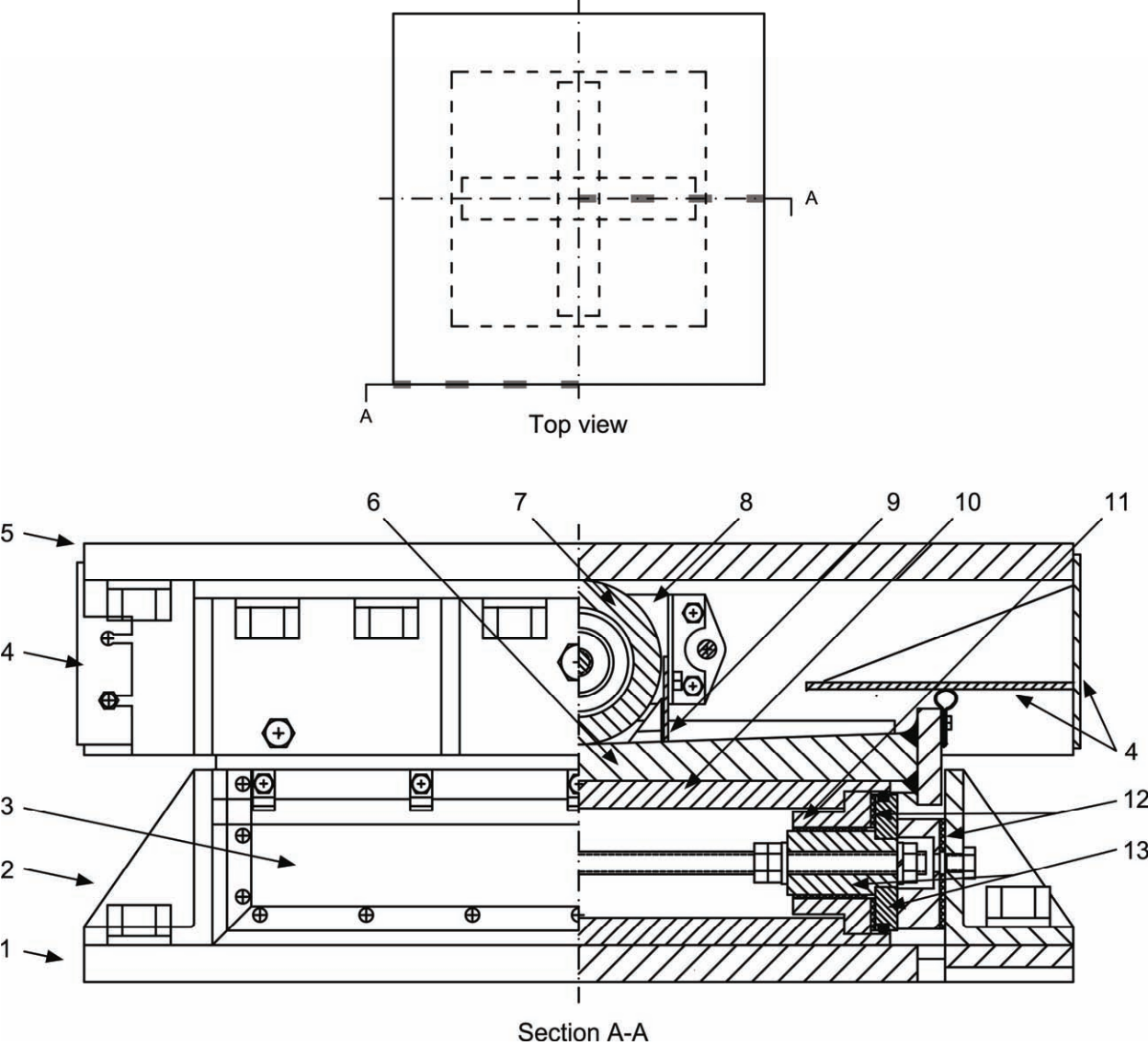
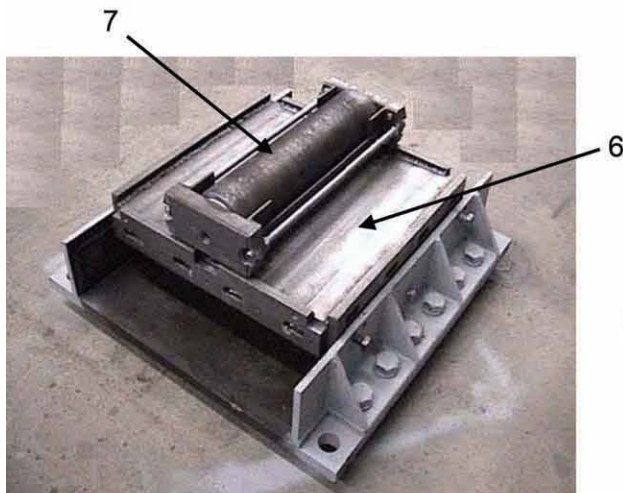


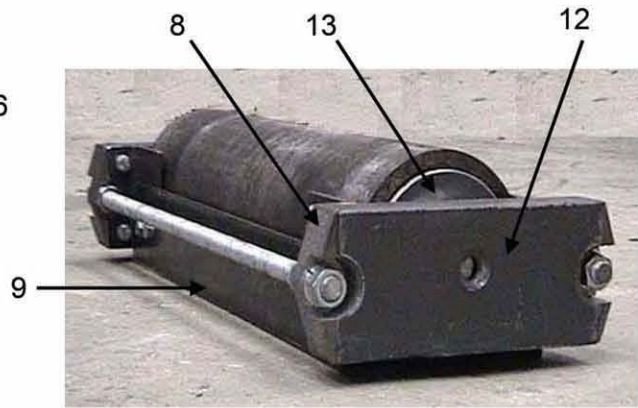
Figure 4-2 Design details of the first prototype roller bearing



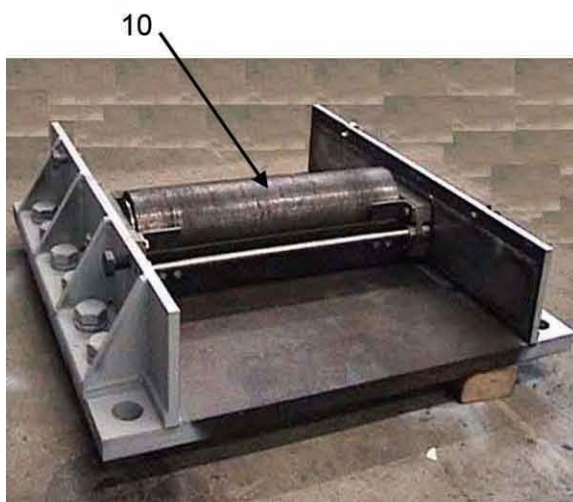
Roller bearing assembly



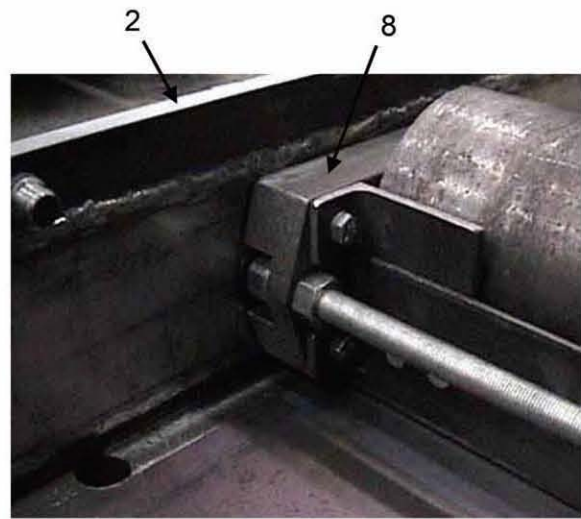
Upper roller and intermediate plate



Roller



Lower roller and lower plate



Close view of roller guide and transverse wall

Figure 4-3 Photos of the first prototype roller bearing

4.2 The Second Prototype Roller Seismic Isolation Bearing

4.2.1 Mechanical Properties

The design parameters of the bearing are listed in Table 4-2. The schematic view of the bearing is shown in Figure 4-4. The second prototype roller bearing has several improvements over the first prototype roller bearing. First of all, it has built-in devices for supplemental friction energy dissipation. In addition, the friction devices could also act to lock the bearing under wind and braking forces and under uplift of the superstructure due to vertical ground motions. Second, the rollers are not guided by the roller guides as seen in the first prototype roller bearing. Tests have shown that the interfaces between the ends of the roller and guide walls in the first prototype roller bearing may produce unexpected large friction forces, which could interrupt the rolling action of the rollers. A gap is designed between each end of the roller and the side wall (see Figure 4-4) in the second prototype bearing. Third, excessive rotations of the superstructure are prevented in this bearing by the side walls. The superstructure is allowed to rotate only until the gaps between the side walls and the bearing plates are exhausted. Lastly, this bearing has an option of adding shear keys to resist wind and braking forces in addition to the previously mentioned friction forces.

Both the upper roller and the lower roller of the prototype bearing have a diameter D , a wall thickness t and a final length L' of 4.92 in (125 mm), 1.06 in (27 mm) and 8.19 in (208 mm), respectively. The design displacement capacity of the bearing, $2D_r$, is 3 in (76.2 mm). The steel used for the rollers and plates has a yield strength σ_y of 175 ksi (1207 MPa). The vertical force capacity P is listed in Table 4-2 and was calculated using equations (2-50) and (2-51).

The rotational capacity of the bearing is 0.06 radians, which is determined by the 0.4 in (10 mm) gap between the side walls and the upper and lower plates.

Both the upper plate and the lower plate of the bearing have a thickness of 1.18 in (30 mm). The intermediate plate has a thickness of 1.18 in (30 mm) at the intersection of section lines A-A and B-B. The thickness is gradually increased towards the edges of the plate along line A-A at the top face of the plate and along line B-B at the bottom face of the plate to form two V-shaped sloping surfaces with a sloping angle of 5 degrees. The restoring forces f_s for responses along the principal directions and along directions 45 degrees from the principal directions were calculated by equations (2-28) and (2-33), respectively. And, the rolling friction forces f_{Dr} were computed by equations (2-29) and (2-34), respectively. Results are listed in Table 4-2. The coefficient of rolling friction μ_r was calculated by equation (2-3) with δ of 0.002 in (0.05 mm).

The sliding friction force for energy dissipation along each of the two principal directions of the bearing is generated by the corresponding pair of friction interfaces (see Figure 4-4) that are parallel to the rolling direction and located at two parallel outer faces of the side walls. There are two pairs of friction interfaces for rolling along the two principal directions of the bearing. If the bearing is displaced along one principal direction, only one pair of friction interfaces will be mobilized; if the bearing is displaced along directions 45 degrees away from the principal directions, both pairs of friction interfaces will be mobilized. Under such a condition, the bearing

will have the maximum friction force. Assume that the friction forces for the rolling directions of the upper roller and the lower roller are $\mu_s N_1$ and $\mu_s N_2$, respectively. The maximum friction force f_{Ds} is

$$f_{Ds} = \sqrt{(\mu_s N_1)^2 + (\mu_s N_2)^2} \quad (4-1)$$

where μ_s is the coefficient of sliding friction; and N_1 and N_2 are normal forces applied to the friction interfaces. Note that the two friction forces can be designed to be different by applying different normal forces to the two pairs of friction interfaces. They are equal in this prototype bearing. Thus, the maximum friction force is defined by equation (3-3).

The normal forces of the friction interfaces are achieved by screws. The mechanism is presented in the next section. The relationship between the torque T applied to a screw and the resulting normal force N_b to the friction interface may be expressed as

$$T = N_b (0.159t + 0.531\mu d) \quad (4-2)$$

where t and d are the pitch and the diameter of the screw, respectively; and μ is the coefficient of friction between the threads (Oberg et al. 2000). For each rolling direction, there are two friction interfaces. Normal forces for each interface are generated by three screws. As a result, the total normal force N for each rolling direction is

$$N = 6N_b \quad (4-3)$$

Table 4-2 Design parameters of the second prototype roller bearing

Vertical force capacity P (kips)		210
Restoring force f_s (mg *)	Principal	0.044
	45°	0.062
Rolling friction force f_{Dr} (mg)	Principal	0.0008
	45°	0.0011
Sliding friction force f_{Ds} (mg)	Principal	$\mu_s N$
	45°	$\sqrt{2}\mu_s N$
Displacement capacity (in)		3
Rotational capacity (rad)		0.06

* seismic weight carried by the bearing

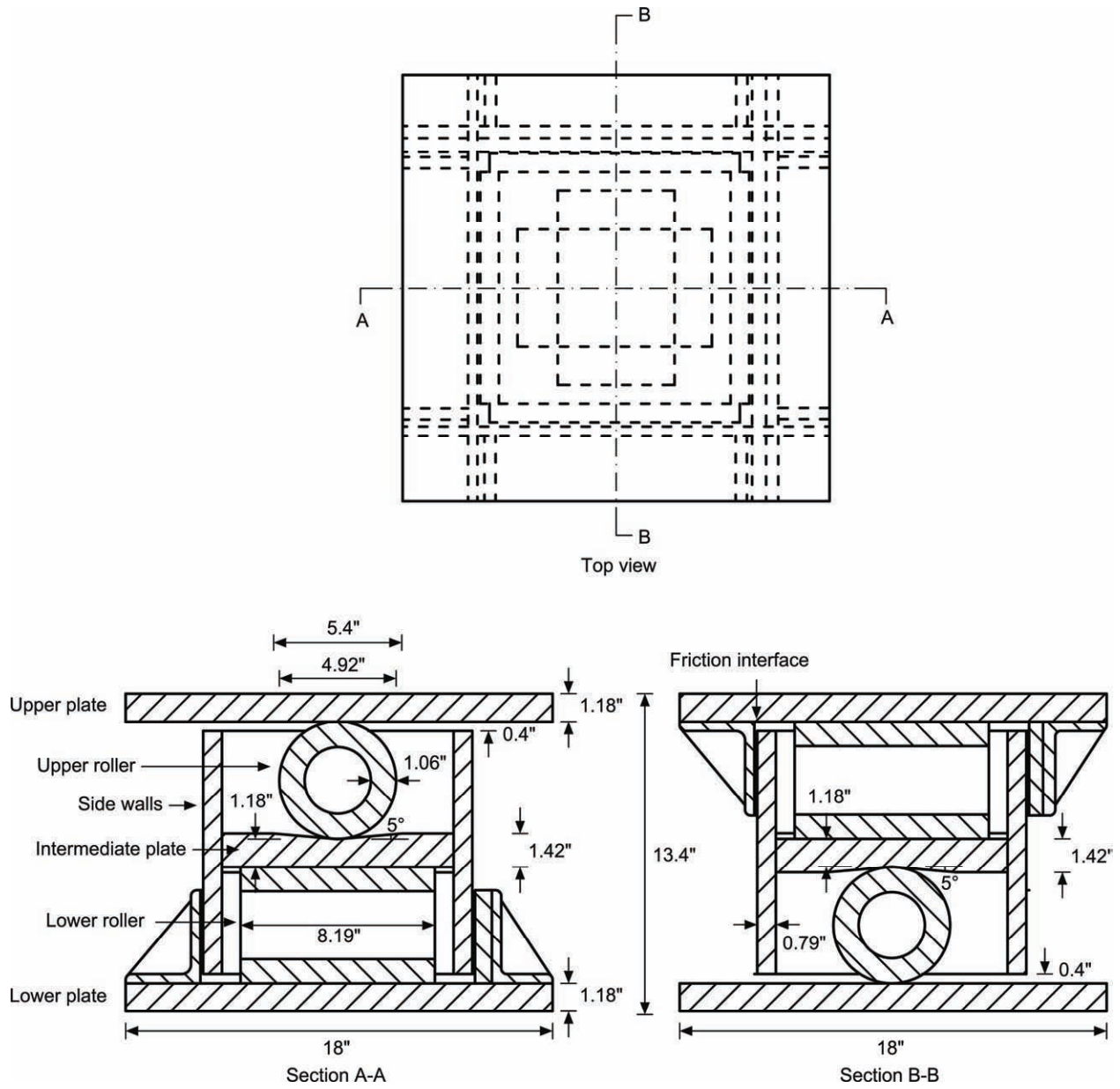


Figure 4-4 Schematic view of the second prototype roller bearing

4.2.2 Components

The design details of the bearing are shown in Figure 4-5. The materials and functions of the components identified in the figure are presented below. Figure 4-6 shows the photos of the bearing and its components.

1. **Upper plate:** a flat alloy steel plate. It is secured to the superstructure.
2. **Reaction wall:** a steel angle with the exterior face strengthened by welded stiffeners. There are two pairs of reaction walls for each of the two rolling directions. One pair of the reaction walls is fixed to the upper plate and the other fixed to the lower plate. Each pair of the reaction walls has a friction plate (see item 8) attached to one of the walls. Three screws (see item 10) anchored at that wall are turned to push the friction plate against the matching face of the side walls (see item 7). By doing this, the friction plate applies a normal force to the matching face of the side walls. For force equilibrium, the same amount of normal force is generated between the other reaction wall and the matching face of the side walls.
3. **Upper roller:** a seamless alloy steel tube. The upper roller is designed to roll between the upper and intermediate plates. The rollers do not touch the side walls as seen in the first prototype bearing. The reason for this has been explained in Section 4.2.1.
4. **Intermediate plate:** a flat alloy steel plate, which has the top face machined to a V-shaped sloping surface and the bottom face machined to an inverted V-shaped sloping surface.
5. **Lower roller:** a seamless alloy steel tube designed to roll between the intermediate and the lower plates.
6. **Lower plate:** a flat alloy steel plate. It is anchored to the top of the pier cap or abutment.
7. **Side walls:** four steel plates welded to each other and to the four edges of the intermediate plate. As previously mentioned, the side walls have multiple functions. They limit the displacements of the rollers and the rotation of the superstructure. Moreover, supplemental energy dissipation is generated through relative displacements between the side walls and reactions walls.
8. **Friction plate:** a steel plate located between one of each pair of the reaction walls and the matching face of the side walls. The face of the plate in contact with the matching face of the side walls is plated with a layer of hard chromium for wear resistance.
9. **Hard chromium layer:** plated to the faces of the friction interfaces for wear resistance, including the interface between the side walls and friction plates as well as that between the side walls and reaction walls.
10. **Fastener for normal force:** consisting of a steel hexagon socket set screw and a steel hex nut. Three fasteners are used to apply a normal force to each friction plate. The amount of normal force depends on the torque applied to the screw.

11. **Fastener for fixing friction plates:** used to prevent relative movement between the friction plate and reaction wall.
12. **Shear keys:** a tapered steel bar used to prevent rolling of the bearing under wind loads and braking forces in addition to the static friction force provided by the friction interfaces. The capacity of the keys is adjusted through the size of the critical section of the key.
13. **Temporary fasteners:** used to fix the bearing for transporting.
14. **Protective rubber sheets:** used to cover the gaps between the side walls and the upper and lower plates to keep dust and moisture from contaminating the rolling surfaces.

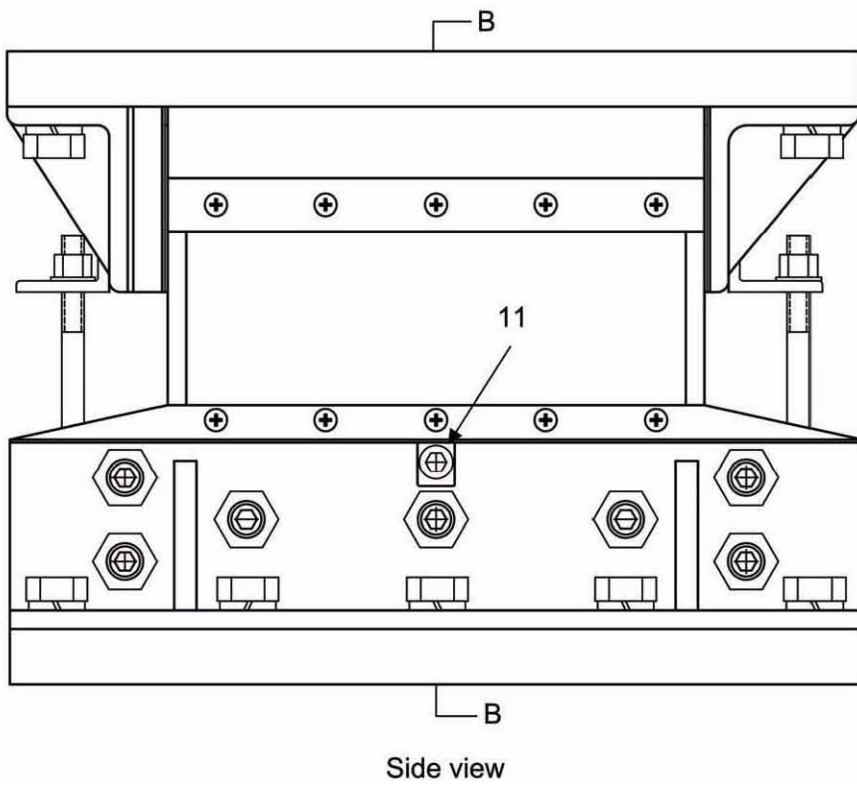
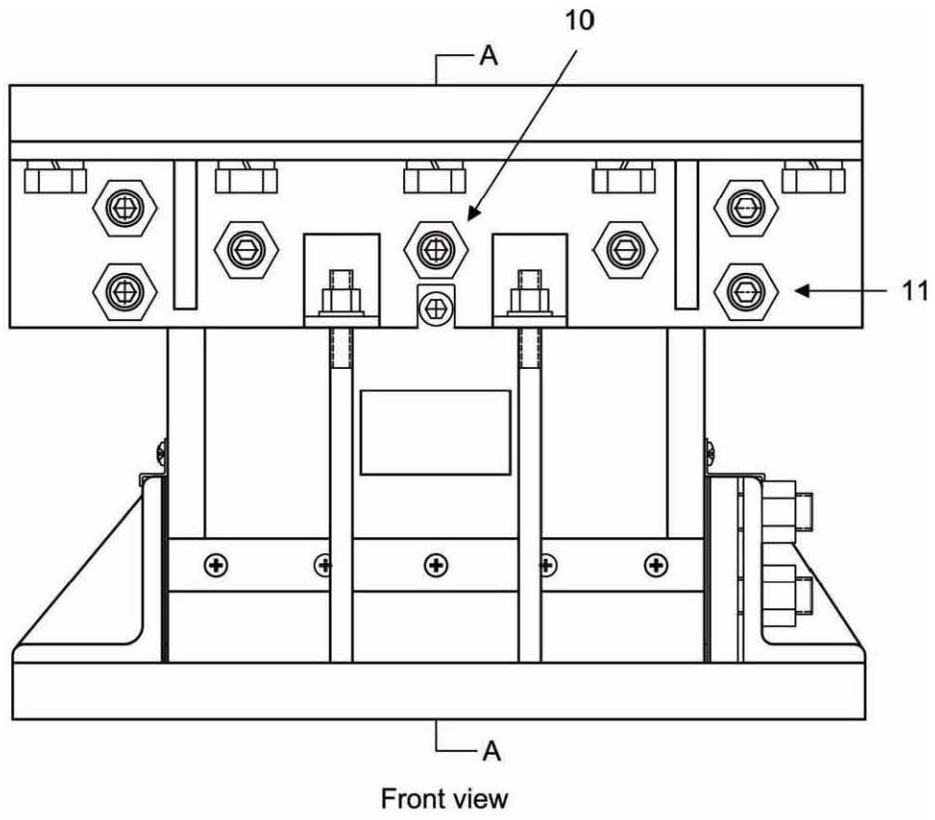
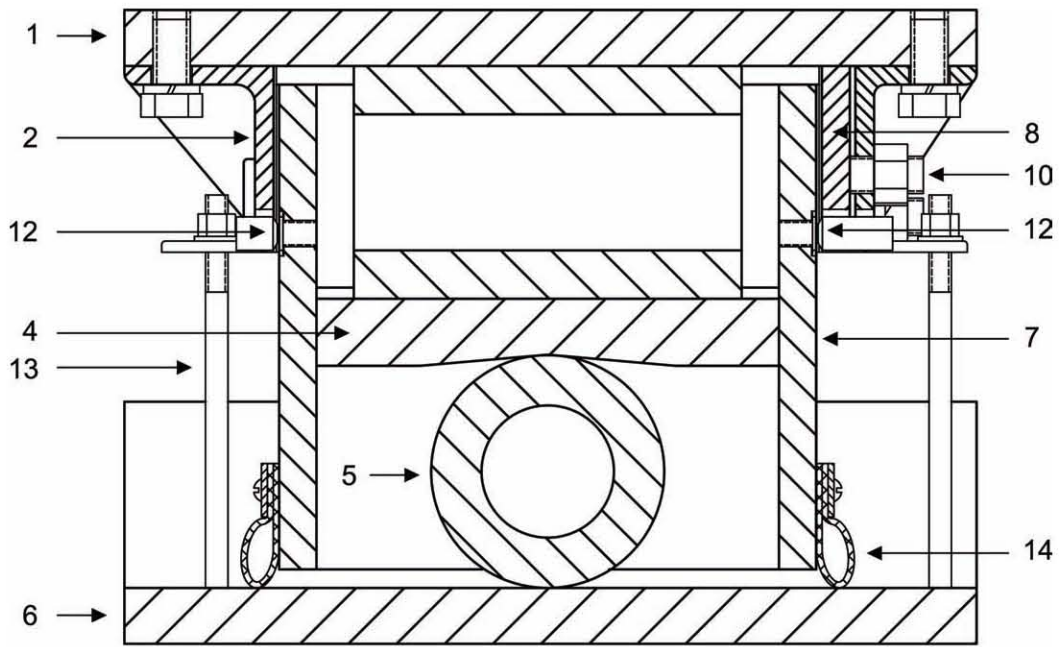
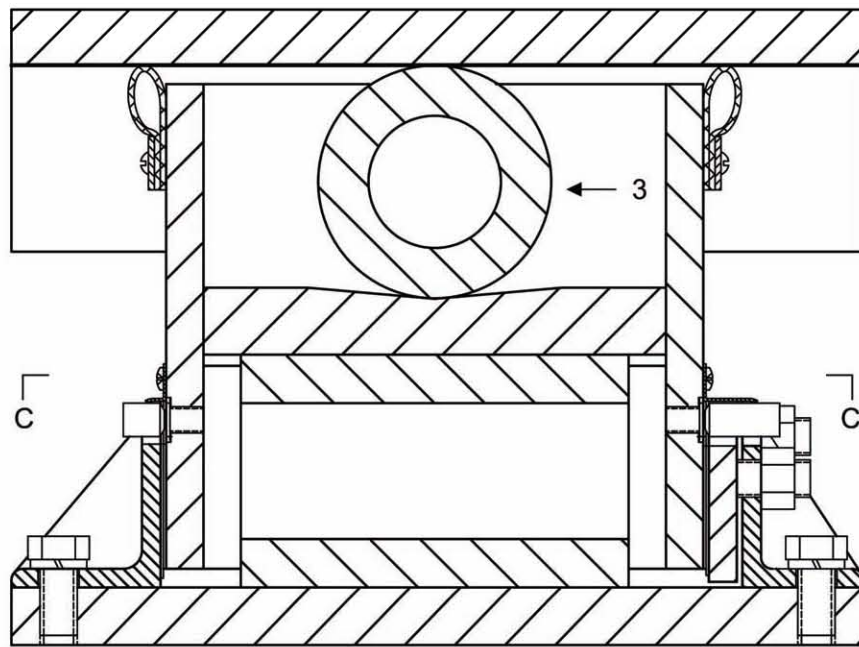


Figure 4-5 Design details of the second prototype roller bearing



Section A-A



Section B-B

Figure 4-5 Design details of the second prototype roller bearing (cont'd)

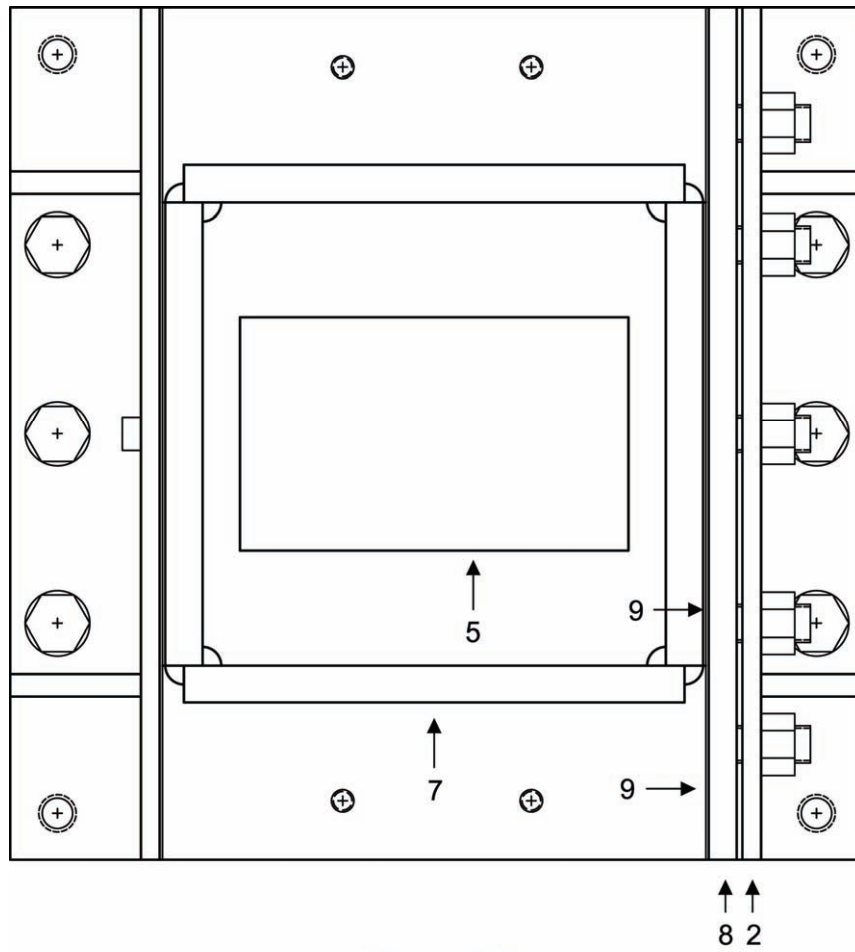
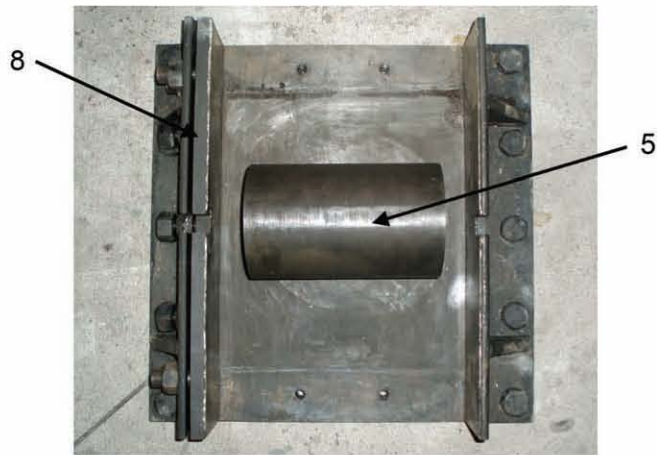


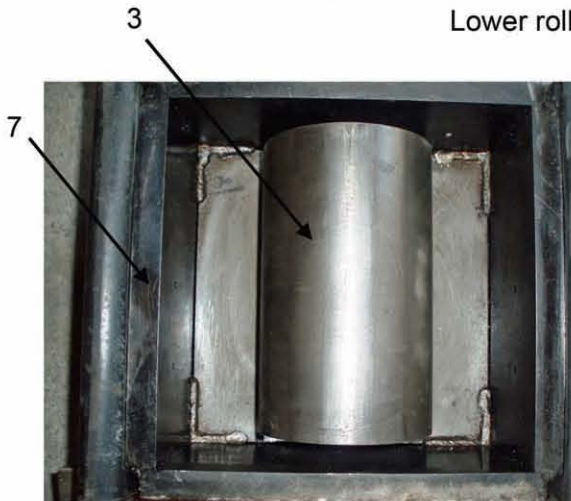
Figure 4-5 Design details of the second prototype roller bearing (cont'd)



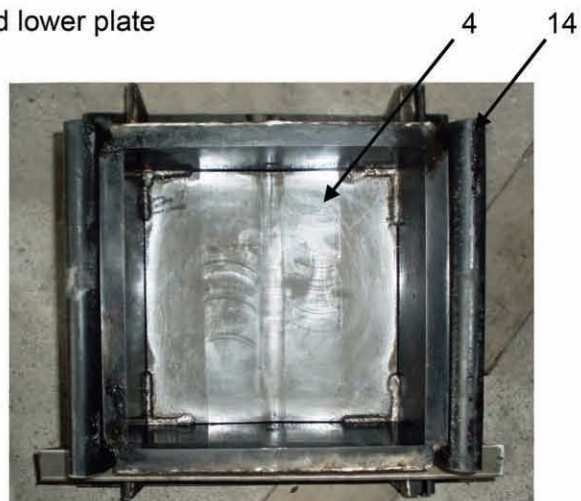
Roller bearing assembly



Lower roller and lower plate



Upper roller



Upper plate and side walls

Figure 4-6 Photos of the second prototype roller bearing

4.2.3 Testing of the Bearing

Pilot tests were carried out to validate the performance of the bearing. The bearing was first subjected to monotonic vertical loading twice up to 1.5 times the design vertical load, 315 kips (1400 kN), to examine the load carrying capacity. Next, the vertical load was maintained for 900 min. to examine the creep behavior of the bearing. Finally, the bearing was subjected to lateral cyclic loading along the principal directions under a constant design vertical load to investigate the lateral force-displacement responses.

Figure 4-7 shows the testing apparatus. The cyclic loading was achieved by moving the lower part of the machine, where the lower plate of the bearing was anchored, relative to the upper part of the machine, where the upper plate was secured. Figure 4-8 shows the bearing at a lateral displacement of 3 in (76 mm). The vertical force-displacement responses to the monotonic vertical loading are shown in Figure 4-9. The bearing showed a smaller stiffness in the early stage of loading. This was likely due to closing of small gaps that existed between components of the bearing. When the load was larger than 90 kips (400 kN), the bearing exhibited a linear relationship between the force and displacement up to the maximum applied load. The design vertical displacement corresponding to the design vertical load, which is 210 kips (935 kN), was 0.056 in (1.44 mm).

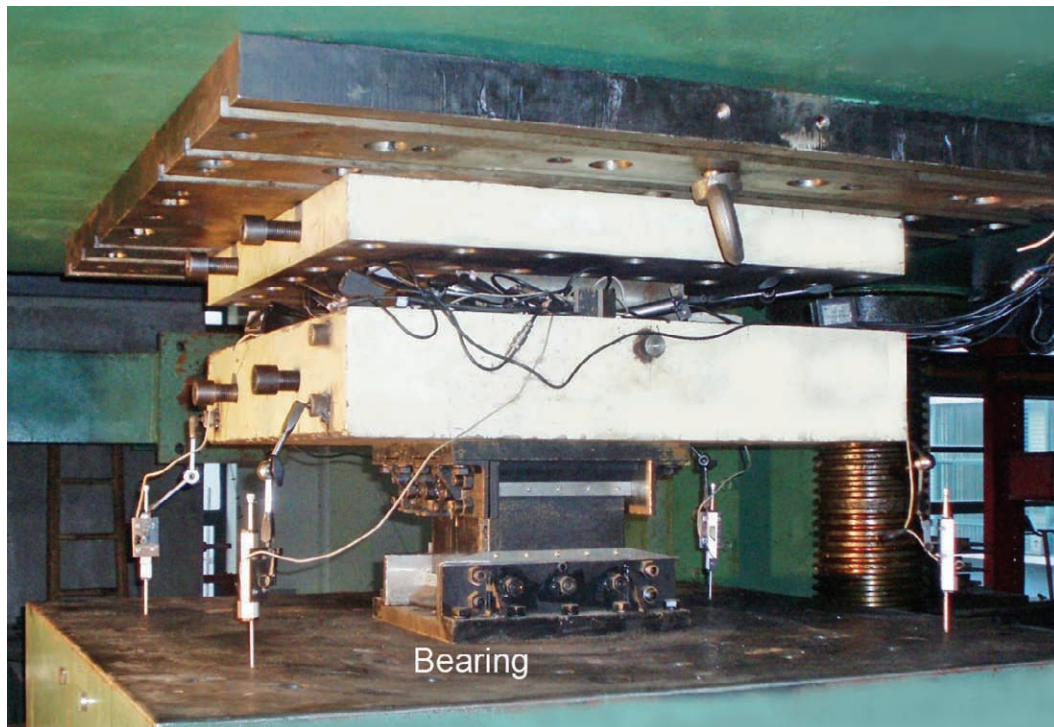


Figure 4-7 Test setup

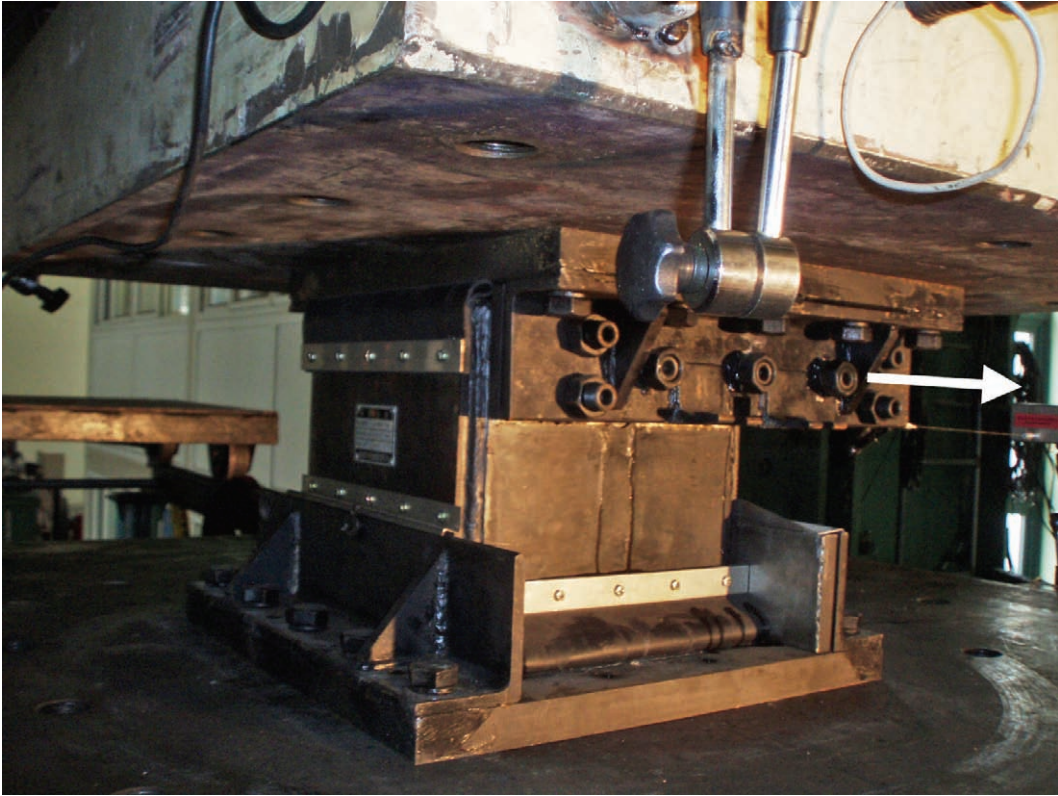


Figure 4-8 Bearing at a displacement of 3 in

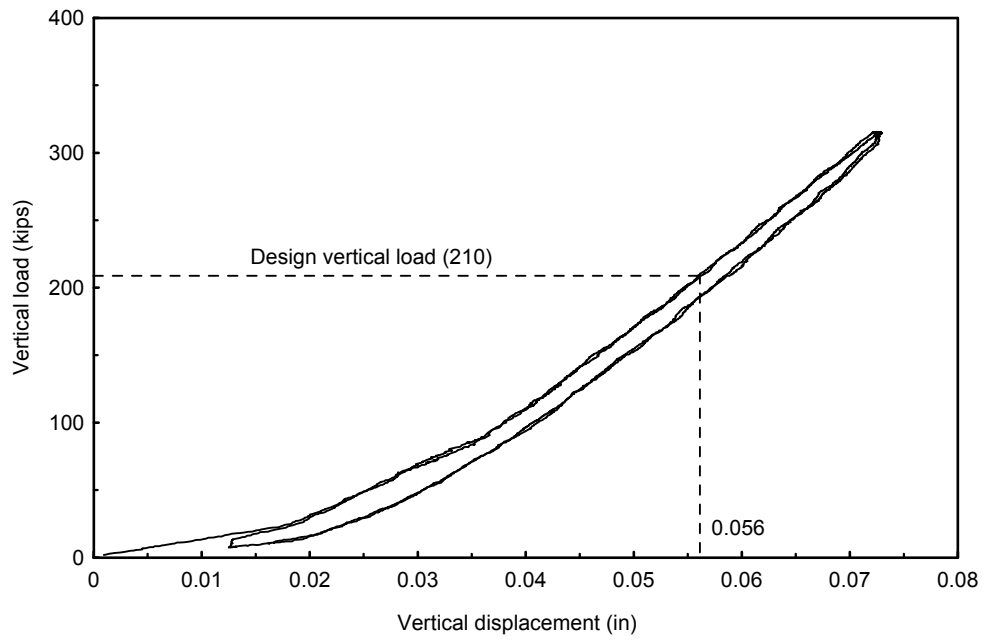


Figure 4-9 Force-displacement responses to vertical loading

The bearing showed very small creep displacements within the time of the sustained loading (see Figure 4-10). The maximum change of the vertical displacement was approximately 0.0006 in (0.015 mm), which was only 1.5% of the design vertical displacement.

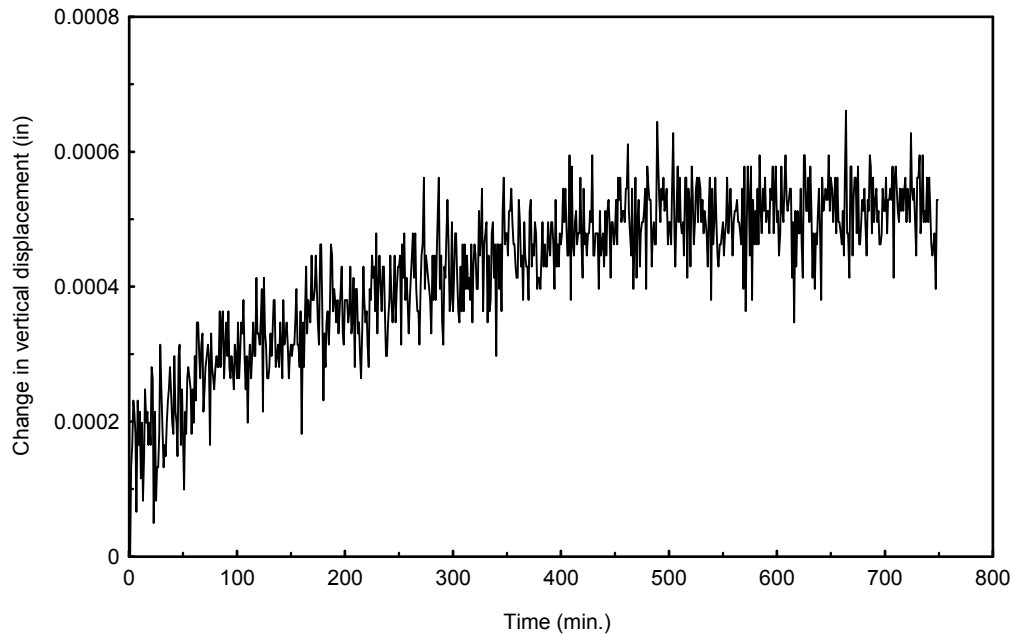


Figure 4-10 Change in the vertical displacement under sustained vertical loading

After the creep test, the bearing was unloaded from 315 kips (1400 kN) to the design vertical load, 210 kips (935 kN) and was subjected to lateral cyclic loading along each of the principal directions with a displacement amplitude of 4.7 in (120 mm). A sample test result is shown in Figure 4-11.

As identified in the figure, the measured restoring force f_s is 9.4 kips (42 kN). According to Table 4-2, the theoretical value of f_s is

$$f_s = 0.044 mg = 0.044 \cdot 210 = 9.2 \text{ (kips)} (= 41 \text{ kN})$$

This value agrees well with the measured value. According to Table 4-2, the theoretic value of the rolling friction force is

$$f_{Dr} = 0.0008 mg = 0.0008 \cdot 210 = 0.2 \text{ (kips)} (= 0.9 \text{ kN})$$

A torque T of 52 lb-ft (71 N-m) was applied to each screw used to produce a normal force to the friction interface. The screw had a diameter of 0.787 in (20 mm) and a pitch of 0.04 in (1 mm). According to equation (4-2), the normal force N_b produced by each screw with that torque is

$$N_b = \frac{T}{(0.159t + 0.531\mu d)} = \frac{52.4 \times 12}{(0.159 \cdot 0.04 + 0.531 \cdot 0.15 \cdot 0.787)} = 9107 \text{ (lb)} = 9.1 \text{ (kips)}$$

The total normal force for each rolling direction is (see (4-3))

$$N = 6N_b = 6 \cdot 9.1 = 54.6 \text{ (kips)}$$

Assume a coefficient of friction of 0.1 for the friction interfaces. The theoretical value of the friction force f_{Ds} along the principal directions is (Table 4-2)

$$f_{Ds} = \mu_s N = 0.1 \cdot 54.6 = 5.46 \text{ (kips)} (= 24 \text{ kN})$$

The theoretical value of the sum of f_{Dr} and f_{Ds} is

$$f_{Dr} + f_{Ds} = 0.2 + 5.46 = 5.7 \text{ (kips)} (= 25 \text{ kN})$$

The measured value of the sum of f_{Dr} and f_{Ds} is approximately 4.7 kips (21 kN) as shown in Figure 4-11. The error is approximately 21%. It may result from uncertainties associated with the coefficient of friction between the threads of the screws μ and that at the friction interfaces μ_s .

A comprehensive testing program is in progress at the time of this writing to further characterize the bearing. It will be conducted to investigate the behavior of the bearings with different design parameters including the sloping angle, sliding friction force, loading frequency, direction of loading and displacement amplitude.

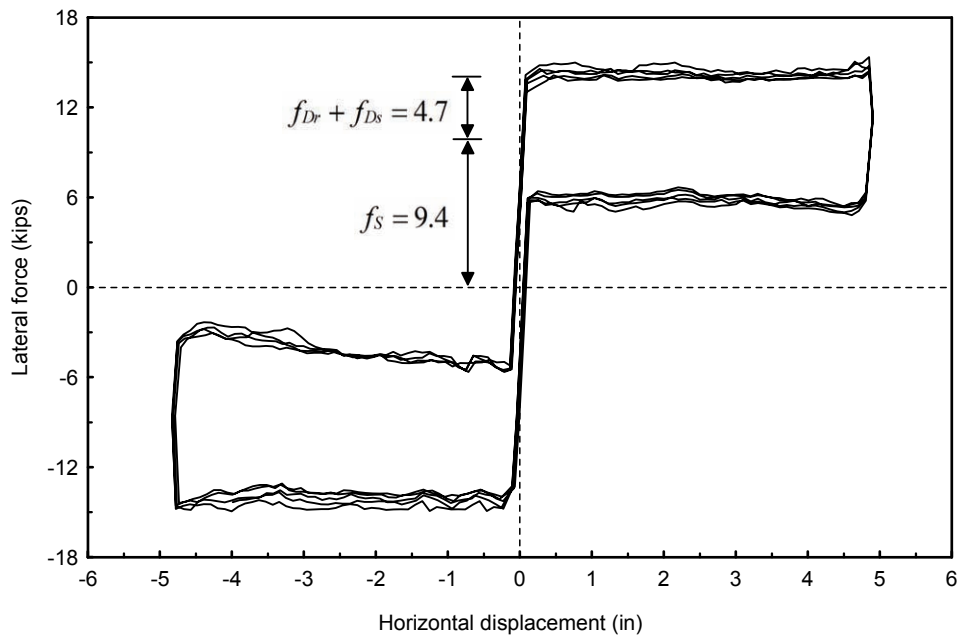


Figure 4-11 Force-displacement responses to lateral cyclic loading

CHAPTER 5 CASE STUDY

Design procedures to implement roller seismic isolation bearings in a bridge in a region of high seismicity are given in this chapter. The design procedures are primarily based on the results presented in this report and AASHTO specifications for LRFD bridge design (AASHTO 2004) and for seismic isolation design (AASHTO 2000).

5.1 Description of the Bridge

The bridge site is assumed to be located at 37.8° N latitude and 122.45° W longitude in the San Francisco area of California. The approximate location of the bridge is shown in Figure 5-1. Also indicated in the figure is the San Andreas Fault, which is the nearest fault to the bridge. The site is assumed to have a soil profile of type I, which is defined in AASHTO (2004). A typical continuous superstructure unit of the bridge consists of two 150 ft (45.7 m) spans over three columns as shown in Figure 5-2.

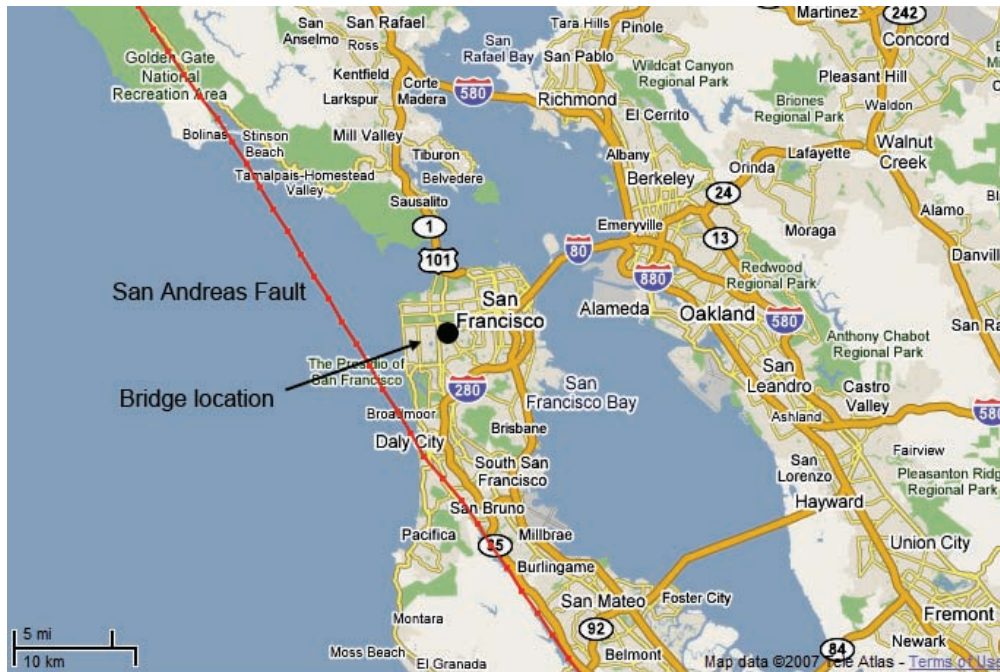


Figure 5-1 Bridge location

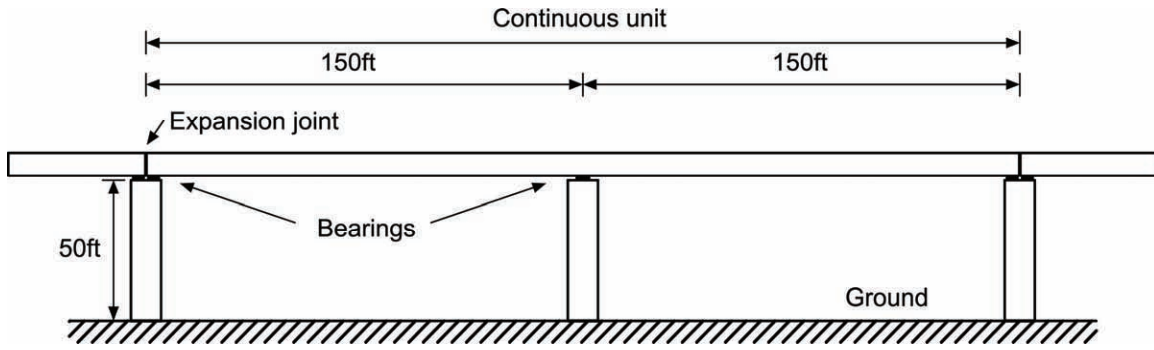


Figure 5-2 A typical continuous unit of the bridge

The bridge is designed with prestressed concrete box girders and reinforced concrete columns. The tributary dead load, vehicular live load, wind load and braking force for each column is assumed to be 2800 kips (12455 kN), 650 kips (2891 kN), 87.5 kips (389 kN) and 35 kips (156 kN), respectively. The lateral stiffness of the column k_c is assumed to be 1400 kips/in (245 kN/mm).

5.2 Design Procedures

5.2.1 Vertical Load Carrying Capacity

5.2.1.1 Vertical factor loads and seismic weight.

Based on strength limit state I in AASHTO (2004), the factored vertical load of the bearings is

$$Q_v = \gamma_p DC + 1.75LL \quad (5-1)$$

where Q_v is the factored vertical load; γ_p is a load factor that ranges from 1.25 to 0.9; DC is the dead load; and LL is the vehicular live load. Here, the value of γ_p is conservatively assumed to be 1.25. The factor vertical load Q_v for each column is

$$Q_v = 1.25 \cdot 2800 + 1.75 \cdot 650 = 4638 \text{ (kips)} (= 20630 \text{ kN})$$

Based on extreme event limit state I in AASHTO (2004), the tributary seismic weight for each column W is

$$W = \gamma_p DC + \gamma_{EQ} LL \quad (5-2)$$

where γ_p is taken as 1.0; and γ_{EQ} is assumed to be 0.5 as suggested by AASHTO (2004). The value of W is

$$W = 1.0DC + 0.5LL = 2800 + 0.5 \cdot 650 = 3125 \text{ (kips)} (= 13900 \text{ kN})$$

Since the distance from the bridge site to the nearest fault is less than 31 mi (50 km), the effect of vertical ground motions on the design vertical load for the bearings need to be considered (see Section 3.3.3). The distance of the site to the nearest fault, i.e., the San Andreas Fault, is approximately 4 mi (6 km), as identified in Figure 5-1. Based on Tables 3-4 and 3-5, 0.9 is conservatively selected for the coefficient C_v to be used in equation (3-18).

The tributary seismic weight considering the effect of vertical ground motions W_{sv} (equation (3-18)) for each column is

$$W_{sv} = (1 + C_v)W = 1.9 \cdot 3125 = 5938 \text{ (kips)} (= 26410 \text{ kN})$$

Since the value of W_{sv} is larger than that of Q_v , W_{sv} is used as the design vertical load of the bearings in each column.

5.2.1.2 Diameter of rollers and thickness of bearing plates.

Each column of the bridge has four roller seismic isolation bearings. There are eight bearings for each continuous unit: four on the interior column and two on each of the two exterior columns. The design vertical load for each bearing is 1485 kips (6603 kN), one-fourth the value of W_{sv} . Steel rollers and steel bearing plates with a yield strength of 240 ksi (1655 MPa) are used. According to equation (2-50), the product of the diameter of the rollers and the initial length L should satisfy

$$DL \geq \frac{W_{sv} / 4E_s}{8 \sigma_y^2} = \frac{1485 \cdot 29500}{8 \cdot 240^2} = 95 \text{ (in}^2\text{)} (= 61290 \text{ mm}^2)$$

Rollers with a diameter D of 8 in (203 mm) and an initial length L of 12 in (305 mm) are used. Note that L is not the final length of the roller, which will be determined later after the displacement capacity of the bearing is determined.

The wall thickness of the roller is taken as 0.25 of the diameter (see Section 2.6.2), namely, 2 in (51 mm). The thickness of the upper and lower plates and the center of the intermediate plate are taken as the same value as the wall thickness of the rollers. The length of the roller is determined later after the maximum displacement demand of the roller under the maximum probable earthquake is determined.

5.2.2 Sloping Angle and Characteristic Strength

To avoid sliding of the rollers, the sloping angle of the bearing θ is set as smaller than 11 degrees (see equation (2-40)). Within this range, a larger sloping angle results in a higher restoring force of the bearing and hence a larger base shear force for the column where the bearing seats. However, as shown in Section 3-2, a larger restoring force allows for the use of a

higher sliding friction force and hence leads to a smaller maximum relative displacement response under a given design earthquake.

A bearing with a sloping angle of 6 degrees and a maximum allowable sliding friction force f_{Dsa} is investigated first.

With the tributary seismic weight W for each column, the restoring force of each of the four bearings f_s (see equation (2-28)) is

$$f_s = \frac{1}{2} \frac{W}{4} \sin \theta = \frac{1}{2} \frac{3125}{4} \sin 6^\circ = 40.8 \text{ (kips)} (= 182 \text{ kN})$$

The sliding friction force f_{Ds} of the bearing is set as the maximum allowable value f_{Dsa} (equation (3-6))

$$f_{Ds} = \frac{f_s}{1.05} - f_{Dr} = 38.5 \text{ (kips)} (= 171 \text{ kN})$$

where the rolling friction force f_{Dr} is calculated as (equations (2-3) and (2-29))

$$f_{Dr} = \mu_r \frac{W}{4} = \frac{\delta}{R} \cdot \frac{W}{4} = \frac{0.002}{8/2} \cdot \frac{3125}{4} = 5 \cdot 10^{-4} \cdot 781.25 = 0.4 \text{ (kips)} (= 2 \text{ kN})$$

5.2.3 Maximum Relative Displacement Demand under the Design Earthquake

The maximum displacement demand is conservatively estimated using properties of the bearings along the principal directions as stated in Section 3.2.1. Moreover, the effect of vertical ground motions is ignored as explained in Section 3.3.3.

5.2.3.1 Equivalent linear system.

Assume an initial value, 10 in, for the maximum relative displacement response of the bearing x_i .

$$x_i = 10 \text{ (in)}$$

The effective stiffness of the bearing k_i (see equation (3-23)) is

$$k_i = \frac{f_s + f_{Dr} + f_{Ds}}{x_i} = \frac{40.8 + 38.5 + 0.4}{10} = 7.97 \text{ (kips/in)}$$

The combined stiffness of four roller bearings and the column K_{eff} (see equation (3-22)) is

$$K_{eff} = \left(\frac{1}{k_c} + \frac{1}{4k_i} \right)^{-1} = \left(\frac{1}{1400} + \frac{1}{4 \cdot 7.97} \right)^{-1} = 31.17 \text{ (kips/in)}$$

Note the stiffness of the surrounding soil is ignored. The effective period of the combined system consisting of one column and four bearings is

$$T_{eff} = 2\pi \sqrt{\frac{W}{gK_{eff}}} = 2\pi \sqrt{\frac{3125}{386.1 \cdot 31.17}} = 3.2 \text{ (s)}$$

$$\omega_{eff} = \frac{2\pi}{T_{eff}} = \frac{2\pi}{3.2} = 1.96 \text{ (rad/s)}$$

The relative displacement of the column x_c due to the force of the bearings is

$$x_c = \frac{4(f_s + f_{Dr} + f_{Ds})}{k_c} = \frac{4(40.8 + 38.5 + 0.4)}{1400} = 0.23 \text{ (in)}$$

This displacement is much smaller than that of the roller bearing as expected. The total relative displacement of the superstructure x_{max} is

$$x_{max} = x_i + x_c = 10 + 0.23 = 10.23 \text{ (in)}$$

The equivalent damping β_c of the combined system (see equation (3-26)) is

$$\beta_c = \frac{2(f_{Dr} + f_{Ds})x_i}{\pi(f_s + f_{Dr} + f_{Ds})x_{max}} = \frac{2 \cdot (38.5 + 0.4) \cdot 10}{\pi(40.8 + 38.5 + 0.4) \cdot 10.23} = 0.3$$

5.2.3.2 Elastic seismic response coefficient.

According to Figure 3.10.2-1 of AASHTO (2004), the acceleration coefficient A representing the design earthquake for the bridge site is

$$A = 0.6 \tag{5-3}$$

The elastic seismic response coefficient C_s is defined by AASHTO (2000) as

$$C_s = \frac{AS_i}{T_{eff} B} < 2.5A \tag{5-4}$$

where S_i is the site coefficient as defined in Table 5-1 (AASHTO 2000); and B is damping coefficient as defined in Table 3-6 (AASHTO 2000). S_i is 1.0 for soil profile type I, and B is 1.7 for β_c of 0.3.

The value of C_s is

$$C_s = \frac{0.6 \cdot 1.0}{3.2 \cdot 1.7} = 0.11 < 2.5 \cdot 0.6 = 1.5$$

Table 5-1 Site soil coefficient S_i (AASHTO 2000)

Soil Profile Type	I	II	III	IV
S_i	1.0	1.5	2.0	2.7

5.2.3.3 Maximum relative displacement demand

The maximum relative displacement demand of the bearing S_{di} is obtained by

$$S_{di} = \frac{C_s g}{\omega_{eff}^2} - x_c = \frac{0.11 \cdot 386.1}{1.96^2} - 0.23 = 10.83 \text{ (in)} \quad (5-5)$$

10.83-in is used as the new value of x_i and S_{di} is recalculated in a similar manner until the calculated value of S_{di} is close to the assumed value of x_i . The final value of S_{di} is

$$S_{di} = 11.72 \text{ (in)} (= 298 \text{ mm})$$

This displacement demand is increased here by 40% to address the fact that the secant stiffness method could underestimate as much as 40% the maximum displacement response of a roller seismic isolation bearing (see Section 3.4.3). The increased maximum displacement demand S'_{di} is

$$S'_{di} = 1.4 S_{di} = 16.4 \text{ (in)} (= 417 \text{ mm})$$

As mentioned in Section 2.3, the relative displacement between the roller and matching bearing plates is half the relative displacement of the bearing. Thus, the maximum displacement demand of the rollers is

$$S'_{dr} = \frac{S'_{di}}{2} = 8.2 \text{ (in)} (= 208 \text{ mm})$$

If a smaller maximum displacement demand is desired, one can raise the sloping angle within the range suggested by equation (2-40). This allows the use of a larger sliding friction force and hence achieves a smaller displacement demand.

5.2.4 Displacement Capacity of the Bearings

To accommodate the displacement demand under the design earthquake (S'_{dr}), 8.5 in (216 mm) is selected as the design displacement capacity of the rollers D_r . The displacement capacity of the bearing is $2D_r$, 17 in (432 mm). According to equation (2-51), the final length of the rollers L' is

$$L' = L + 2D_r = 12 + 2 \cdot 8.5 = 29 \text{ (in)} (= 737 \text{ mm})$$

5.2.5 Fasteners for Normal forces on the Friction Interfaces

The sliding friction force f_{Ds} for each rolling direction is 38.5 kips (171 kN) (see Section 5.2.2). Thus, each of two friction interfaces for each rolling direction needs to provide a friction force of 19.3 kips (86 kN). Assume a coefficient of friction of 0.1 for the interface and three screws for applying normal forces to the interface. The normal force required by each bolt is

$$N_b = \frac{19.3}{0.1 \cdot 3} = 64.3 \text{ (kips)} (= 286 \text{ kN})$$

Screws are used with a diameter of 1 in (25 mm), a pitch of 1/12 in (2 mm) conforming to UNF/UNRF series and a tensile area of 0.663 in² (428 mm²) (Oberg et al. 2000). The yield strength of the screw is 150 ksi (1034 MPa). To achieve the normal force N_b , the required torque for each screw T is estimated to be (equation (4-2))

$$\begin{aligned} T &= N_b (0.159t + 0.531\mu d) = 62.3(0.159 \cdot 1/12 + 0.531 \cdot 0.15 \cdot 1) \\ &= 6 \text{ (kips} \cdot \text{in)} (= 678 \text{ N} \cdot \text{m}) \end{aligned}$$

where the coefficient of friction between the threads is assumed to be 0.15. Note that testing such as shown in Section 4.2.3 should be conducted to verify this result.

5.2.6 Serviceability Limit State

According to AASHTO (2004), the load combination for the lateral forces for each bearing associated with the normal operational use of the bridge is

$$Q_{ls} = BR + 0.3WS \quad (5-6)$$

where Q_{ls} is the factored lateral load for each bearing; BR is the vehicular braking force; and WS is the wind load.

$$Q_{ls} = \frac{35}{4} + 0.3 \cdot \frac{87.5}{4} = 15.3 \text{ (kips)} (= 68.1 \text{ kN})$$

This force is smaller than the restoring force of each bearing, 40.8 kips (182 kN). Therefore, rolling of the rollers of the bearing will not occur under the serviceability limit state. Alternatively, shear keys can be added to resist this force.

5.2.7 Column Base Shear

The maximum column base shear occurs when the responses of the bearing are along directions 45 degrees away from the principal directions. Based on equation (3-17), the maximum base shear for each column is

$$\begin{aligned} V &= \frac{\sqrt{2}}{2} W (1 + C_v) \sin \theta + \sqrt{2} \mu_r W (1 + C_v) + \sqrt{2} \cdot 4 f_{Ds} \\ &= \frac{\sqrt{2}}{2} 3125 (1 + 0.9) \sin 6^\circ + \sqrt{2} \cdot 5 \cdot 10^{-4} \cdot 3125 (1 + 0.9) + \sqrt{2} \cdot 4 \cdot 38.5 \\ &= 661 \text{ (kips)} (= 2941 \text{ kN}) \end{aligned}$$

This is the base shear force for each column and is approximately 21% the seismic weight W . Note that under this force, the column should not yield to ensure proper functioning of the bearings. The connections of each of the four bearings to the superstructure and the column will have to be designed to resist one fourth of this force, that is, 165 kips (734 kN).

5.2.8 Uplift of the Superstructure

The value of $C_v \cdot g$ represents the maximum downward vertical acceleration response expected for the site (see equation (3-16)). Use equation (2-44) to check the limit state associated with the uplift of the superstructure.

$$|\ddot{z}_{3-}| = C_v g = 0.9g < \left(g + \frac{4f_{Ds}}{W} g \right) = \left(g + \frac{4 \cdot 38.5}{3125} g \right) = 1.05g$$

Thus, uplift of the superstructure is not likely to occur. However, since the bridge is very close to a major fault, a response-history analysis of the bridge is suggested to verify this conclusion.

5.3 Schematic View of the Bearing

The schematic view and dimensions of the bearing is shown in Figure 5-3. The bearing uses the same design concepts as presented in Section 4.2. Refer to Section 4.2.2 for more information on the detailed design of the bearing.

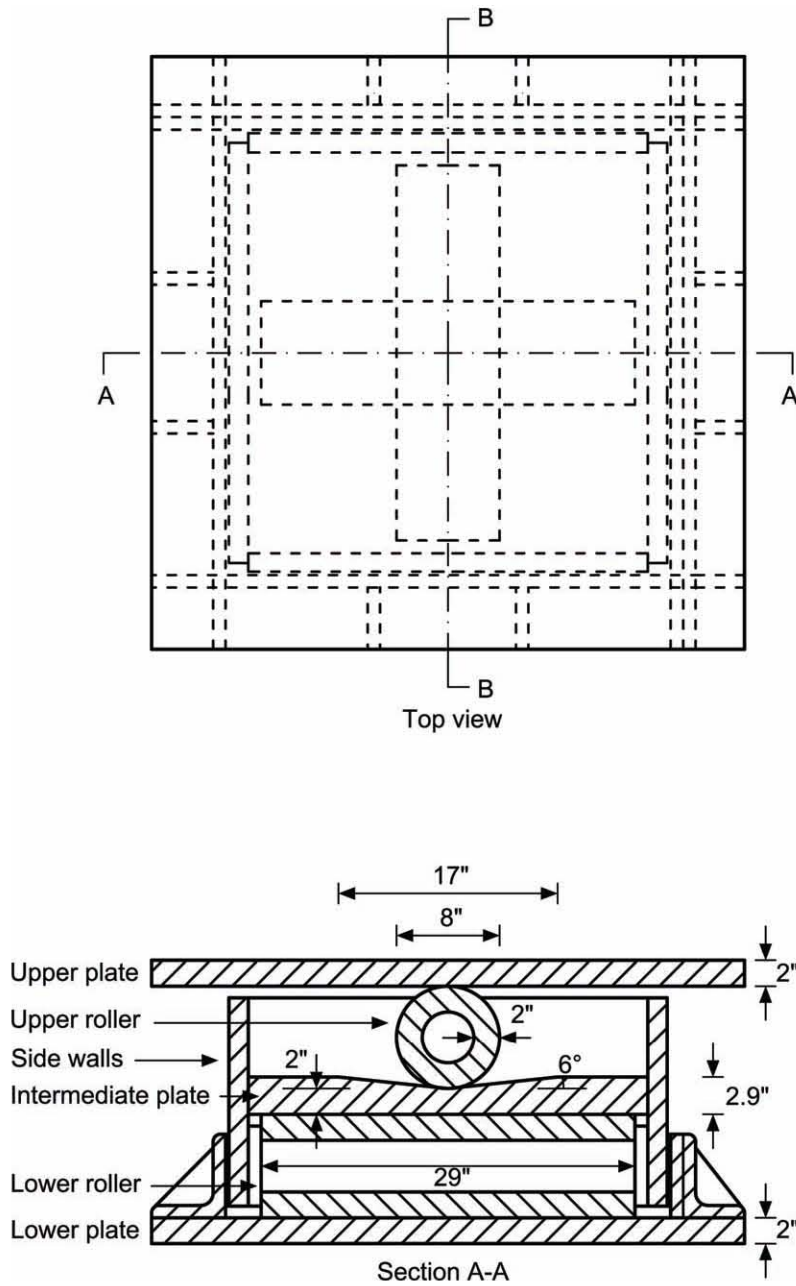


Figure 5-3 Schematic view of the bearing

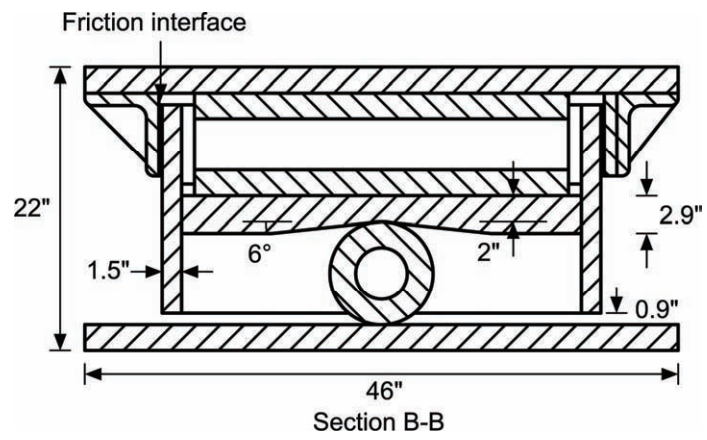


Figure 5-3 Schematic view of the bearing (cont'd)

CHAPTER 6 SUMMARIES AND CONCLUSIONS

6.1 Summaries and Conclusions

This report presents a new roller seismic isolation bearing for use in highway bridges. The bearing uses rolling motions of cylindrical rollers between sloping surfaces to achieve seismic isolation. Principles of the bearing under vertical loading and earthquake excitation are analytically and experimentally investigated. Two prototype roller isolation bearings have been developed with and without built-in friction devices for supplemental energy dissipation. A case study illustrating design procedures of the bearing is presented. A number of important conclusions are shown as follows:

- (1) The bearing has a constant spectral acceleration independent of the amplitude and the frequency content of horizontal ground motions. This means resonance between the bearing and the horizontal ground motions will not occur and the column base shear can be predicted with more certainty. In addition, the bearing also possesses a self-centering capability when the earthquake ends. This means the bridge superstructure can return to its original position after an earthquake.
- (2) To prevent sliding of the rollers, the sloping angle of the bearing needs to be smaller than a certain value depending on the coefficient of static friction and coefficient of rolling friction between the roller and sloping surface. For steel rollers and steel bearing plates, the sloping angle may need to be smaller than 11 degrees for greasy contact interface.
- (3) The bearing has the maximum restoring force, rolling friction force and sliding friction force when responses are along directions 45 degrees away from the principal directions. To be conservative, properties of the bearing along the principal directions are used in estimating the maximum displacement response of the bearing while those along directions 45 degrees away from the principal directions are used to predict the maximum base shear.
- (4) A larger sloping angle of the bearing results in a larger restoring force and hence a higher lateral strength of the bearing. However, based on the results of nonlinear response-history analyses, this does not result in a smaller maximum displacement response in most cases if friction devices are not incorporated into the bearing. If friction devices are included into the bearing, a larger restoring force permits the use of a larger sliding friction force of the bearing while maintaining a self-centering capability, which leads to a smaller maximum displacement response.
- (5) Vertical ground motions have little influence on the maximum displacement response of the bearing with friction energy dissipation devices. However, they could significantly increase the maximum acceleration response and hence the column base shear. A coefficient to account for this effect has been incorporated into the calculation procedure for the column base shear.

- (6) An equivalent linear method based on relative displacement, relative velocity and absolute acceleration spectra has been developed. The method provides a better prediction of the maximum displacement demand of the bearing under earthquakes than the secant stiffness method. Results from nonlinear response-history analyses showed that the proposed method and the secant stiffness method could underestimate the maximum displacement response by approximately as much as 20% and 40%, respectively, under the 28 ground motions examined.

6.2 Future Research

- (1) In addition to the displacement spectrum, the proposed equivalent linear method also uses relative velocity and absolute acceleration spectra. However, existing building codes and bridge specifications only provide 5% damped relative displacement spectra. Research should be conducted to develop a simplified method to establish absolute acceleration and relative velocity spectra from a 5% damped relative displacement spectrum.
- (2) The durability of the friction interface of the bearing's friction devices subjected to thermal cycles should be investigated. Alternatively, methods of demobilizing the friction devices under thermal cycles can be developed to address this issue.
- (3) The bearing may exhibit a large permanent displacement when uplift of the superstructure occurs. Although the friction force from the friction energy dissipation device could help resist the uplift, it typically occupies only a small fraction of the resistance against uplift as compared to the gravity force. A mechanism to increase the resistance needs to be developed if the bearing is to be used in places where uplift is likely to occur.
- (4) The properties of the bearing will change over time due to wear under repeated loading cycles and weathering due to environmental factors. Moreover, the bearing may have an initial displacement prior to earthquakes due to thermal displacements and long-term effects such as creep and shrinkage of concrete if a concrete superstructure is used. These effects on the seismic performance of the bearing should be studied.

CHAPTER 7 REFERENCES

- AASHTO. (2004). *AASHTO LRFD bridge design specifications*, 3rd Ed., Washington, DC.
- AASHTO. (2000). *Guide specifications for seismic isolation design*, Washington, DC.
- Avallone, E.A., and Baumeister, T., III. (1996). *Marks' standard handbook for mechanical engineers*, 10th Ed., McGraw-Hill, London, U.K.
- California Buildings Standards Commission. (2001). *California building code*. Sacramento, CA.
- Constantinou, M. C., Whittaker, A. S., Kalpakidis, Y., Fenz, D. M., and Warn, G. P. (2007). "Performance of seismic isolation hardware under service and seismic loading." *Report No. MCEER-07-0012*, Multidisciplinary Center for Earthquake Engineering Research, University at Buffalo, State University of New York, Buffalo, NY.
- Earthquake Protection Systems, Inc. (2007). "Friction Pendulum seismic isolation bearings." <<http://www.earthquakeprotection.com/product2.html>> (Nov. 17, 2007).
- HKS (Hibbitt, Karlsson, & Sorensen, Inc.). (2002). *ABAQUS user's manual*, Version 6.3, Pawtucket, RI.
- Jones, F., Ryffel, H., McCauley, C., Green, R., and Heald, R. (2000). *Machinery's handbook guide 26*, Industrial Press, Inc., New York, NY.
- Kemeny, Z. A. (1997). *Ball-in-cone seismic isolation bearing*, US Patent No. 194170, February 4.
- Lee, G. C., Liang, Z., and Niu, T.-C. (2000). "International patent application serial no. PCT/US00/42377: seismic isolation bearing."
- Lee, G. C., and Liang, Z. (2003). "A sloping surface roller bearing and its lateral stiffness measurement." *Proc., 19th US-Japan Bridge Engineering Workshop*, Tsukuba, Japan, October 27-28.
- Lee, G. C., Liang, Z., and Niu, T.-C. (2005). *Seismic isolation bearing*, US Patent No. 6971795 B2.
- Lin, T., and W., Hone, C. C. (1993). "Base isolation by free rolling rods under basement." *Earthquake Engineering and Structural Dynamics*, 22(3), 261–273.
- MCEER/ATC. (2003). "Recommended LRFD guidelines for the seismic design of highway bridges, part 1: specifications." *MCEER-03-SP03*, Multidisciplinary Center for Earthquake Engineering Research, University at Buffalo, State University of New York, Buffalo, NY.

Naeim, F., and Kelly, J. M. (1999). *Design of seismic isolated structures: from theory to practice*, John Wiley & Sons Inc., New York, NY.

Oberg, E., Jones, F.D., Horton, H.L., and Ryffell, H.H. (2000). *Machinery's handbook*, 26th Edition, Industrial Press Inc., New York.

Touaillon, J. (1870). *Improvement in buildings*. U.S. Patent No. 99973, February 15.

USGS. (2007). "Conterminous states probabilistic maps & data."
<http://earthquake.usgs.gov/research/hazmaps/products_data/48_States/index.php>
(Dec. 1, 2007).

R. J. Watson, Inc. (2007). "The EradiQuake System."
<http://www.rjwatson.com/eqs_bearing.htm> (Nov. 17, 2007).

WorkSafeTechnologies. (2007). "ISO-Base seismic isolation platform."
<<http://www.worksafetech.com/pages/ISO%5FBase.html>> (Nov. 17, 2007).

Young, W. C., and Budynas, R. G. (2002). *Roark's formulas of stress and strain*, McGraw-Hill, Columbus, OH.

APPENDIX A

This appendix contains experimental data on roller seismic isolation bearings from tests conducted at the University of California at San Diego, National Center of Research on Earthquake Engineering, Taipei, Taiwan and Institute of Engineering Mechanics, Harbin, China. In addition, it also contains results of tests on the coefficient of rolling direction under rusty conditions.

UCSD Tests

The objectives of the tests are to introduce a new friction damper to regulate the bearing displacement and to use the HITEC test protocol.

1. ISOLATORS USED IN UCSD TESTS

The bearings tested belong to the first prototype bearing as presented in Section 4.1 of the report. The friction damper tested is a dry friction damper. This damper uses small angle edge to increase the effective friction coefficient with magnification factor about 5.75 so that the designed friction coefficient μ is about 2.87.

This kind of friction damper has a notable advantage for the effective friction coefficient can be magnified significantly. In so doing, the normal force used to generate the friction damping can be considerably small. Otherwise, since the regular friction coefficient is often smaller than 1, the normal force will be greater than the friction force. Such a large force is difficult to control as well as difficult to maintain in the constant level. The resulted damping force will fluctuated accordingly.

2. FRICTION DAMPER

The damper used has a small angle edge to increase the effective friction coefficient with magnification factor about 5.75 so that the designed friction coefficient μ is about 2.87.

This kind of friction damper has a notable advantage for the effective friction coefficient can be magnified significantly. In so doing, the normal force used to generate the friction damping can be considerably small. Otherwise, since the regular friction coefficient is often smaller than 1, the normal force will be greater than the friction force. Such a large force is difficult to control as well as difficult to maintain in the constant level. The resulted damping force will fluctuated accordingly.

The mechanism of the coefficient magnification can be seen in figure 2-1(a). Since T can be omitted, we have

$$P = 2N\sin\alpha \quad (2-1)$$

The friction force is

$$F_f = \mu \times 2N = \mu \times P/\sin\alpha \quad (2-2)$$

where μ is the friction coefficient of friction pairs.

Since the quantity $1/\sin\alpha$ can be very large if the angle α is sufficiently small. The effective friction coefficient can be fairly large. In our case, we use construction steel A36, the friction coefficient is between 0.5 to 0.7. We use the channel steel to provide the edge angle α , see figure 2-1 (b). The angle of the channel steel is about 10° . So that $1/\sin\alpha = 5.75$.

$$\mu_{\text{eff}} = \mu / \sin\alpha \quad (2-3)$$

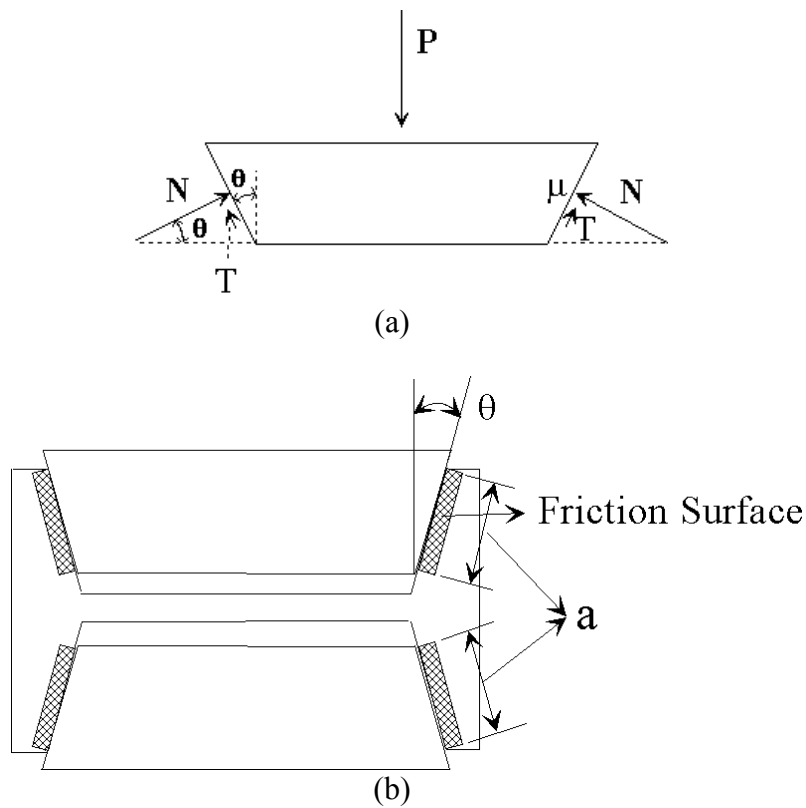


Figure 2-1 Friction damper

The conceptual working scheme of the friction damper is shown in figure 2-2. The drawings of the friction damper are shown in figure 2-3. Table 1-1 lists the technical specifications and table 2-2 lists the detailed parts of the damper. The photo of the prototype damping under assembling is shown in figure 2-4.

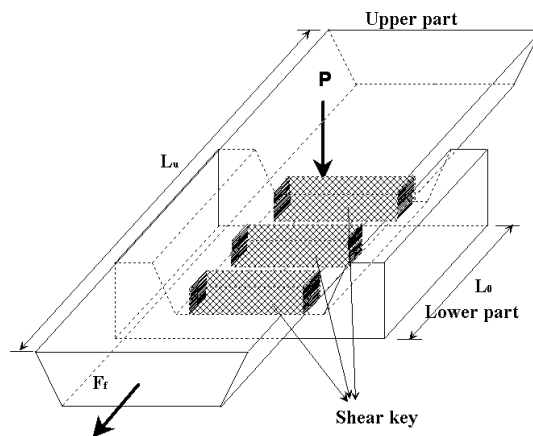


Figure 2-2. Working Principle of friction damper



Figure 2-3 Assembling friction damper

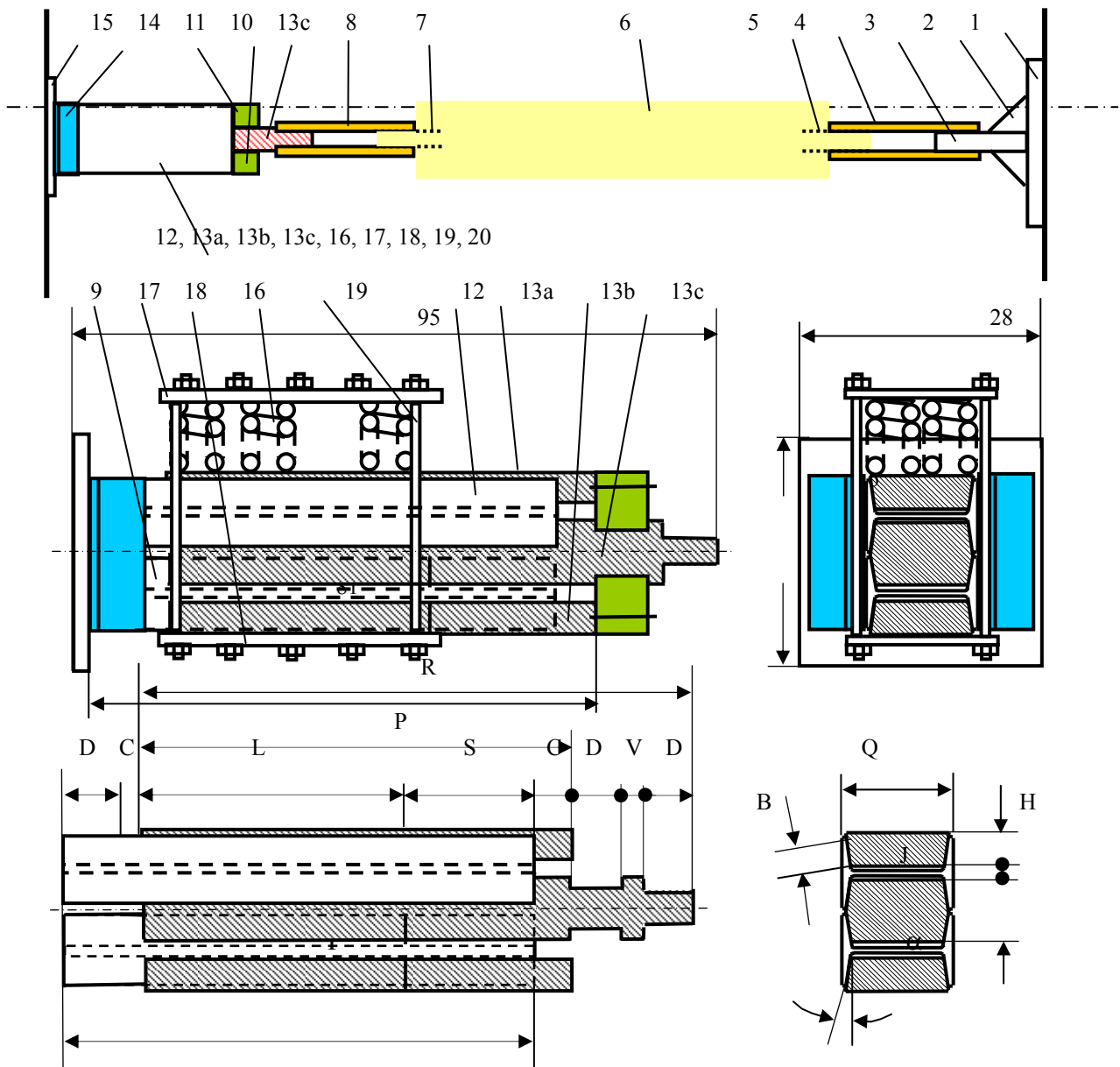


Figure 2-4 Drawings of a friction damper

Table 2-1 Specifications of the friction damper

Total friction force: $F_t = 120 \text{ kips}$
 Friction force of each side: $F = F_t / 8 = 15 \text{ kips}$
 Material friction coefficient: $\mu_m = 0.5$
 Assumed angle $\alpha = 10^\circ$
 Designed magnification factor: $m = \sin^{-1}(\theta) = 5.75$
 Designed friction coefficient: $\mu = m \mu_m = 0.5 \times 5.75 = 2.87$;
 Normal force: $N = 2F / \mu \approx 11 \text{ Kips}$ (# of springs = $11000 / 1100 \approx 10 < 14$)
 Allowed pressure $\sigma = 1.0 \text{ Kips/in}^2$
 Working area $A = 2F / \sigma = 30 \text{ in}^2$

Working width $B = 1.145 \text{ in} \approx 1 \text{ in}$
 Working length $L = 29 \text{ in} > A/B = 26 \text{ in}$
 Stroke $S = 28 \text{ in}$
 Allowance $C = 2 \text{ in}$
 Length of fixture $D = 5.25 \text{ in}$
 Length of fitting edge $V = 1.75$
 Length of I-beam $I = 64.25 \text{ in}$;
 I – beam: S8 x 23
 Width of I – beam = 8 in
 Height of I – beam = 4.171 in
 Length of upper/lower friction plates $P = 59 \text{ in}$
 Length of middle friction plate $R = 71.25 \text{ in}$
 Width of friction plate $Q = 7.25 \text{ in}$ (7.15 in)
 Height of upper/lower friction plate $H = 1.5 \text{ in}$
 Height of middle friction plate $J = 3 \text{ in}$

Table 2-2 Detailed Parts of the Friction Damper

No.	Item	Quantity
1.	Strong wall connection plate	1
2.	Triangle strengthen plate	8
3.	Connection plate	1
4.	Yielding connectors	4
5.	Adapting plate	2
6.	Connection I-Beam	1
7.	Adapting plate	2
8.	Yielding connectors	4
9.	Lower friction I- beam S8x23	1
10,11.	Adapting block	2
12.	Upper friction I –beam S8X23	1
13a.	Upper friction plate	1
13b.	Lower friction plate	1
13c.	Middle friction plate	1
14.	Angle steel connector	2
15.	Table connection plate	1
16.	Springs	14
17.	Upper spring fixture plate	1
18.	Lower spring fixture plate	1
19.	Pressure bolt assembly	10
10, 11	Adapting block 5.25 x 6.5 x 4.5 (2)	

3. HITEC PROTOCOL

In 1994, the California Department of Transportation (Caltrans) the Highway Innovative Technology Evaluation Center (HITEC) and the Federal Highway Administration began a collaborative process to formulate plans to test and evaluate seismic isolation devices for highway bridges. In 1995, AASHTO's highway Subcommittee on Bridge and Structure appointed an ad hoc panel to review specifications for seismic isolation design. In 1996, HITEC published the "Guidelines for the Testing of Seismic Isolation and Energy Dissipation Devices", which is often referred to as the HITEC testing protocol. In this document, the test procedure on seismic isolation bearings is specified. In 2002 HITEC published an alternative Guideline for large sized bearings. A few changes were made to improve the test protocol on larger isolation devices.

Generally speaking, the isolation bearing test includes the performance, the effect of temperature, fatigue and wear as well as environmental degradation.

The bearing test is carried out by cyclic load. The performance characteristics are determined at harmonic frequencies of 0.05 Hz, 0.2 Hz 0.5 Hz 1.0 Hz and 2.0 Hz. The load-deflection characteristics of the bearing are then measured as the basic test data. The possible variation of load-deflection loop due to inelastic response is then examined by using numbers of cycles. Possible device damage such as /fail/yield during the operation is also checked.

Testing protocol for roller bearings

In the following, we list the requirements and control parameters of the bearing test in the HITEC 1996 and 2002 documents.

CHARACTERISTICS TO BE EXAMINED

HITEC 1996, 1999 (Hitec 96-02)	HITEC 2002 (CERF 40600)
Stability	Benchmark, pseudo-static response
Range	Dynamic response
Capability	Influence of axial load
Resilience	Bi-directional loading
Resistance to service loads	Restoring force
Energy dissipation	Service-life
Survivability in extreme environments	Uni-directional re-characterization
Resistance to aging and creep	Ultimate displacement
Predictability of response	
Fatigue and wear	
Size effects	

DESIGN PARAMETERS

Design Compressive Load (DCL)	Rated Compressive Load (RCL)
Design Displacement (DD)	Rated Displacement (RD)
Design Velocity (DV)	Ultimate Displacement (UD)
Movement Rating (MR)	

Design Lateral Load (DLL)
Design Rating (DR) (energy dissipater only)

The Test Plan

Due to the test apparatus at the ETEC lab in UC San Diego, certain tests were not conducted, which are marked right after the list of each testing tasks. Yet certain other test plans are altered due to the limitation of the testing apparatus, which will be explained in the corresponding result analyses.

Performance Benchmark (Hitec 96 Test 1, Hitec 02 IC1, IC3)

Purpose: Initial stiffness;
Damping/friction;
NSD (number of shake-down cycles)

Procedure: Full unilateral loading cycle = 10
DD (RD) = 12”
Driving frequency = 0.5 Hz
DCL (RCL) : 320 (40%), 560(70%), 800(100%) Kips
(80, 140, 200 Kips per bearing)
Mounting Position: 45 degree
Temperature: ambient

Measurement: Vertical force
Lateral force
Displacement
Ambient temperature

Load-Deflection, Bi-lateral Test (Hitec 96 Test 2, Hitec 02 IC4)

Purpose: Determine load-deflection performance

Procedure: Full bi-lateral loading cycle = 3
DD (RD) = 12”
Driving frequency = 0.5 Hz
DCL (RCL): 320 (40%), 560(70%), 800(100%) Kips
(80, 140, 200 Kips per bearing)
Mounting Position: 45 degree
Temperature: ambient

Measurement: Vertical force
Lateral force
Displacement
Ambient temperature

Frequency Dependent (Hitec 96 Test 3, Hitec 02 IC2)

Purpose: Determine static and dynamic performance

Procedure: Full unilateral loading cycle = 3
DD = 6"
Driving frequency = 0.05, 0.2, 1.0 Hz
DCL (RCL) = 800(100%) Kips (200 Kips per bearing)
Mounting Position: 45 degree
Temperature: ambient

Measurement: Vertical force
Lateral force
Displacement
Ambient temperature

Fatigue and Wear (Hitec 96 Test 4, Hitec 02 IC6)

Purpose: Determine possible deterioration

Procedure: Without damper
Full unilateral loading cycle = 131,250 (travel > 1600m)
DD = 1.2" (DV > 4.5"/min)
Driving frequency = 0.1 Hz
DCL (RCL) = 800(100%) Kips (200 Kips per bearing)
Mounting Position: 45 degree
Temperature: ambient

Measurement: Vertical force
Lateral force
Displacement
Ambient temperature

Note that, this test plan was not carried out due to the limitation of the test facility in ETEC lab.

Environmental Aging (Hitec 96 Test 5)

Purpose: Verify performance in a salt spray environment

Procedure: Salt spray 1000 hours

Note that, this test plan was not carried out due to the limitation of the test facility in ETEC lab.

Dynamic Performances at Temperature Extremes (Hitec 96 Test 6)

Note that, this test plan was not carried out due to the limitation of the test facility in ETEC lab.

Purpose: Effect of temperature
Procedure: Full unilateral loading cycle = 3

DD (RD) = 12"
Driving frequency = 0.5 Hz
DCL (RCL) = 800(100%) Kips (200 Kips per bearing)
Mounting Position: 45 degree
Temperature: -40 – 120 F

Measurement: Vertical force
Lateral force
Displacement
Ambient temperature

Durability (Hitec 96 Test 7 Hitec 02 IC7)

Purpose: Durability
Procedure: Full unilateral loading cycle = 20
DD (RD) = 12"
Driving frequency = 0.5 Hz
DCL (RCL) = 800(100%) Kips (200 Kips per bearing)
Mounting Position: 45 degree
Temperature: ambient

Measurement: Vertical force
Lateral force
Displacement
Ambient temperature

Displacement Stability Test to Failure (Hitec 96 Test 9 Hitec 02 IC8)

Purpose: Maximum allowed displacement (failure load) [last test]
Procedure: DD (RD) = 14" (design maximum allowed displacement)
Driving frequency = 0.5 Hz
DCL (RCL) = 800(100%) kips
Mounting Position: 45 degree
Temperature: ambient

Measurement: Vertical force
Lateral force
Displacement
Ambient temperature

Restoring Force (test 10 Hitec 02 IC5)

Purpose: Restoring performance
Procedure: Without the friction damper
DD (RD) = 12" , quickly release
DCL (RCL) = 800(100%) kips
Mounting Position: 45 degree
Temperature: ambient

Measurement: Vertical force

Lateral force
 Displacement
 Ambient temperature

The test apparatus in the ETEC lab is designed for regular bearings, which have considerably large lateral stiffness. However, for the bearing, the lateral force is very small. Therefore, the test apparatus is not exactly suitable for the roller bearing. This is because the test shaking table is controlled by the lateral force feedback but the lateral roller bearing is so small that it is close to the resolution of the load cell. In this case, the control of the lateral force becomes very difficult, especially when the testing speed becomes higher. Therefore, during the test, the driving frequency must be lower than the HITIC protocol.

Lowering the driving frequency in the test should not be a major problem because the movement of the bearing is controlled by its geometrical configuration, instead of material properties like elastomeric bearings.

The second problem is that the vertical load is difficult to control. Therefore, we try to use a lower amount of vertical load and monitor the real readings. If the measured forces reach or even exceed the requirement of HITEC's requirement, then the test is considered to be valid, even the setup load is not as high as the HITEC's standard.

Due to the above practical difficulties, the test plans are modified and listed in Table 3-1.

Table 3-1 Test Plan

Test #	Cycle #	Disp. (in)	Vel. (in/s)	Driving Freq. (Hz)	V. load proposed	Max. V. Load single bearing	HITIC equivalent
1	3	10	0.628	0.01	120 (Kips)	> 80 (Kips)	1, 3
2	3	10	6.28	0.1	120 (Kips)	> 80 (Kips)	2, 3
3	3	10	0.628	0.01	210 (Kips)	> 140 (Kips)	1, 3
4	3	10	6.28	0.1	210 (Kips)	> 140 (Kips)	2, 3
5	3	10	0.628	0.01	300 (Kips)	> 200 (Kips)	1, 3
6	3	10	3.14	0.05	300 (Kips)	> 200 (Kips)	2, 3
7	3	10	12.56	0.2	150 (Kips)	> 200 (Kips)	3,
8	3	10	21.97	0.35	150 (Kips)	> 200 (Kips)	3,
9	3	10	6.28	0.1	300 (Kips)	> 200 (Kips)	10,
10	20	10	31.42	0.5	300 (Kips)	> 200 (Kips)	1, 7, 9, 10
11	5	1	3.142	0.5			10

4. TEST SETUP

In the following, the test and result analysis on the roller bearing with the damper will be listed and discussed.

The test apparatus are equipped in the Energy Technology Engineering Center (ETEC). Figure 4-1. The test tables and bearings are shown in figure 4-2. The mounting or bearings are shown in figure 4-3.

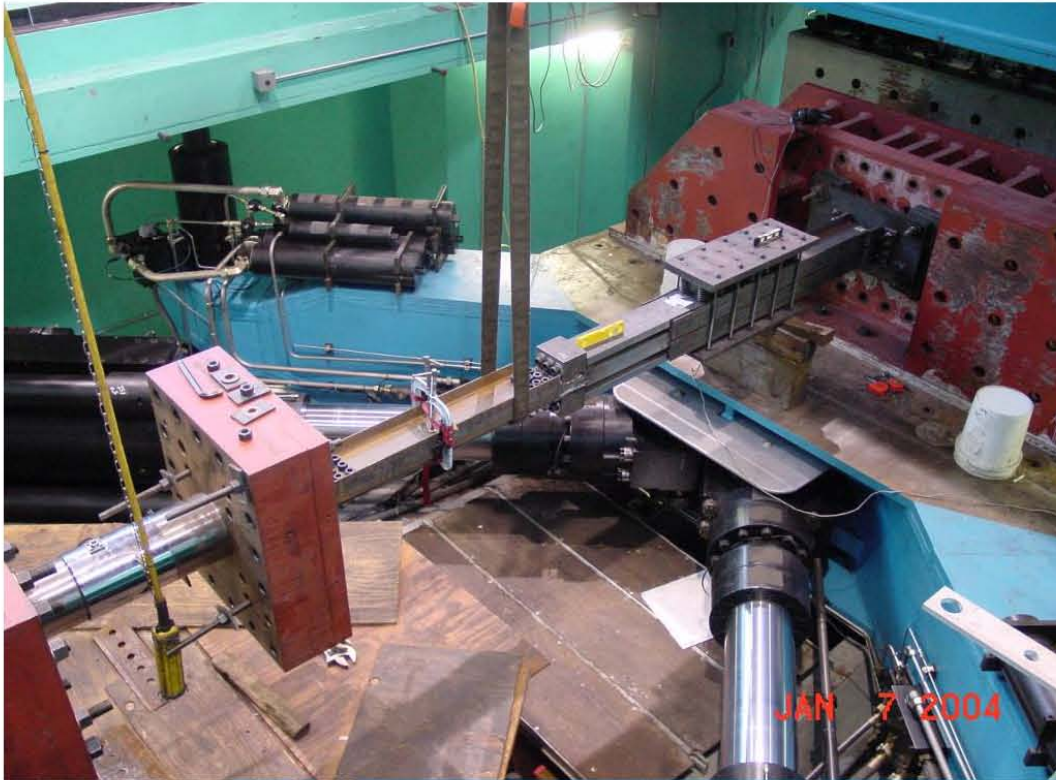


Figure 4-1 Test setup



Figure 4-2 Test table and bearings



Figure 4-3 Bearing mounting

5. TEST RESULTS

Two test results for test #1 are shown in figure 5-1.

Figures 5-2 shows the results of test #2, (see Table 3-1.)

Figures 5-3 shows the results of test #3, (see Table 3-1.)

Figures 5-4 shows the results of test #4, (see Table 3-1.)

Figures 5-5 shows the results of test #5, (see Table 3-1.)

Figures 5-6 shows the results of test #6, (see Table 3-1.)

Figures 5-7 shows the results of test #7, (see Table 3-1.)

Figures 5-8 shows the results of test #8, (see Table 3-1.)

Figures 5-9 shows the results of test #9, (see Table 3-1.)

Figures 5-10 shows the results of test #10, (see Table 3-1.)

Figures 5-11 shows the results of test #11, this is a damping only test realized by not applying any vertical to the bearings. (also see Table 3-1.)

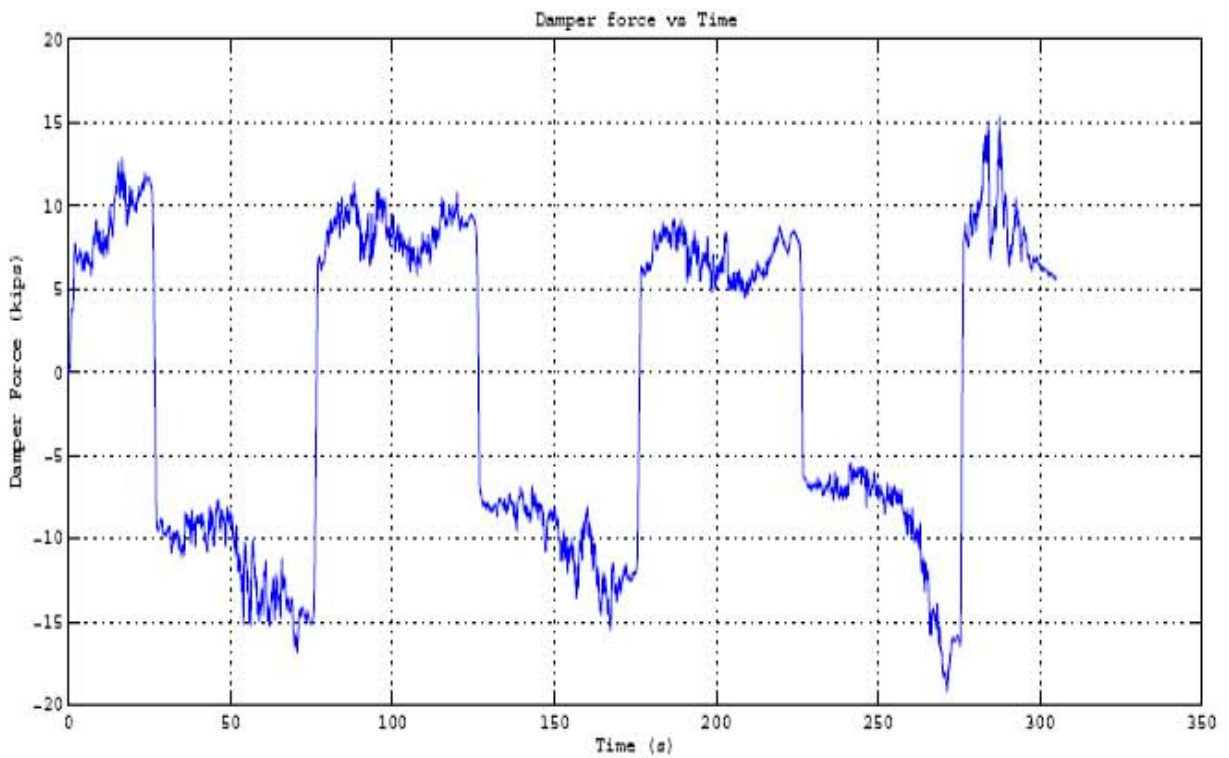
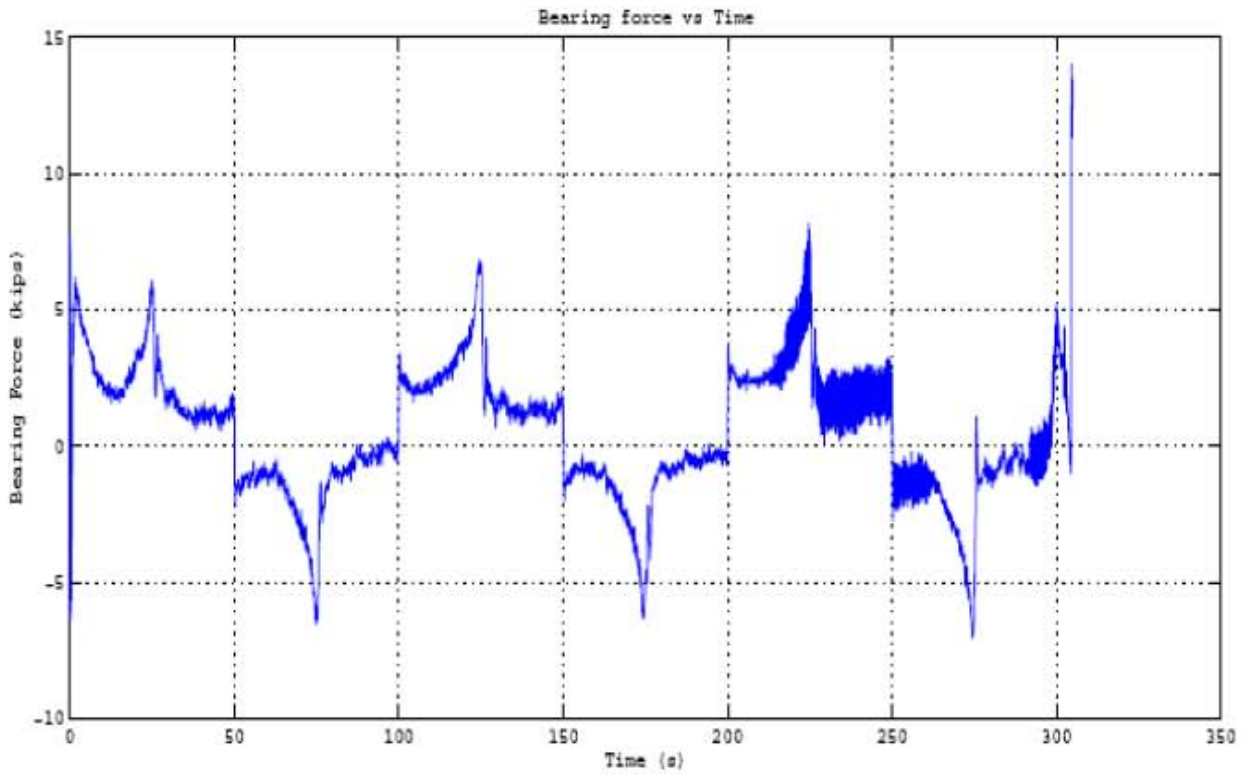


Figure 5-1 Results of Repeated Test #1.

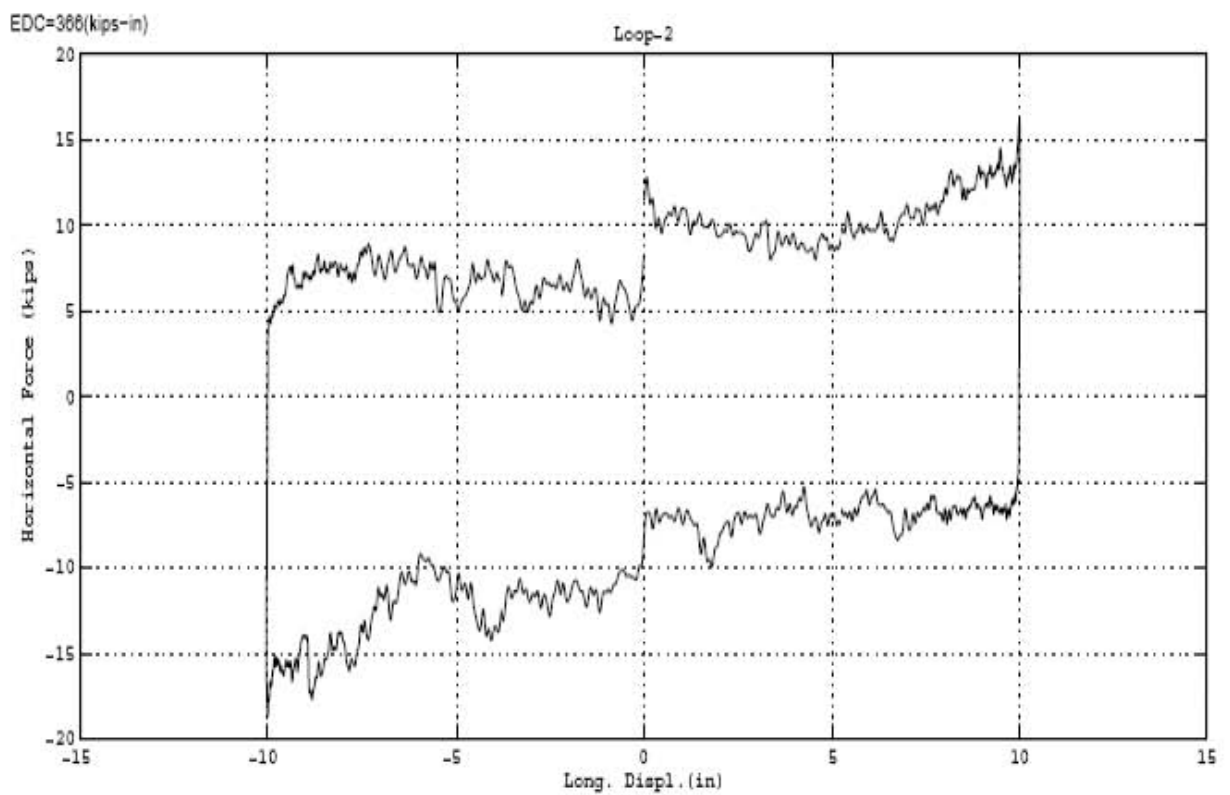
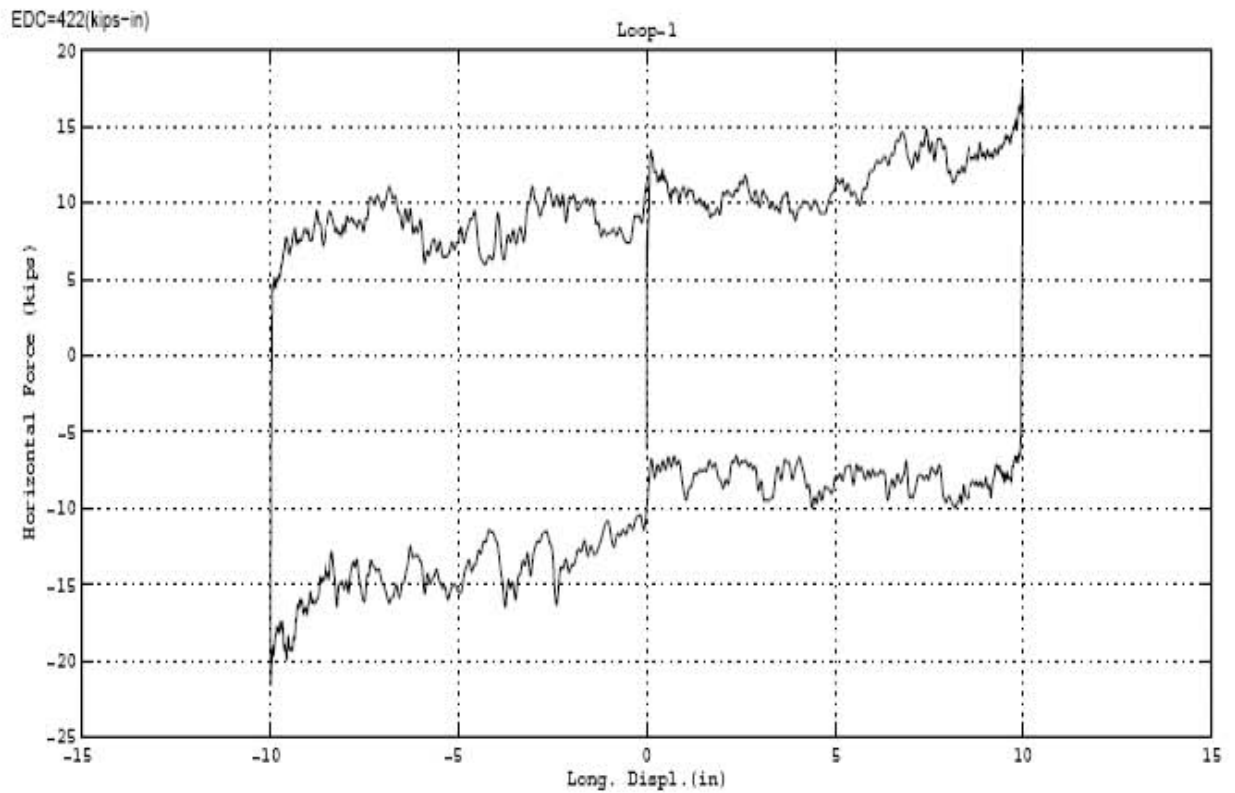


Figure 5-1 Results of Repeated Test #1 (continued).

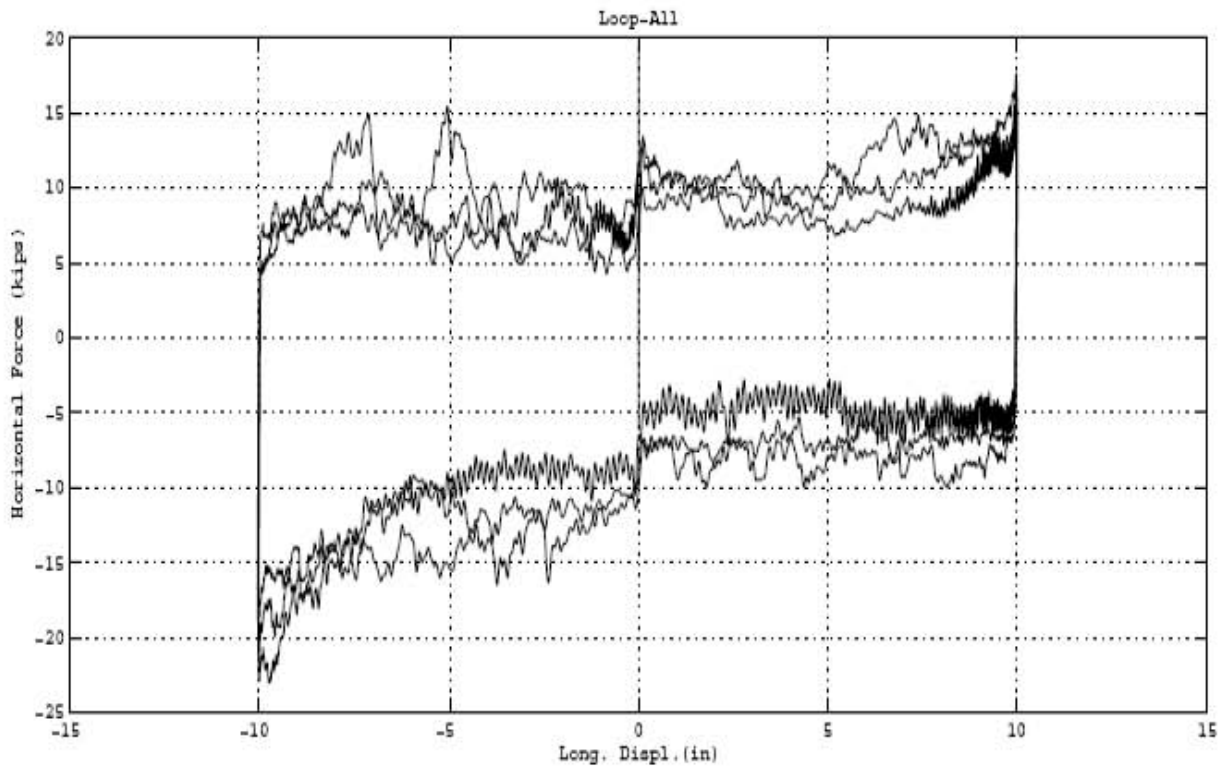
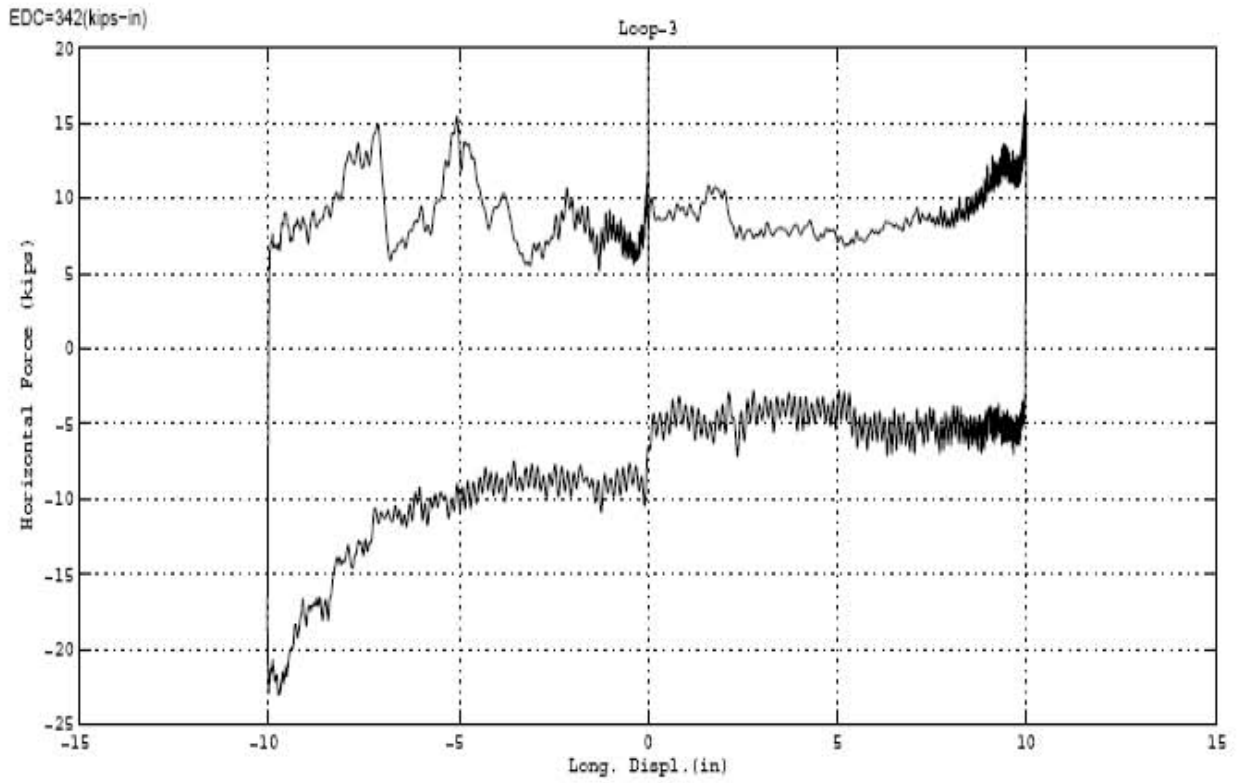


Figure 5-1 Results of Repeated Test #1 (continued).

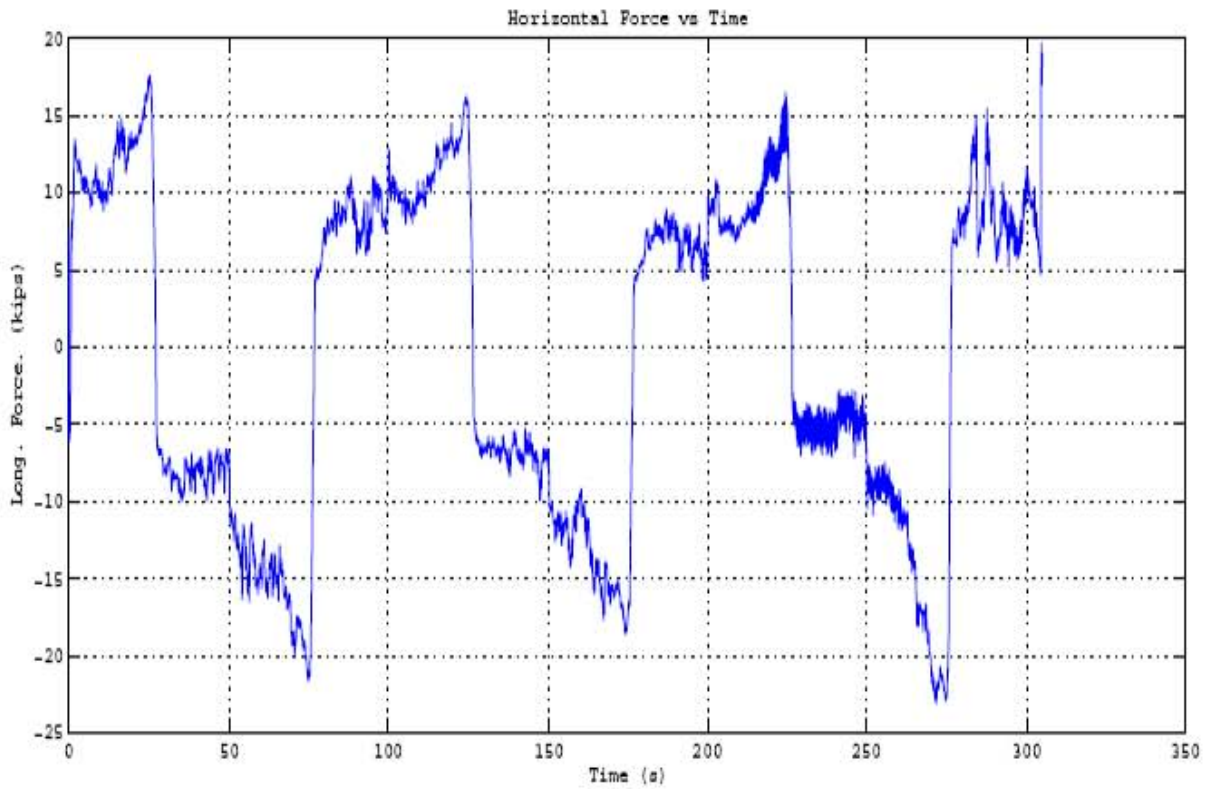
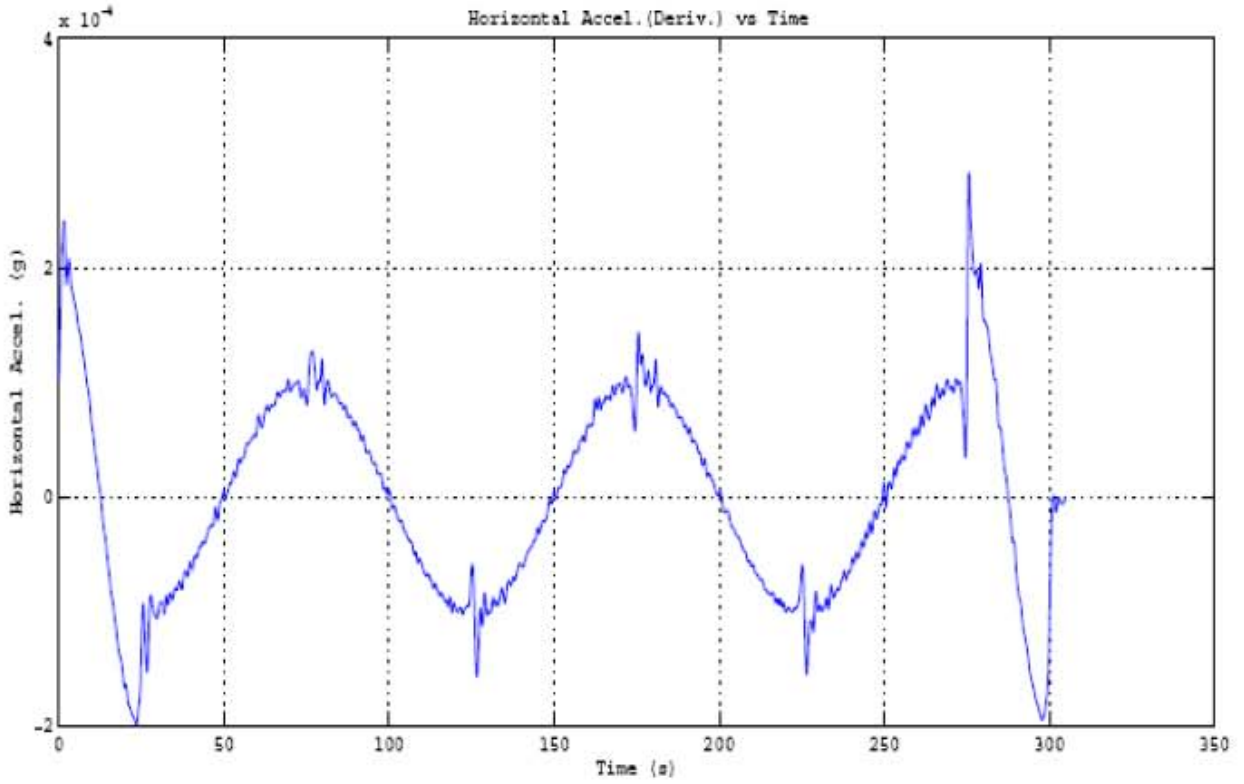


Figure 5-1 Results of Repeated Test #1 (continued).

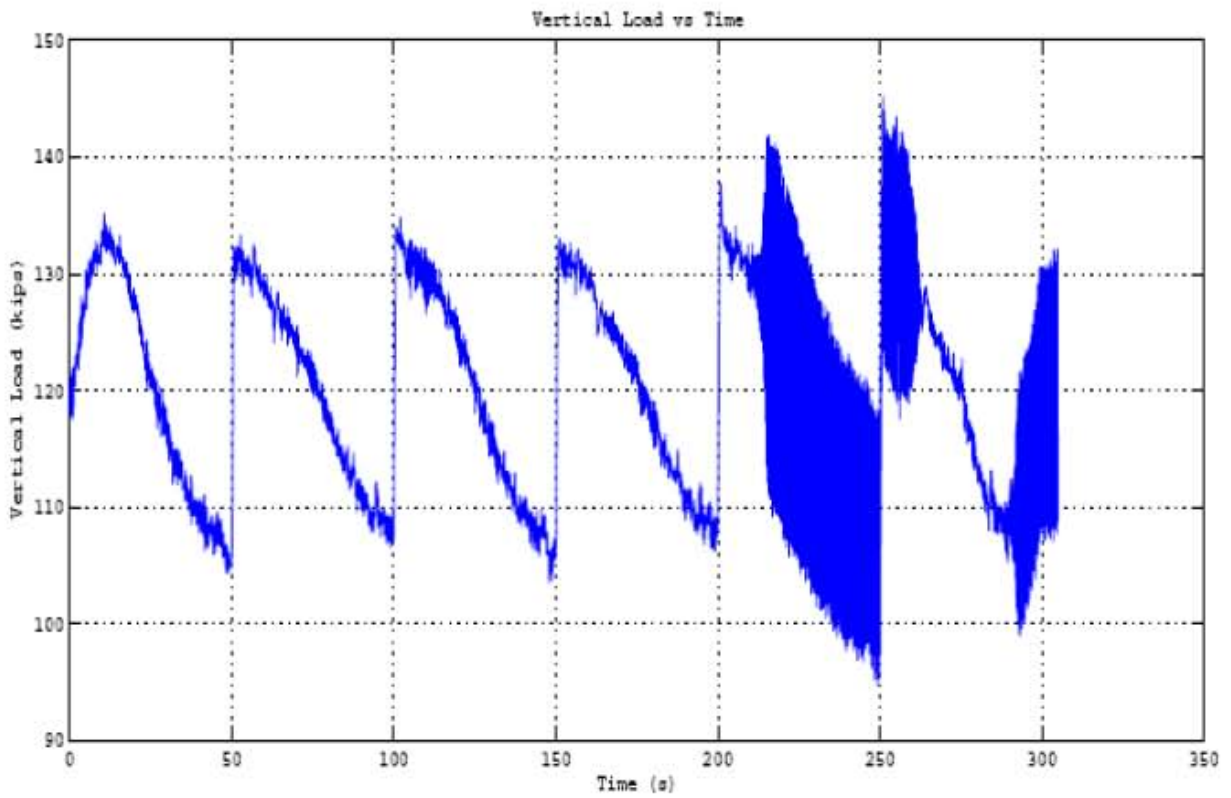
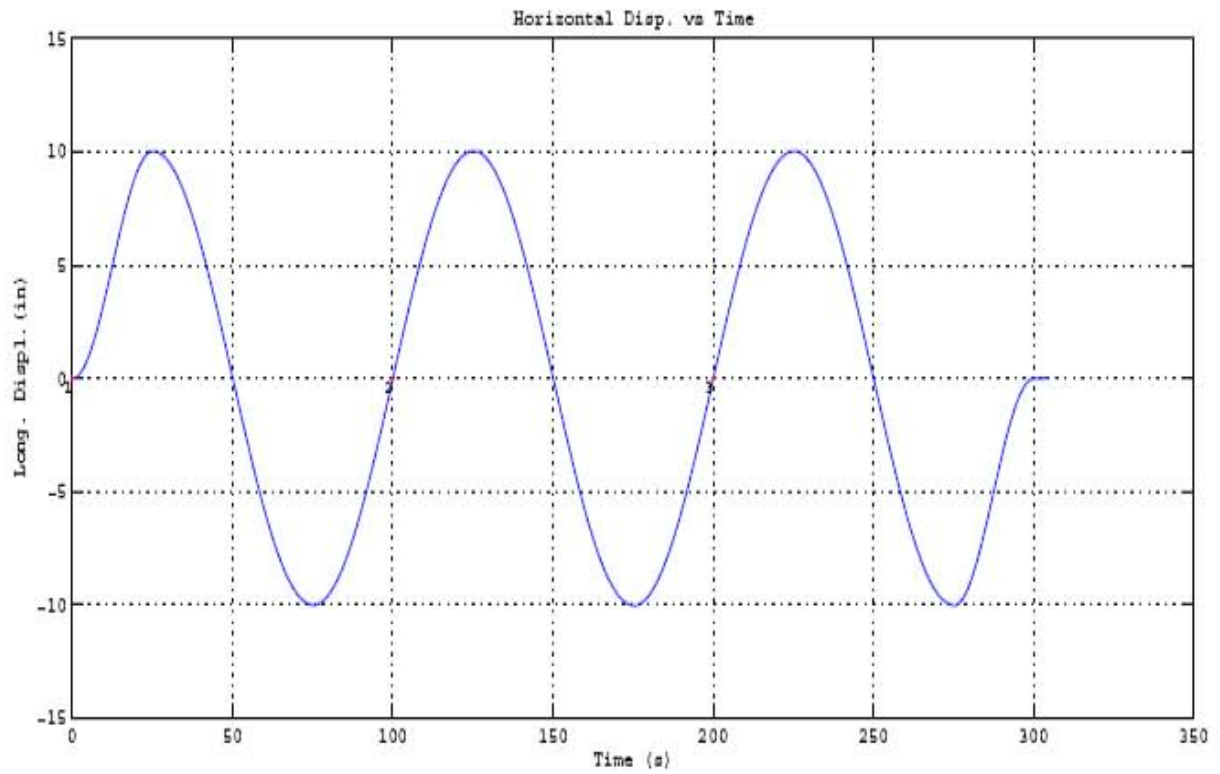


Figure 5-1 Results of Repeated Test #1 (continued).

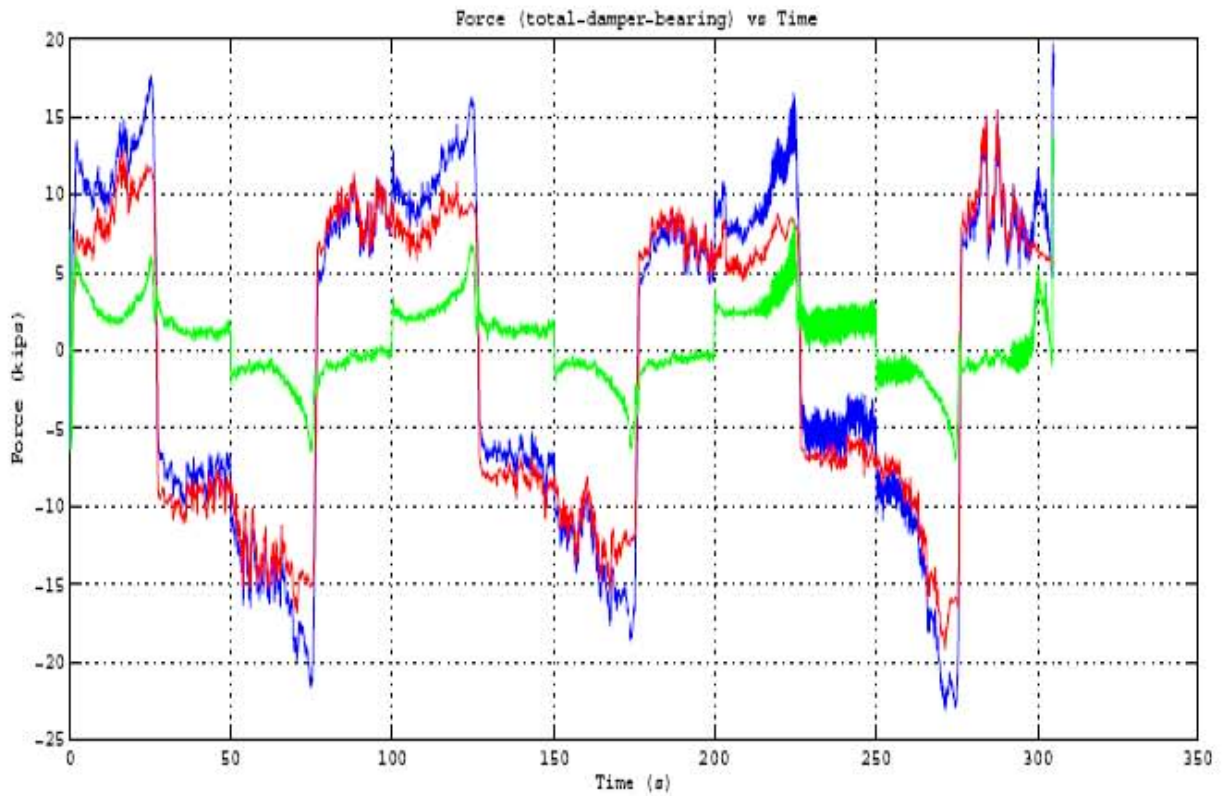
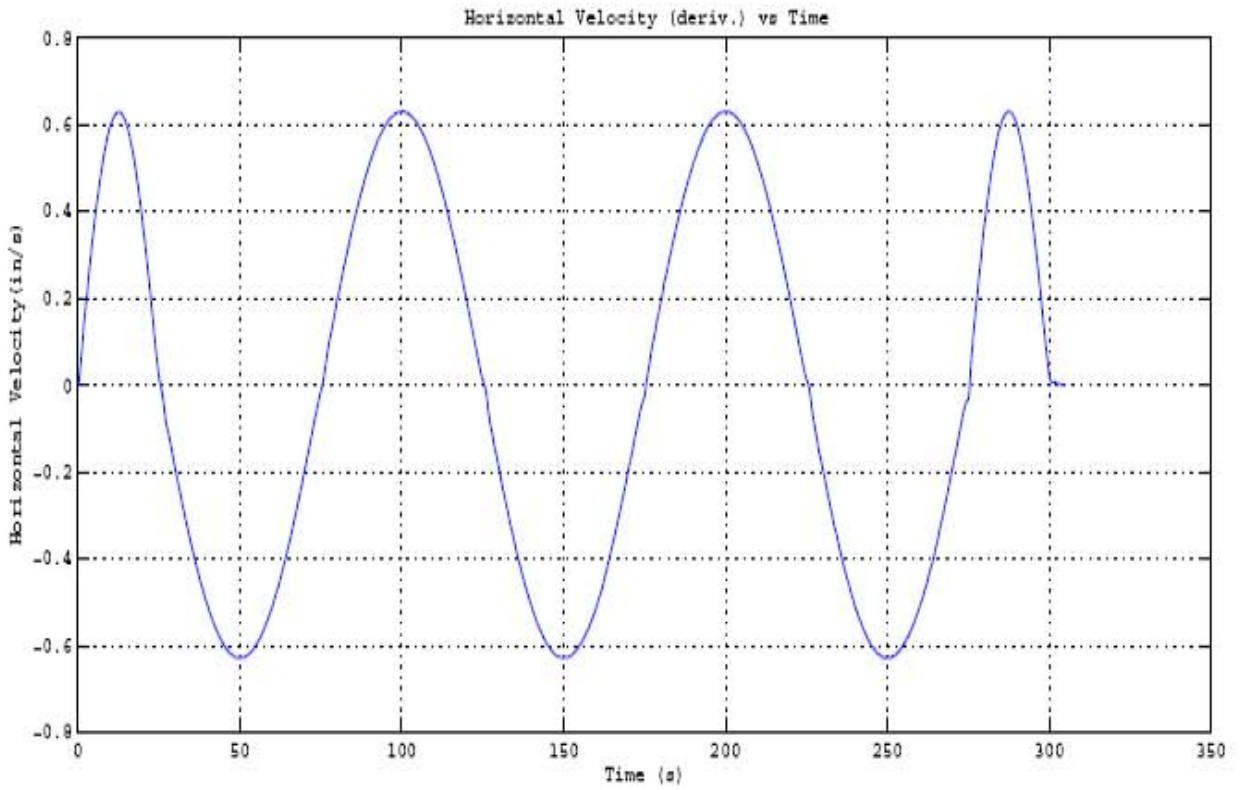


Figure 5-1 Results of Repeated Test #1 (continued).

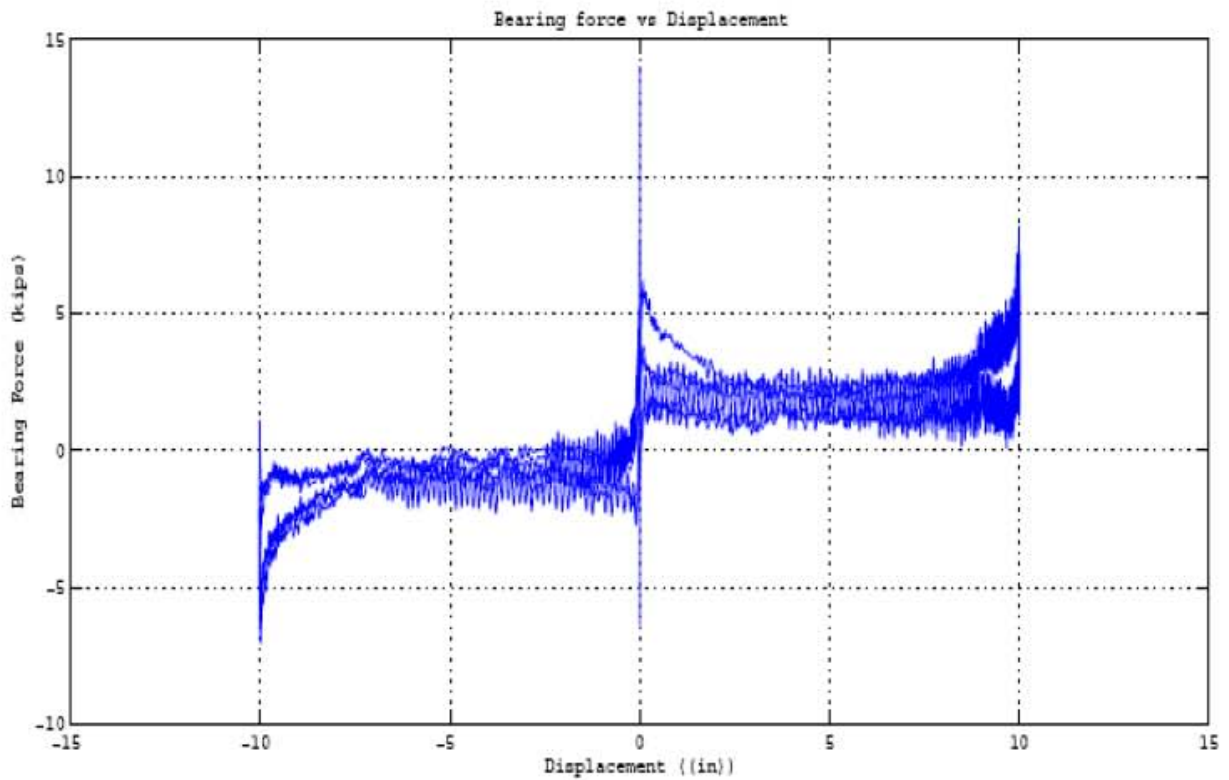
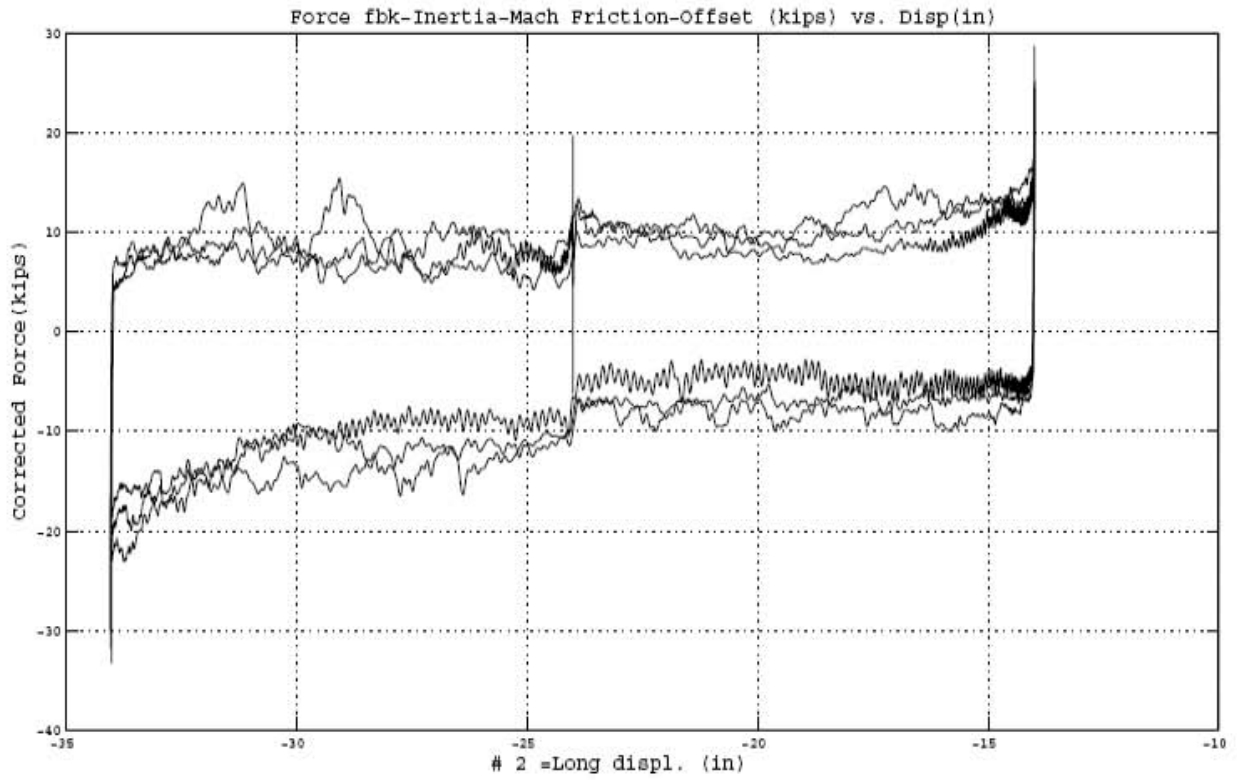


Figure 5-1 Results of Repeated Test #1 (continued).

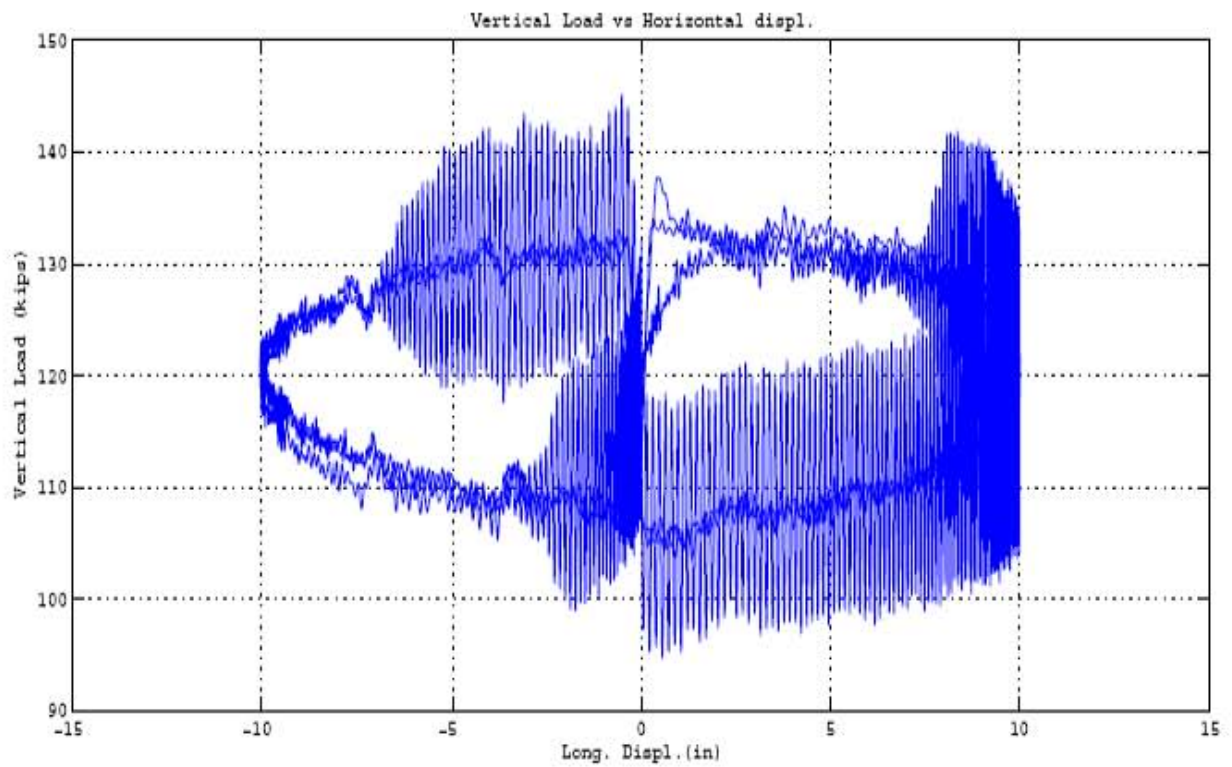
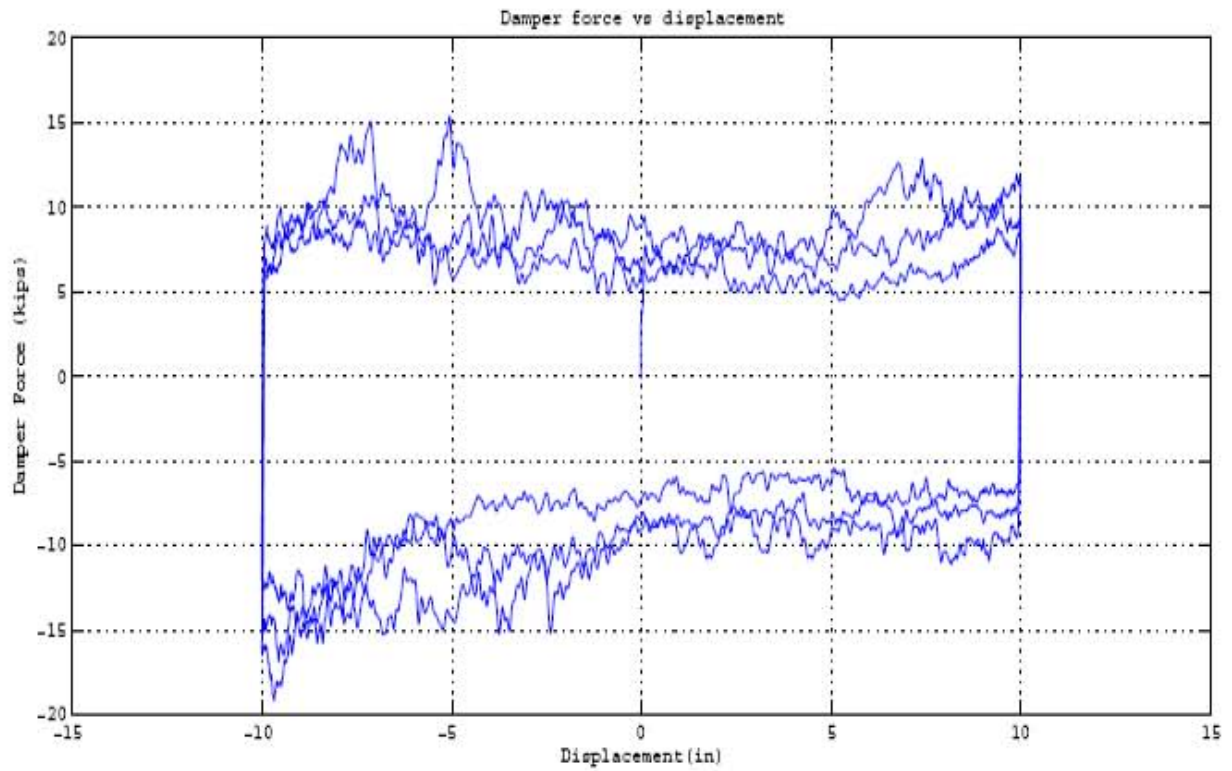


Figure 5-1 Results of Repeated Test #1 (continued).

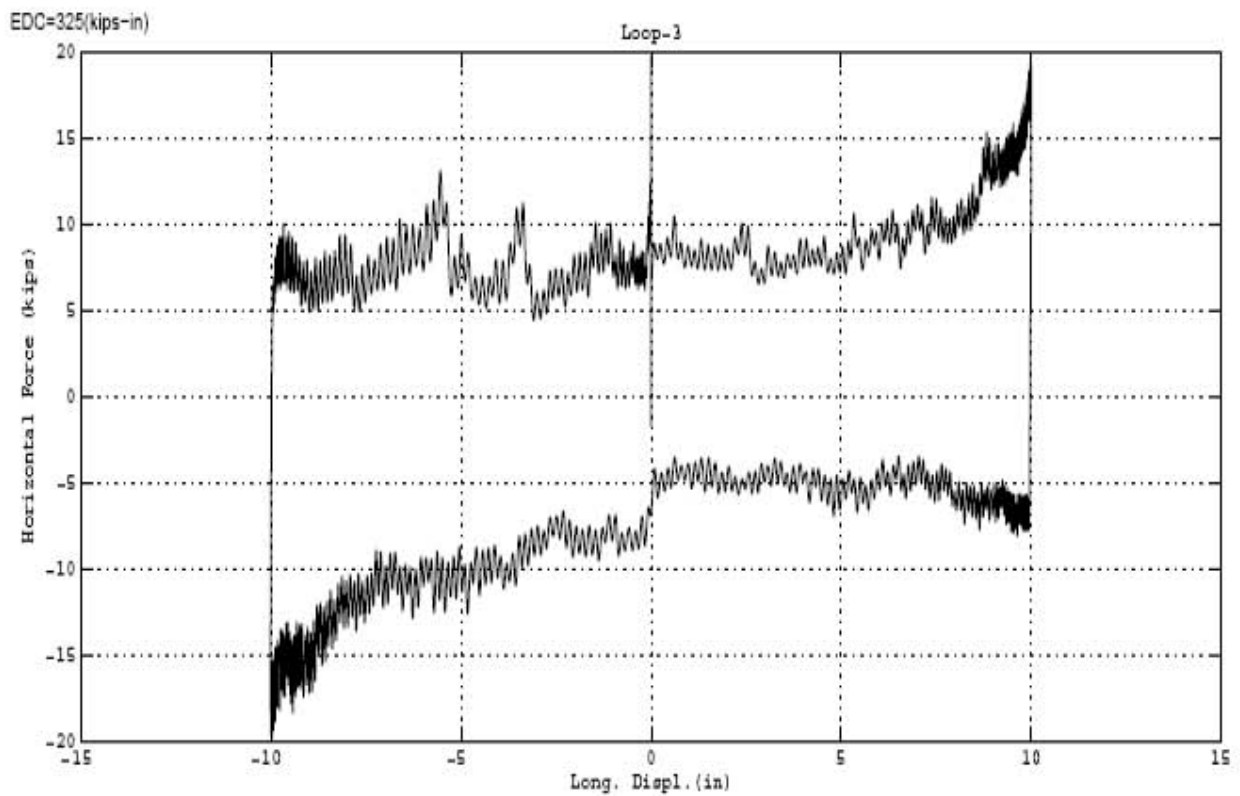
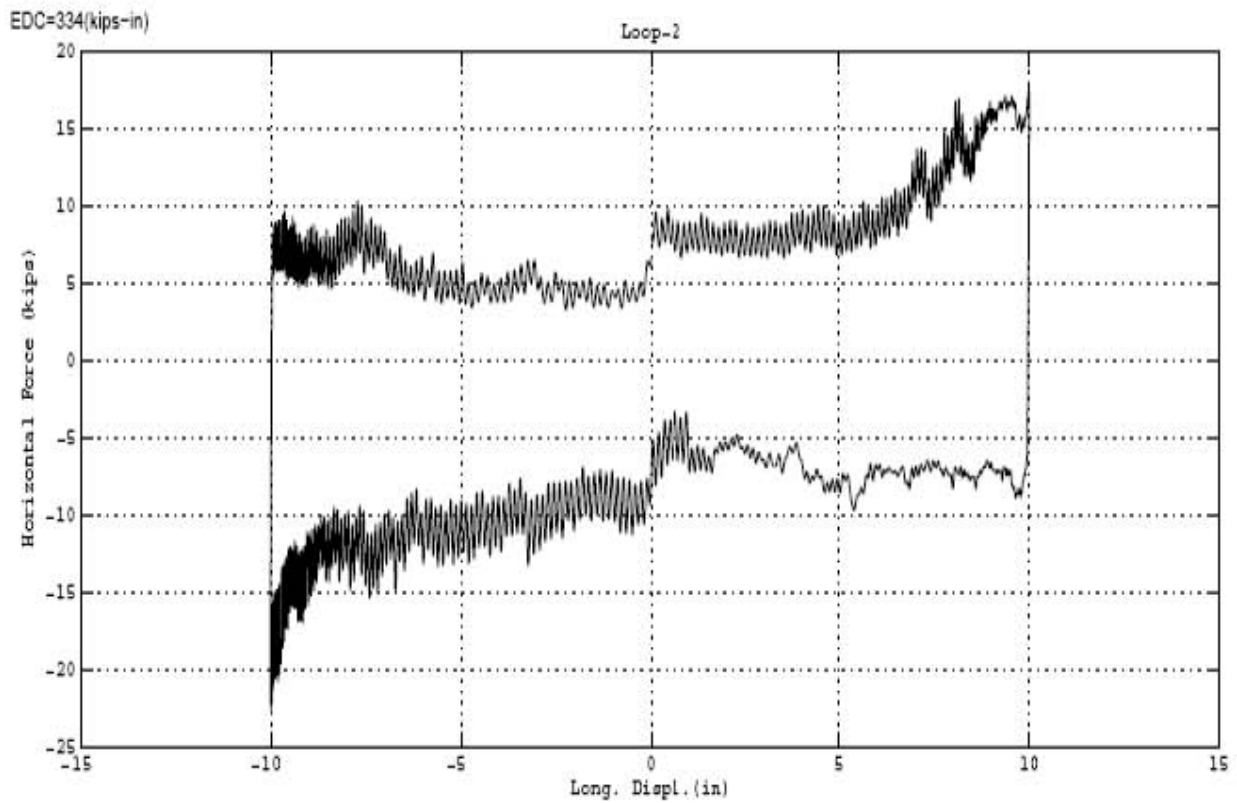


Figure 5-1 Results of Repeated Test #1 (continued).

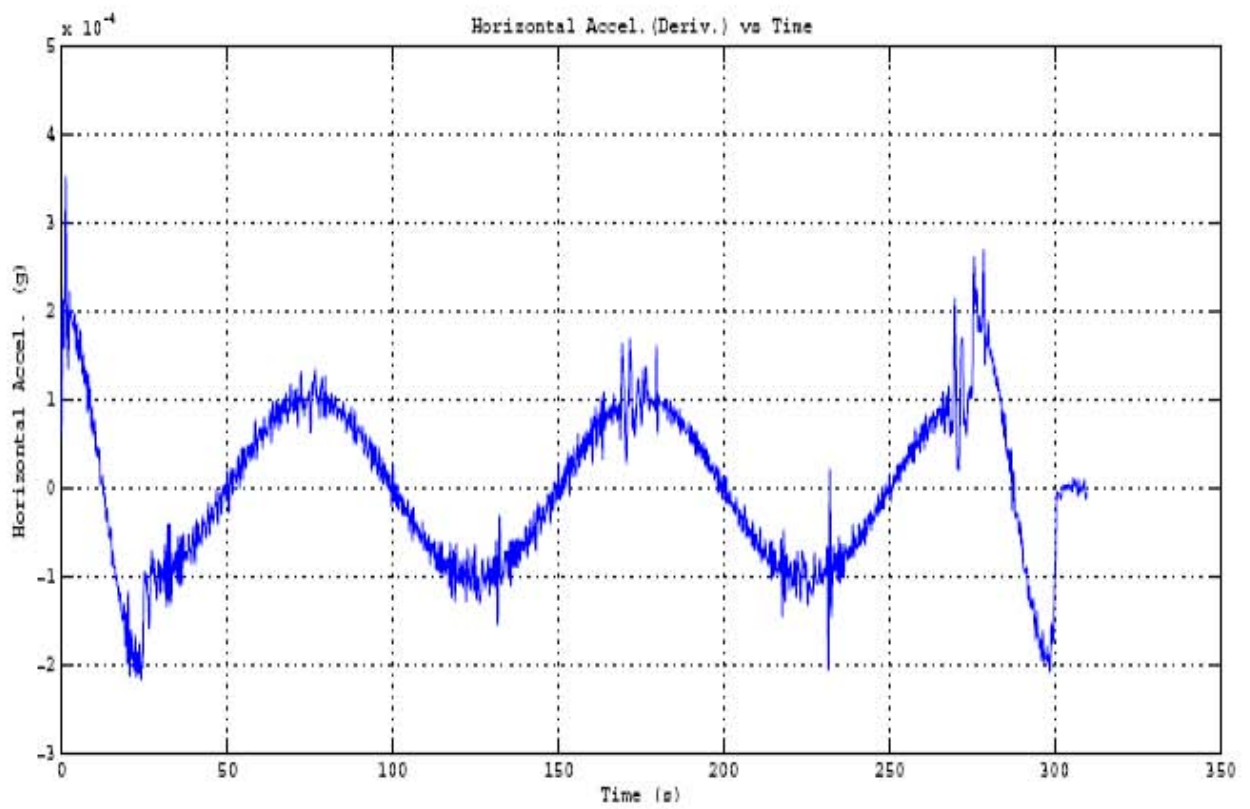
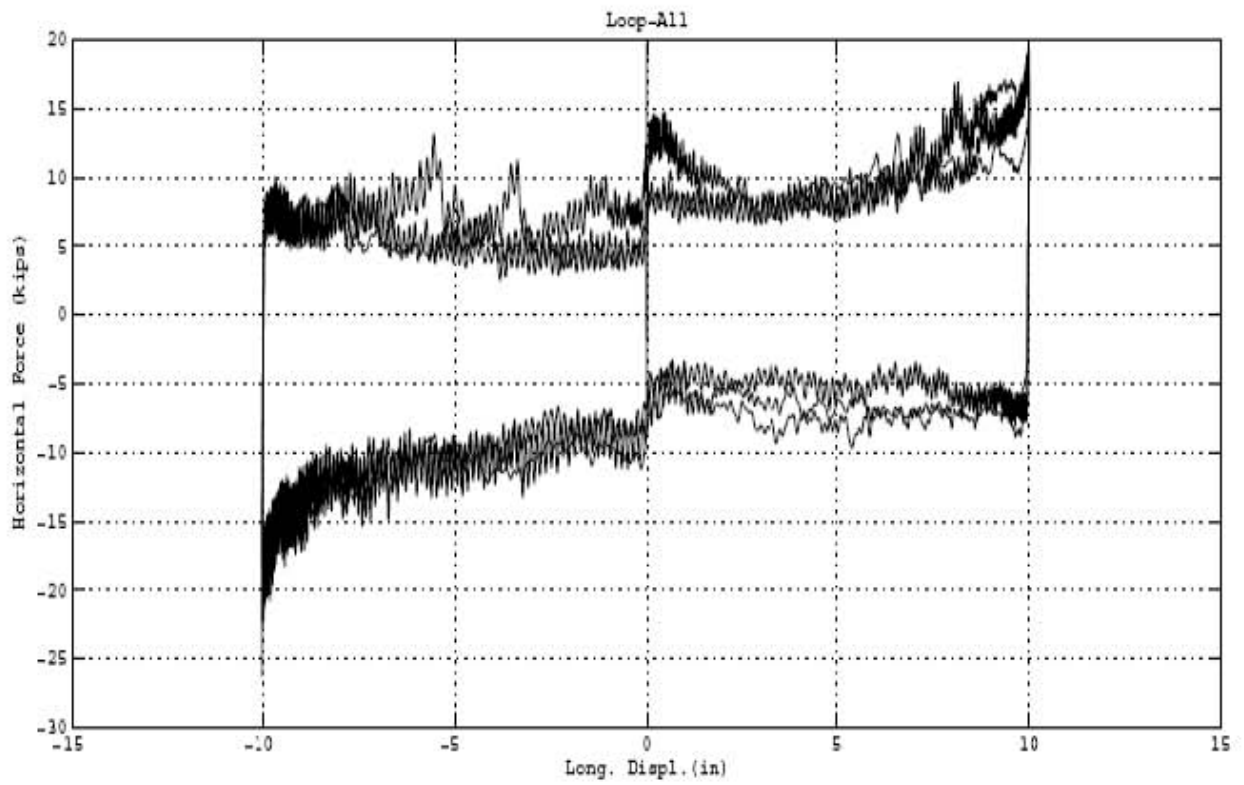


Figure 5-1 Results of Repeated Test #1 (continued).

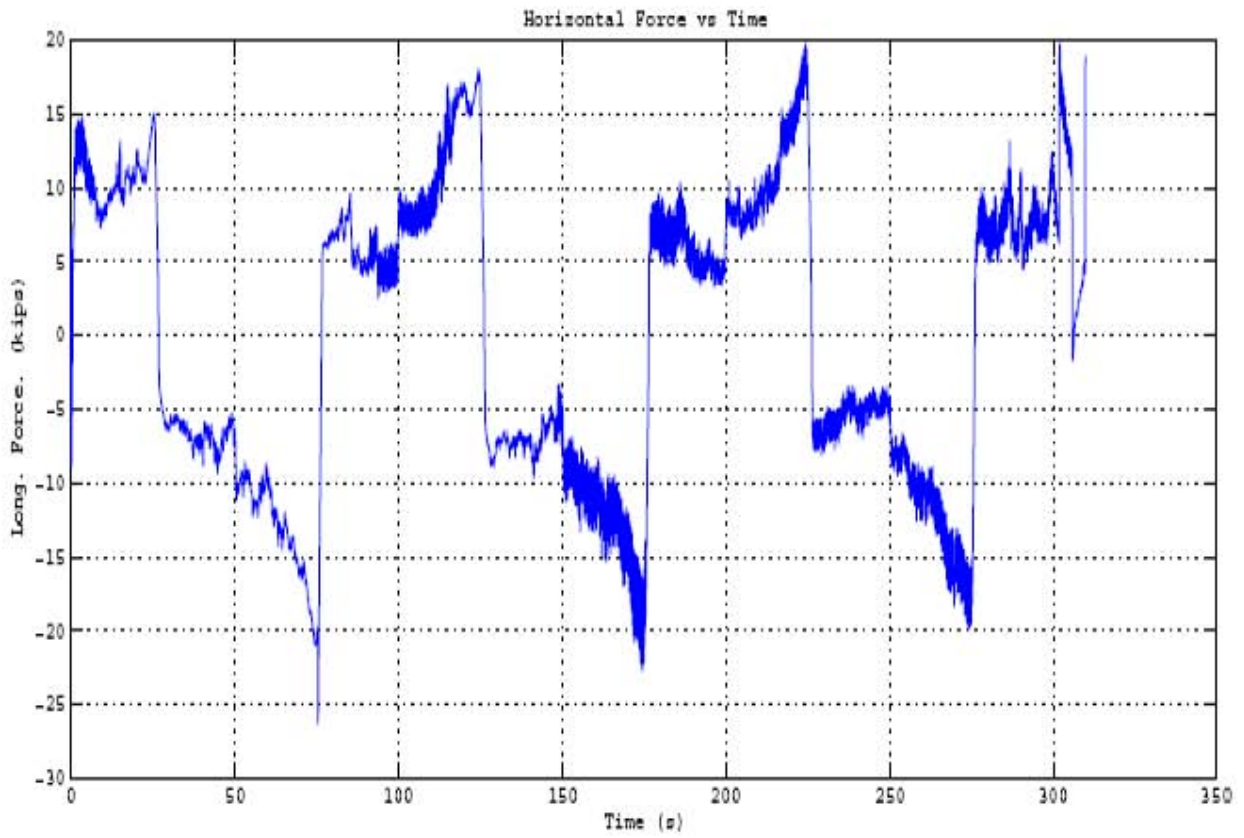
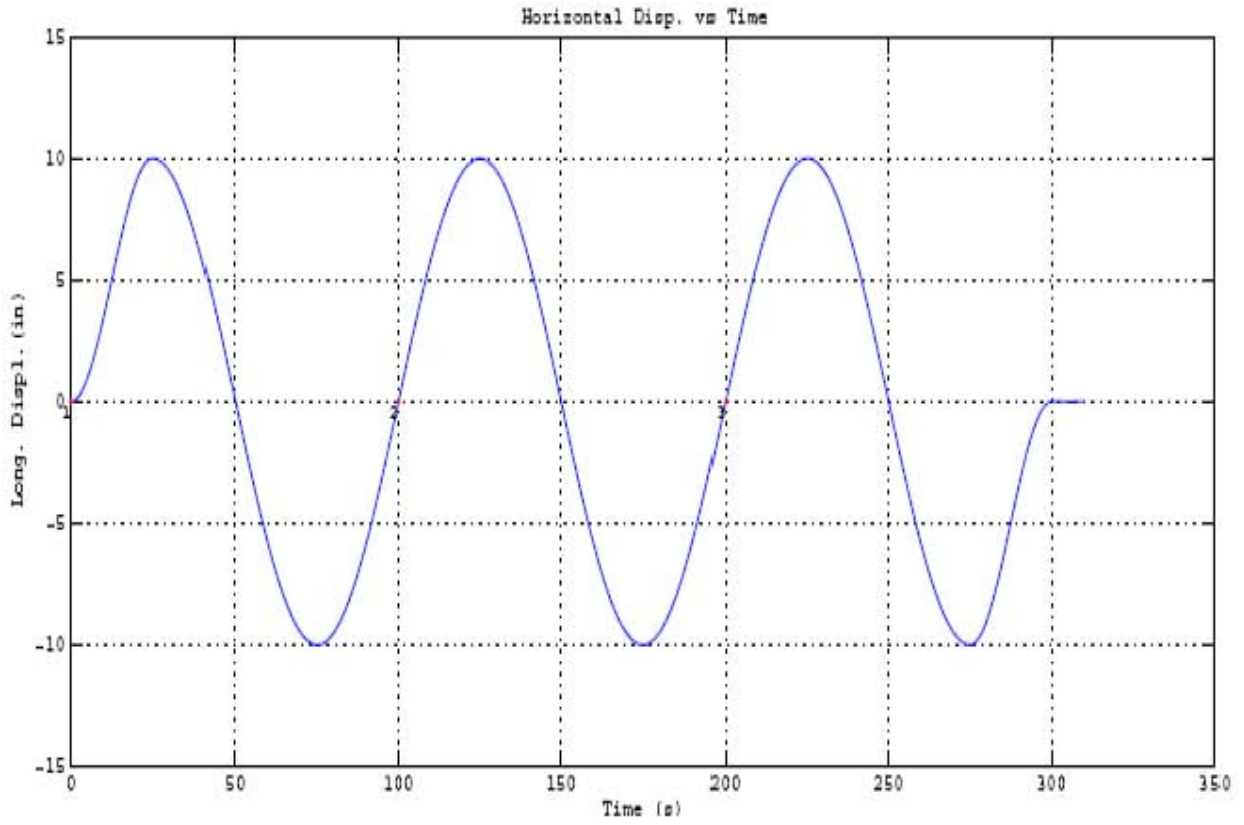


Figure 5-1 Results of Repeated Test #1 (continued).

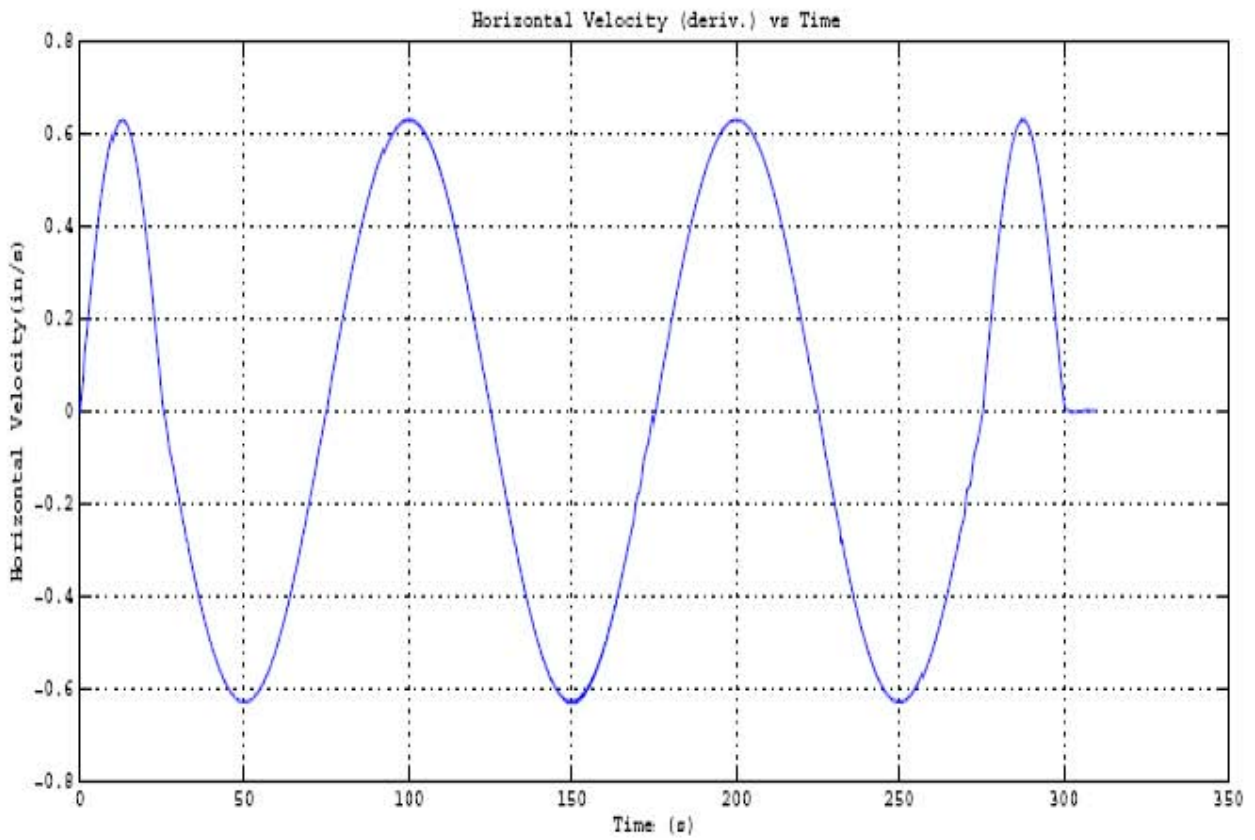
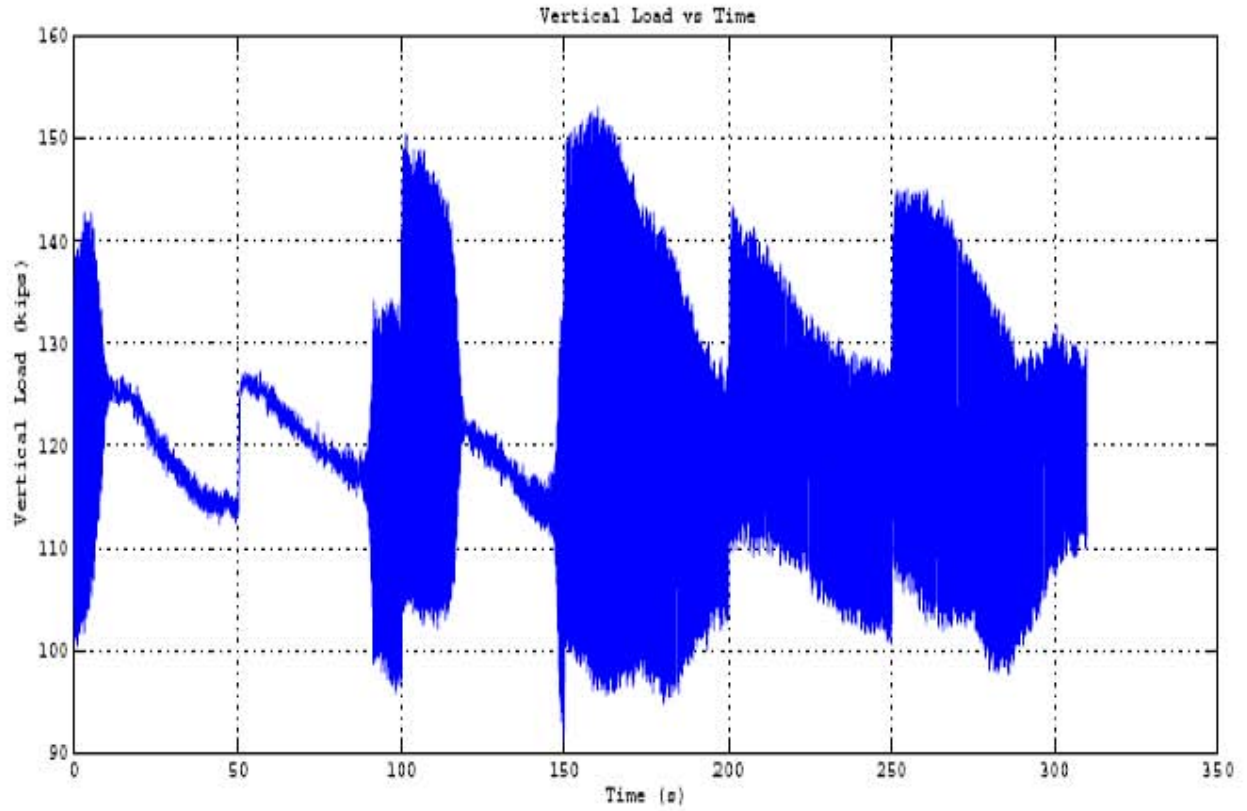


Figure 5-1 Results of Repeated Test #1 (continued).

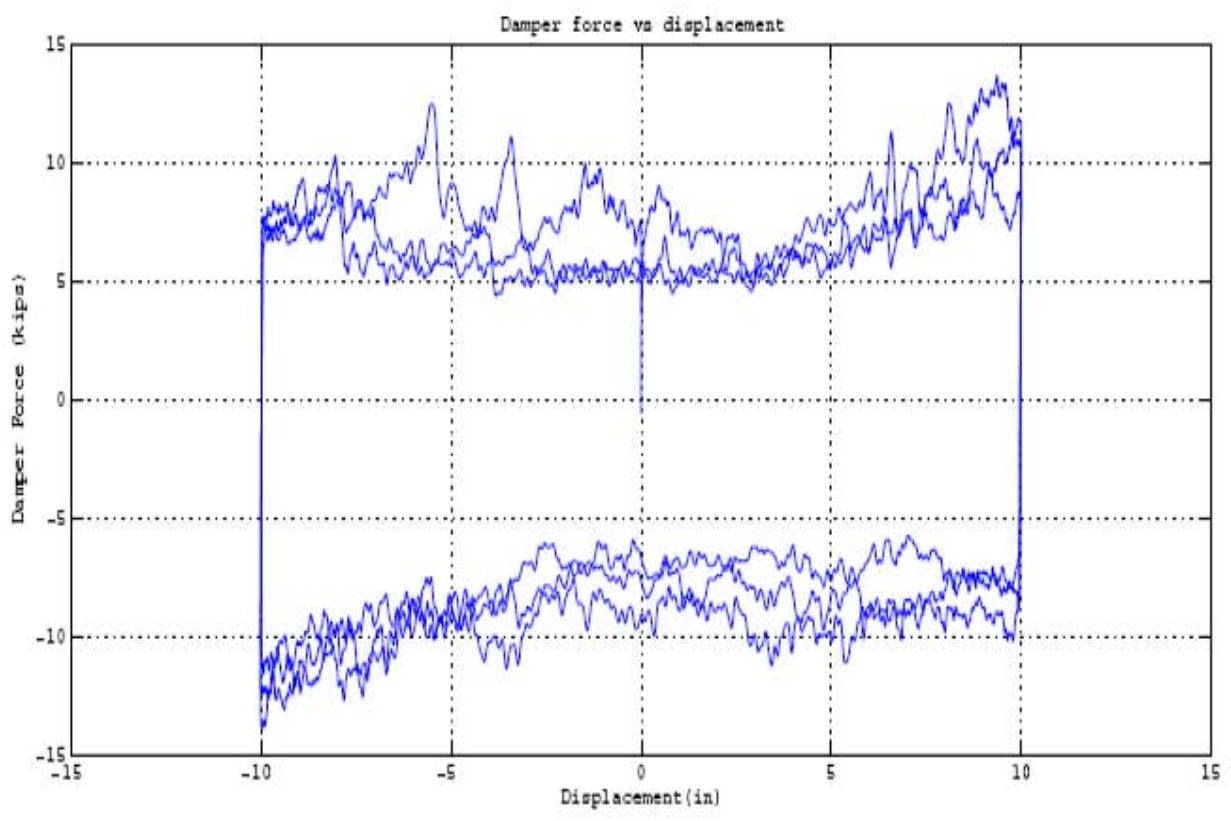
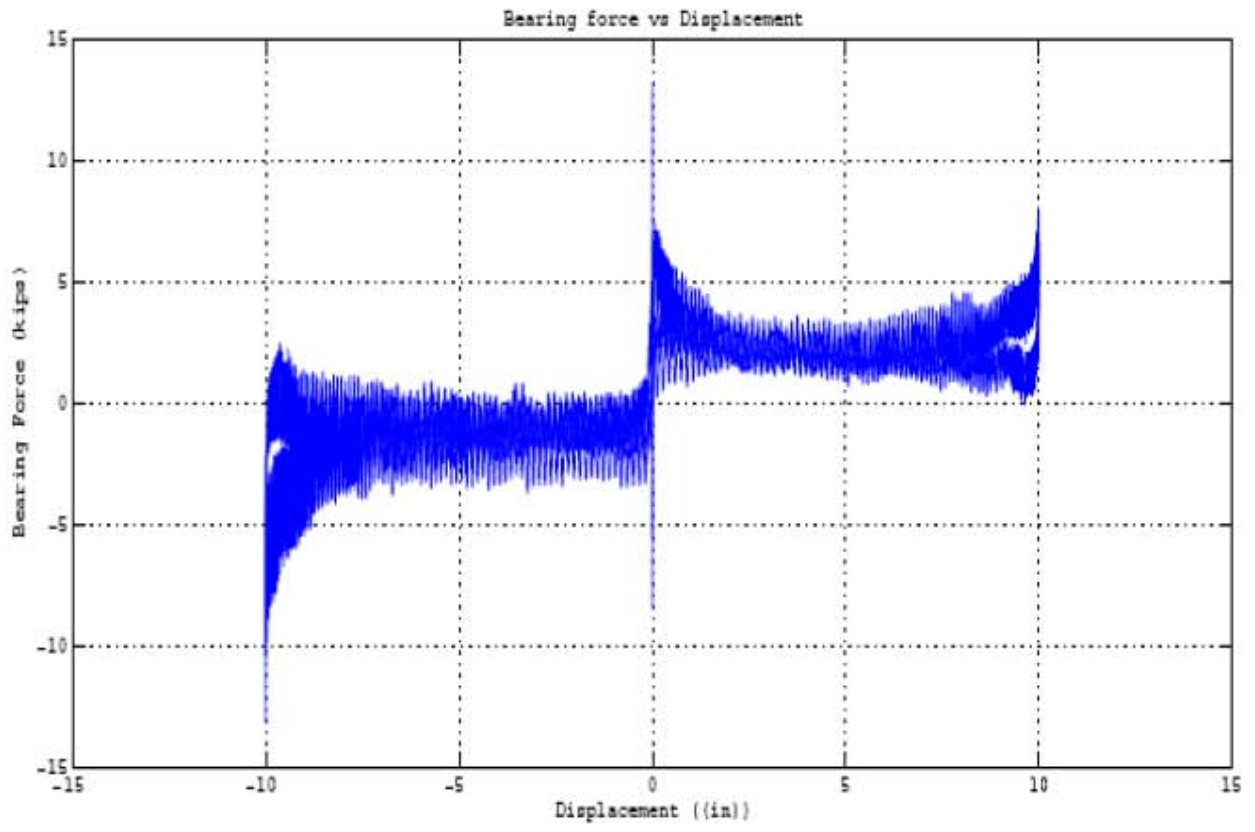


Figure 5-1 Results of Repeated Test #1 (continued).

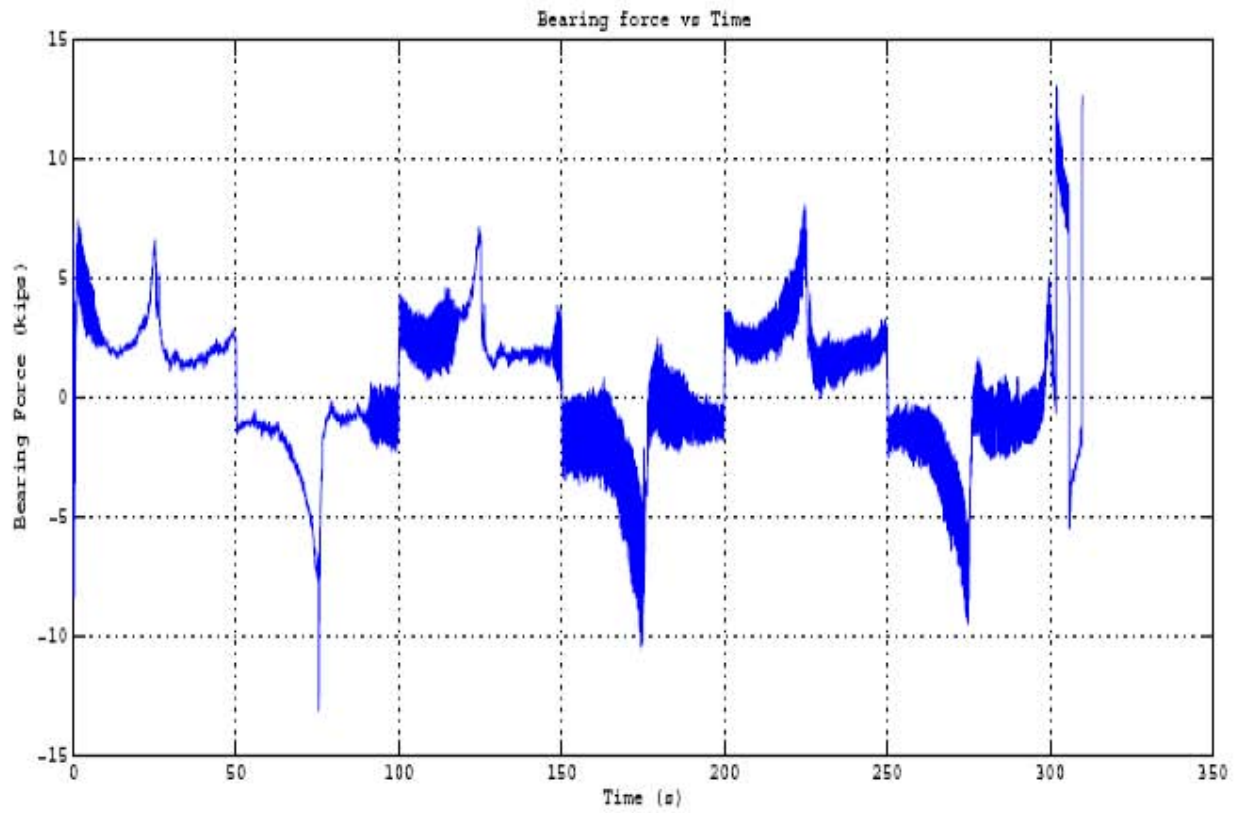
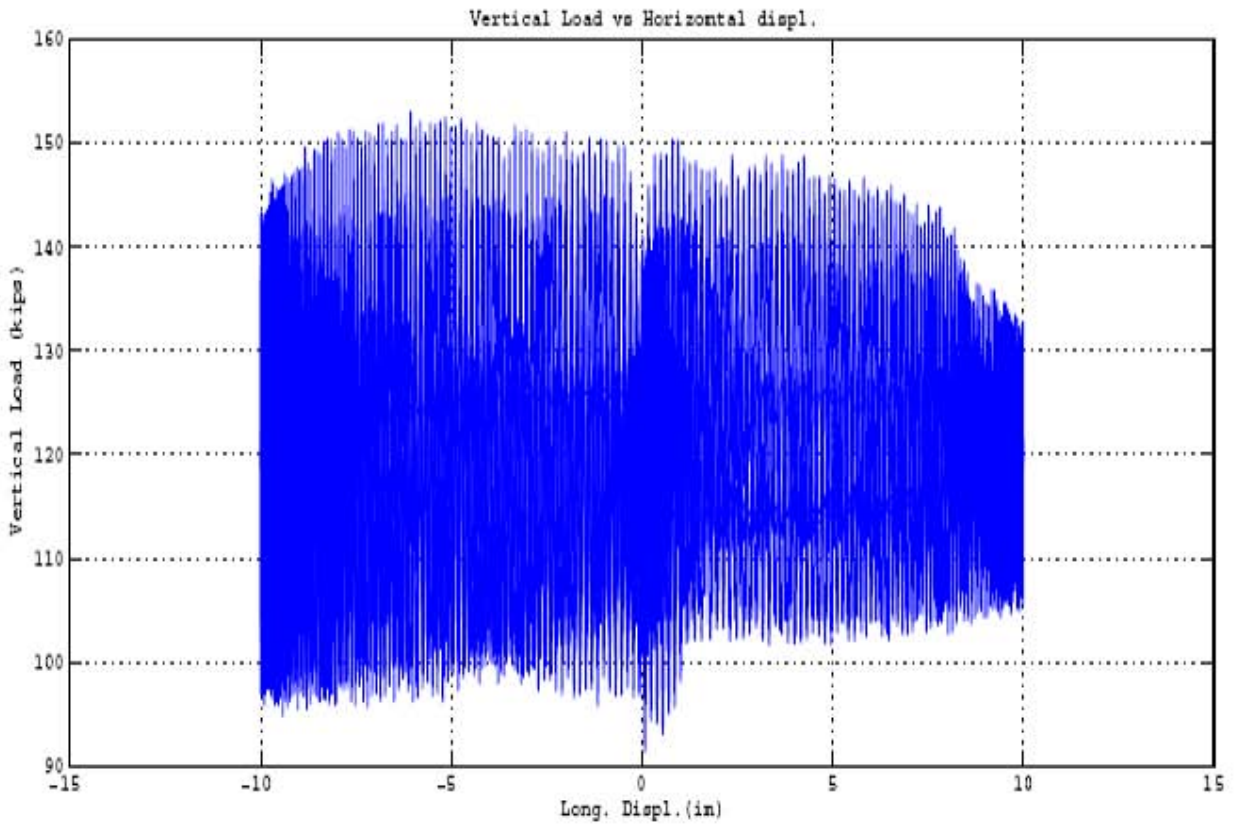


Figure 5-1 Results of Repeated Test #1 (continued).

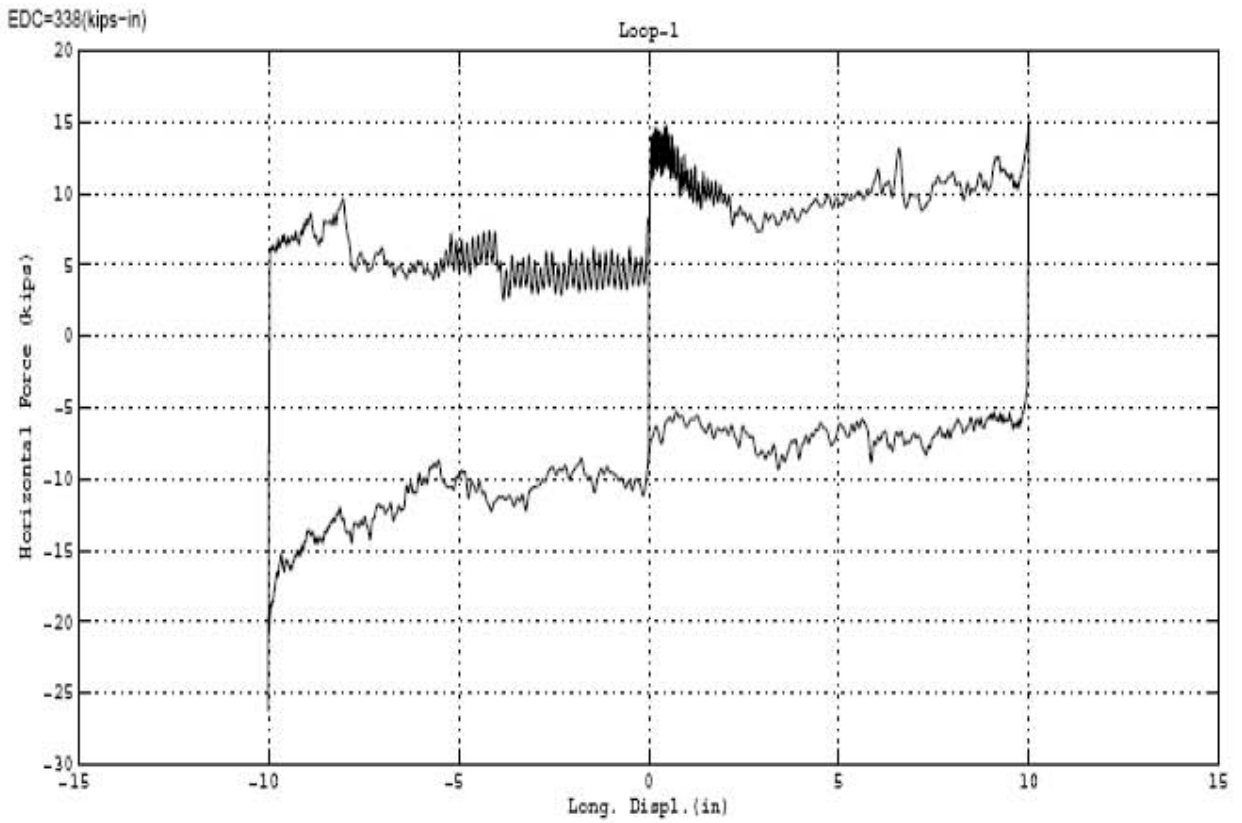
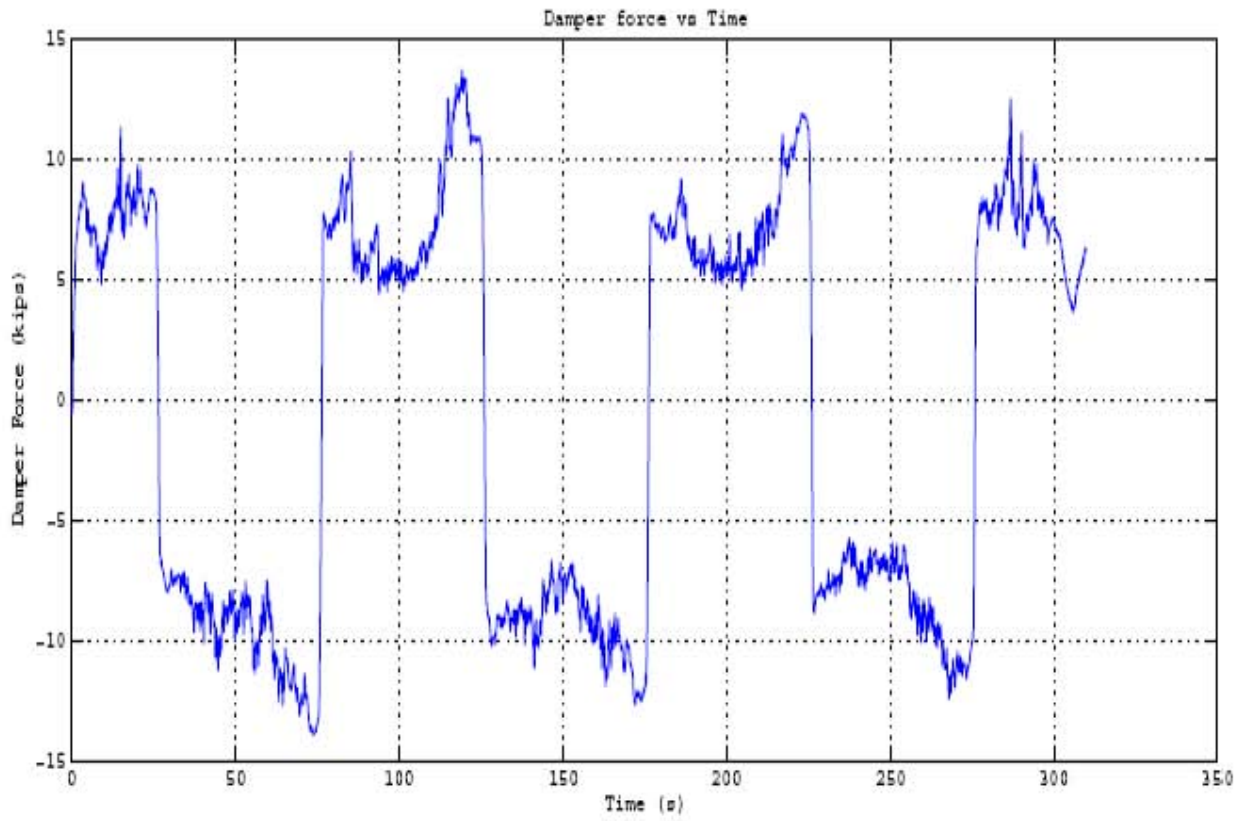


Figure 5-1 Results of Repeated Test #1 (continued).

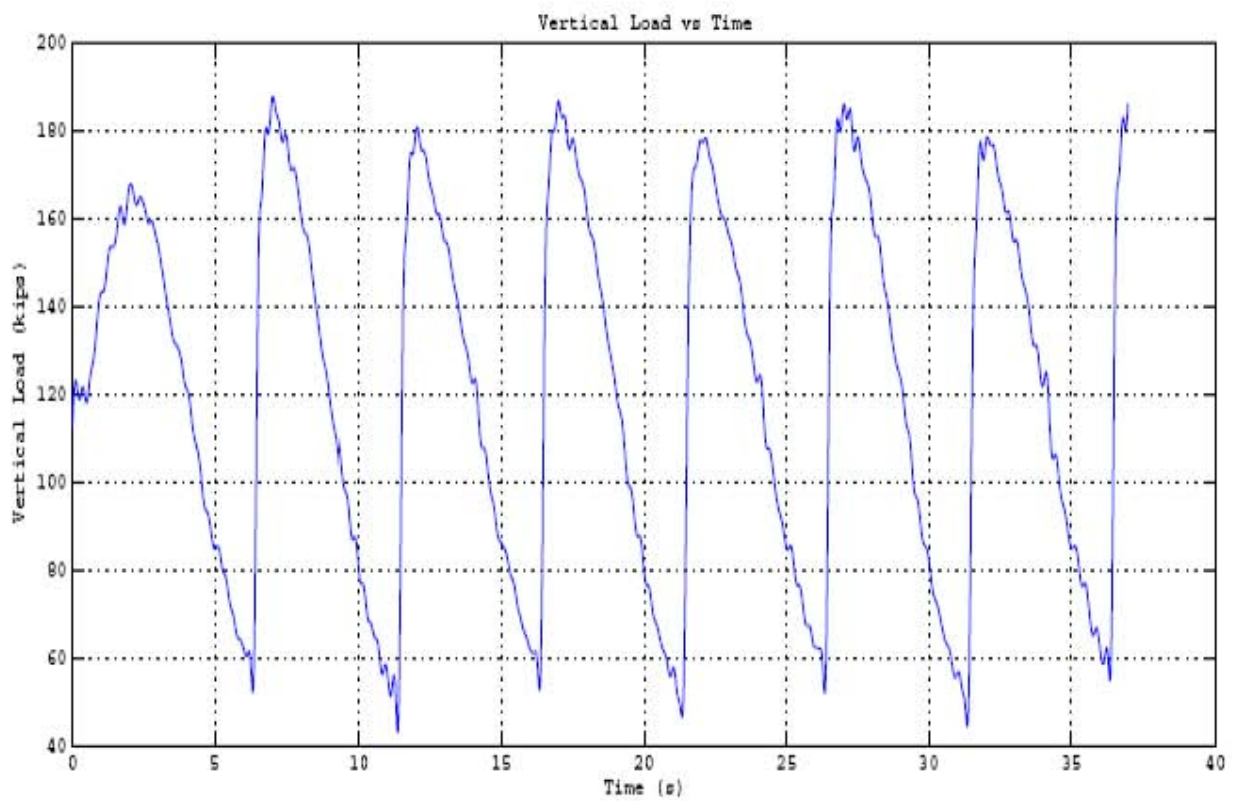
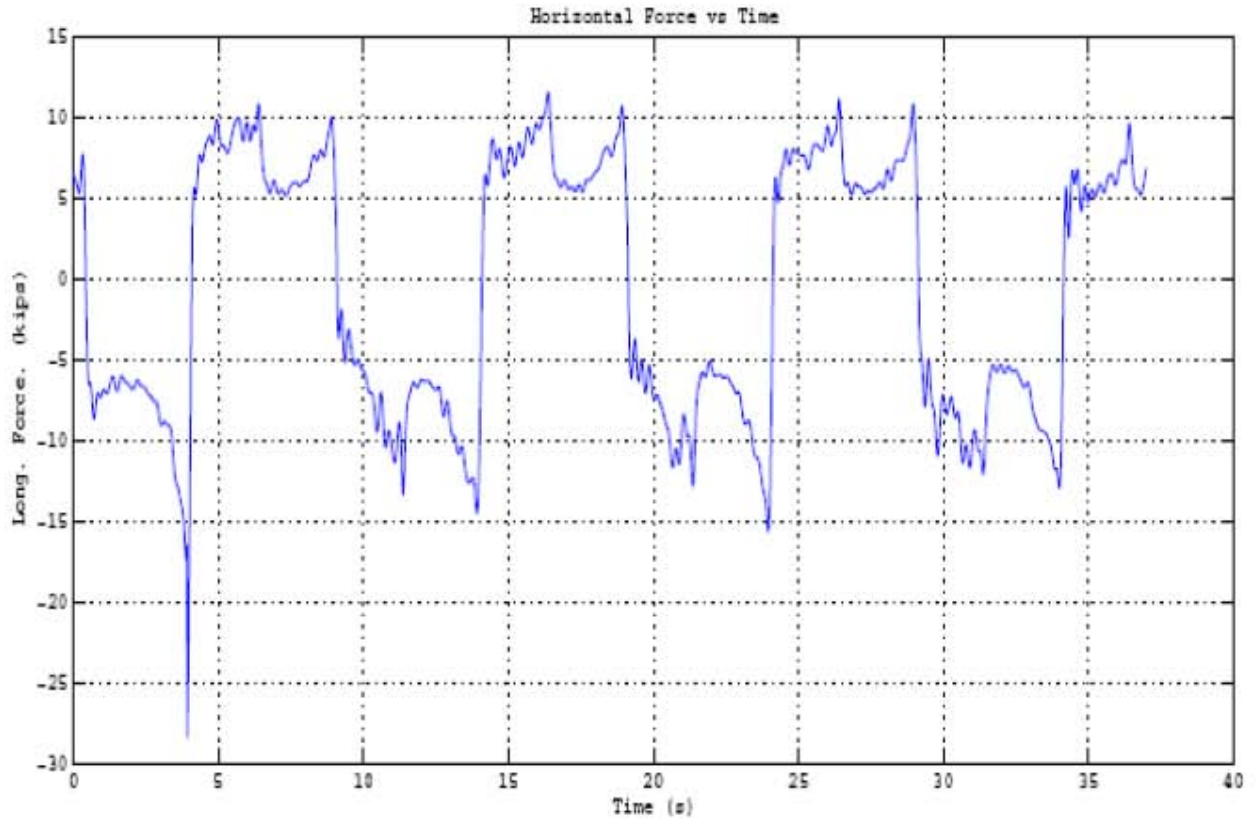


Figure 5-2 Results of Repeated Test #2.

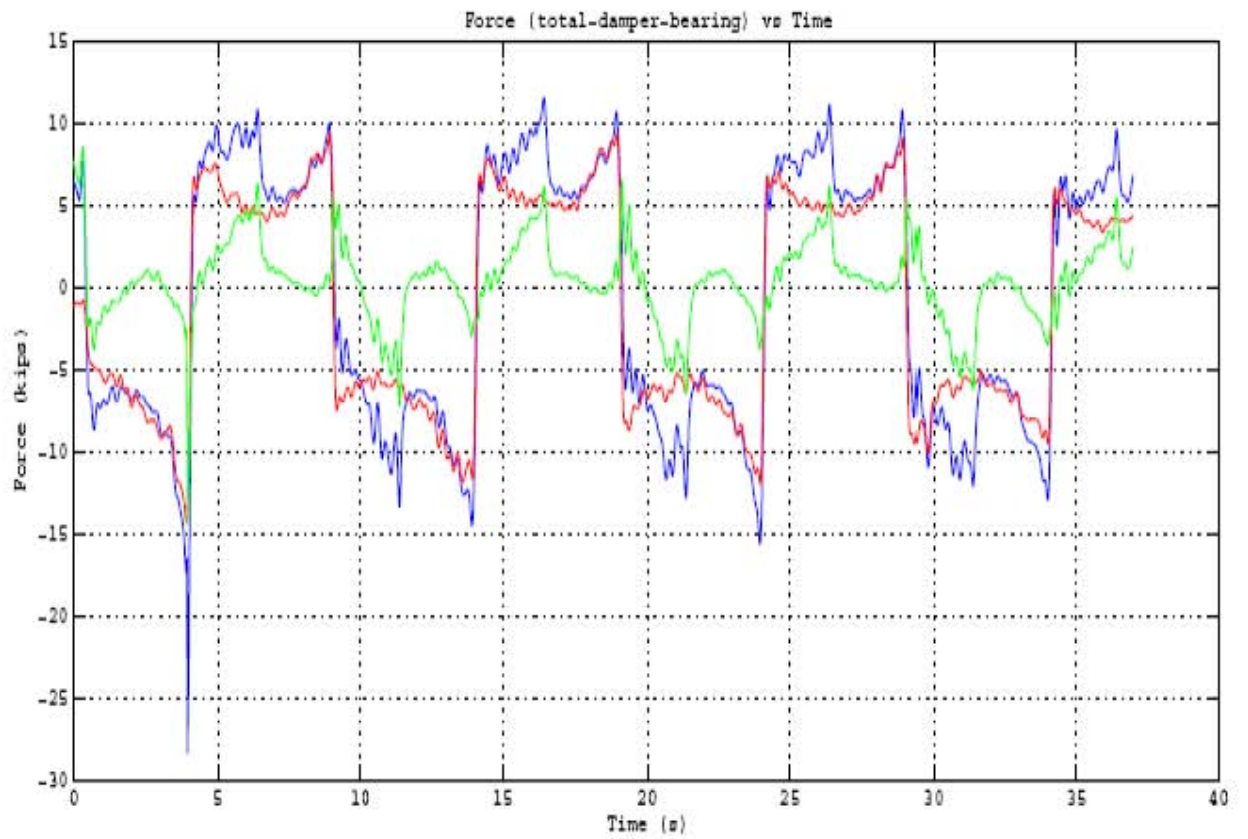
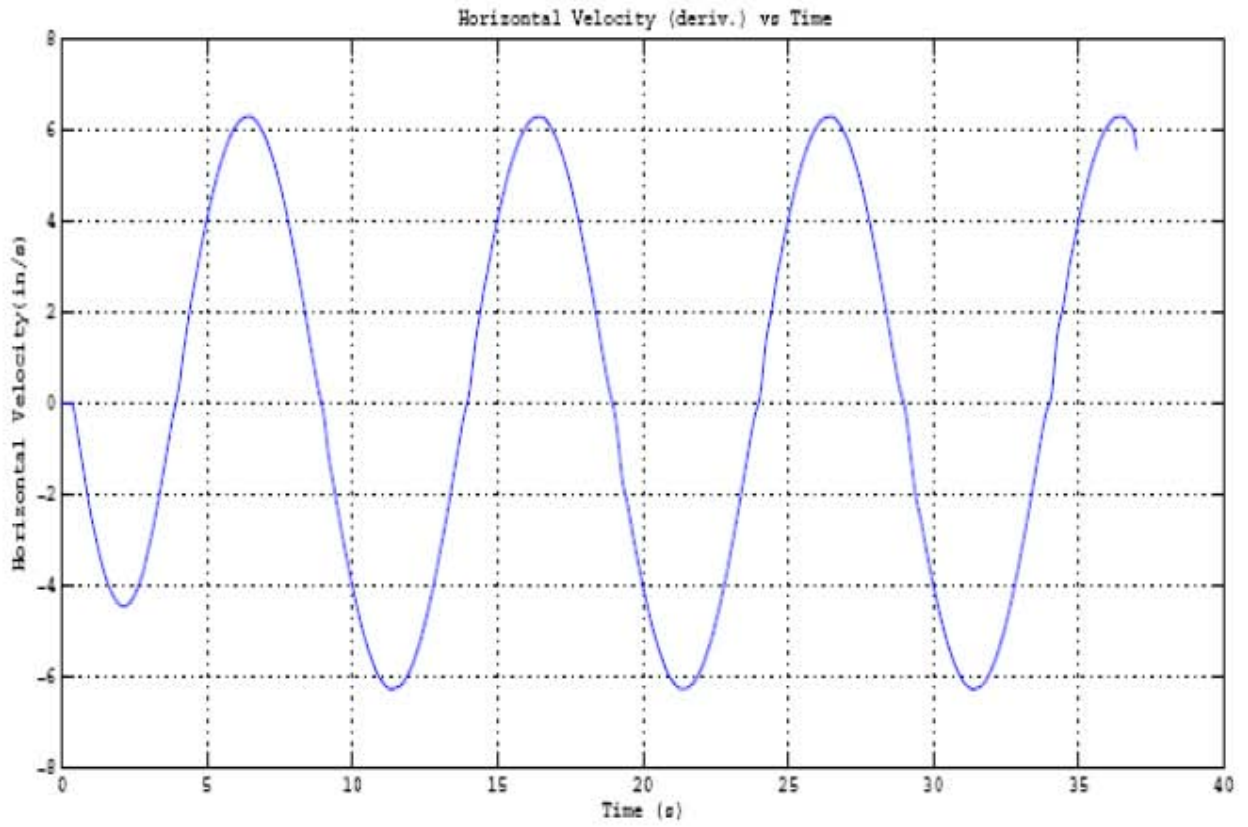


Figure 5-2 Results of Repeated Test #2 (continued).

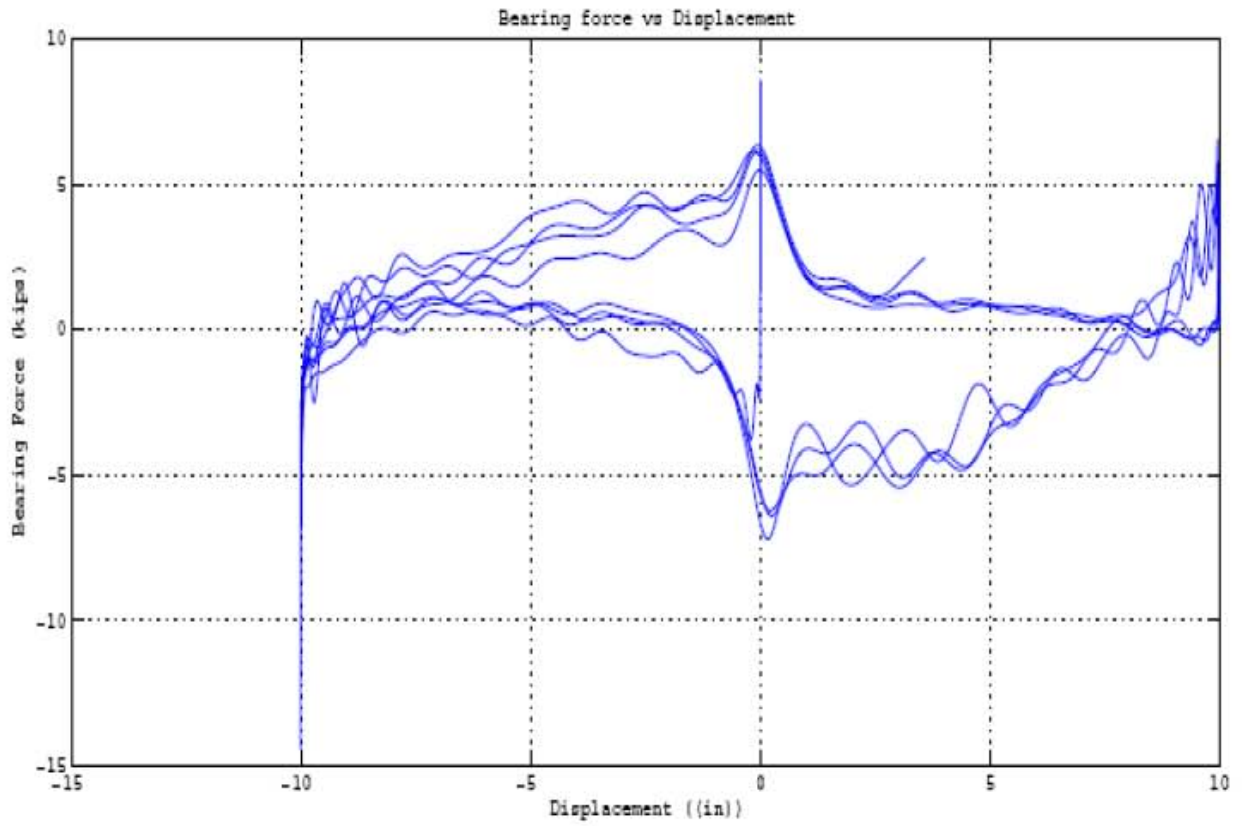
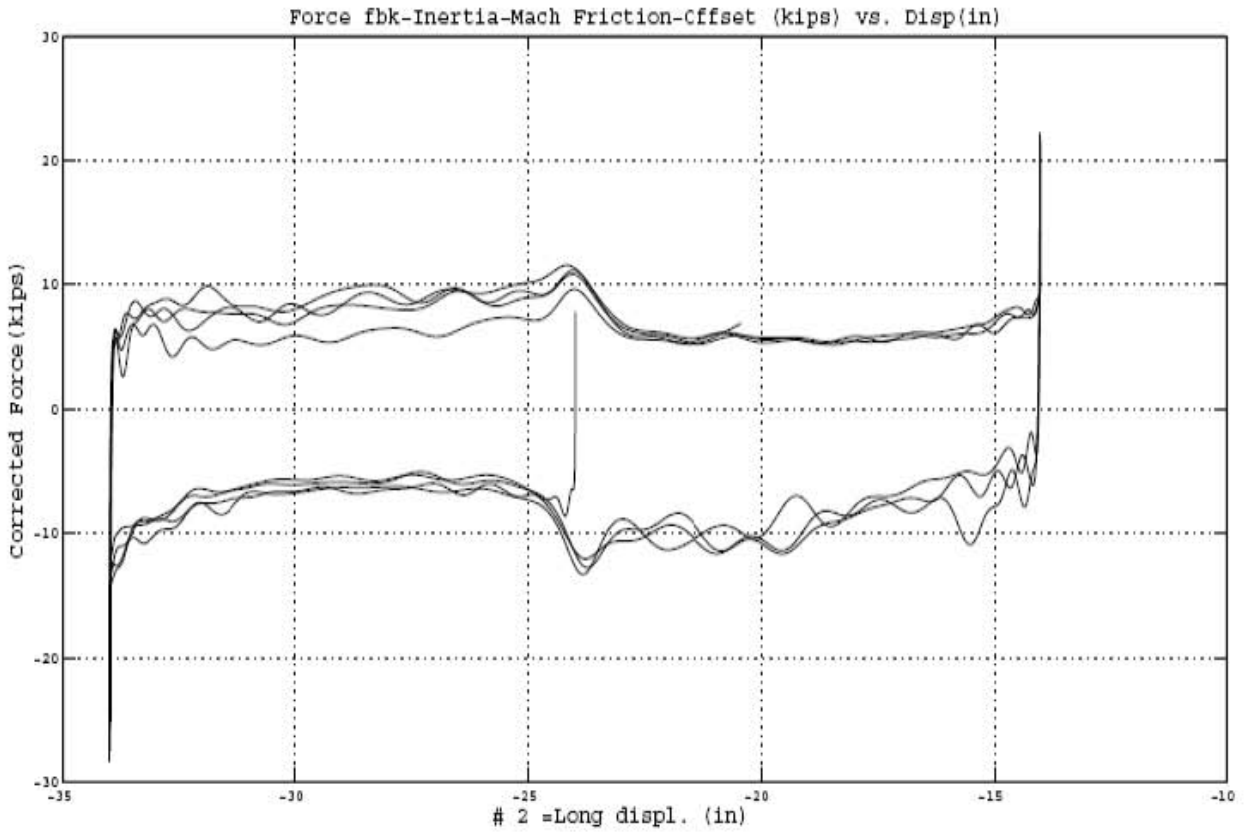


Figure 5-2 Results of Repeated Test #2 (continued).

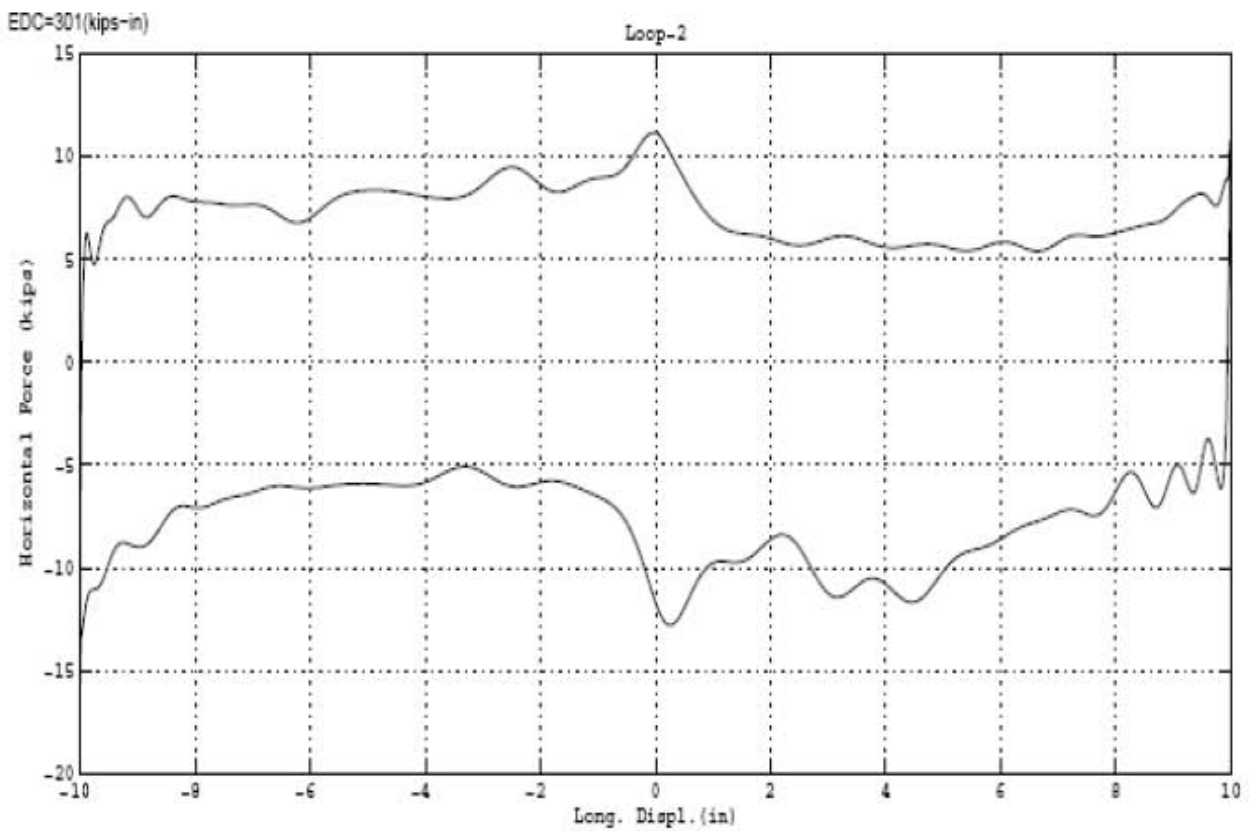
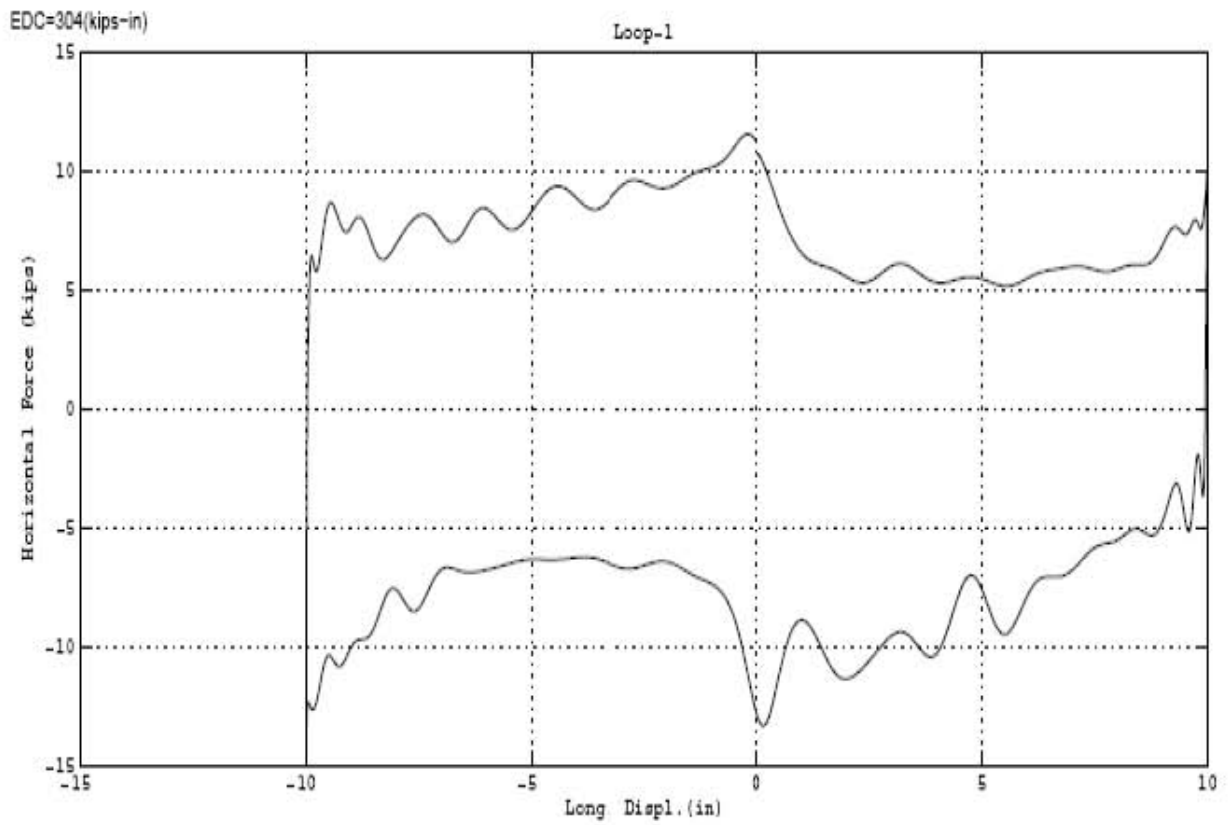


Figure 5-2 Results of Repeated Test #2 (continued).

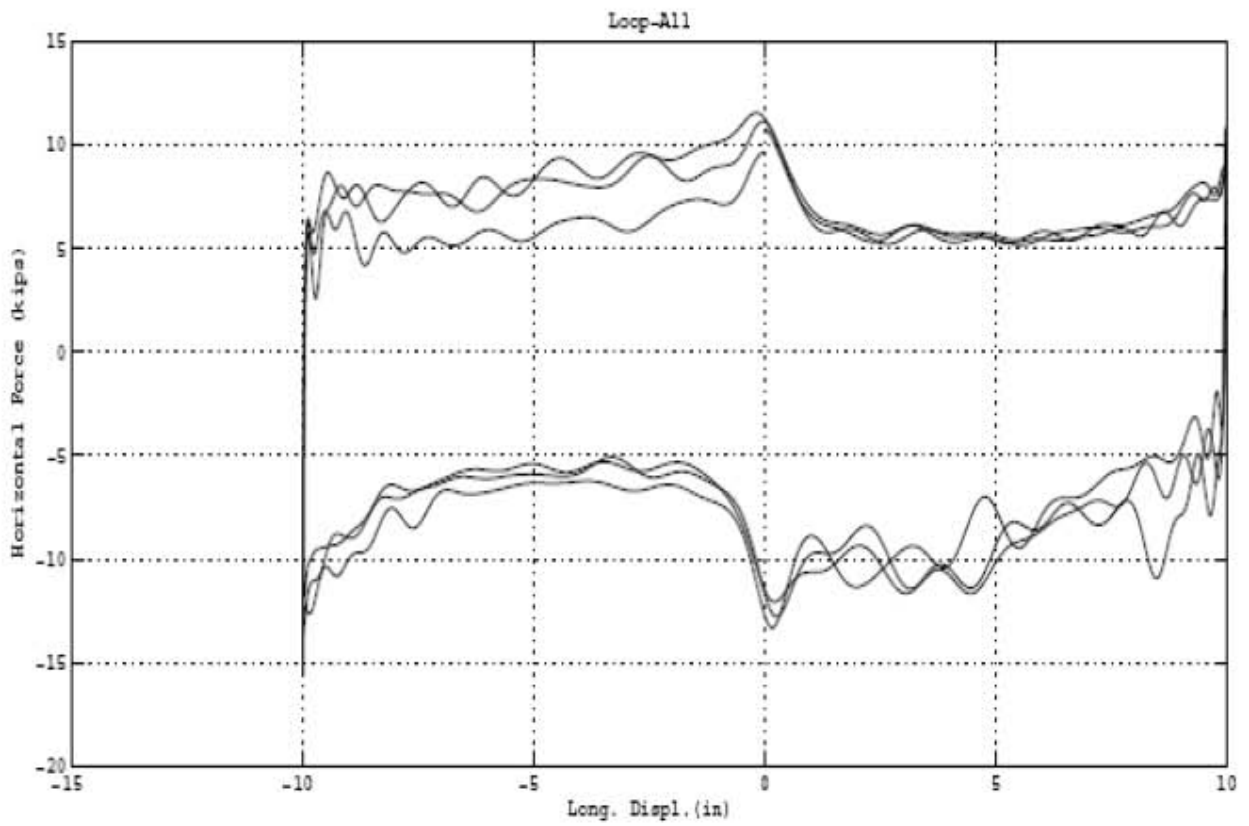
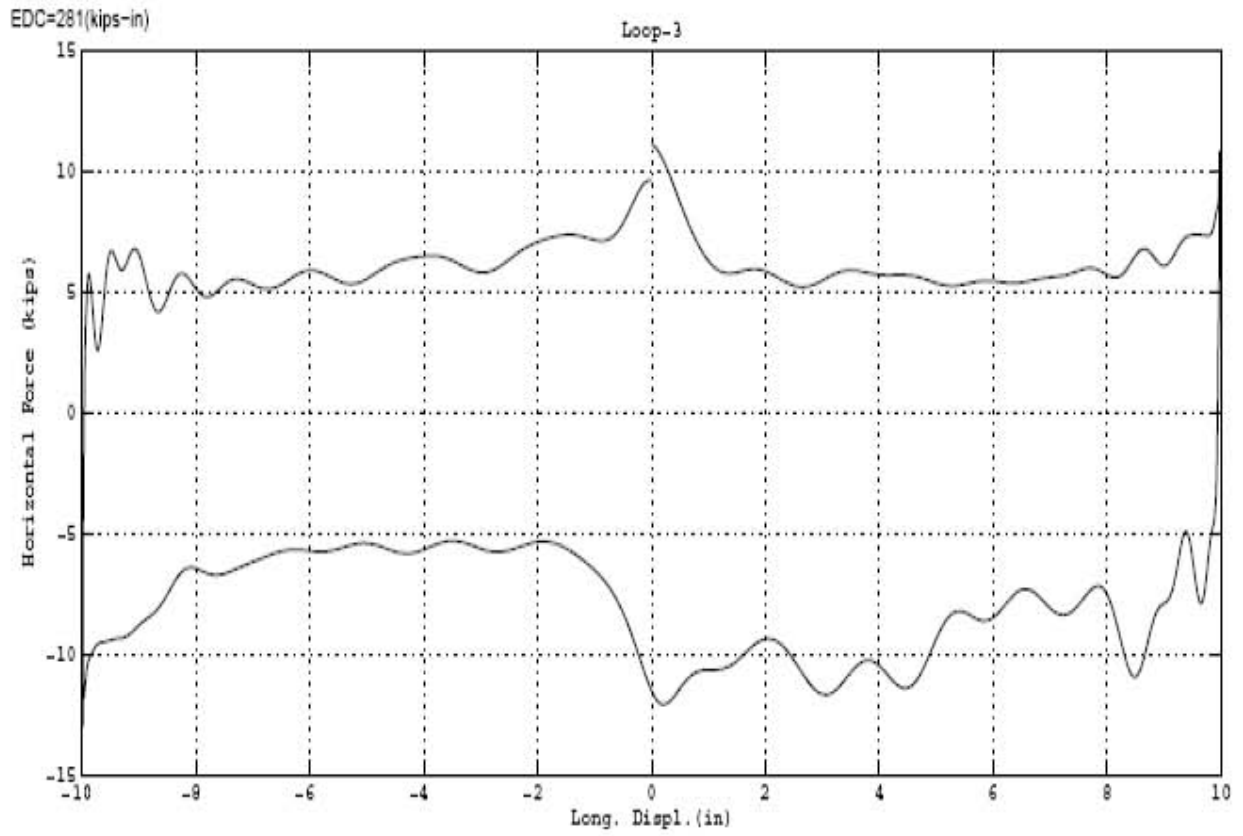


Figure 5-2 Results of Repeated Test #2 (continued).

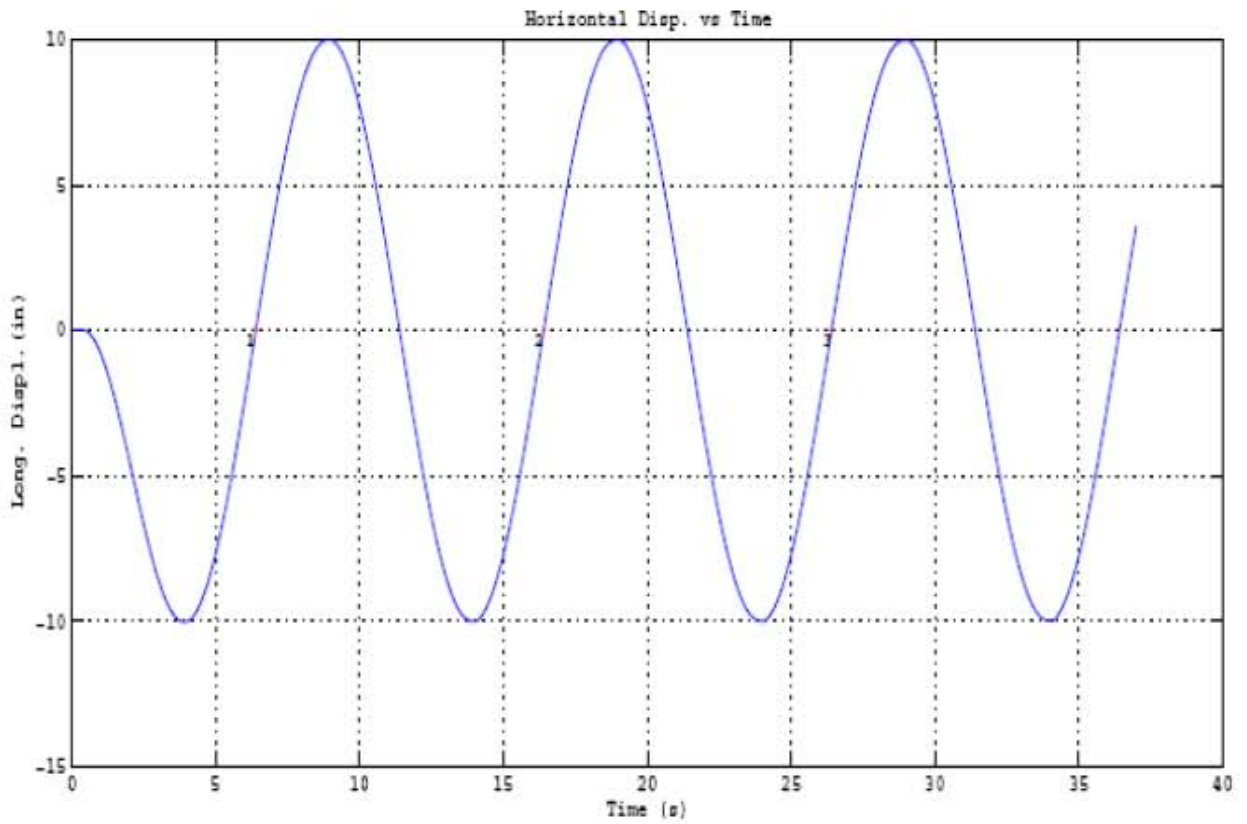
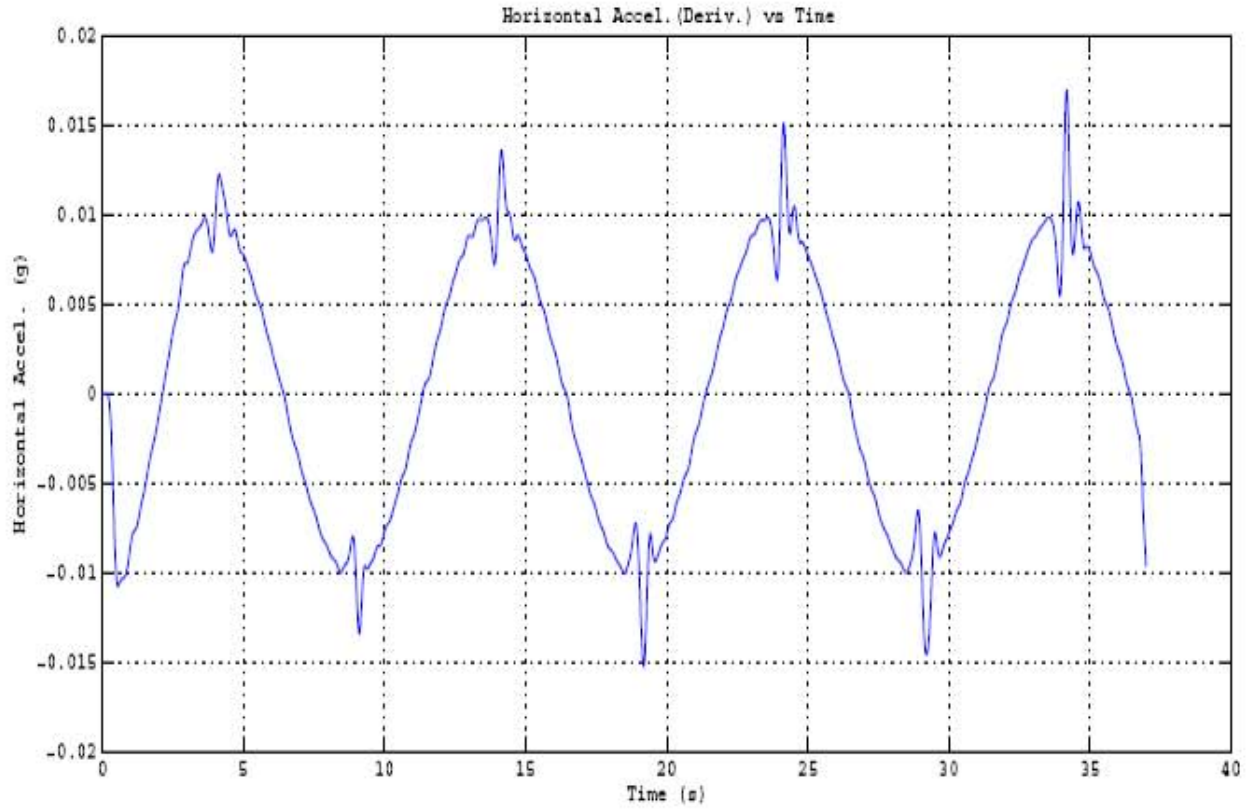


Figure 5-2 Results of Repeated Test #2 (continued).

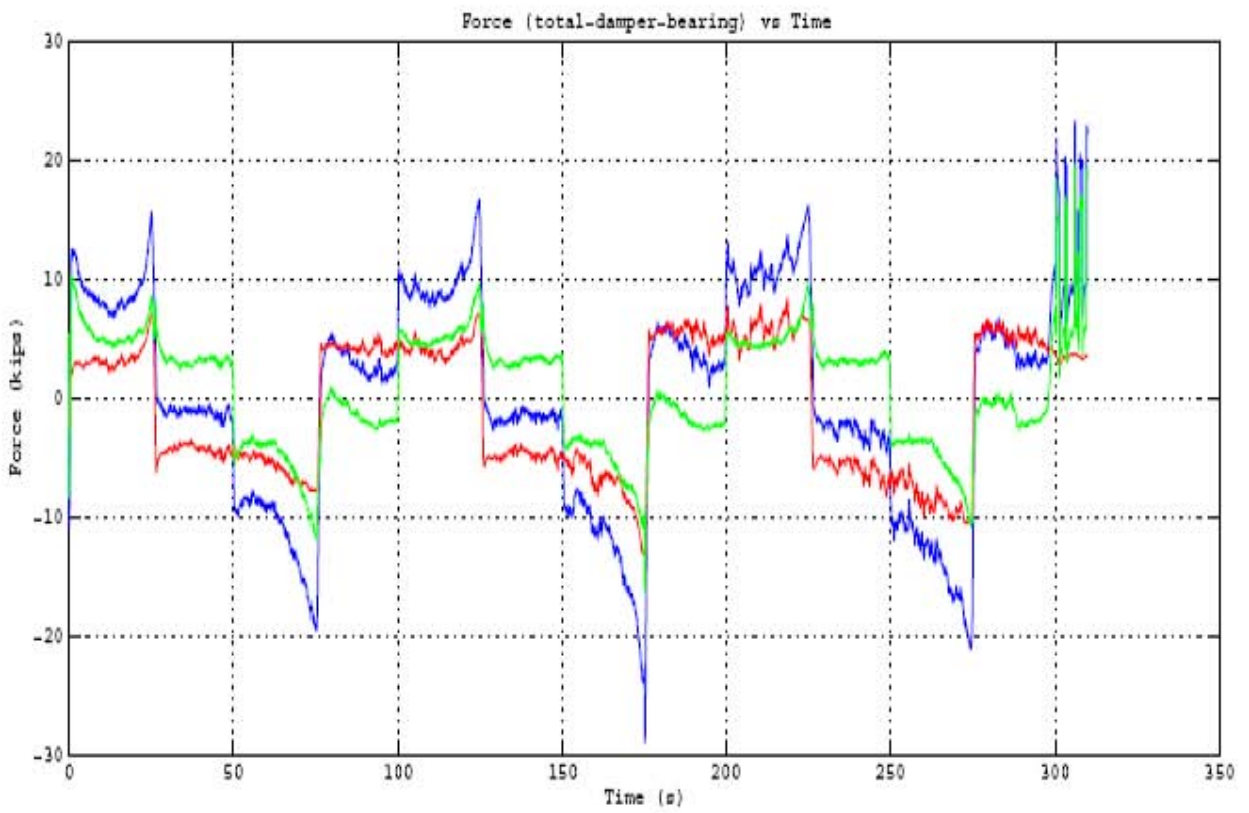
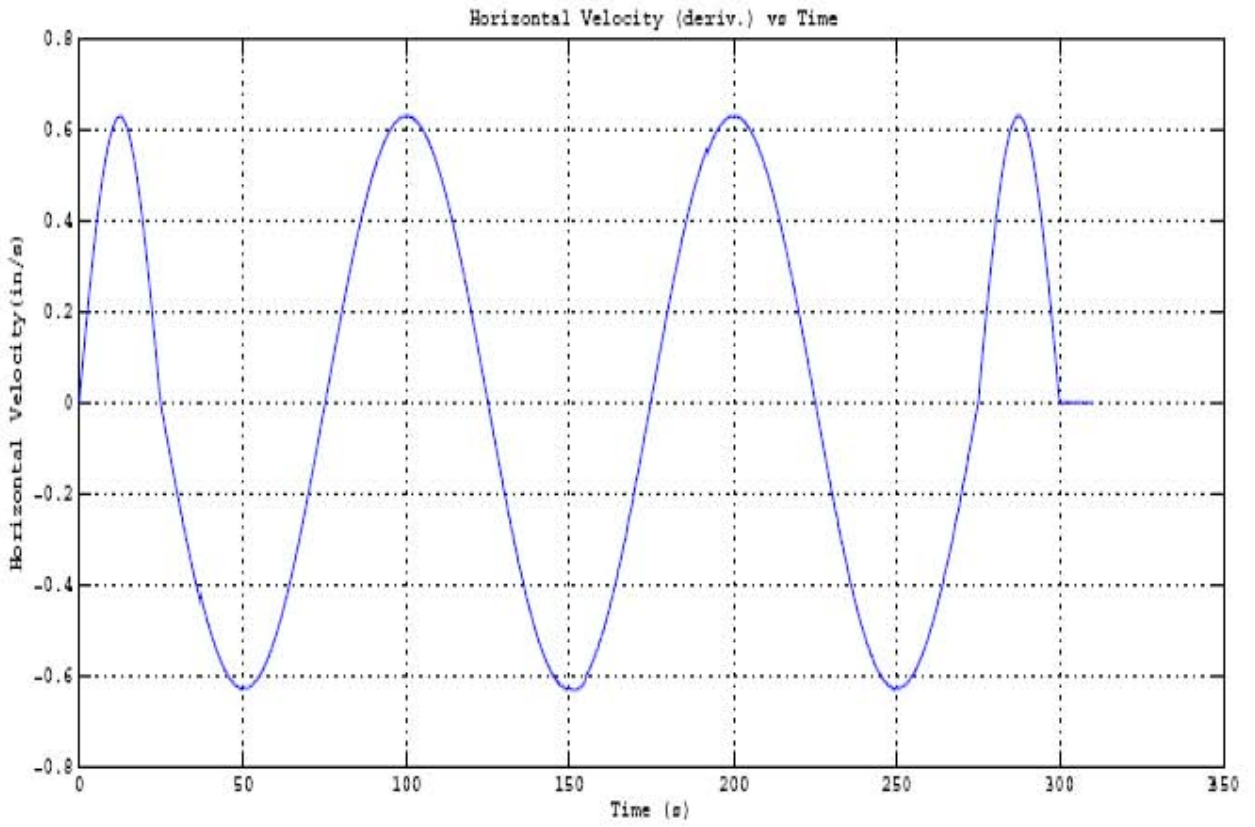


Figure 5-3 Results of Repeated Test #3.

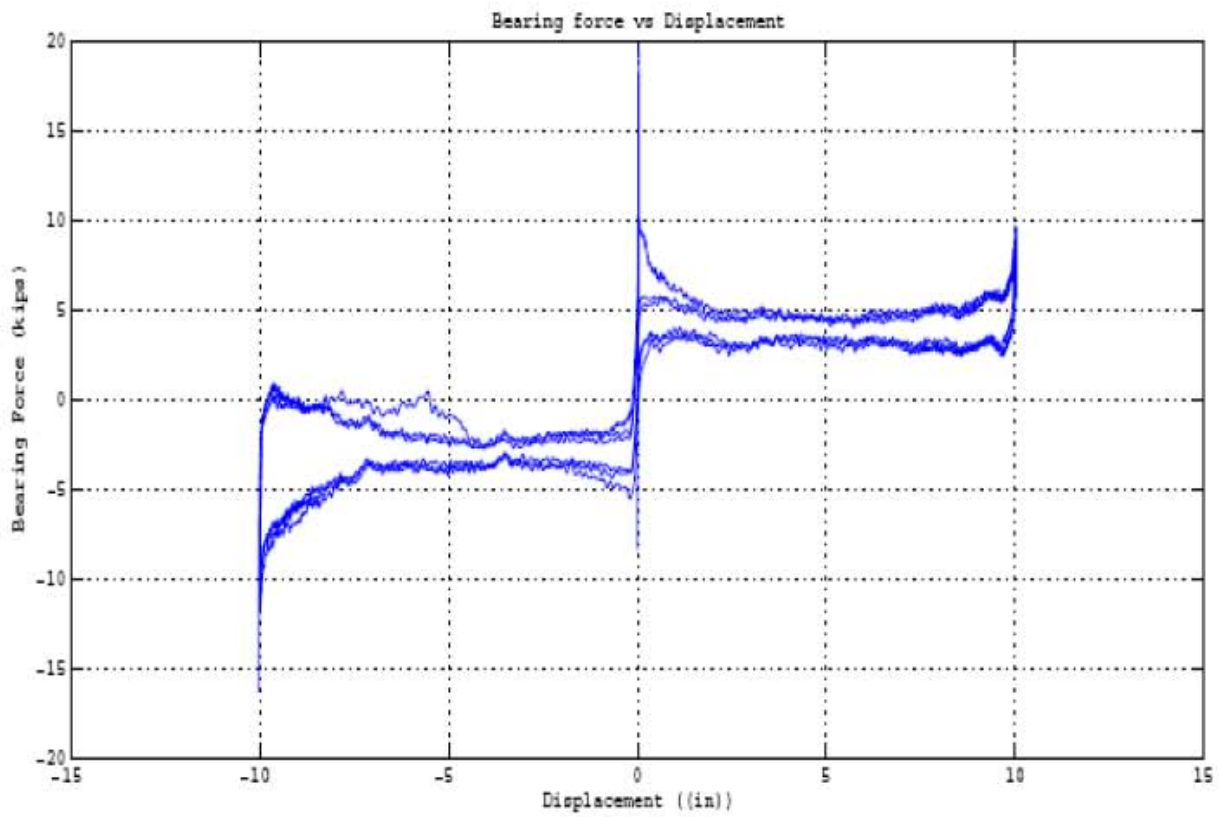
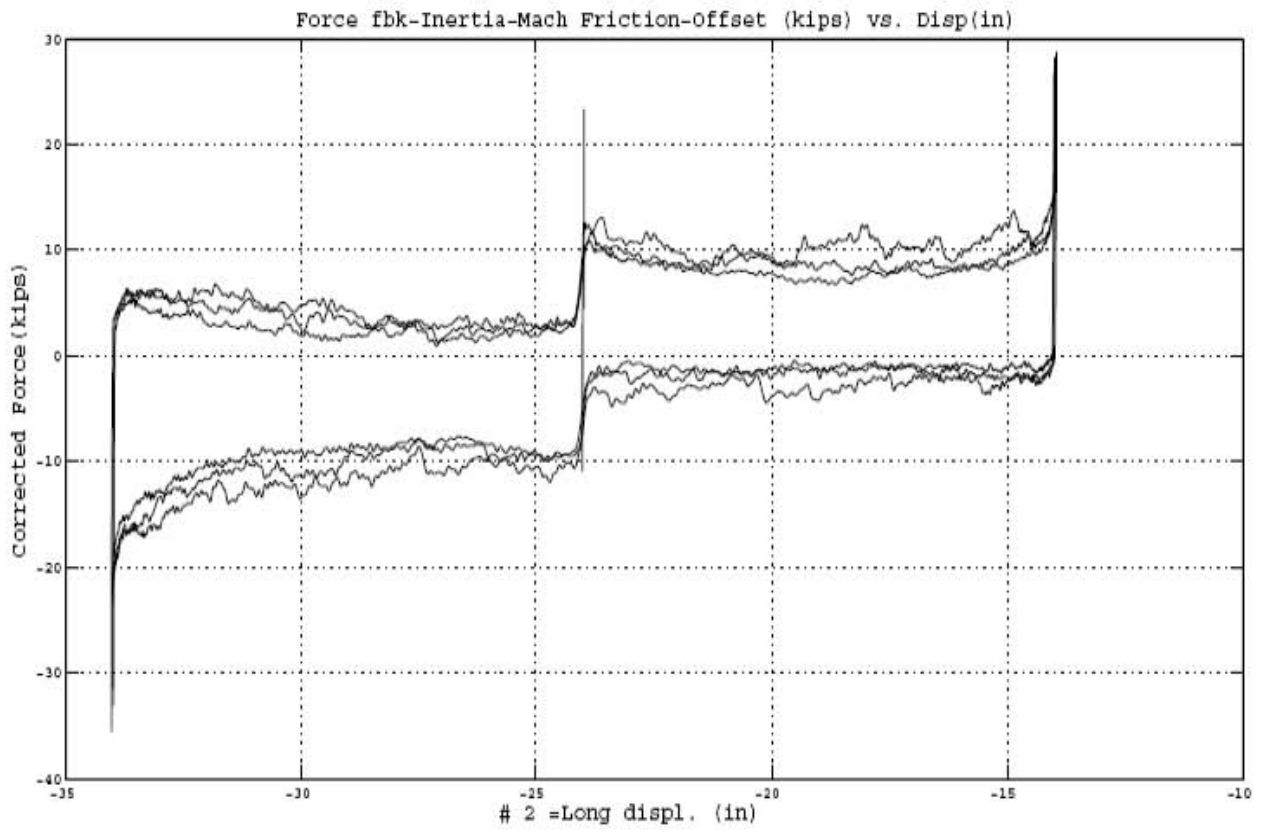


Figure 5-3 Results of Repeated Test #3 (continued).

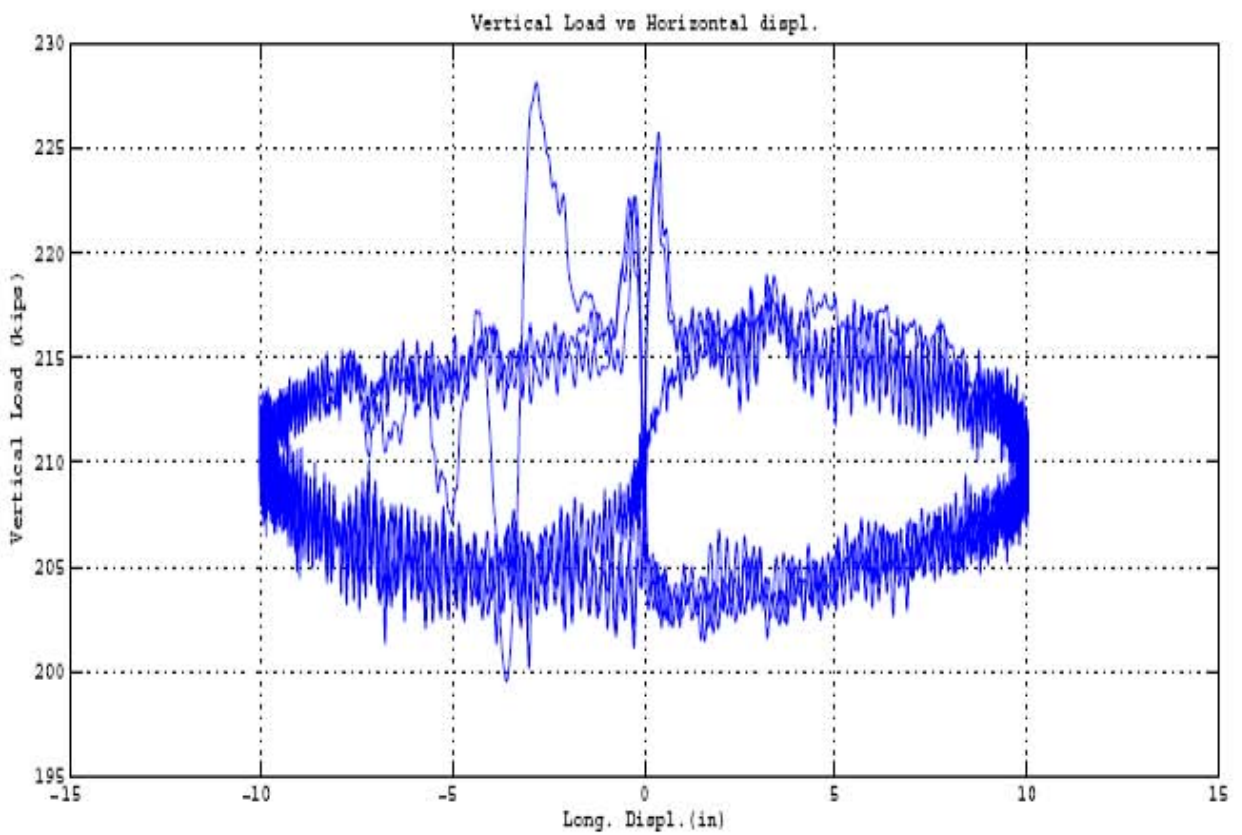
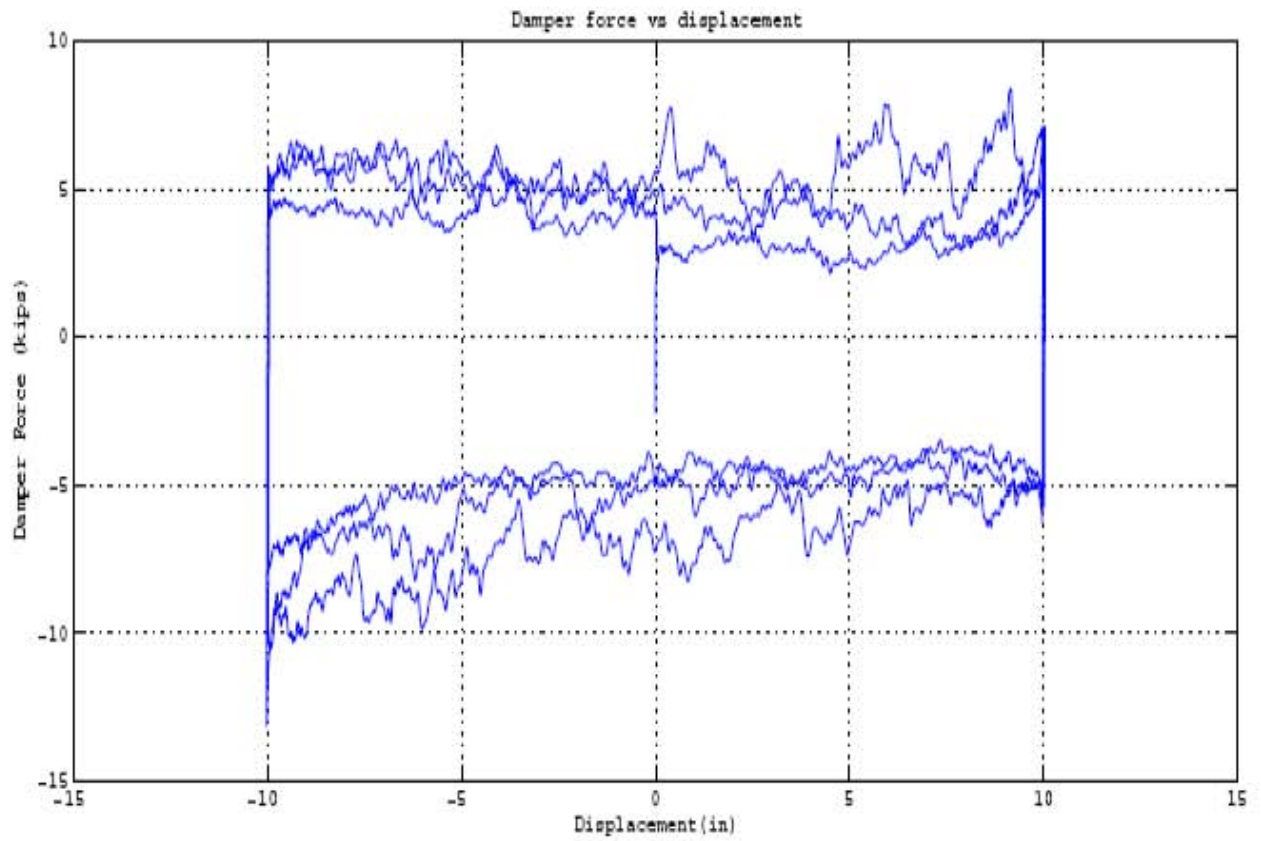


Figure 5-3 Results of Repeated Test #3 (continued).

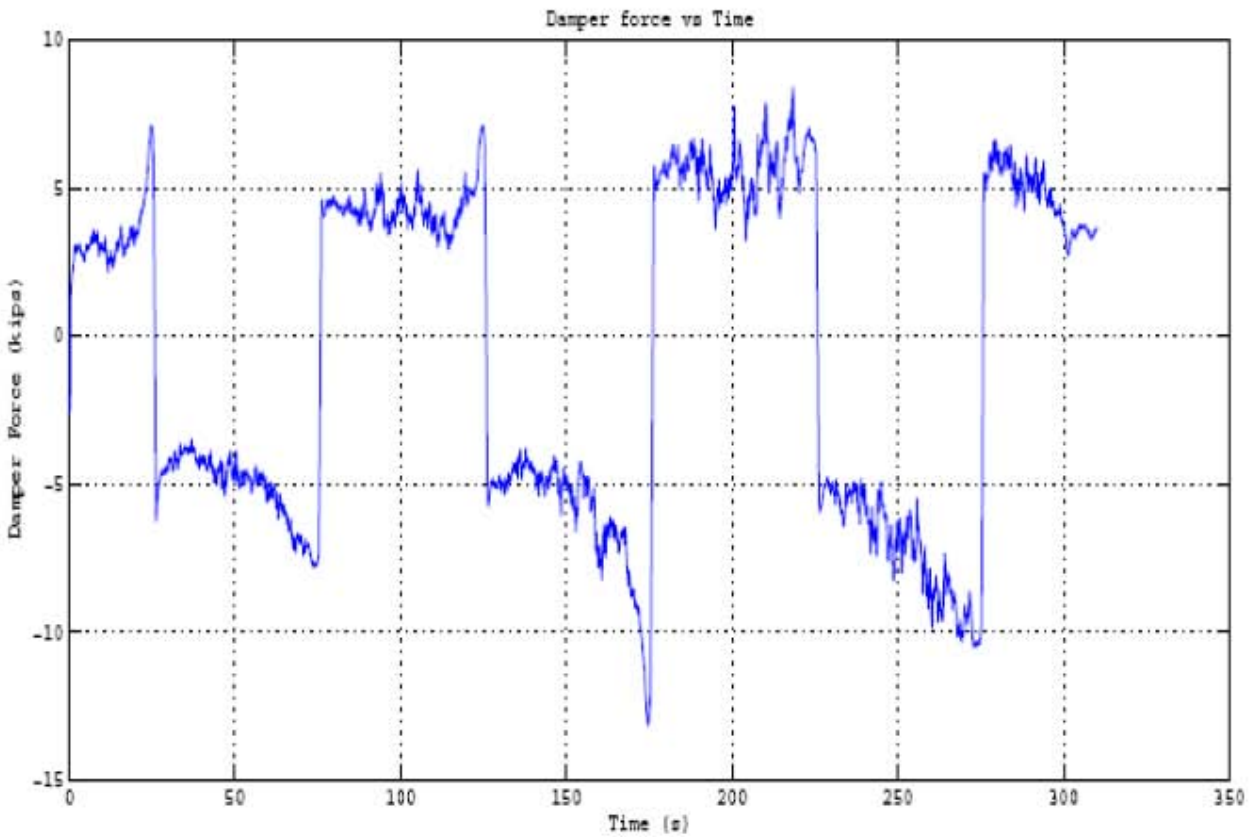
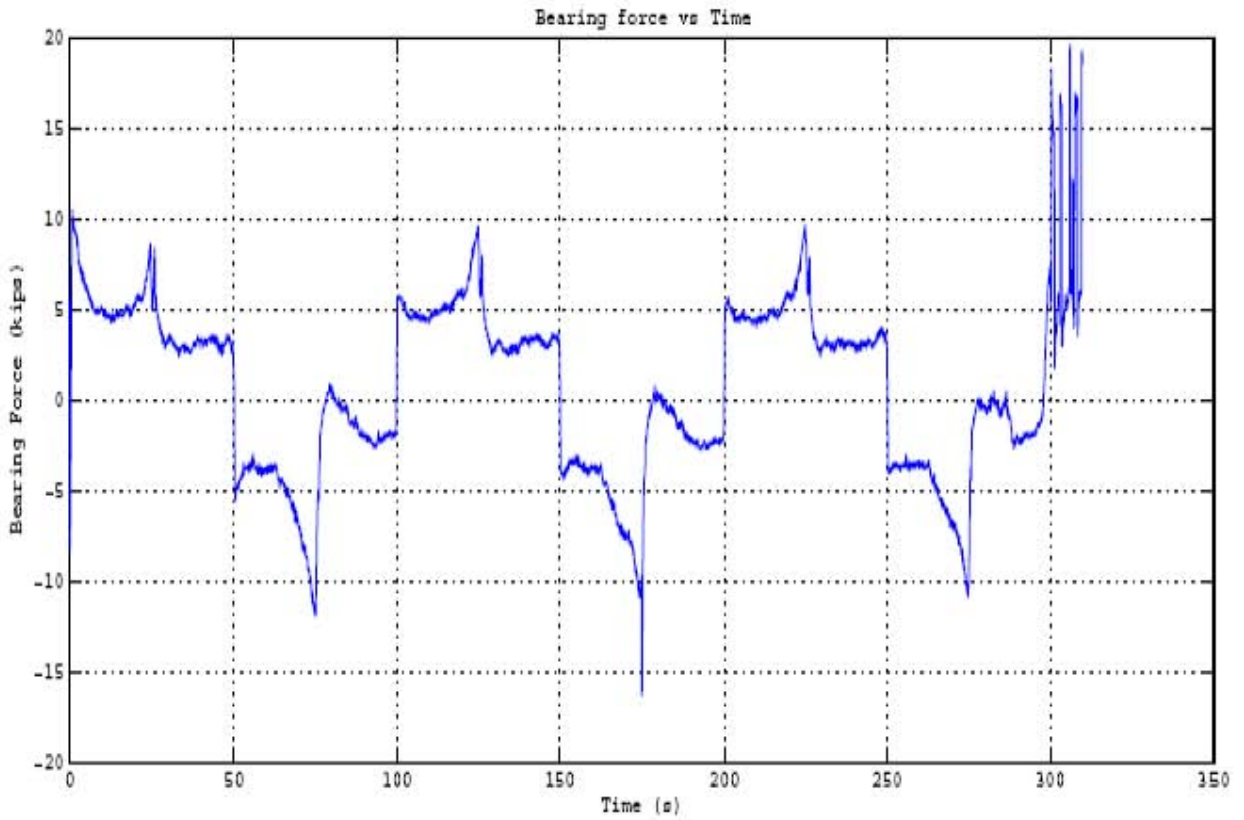


Figure 5-3 Results of Repeated Test #3 (continued).

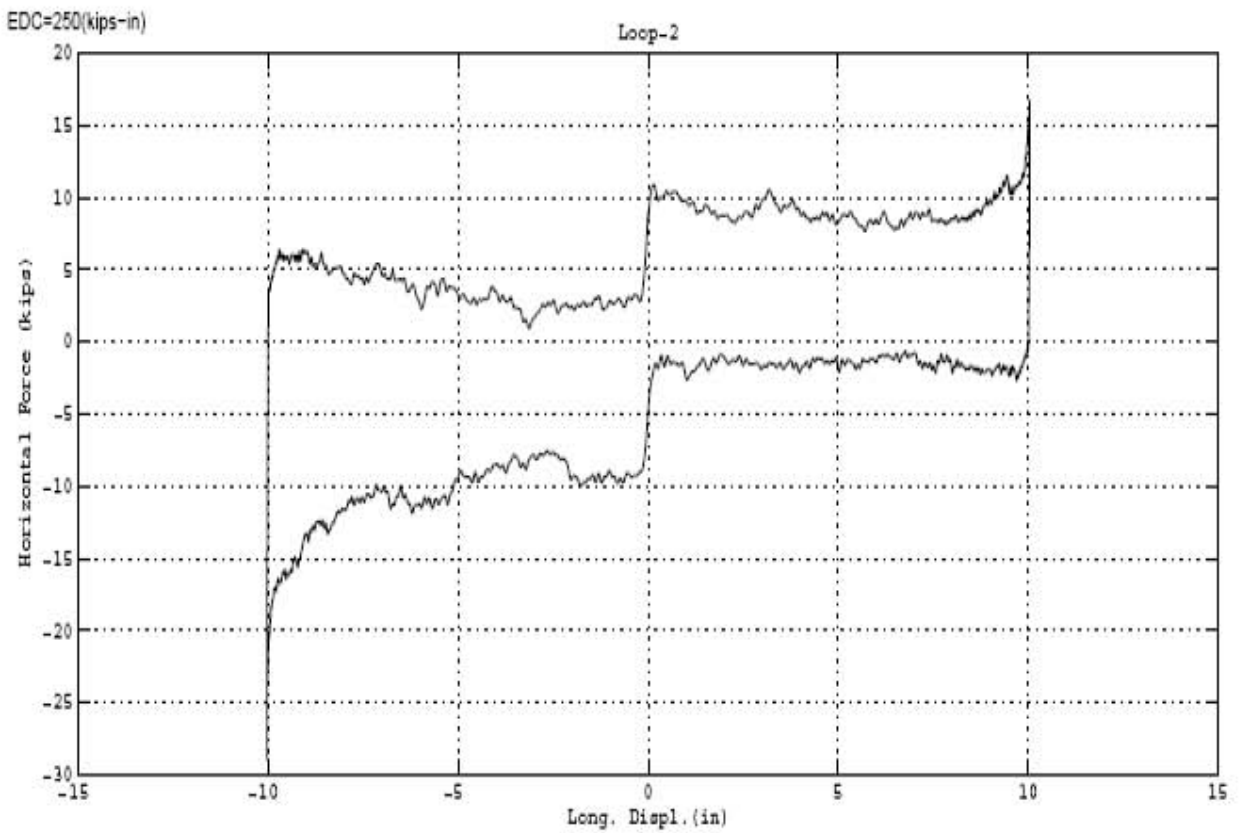
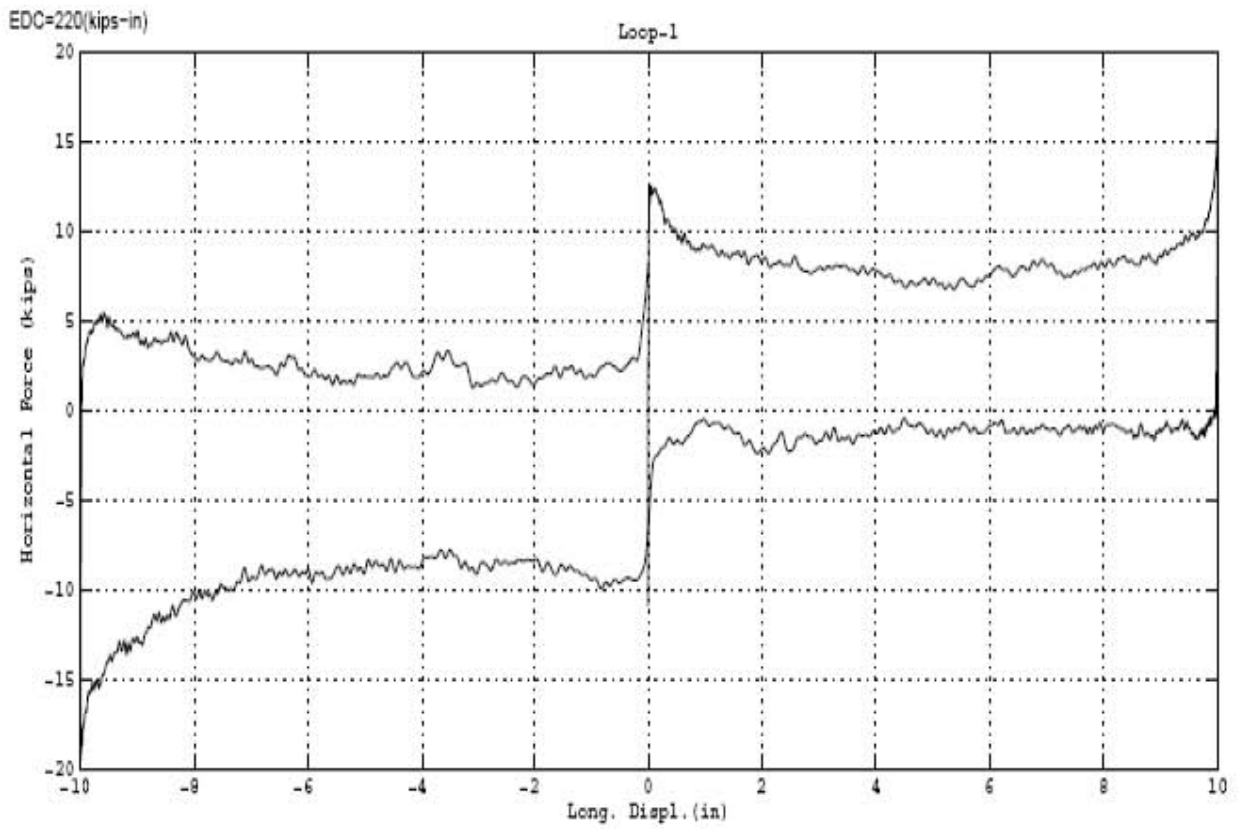


Figure 5-3 Results of Repeated Test #3 (continued).

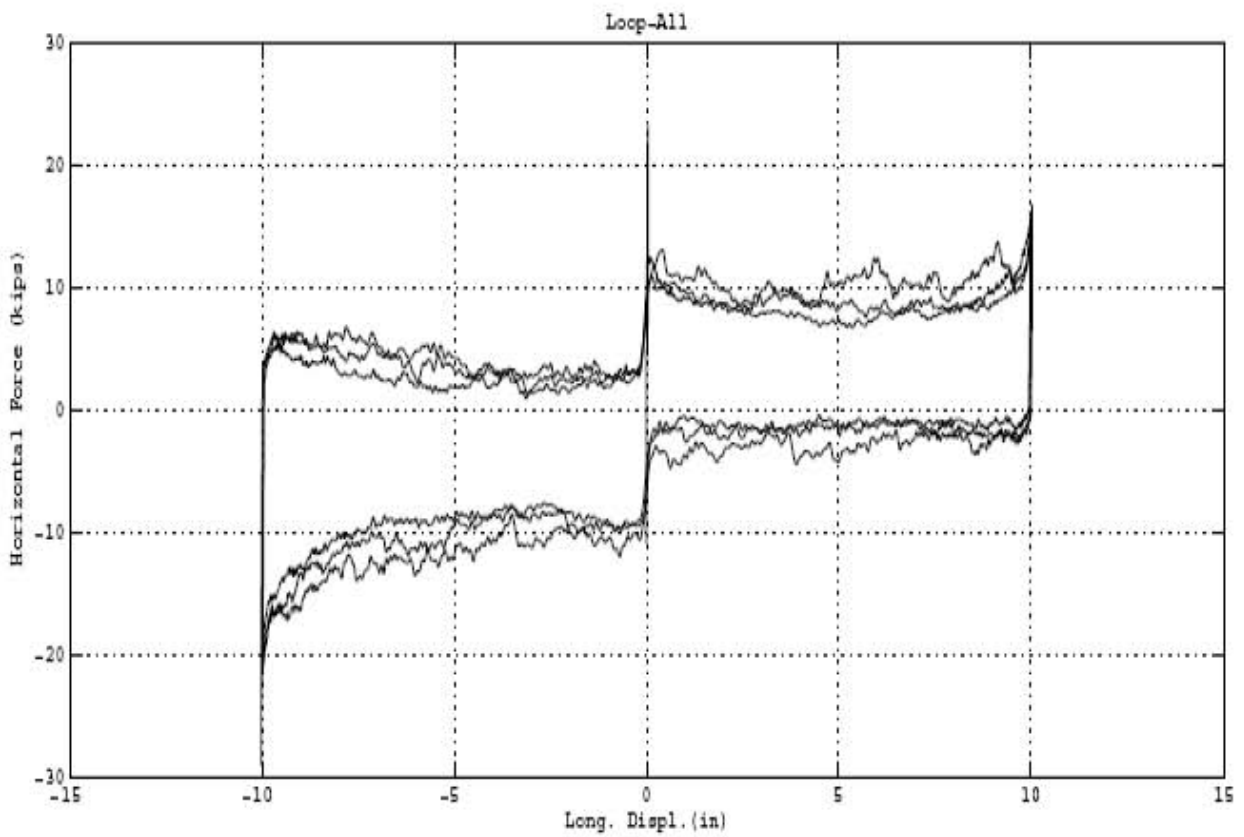
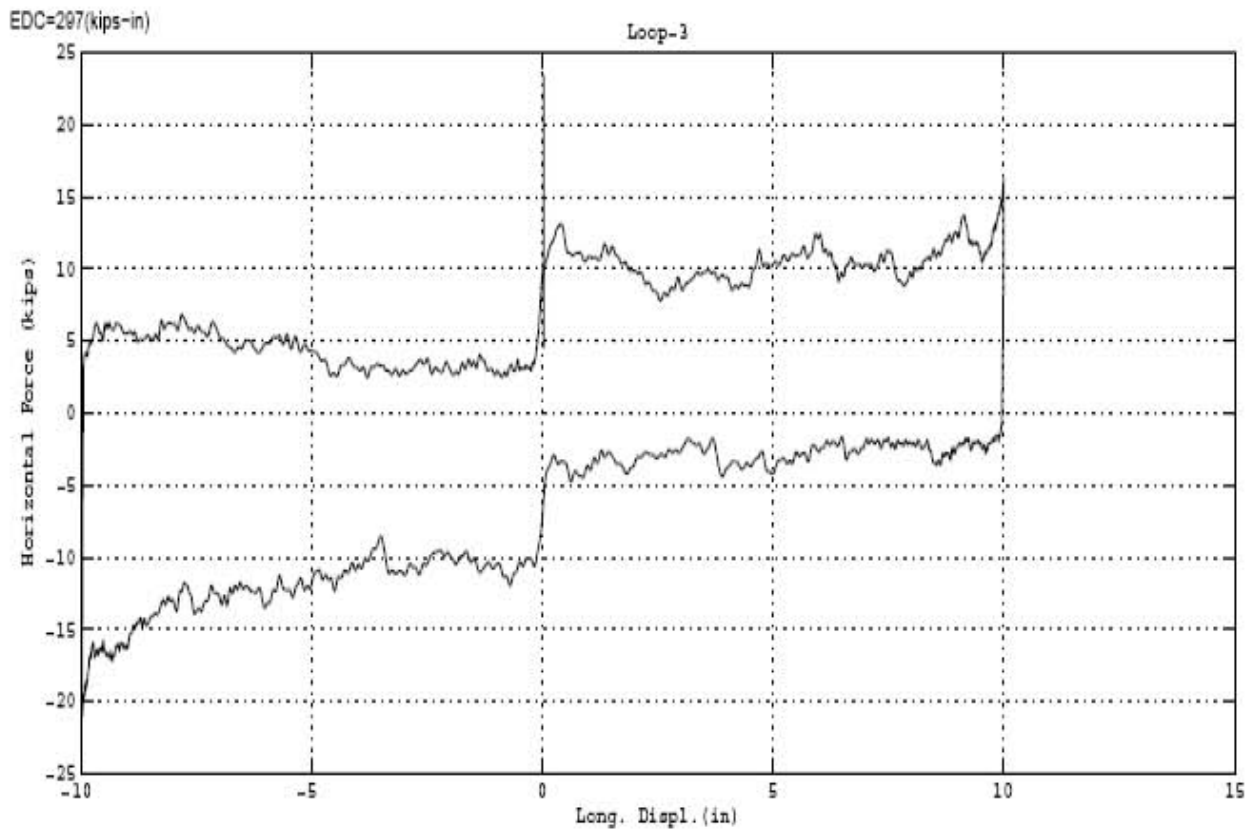


Figure 5-3 Results of Repeated Test #3 (continued).

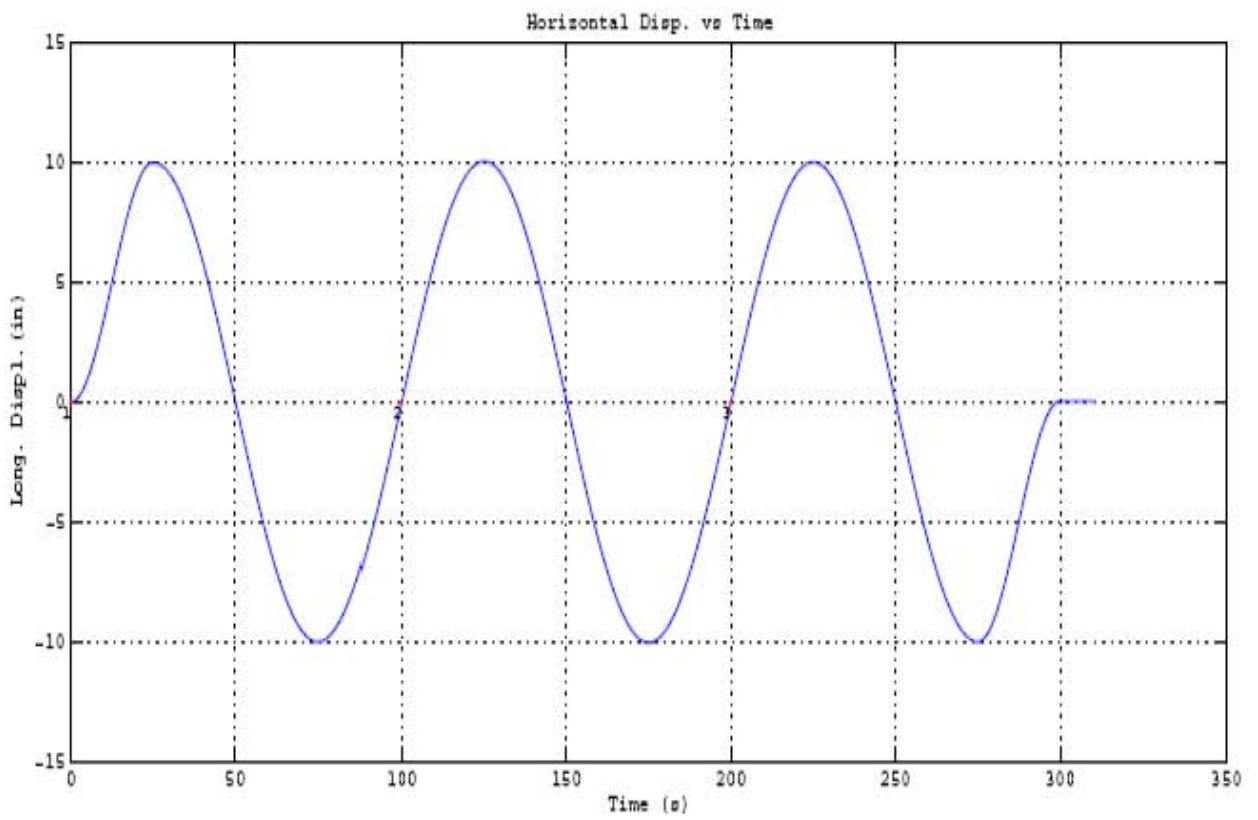
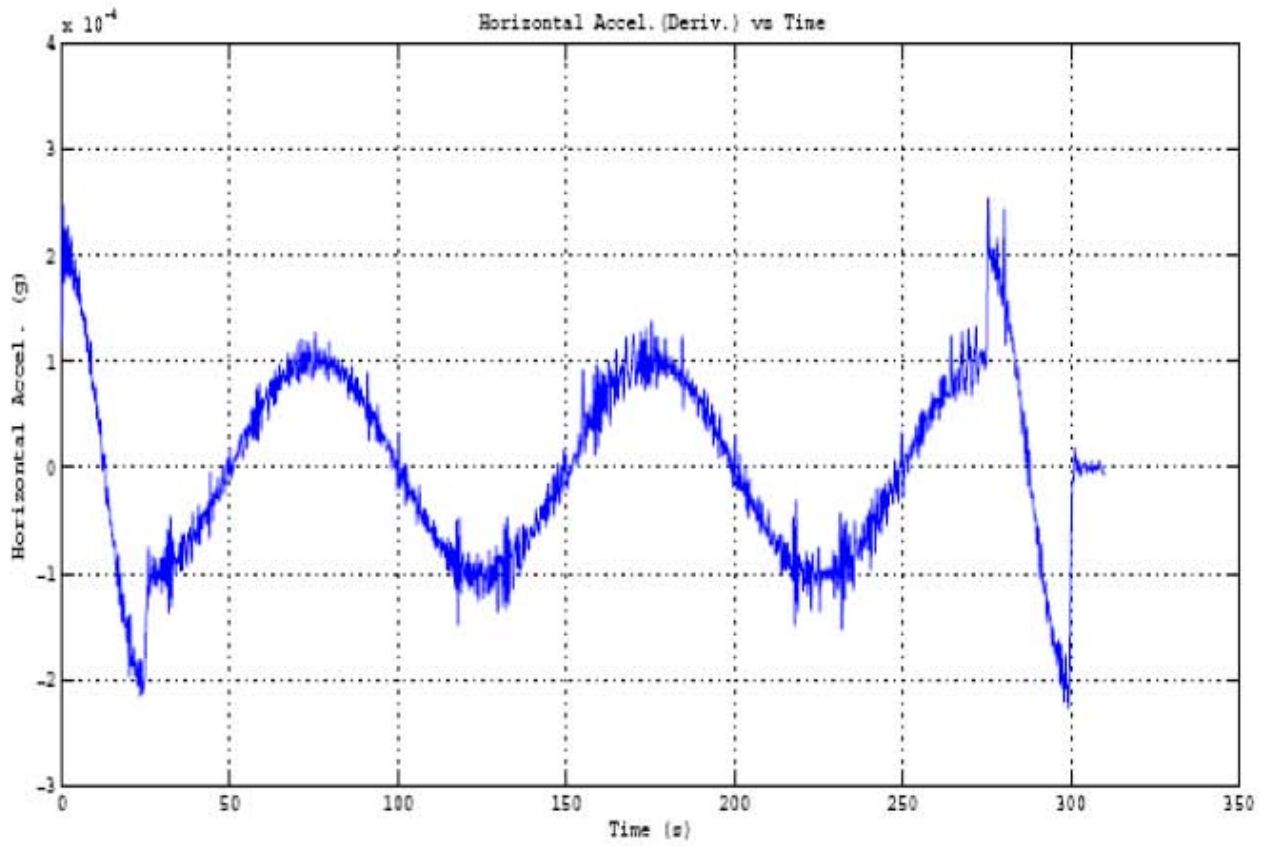


Figure 5-3 Results of Repeated Test #3 (continued).

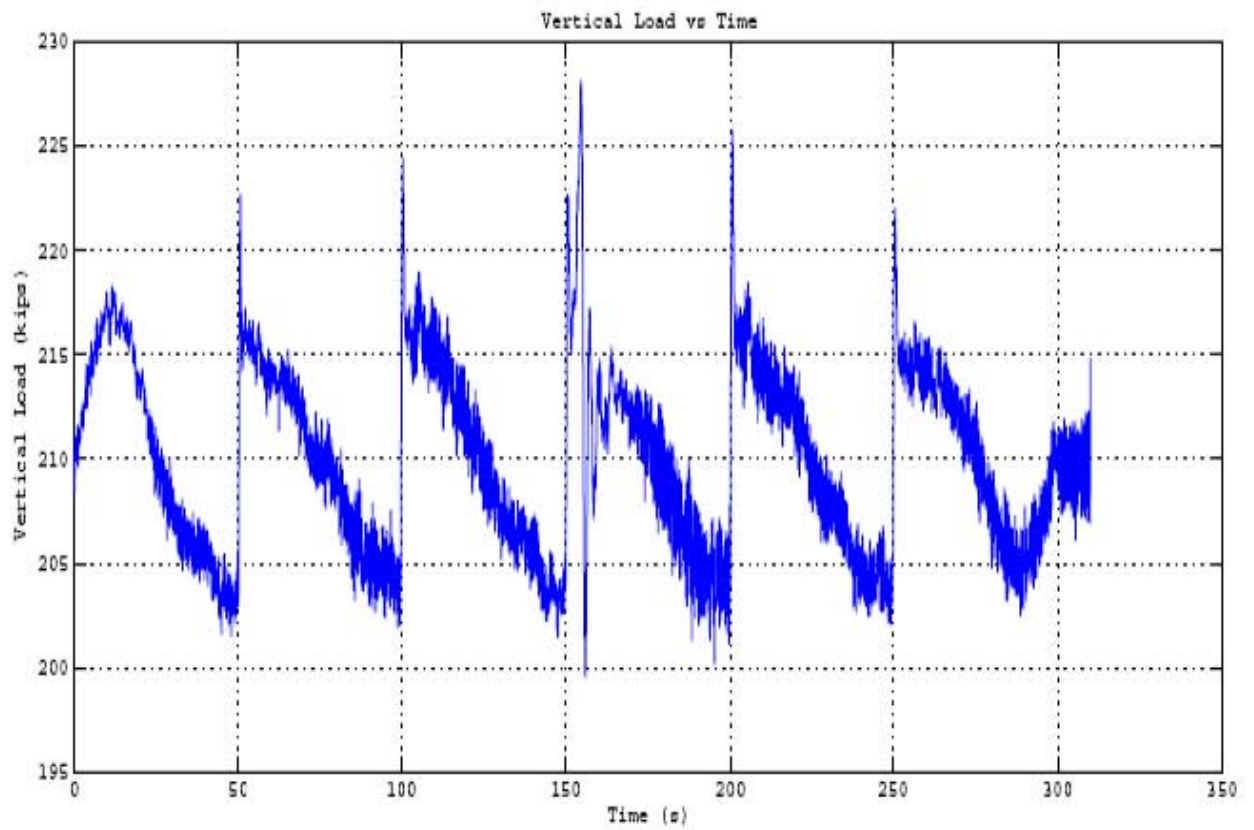
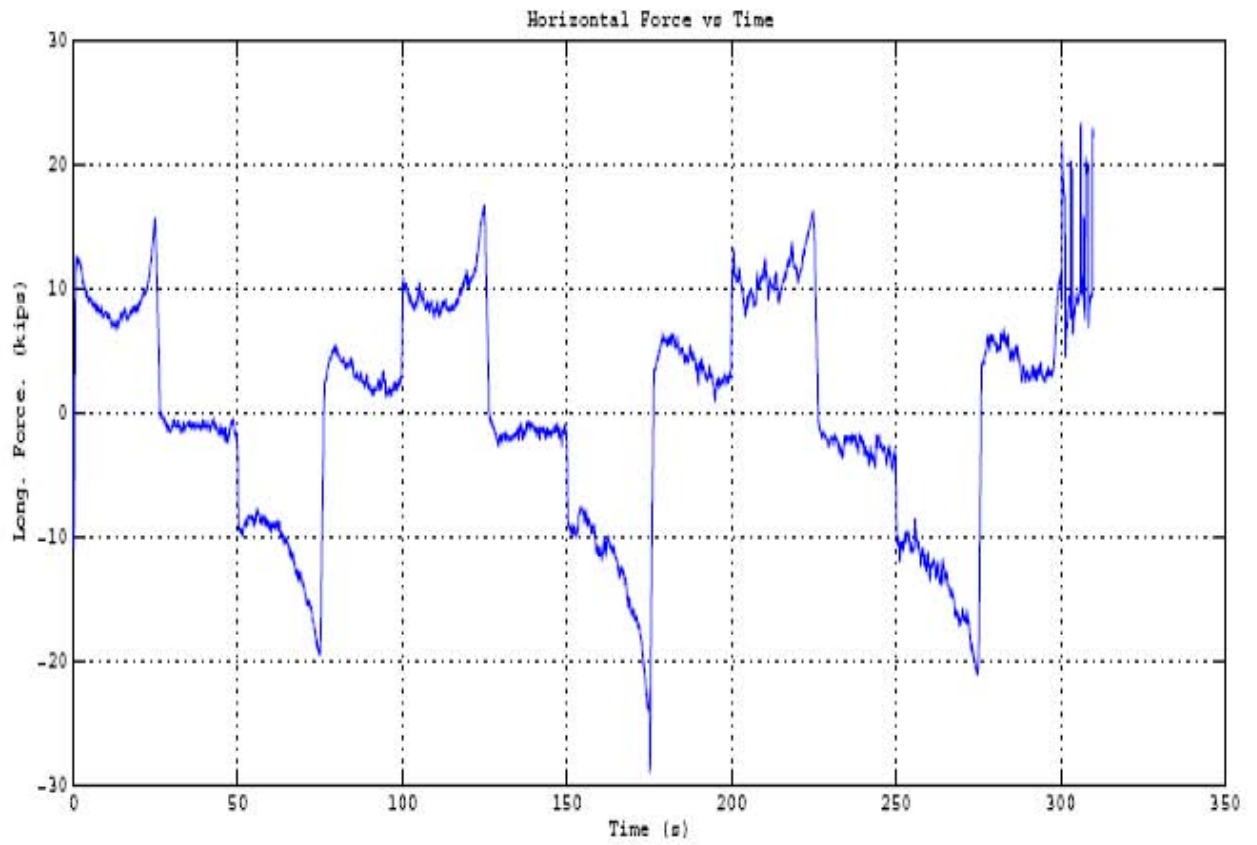


Figure 5-3 Results of Repeated Test #3 (continued).

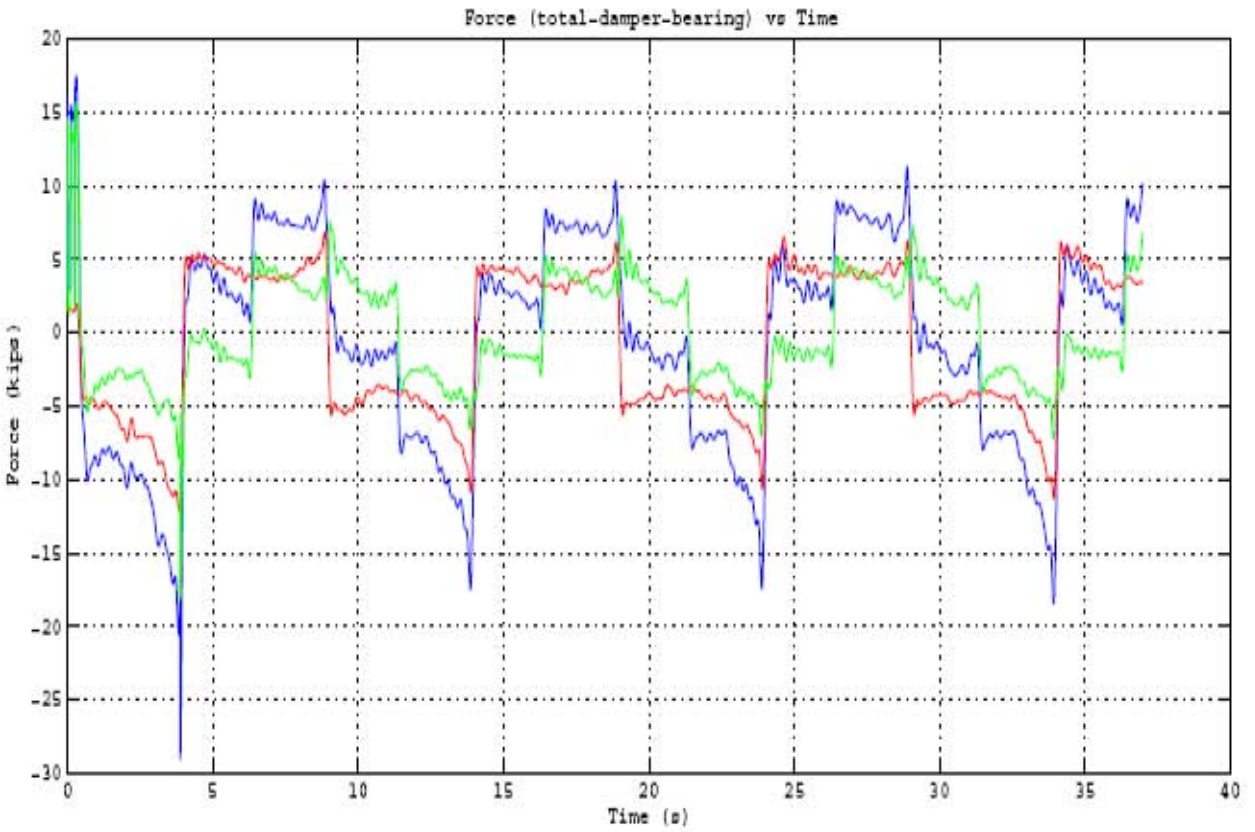
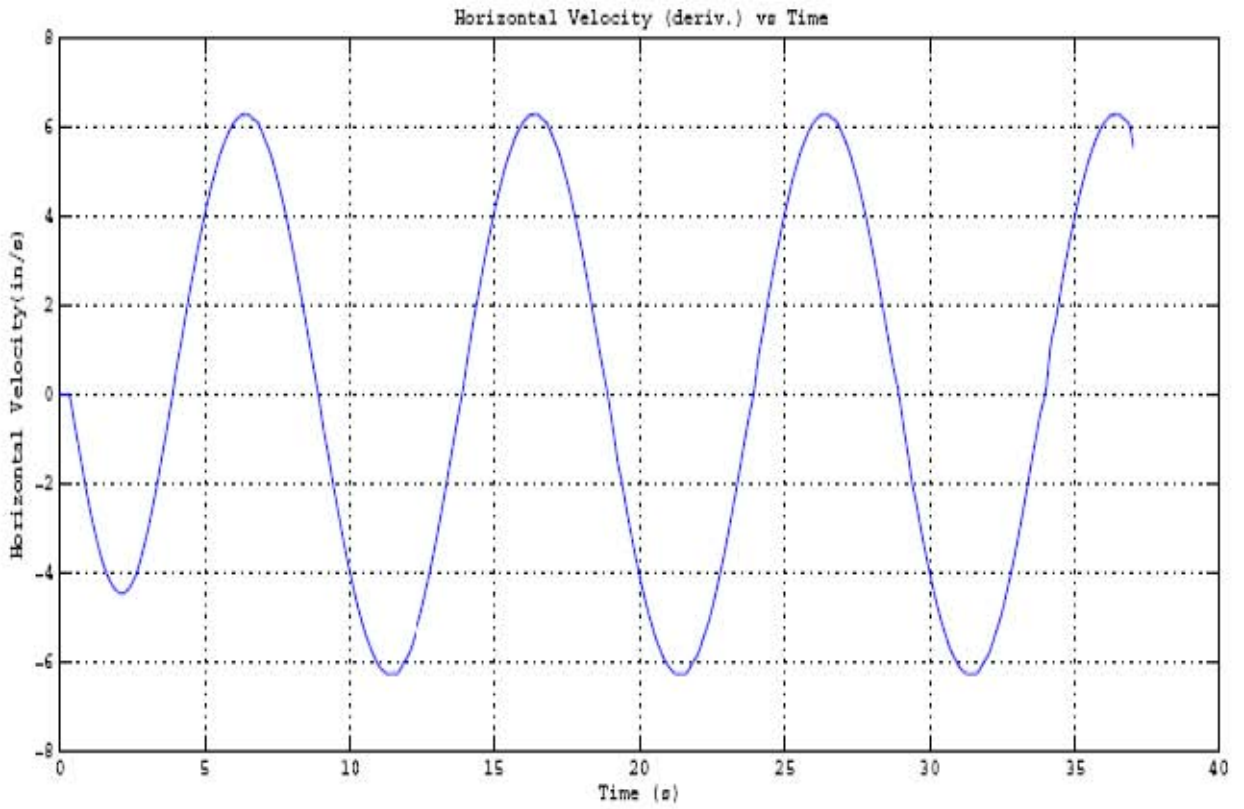


Figure 5-4 Results of Repeated Test #4.

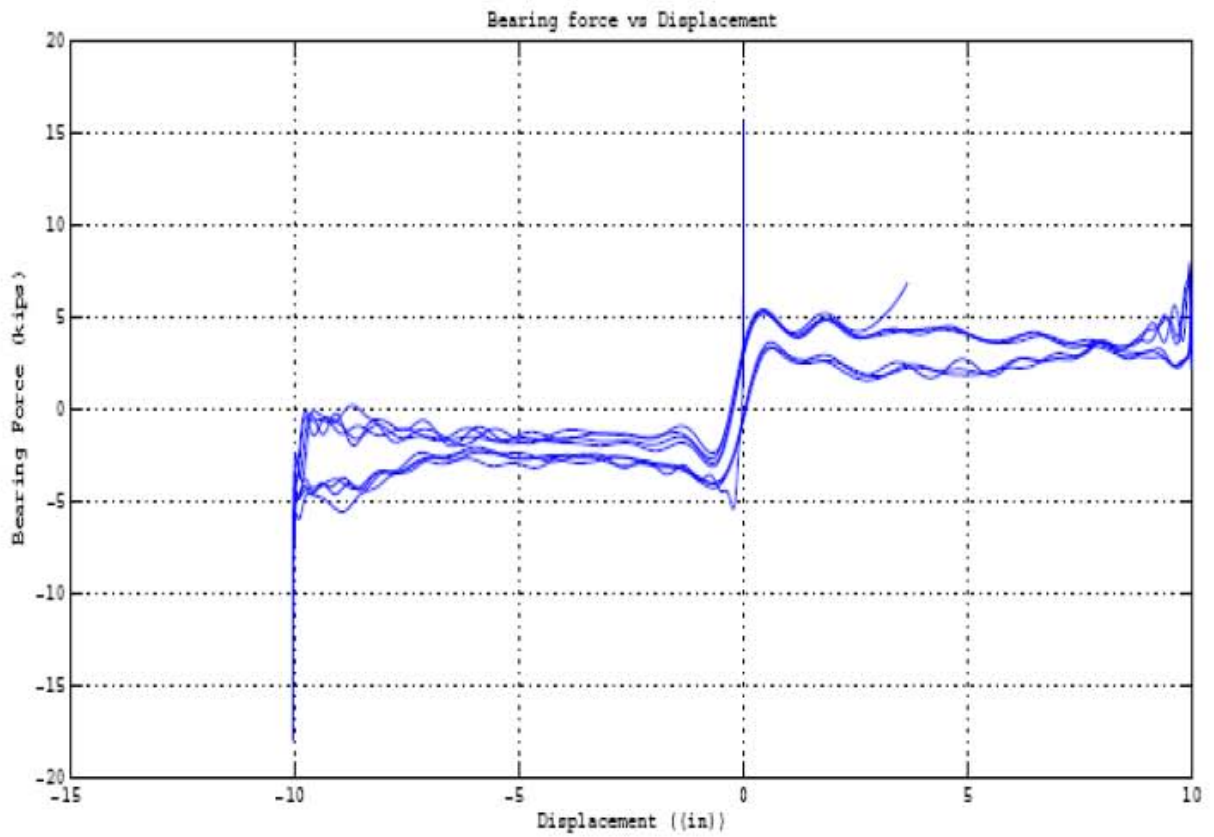
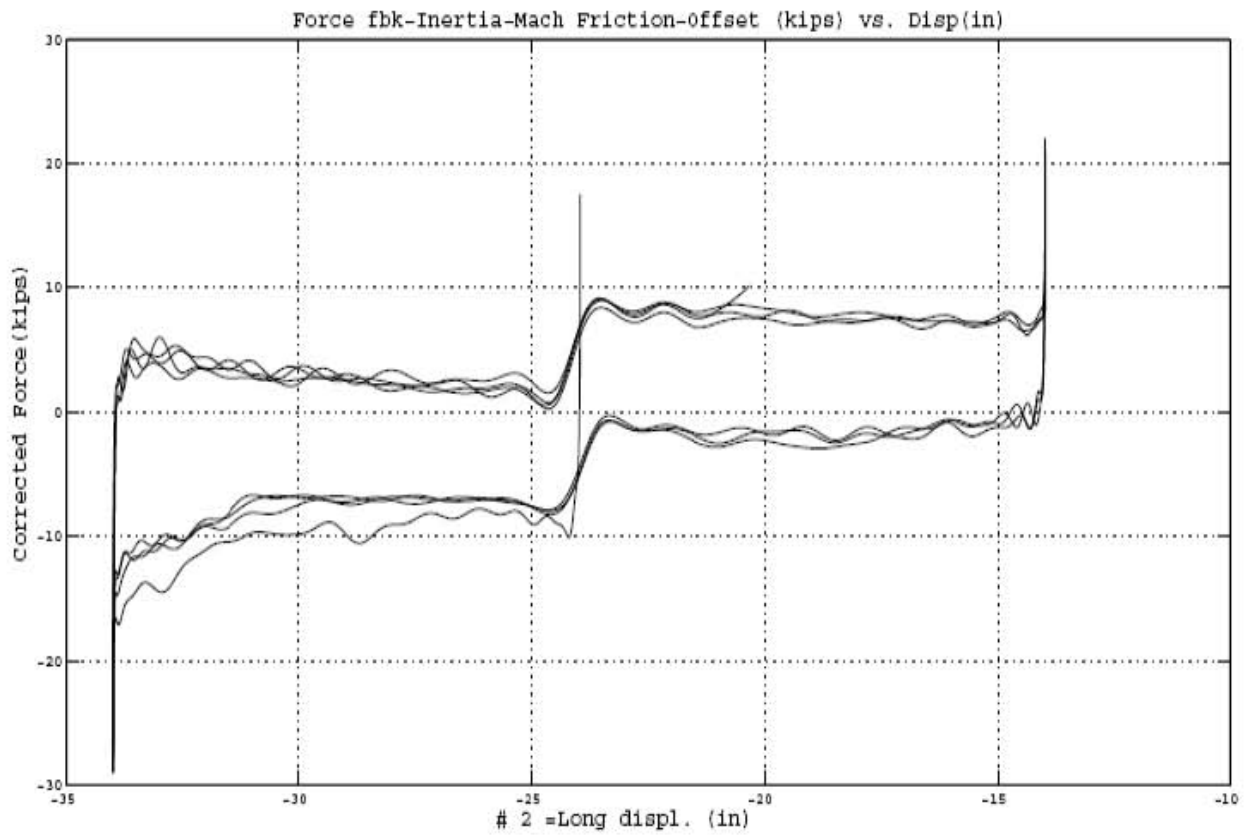


Figure 5-4 Results of Repeated Test #4 (continued).

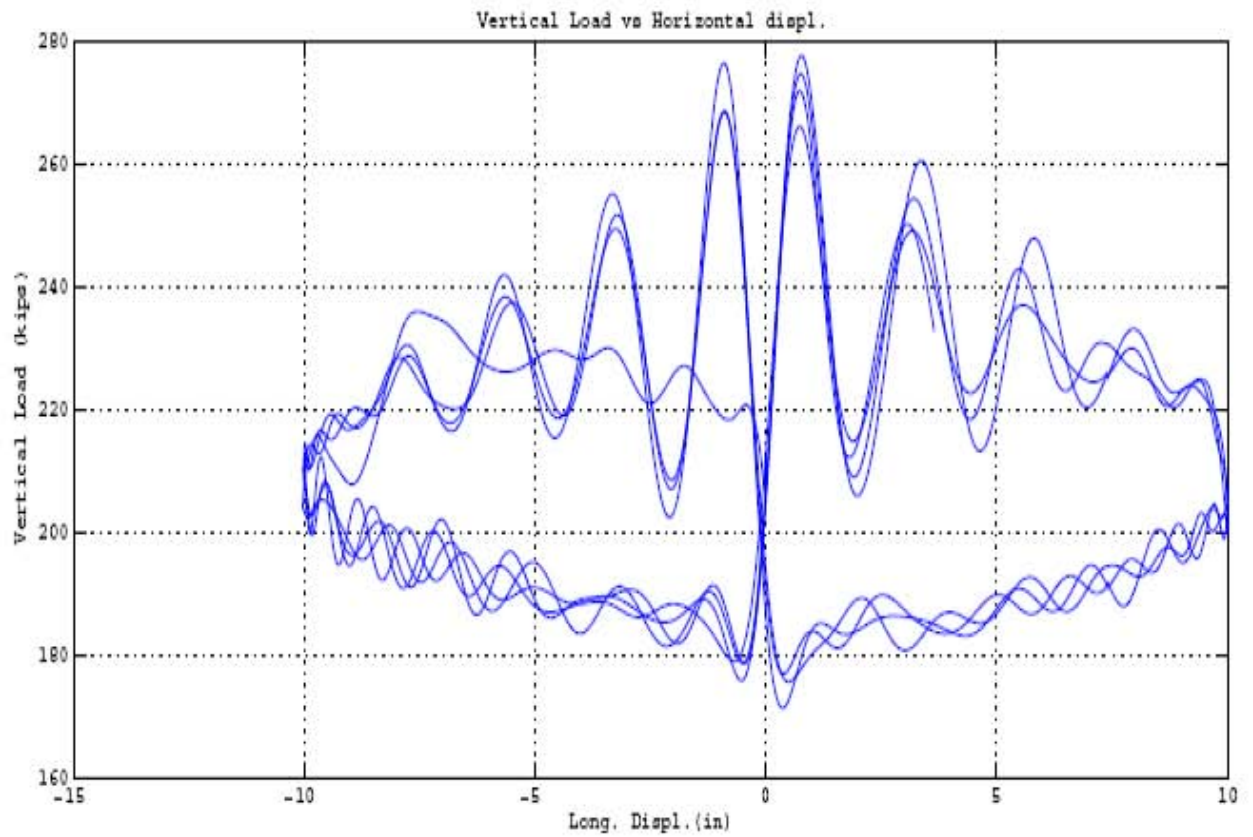
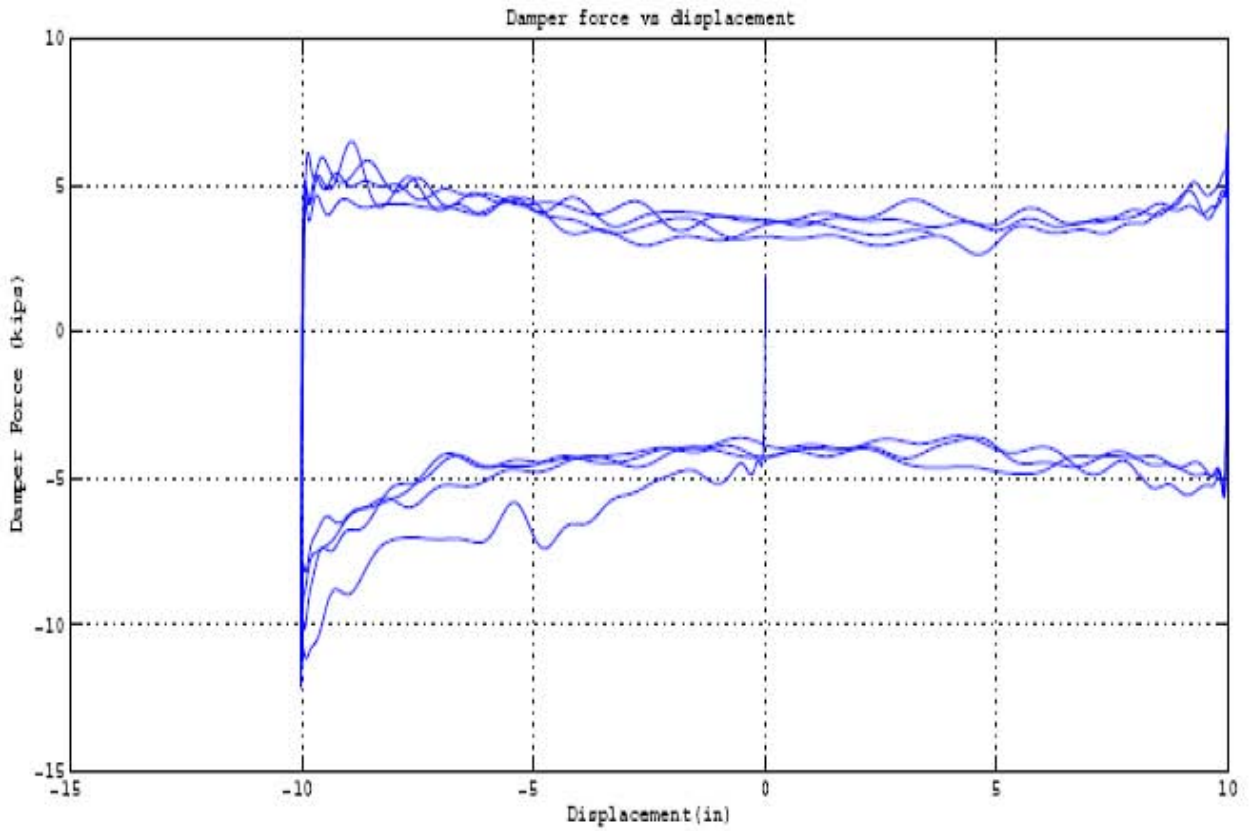


Figure 5-4 Results of Repeated Test #4 (continued).

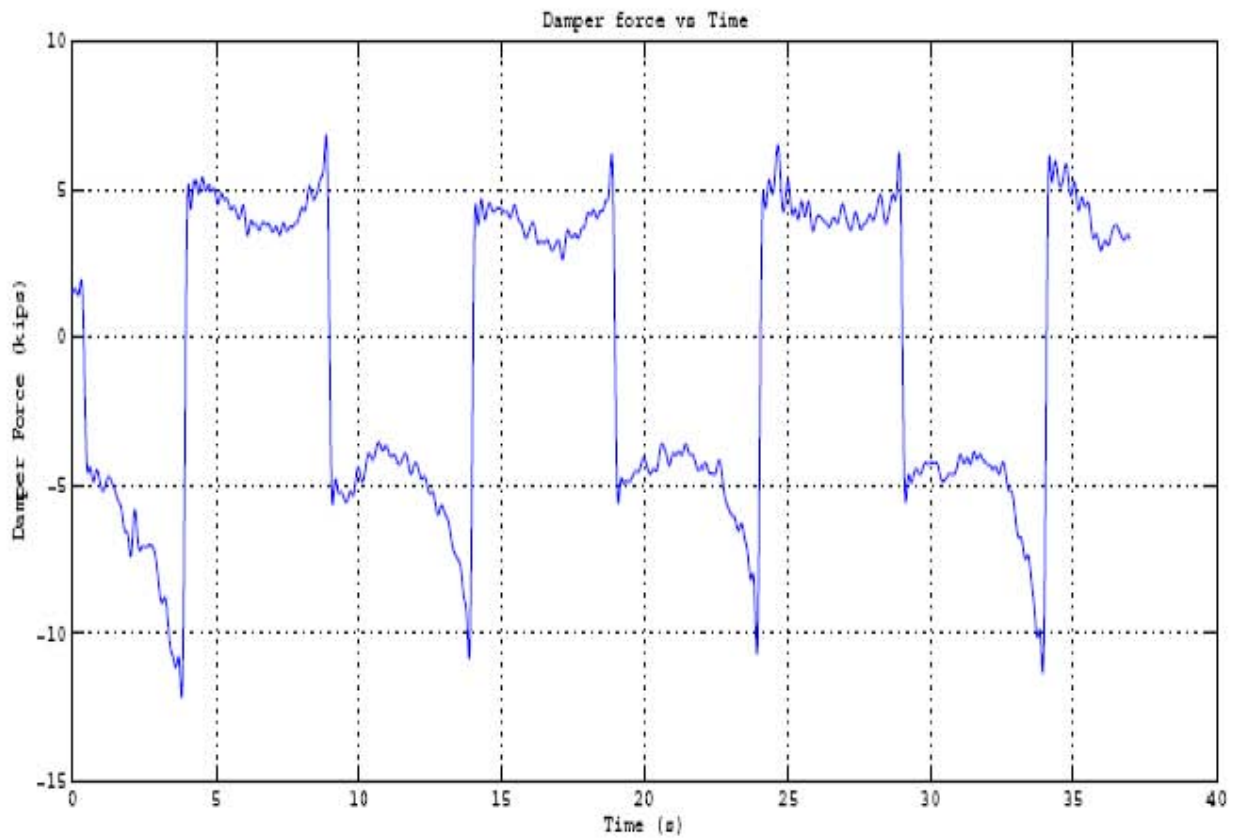
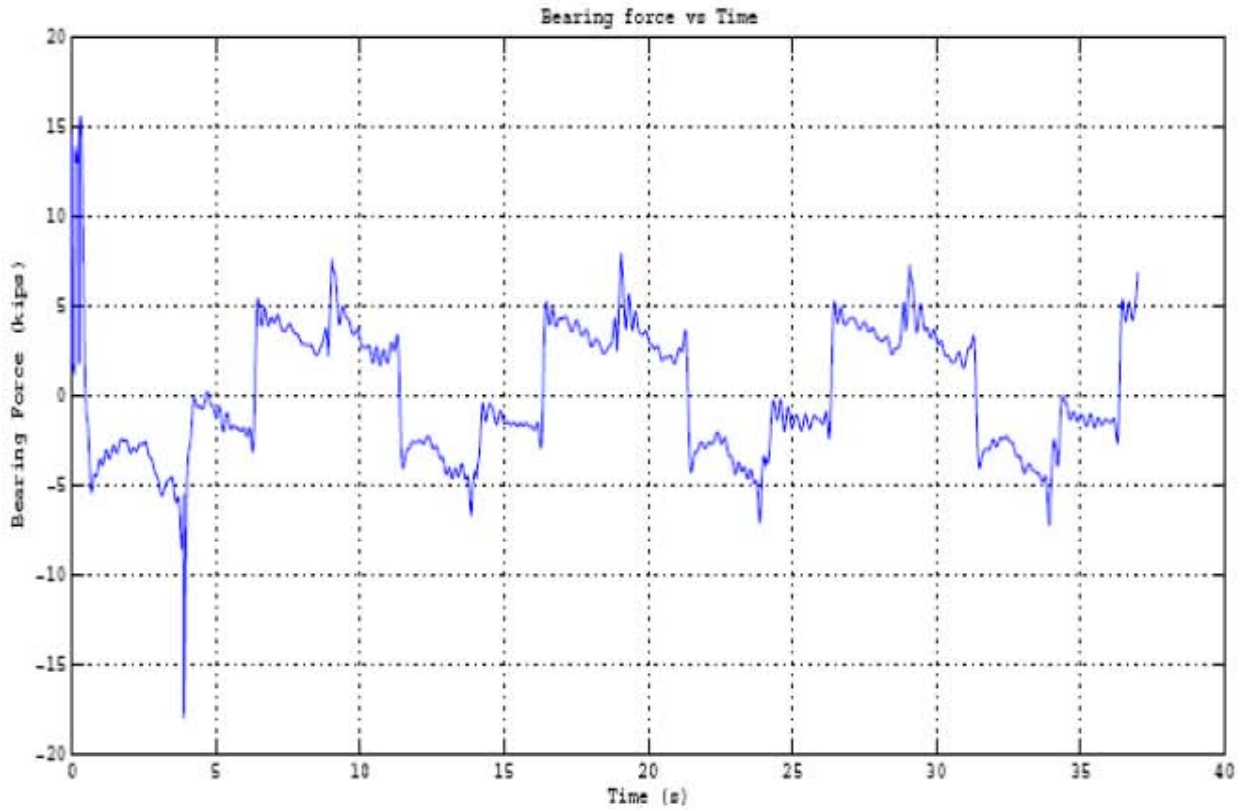


Figure 5-4 Results of Repeated Test #4 (continued).

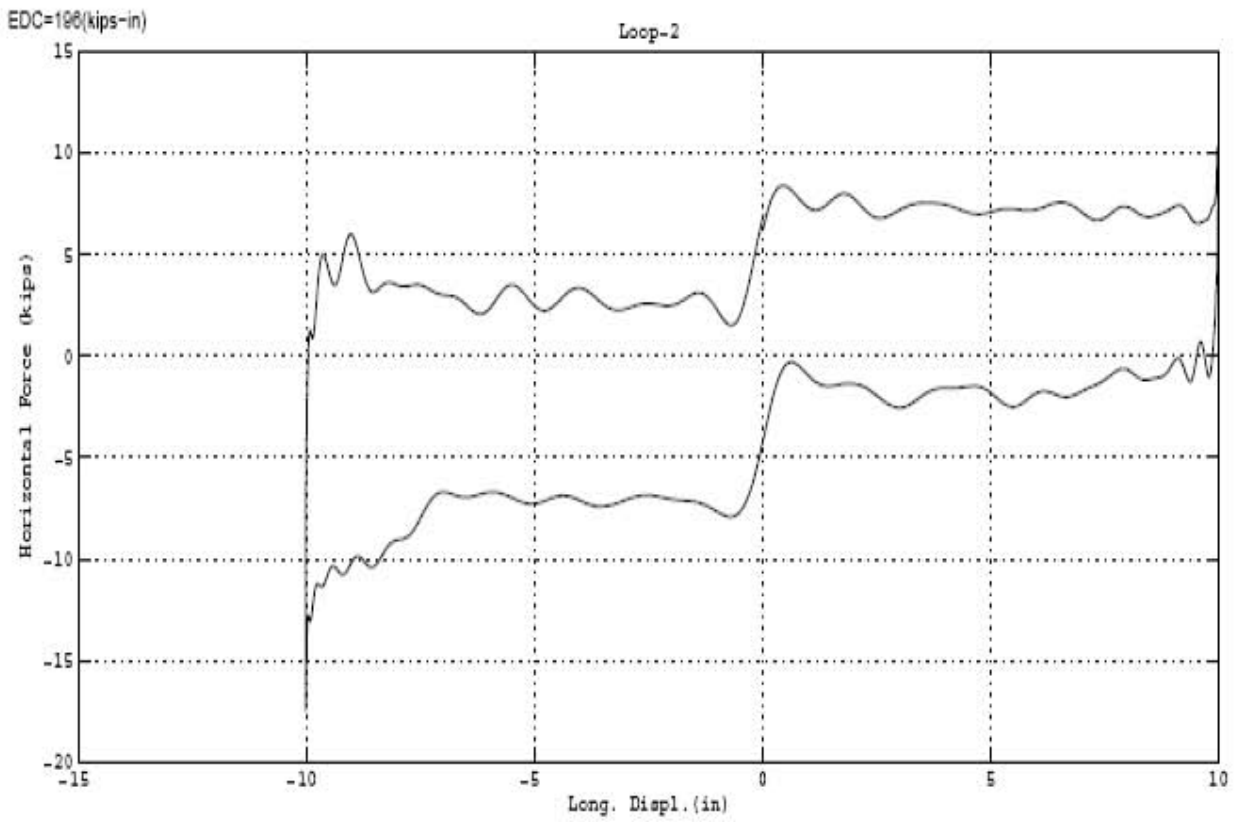
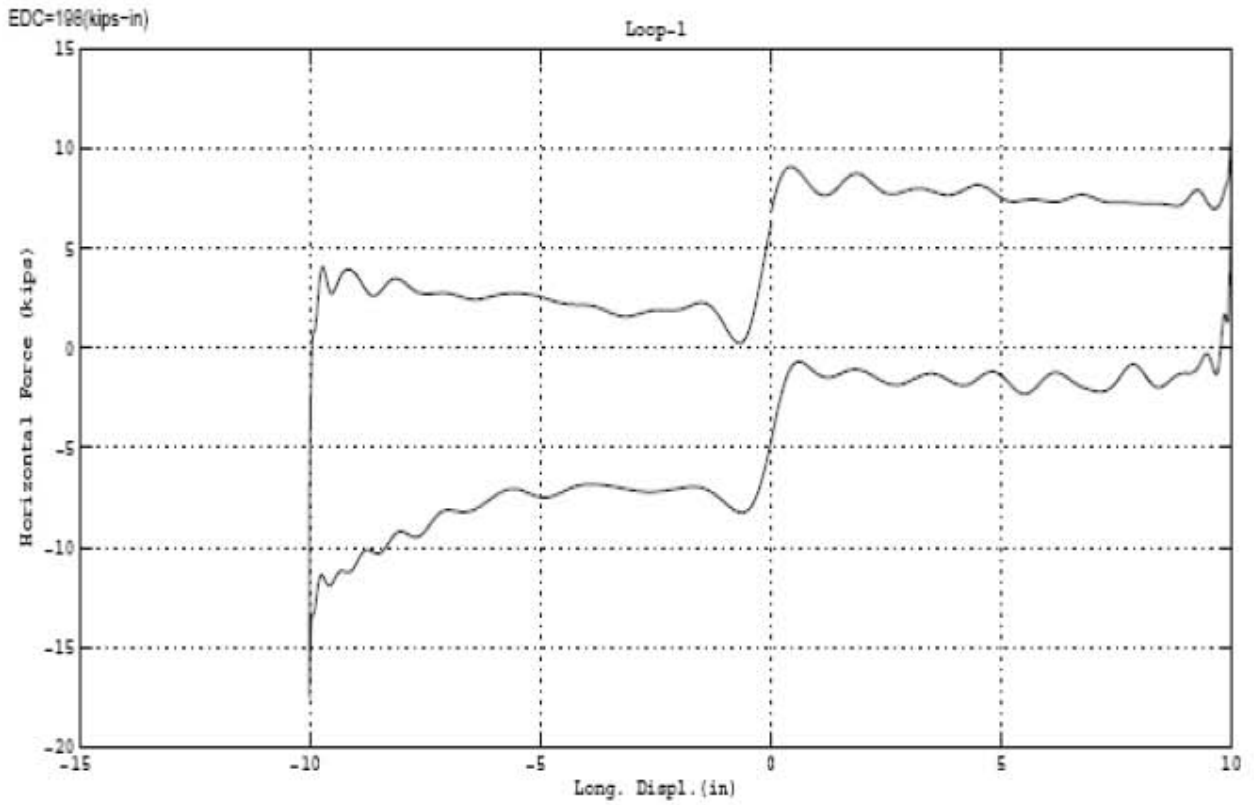


Figure 5-4 Results of Repeated Test #4 (continued).

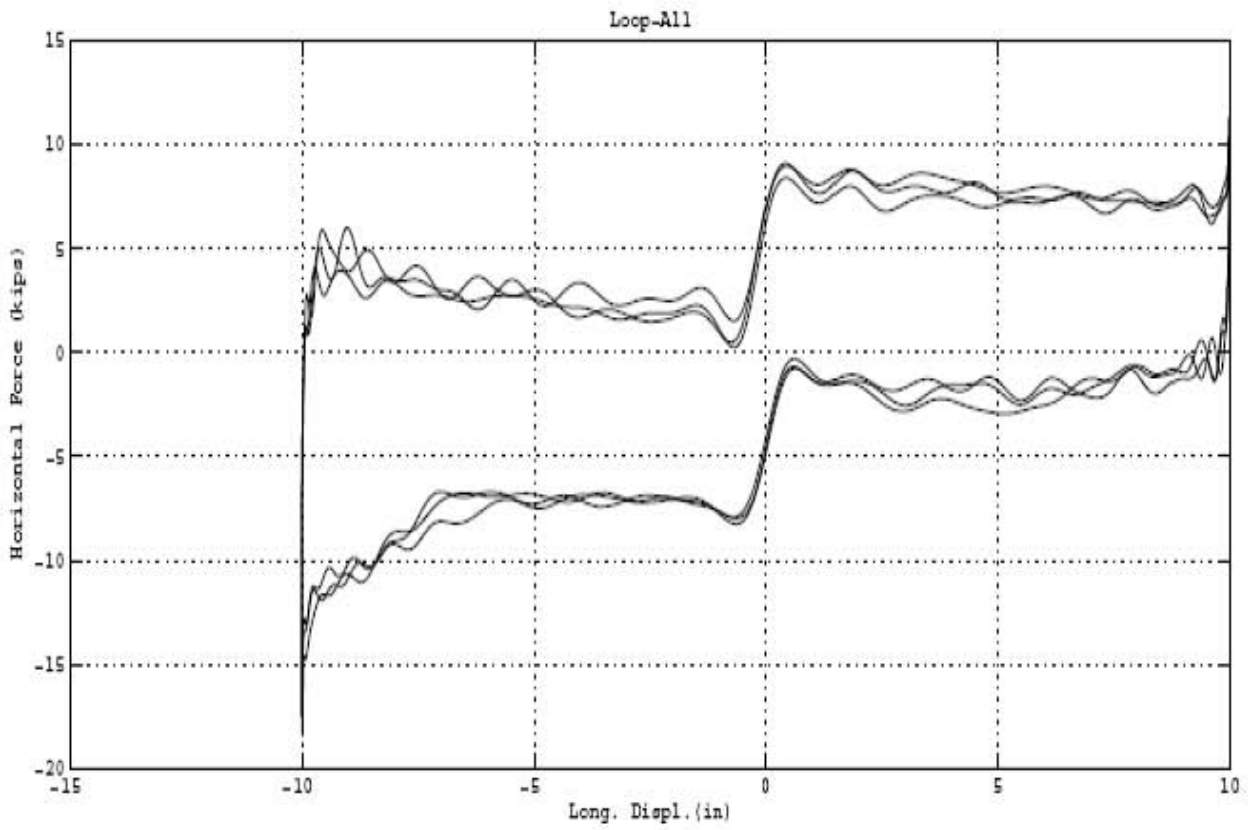
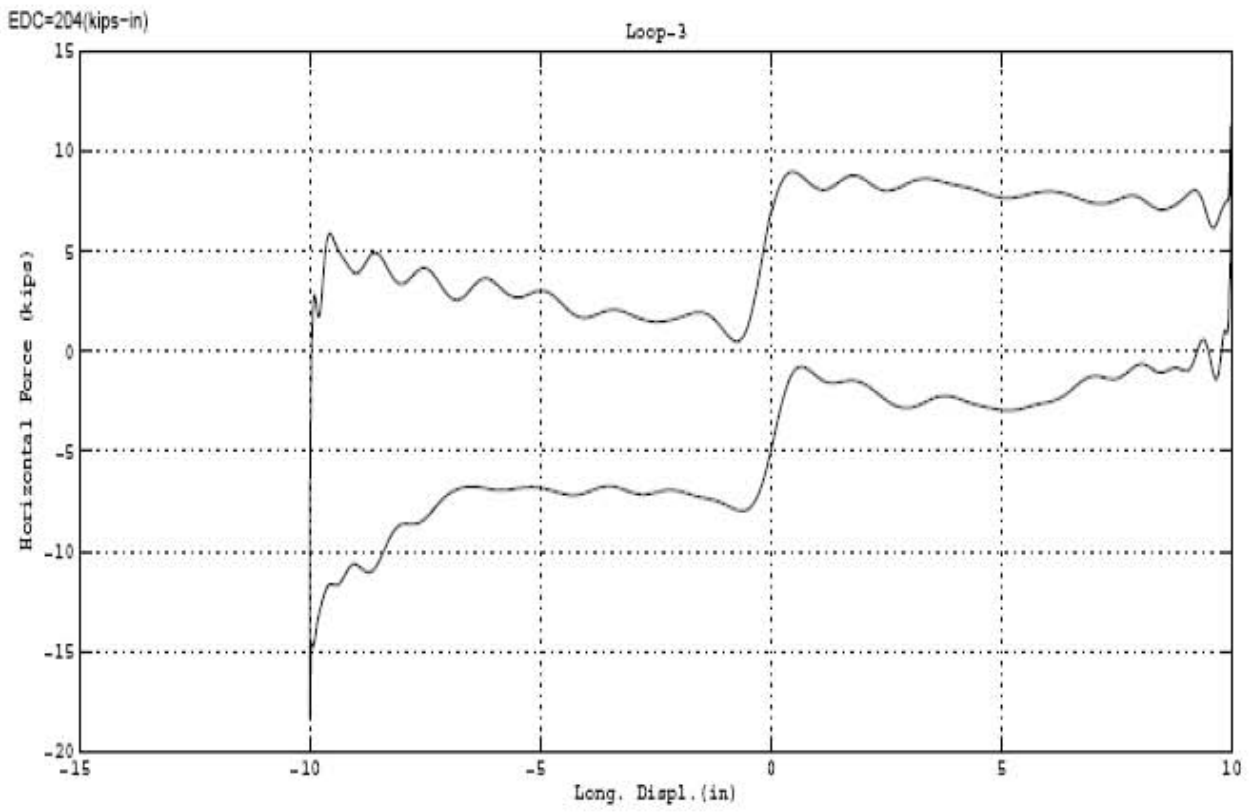


Figure 5-4 Results of Repeated Test #4 (continued).

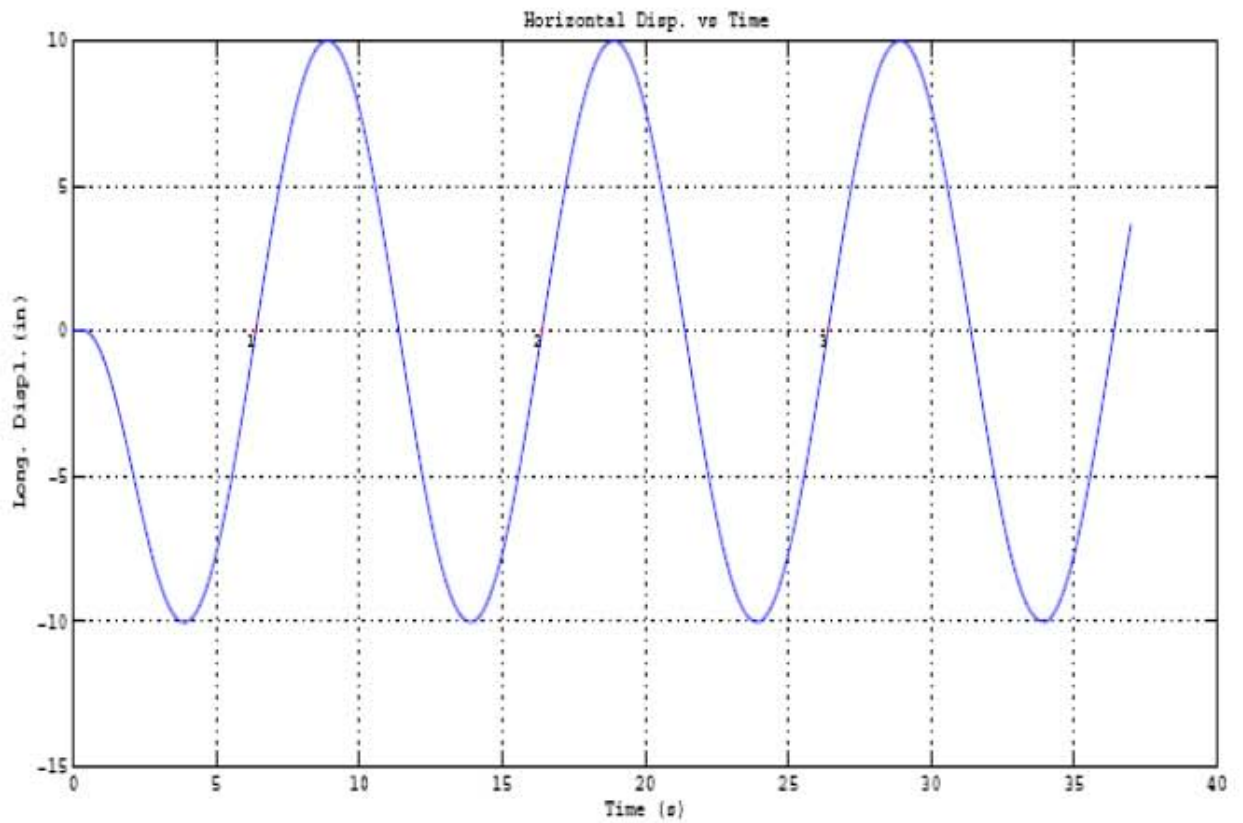
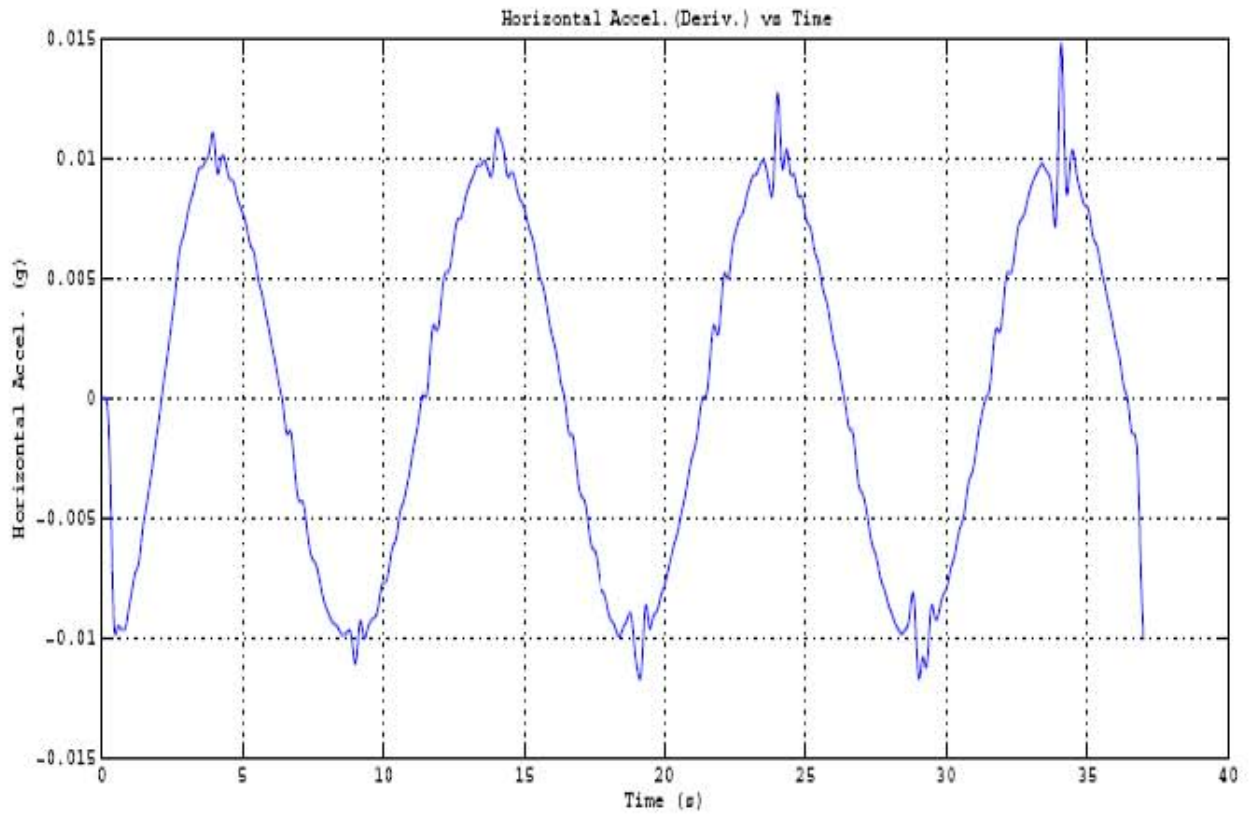


Figure 5-4 Results of Repeated Test #4 (continued).

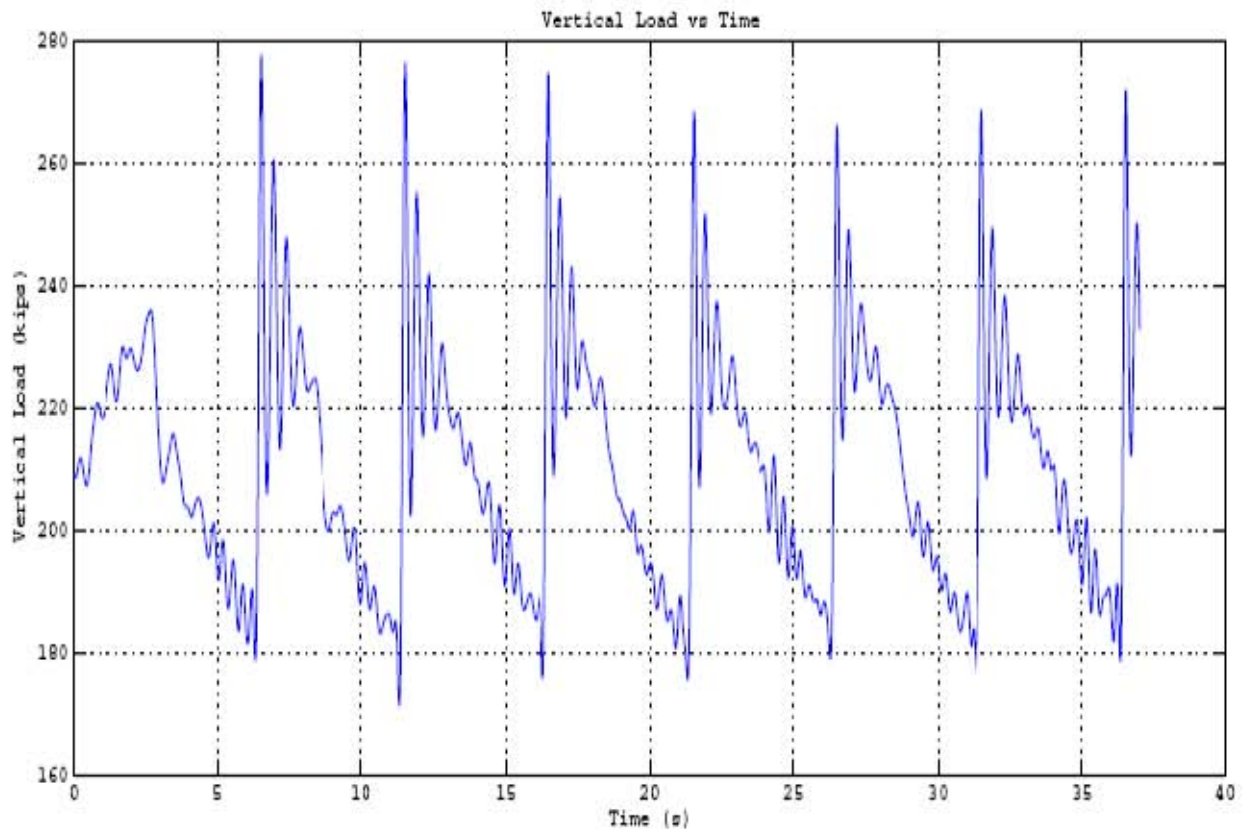
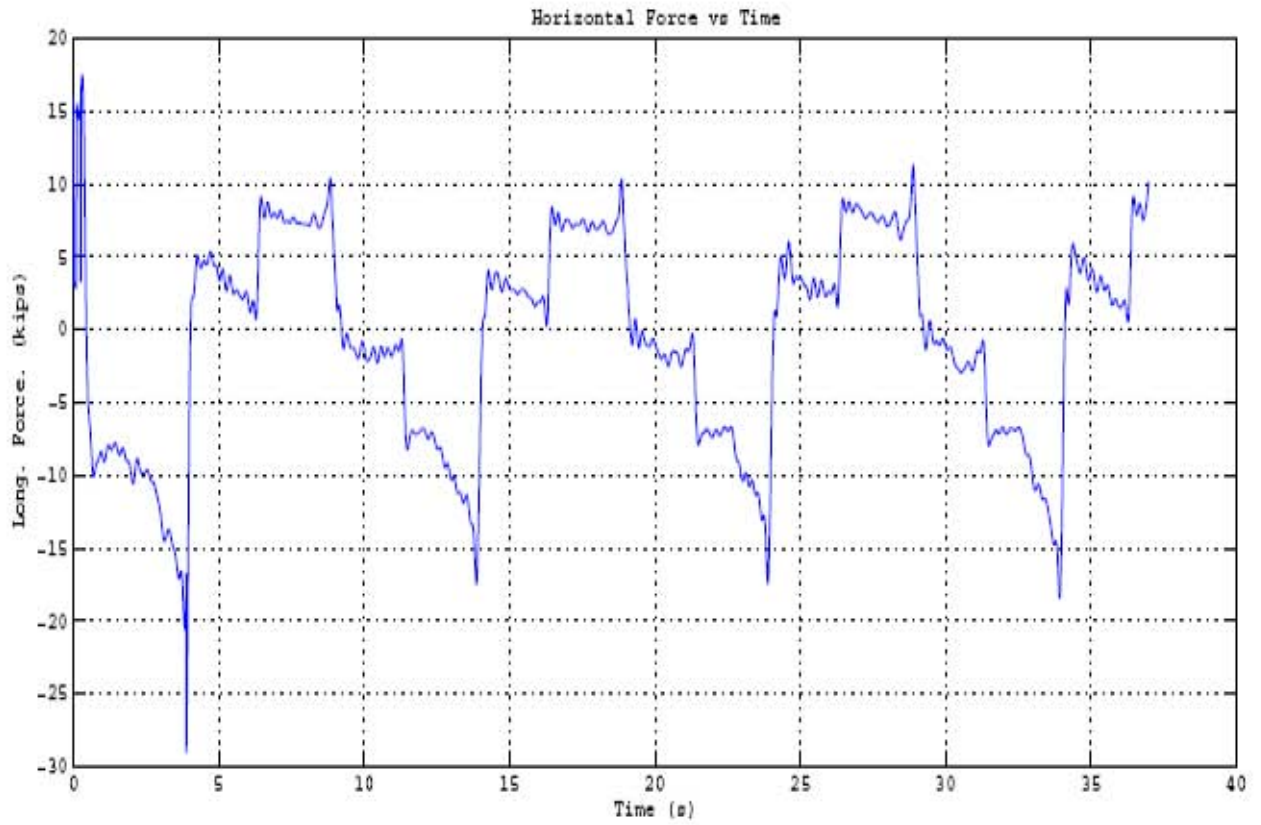


Figure 5-4 Results of Repeated Test #4 (continued).

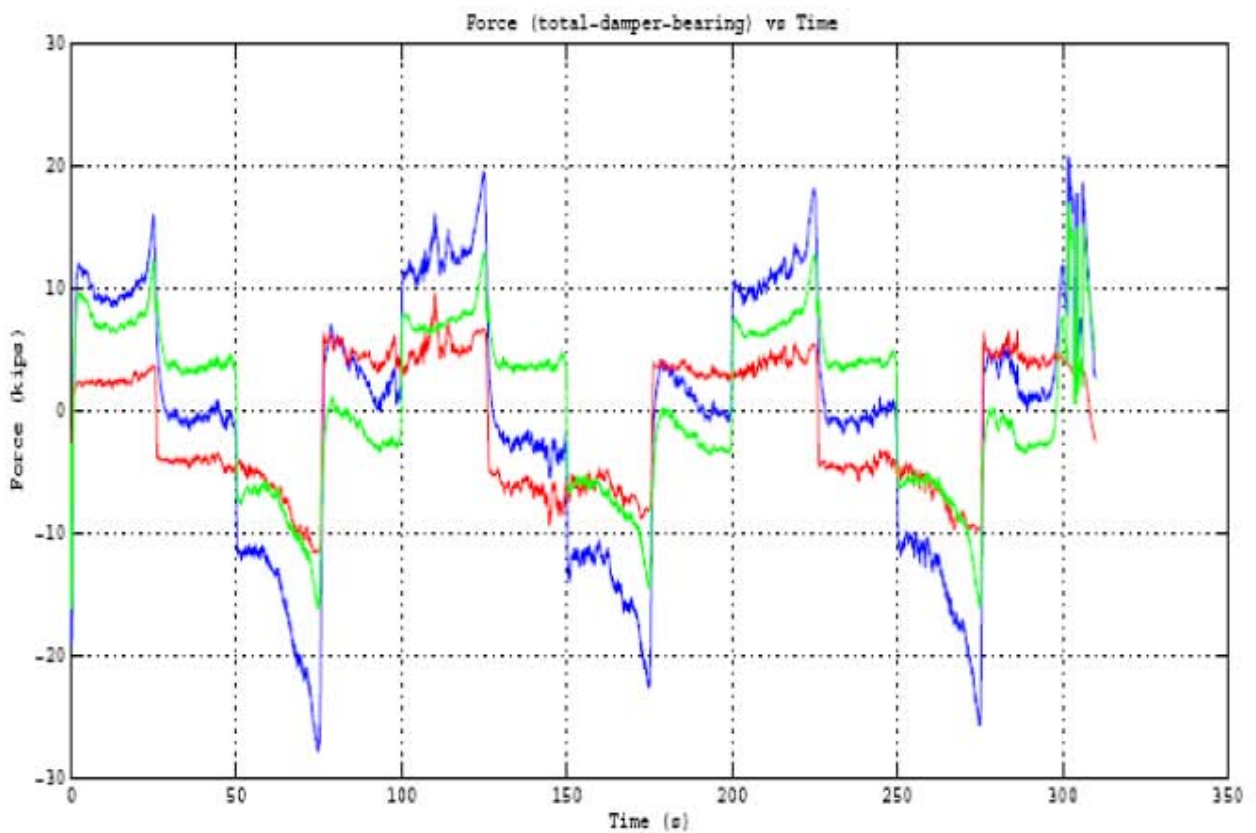
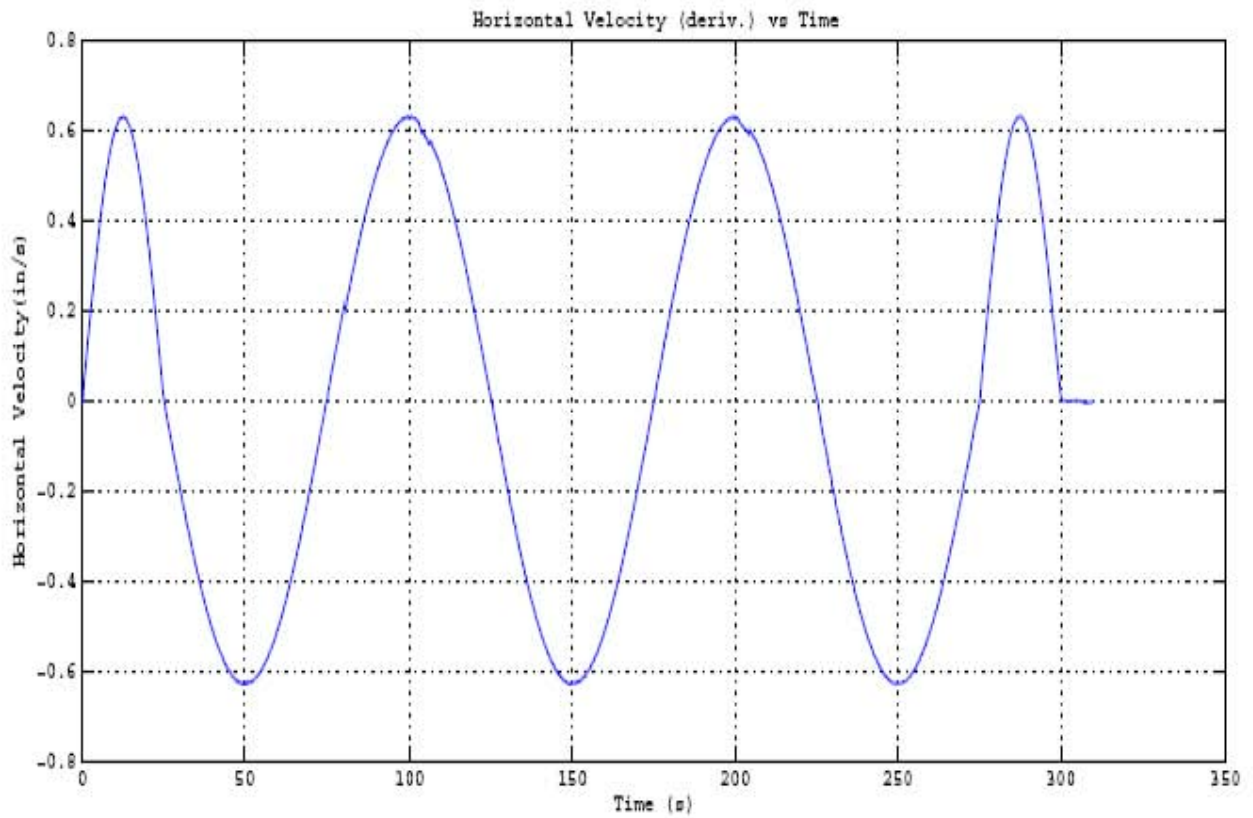


Figure 5-5 Results of Repeated Test #5.

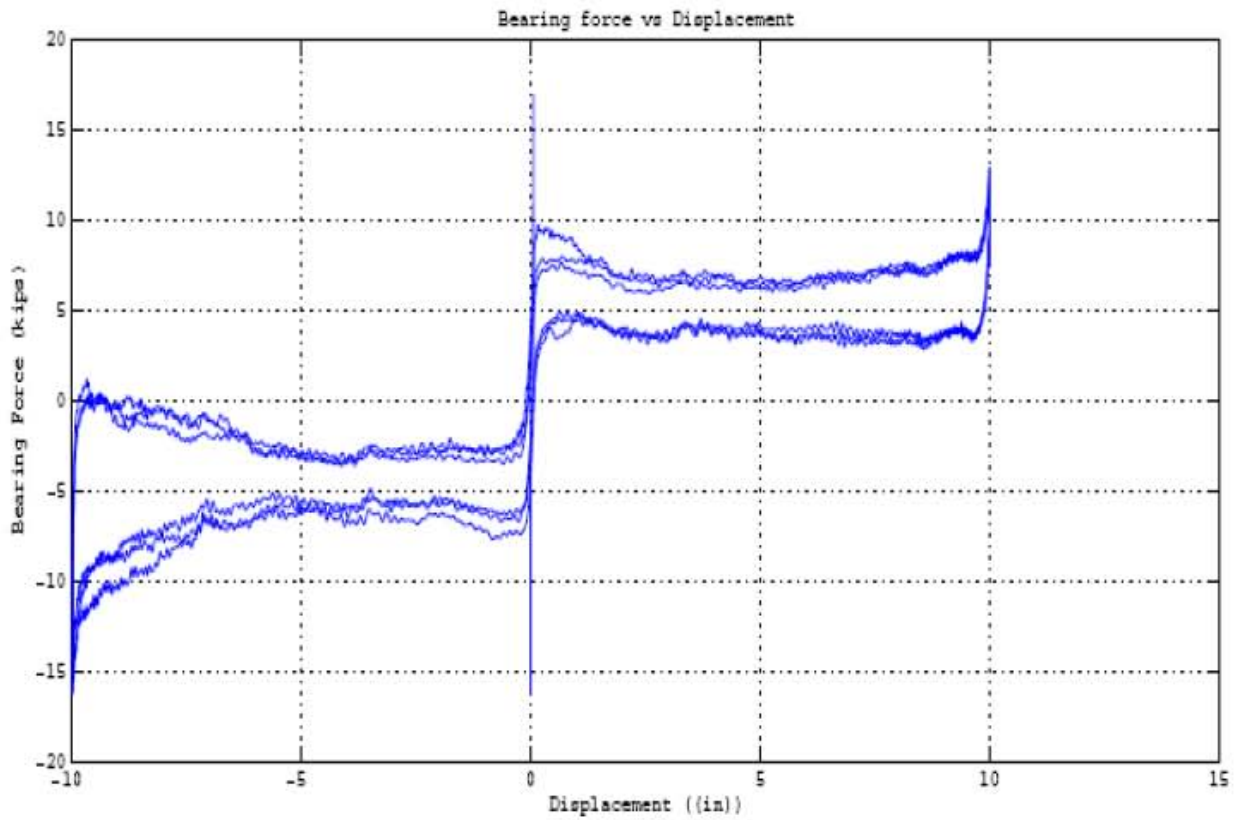
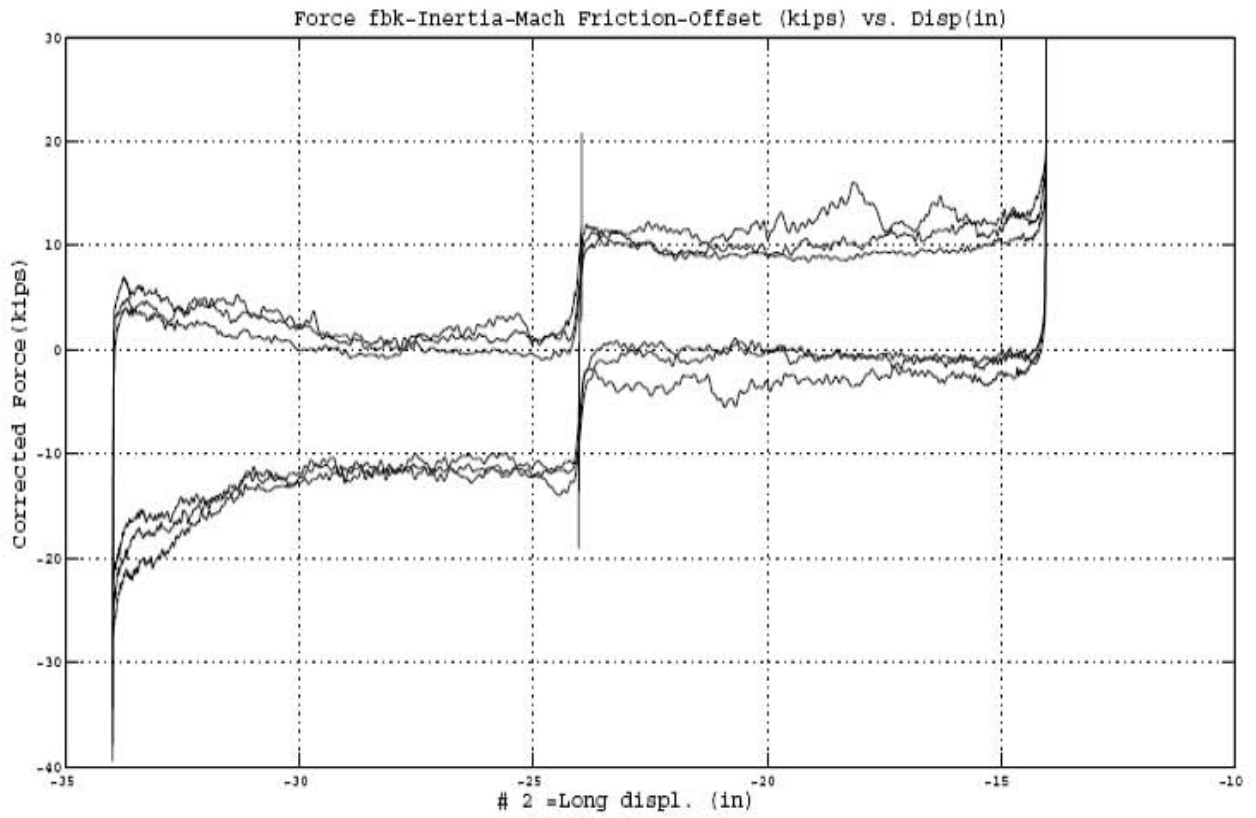


Figure 5-5 Results of Repeated Test #5 (continued).

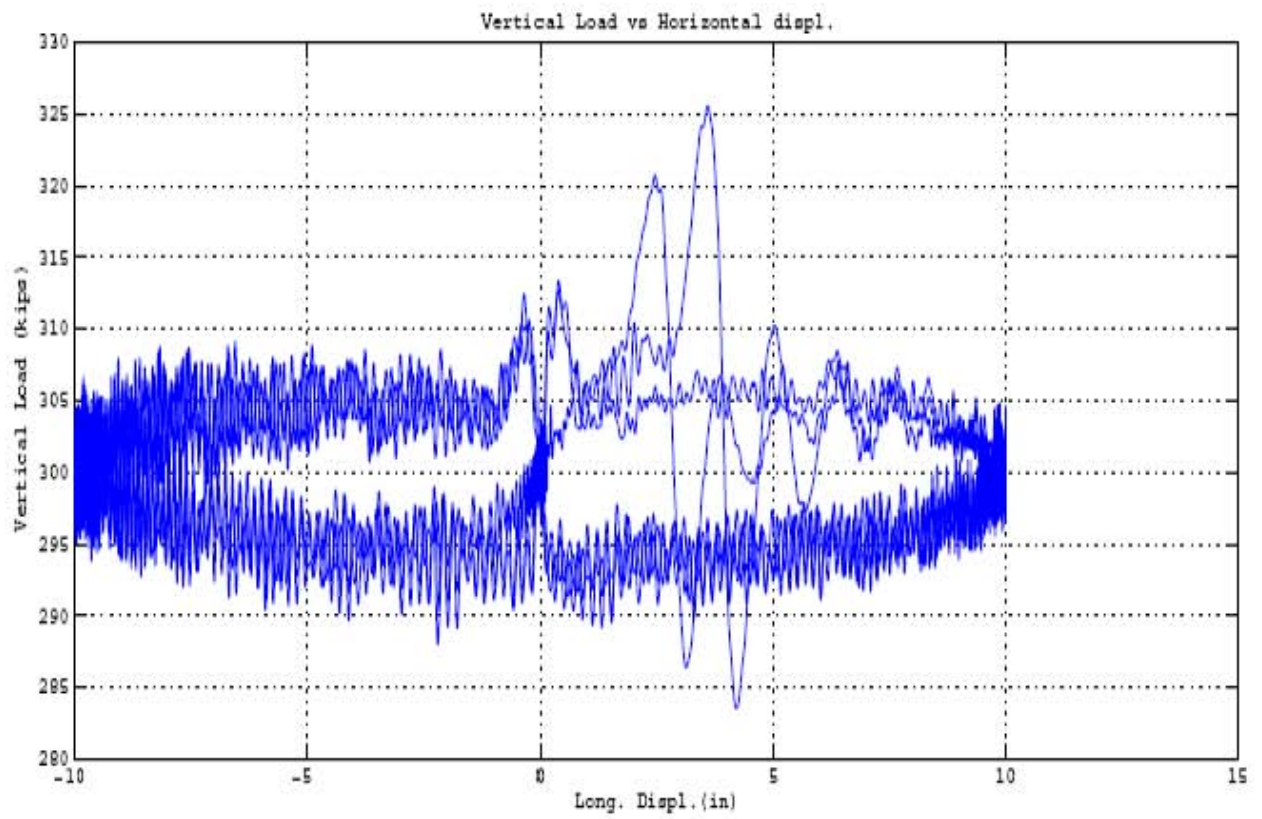
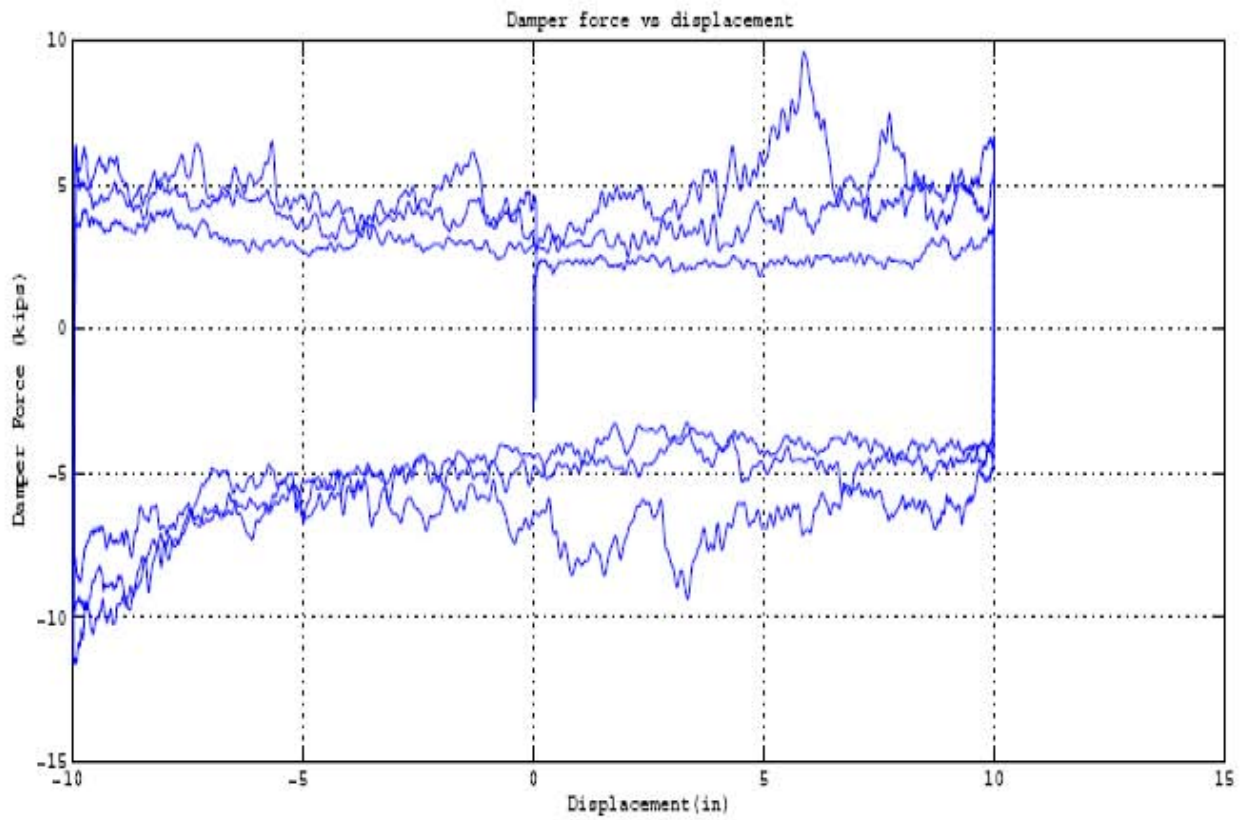


Figure 5-5 Results of Repeated Test #5 (continued).

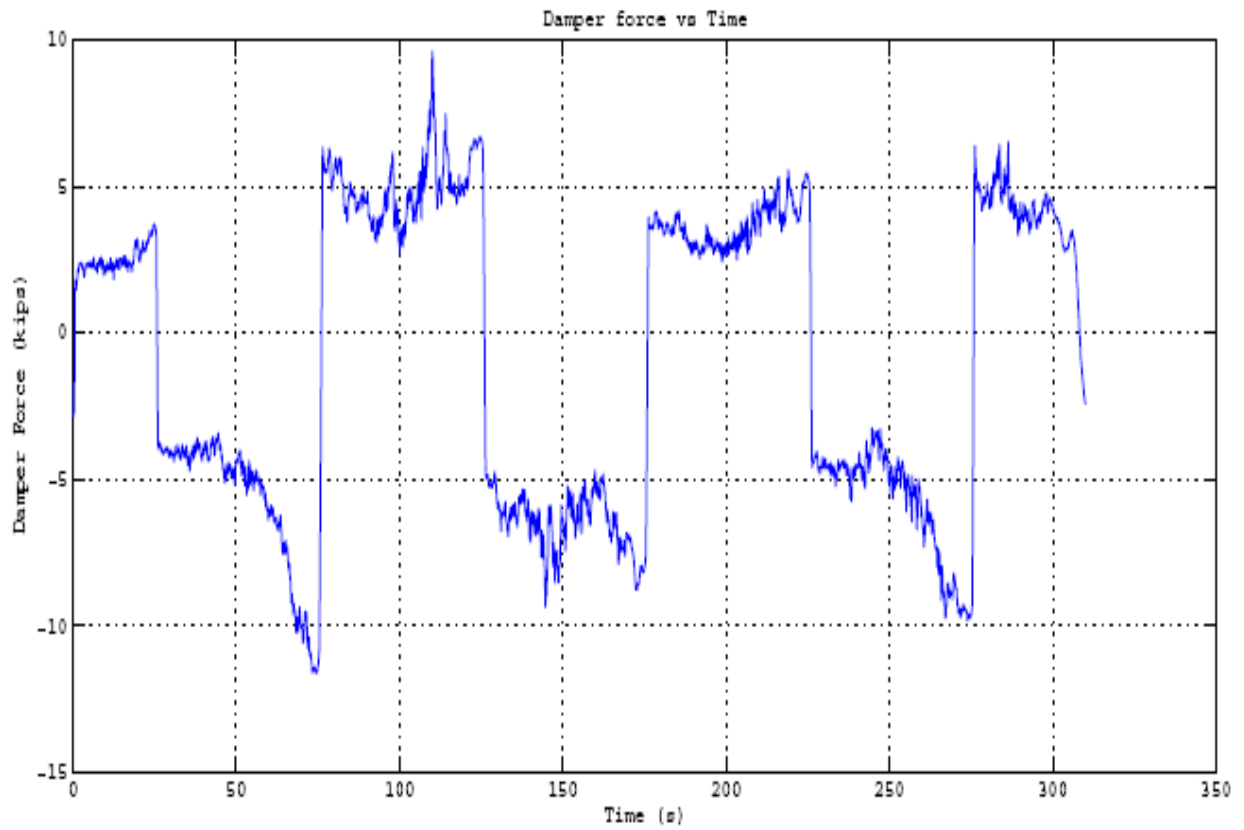
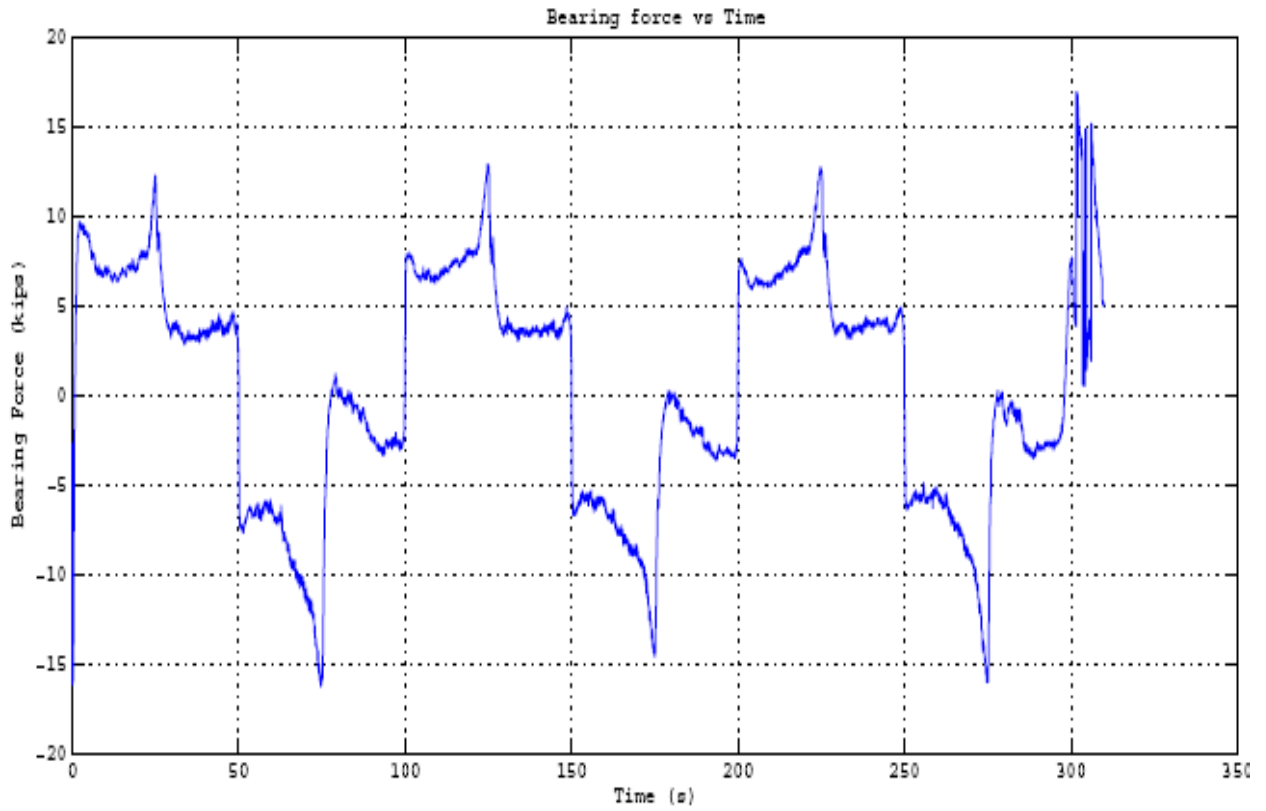


Figure 5-5 Results of Repeated Test #5 (continued).

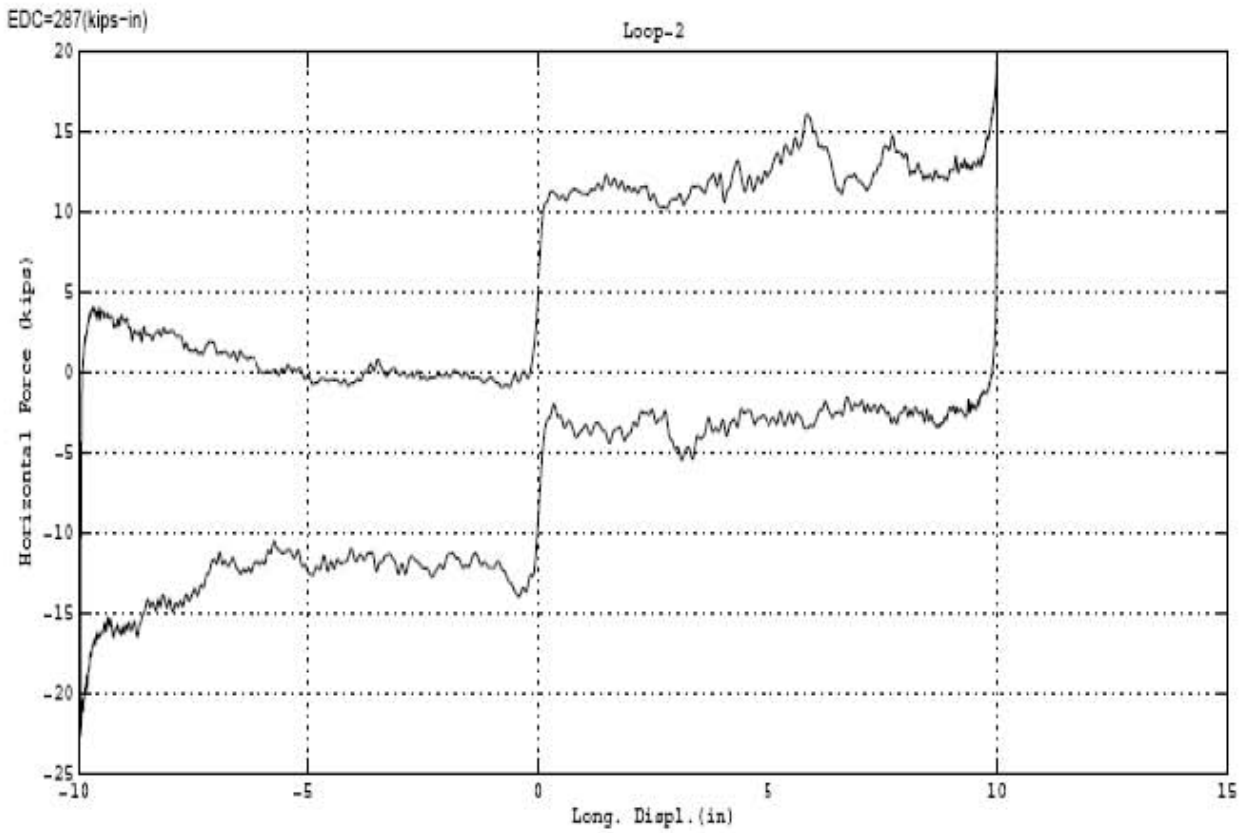
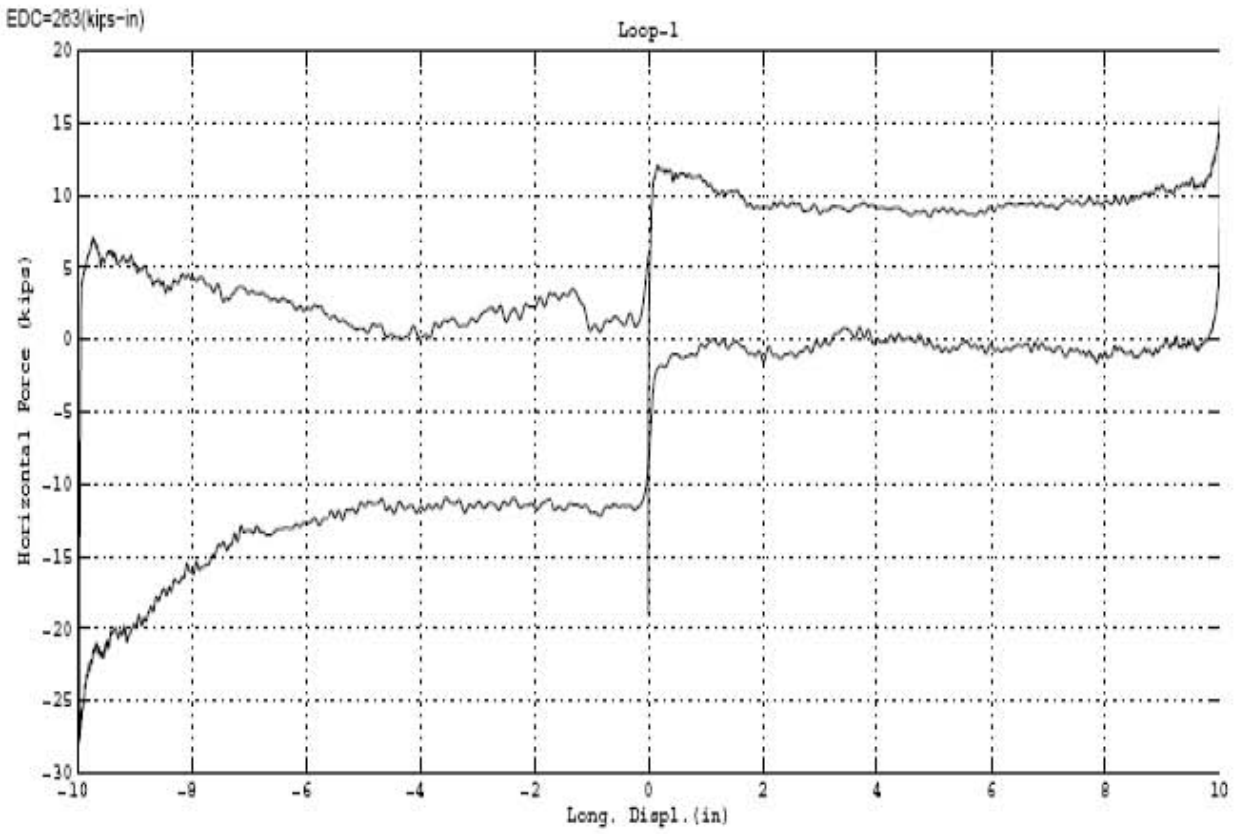


Figure 5-5 Results of Repeated Test #5 (continued).

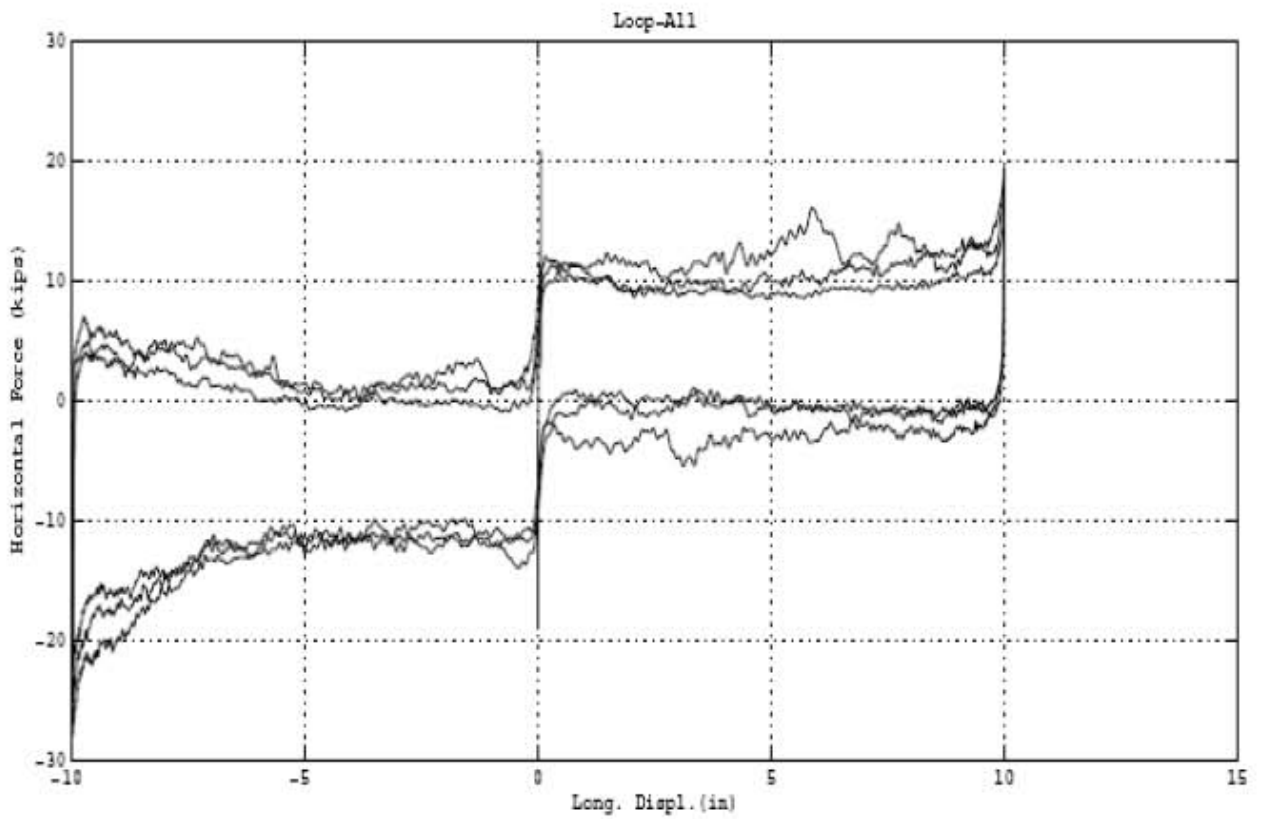
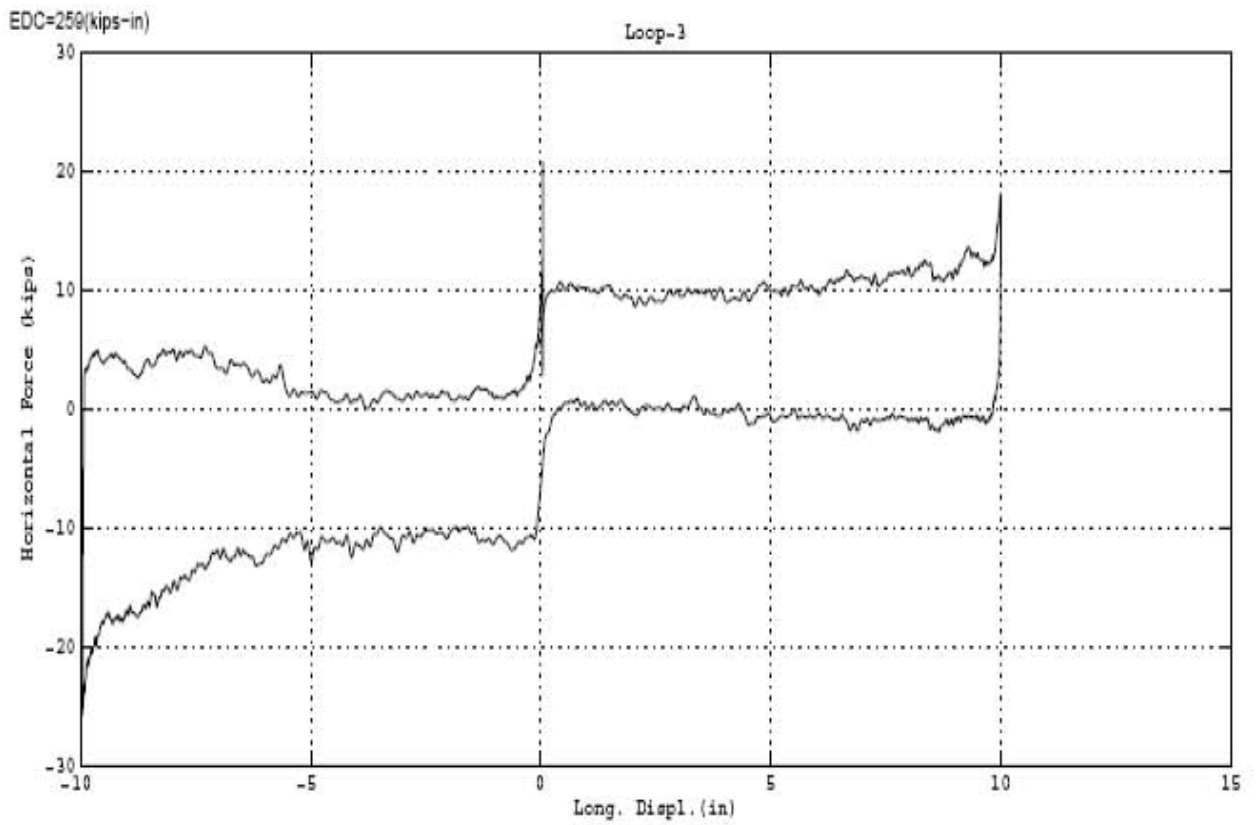


Figure 5-5 Results of Repeated Test #5 (continued).

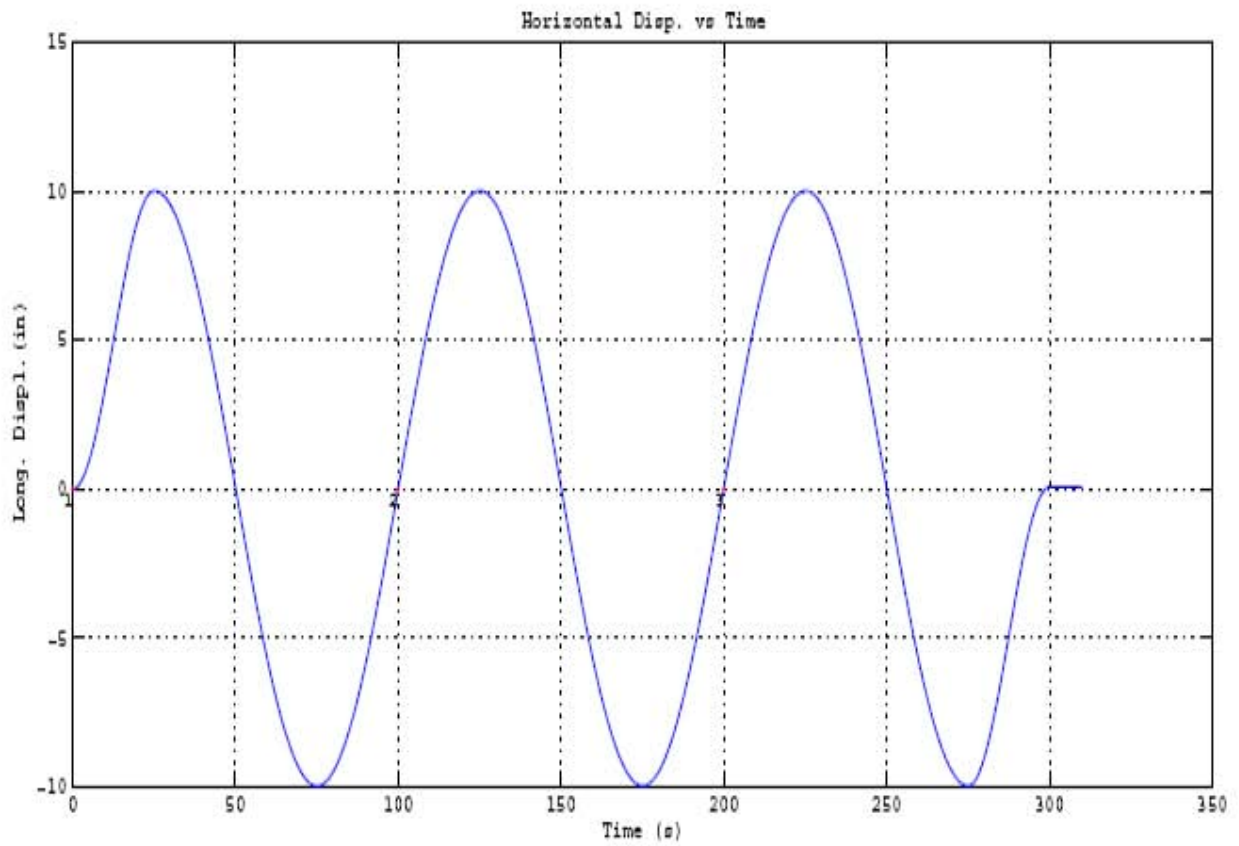
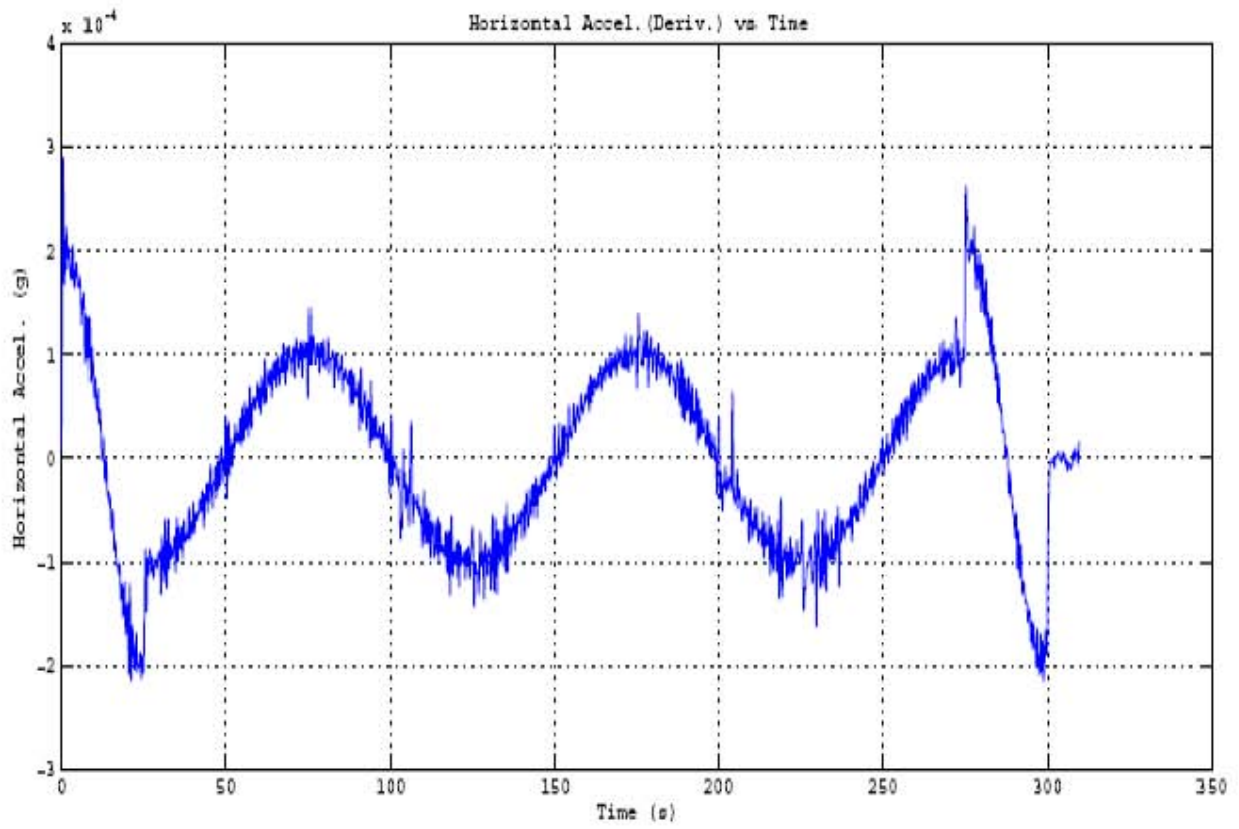


Figure 5-5 Results of Repeated Test #5 (continued).

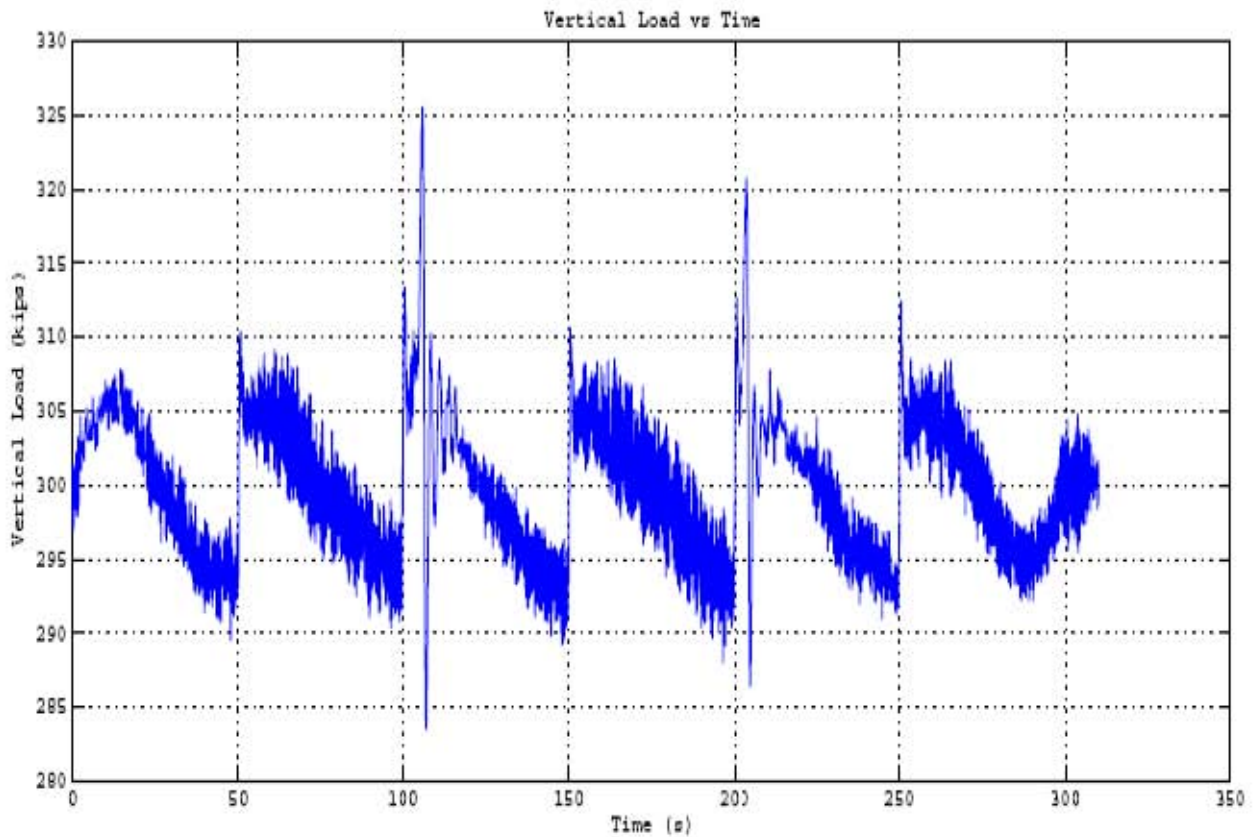
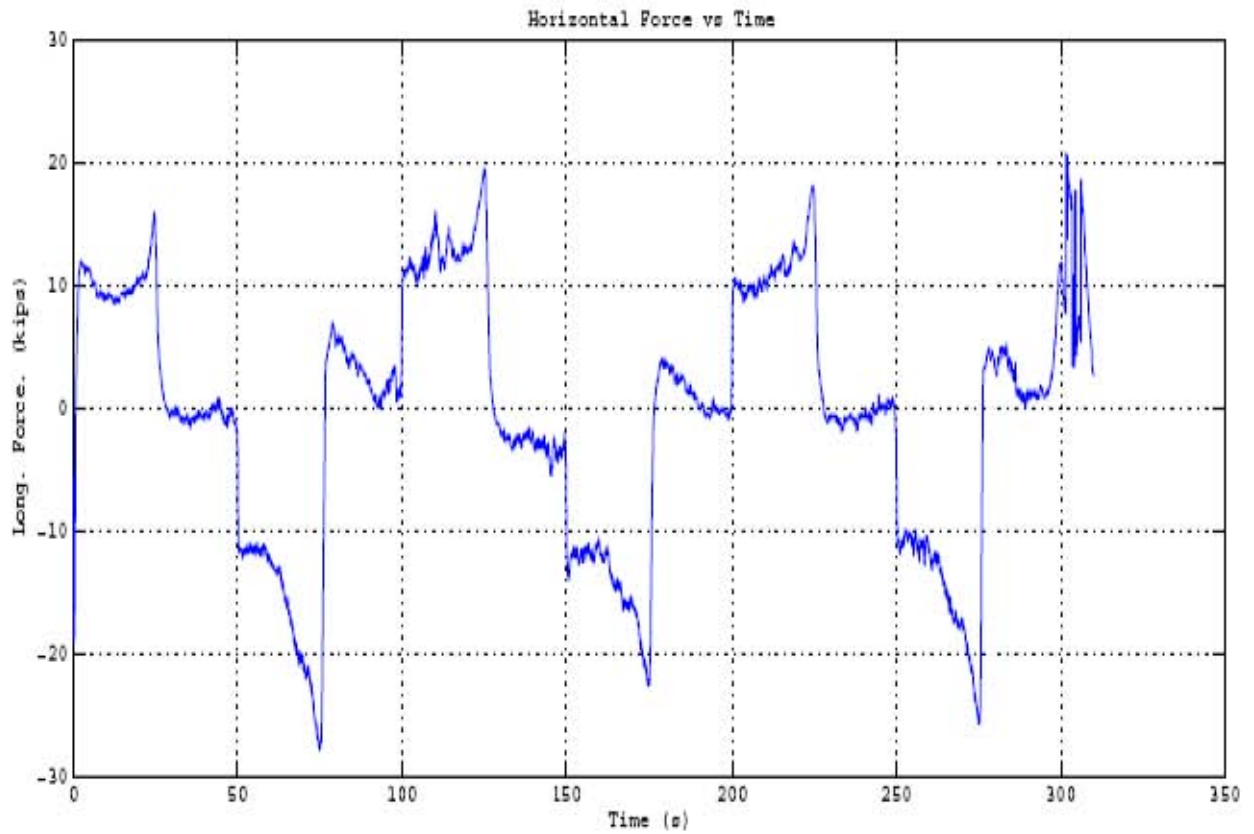


Figure 5-5 Results of Repeated Test #5 (continued).

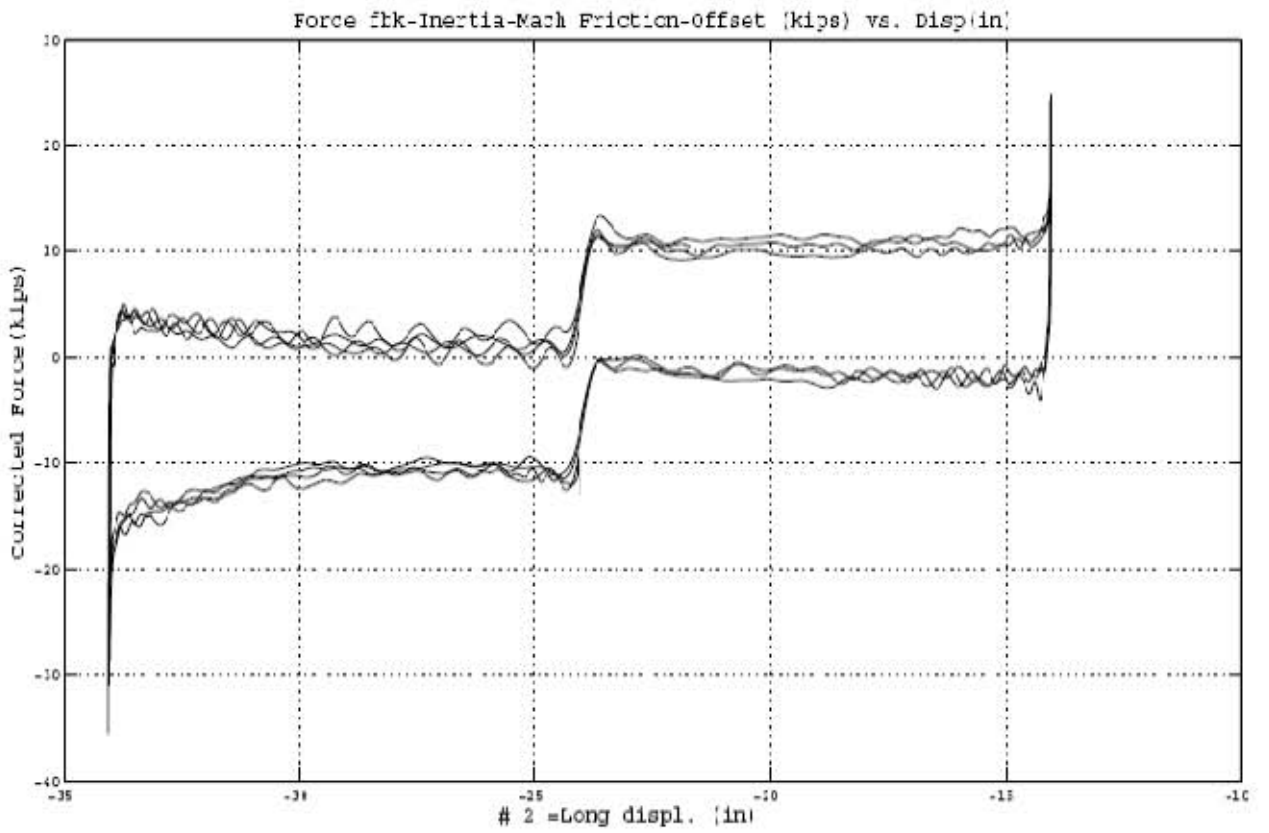
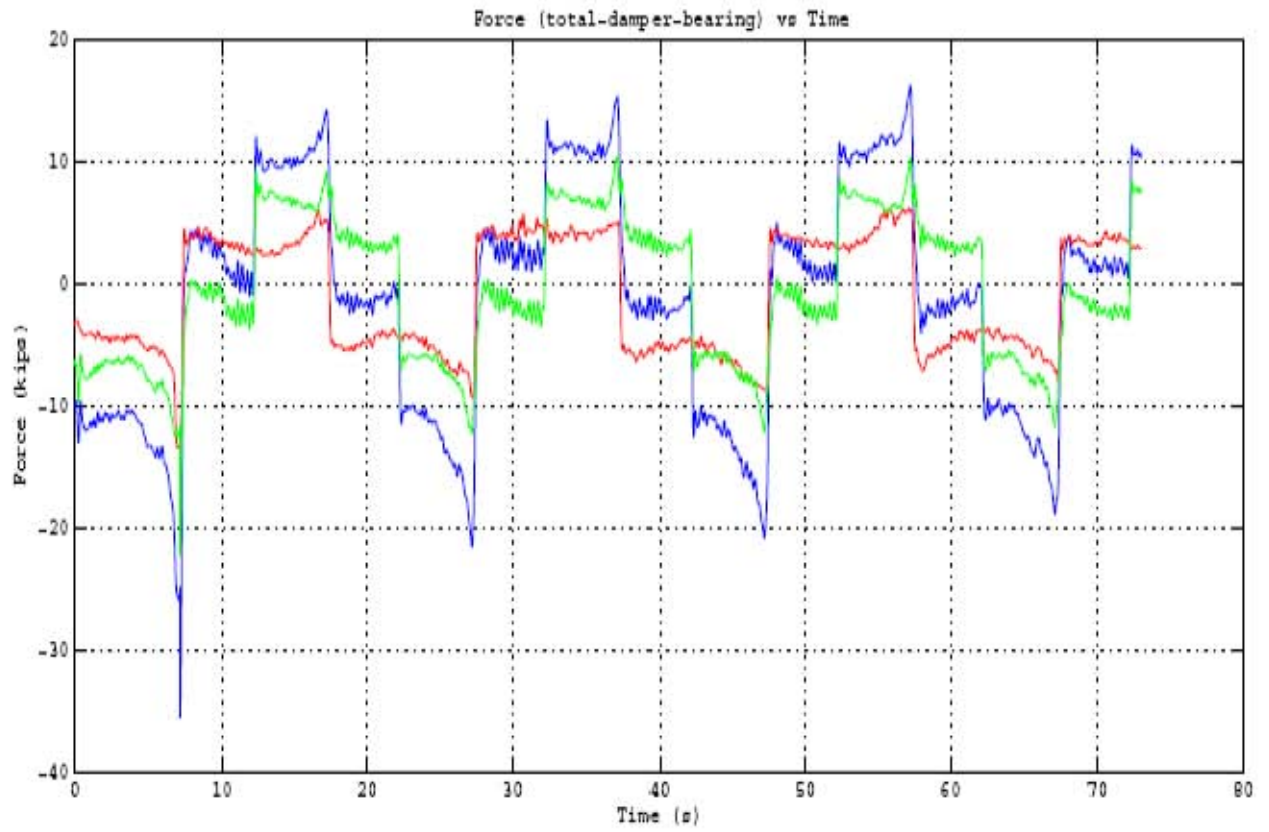


Figure 5-6 Results of Repeated Test #6.

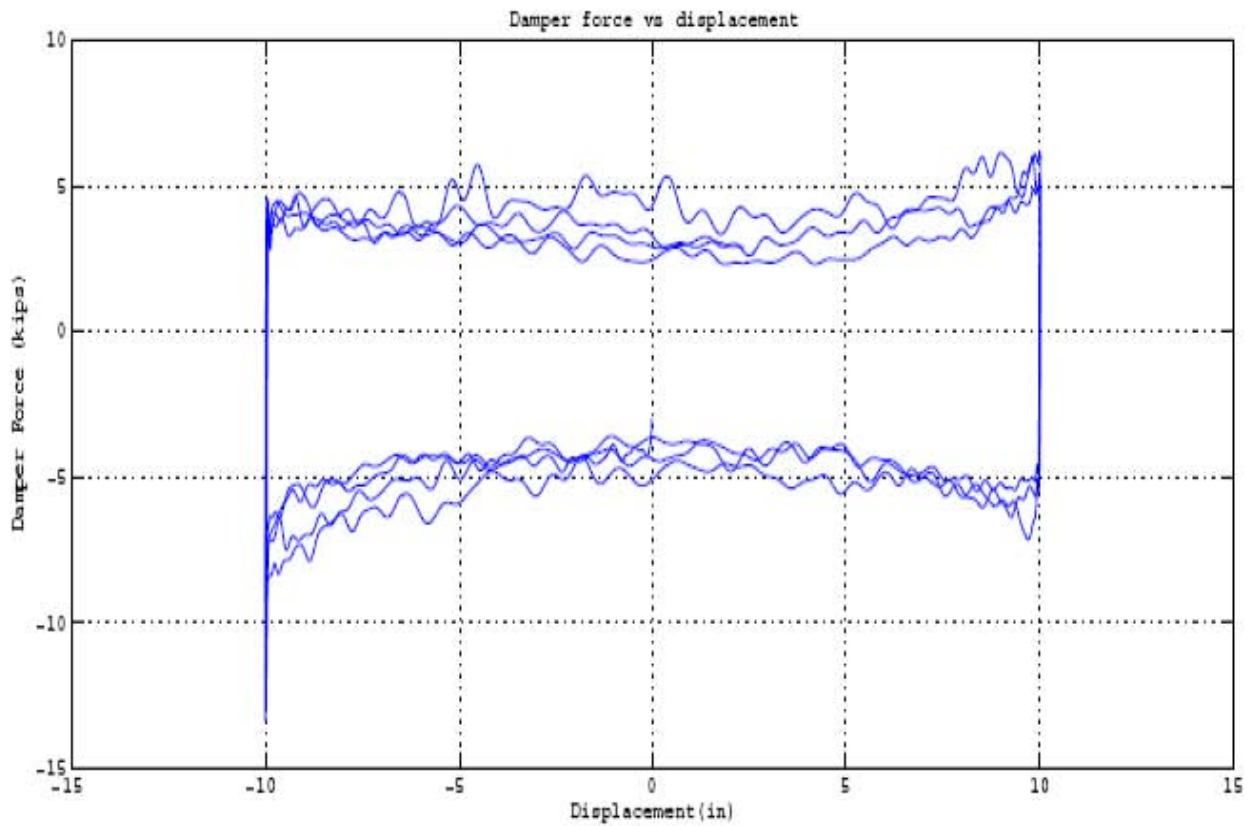
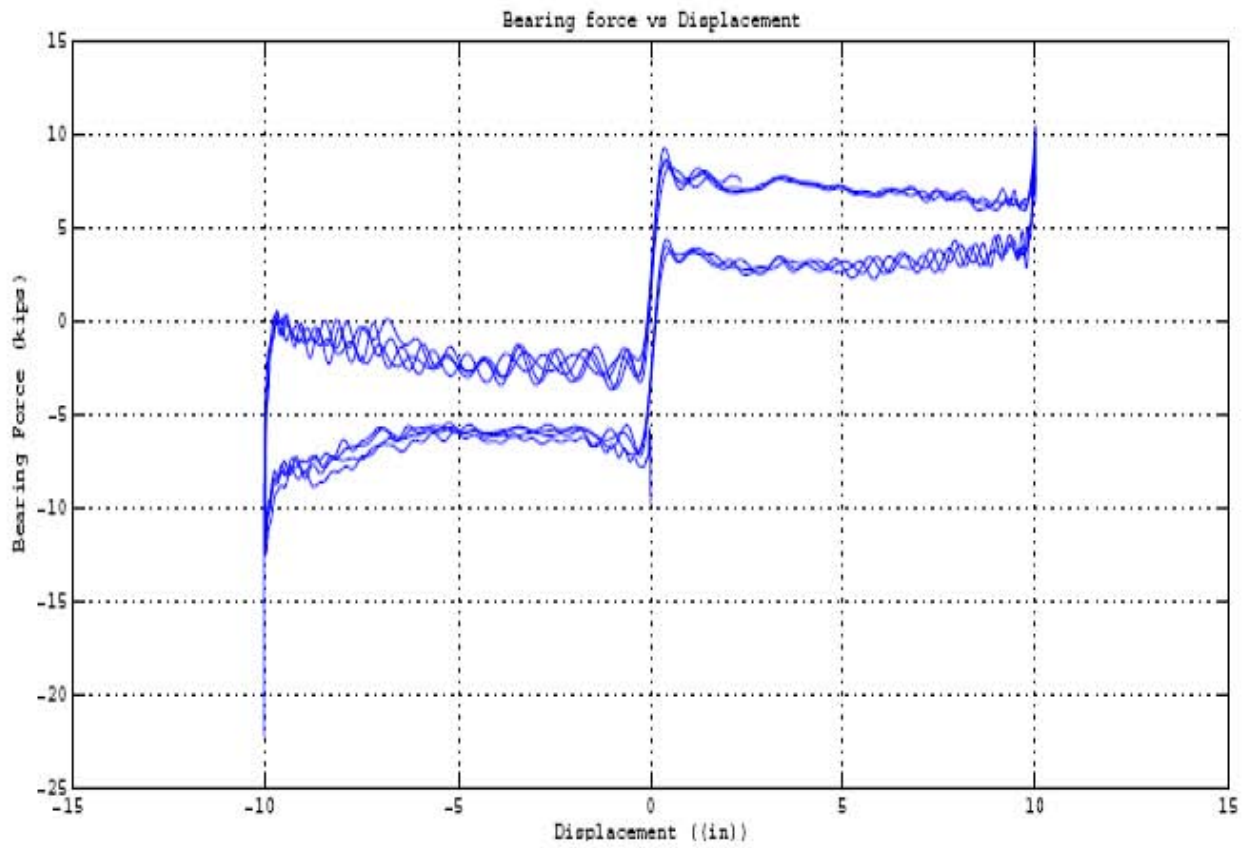


Figure 5-6 Results of Repeated Test #6 (continued).

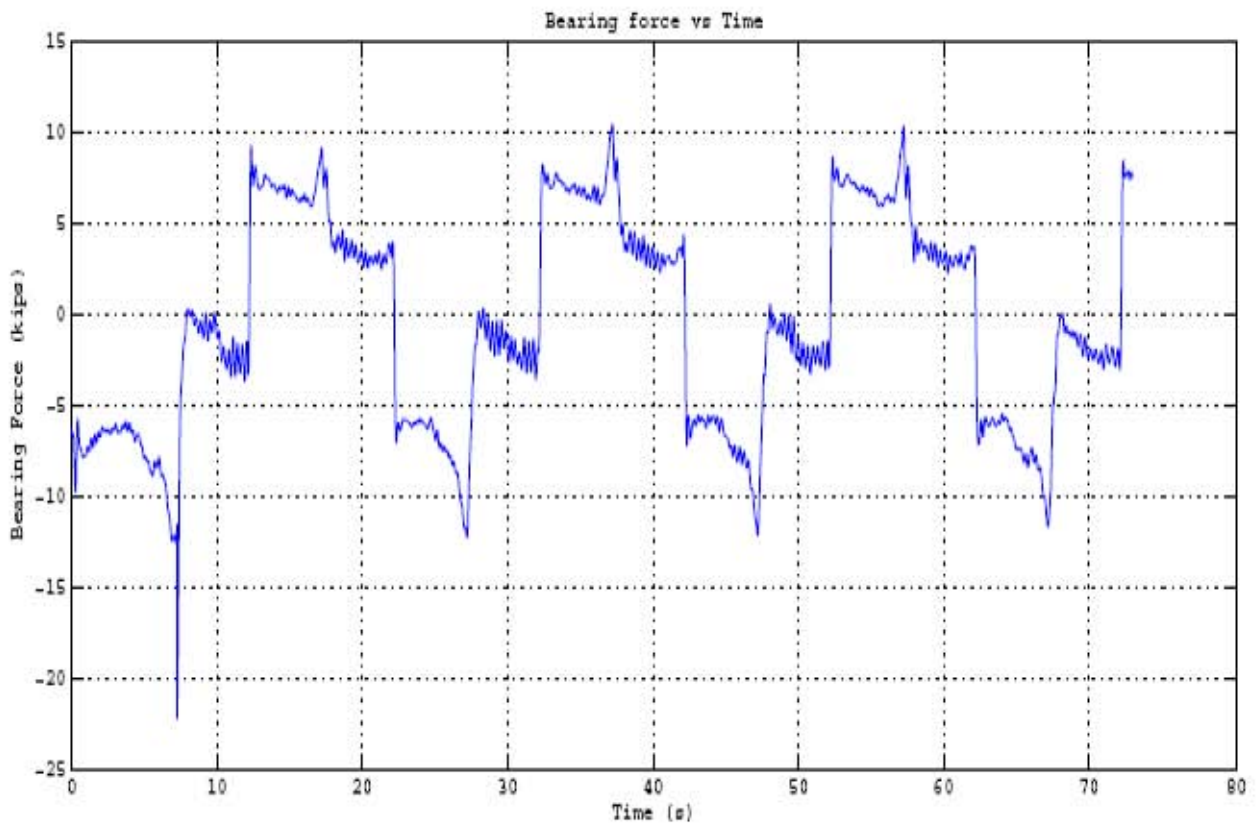
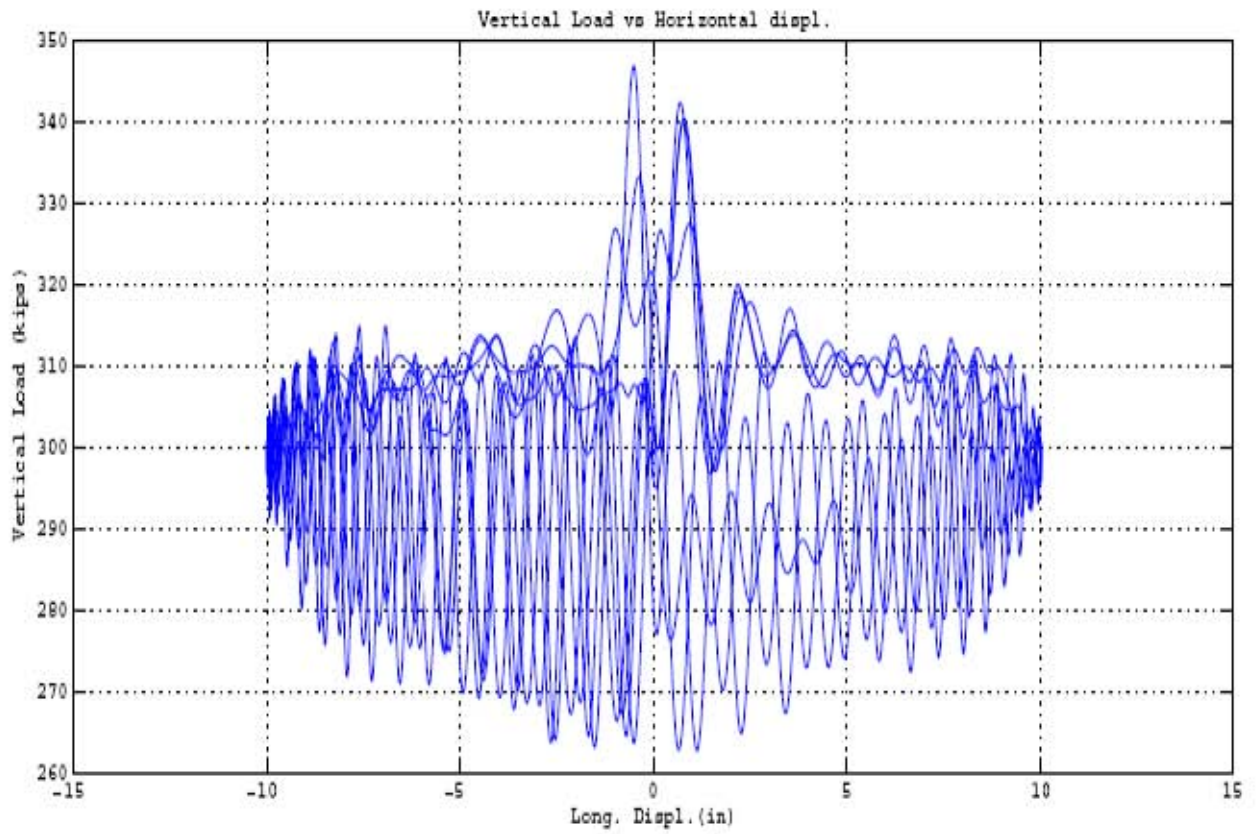


Figure 5-6 Results of Repeated Test #6 (continued).

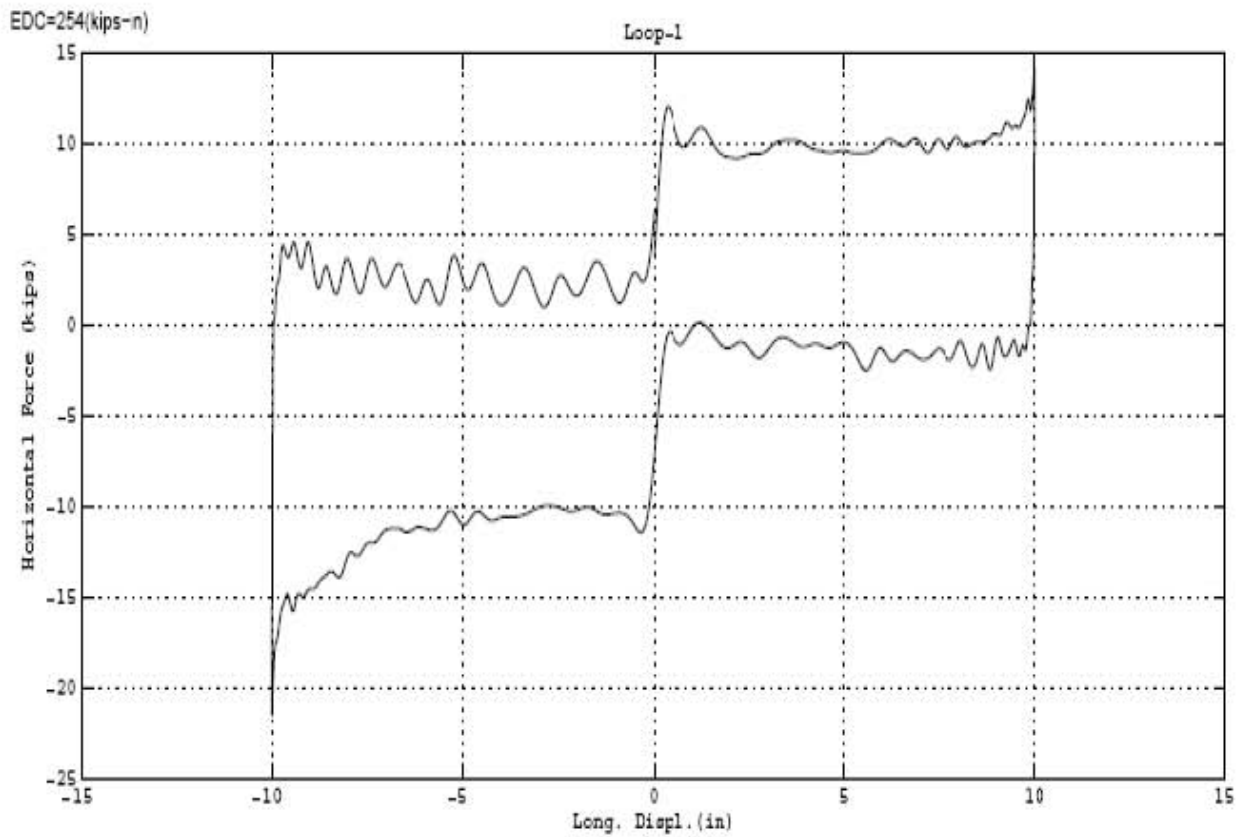
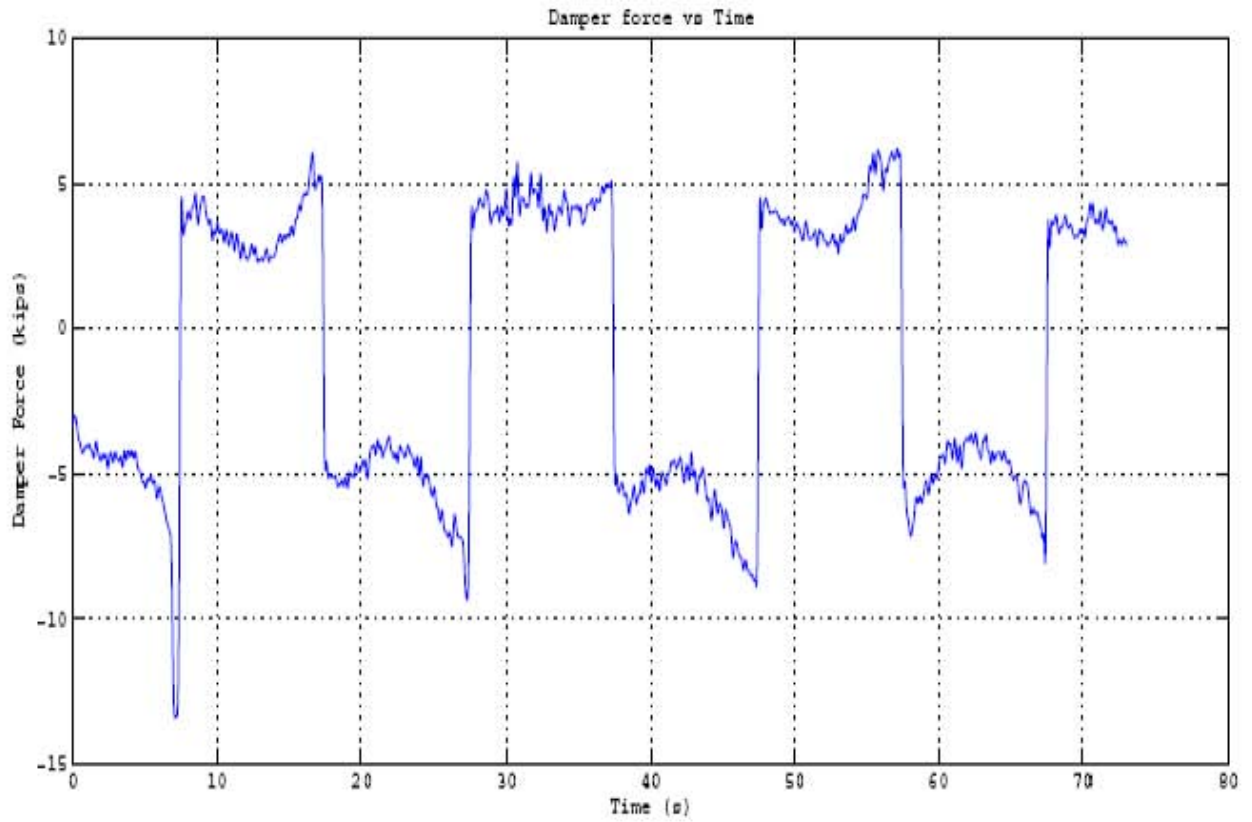


Figure 5-6 Results of Repeated Test #6 (continued).

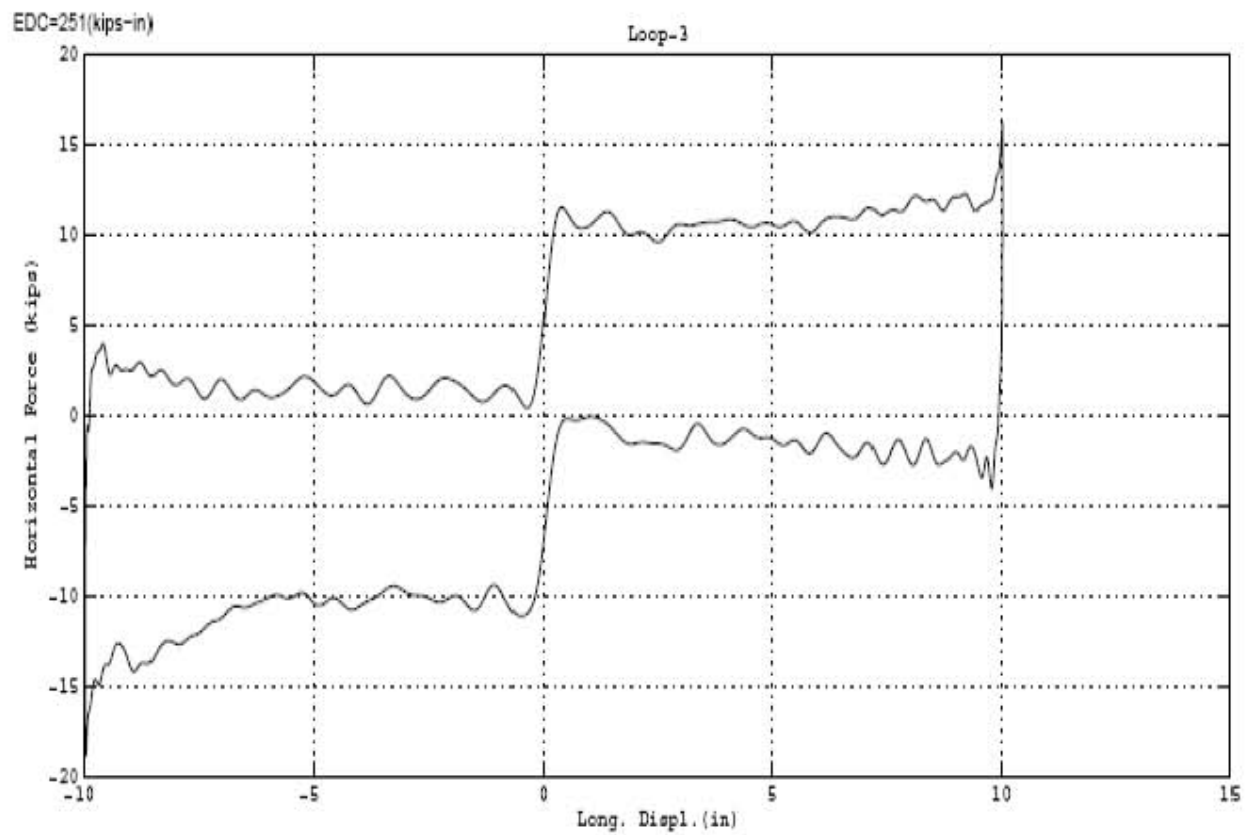
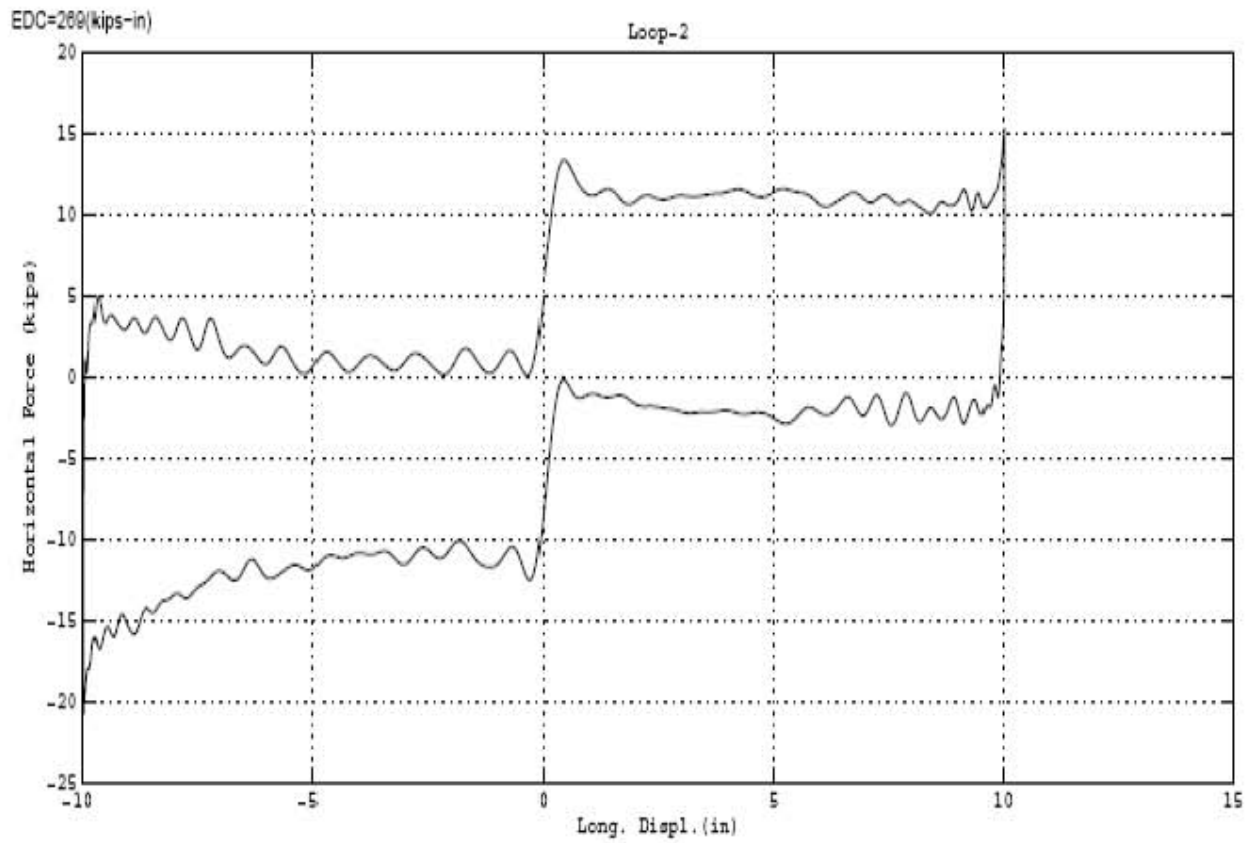


Figure 5-6 Results of Repeated Test #6 (continued).

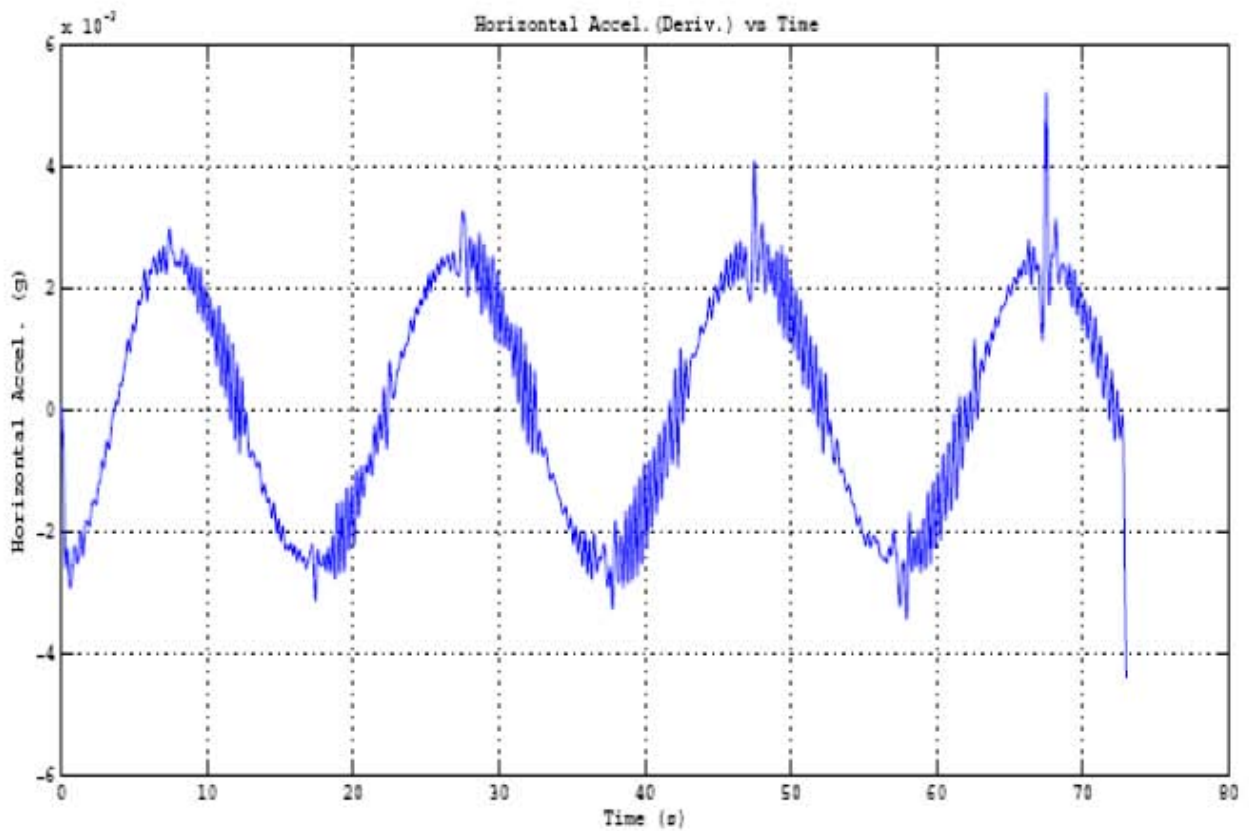
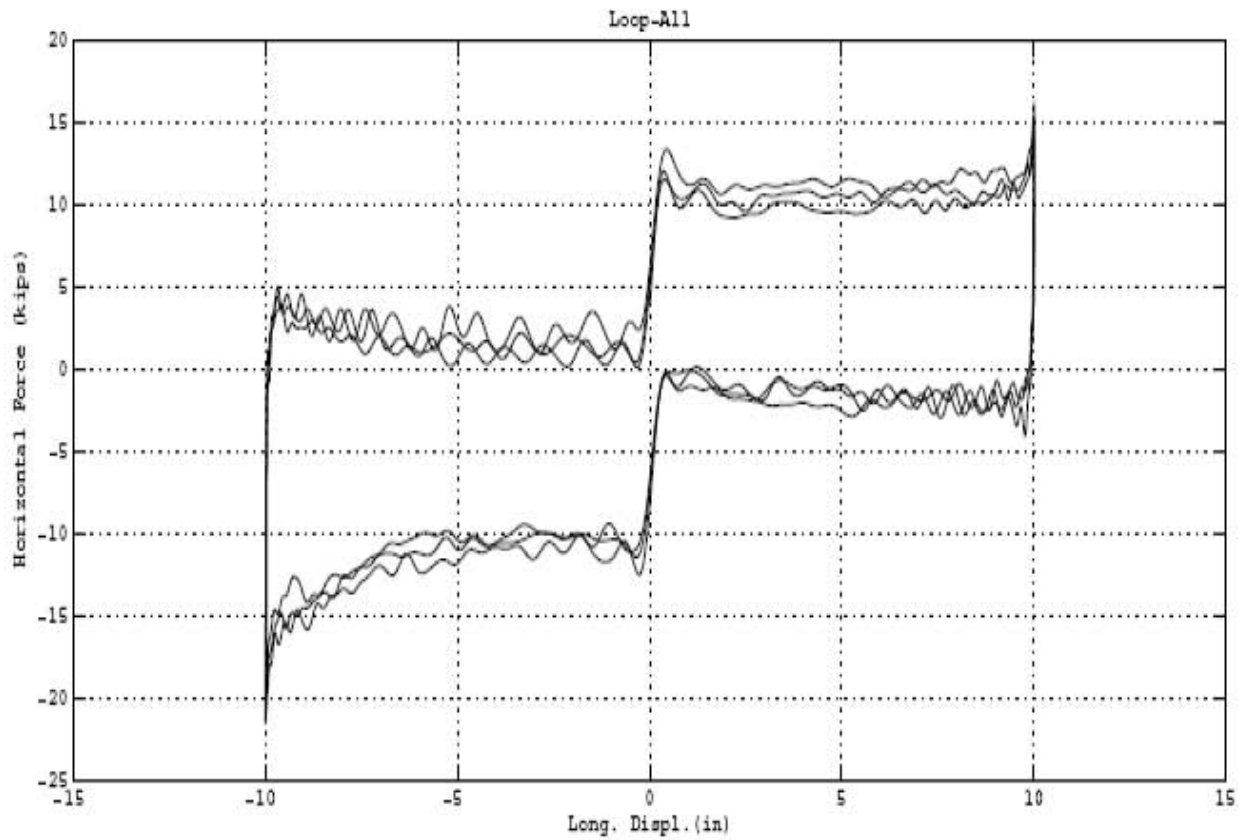


Figure 5-6 Results of Repeated Test #6 (continued).

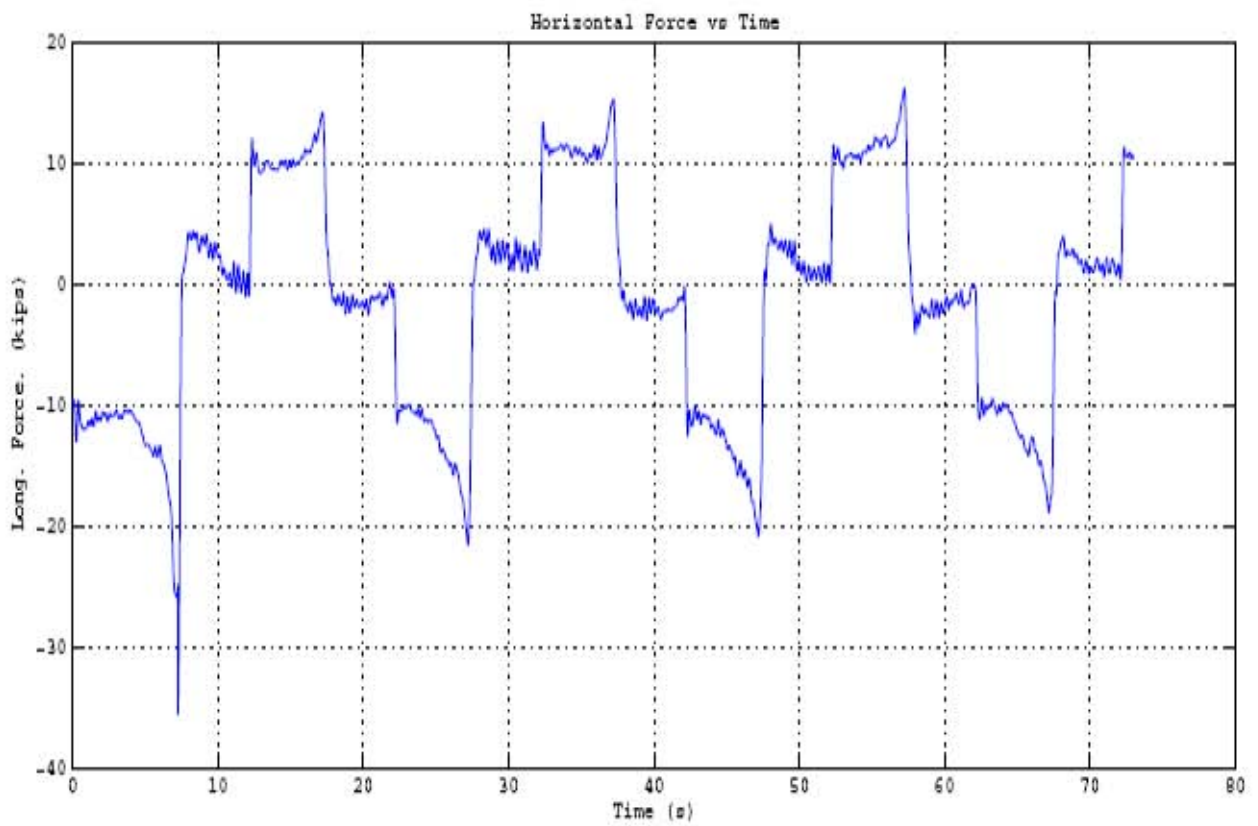
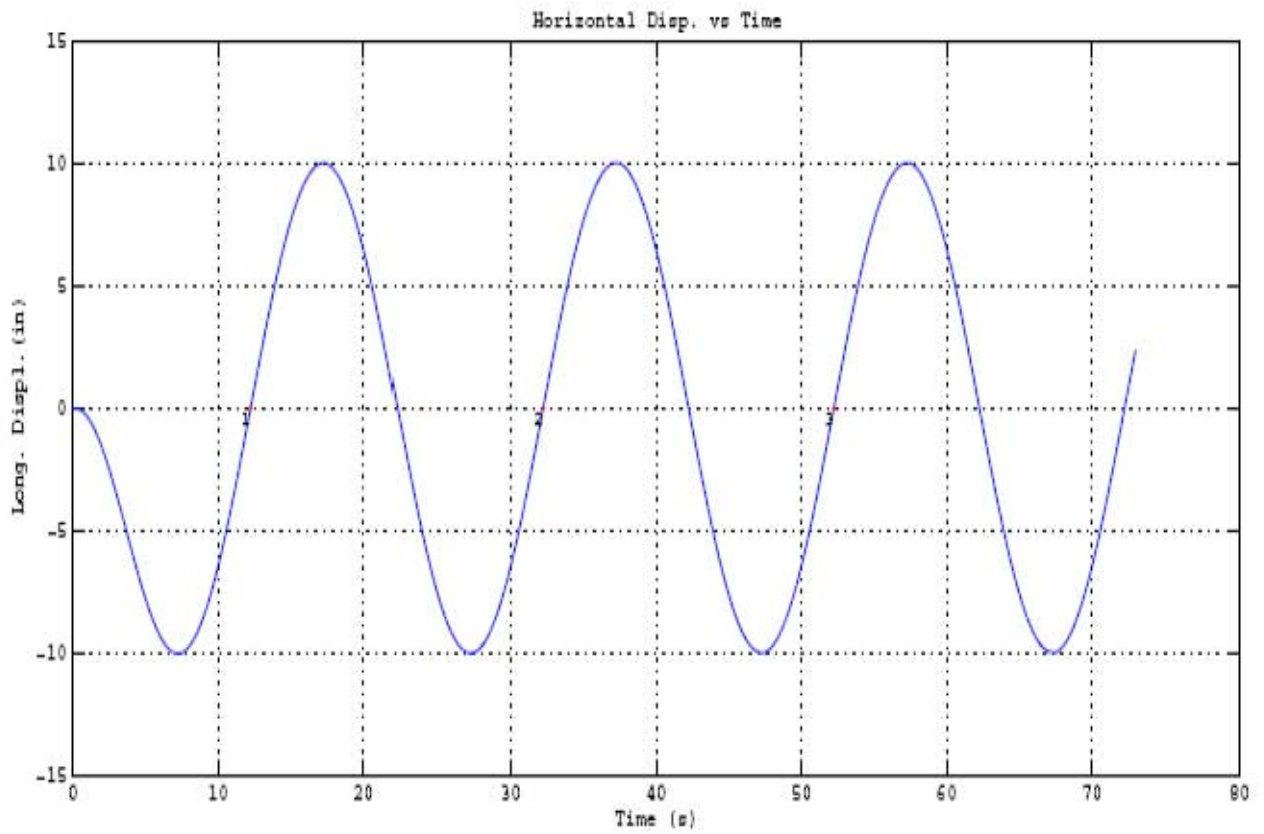


Figure 5-6 Results of Repeated Test #6 (continued).

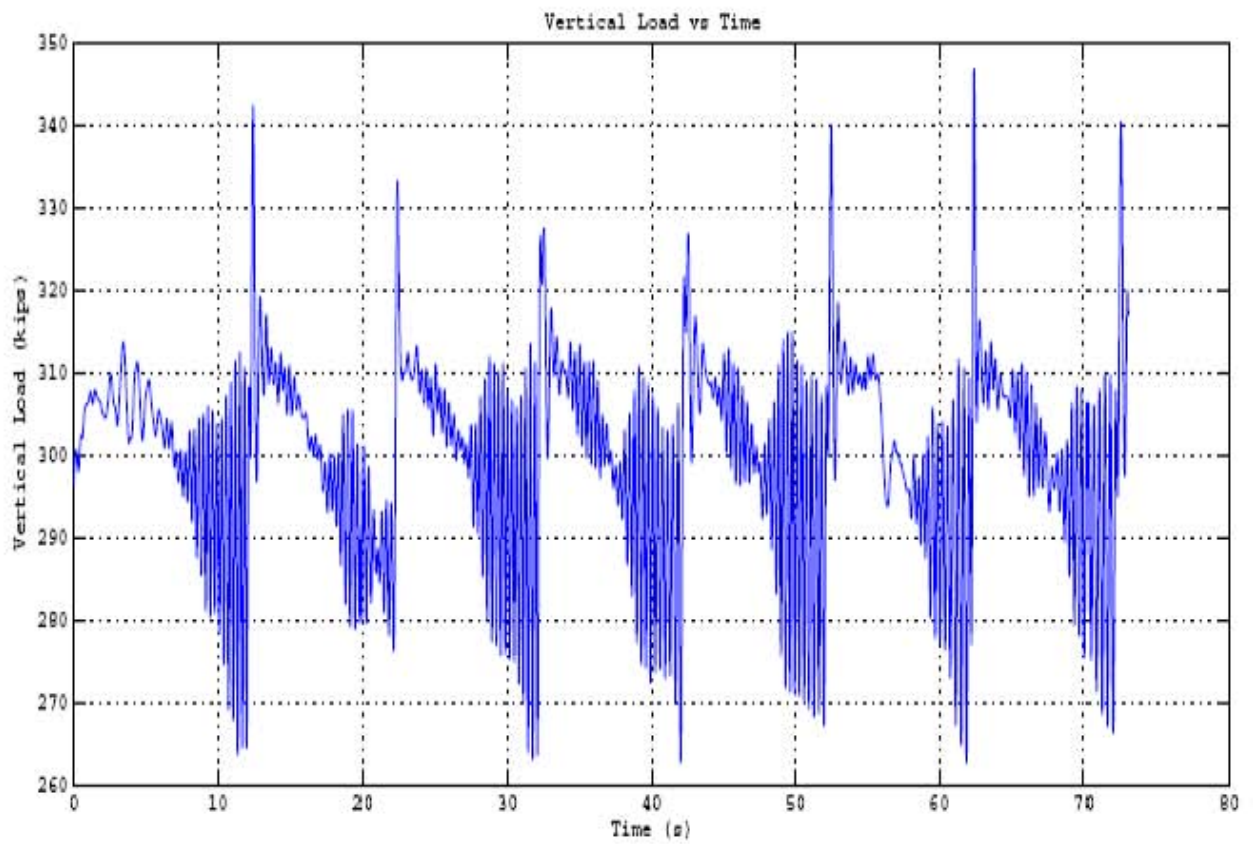
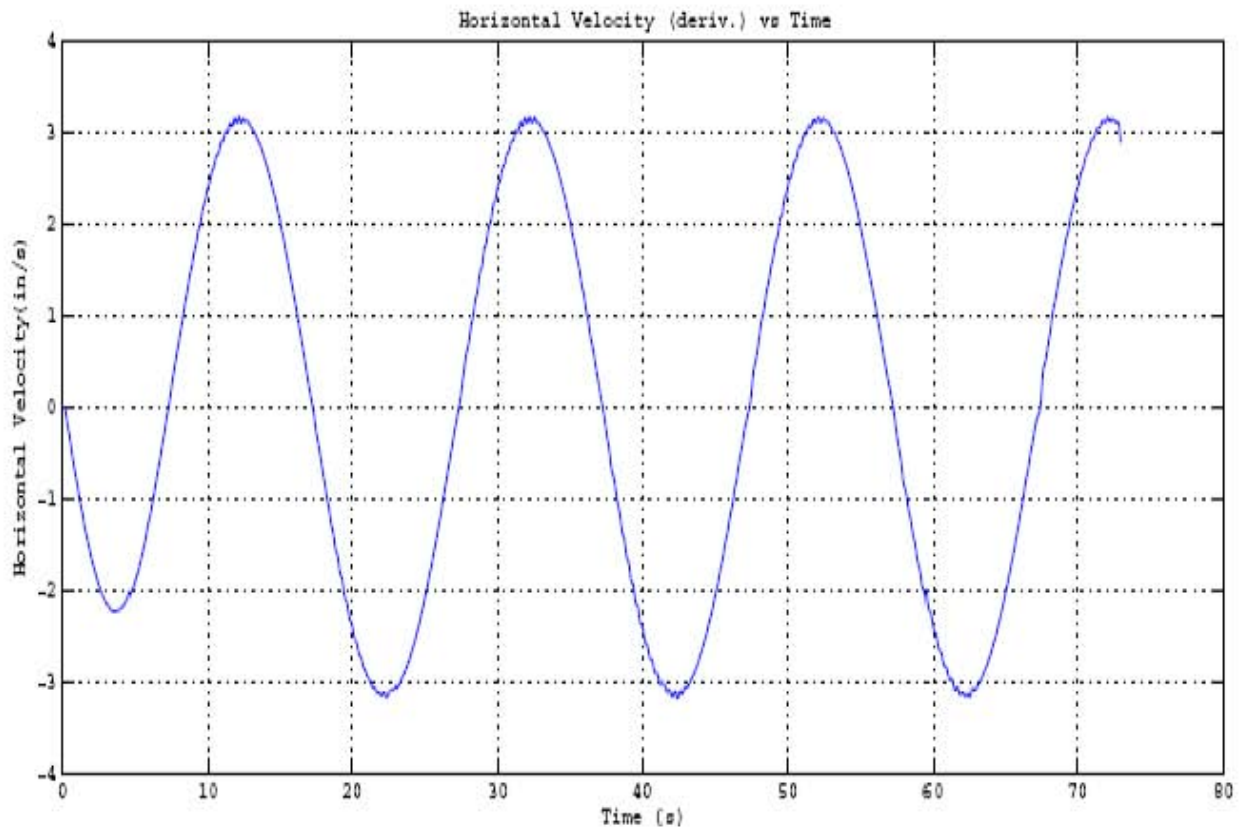


Figure 5-6 Results of Repeated Test #6 (continued).

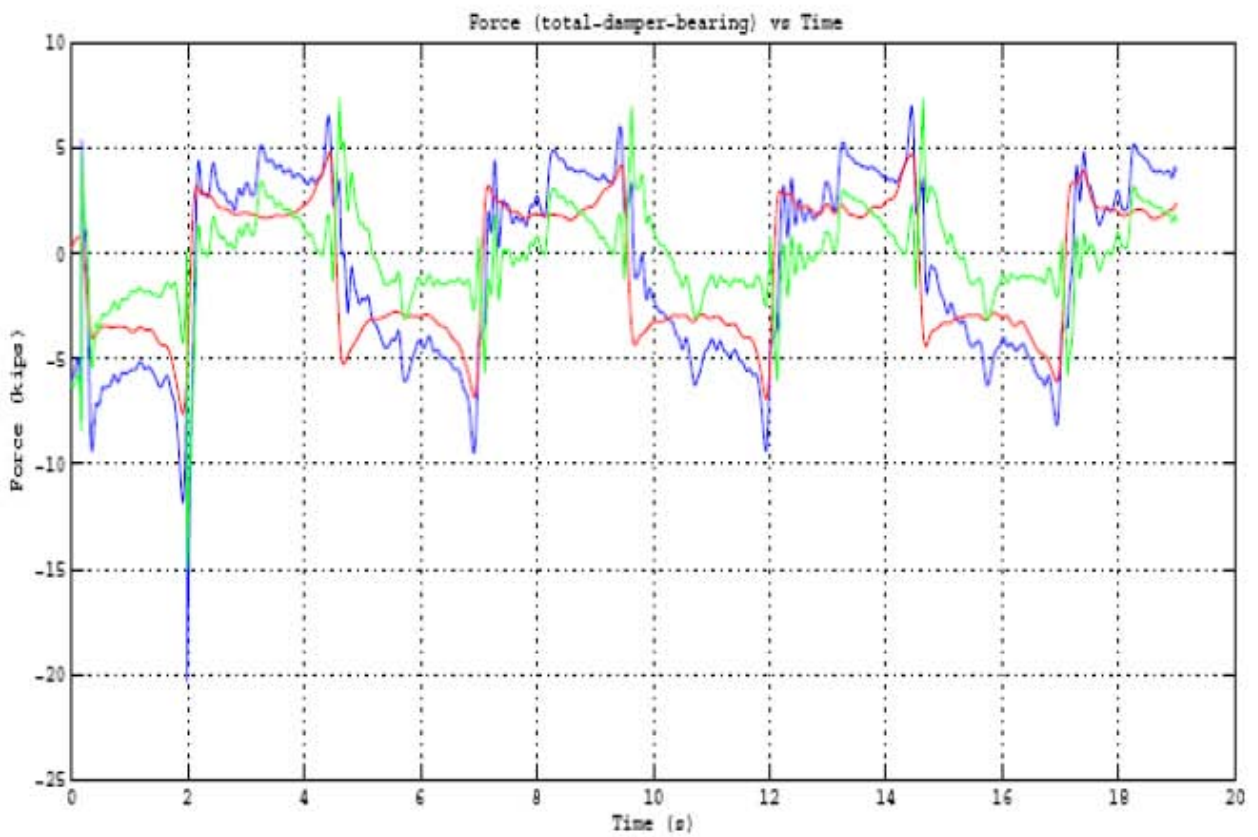
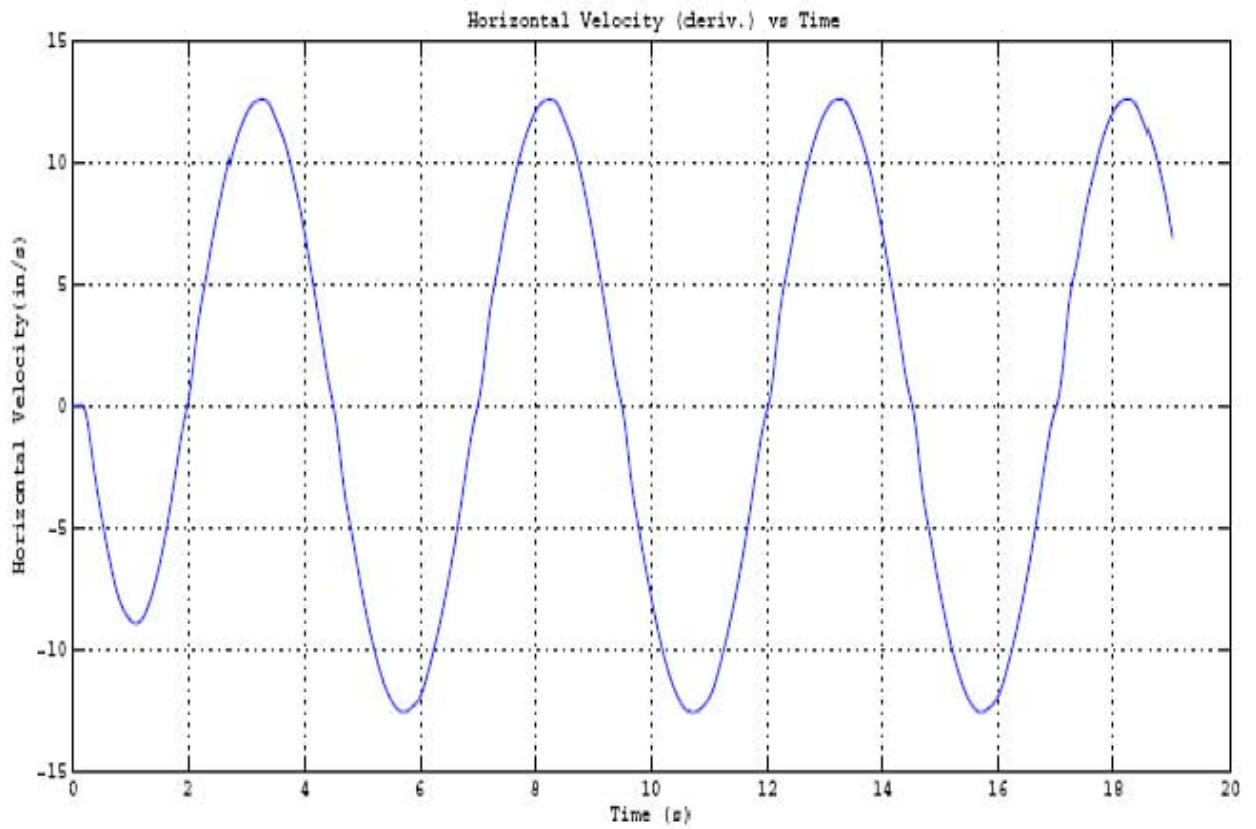


Figure 5-7 Results of Repeated Test #7.

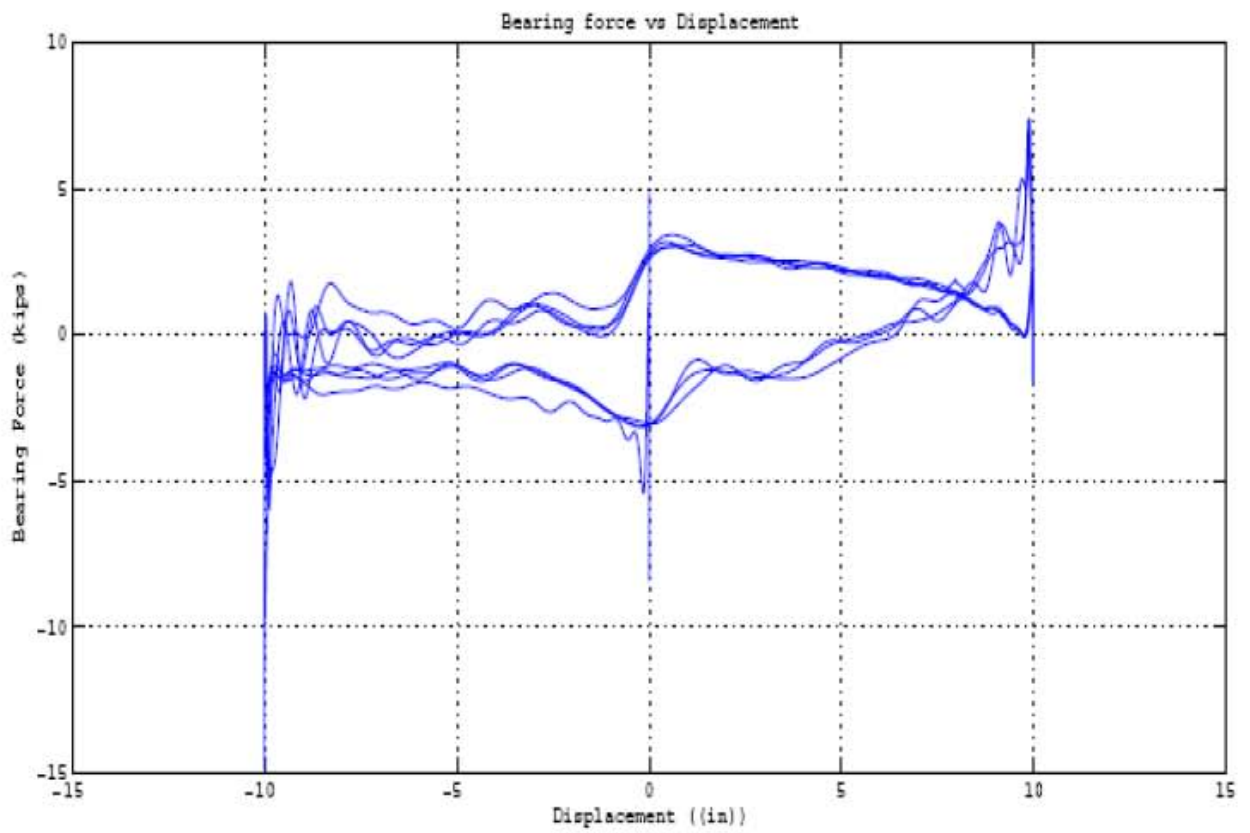
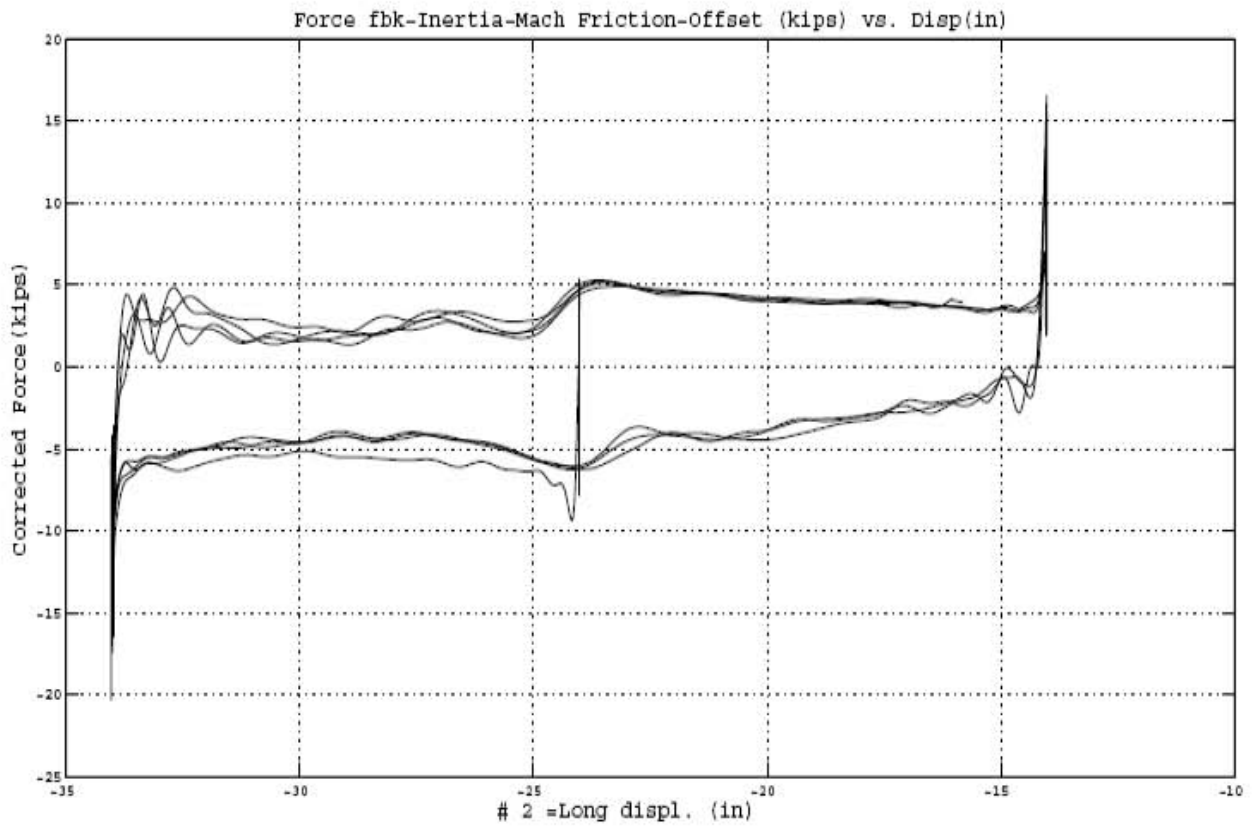


Figure 5-7 Results of Repeated Test #7 (continued).

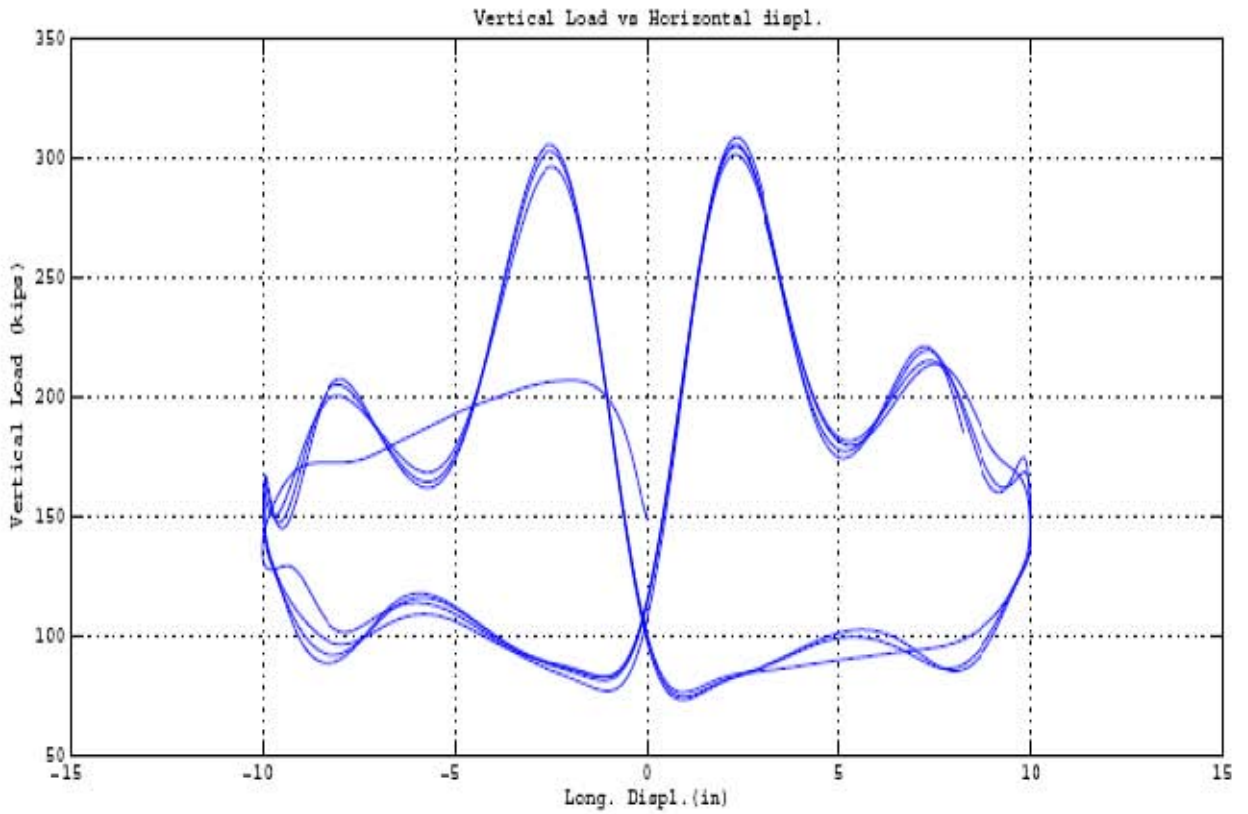
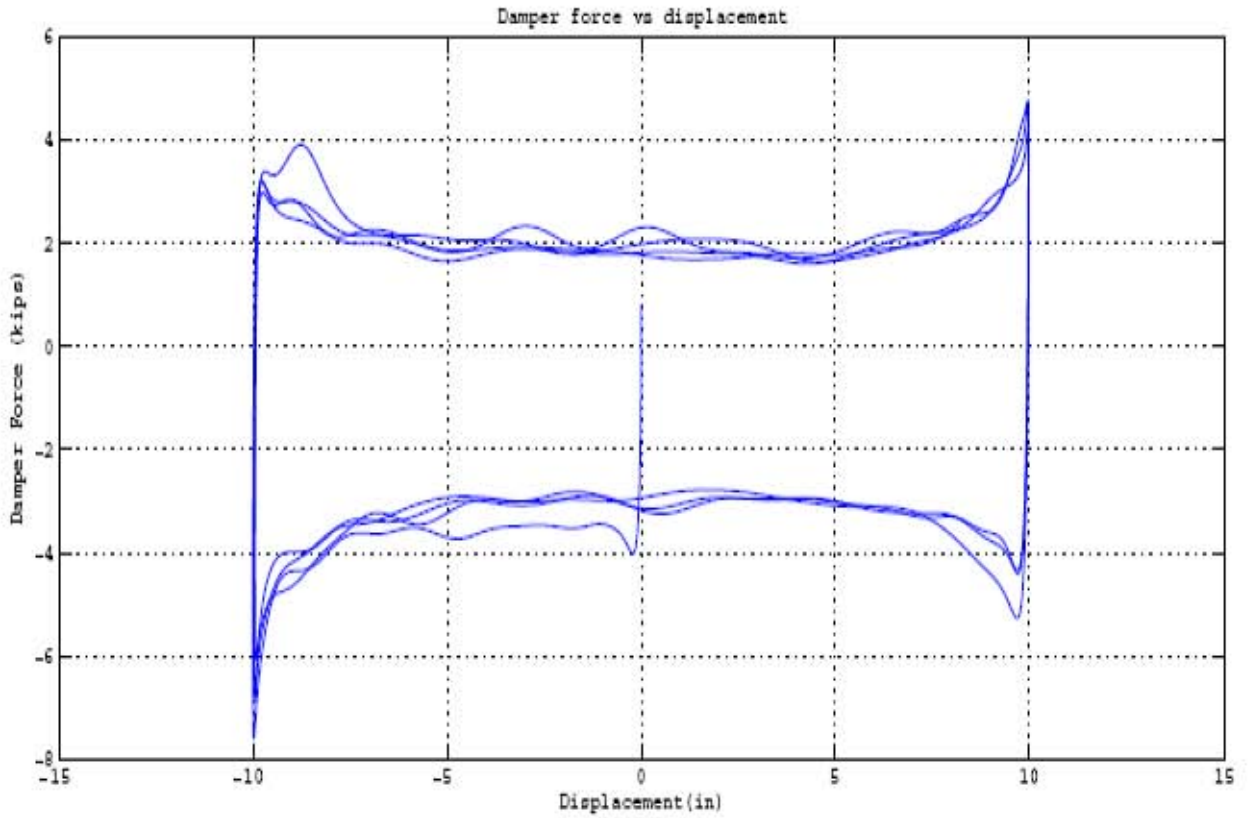


Figure 5-7 Results of Repeated Test #7 (continued).

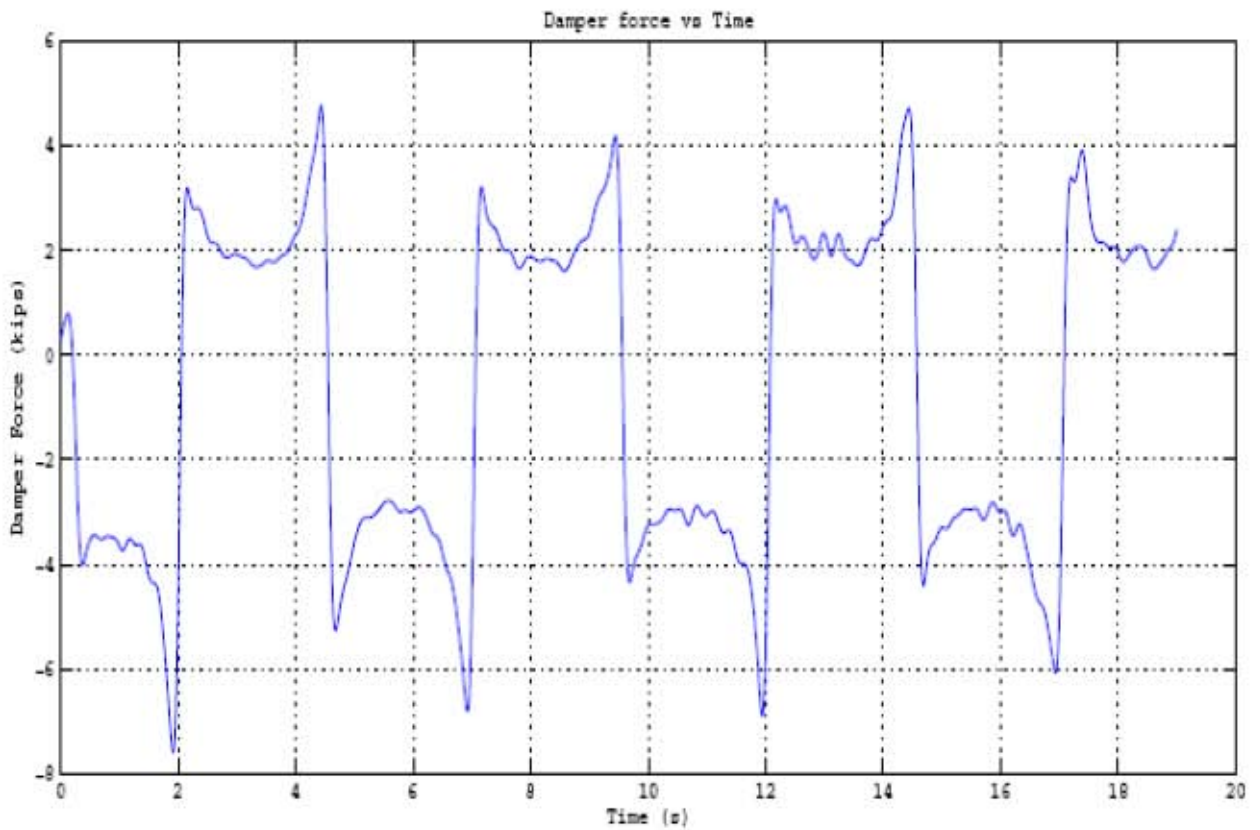
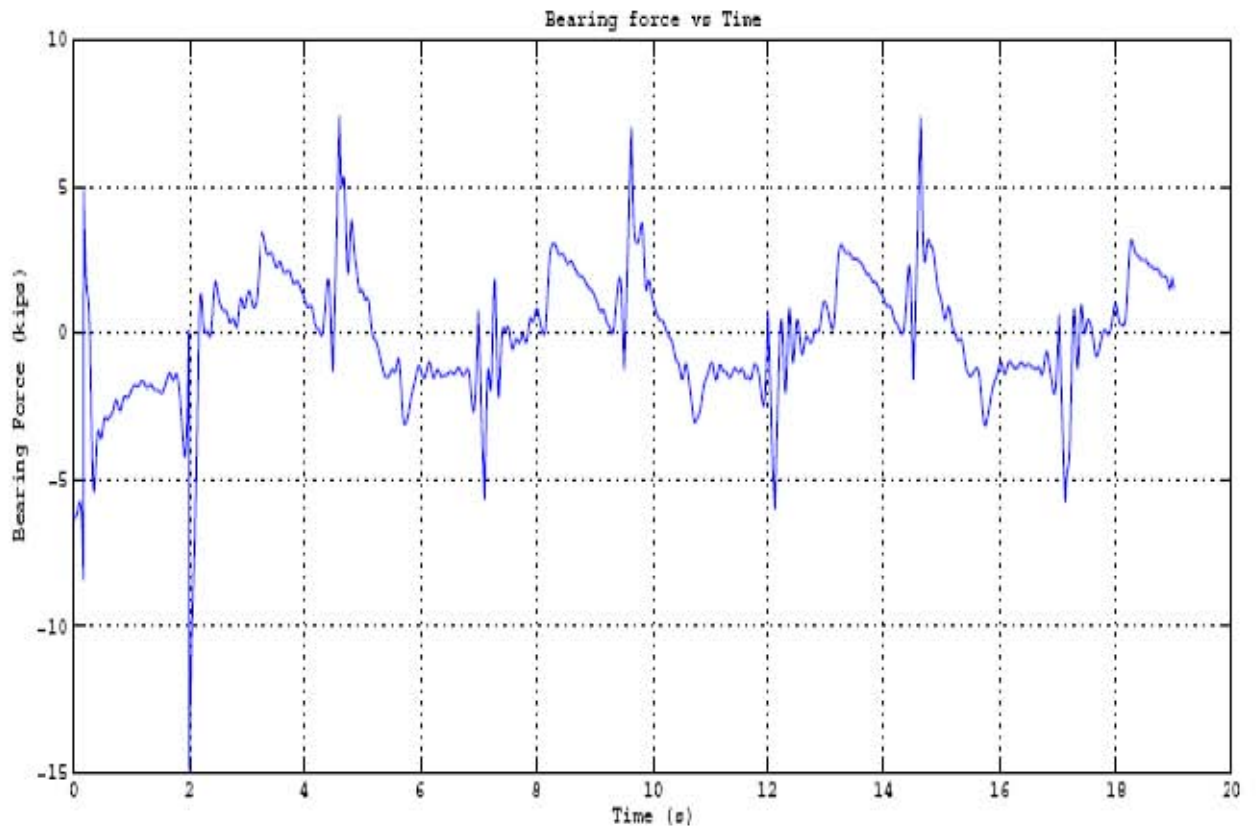


Figure 5-7 Results of Repeated Test #7 (continued).

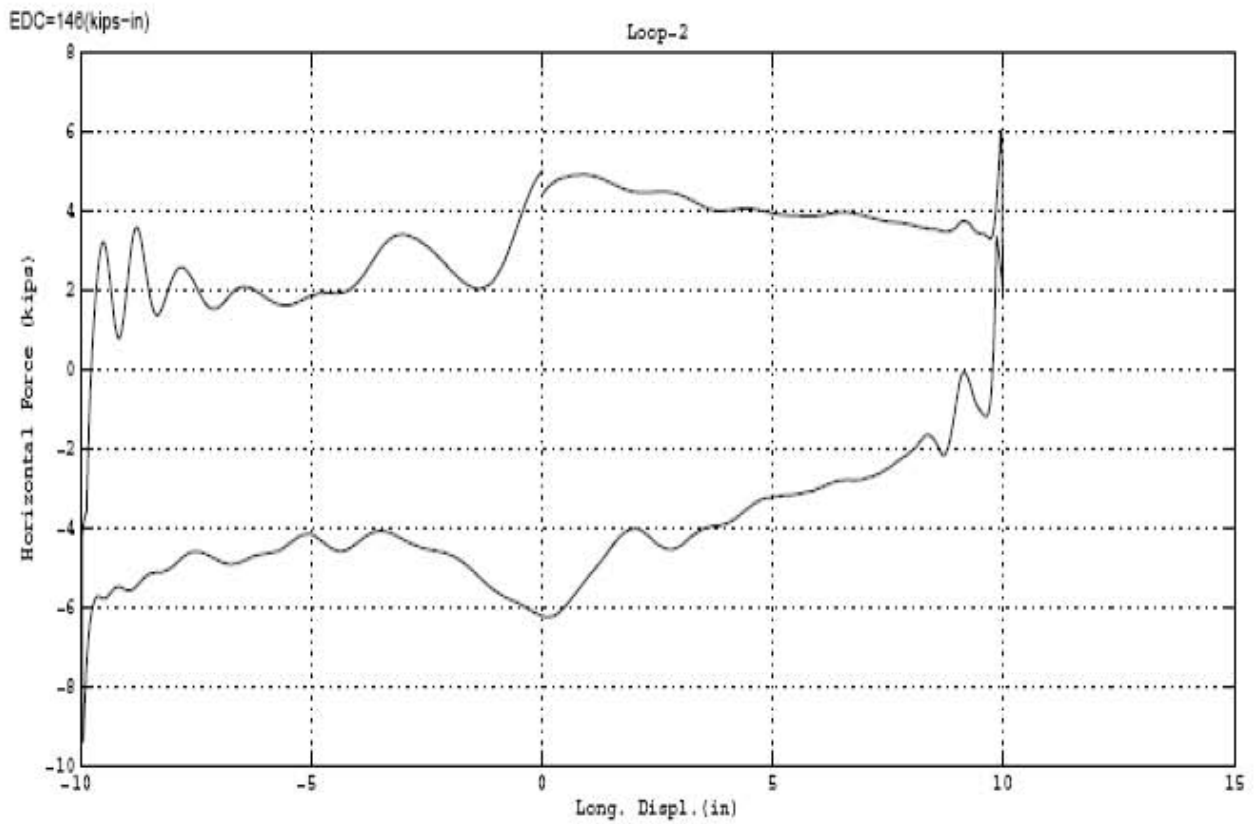
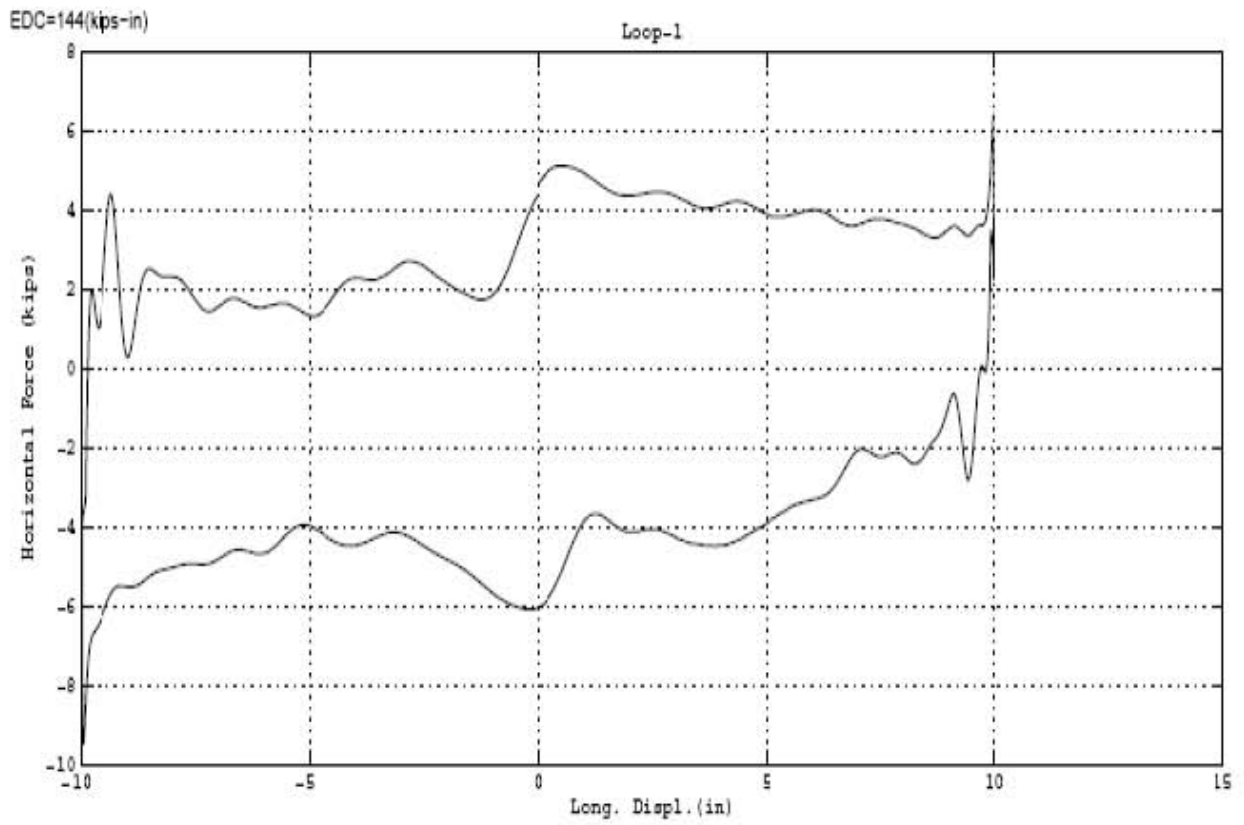


Figure 5-7 Results of Repeated Test #7 (continued).

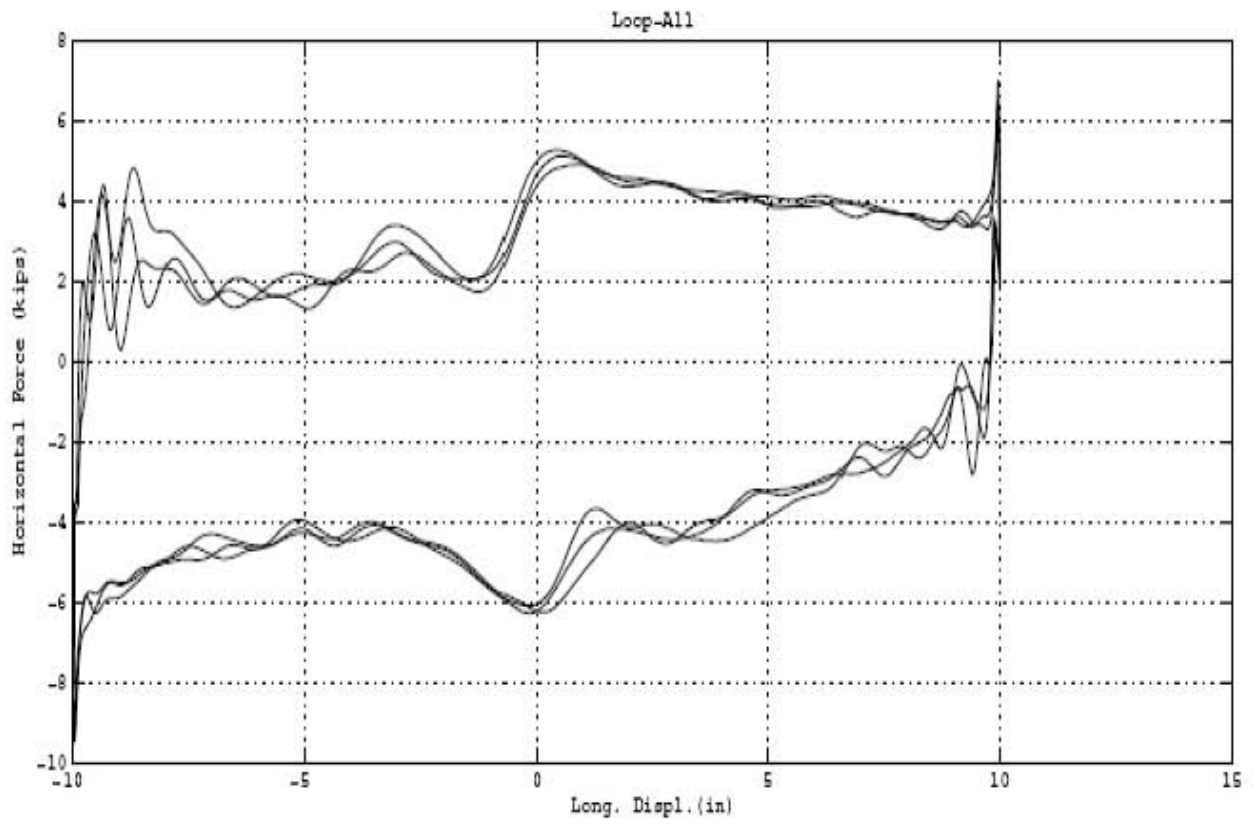
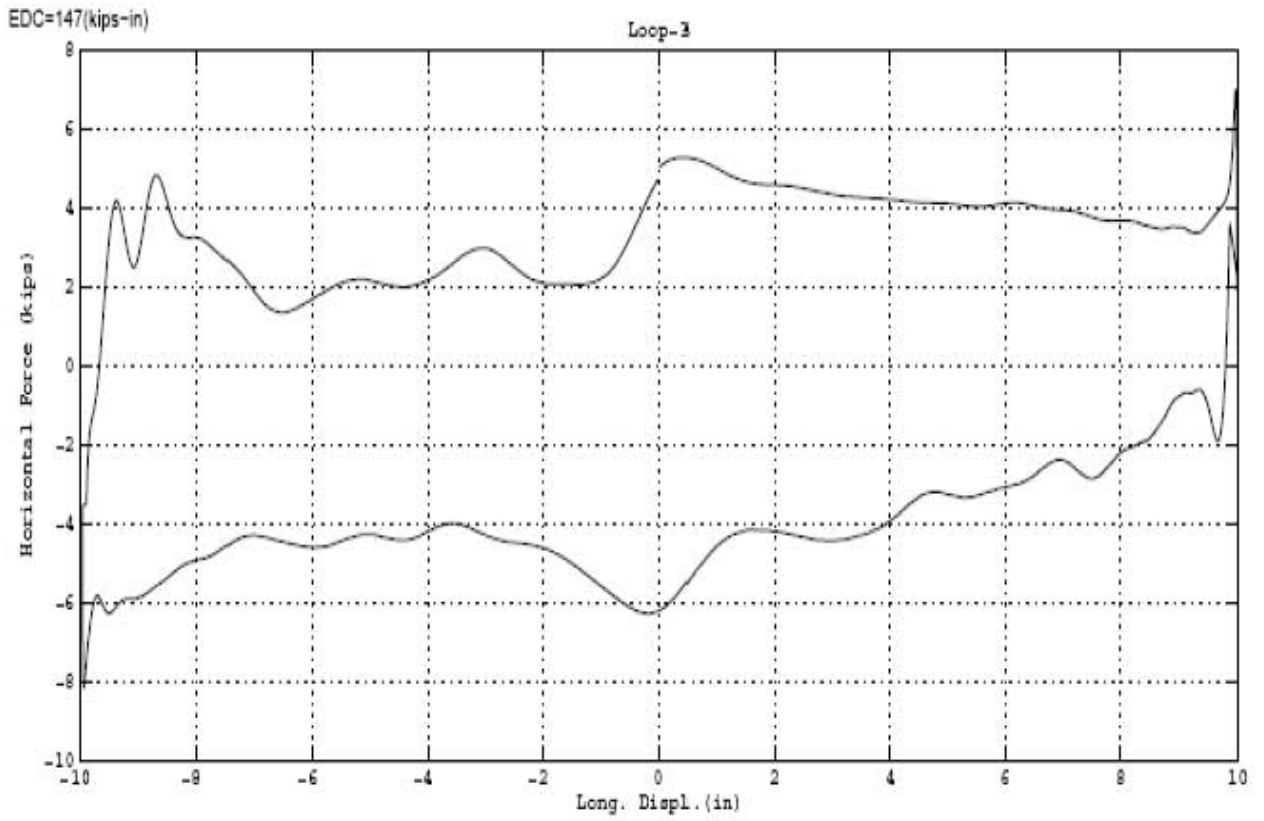


Figure 5-7 Results of Repeated Test #7 (continued).

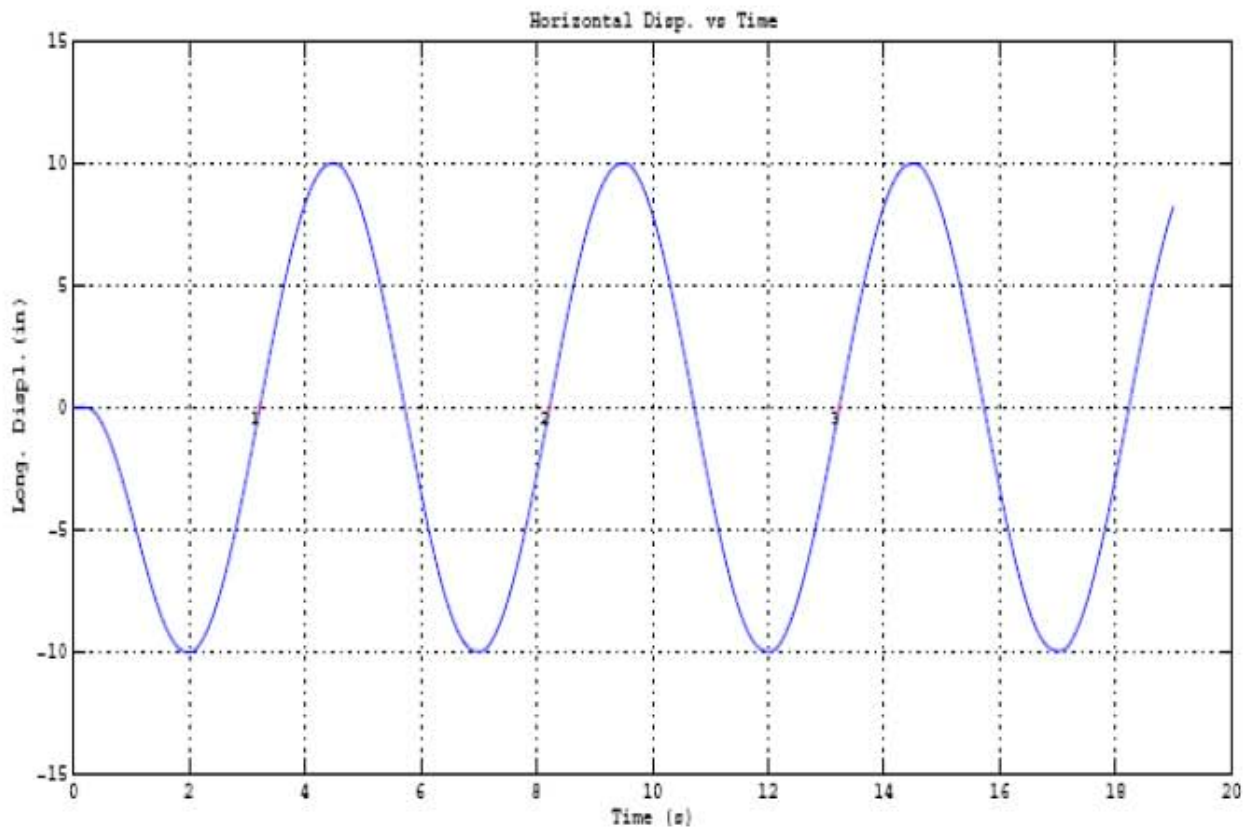
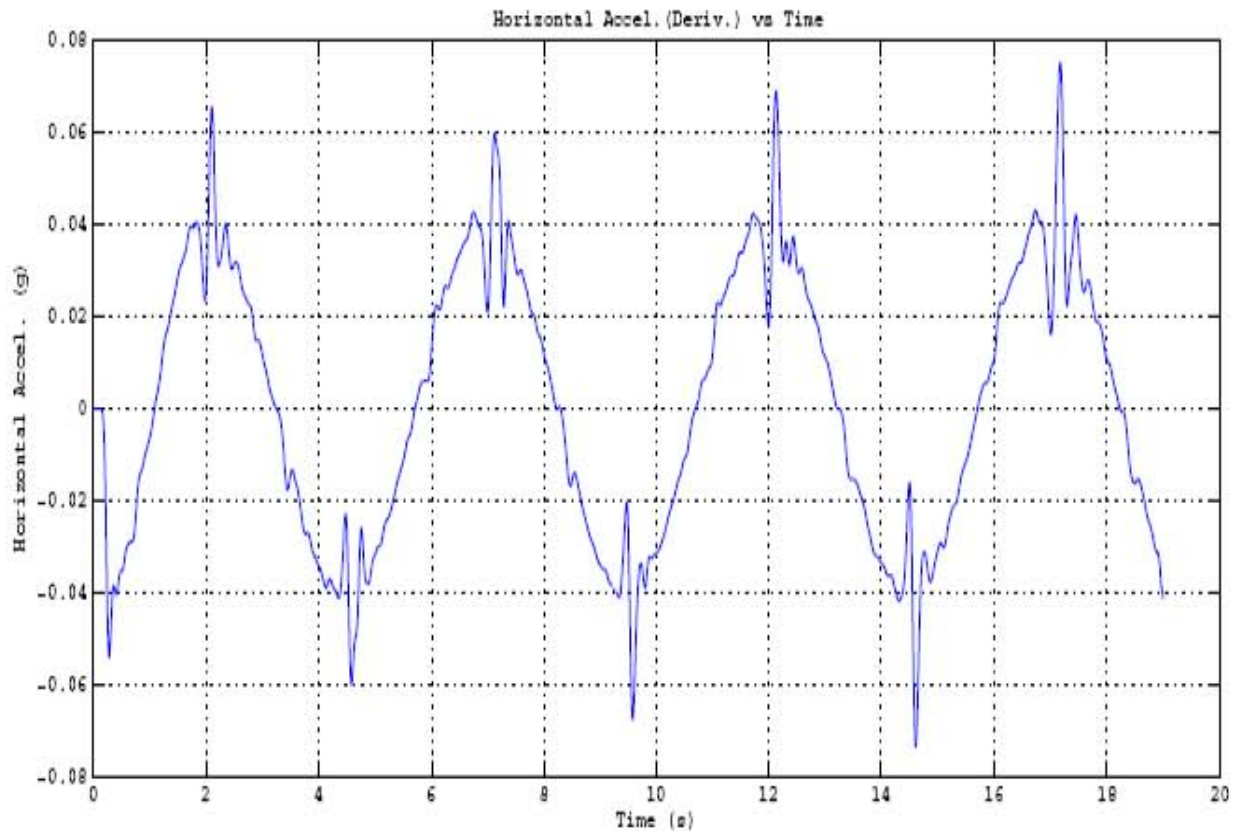


Figure 5-7 Results of Repeated Test #7 (continued).

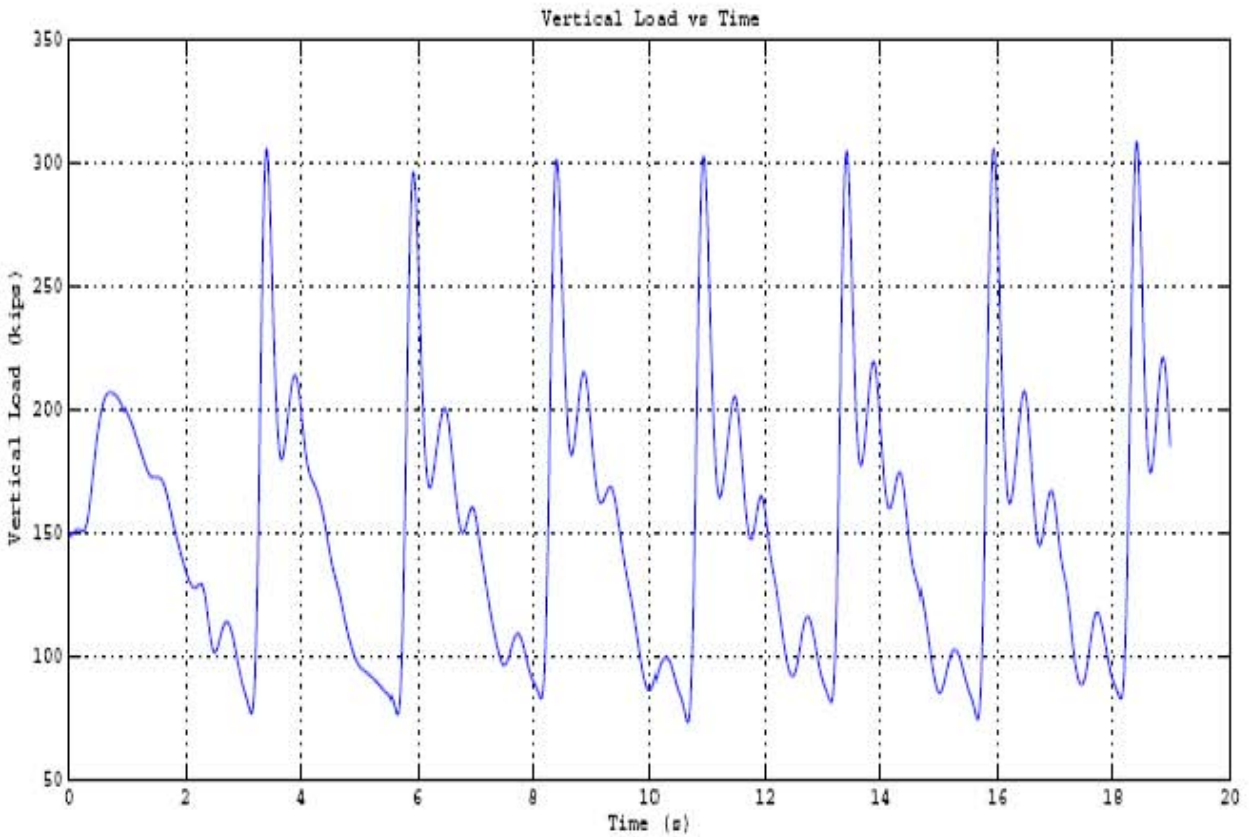
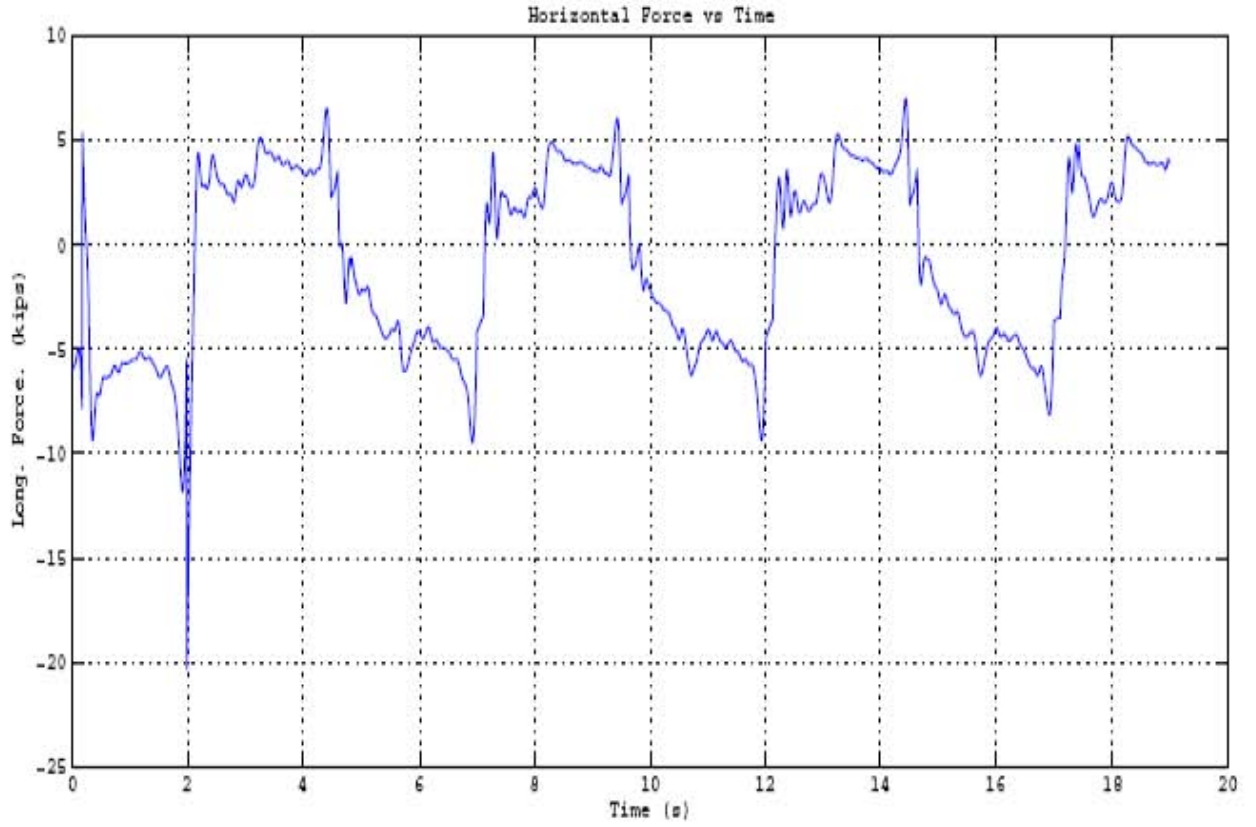


Figure 5-7 Results of Repeated Test #7 (continued).

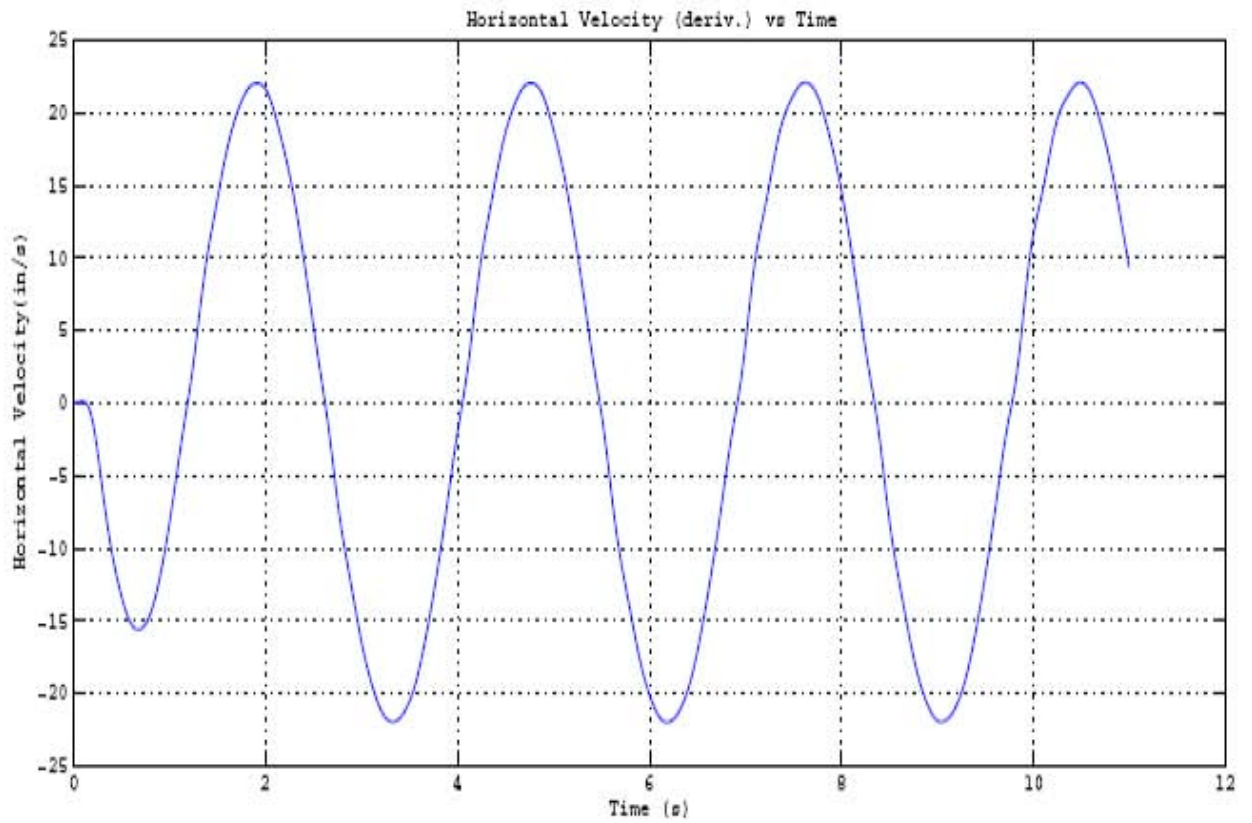
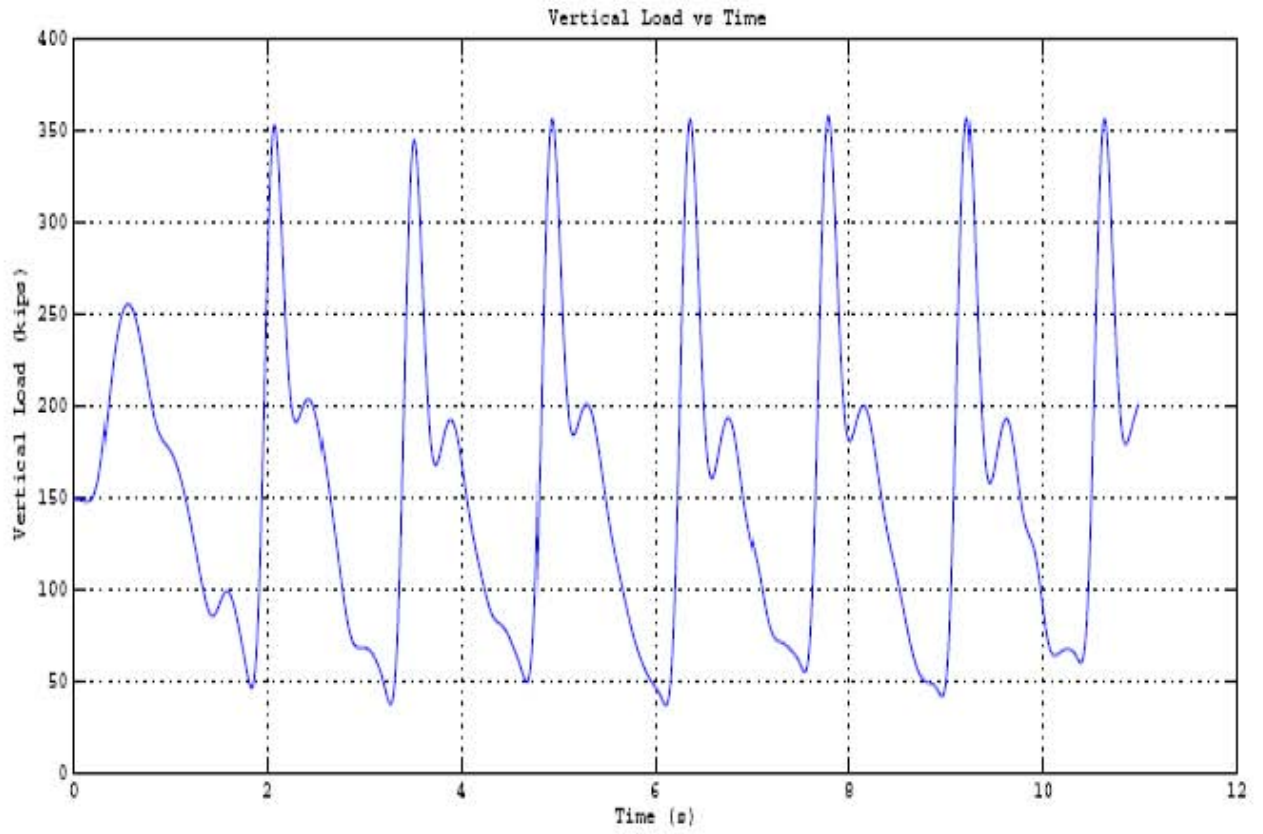


Figure 5-8 Results of Repeated Test #8.

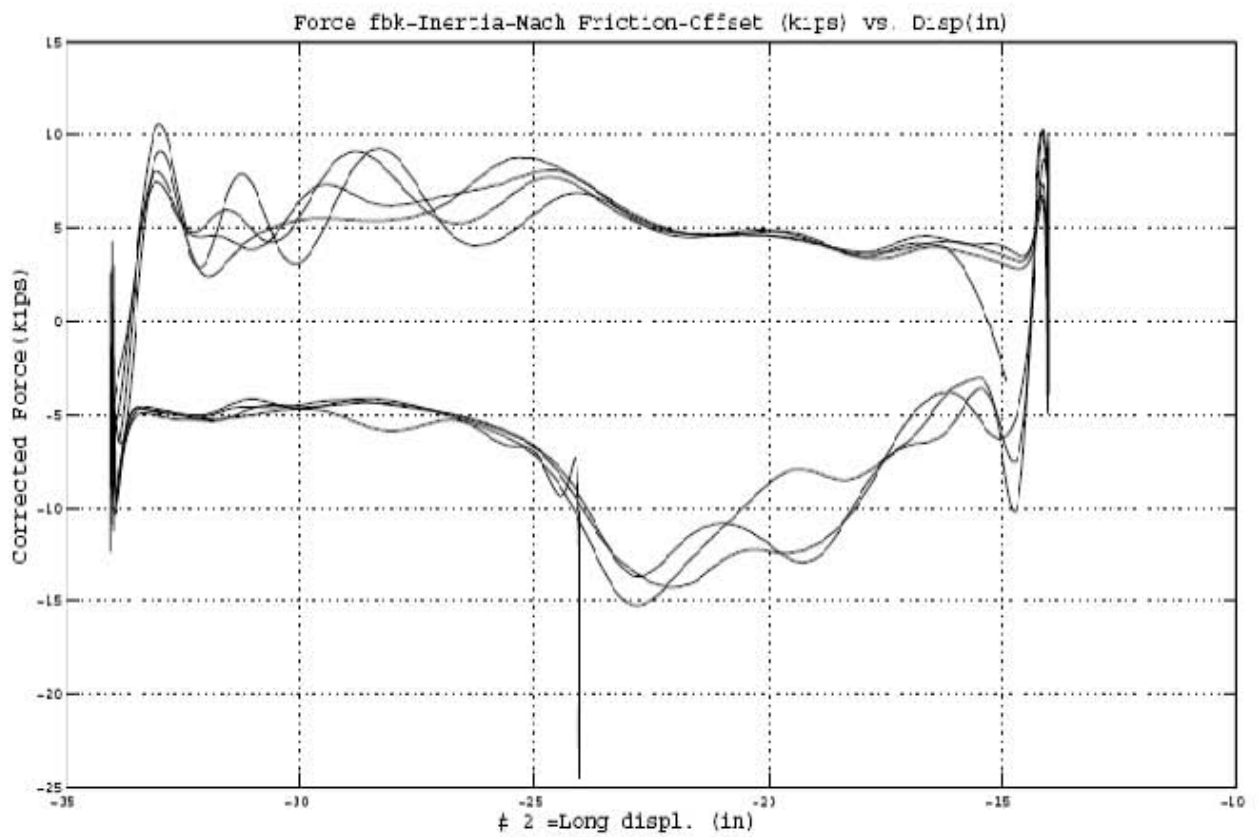
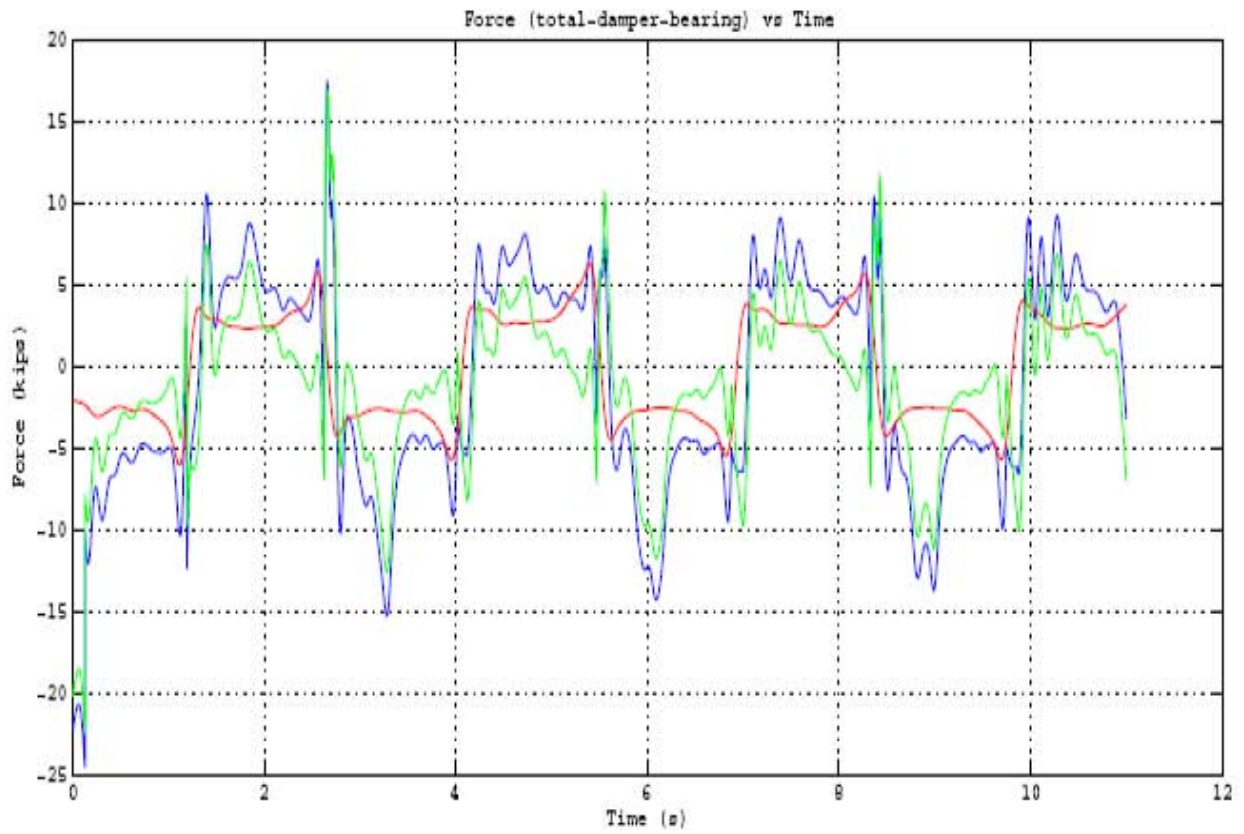


Figure 5-8 Results of Repeated Test #8 (continued).

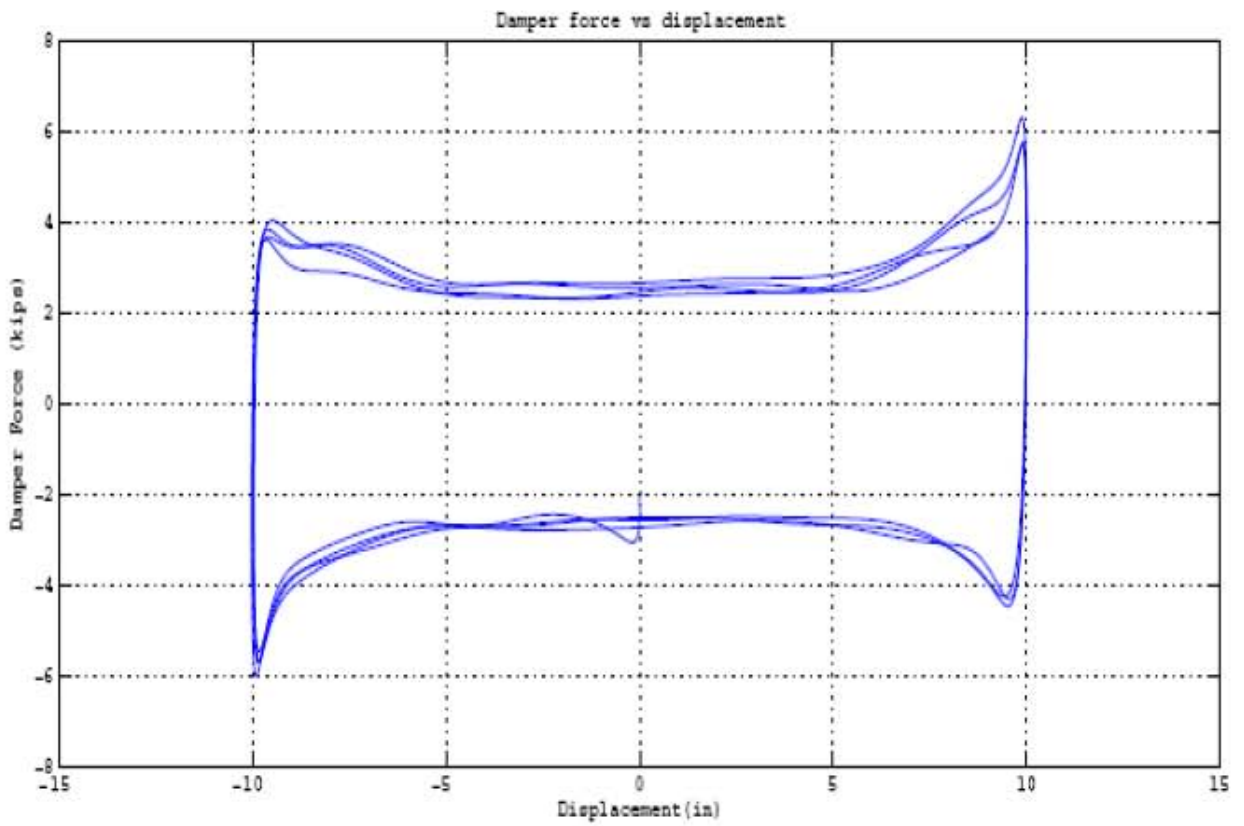
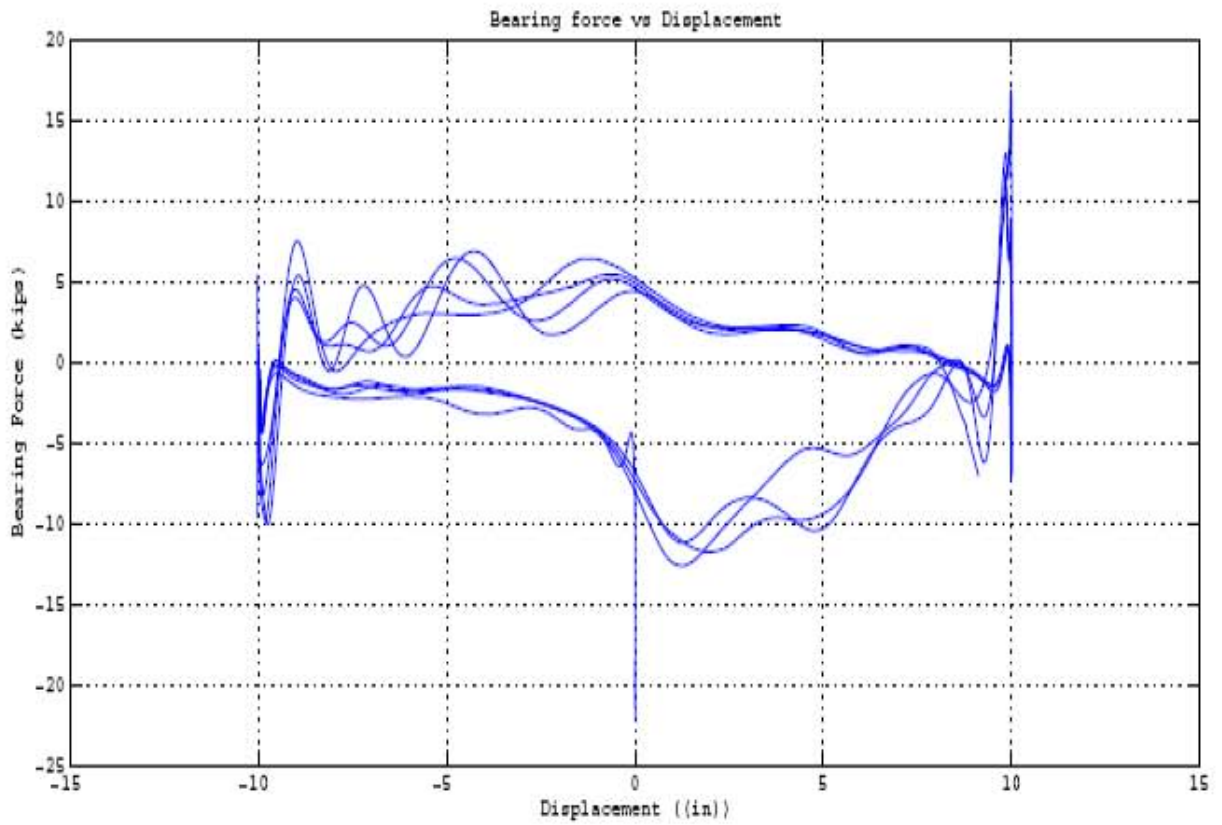


Figure 5-8 Results of Repeated Test #8 (continued).

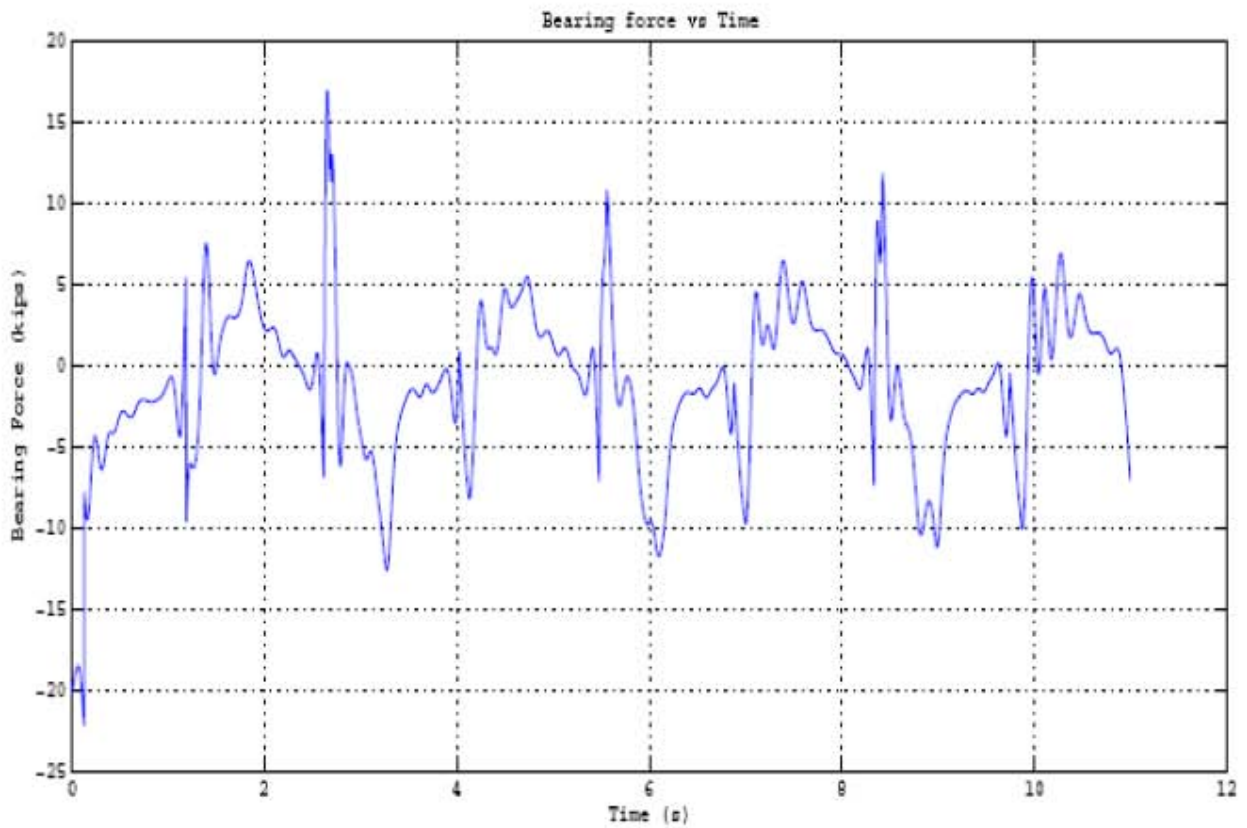
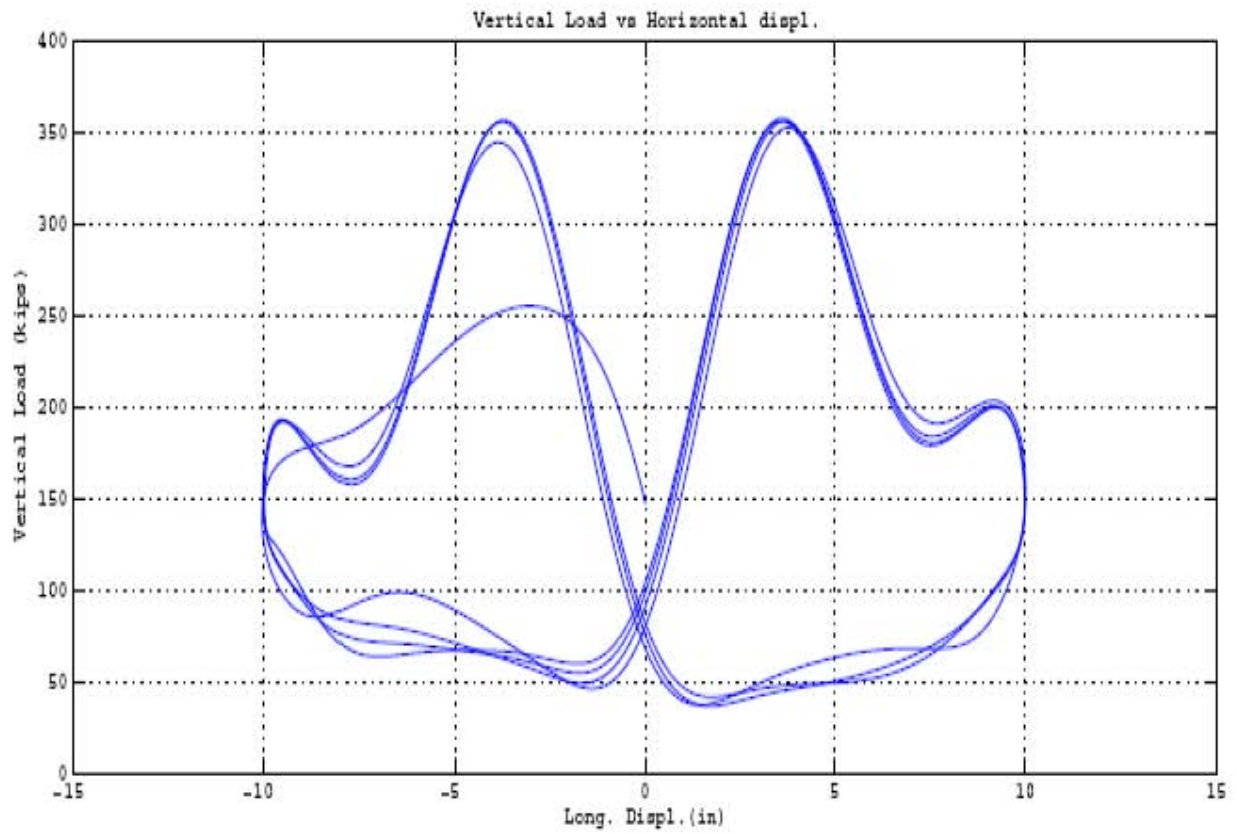


Figure 5-8 Results of Repeated Test #8 (continued).

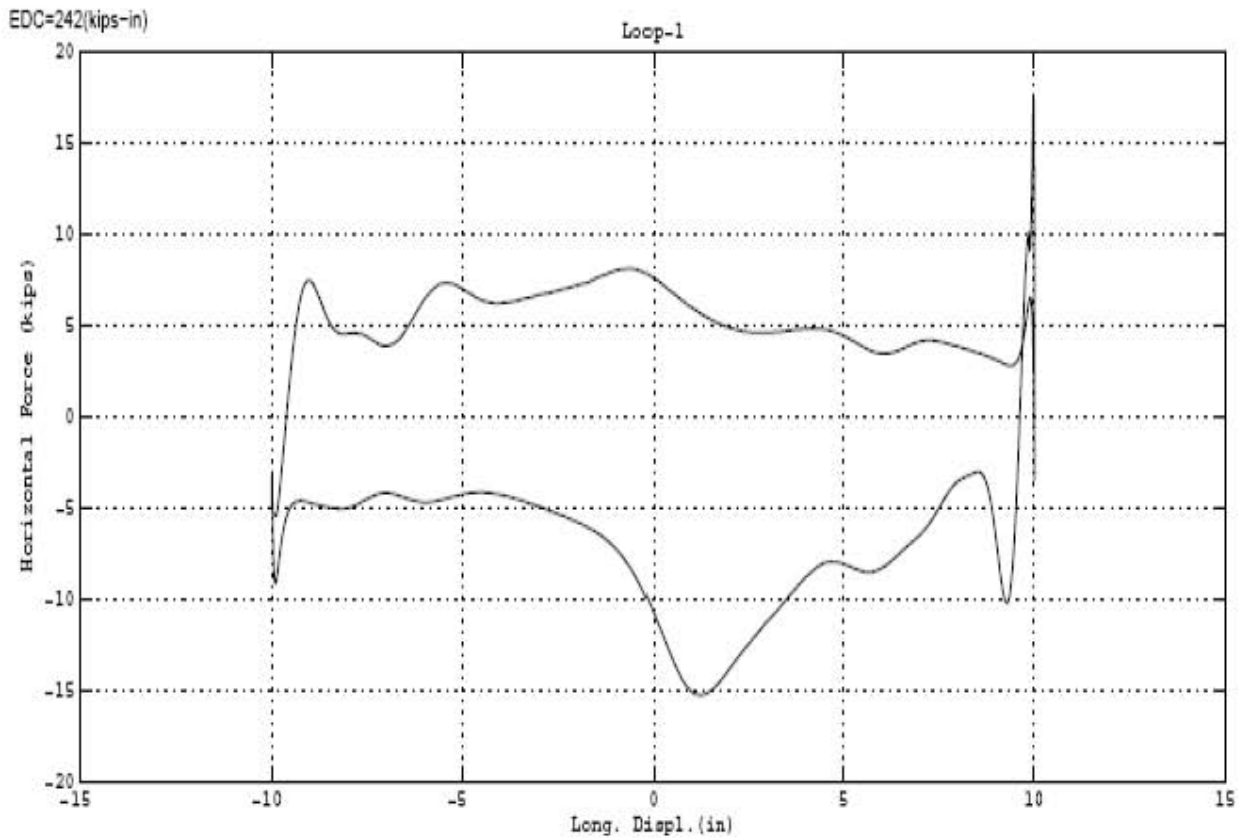
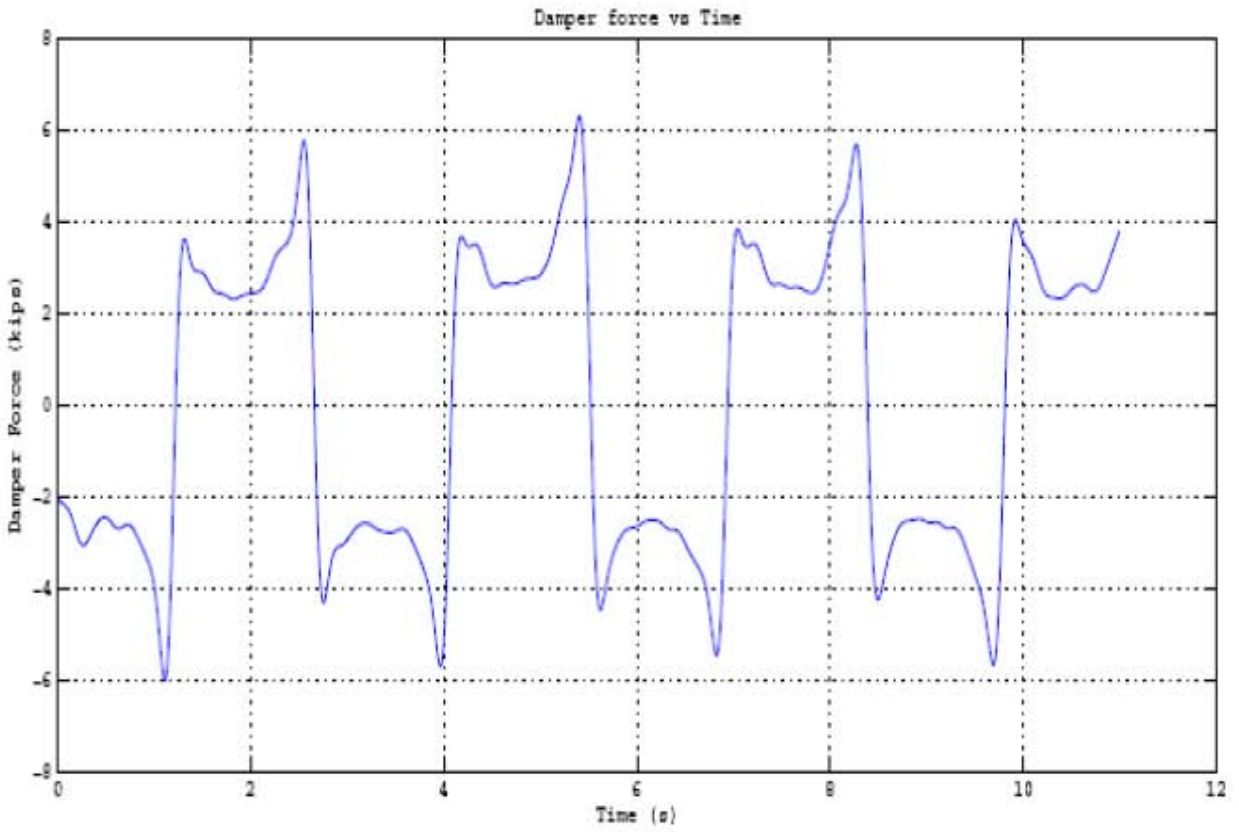


Figure 5-8 Results of Repeated Test #8 (continued).

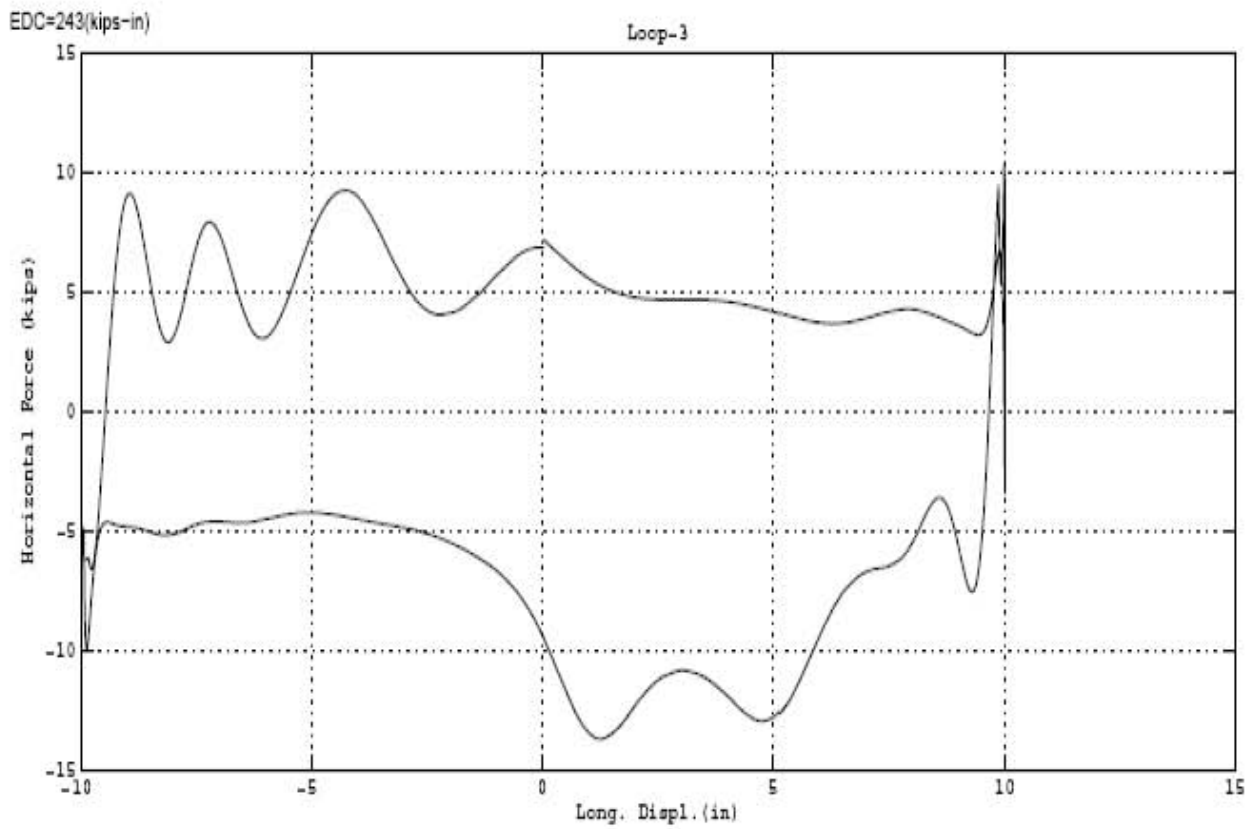
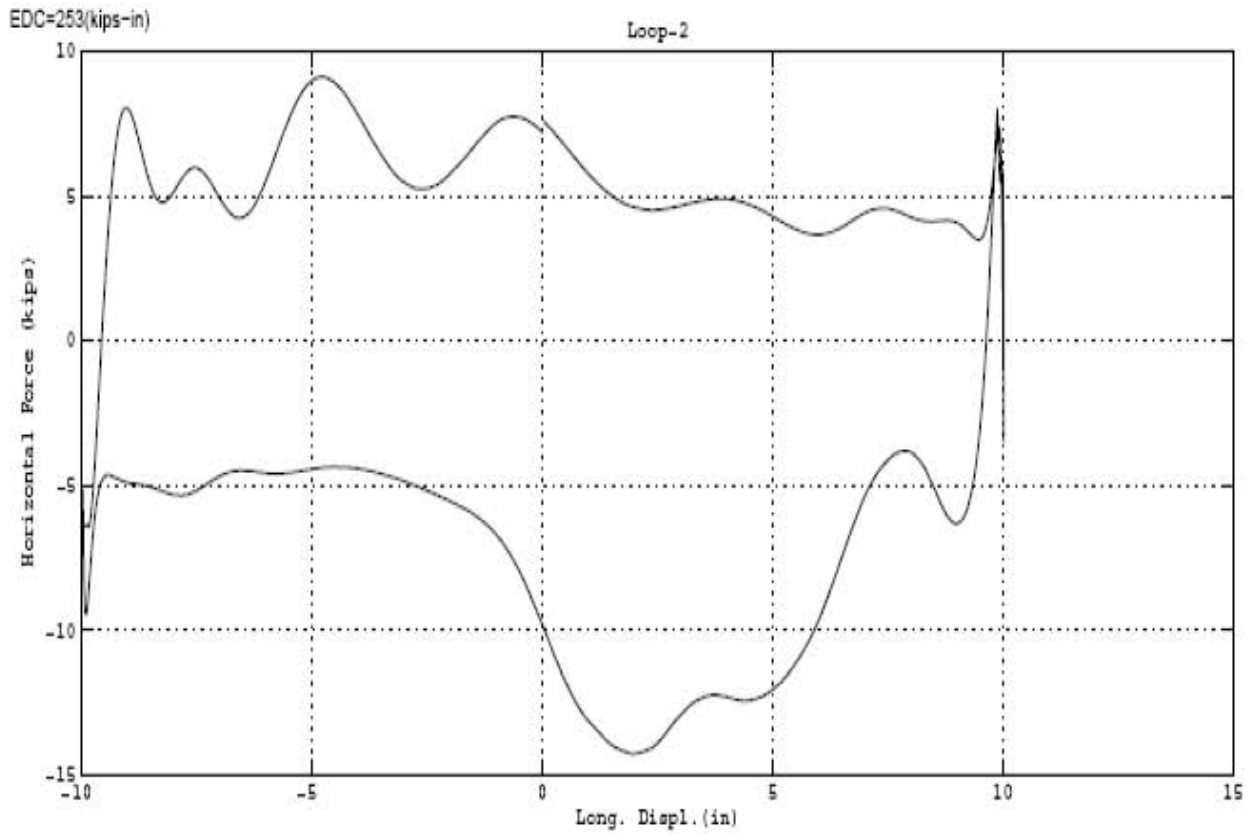


Figure 5-8 Results of Repeated Test #8 (continued).

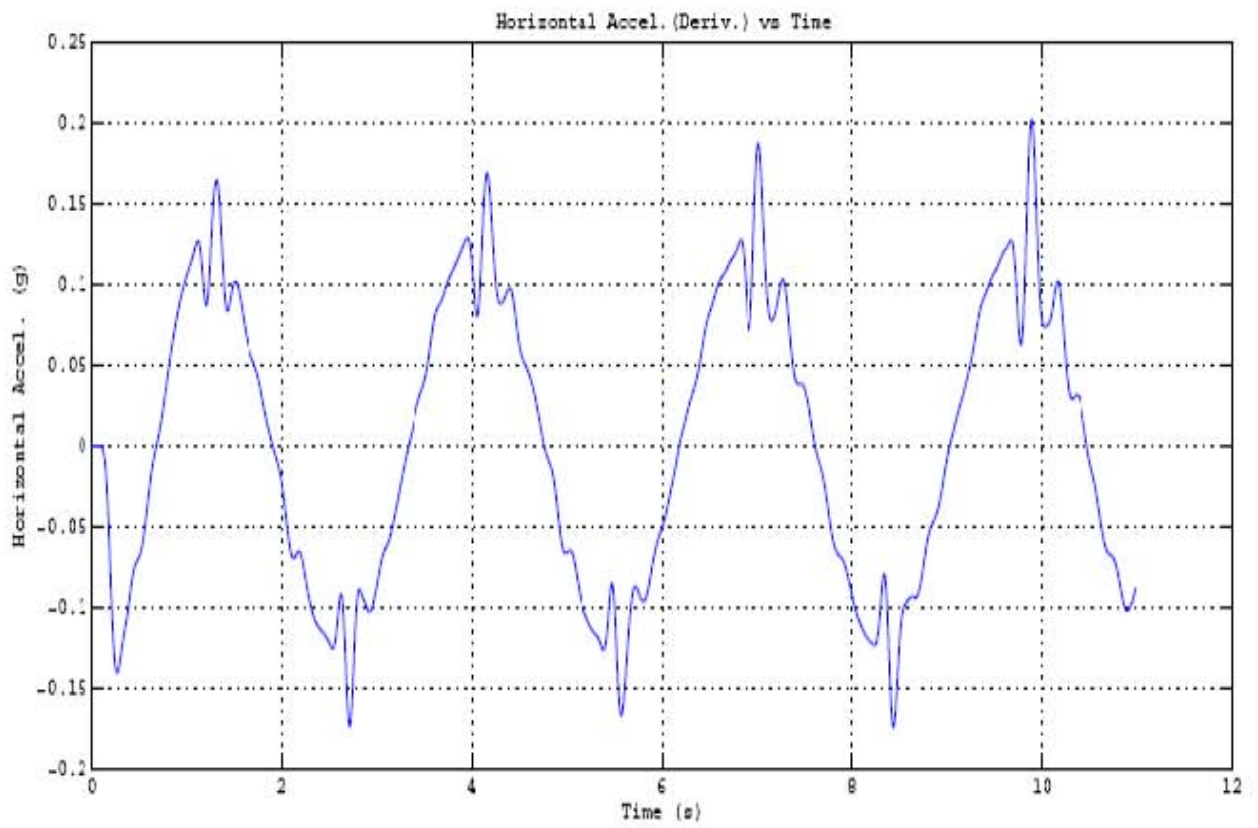
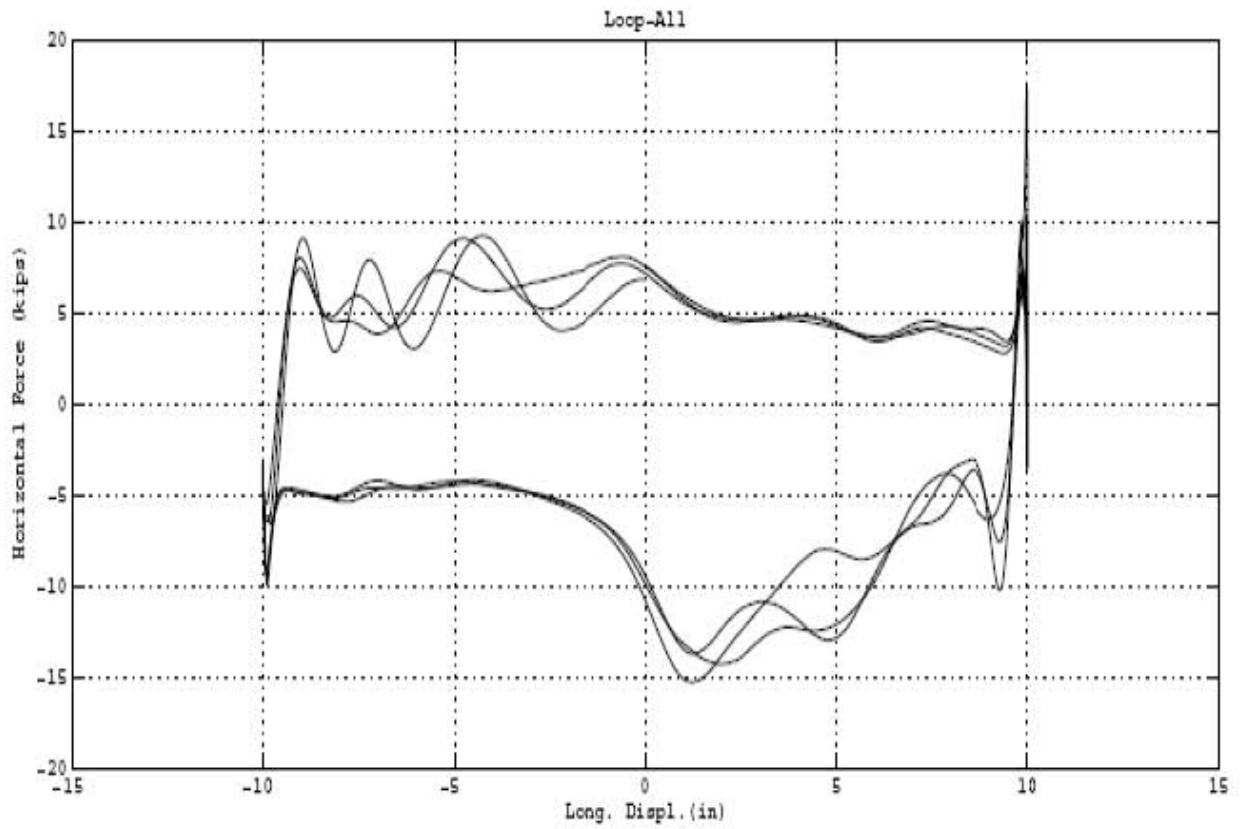


Figure 5-8 Results of Repeated Test #8 (continued).

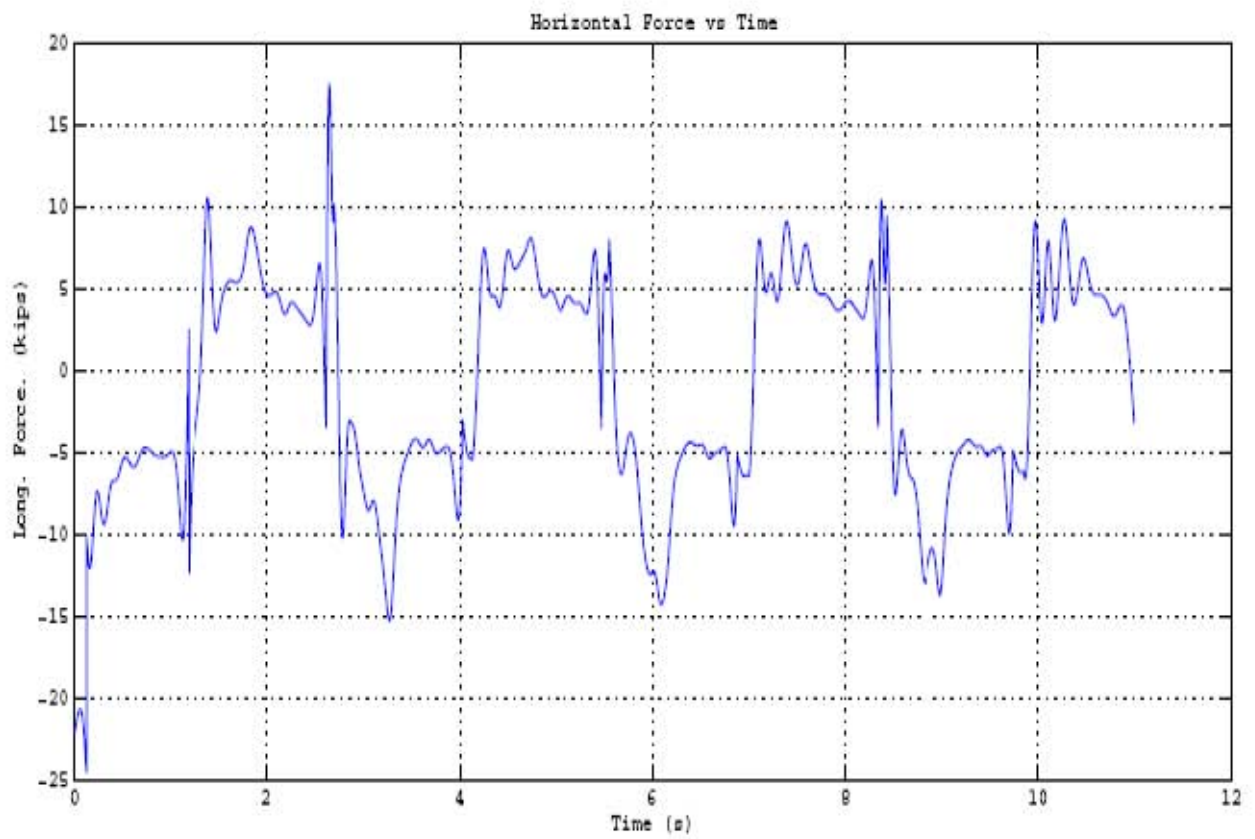
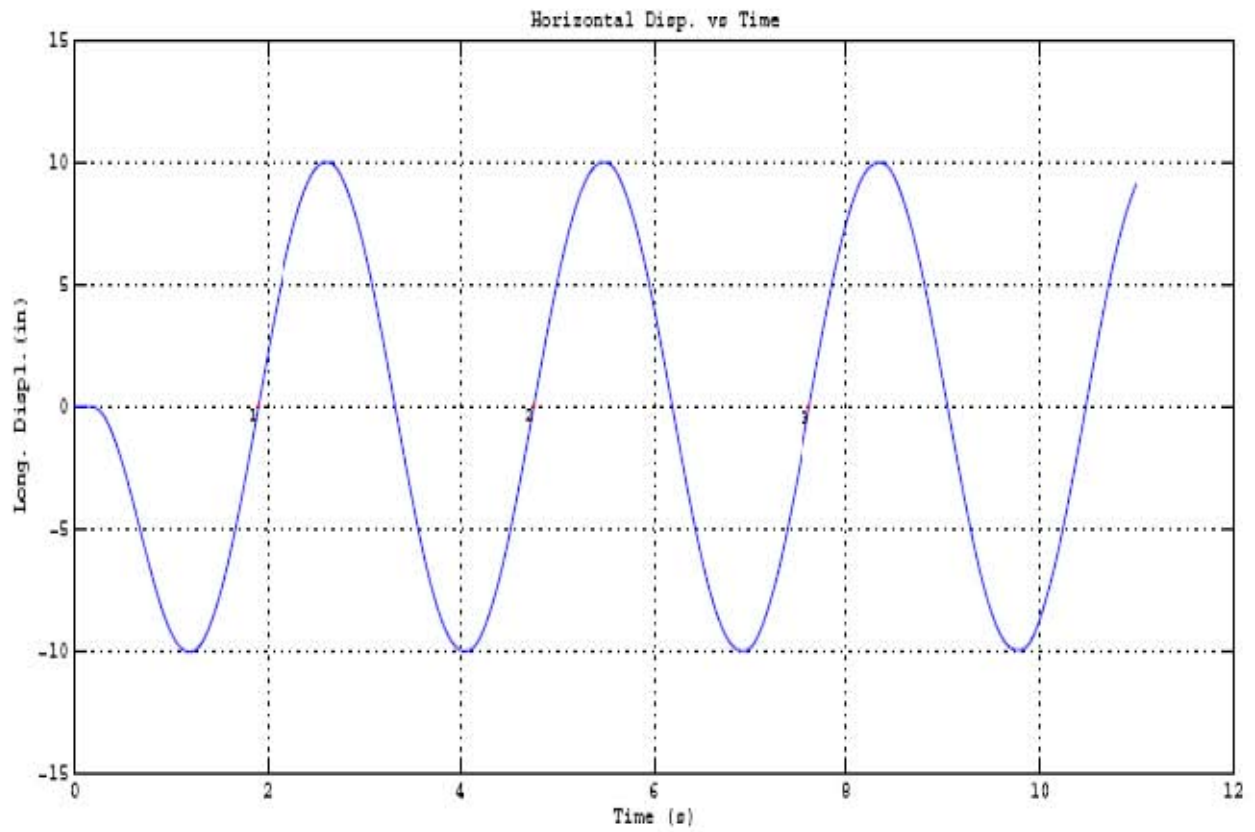


Figure 5-8 Results of Repeated Test #8 (continued).

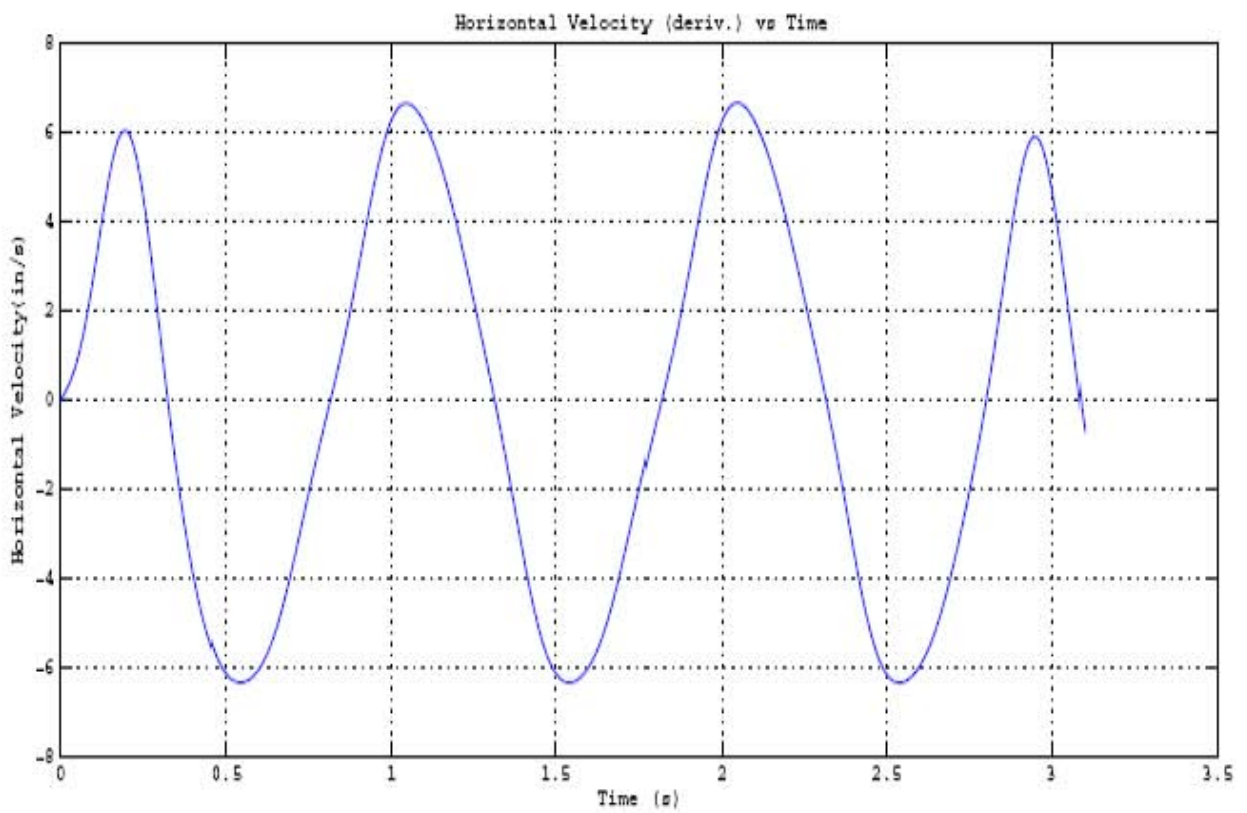
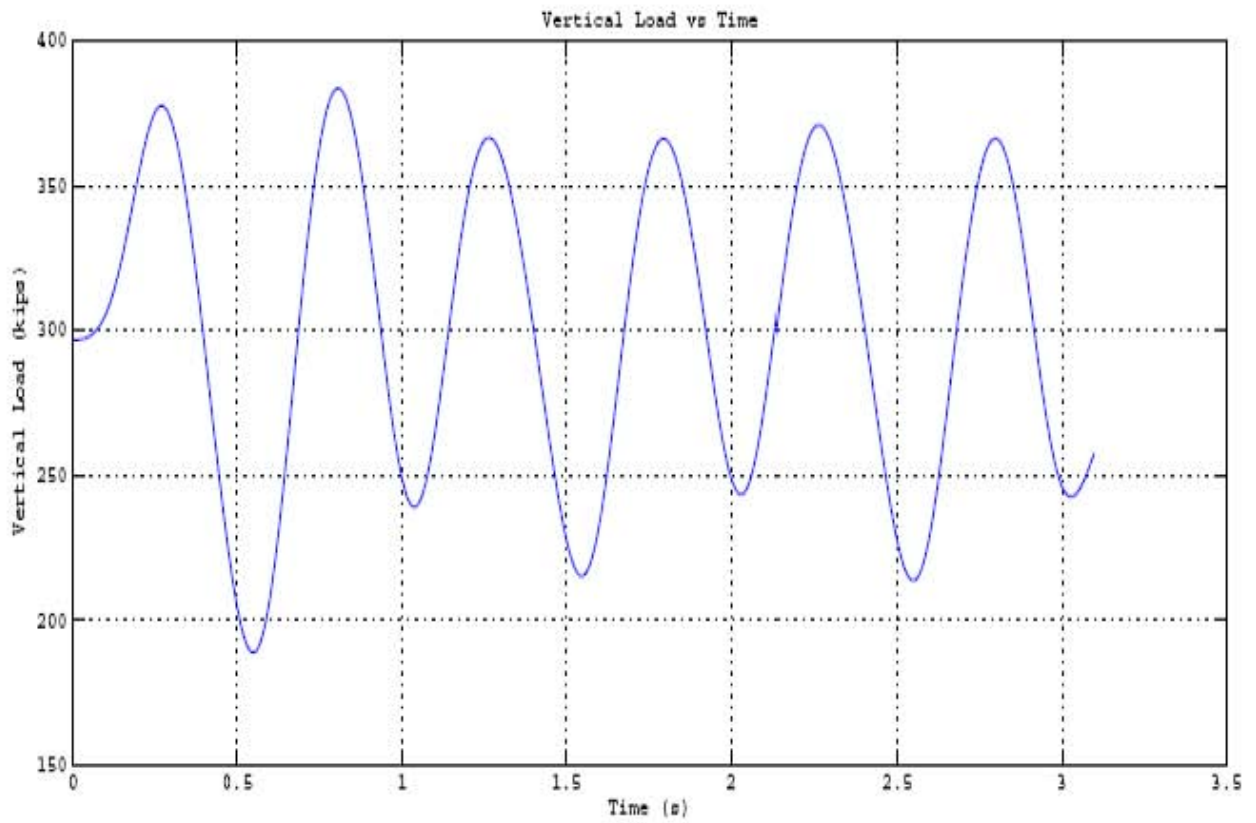


Figure 5-9 Results of Repeated Test #9.

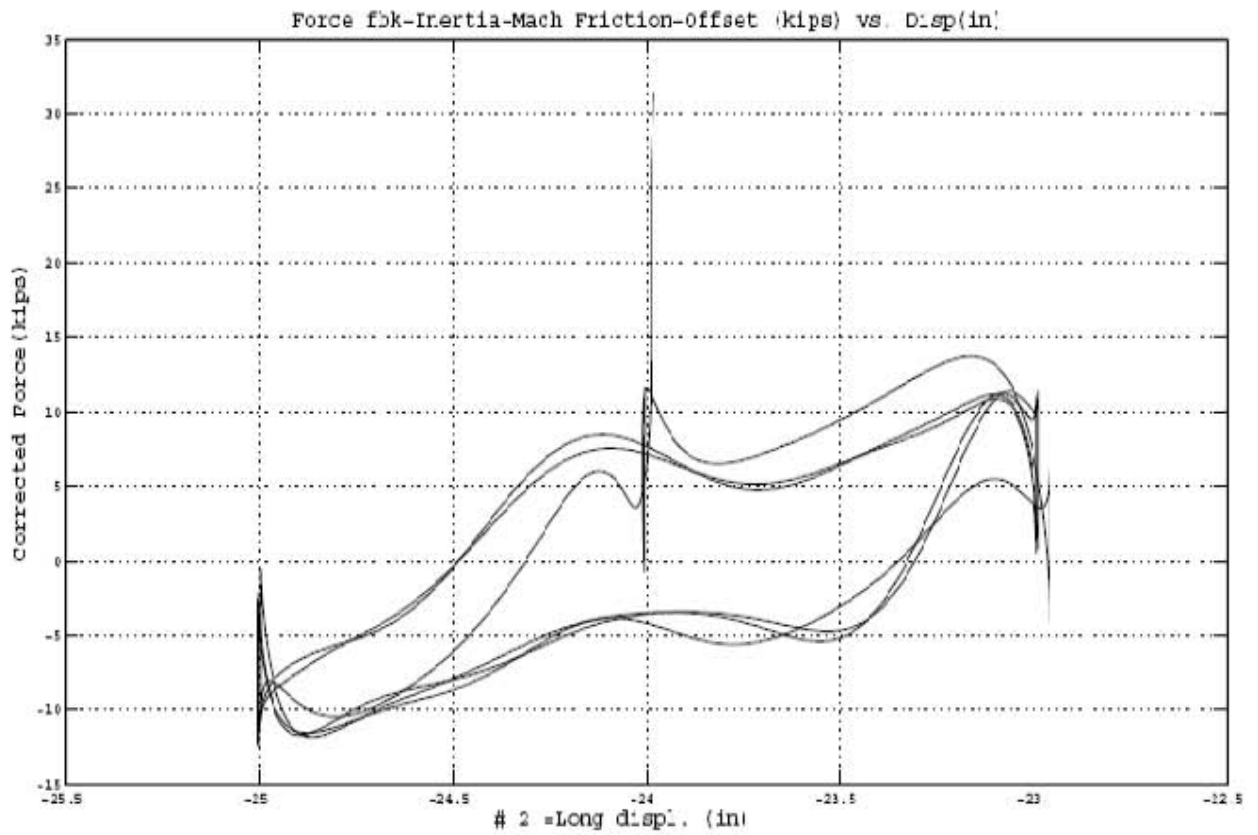
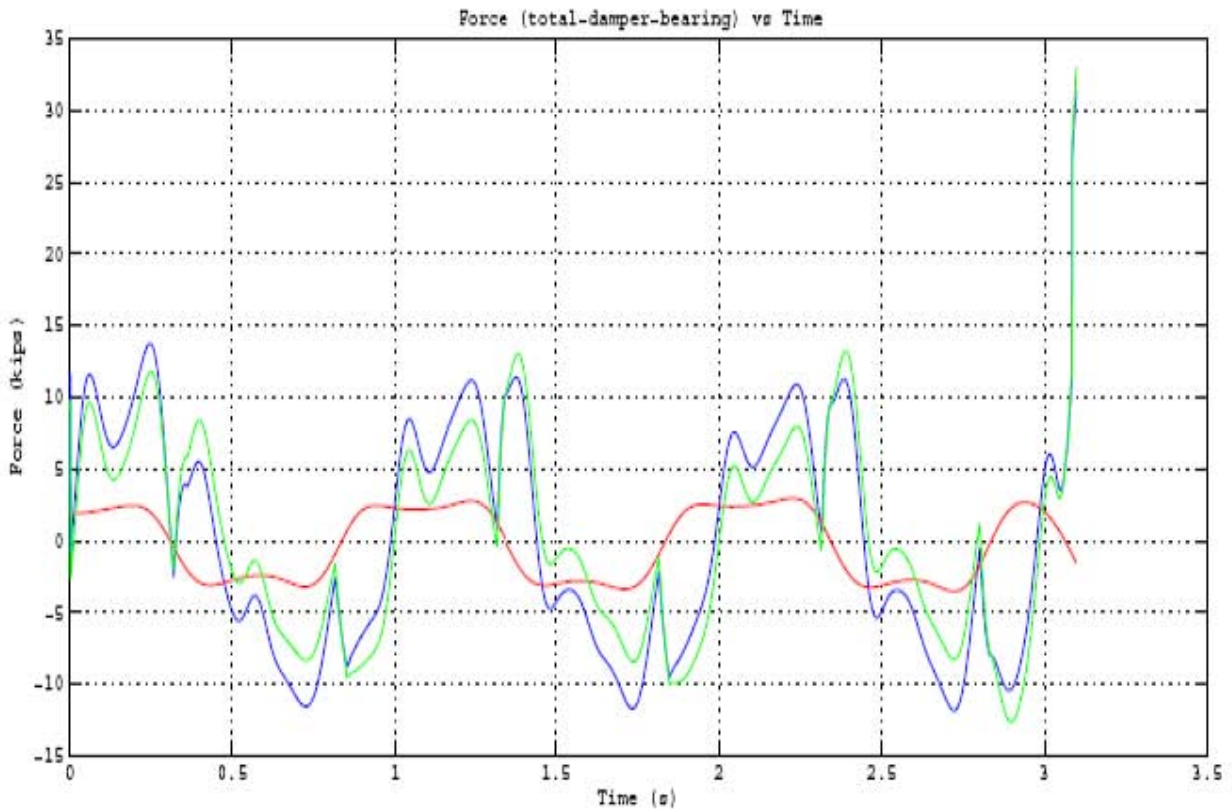


Figure 5-9 Results of Repeated Test #9 (continued).

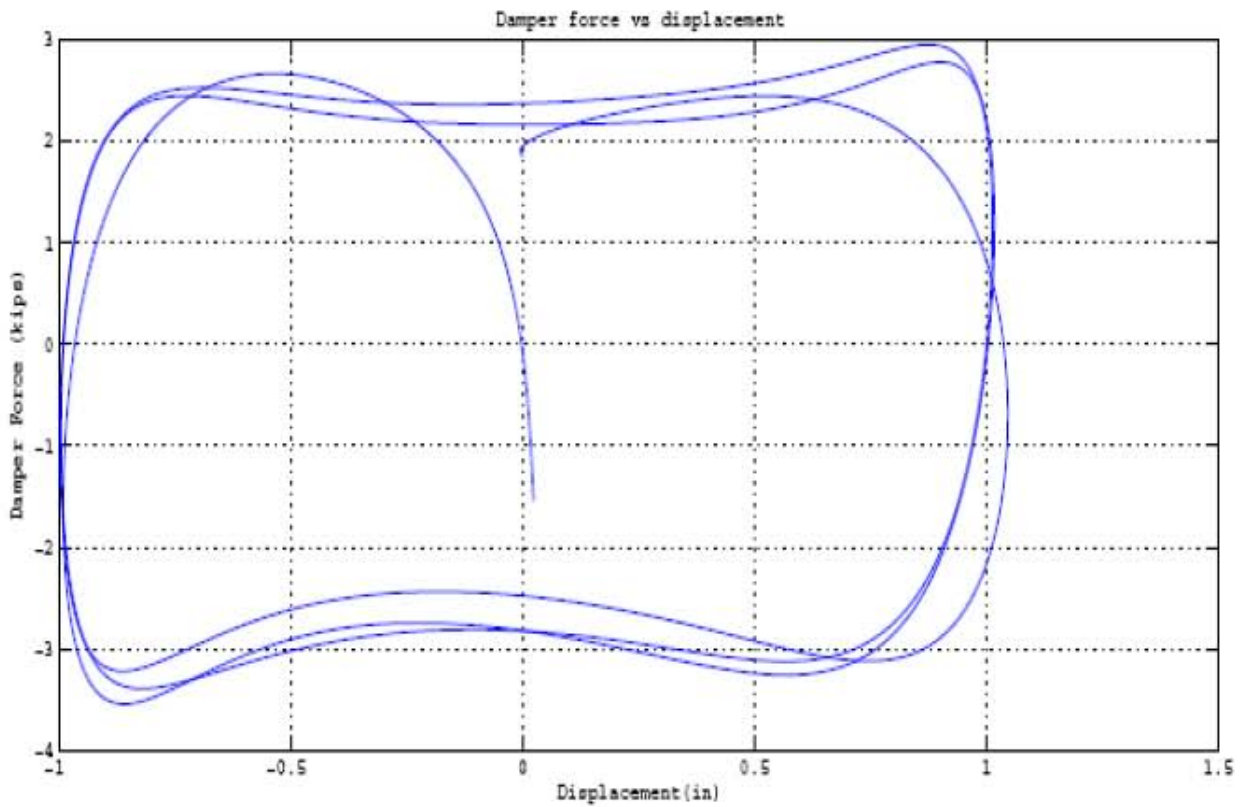
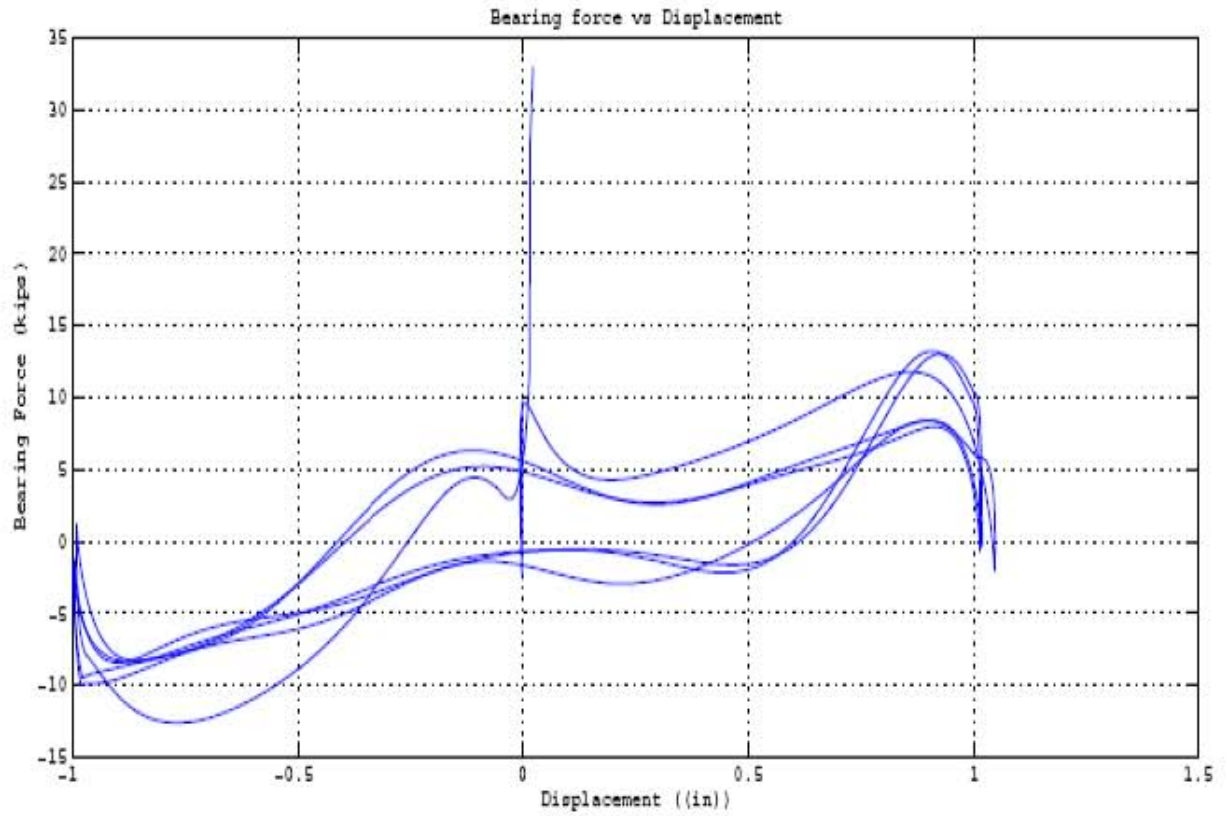


Figure 5-9 Results of Repeated Test #9 (continued).

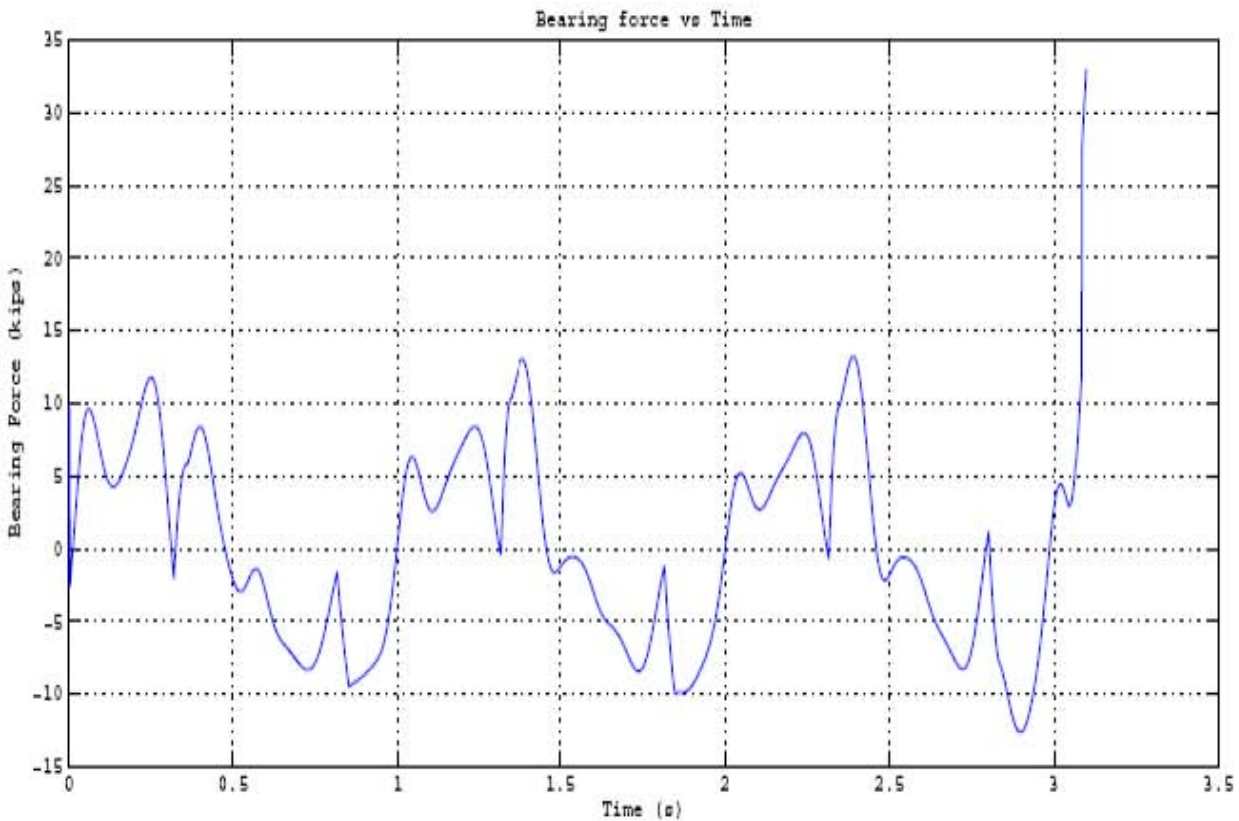
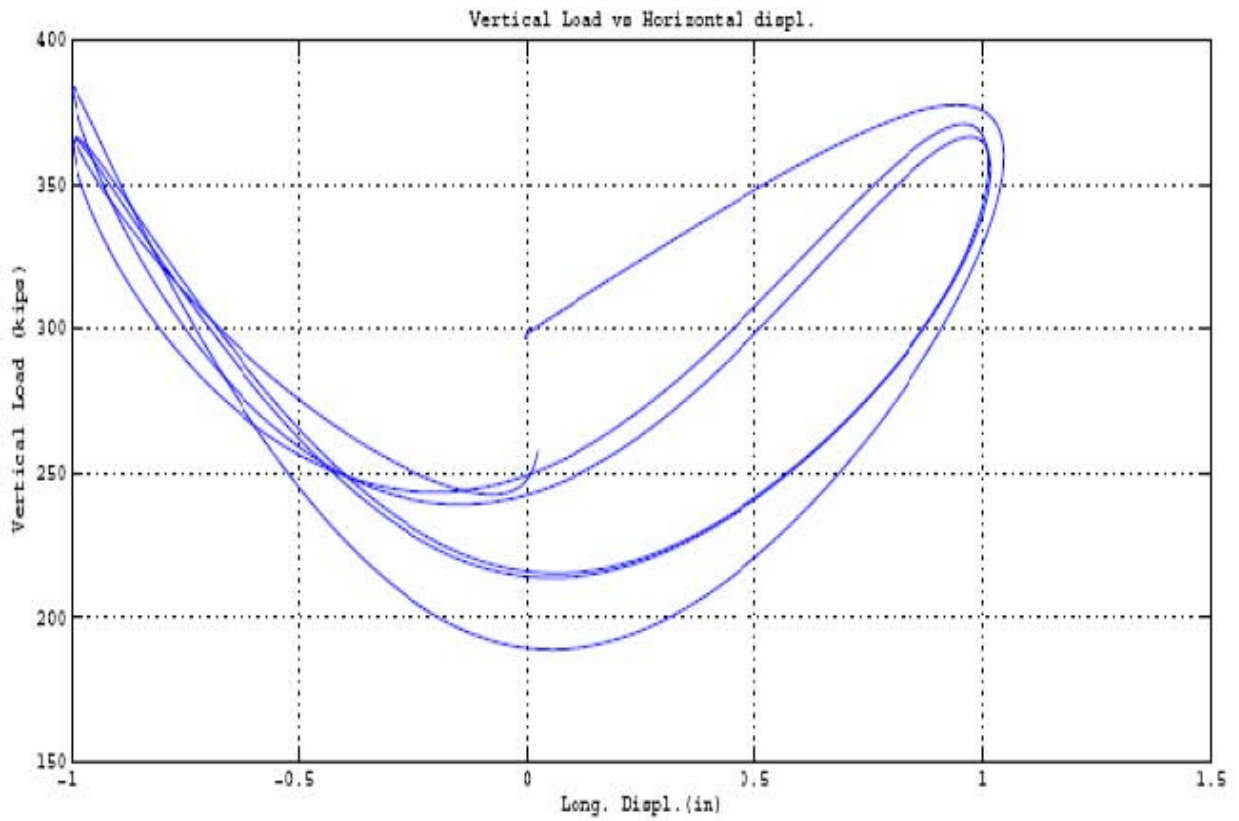


Figure 5-9 Results of Repeated Test #9 (continued).

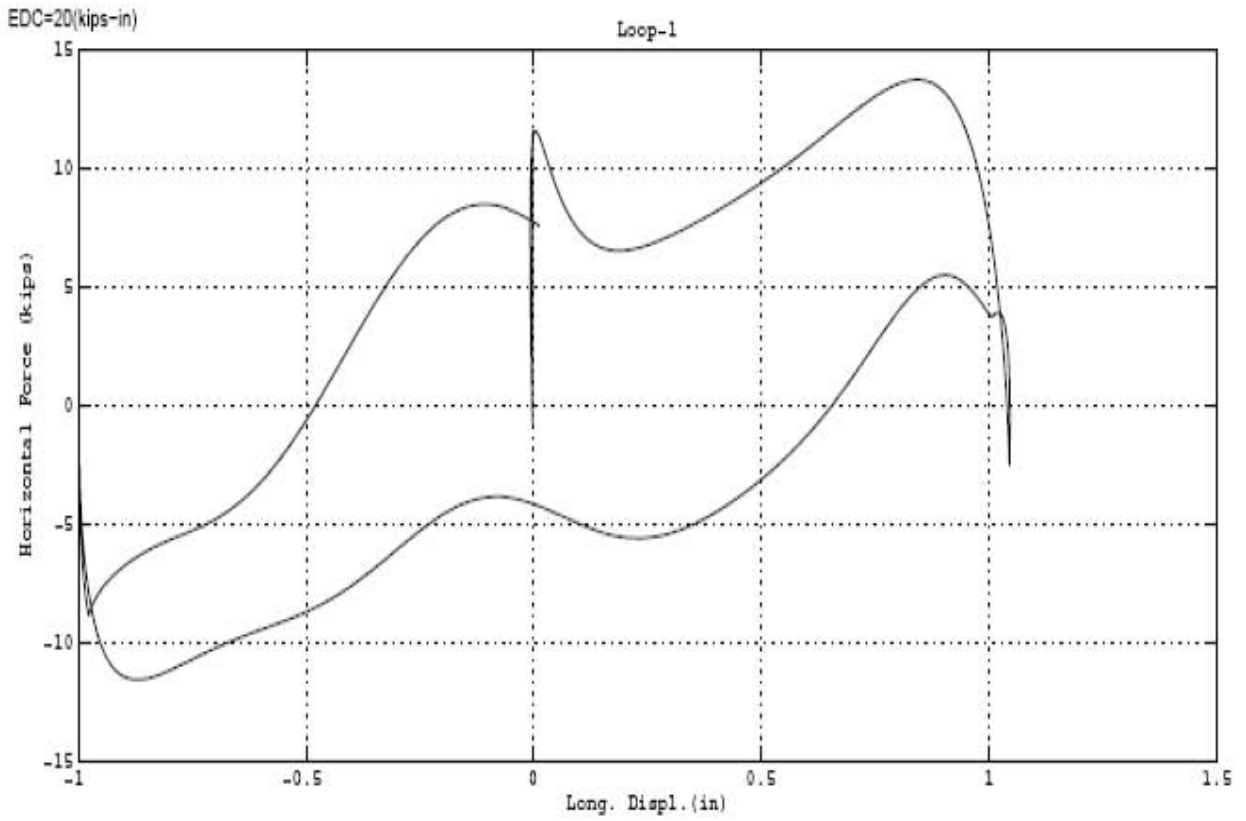
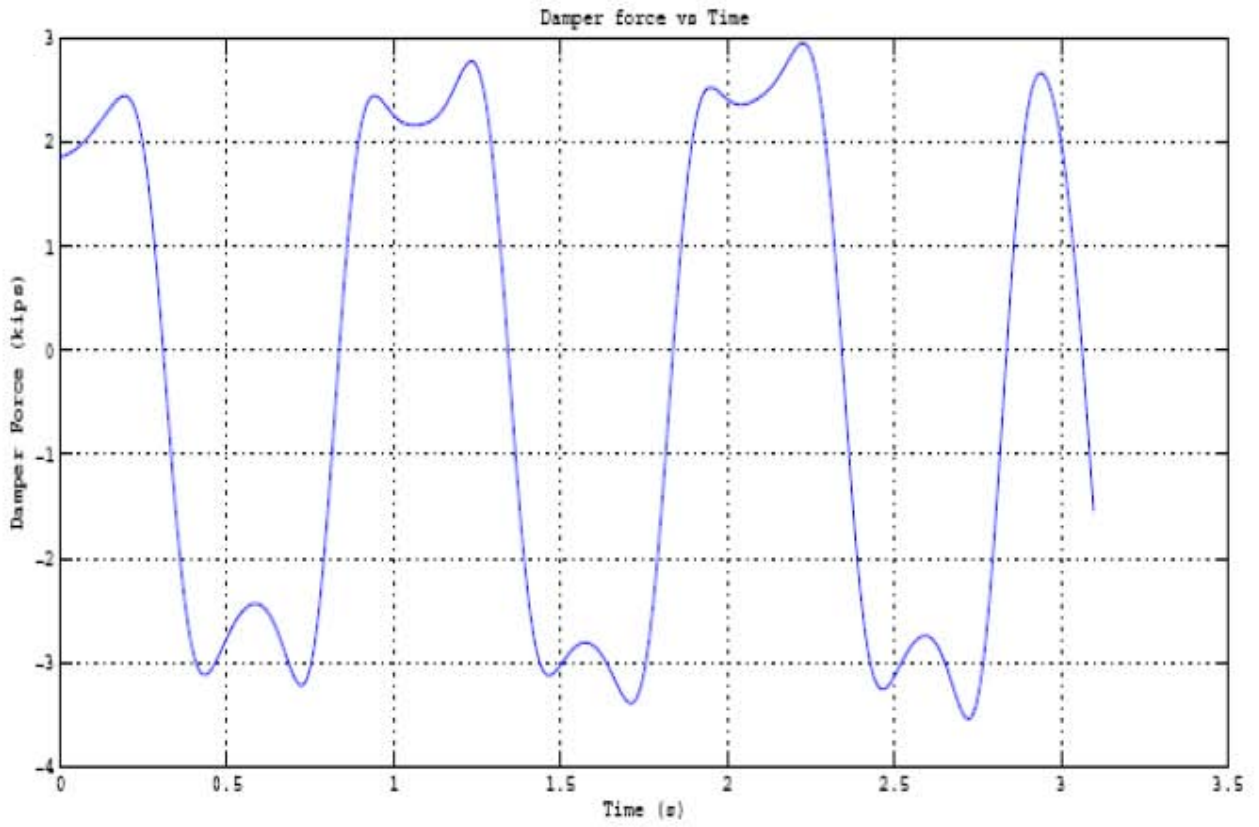


Figure 5-9 Results of Repeated Test #9 (continued).

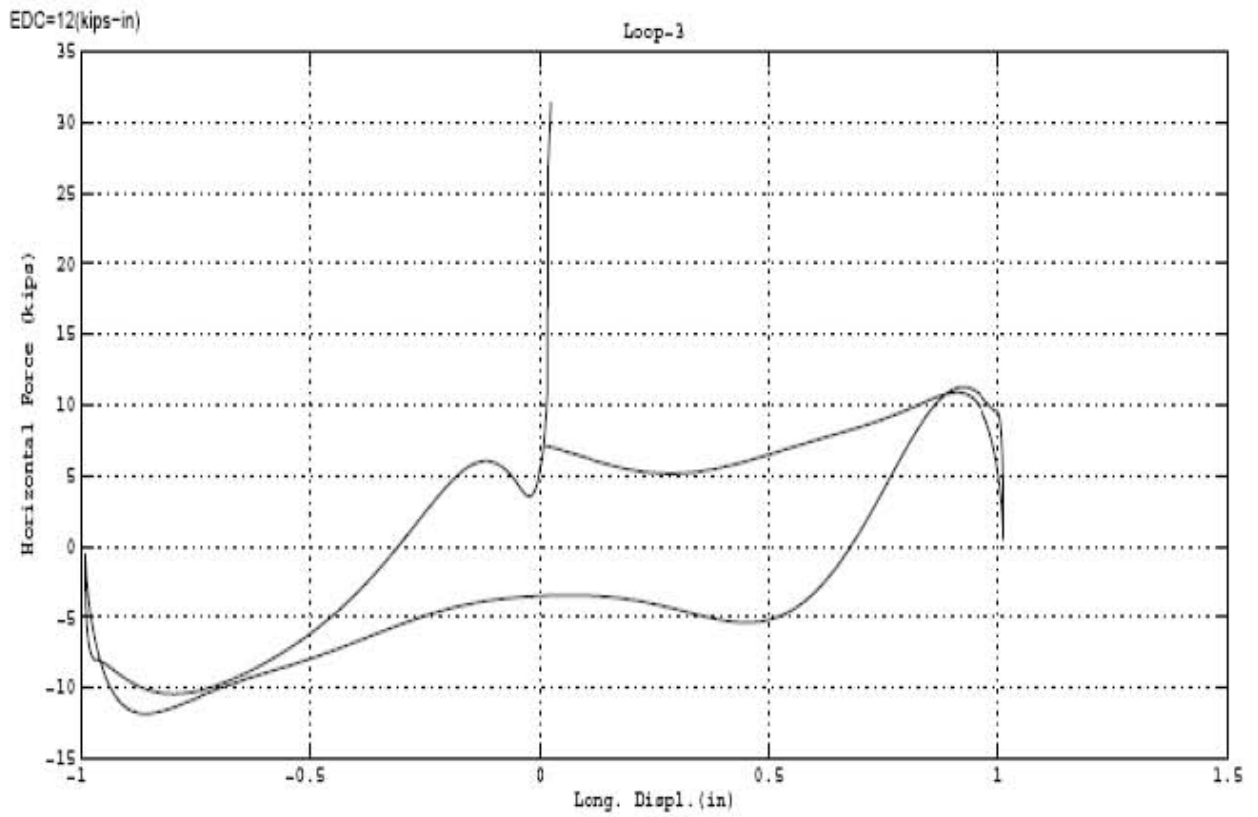
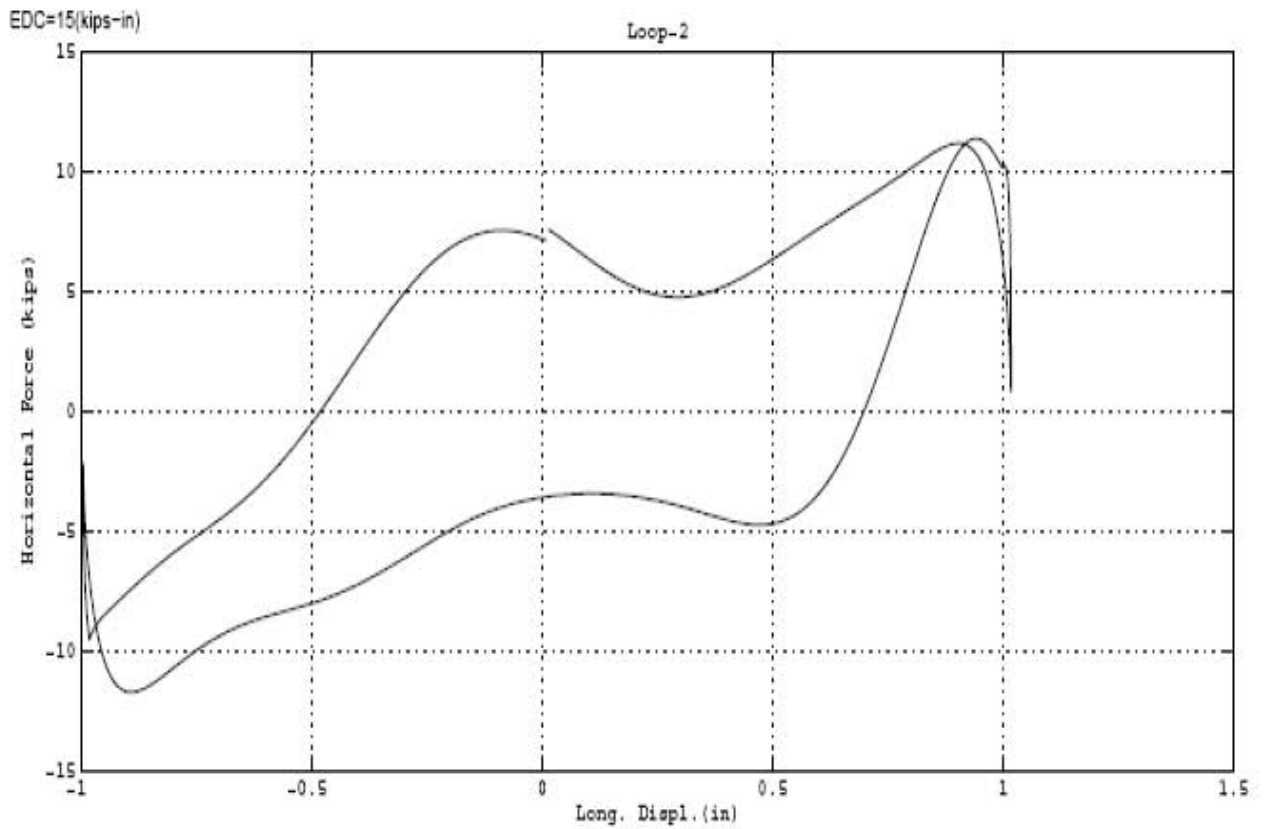


Figure 5-9 Results of Repeated Test #9 (continued).

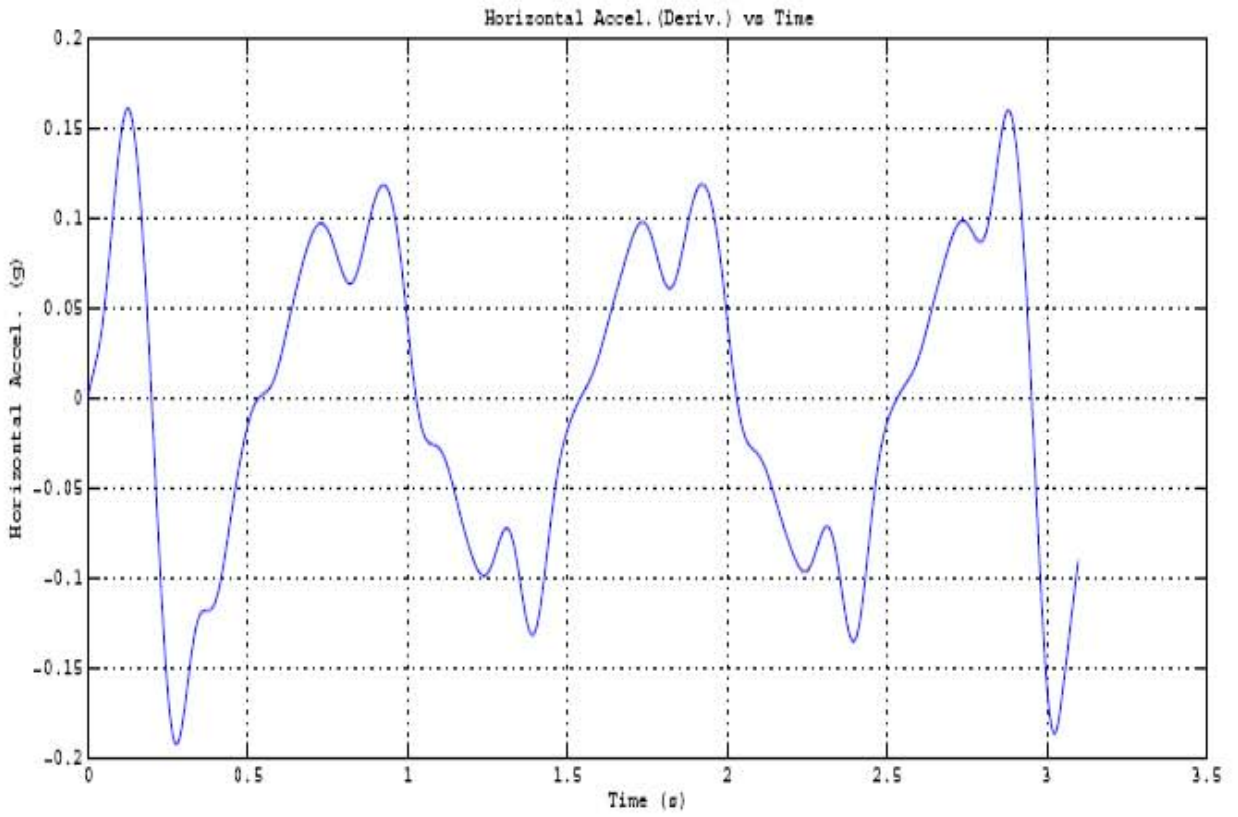
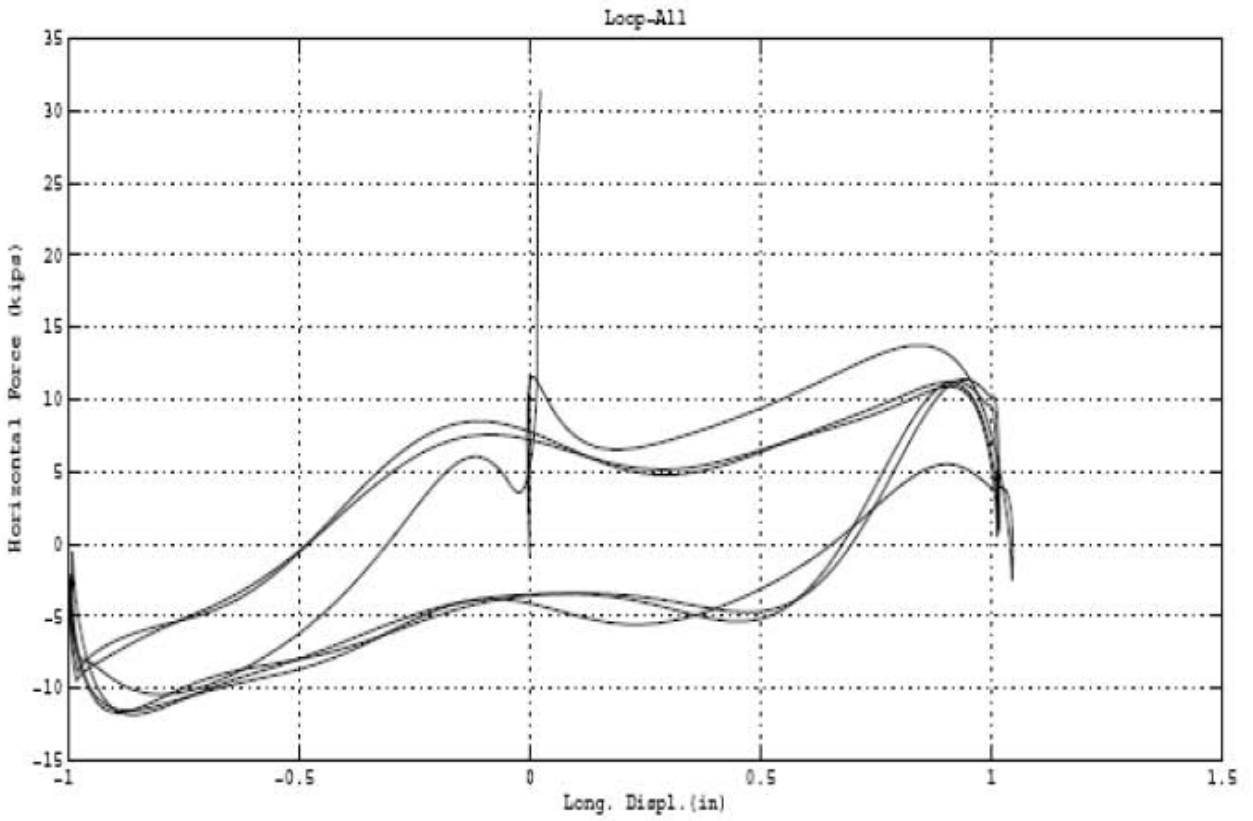


Figure 5-9 Results of Repeated Test #9 (continued).

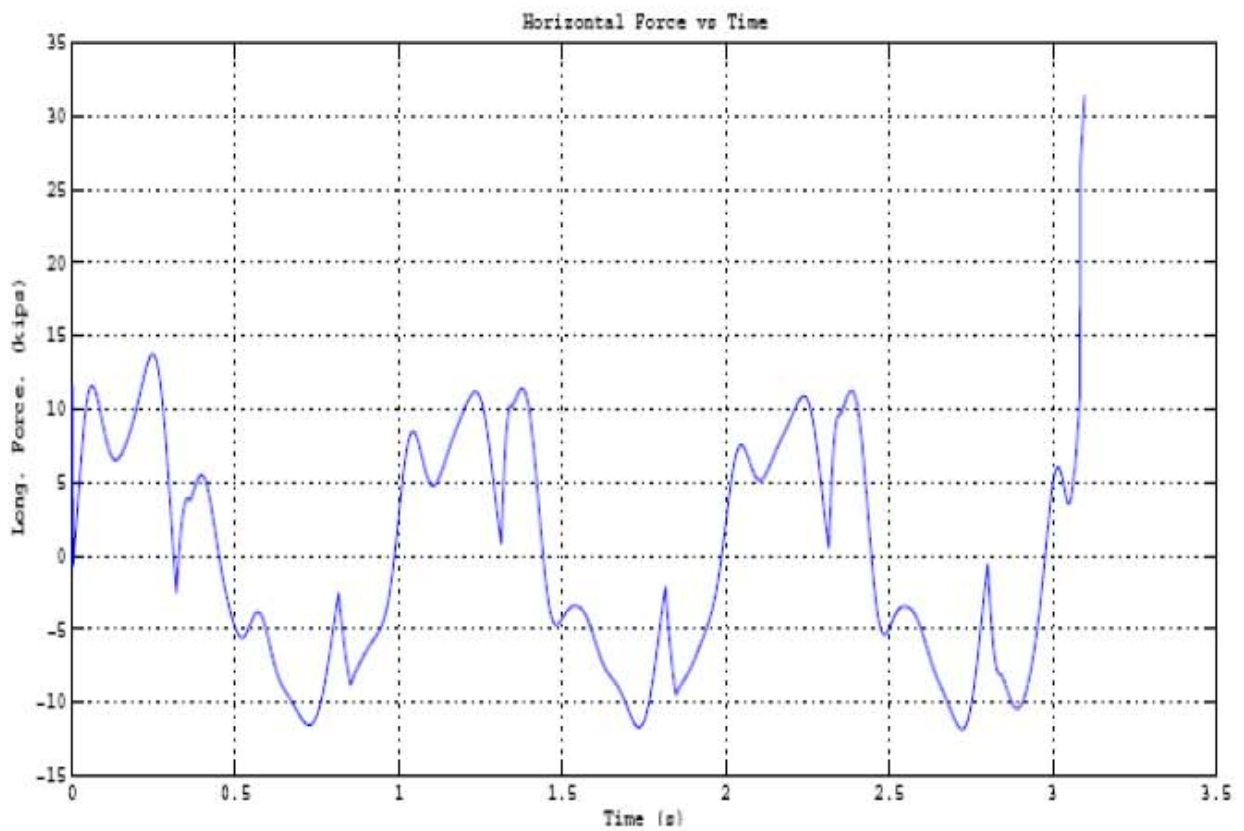
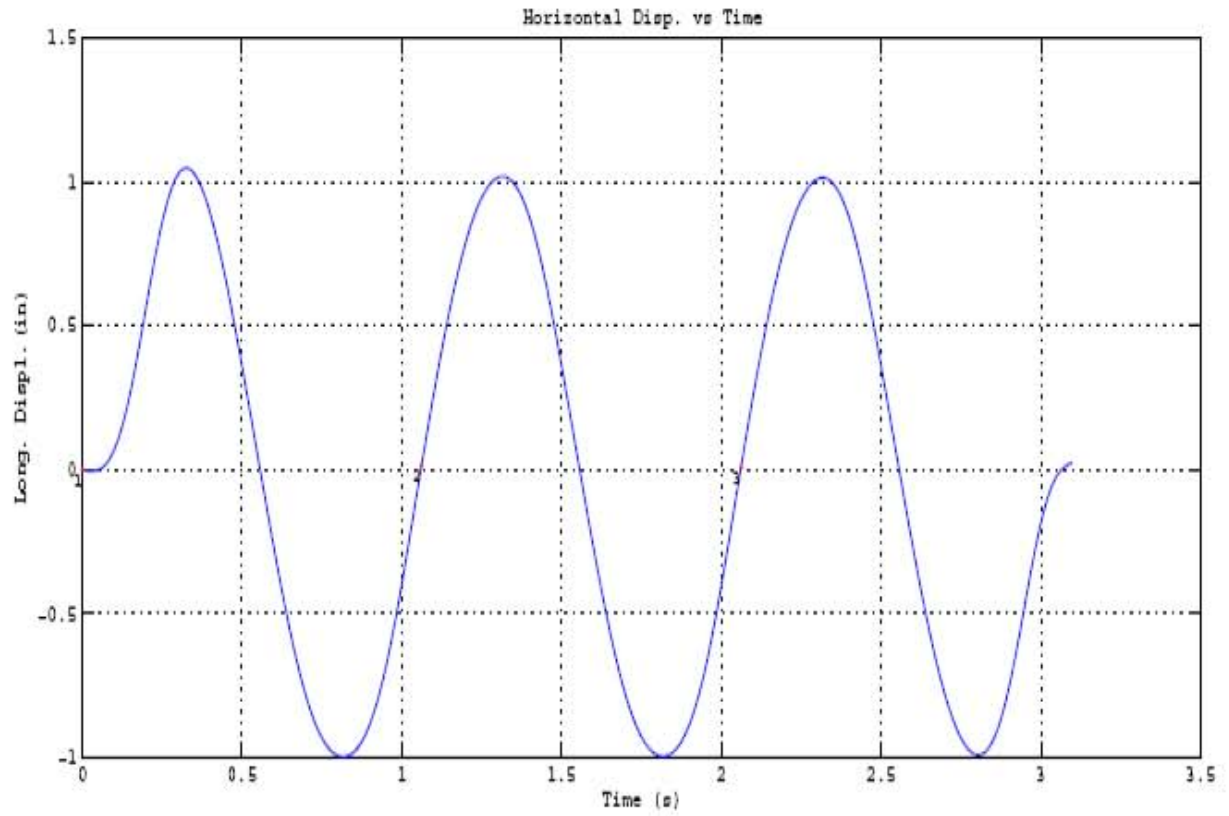


Figure 5-9 Results of Repeated Test #9 (continued).

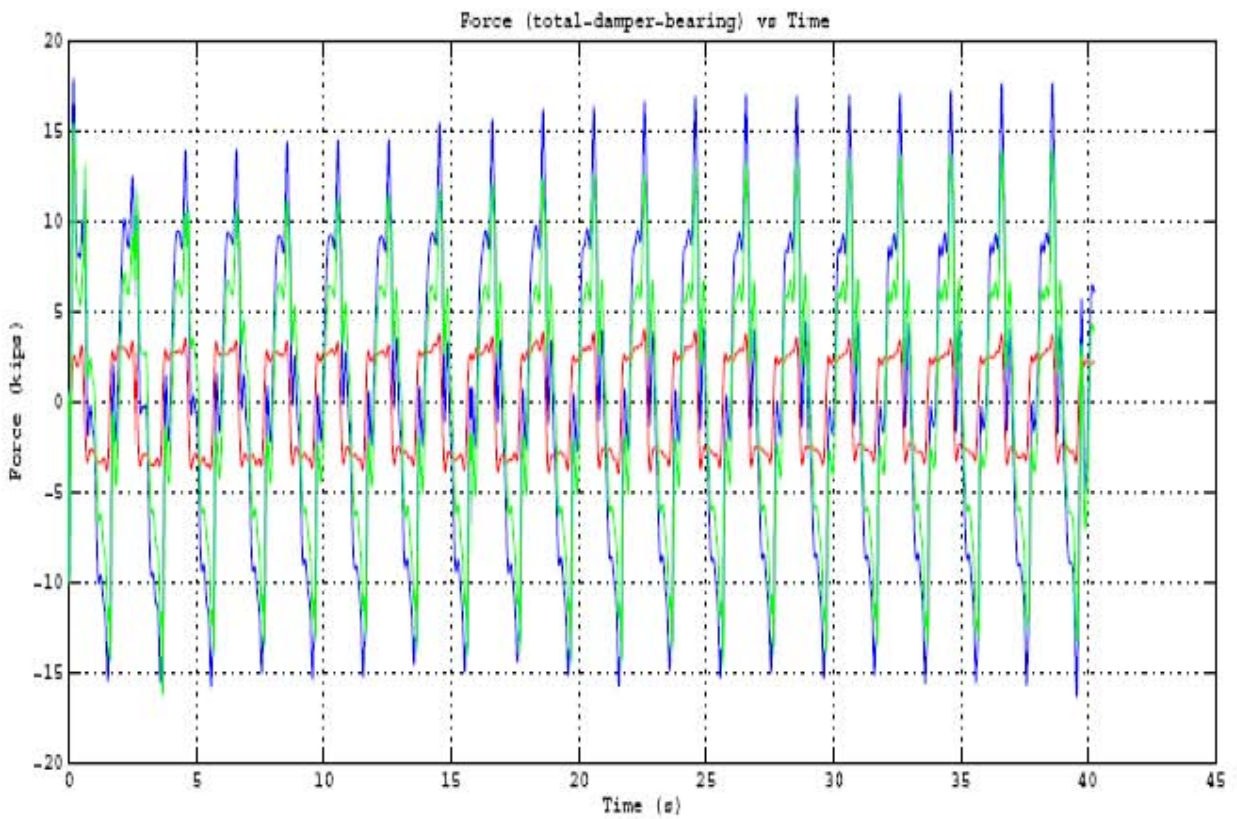
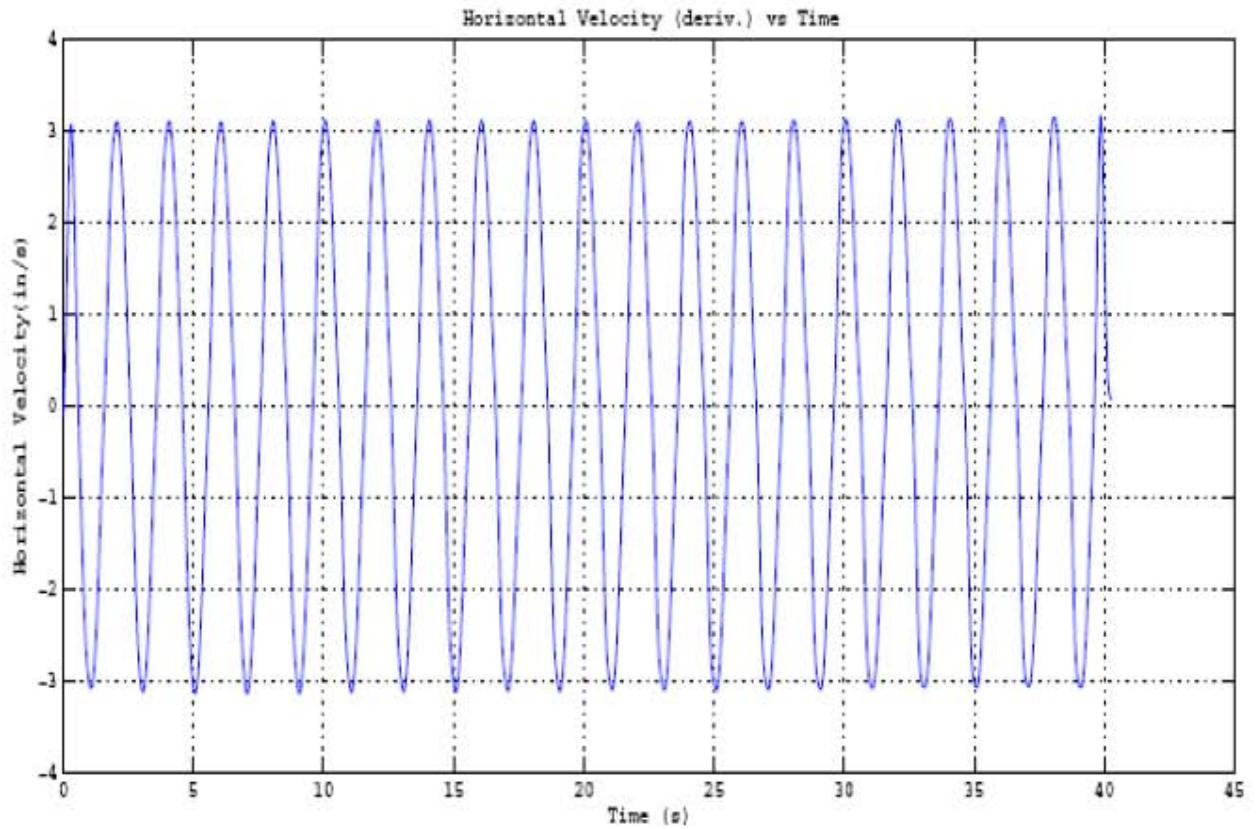


Figure 5-10 Results of Repeated Test #10.

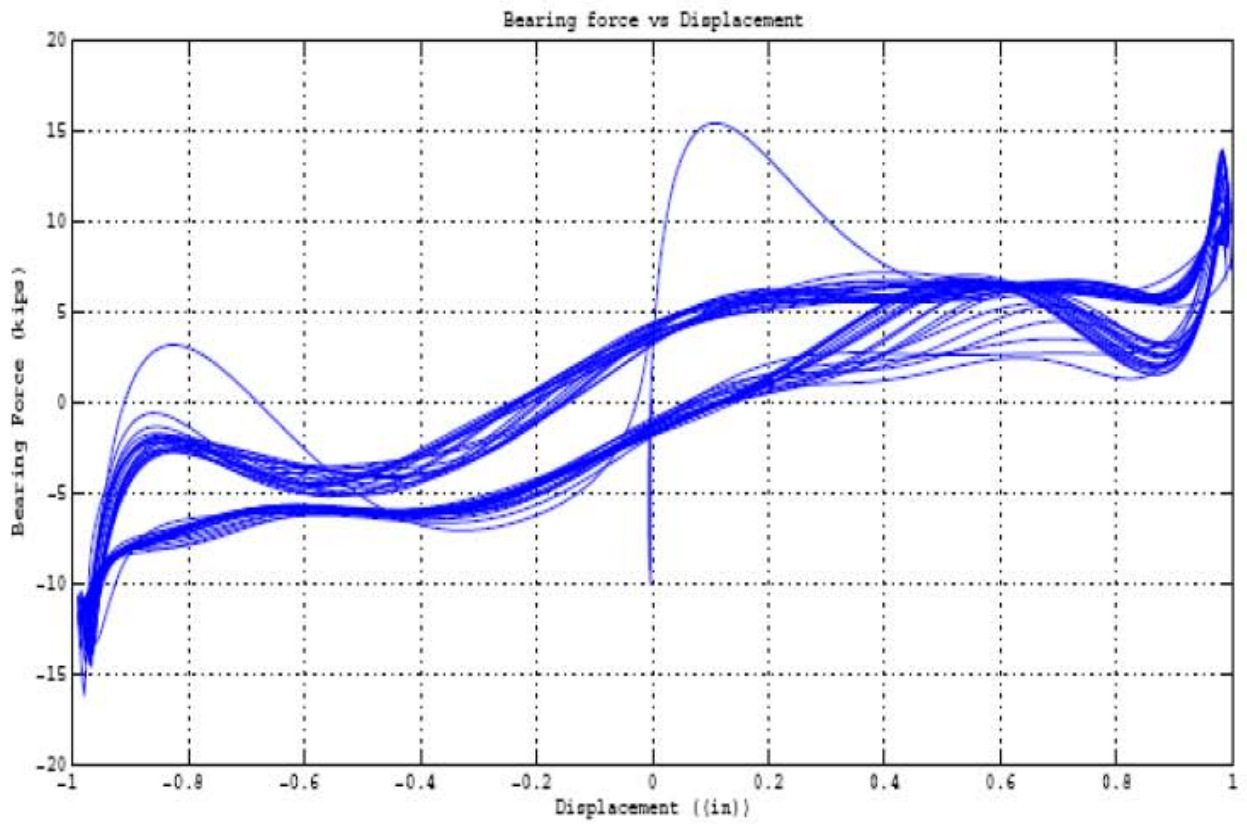
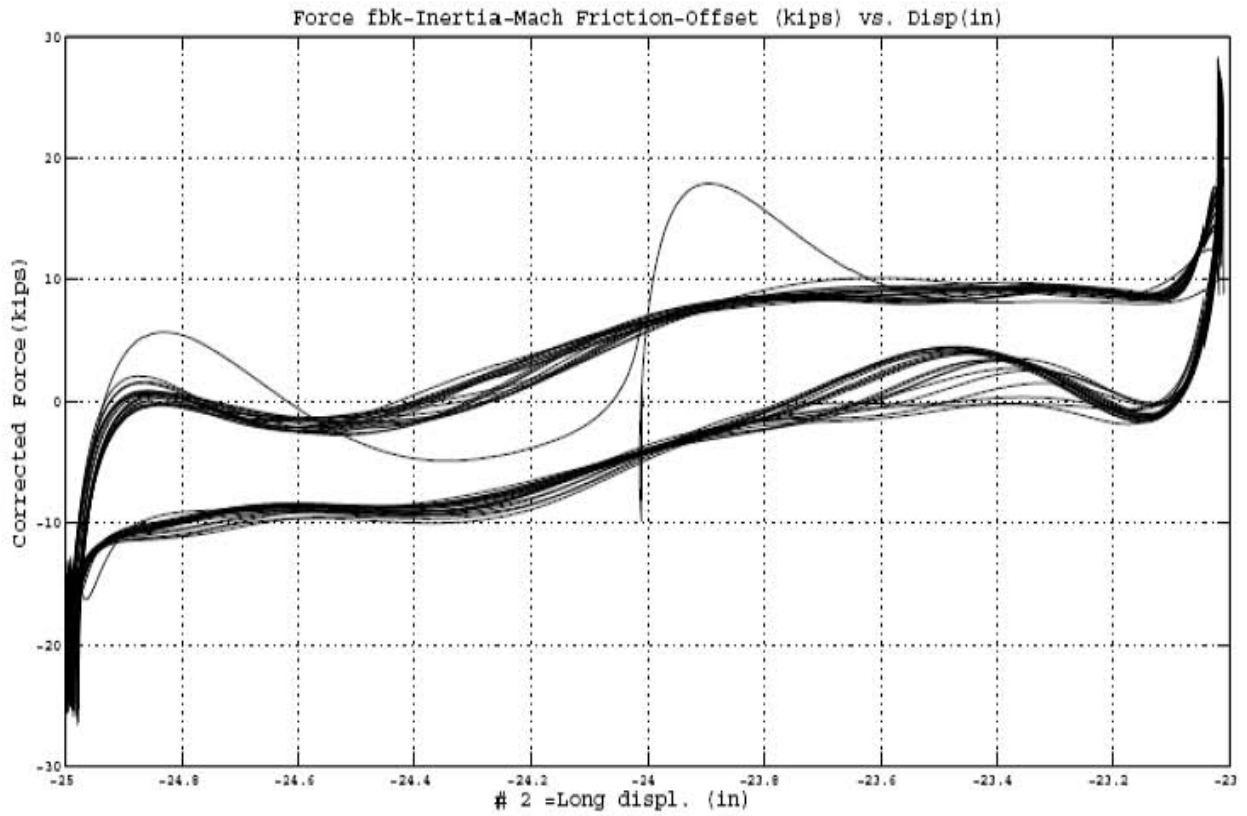


Figure 5-10 Results of Repeated Test #10 (continued).

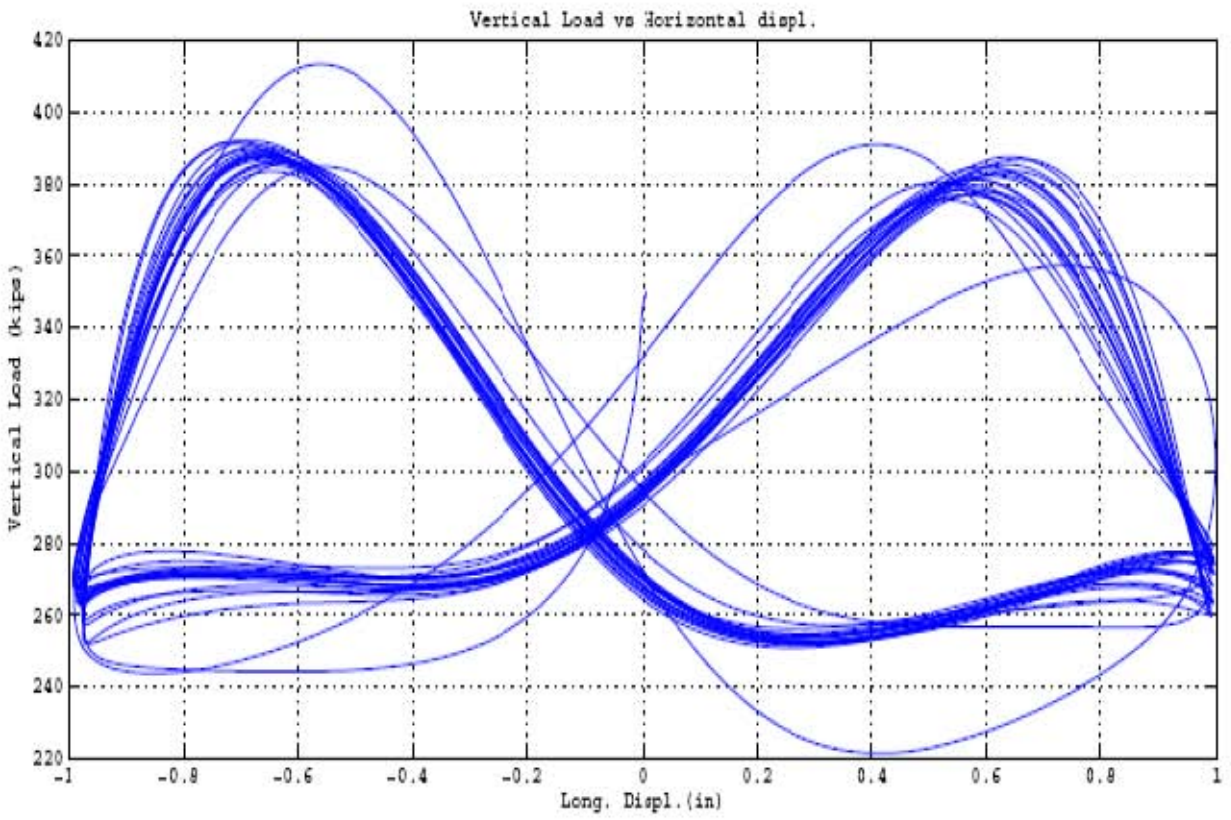
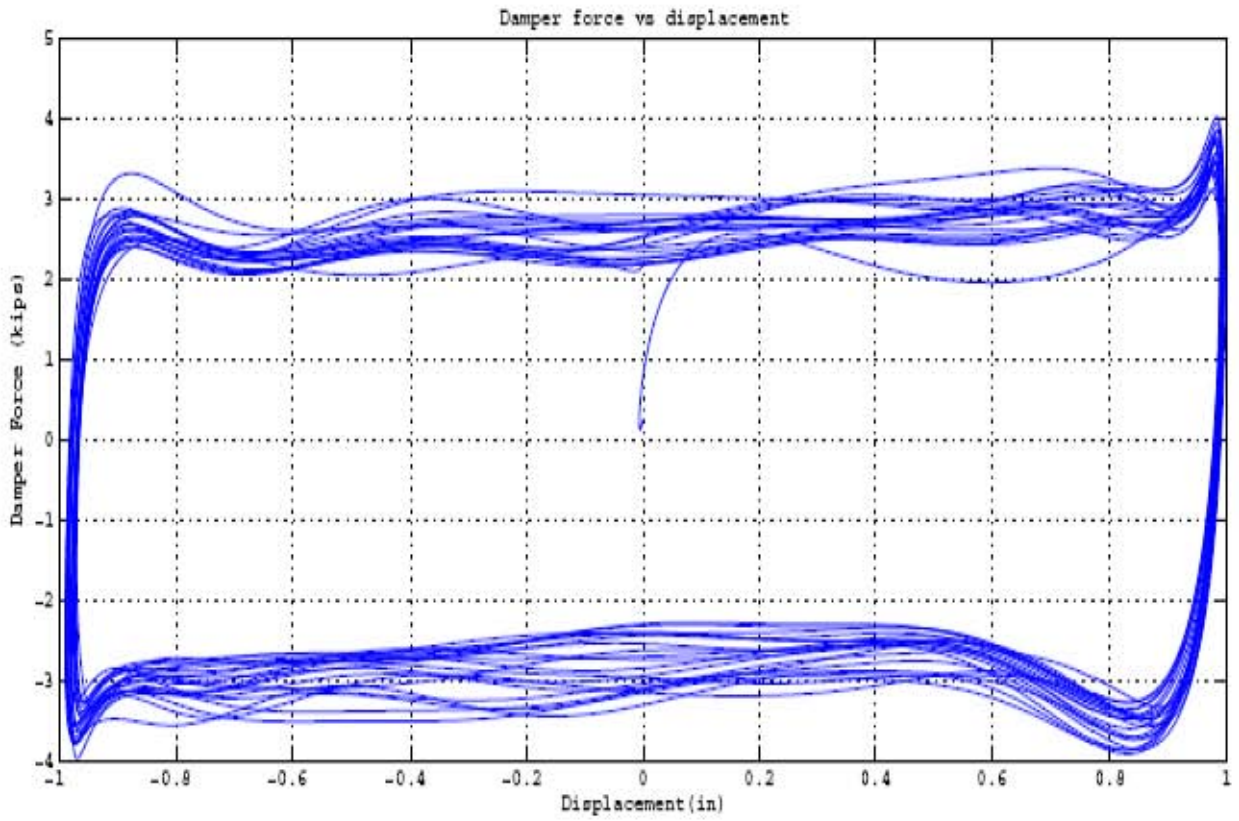


Figure 5-10 Results of Repeated Test #10 (continued).

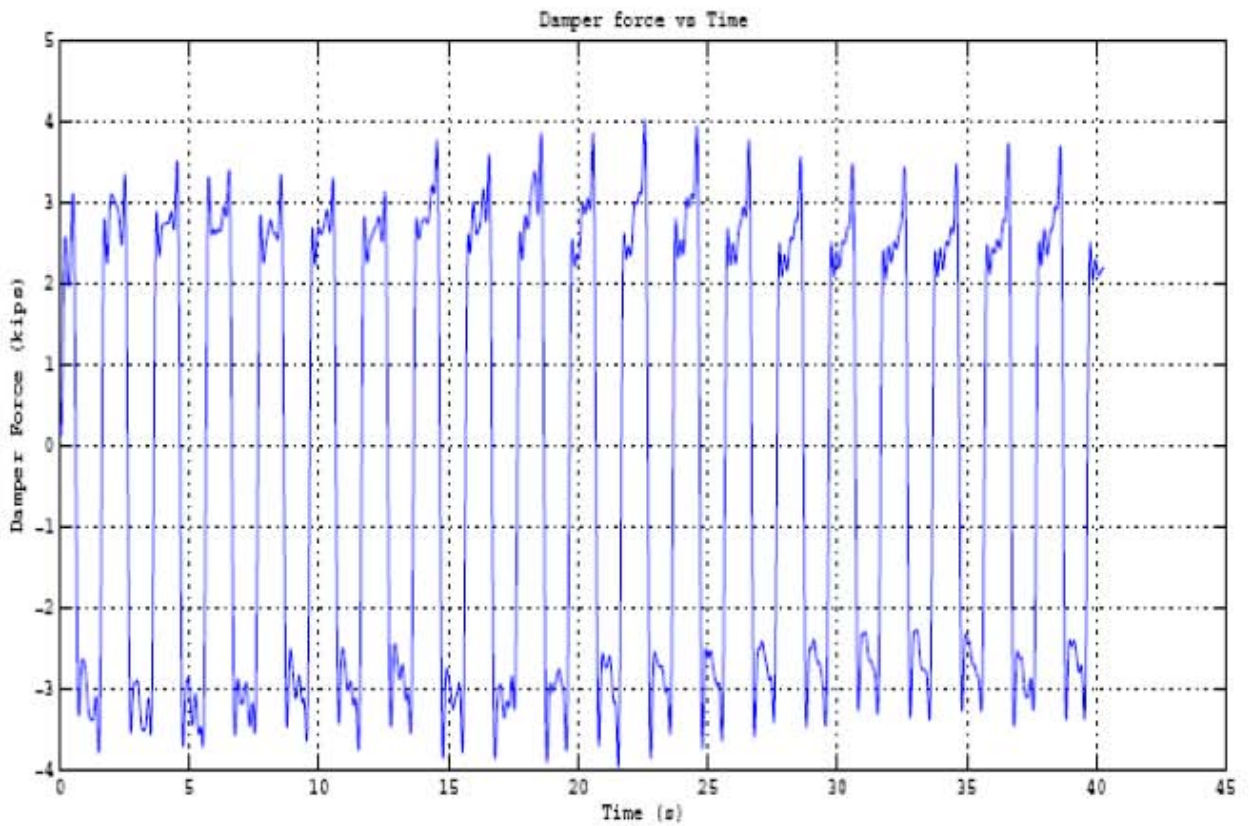
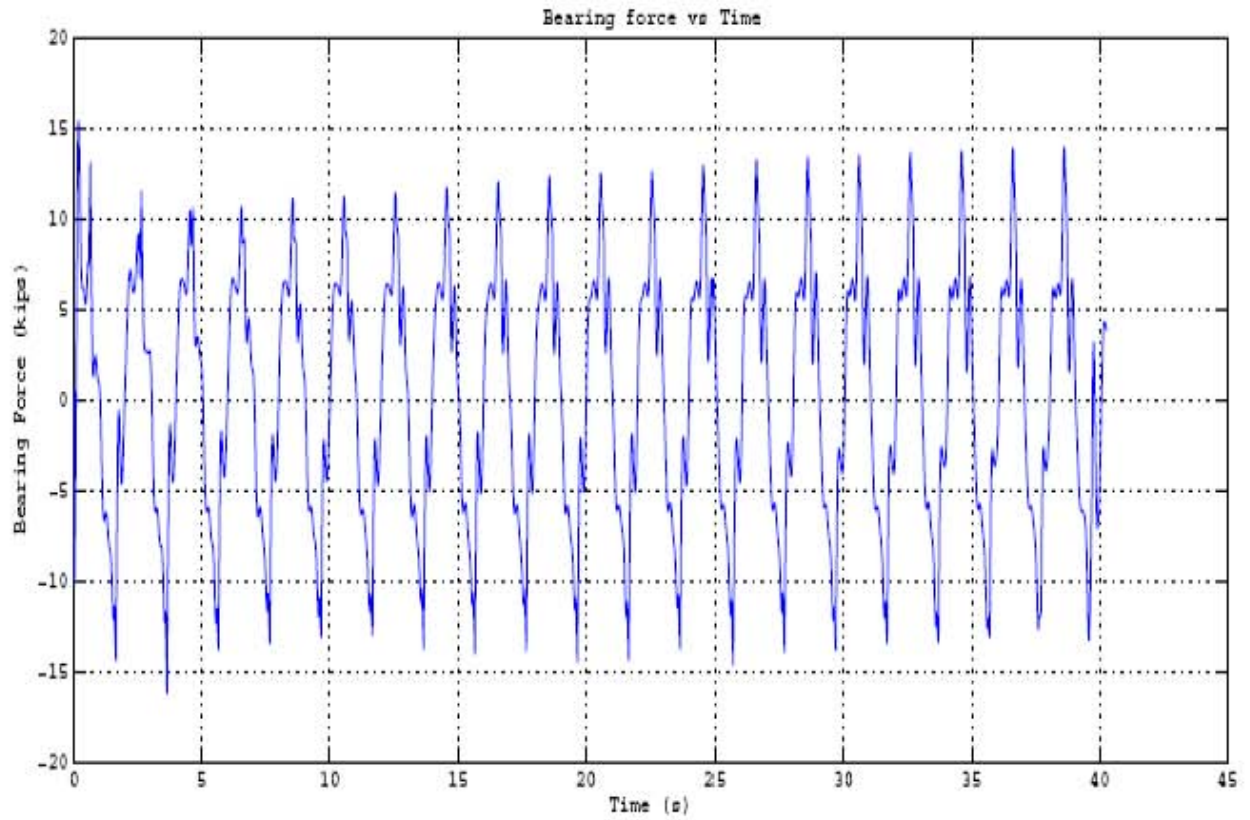


Figure 5-10 Results of Repeated Test #10 (continued).

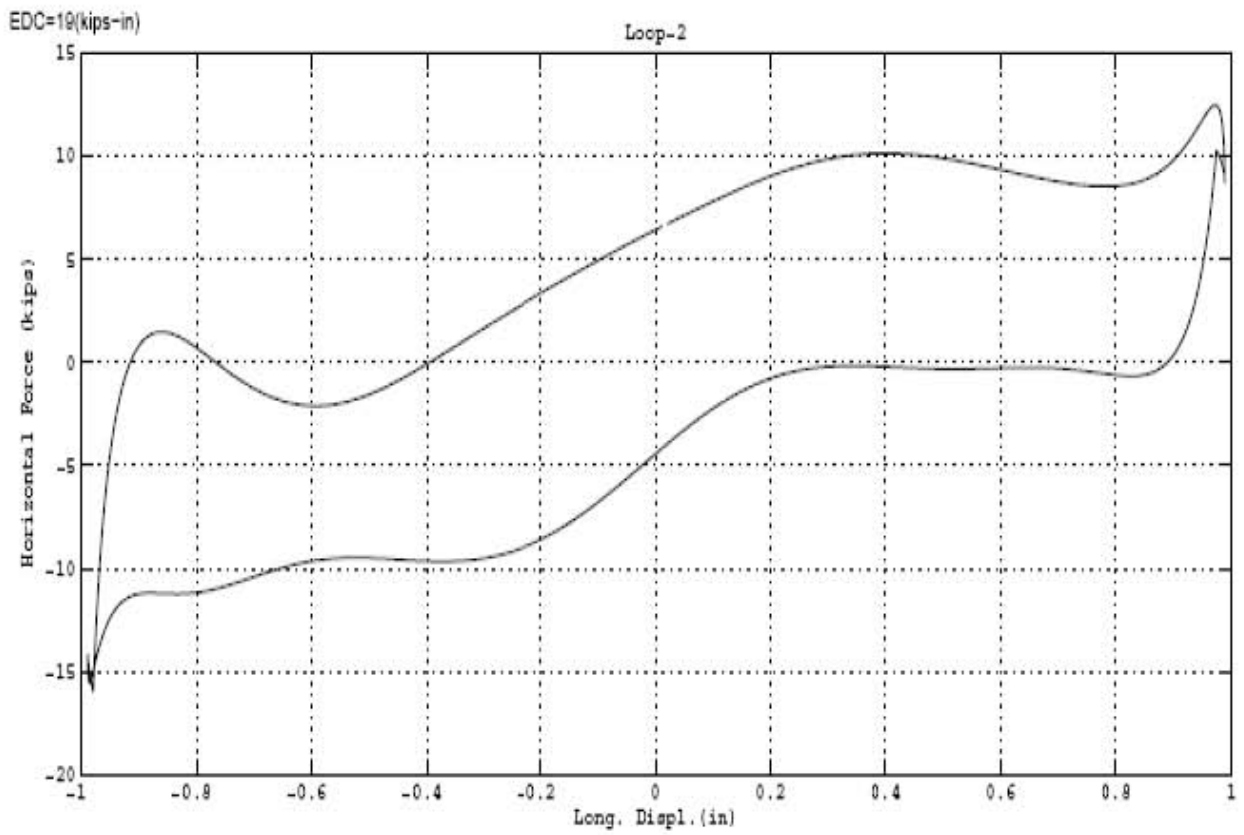
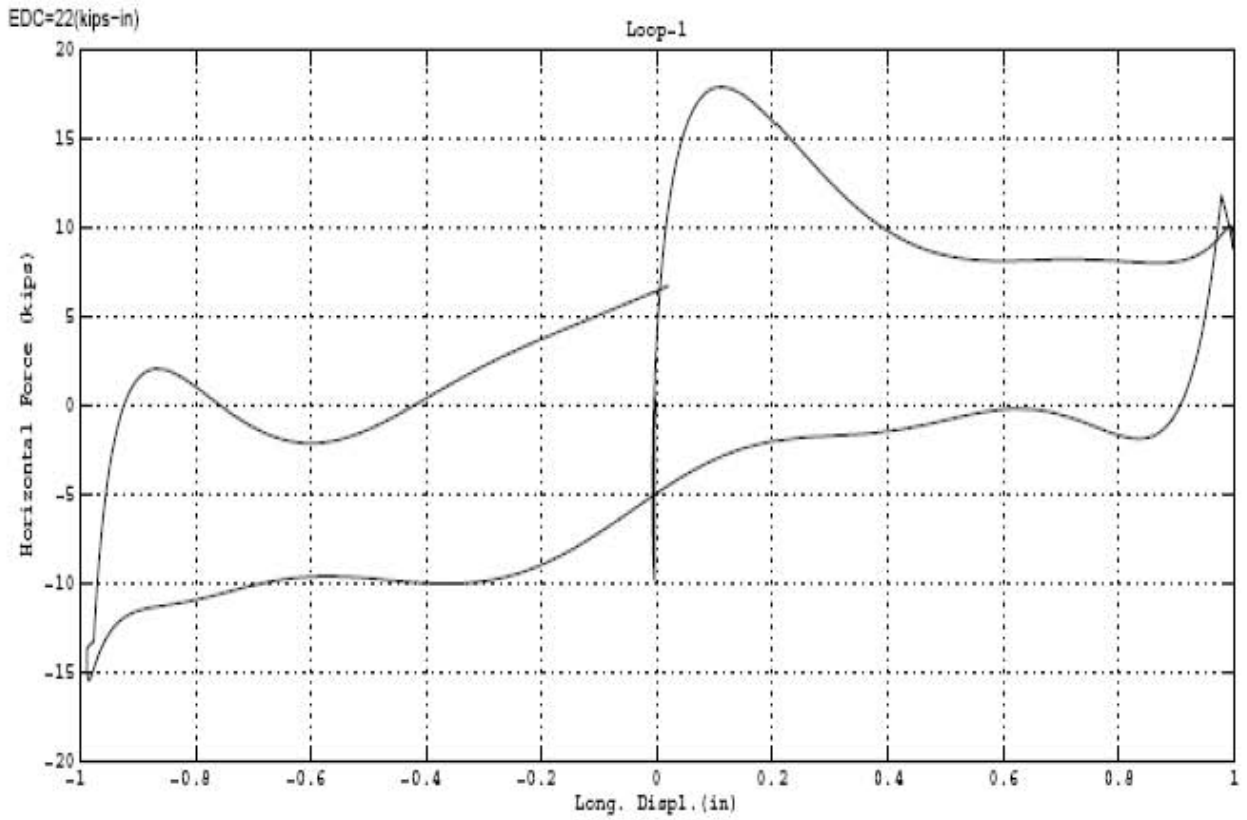


Figure 5-10 Results of Repeated Test #10 (continued).

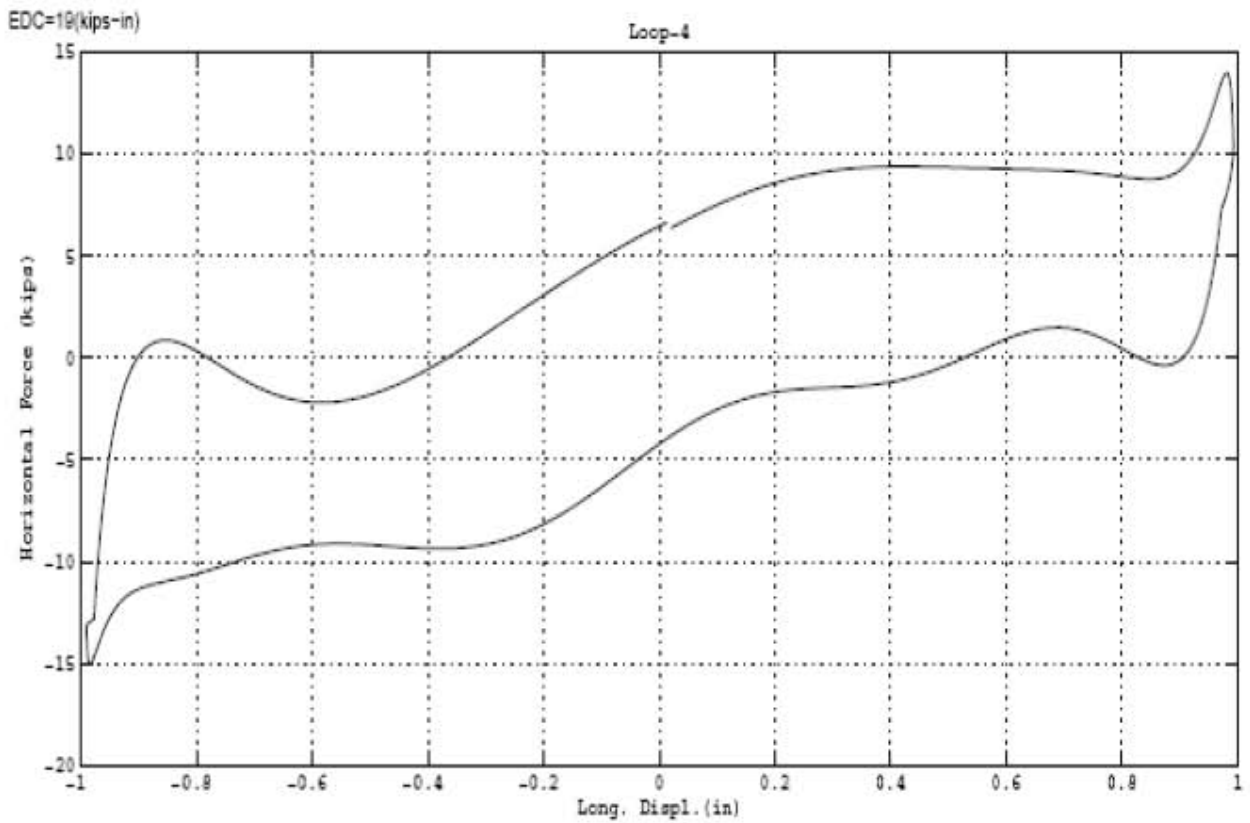
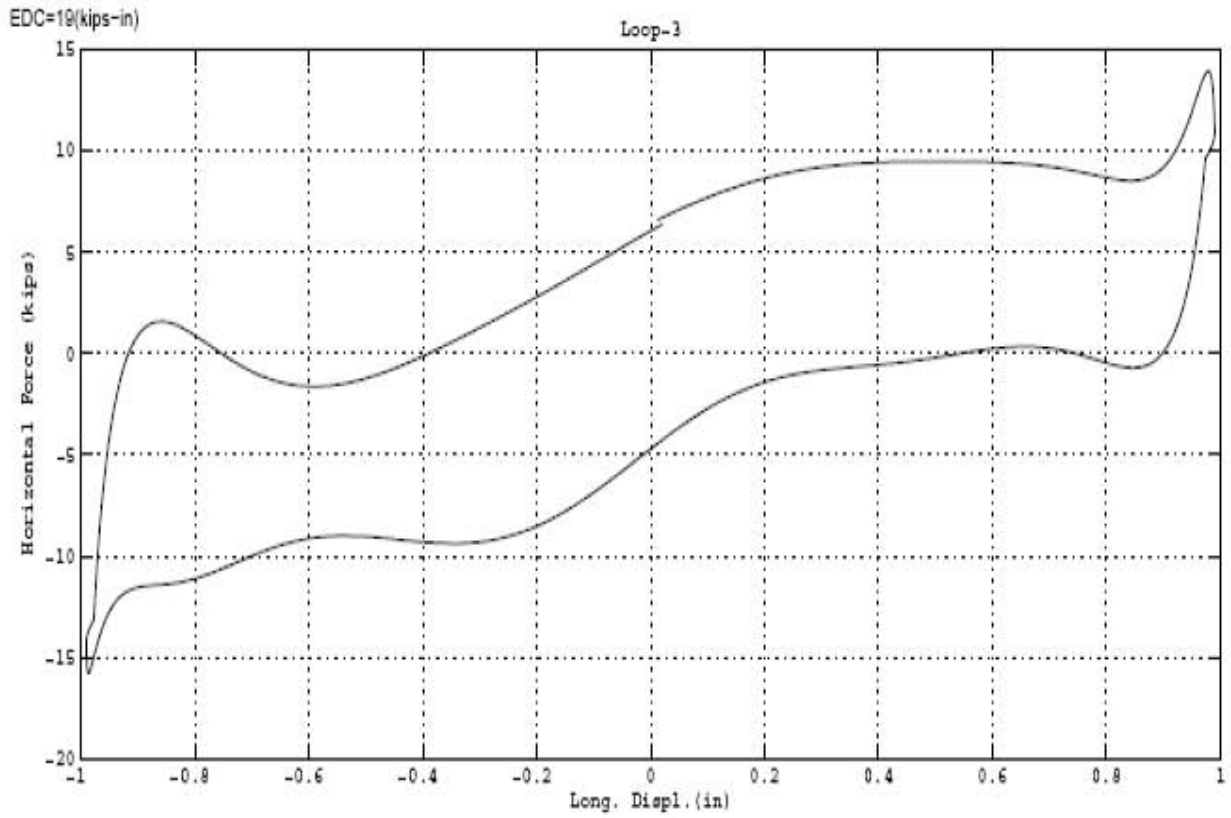


Figure 5-10 Results of Repeated Test #10 (continued).

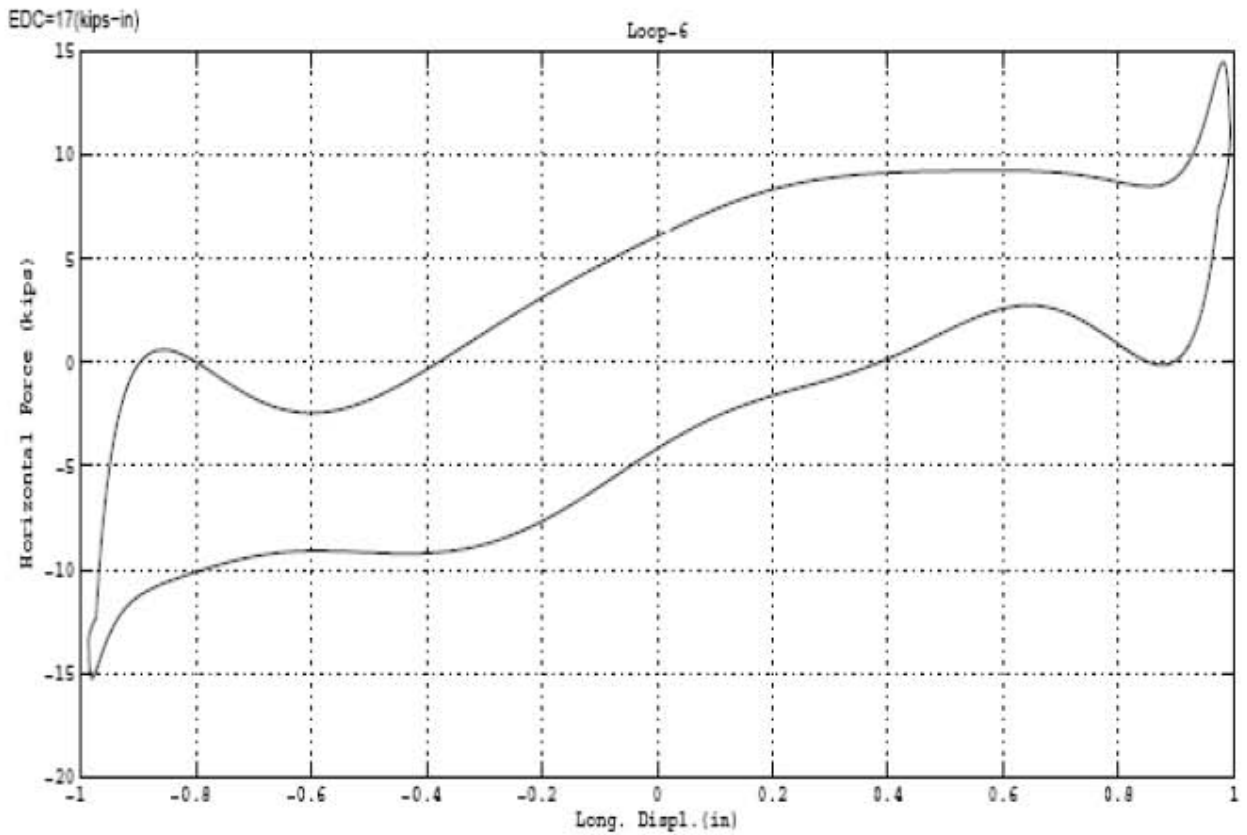
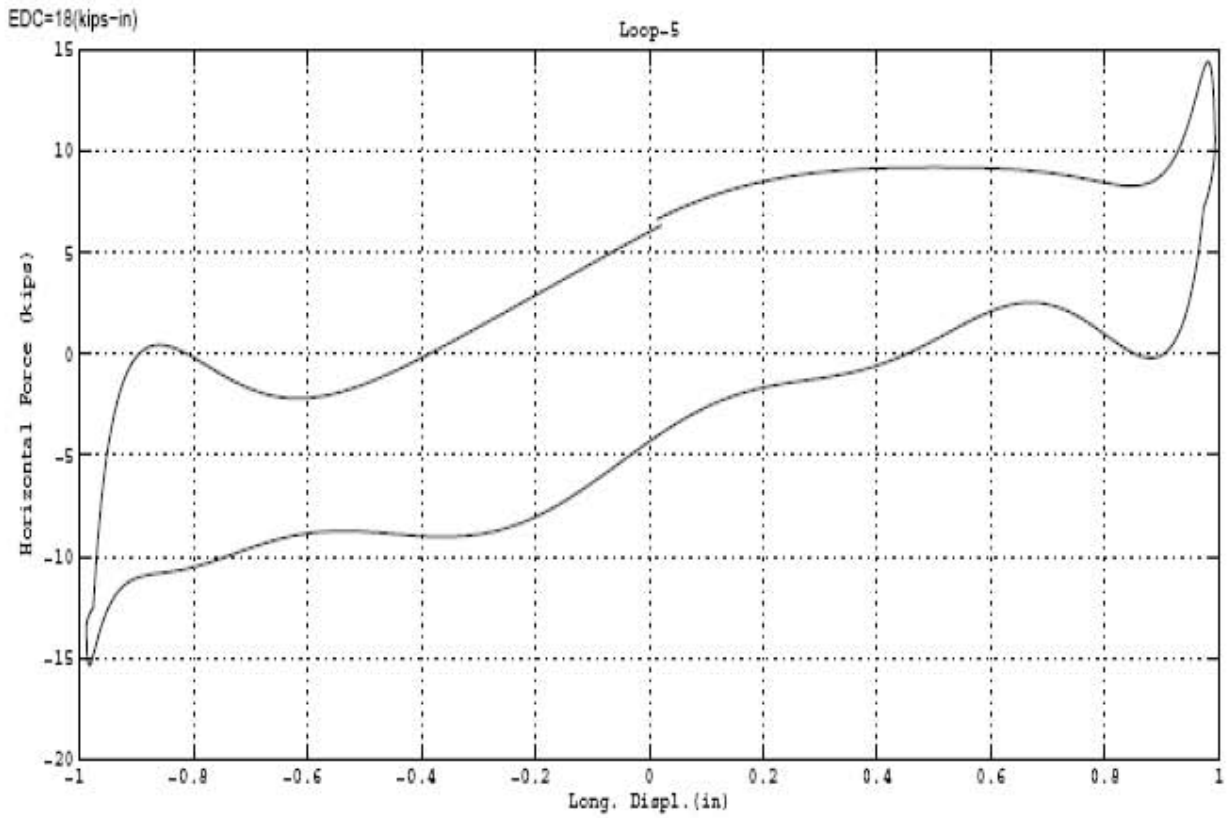


Figure 5-10 Results of Repeated Test #10 (continued).

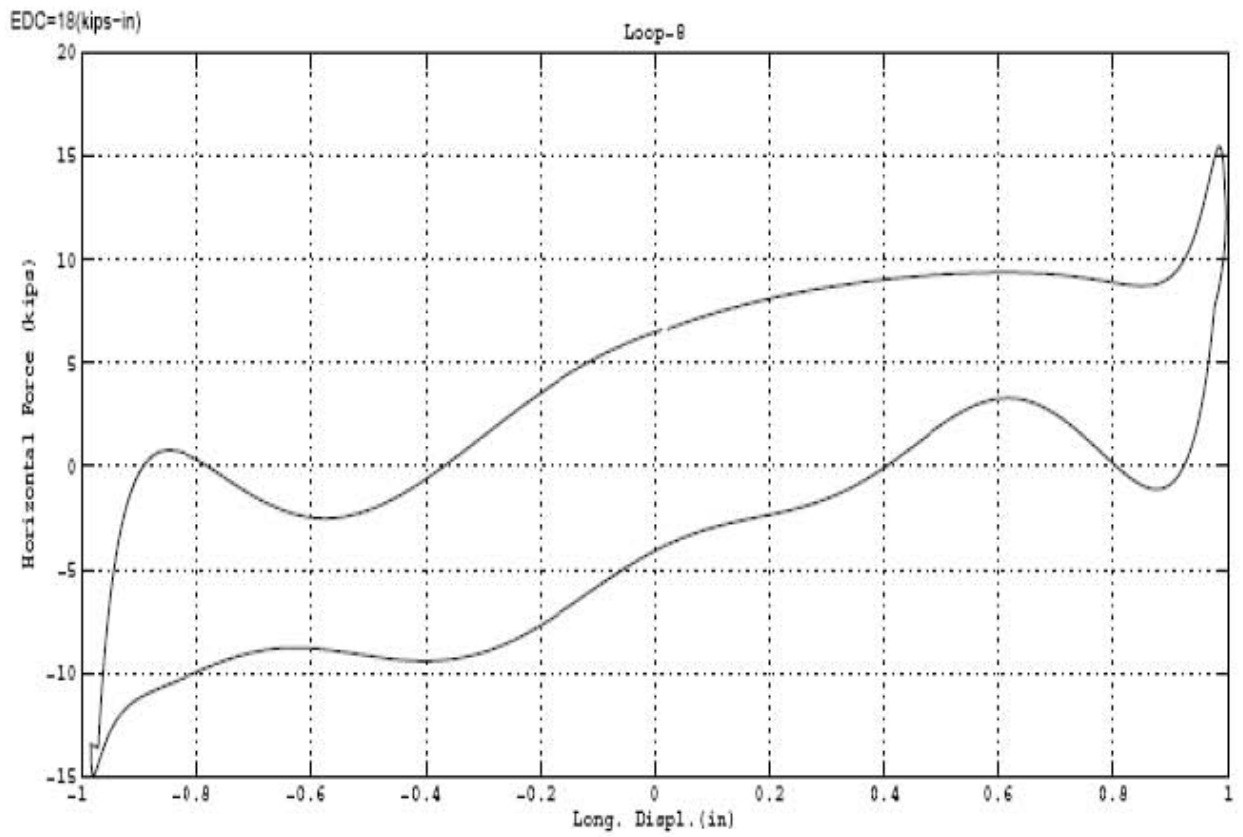
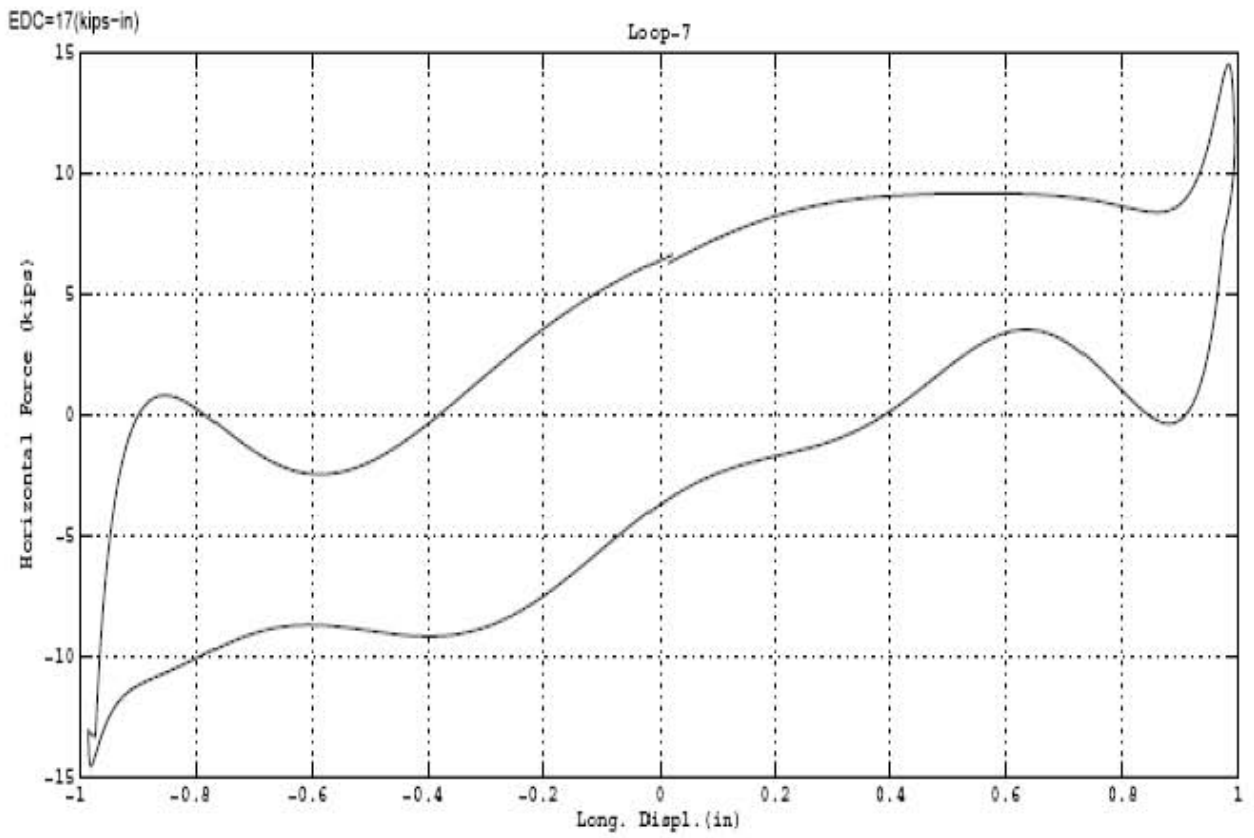


Figure 5-10 Results of Repeated Test #10 (continued).

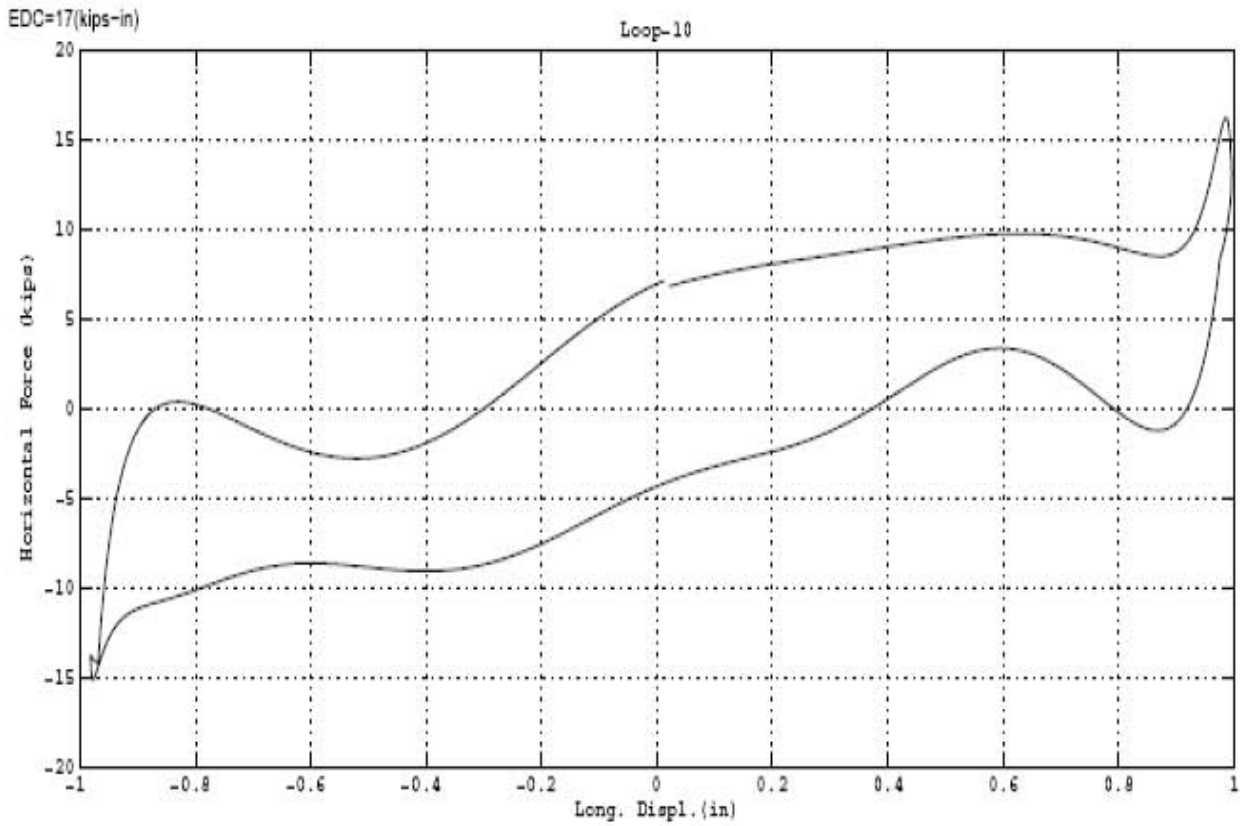
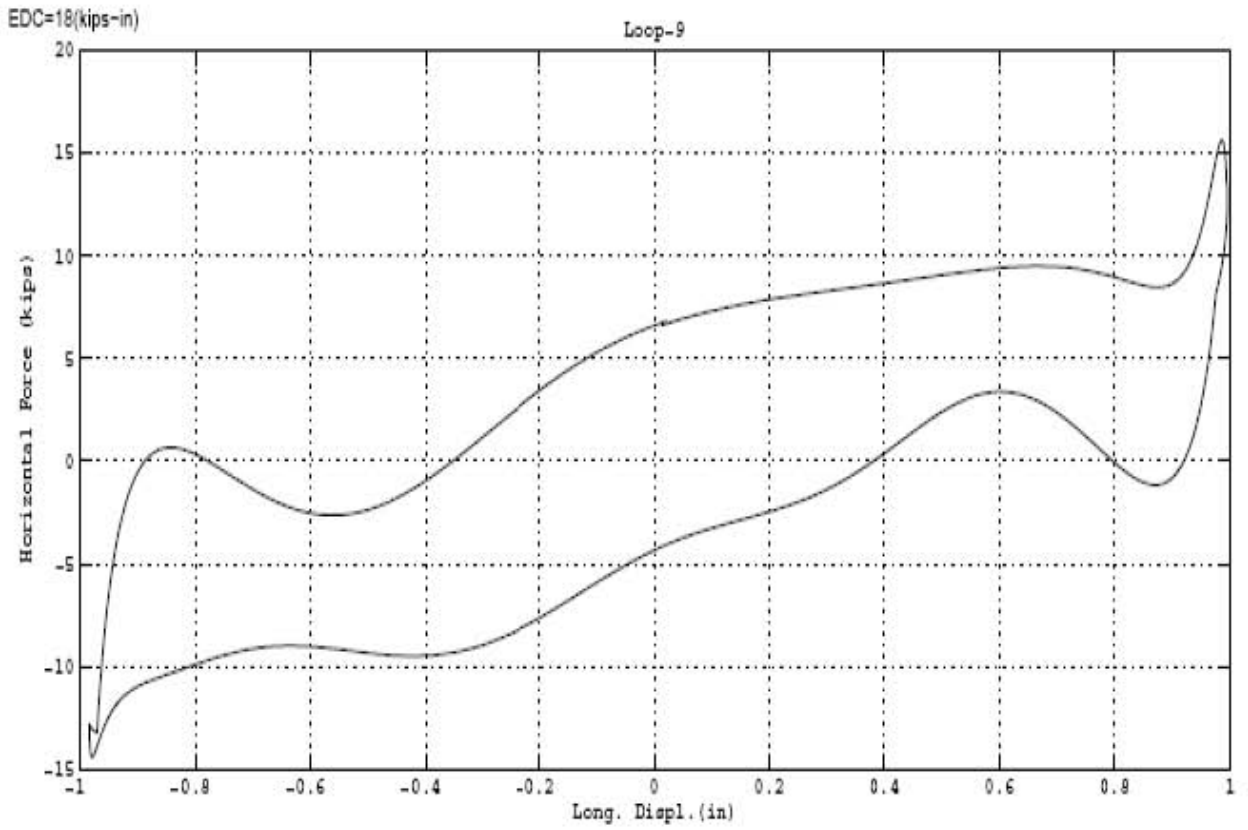


Figure 5-10 Results of Repeated Test #10 (continued).

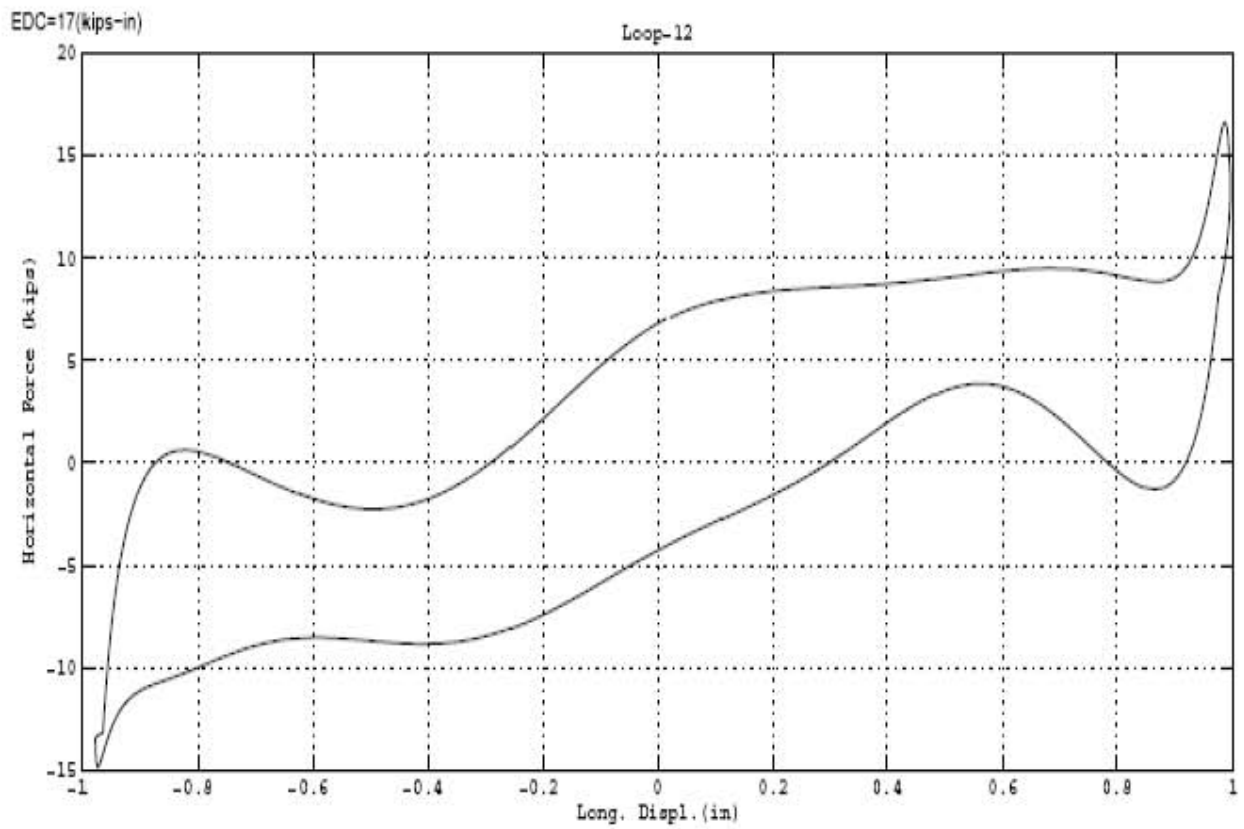
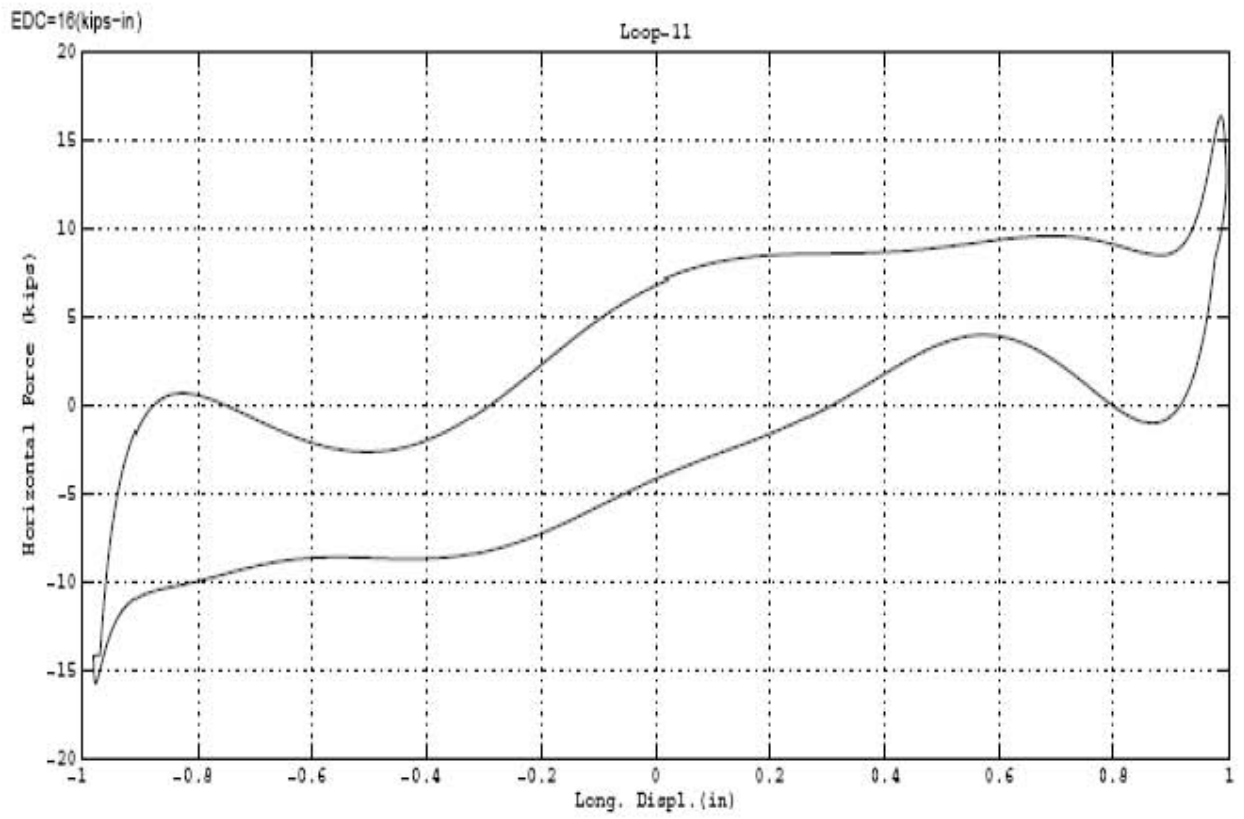


Figure 5-10 Results of Repeated Test #10 (continued).

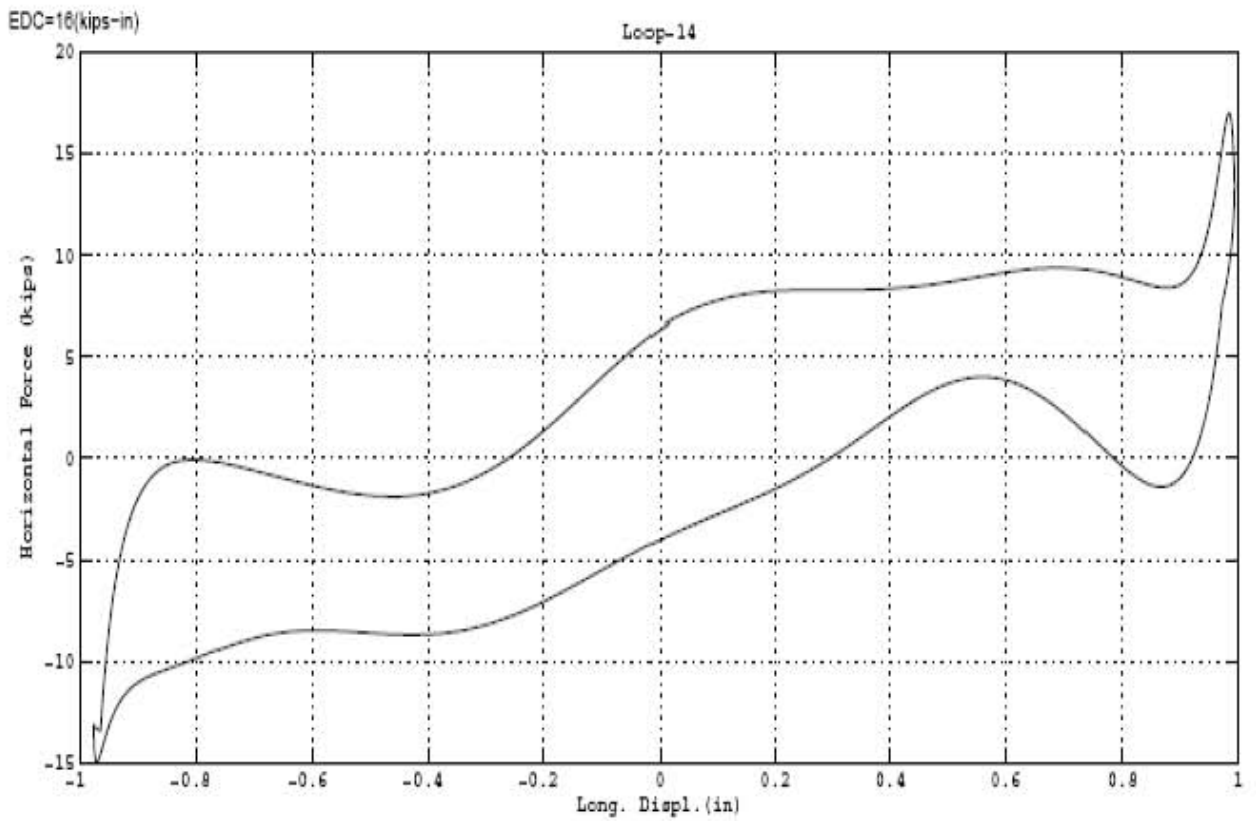
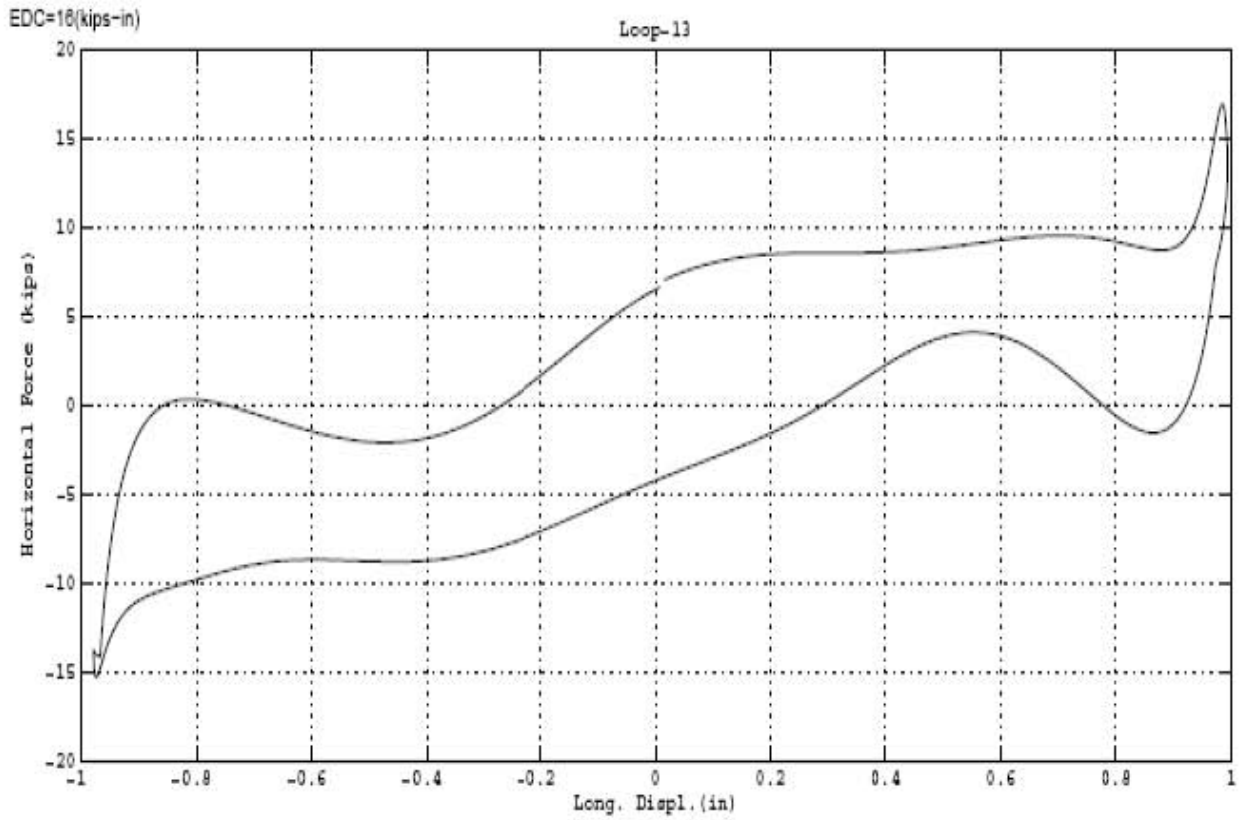


Figure 5-10 Results of Repeated Test #10 (continued).

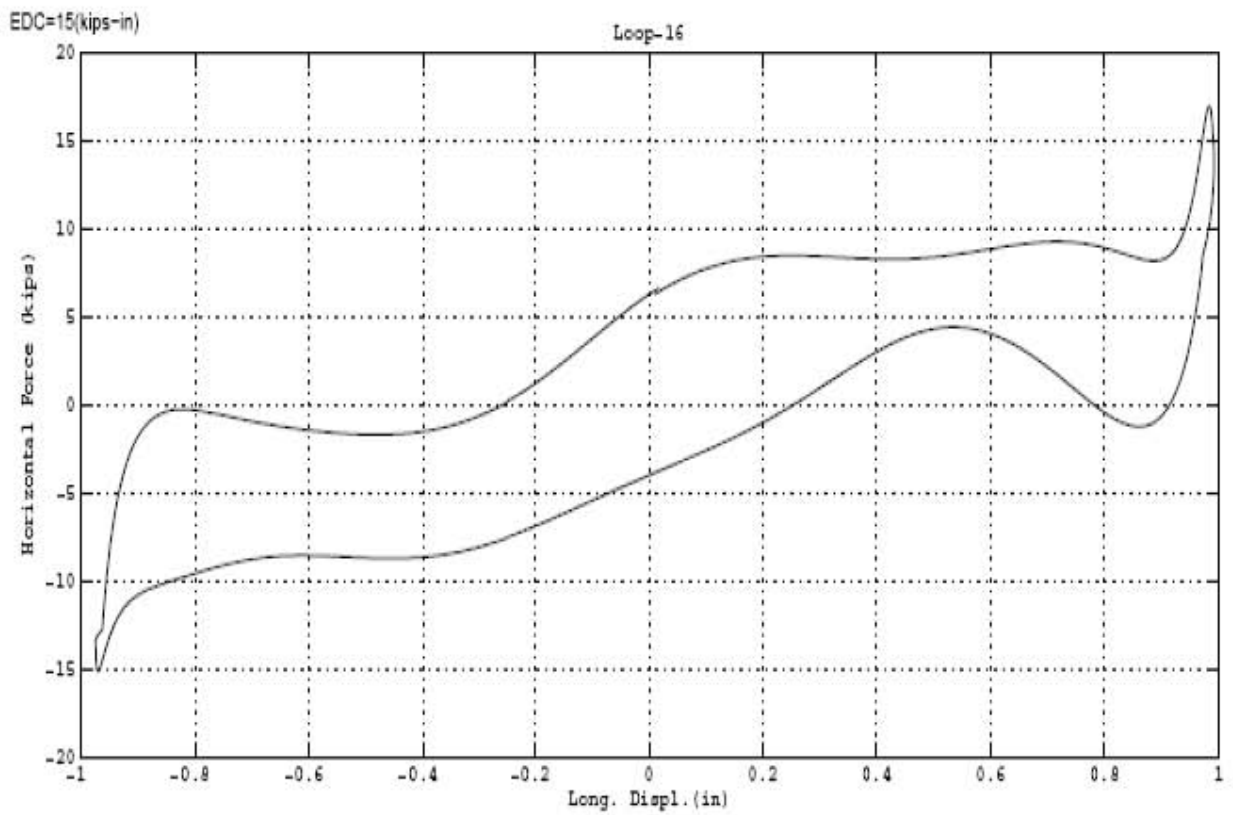
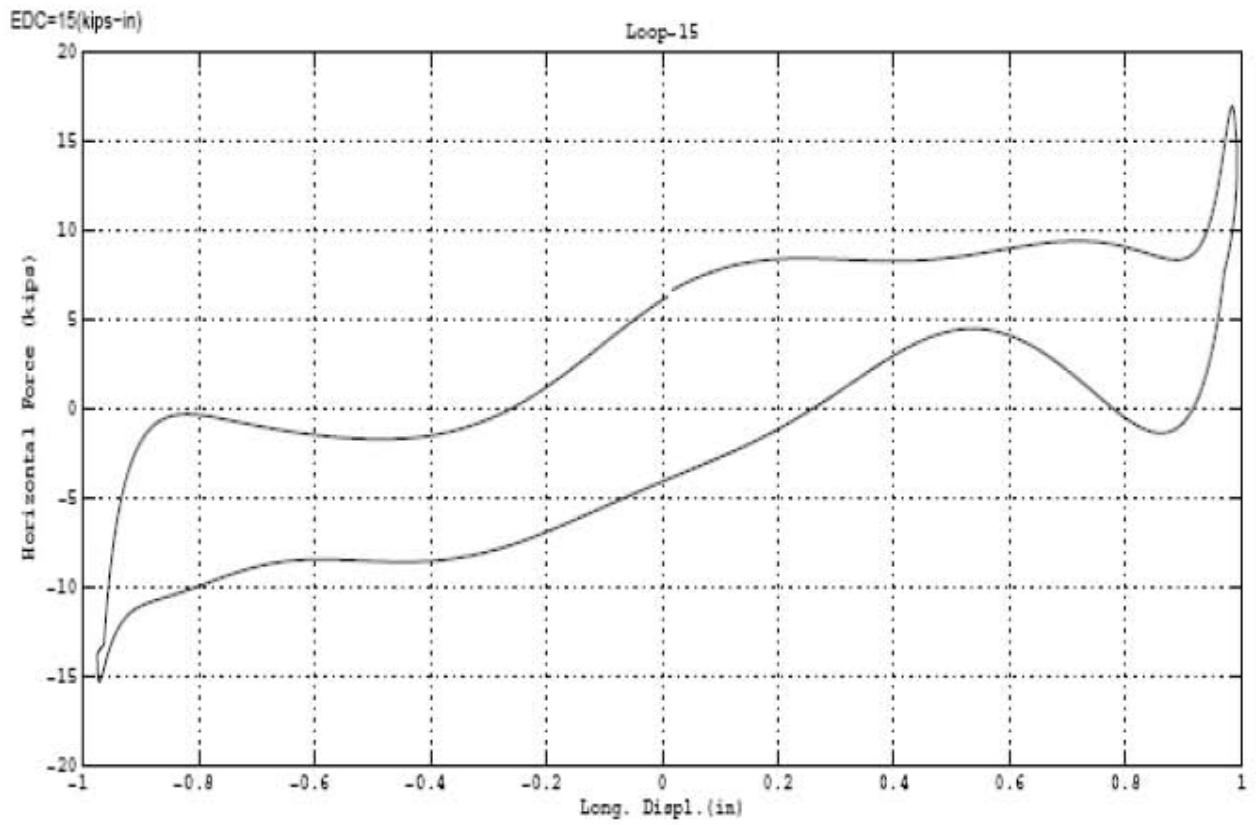


Figure 5-10 Results of Repeated Test #10 (continued).

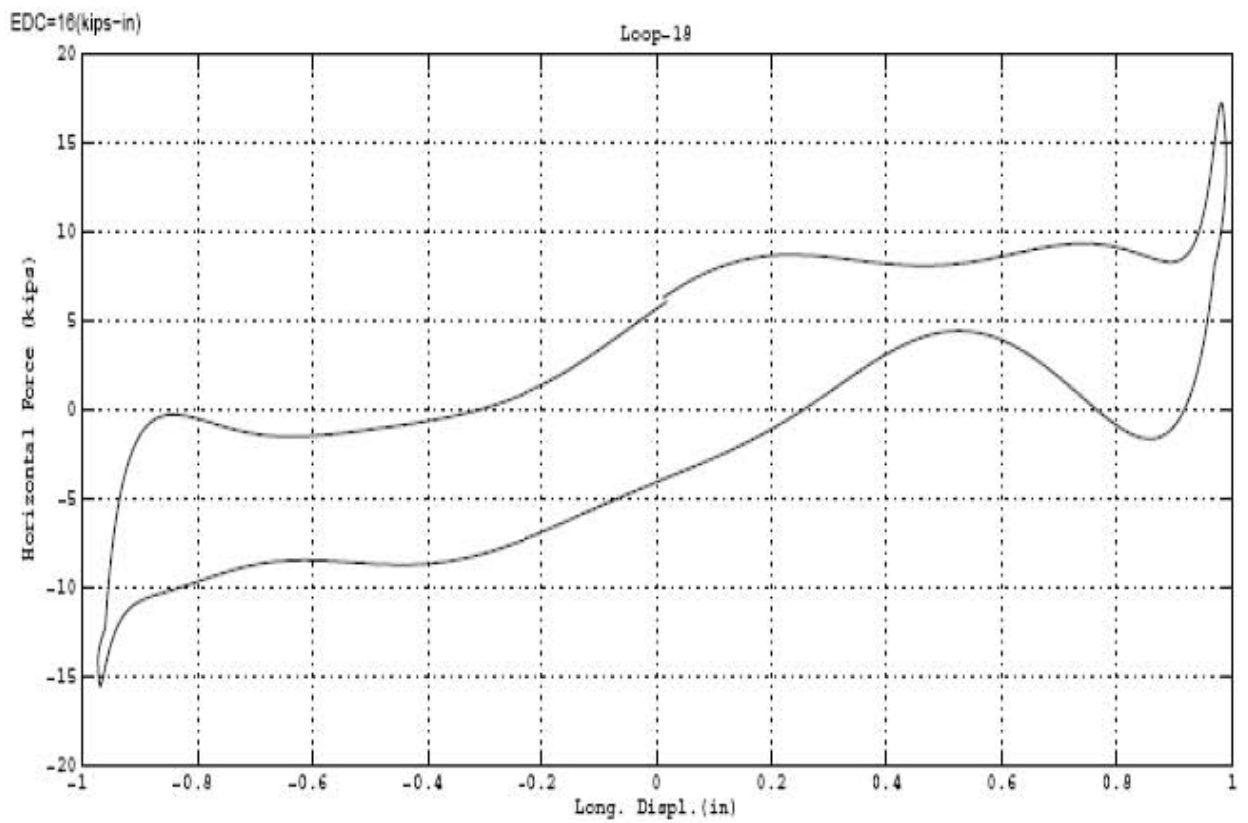
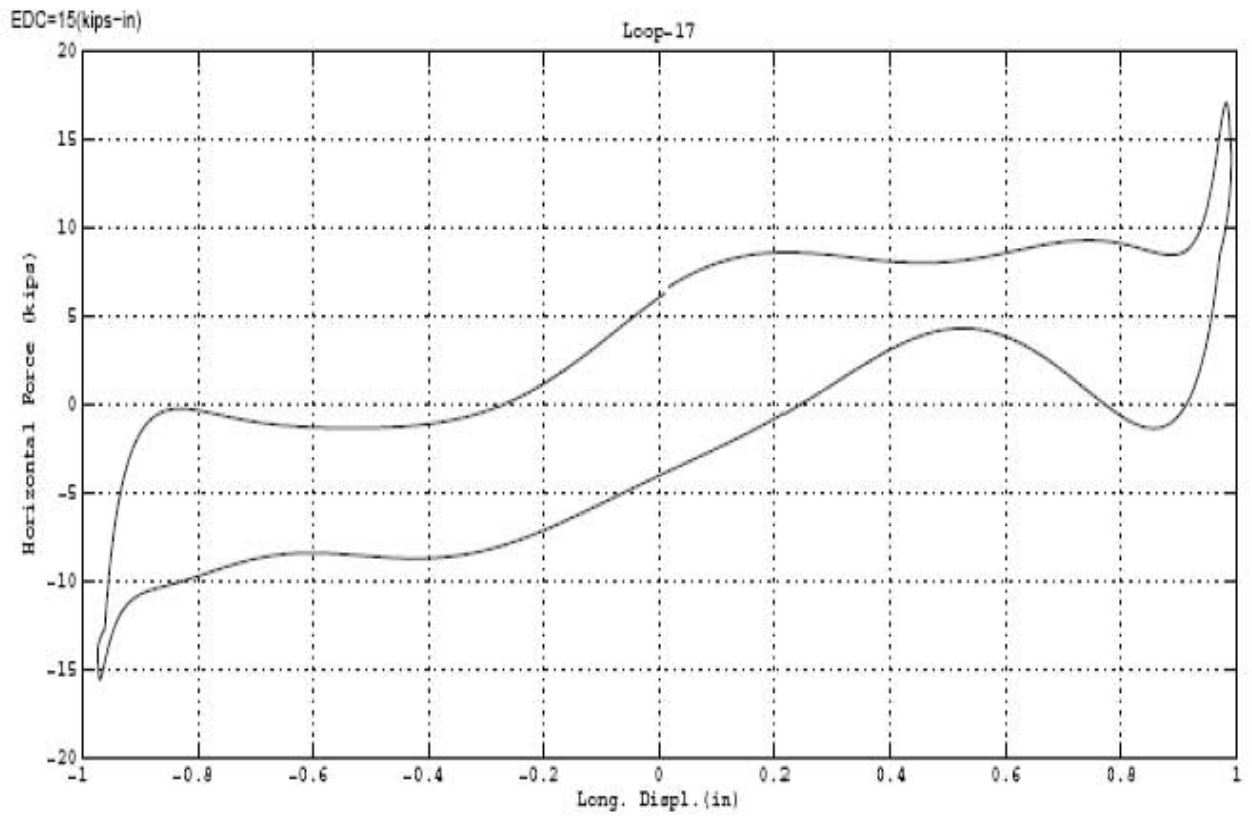


Figure 5-10 Results of Repeated Test #10 (continued).

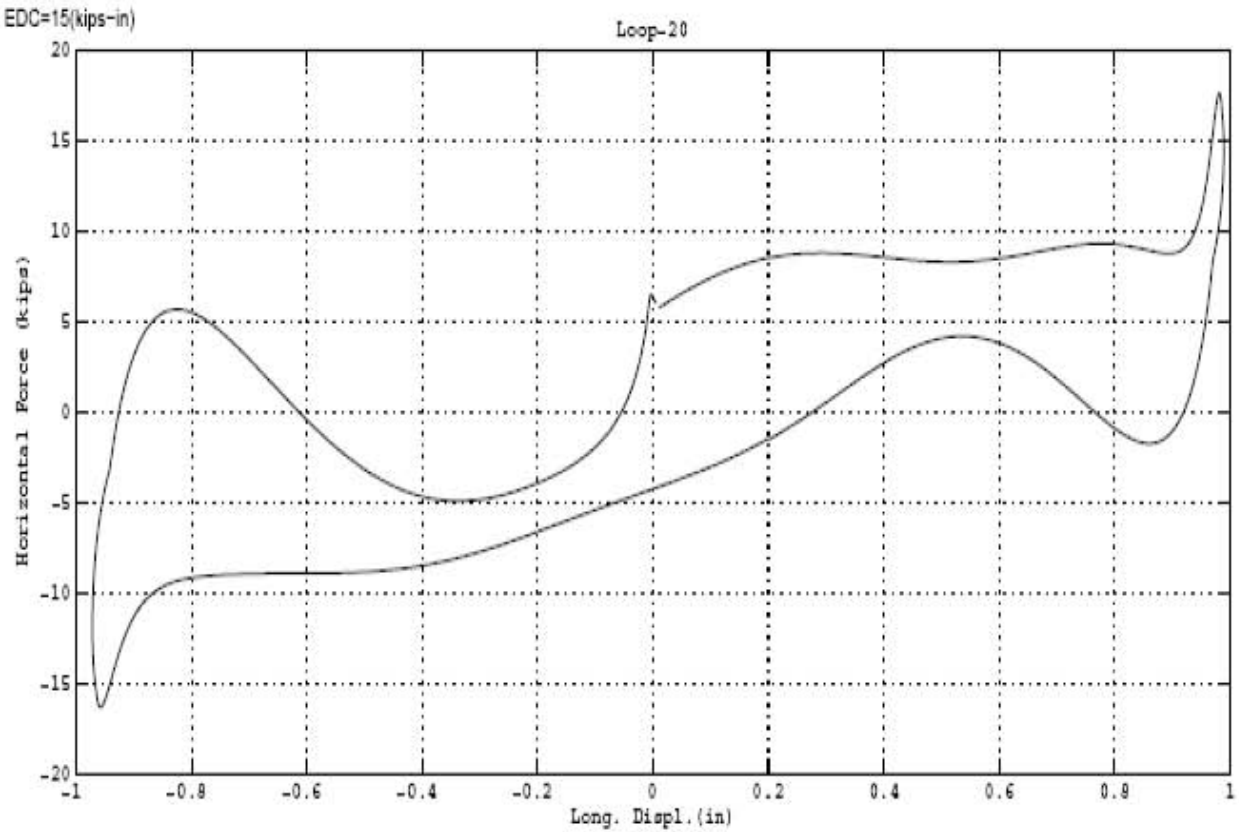
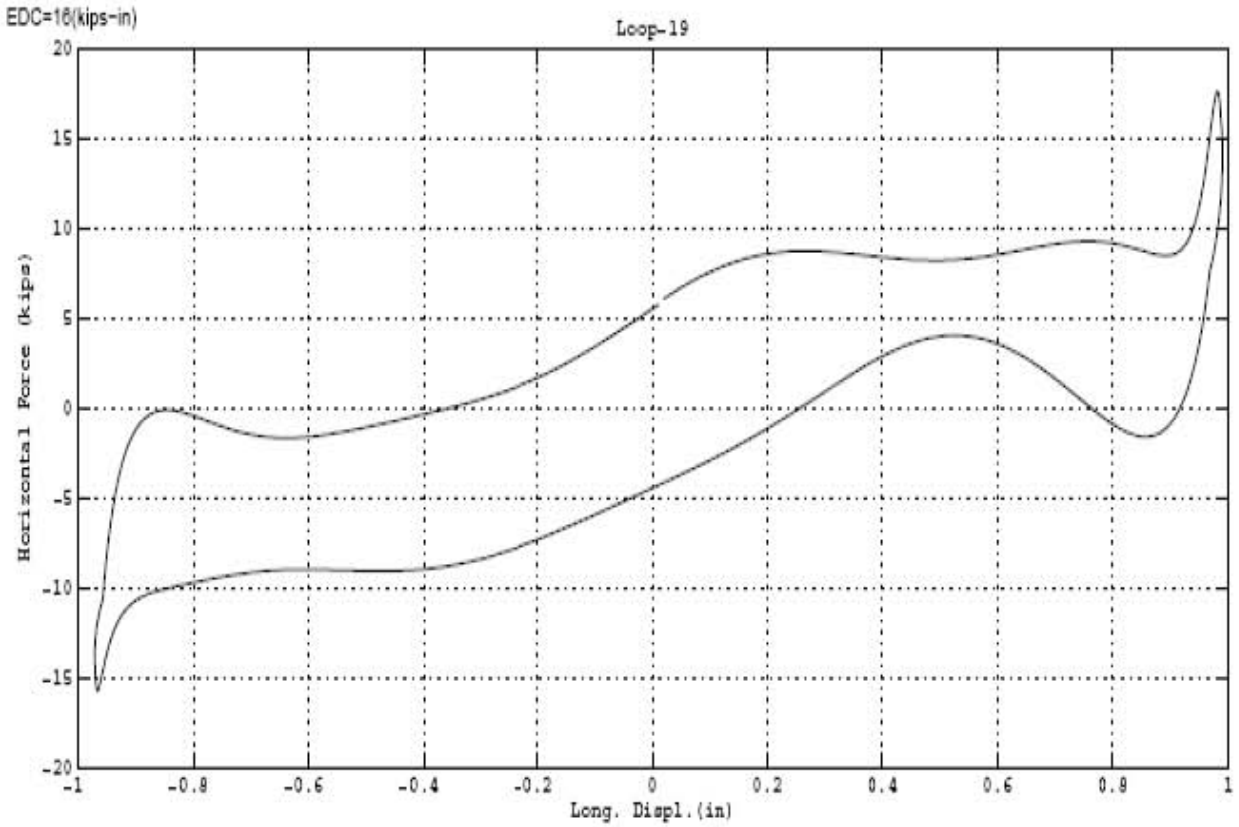


Figure 5-10 Results of Repeated Test #10 (continued).

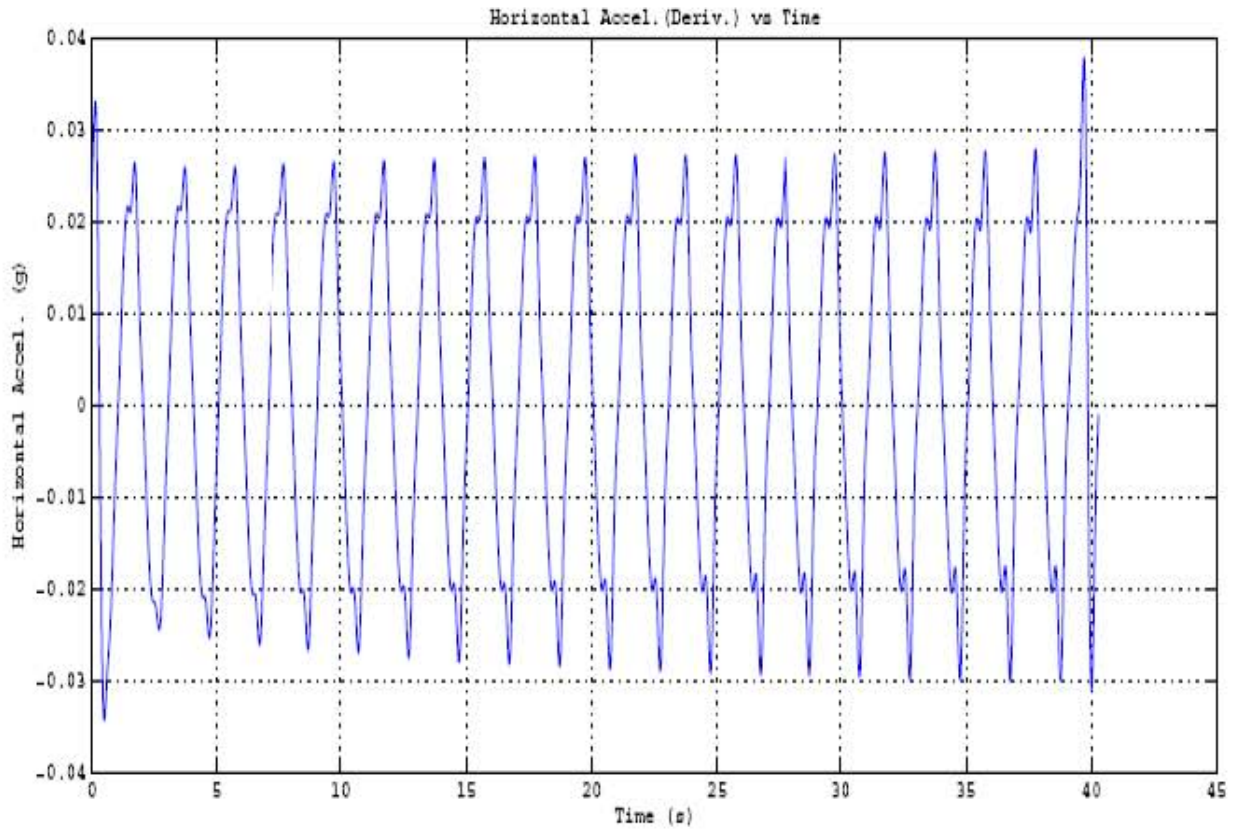
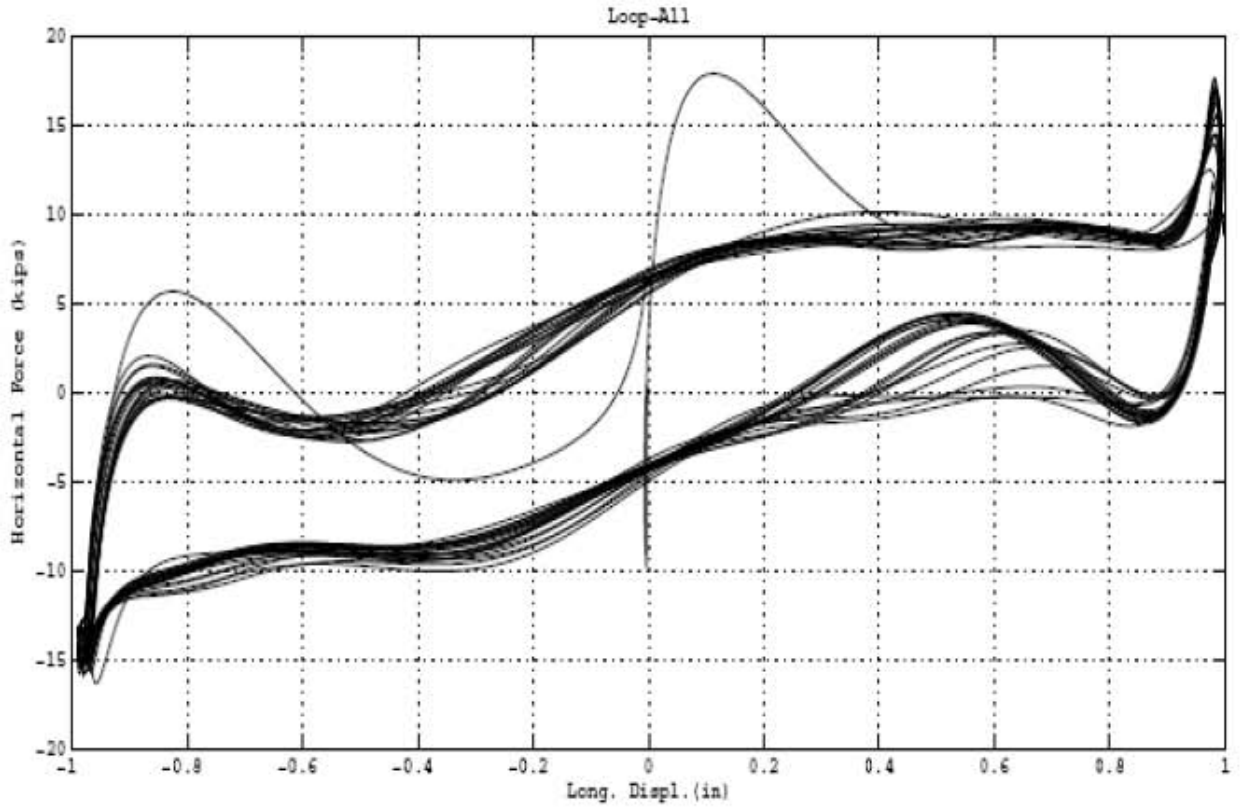


Figure 5-10 Results of Repeated Test #10 (continued).

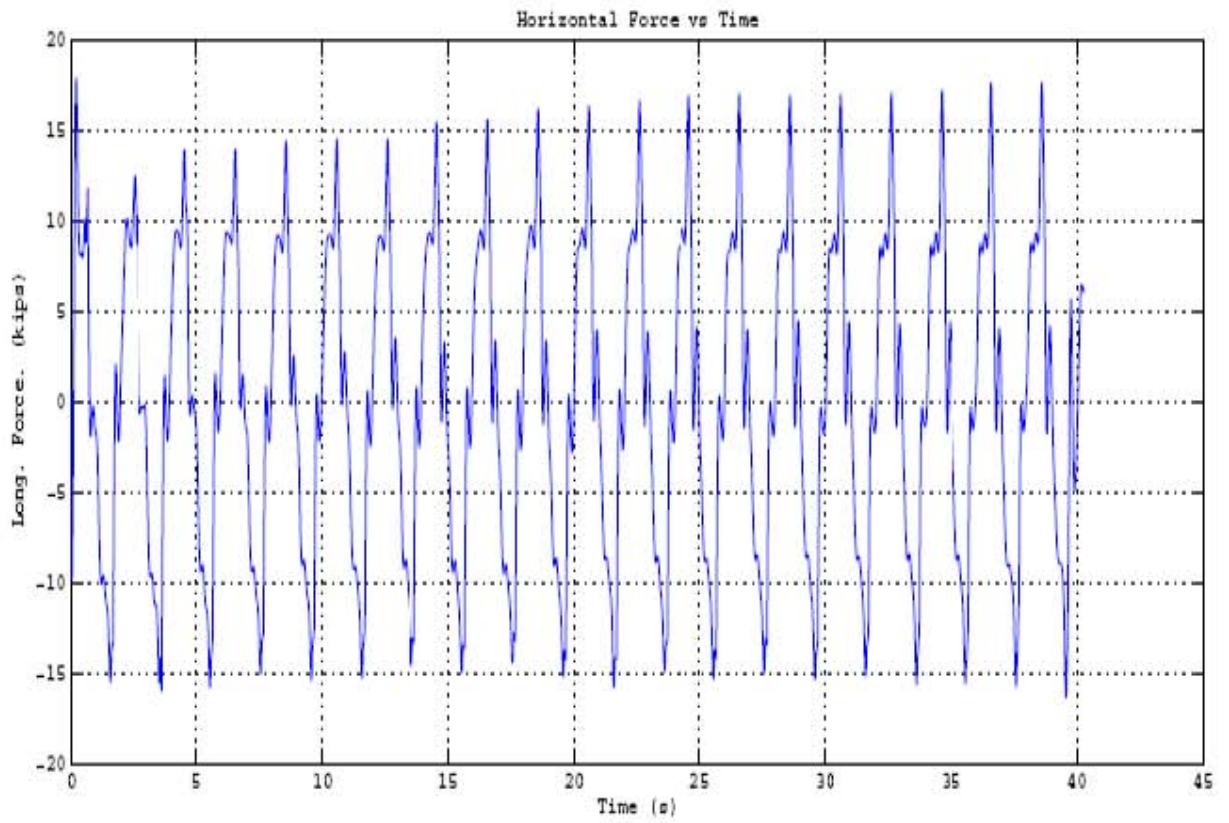
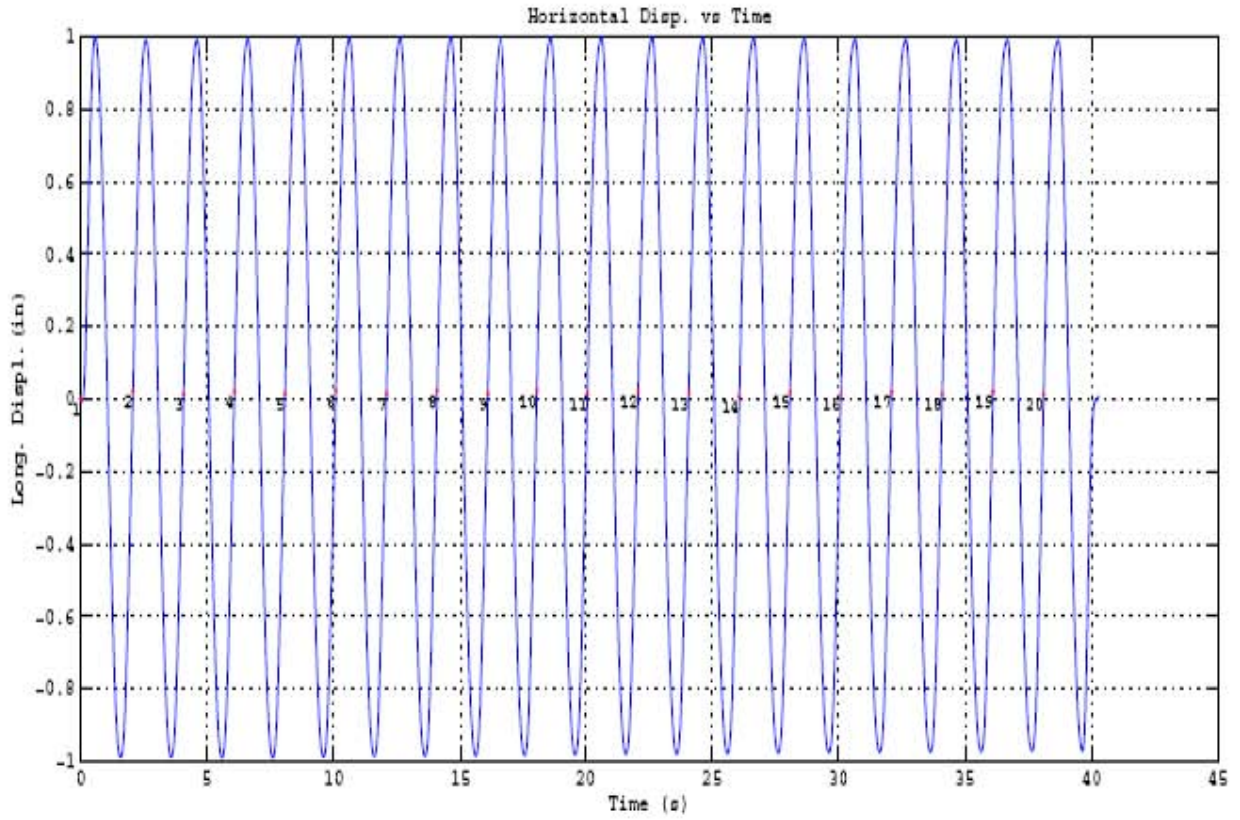


Figure 5-10 Results of Repeated Test #10 (continued).

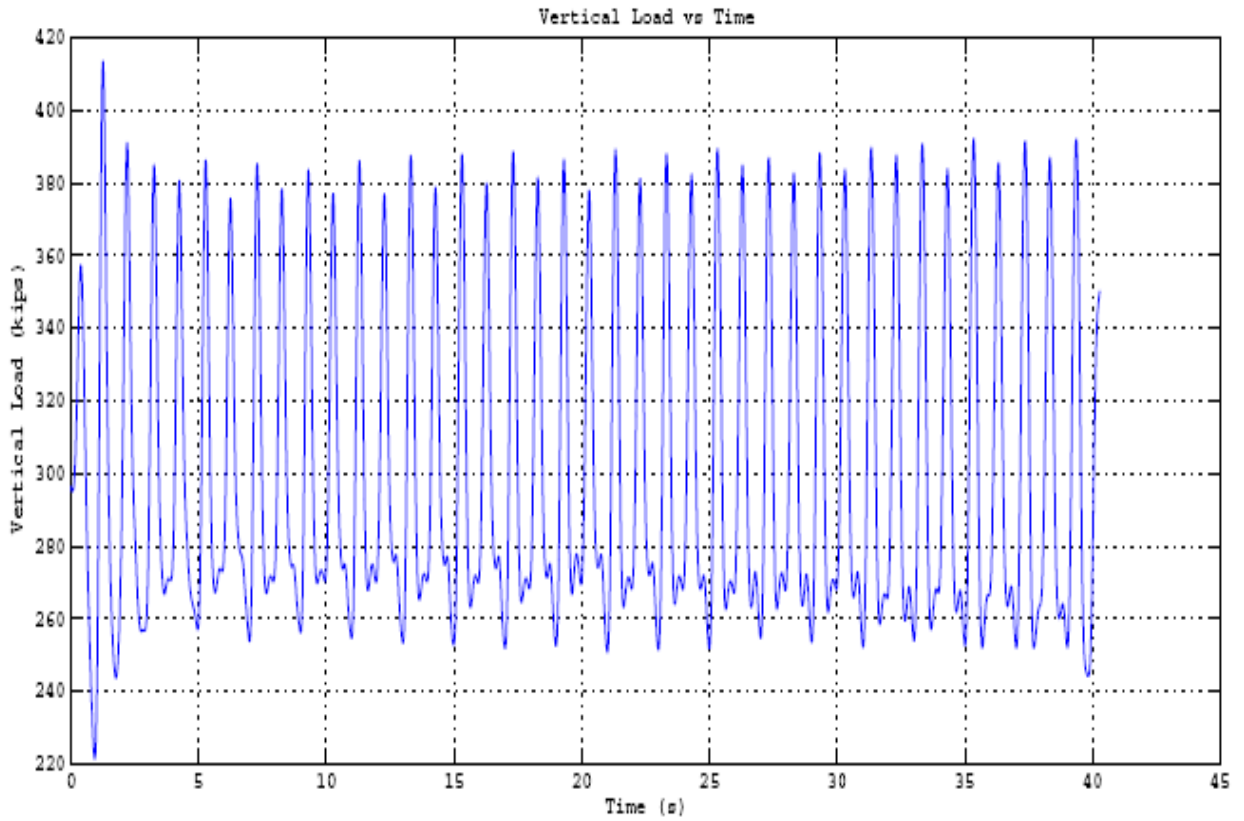


Figure 5-10 Results of Repeated Test #10

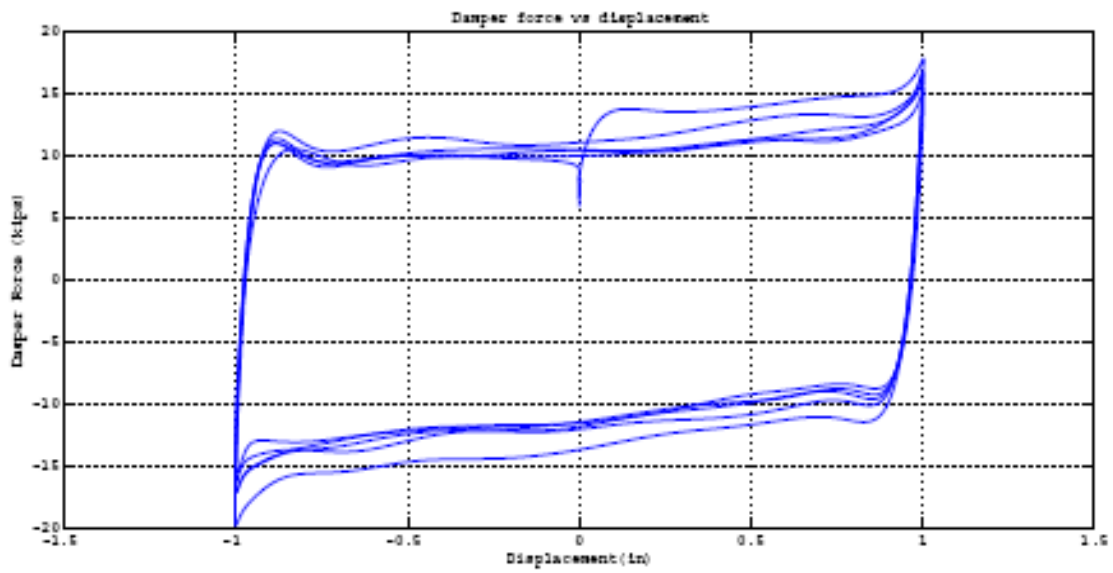


Figure 5-11 Results of Repeated Test #11 (continued).

6. DISCUSSIONS OF TEST RESULTS

Basic Requirement of HITEC

The purpose of HITEC test 1 is to estimate the effective stiffness in one direction. In the following, we shall explain why the stiffness of the roller bearing cannot be measured using the HITEC protocol. However, the performances of the roller bearing, in terms of relationship between the horizontal (lateral) force and the displacement are observed through tests # 1, 3 and 5. The total number of cycles for each test with different vertical load is required to be 10. In our tests, we use 12. It is seen that, during the 12 cycles, the relationship of the horizontal force and the displacement is unchanged. In fact, it should not be changed for this relation is guaranteed by the geometrical configuration of the bearing and during the testing, which is not changed at all.

The purpose of HITEC test 2 is to examine the bi-directional force-displacement relationship. The performances of the roller bearing, in terms of the horizontal (lateral) force and the displacement are tested through tests # 2, 4 and 6. The total number of cycles for each test with different vertical load is required to be 3. In our tests, we use 12. It is seen that, during the 9 cycles, the relationship of the horizontal force and the displacement is unchanged.

The purpose of HITEC test 3 is to examine if the driving frequency can affect the performance. This test is realized partially by test # 1 through 8. Although due to the limitation of the test apparatus, which cannot provide the driving frequency as high as 1.0 Hz, we can clearly see that the performance in terms of the relationship of the horizontal force and the displacement is unchanged. Again, it should not be changed for this relation is guaranteed by the geometrical configuration of the bearing. Test results clearly substantiate it.

In HITEC test 7 20 cycles are used to examine the variation of the performance of the bearing. This test is realized by test #10, where 60 cycles were used altogether. Again, results show clearly that the performance in terms of the relationship of the horizontal force and the displacement is unchanged, which is guaranteed by the geometrical configuration of the bearing, as theoretically predicted.

The purpose of HITEC test 9 is to examine the maximum load and the maximum displacement. Due to a control problem of the test machine, the maximum displacement is limited to 10". The maximum load per bearing is more than 400 Kips, which is about twice of the designed value. During the test, the bearing survived and performed quite stable.

HITEC test 10 is the quick release test. The purpose is to check the capability of the bearing to return to its original centering position. Due to the limitation of the testing apparatus, this test cannot be carried out. However, the capability of self centering can be partially observed through results of test # 9, 10 and 11. Because a friction damper is always connected to the bearing in order to increase the lateral force for control purposes, the total set of bearings cannot be expected to return back to the center position. Note that, the friction force is more than 20 Kips, with the average vertical load of 300 Kips. The component returning force is,

$$300 \times (0.5\theta) = 5.24 \text{ (kips)}$$

Through tests # 9 and #10, we can measure the total horizontal forces. From test 11, we can measure the damper force only. In this measure, the lateral force of the bearing only is about

5 Kips. From the recorded test results, we can see the measured data agree with the theoretical value. On the other hand, the rolling friction coefficient is less than 0.005, therefore, the resistance of that due to the average load equals to 120 Kips is about $300 \times 0.005 = 1.5$ kips

This number is considerably smaller than 5 Kips so that the roller bearing should be able to return to the center position easily. Note that, this is only a theoretical calculation. The test apparatus cannot be controlled with such a small force.

According to the above discussion, the basic requirements of HITEC are satisfied, except the following:

1. HITEC test 4, the fatigue test cannot be conducted due to the limitation of the test apparatus.
2. HITEC test 5, the salt-spray test cannot be conducted due to the limitation of the test apparatus.
3. HITEC test 6, the extreme temperature test cannot be conducted due to the limitation of the test apparatus.

Stiffness Estimation

In this session we address why the HITEC procedure is unsuitable to determine the lateral stiffness of roller isolation bearings.

The effective stiffness is supposed to be calculated by using the AASHTO's or HITEC's formula

$$K_{eff} = \frac{F_{max} - F_{min}}{D_{max} - D_{min}}$$

From test # 1, we can see that the maximum and minimum forces F_{max} and F_{min} measured by the test load cell are about 17 kips and - 21 kips, respectively. The maximum and minimum displacement D_{max} and D_{min} measured by the test LVTD are 10" and - 10", respectively. Therefore, the calculated effective stiffness seems to be 19 kips/in. This number is obviously incorrect because the equivalent lateral stiffness of the roller bearing is zero.

Overload of Vertical Force

Due to the limitation of test apparatus' control, the vertical force is overload. The four bearings are closely planed in the test. Thus, among the four bearings can't be expected to share equally the vertical load. Since there is no load cell installed for the individual bearings, it is reasonable to assume at least one half of the vertical load is taken up by one of the four bearings. In this case, this particular bearing is at least four times overloaded.

This test condition actually provided a much more stringent situation than HITEC's requirement, which give us a chance to examine if this bearing can survive a large vertical load.

Upon examining the bearing after the total 12 tests, no bearing was damaged. This provides an extra confidence on the capacity of the roller bearings to resist possible vertical overload.

NCREE TESTS

The main purpose of this test program is to examine the performance of the roller bearings with added friction dampers.

1. BEARINGS AND DAMPERS USED IN THE NCREE TEST PROGRAM

Design of Roller

The size of the roller is the most important design parameter, which is chosen by using the following formula.

$$F = 6 DL \sigma_u^2 / E$$

where

F : required load per bearing, $F = 25T = 56$ kips (with safety factor = 2)

D : diameter of the roller, chosen to be 3";

L : working length of the roller, chosen to be 10"

σ_u : Ultimate Strength

E : Young's Modulus

Material:

Gray cast iron

ATSM Class 40: Standard Gray test cast iron bars: $\sigma_u \rightarrow 140$ ksi; $E \rightarrow 20000$ ksi

Carbon steel, $\sigma_u \rightarrow 100$ ksi; E- 16. $\rightarrow 30000$ ksi

therefore

$$F_{40} = 6 \times 3 \times 10 \times (140)^2 / 20000 = 176 \text{ kips (79T)} > 56 \text{ kips}$$

$$F_{cs} = 6 \times 3 \times 10 \times (100)^2 / 30000 = 60 \text{ kips (27T)} > 56 \text{ kips}$$

Conceptual Design and Drawings

Lower Plate, Roller Assembly

Design returning acceleration = 0.09g

Slop: 2°

Thickness: $C = 1''$ (25 mm)

Width: $W = L + 2(T + M) = 14''$

$T =$ Width of track = 1.5''

$M =$ Mount = .5''

Length: $H = D + 2(B + S) = 14''$

$B =$ Bearing displacement/2 = 5''

$S =$ Safety distance = 0.5''

Figure 1-1 shows the general view of the bearing.

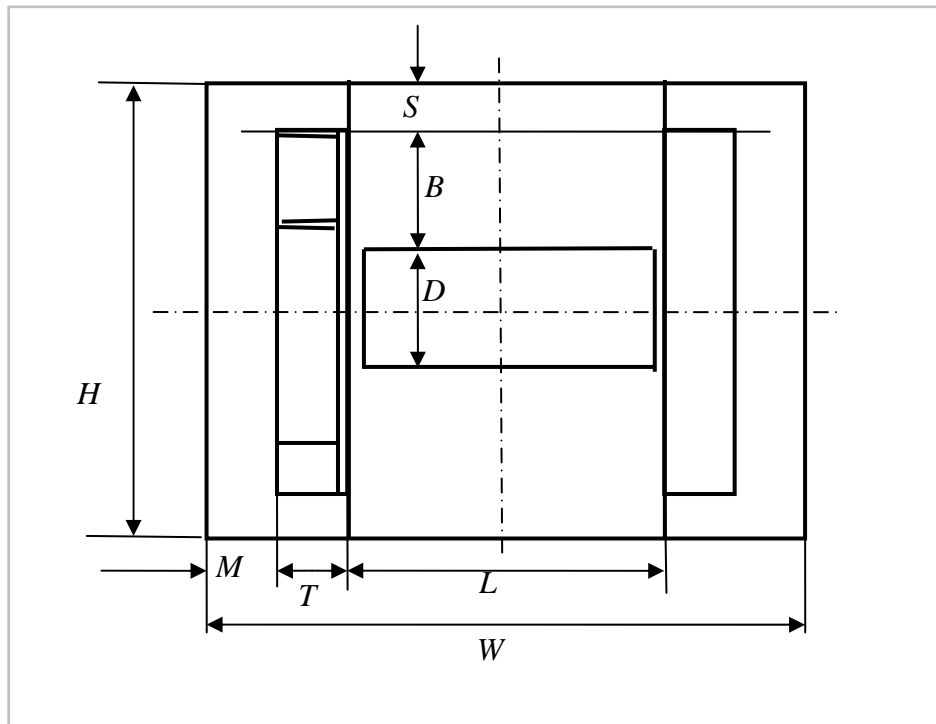


Figure 1-1 General view of the roller bearing

The lower plate is shown in figures 1-2

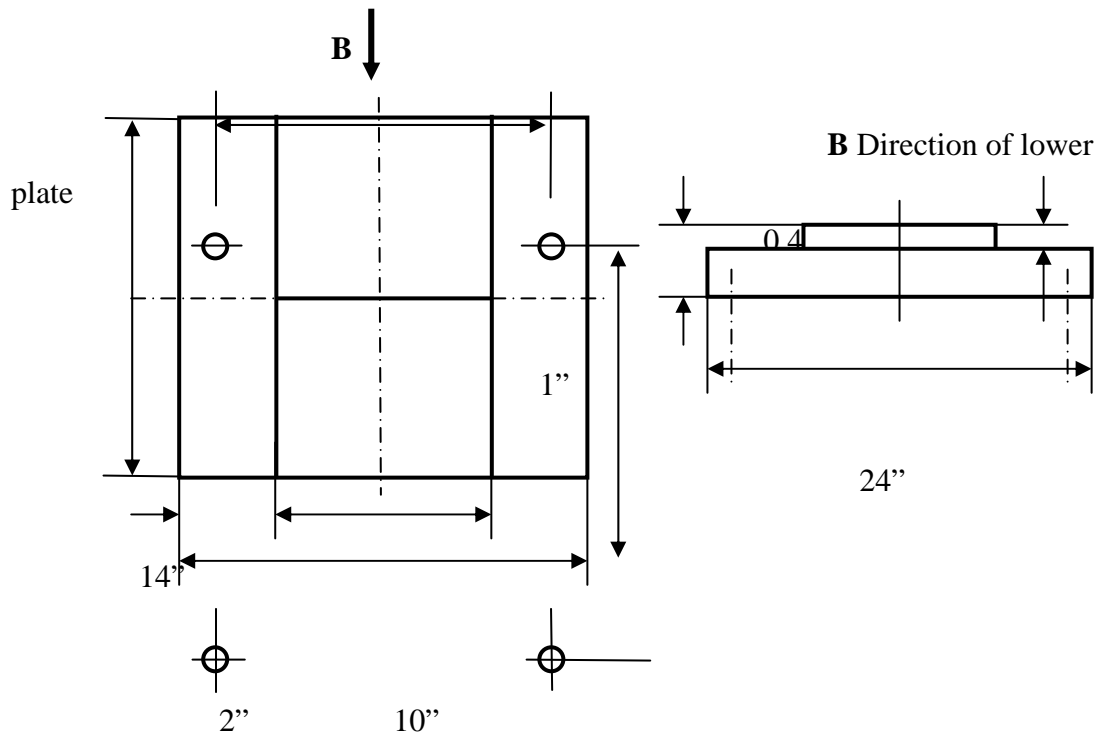


Figure 1-2 Lower plate

The drawing is the B direction is shown in figure 1-3

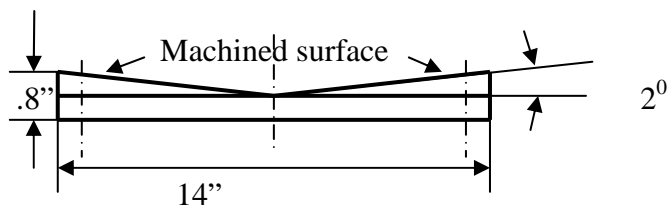


Figure 1-3 B-direction of lower plate

The drawing of roller is shown in figure 1-4

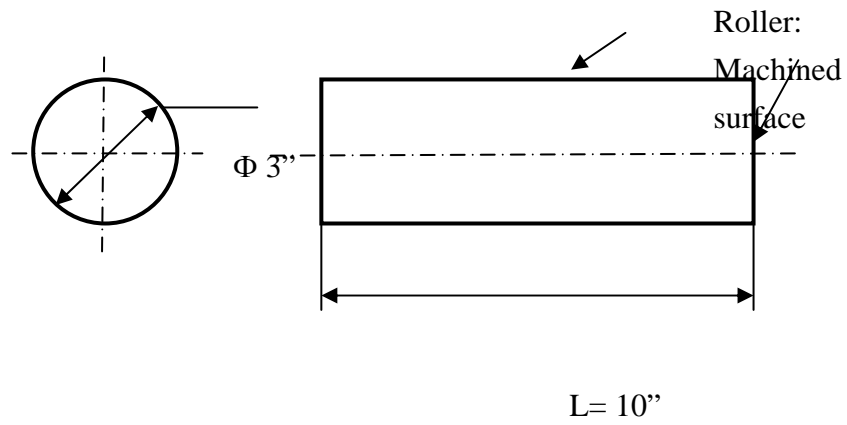


Figure 1-4 Drawing of roller

The drawing of the upper plate is shown in figure 1-5. Figure 1-6 shows the lower rolling surface.

Upper plate

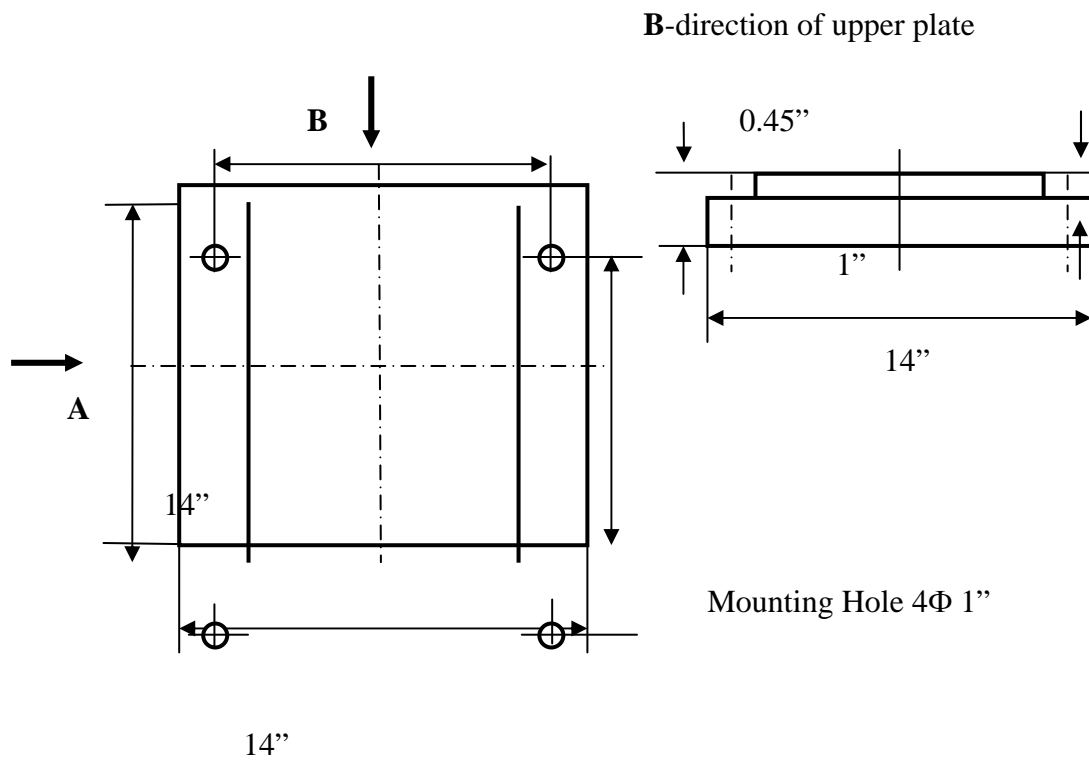


Figure 1-5 Upper plate

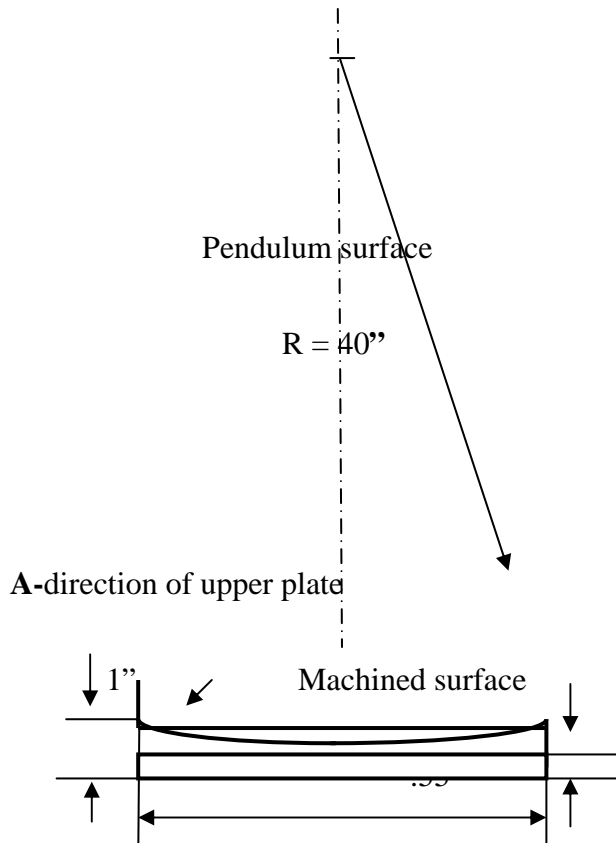
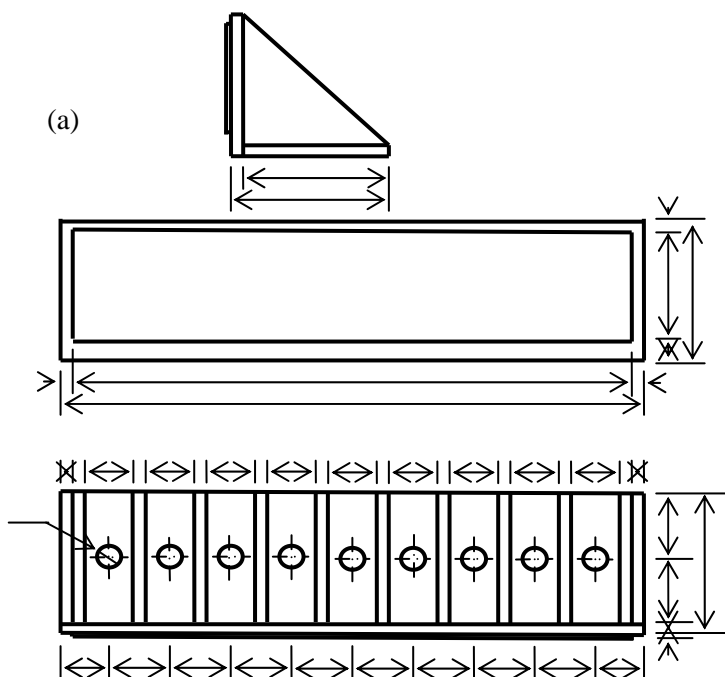


Figure 1-6 Lower rolling surface

Figure 1-7(a) conceptually shows the guidance of the bearing. Figure 1-7(b) shows an alternative design of the guidance.



(b)

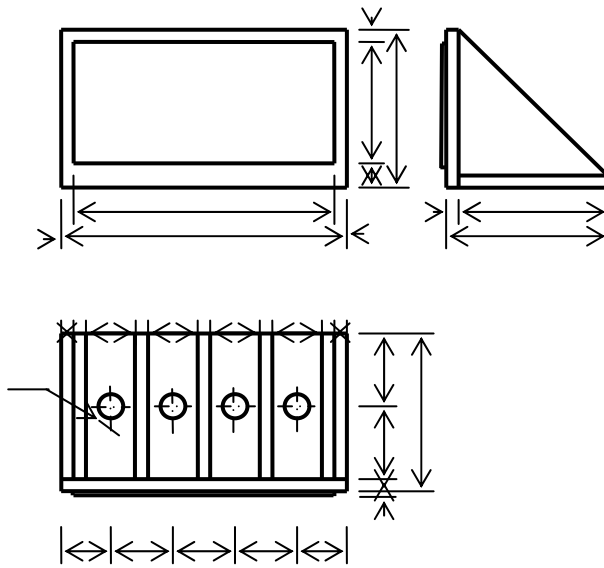


Figure 1-7 Guidance of the bearing

The material and machining requirement of the bearing are expressed as follows

Material

1. Plate

Steel: A36

Stainless Steel Type 304 with # 3 Finish (see McMaster-Carr 89815K47-12" x 12' x 24' for instance)

2. Parts of damper/guides

Steel: A36, PTFE (see McMaster-Carr 8801KAC 8801K512 - 1/4" x 12" x24" for instance)

Friction Coefficient $\mu \leq 0.05$

Max. friction force $0.33 \mu W = 0.017 W$

The photos of the bearing and damper are shown in figures 1-8 and 1-9 respectively

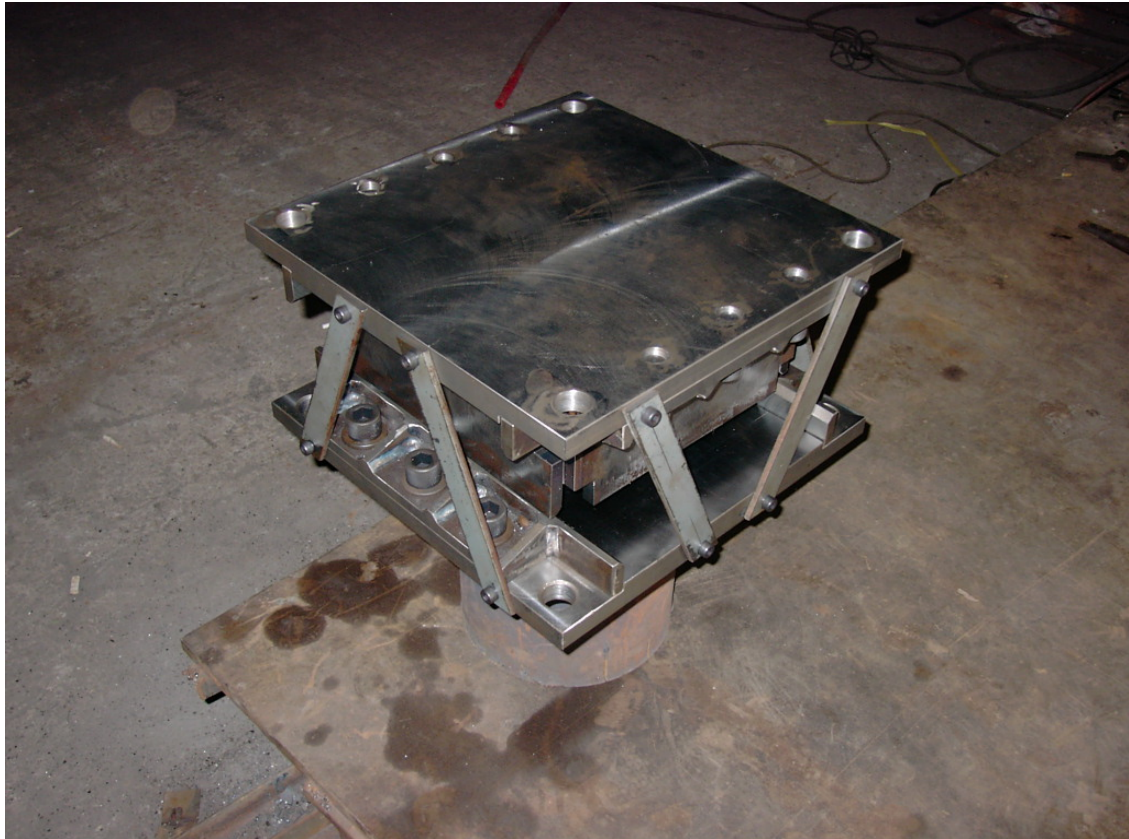


Figure 1-8 Roller bearing used in NCREE test



Figure 1-9 Damper used in NCREE test

2. TEST SETUP

The isolator test is carried out by using existing down-scaled test structures available at NCREE, shown in figure 2-1.

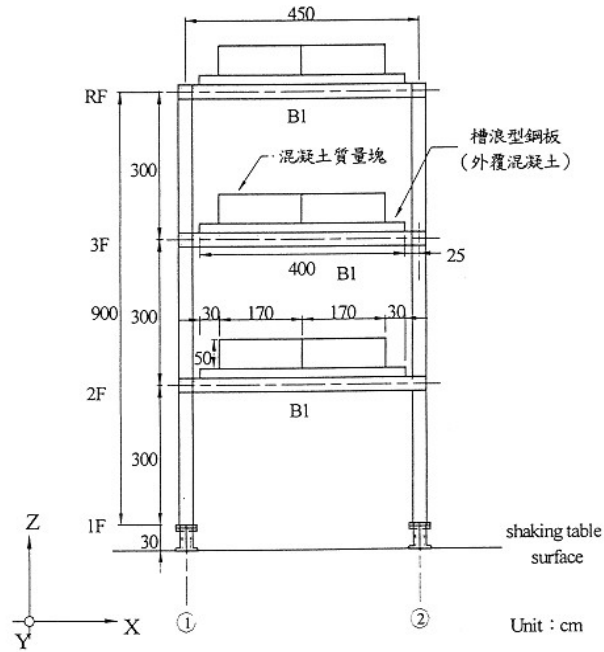


Figure 2-1(a), Test set up, front elevation

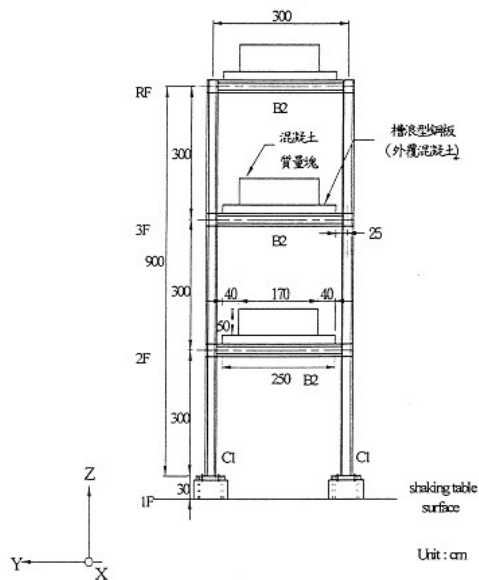


Figure 2-1 (b), Test set up, side elevation

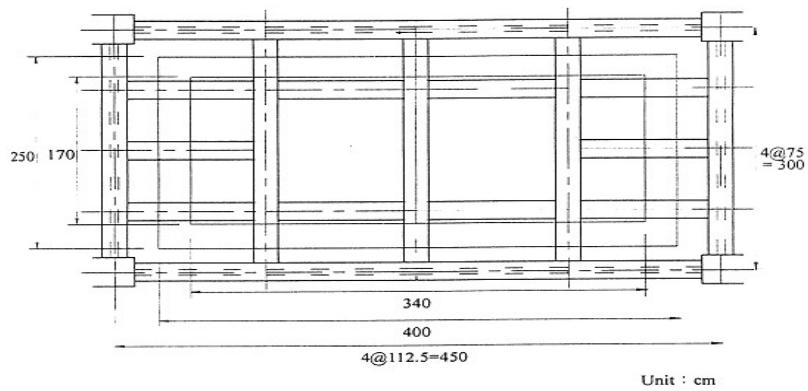


Figure 2-1(c), Test set up, top-view

The structure is made by H steel beam (ASTM A36). The column is H200 × 200 × 8 × 12 and the beam is H200 × 150 × 6 × 9. The added mass are made by concrete block and weighted 29.8 T.

3. TEST RESULTS

The test results are shown and explained in the following

Damper Test

The friction damper is tested using cyclic loading. Figure 3-1 shows the selected force-displacement plots.

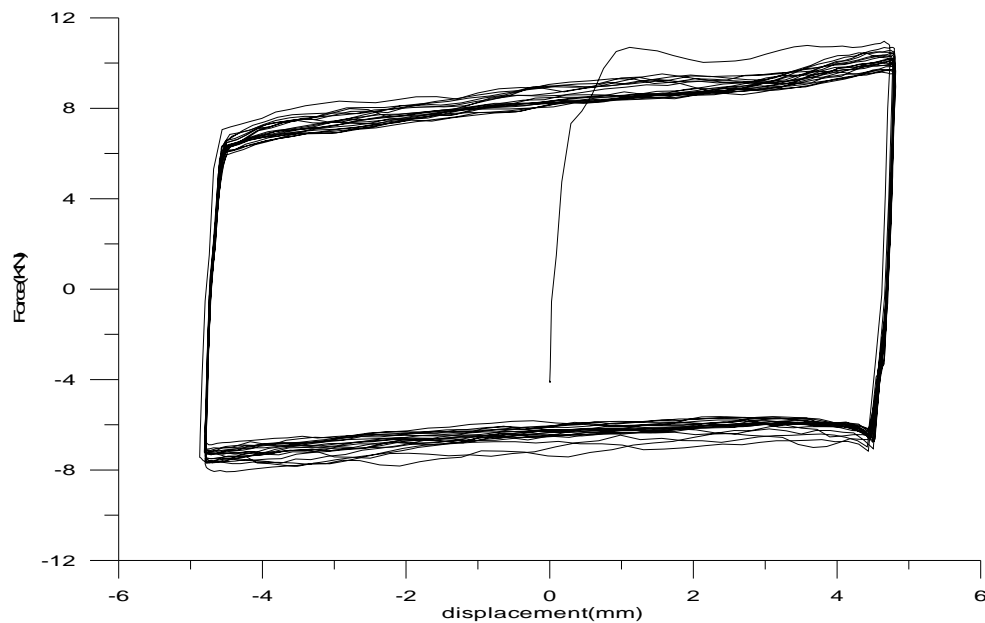


Figure 3-1 Test results of friction damper

These results show that the friction damper can deliver the rectangular energy dissipation loops. And it works rather stably. The results are used to adjust the damper to provide necessary friction forces.

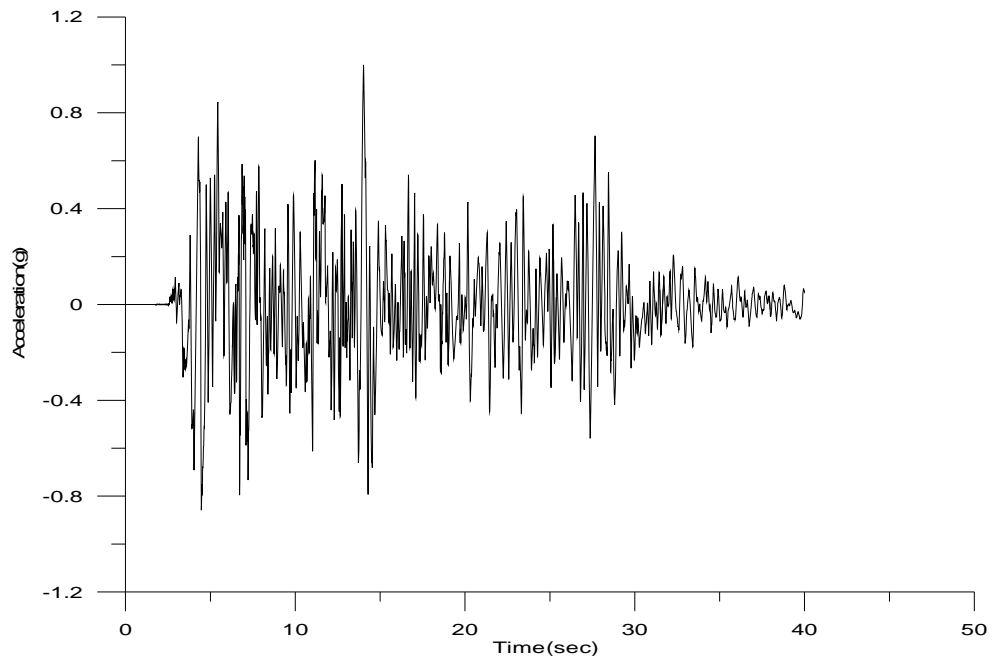
Input Records

In the NCREE tests, we use bi-directional earthquake ground excitations. To examine possible distortion caused by the shaking table, we show the two records in X and Y directions respectively in figures 3-2. From the time histories and response spectra, it is seen that the distortions are small.

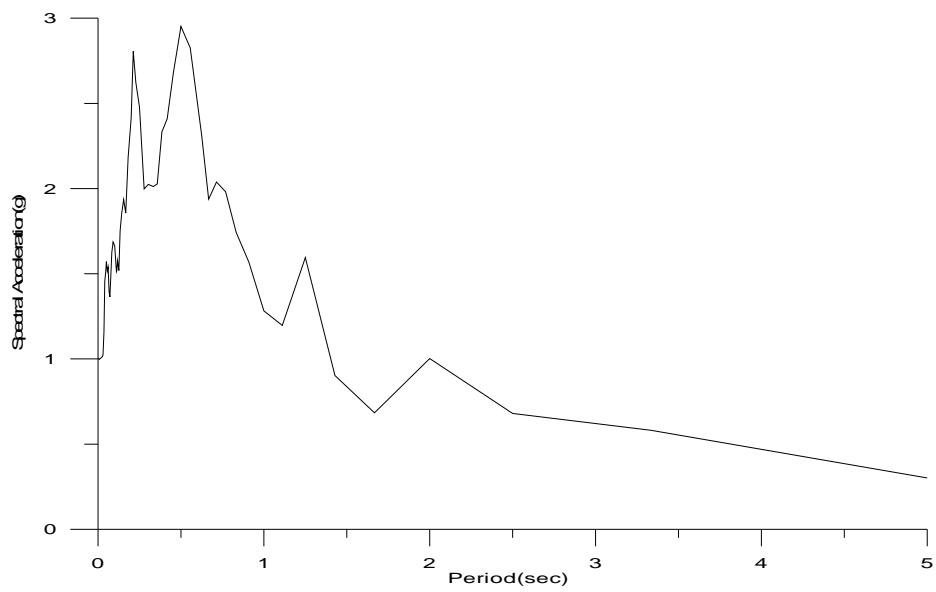
Test Results

The selected test results are shown in figures 3-2 and 3-3. From these test data, it is

seen that the newly designed roller bearing performs well.

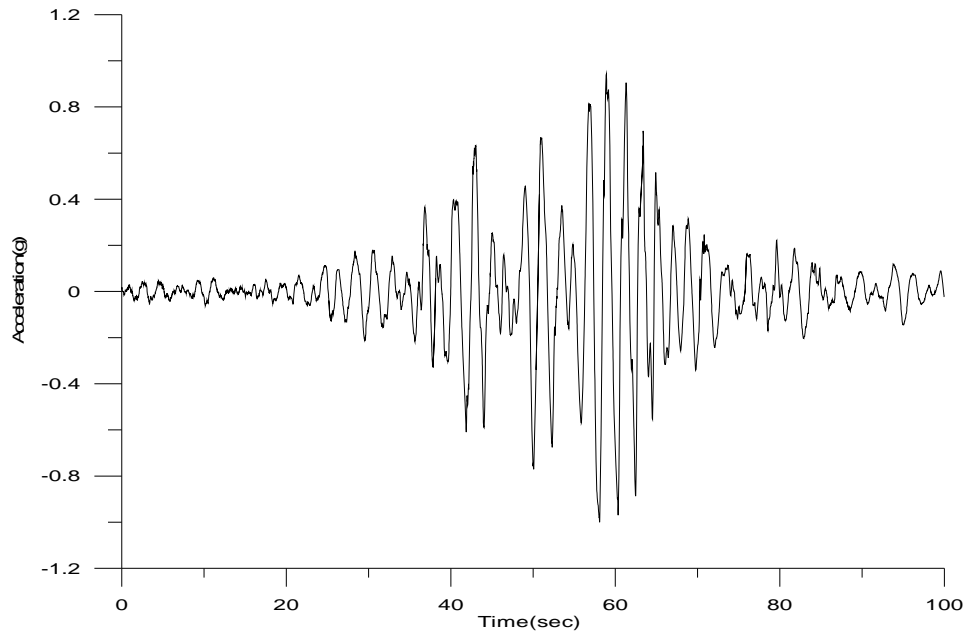


El Centro time history

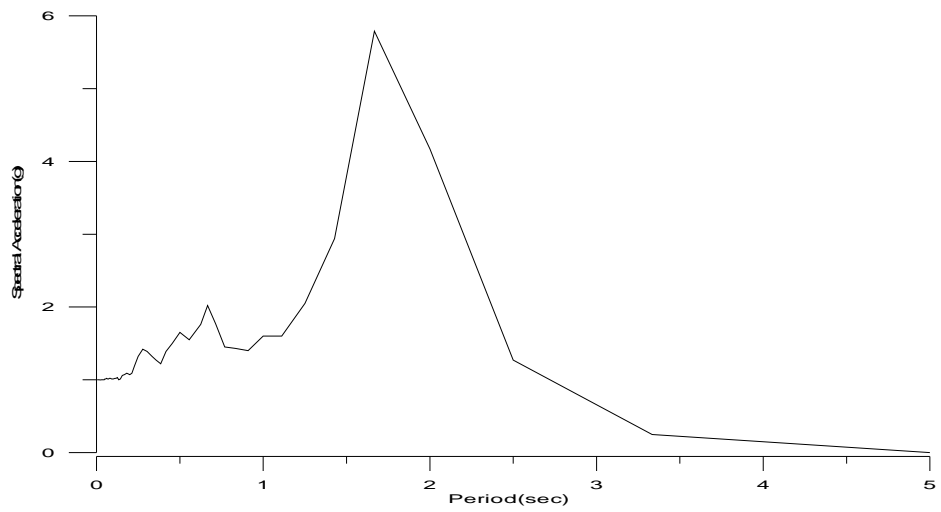


El Centro response

Figure 3-2 Measured ground motions (Mexico earthquake) (continued)

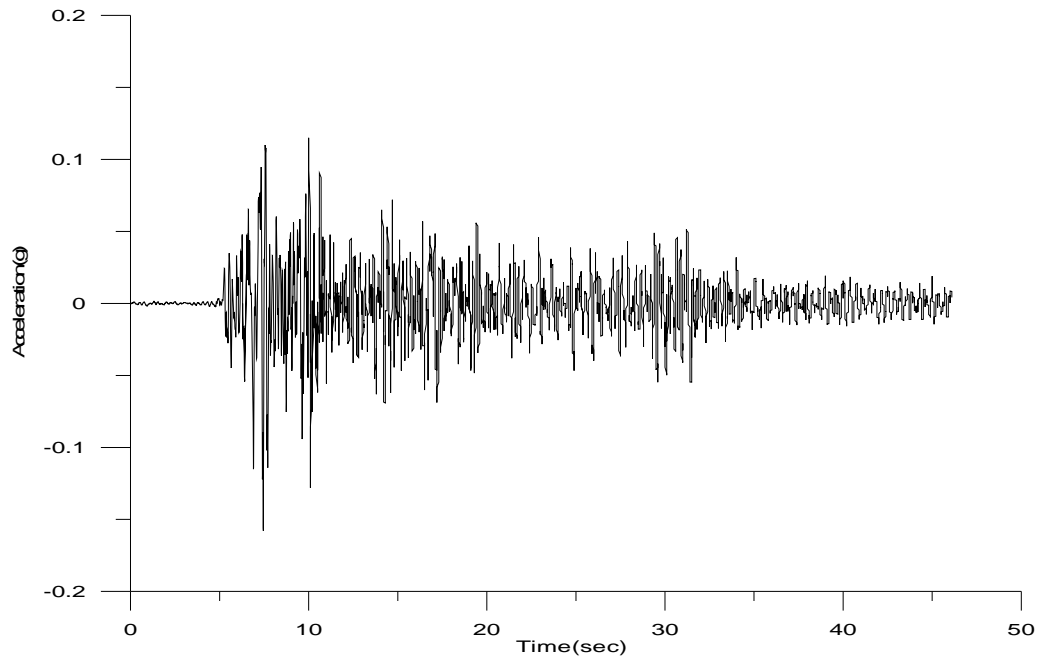


Mexico Time History

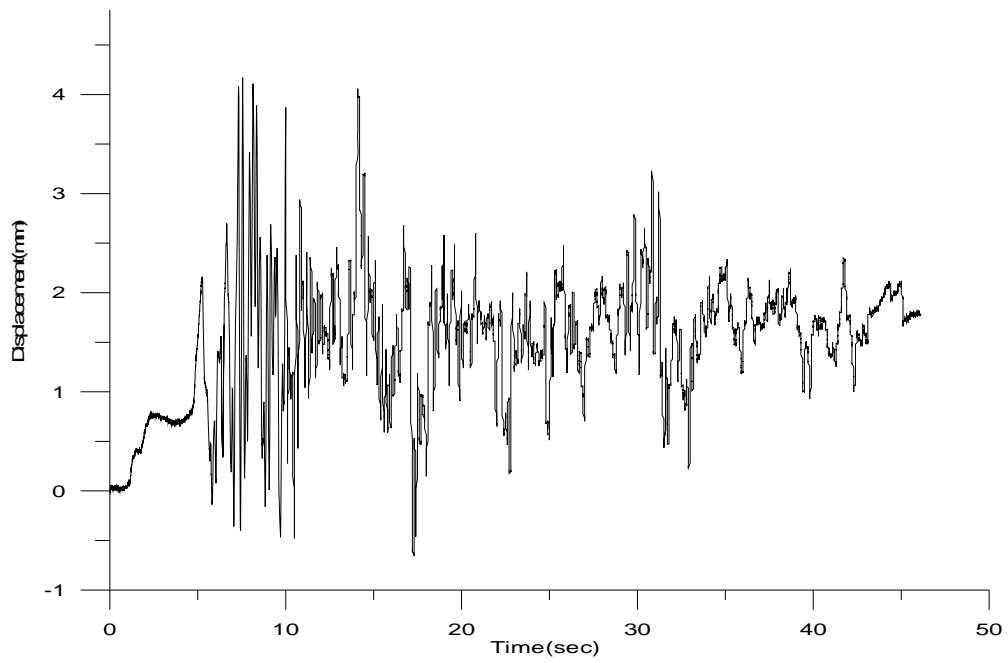


Mexico response spectrum

Figure 3-2 Measured ground motions (Mexico earthquake)



El Centro (X direction only) Top story acceleration



EL Centro (X direction only) Top Story displacement

Figure 3-3 Measured ground motions (El Centro earthquake)

4. BRIEF SUMMARY

In the NCREE tests, we first combined the roller bearing together with the friction damper. It is seen that maximum returning force of the roller bearing is about 0.05 Mg. The maximum damping force of the friction damper is about 0.10 Mg. The total seismic force is about 0.15g. Thus, the damping force is twice as high as the returning force. In other words, this isolated system is definitely an over-damped system.

From the measured data, we can realize that the performances of the over-damped system agree with the theoretically predicted values. Furthermore, the performances of the isolators are quite good. The maximum acceleration of the superstructure is low and vertically unchanged in the vertical direction under different earthquake excitations.

IEM TESTS

An improved isolator combined with roller bearing and friction damper were further tested. The purpose of this test is to examine the performance of the isolation system. The second objective is to compare the performance with a commercially available lead-rubber bearing.

1. TEST SETUP

The roller bearings used in the IEM test program belong to the first prototype bearing as described in Section 4.1 of the report. However, the bearing rolling guides were modified to generate friction damping to reduce displacement responses.

The characteristic of the IEM shake table is listed as follows:

- Degree of freedom : 6, 3-D (XYZ)
- Size of table : mx5m
- Maximum payload : 30 Ton
- Weight of table : 20 Ton
- Maximum displacement : X&Y 80mm , Z 50mm
- Maximum velocity : 50cm/s
- Maximum acceleration : X&Y 1.0g , Z 0.7g
- Frequency range : 0.5~40Hz

The test setup is shown in figure 1-1.

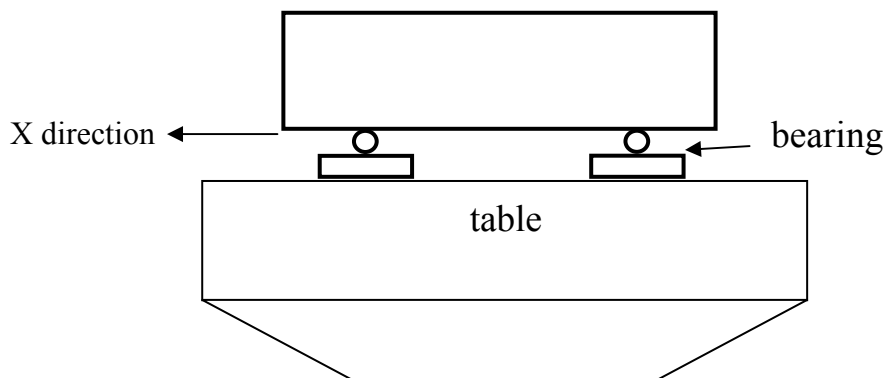
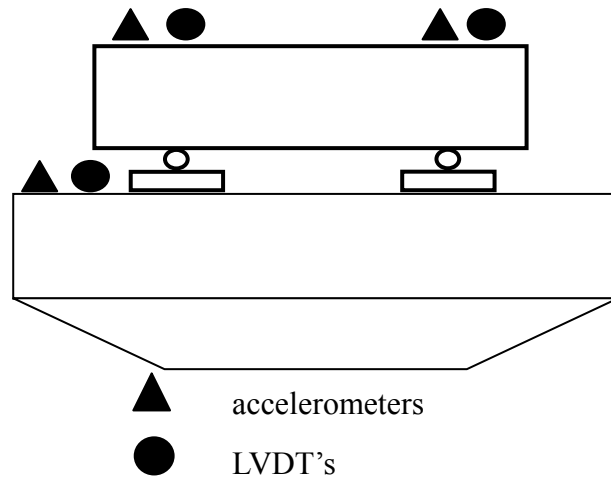
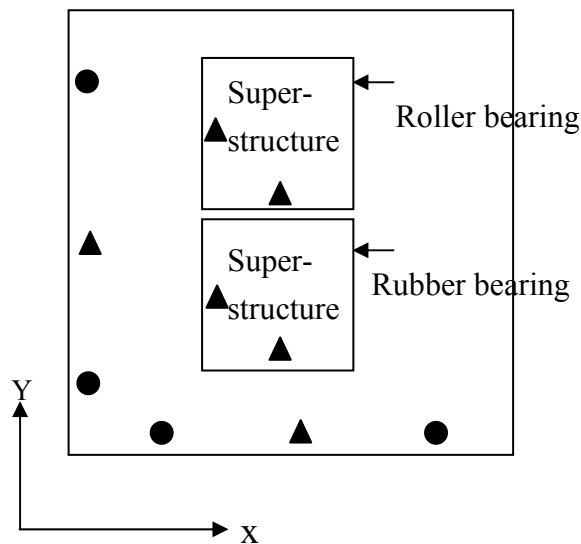


Figure 1-1 Test setup



(a) side elevation



(b) front elevation

Figure 1-2 Sensors

The equivalent superstructure is a 2.0×2.0×1.0M concrete block weighted around 9.5 ton and four roller isolators are used to support the block. Figures 1-3(a) and 1-3(b) show the photos of the test setup.

The isolation system is mounted on the shaking table of IEM test laboratory (see figure 1-4(a)). To compare the performance with lead-rubber bearings, the elastomeric bearings are also installed under the same concrete block. Since the displacement of the shaking table is limited to 10 cm, the time during of the earthquake records was scaled down. Another reason of using shorter time interval in the application of

similitude law for the elastomeric bearings tested. Note that the period of the roller bearing is infinite so that it will not be affected by the issue of time scaling.

The photos of the installation are shown in figure 1-4(b).



(a)



(b)

Figure 1-3 Test setup



(a)



(b)

Figure 1-4 Installation of bearing

2. TEST RESULTS

Figure 1-5 shows the selected accelerations of certain excitation time histories measured during the test. Figure 1-6 shows the measured corresponding accelerations of the superstructures.

Selected test results are shown in table 2-1. It is seen that the performance of the roller bearing agrees with the previous test. And, it also agrees with theoretical predictions.

From this table, we can see the good performance of the roller isolator. We know that the rolling slope provides about 0.035g acceleration of the superstructure. The friction coefficient, however, generates about the same amount of accelerations when the dampers are installed with first adjustment on smaller friction forces and comparatively larger acceleration when the dampers are adjusted to have larger friction forces, which are clearly shown in table 2-1.

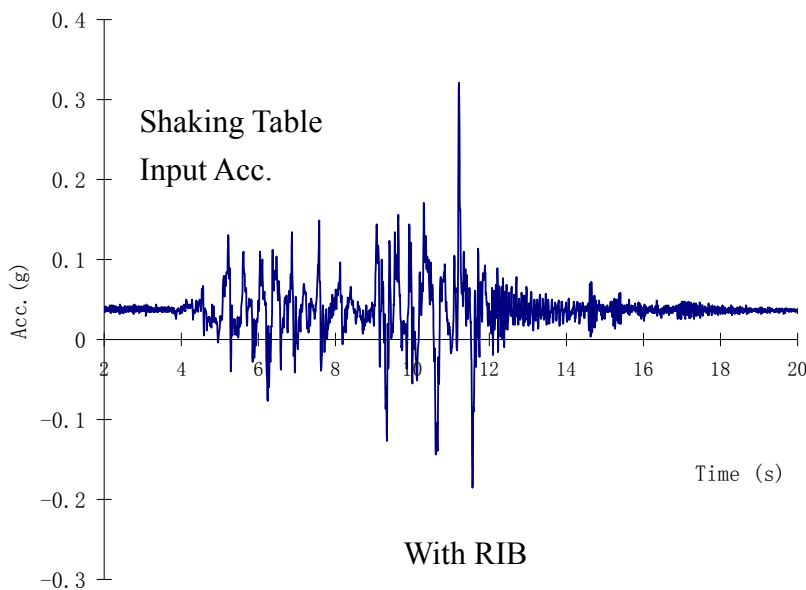


Figure 1-5 Record B5, Shaking table acceleration X direction

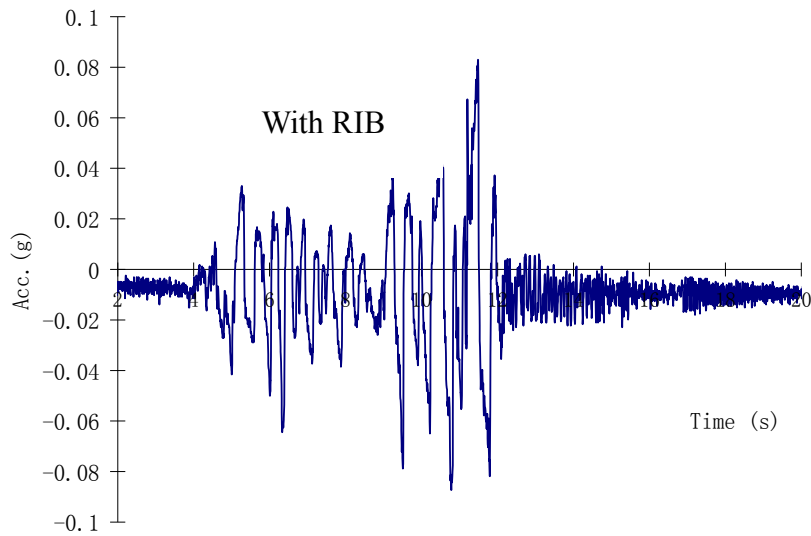


Figure 1-6 Record B5, superstructure acceleration X direction

Table 2-1 Accelerations of superstructure

Record	Level (g)	Direction	Acc. (g)	R (%)
ELC	0.184	X	0.062	66
E2	0.283	X	0.085	70
Q1	0.111	X	0.065	42
E3	0.245	X	0.051	79
E5	0.148	Y	0.085	42
E7	0.274	Y-X	0.075	73
E7	0.395	X-Y	0.060	85
B1	0.281	X	0.058	79
B5	0.084	X	0.084	68
B3	0.206	Y	0.126	39
L4	0.180	X	0.107	41

ROLLING FRICTION UNDER RUSTY CONDITION

In order to examine the performance of steel roller bearings under severe rusty conditions, an experimental program is conducted.

1. RESEARCH OBJECTIVES

The ability for a bearing to return to the centered position and the amount of the restoring force depend strongly on the coefficient of rolling friction between the rollers and the surface of the track. Since the coefficient of roller friction varies dramatically for different surfaces conditions, the performance of the bearing system in actual environmental condition of real bridges has not been thoroughly understood. There are questions on the ability for the system to continue perform after the steel became rusted. A mathematical modal has been formulated to correctly predict the performance of the isolation system. However the coefficient of roller friction between the rollers and the surface of the track still played an important roll in determine the mathematical result.

With numerous uncertainties in assuming the coefficient of roller friction under different surface conditions, A test program was designed and carried out to determine the coefficient of roller friction between the rollers and the surface of the track, specially tailored for the roller experiment. The objective of this experiment study is to identify the critical surface conditions, which might be experience in the lifetime of the roller isolation system, and to determine the coefficient of roller friction between the rollers and the track. The experimental result will then be tabulated and used in the mathematical model to predict and verify the theoretical performance of the roller isolation system in real-world bridges.

2. EXPERIMENTAL PROGRAM

Design Drawings for the Prototype

In order to achieve this experiment result, a roller and track prototype has been fabricated and the coefficients of roller friction tests were carried out. (see Figure 2-1) The actual experimental sets up were shown in figures 2-2 and 2-3.

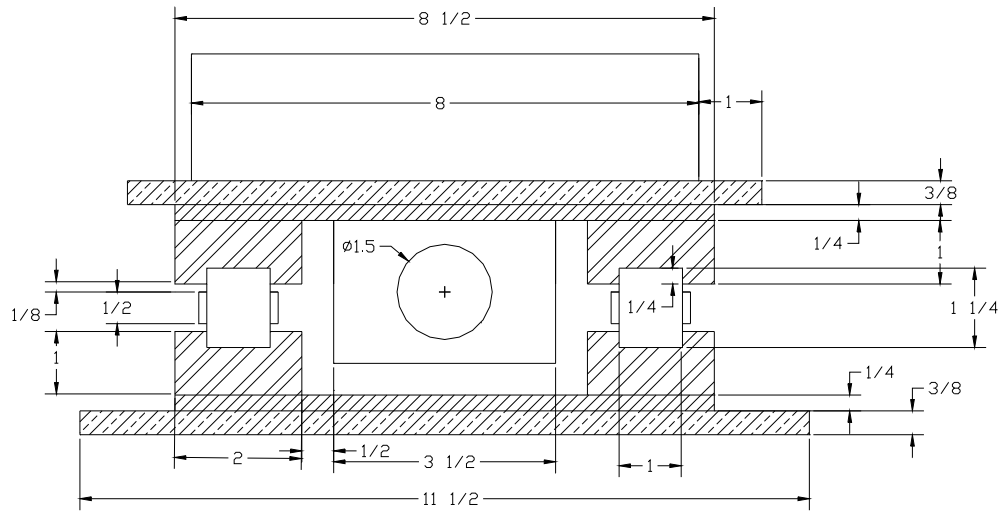


Figure 2-1 Front view of the prototype (Dimension in inches)



Figure 2-2 The first experiment set up for the roller friction test

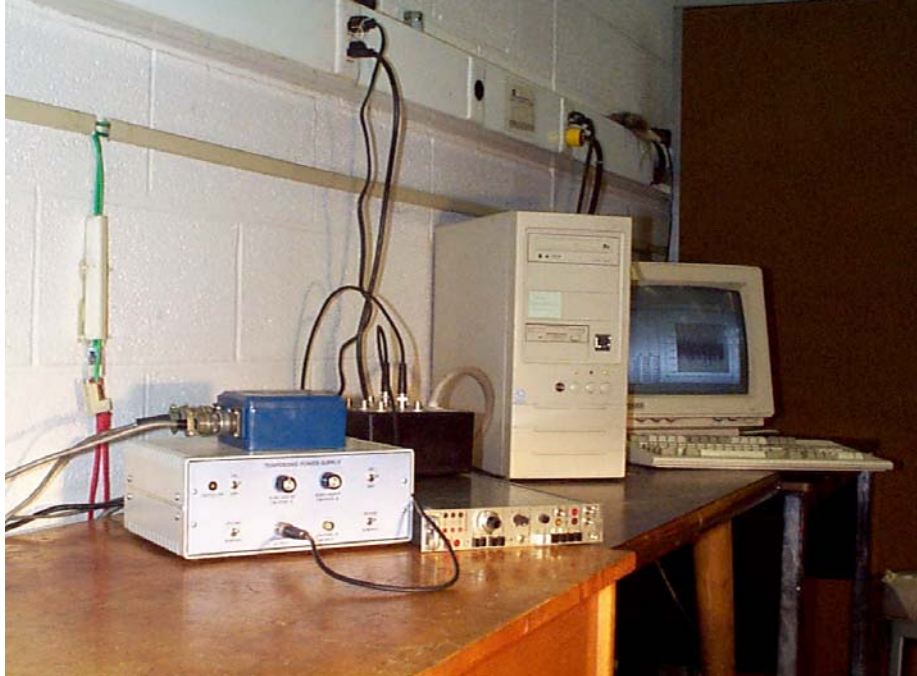


Figure 2-3 Experiment instrument (The Visual Bench software has been used in record the restoring force and the displacement.

Test Conditions

Three different surfaces condition have been identified and tested in this experimental program.

- (1) Clean track –To experimentally calculate the roller friction coefficient for the steel roller under idea working conditions. The coefficient of roller friction will be used in mathematical modal of the system to mimic the real world performance.
- (2) Oily track – In order to minimize the chance that the isolation system been oxidized excessive lubrication oil will be used to protect the steel. However sliding of the isolation track might happen when the sliding friction force is less than the roller friction force. This experiment was focused on calculating the roller friction coefficient for the steel roller under excessive lubrication and verified that sliding would not happen under excessive lubrication.
- (3) Rusting test – One of the key targets for conducting this experiment was to test the ability for the isolation system to perform under extreme weathered condition and ultimately will the system still perform satisfactory if the roller system were severely rusted. This experiment will be dedicated to calculate the roller friction coefficient for the steel rollers when both the steel track and rollers have been severely rusted. Three potential rusting conditions have been verified

- (1) Uniform rusting:
since the isolation system was designed to be exposed to the atmosphere, rust might form on the surface the rollers and the tracks. (Shown in Figure 2-4)

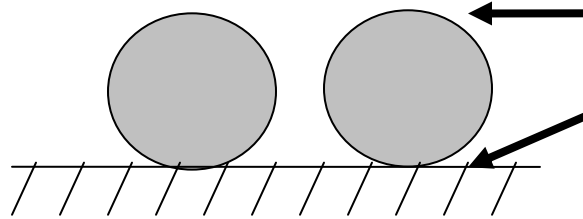


Figure 2-4 Uniform Rusting

- (2) Severe rust at the lower part of the roller only:
Severe rusting might happen only at the lower slot that stops the roller from rolling. Hence the top plate might simply slide. The lateral resistant force will changes from roller friction to kinetic friction; an experiment will be used to determine the kinetic friction. (Shown in Figure 2-5)

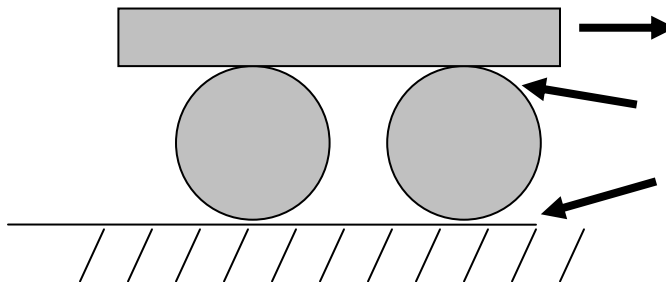


Figure 2-5. Sliding occurs when kinetic friction < Roller friction

- (3) Corrosion:
When severe rust occurred to the roller, part of the roller might fall apart and stop the base isolation form performing. (Shown in Figure 2-6)

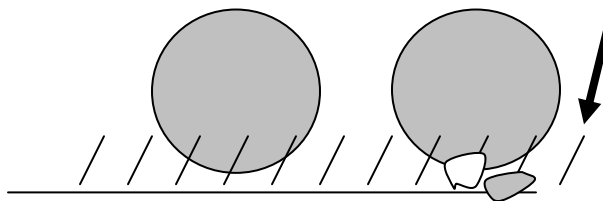


Figure 2-6 Corrosion

3. THEORETICAL BASE

Previous experiments have been conducted to calculate the coefficient of roller friction between different types of material surfaces. (Ref. "Mark's Standard handbook for Mechanical Engineers, the 10th Edition by Eugene A. Avallone Theodore Barumeister"). However, no actual experimental results are available to verify the coefficient of roller friction between steel at a slope with different surface conditions for the roller isolation system. Coefficient of roller friction for the system has been experimentally calculated and tabulated.

Rolling friction Theory:

The friction force transmitted through the roller system is governed by Equation 3-1 (see Figure 3-1)

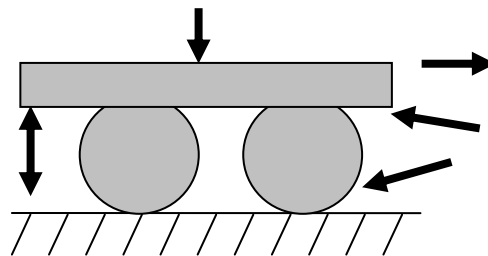


Figure 3-1 Theoretical model

$$P = (\mu + \mu') L/d \quad (3-1)$$

where

L : vertical Loads

P : roller friction force

d : diameter of the roller

μ' : coefficient of roller friction on the upper track

μ : coefficient of roller friction on the lower track

Referring to "Mark's Standard handbook for Mechanical Engineers, the 10th Edition by Eugene A. Avallone Theodore Barumeister"

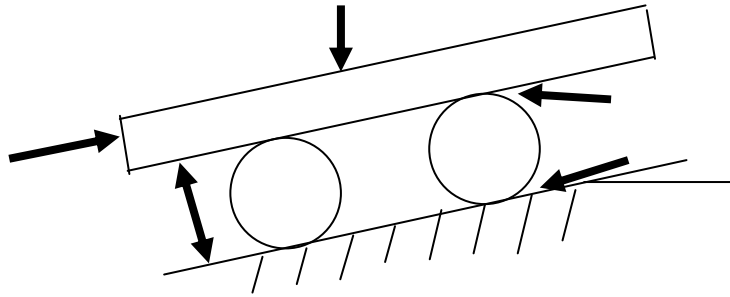


Figure 3-2 Coefficient of Roller friction test at an angle

The coefficient of roller friction shown in Figure 3-2 will hence be calculated by equation 3-2.

$$\mu = \mu' = \frac{\Delta P d}{4L \cos \theta} \quad (3-2)$$

in which

$\mu = \mu'$: the coefficient of roller friction between the track and the roller. Assuming the surface condition between the upper and lower track are identical.

ΔP : two times the Roller friction force. (lb) (difference of the forwarding force and the down warding force measured.)

d : diameter of the roller (in)

L : vertical load (lb)

θ : angle of inclining. (Degree)

4. EXPERIMENT SETUP

Four different surface conditions have been tested for the roller friction test.

- (1) Clean track test (TN)
- (2) Oily track test (TNO)
- (3) Fine sandy track test (TNS)
- (4) Ultimate rust for both the roller and the track test (TNRUST)

Test procedure:

A vertical load of 470 lb was placed on the prototype while the track was inclining at an angle of 6° with respect to horizon. A hydraulic jack was used to push the prototype up the slope then allow the prototype to freely return to the original position down the slope with only the gravity load. A load cell at the end of the track measured the forwarding and returning resistance force at all time.

Experiment Condition:

- (1) Clean track test (TN):
Load = 470lb, $\theta = 6^\circ$, $d=1''$. Both the upper, lower track and the roller are prepared at a clean normal condition. (Shown in Figure 4-1)



Figure 4-1 Experiment set up for clean track test (TN)

- (2) Oily track test (TNO):
Load = 365lb, $\theta = 6^\circ$, $d=1''$. Lubricant oil was applied between the rollers and the tracks. (Shown in Figure 4-2)

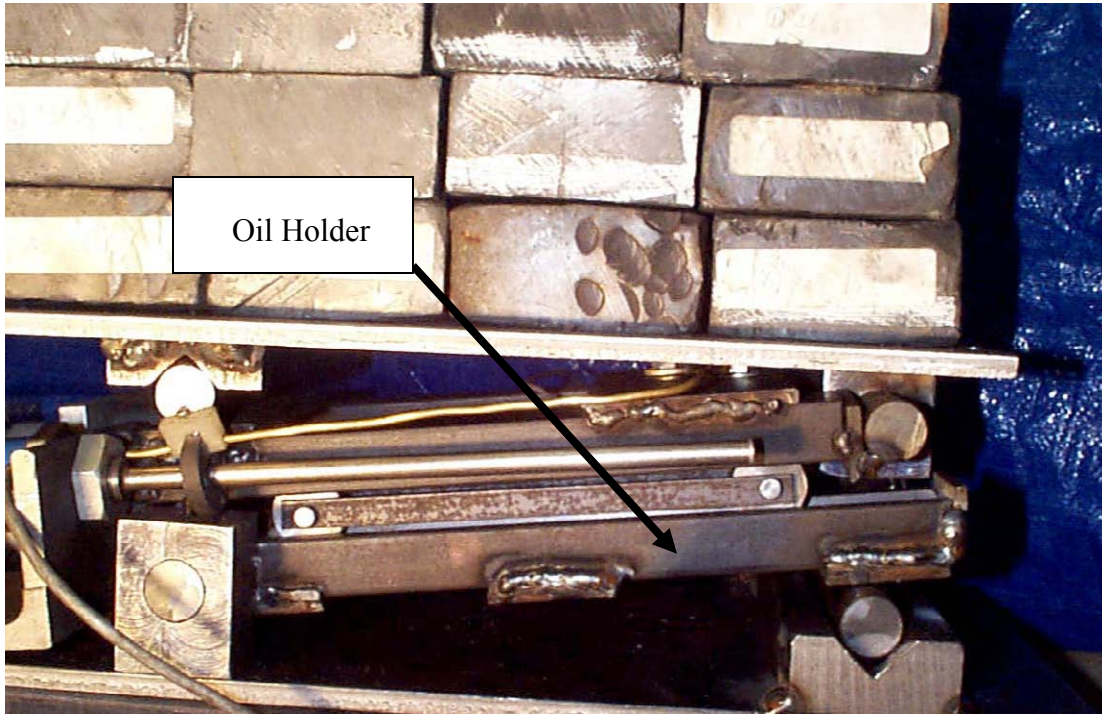


Figure 4-2 Experiment set up for oily track test (TNO)

- (3) Fine sandy track test (TNS):
Load = 365lb, $\theta = 6^\circ$, $d=1''$.
Sand papers were used to provide the rolling surface along the tracks.

(4) Ultimate rust for both the roller and the track test (TNRUST):

Load = 470 lb, $\theta = 6^\circ$, $d=1''$.

Both the tracks and the rollers have been electrically oxidized to stimulate the rusty conditions for the steel as if it has been exposed to the atmosphere after years. In order to test the roller friction for the prototype under extreme rusting condition, DC current has been applied to the prototype to accelerate the rusting process. The actual set up has been shown in Figure 4-3

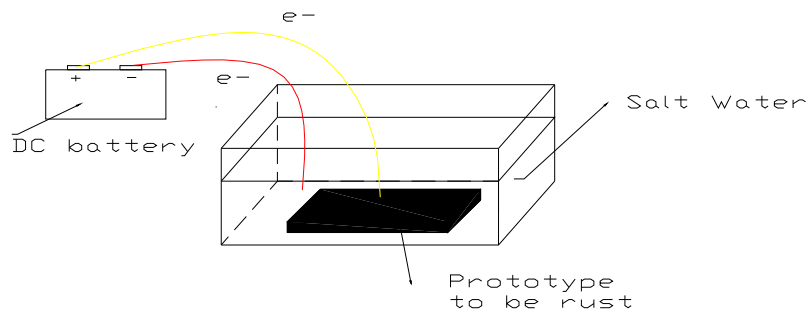


Figure 4-3 laboratory set up for the rusting test.

Figure 4-4 through 4-7 show the pictures taken during the rusting process.



Figure 4-4 Rusting Process



Figure 4-5 Over view of the rust process.



Figure 4-6 Close view of the rust track and rollers



Figure 4-7 View of rusty parts

5. EXPERIMENT RESULT:

Ten experiments have been conducted to calculate the coefficient of the roller friction on the bearing prototype. In each experiment the resistance force vs. the displacement was measured and plotted. The coefficient of roller friction was computed immediately and tabulated for each experiment test.

Clean Track Test (TN)

The results of the Clean Track tests are presented as TN1 to TN10. (In figure 5-1 and Table 5-1)

Experiment result:

The resisting force data measured was collected and plotted against the displacement, shown in Figure 5-1 and table 5-1.

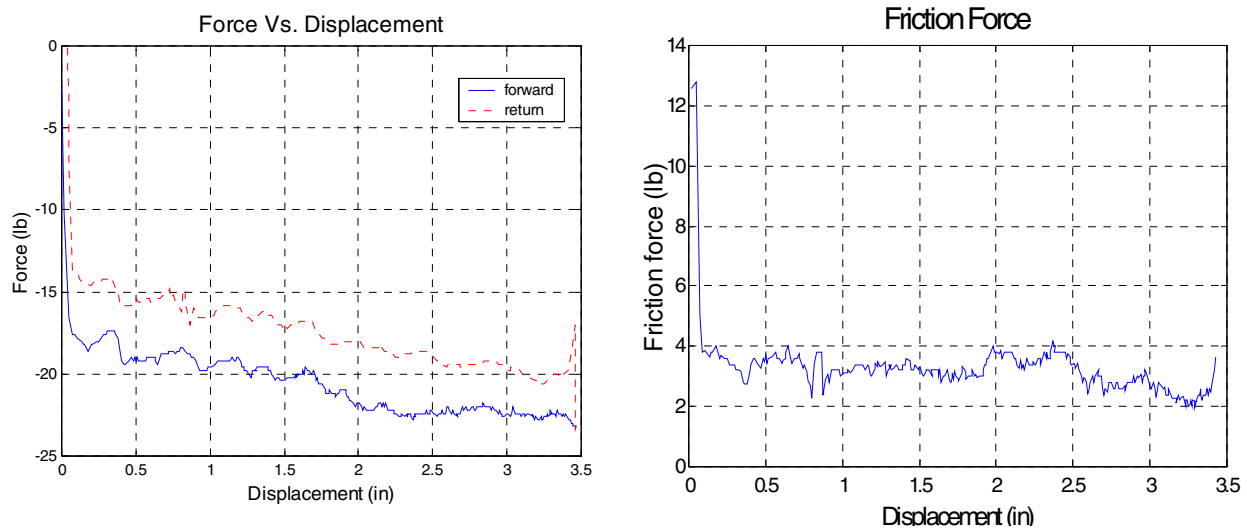


Figure 5-1 TN1 test results

Table 5-1 Friction force

Max (lb)	Min (lb)	Mean (lb)	Standard Deviation (lb)
12.8	1.95	3.2	0.89

Average Friction Force = 3.2 lb \ll $L \sin 6 = 49.2$ lb (will restoring to center of gravity.)

Roller friction coefficient

$$L \cos 6 (\mu + \mu') = \text{friction force} \Rightarrow k = 0.0034$$

Theoretical value for Roller friction coefficient

$$0.0005 < \mu < 0.001 \text{ (Clean steel on Clean steel)}$$

Referring to “Mark’s Standard handbook for Mechanical Engineers, the 10th Editions by Eugene A. Avallone Theodore Barumeister”

Rust Track Test

Here, only selected results are shown. The rest of the results can be seen in figure 5-2 and Table 5-2.

Experiment result:

The resisting force data measured was collected and plotted against the displacement.

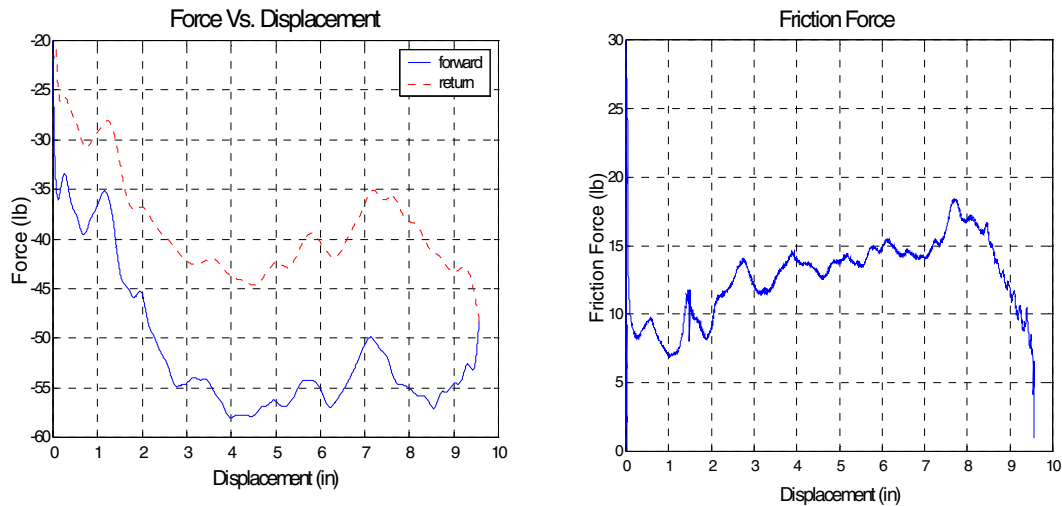


Figure 5-2 TNRUST1

Table 5-2 Friction force

Max (lb)	Min (lb)	Mean (lb)	Standard Deviation (lb)
27.29	0.96	12.23	18.62

Average Friction Force = 12.23 lb << $L \sin 6 = 49.2$ lb (will restoring to center of gravity.)

Roller friction coefficient

$$L \cos 6 (\mu + \mu') = \text{friction force} \Rightarrow k = 0.013$$

Theoretical value for Roller friction coefficient

$$0.005 < \mu < 0.01 \text{ (Rusty surface)}$$

Referring to “Mark’s Standard handbook for Mechanical Engineers, the 10th Editions by Eugene A. Avallone Theodore Barumeister”

6. DISCUSSION OF TEST RESULTS

Table 6-1 Summary of the coefficient of Roller Friction

	Normal Condition	Oily Track	Sandy Track	Rusty Condition
6°	0.0034	-	-	0.0074

Clean Track Test

The friction Force for all the 10 tests are plotted as shown in Figure 6-1

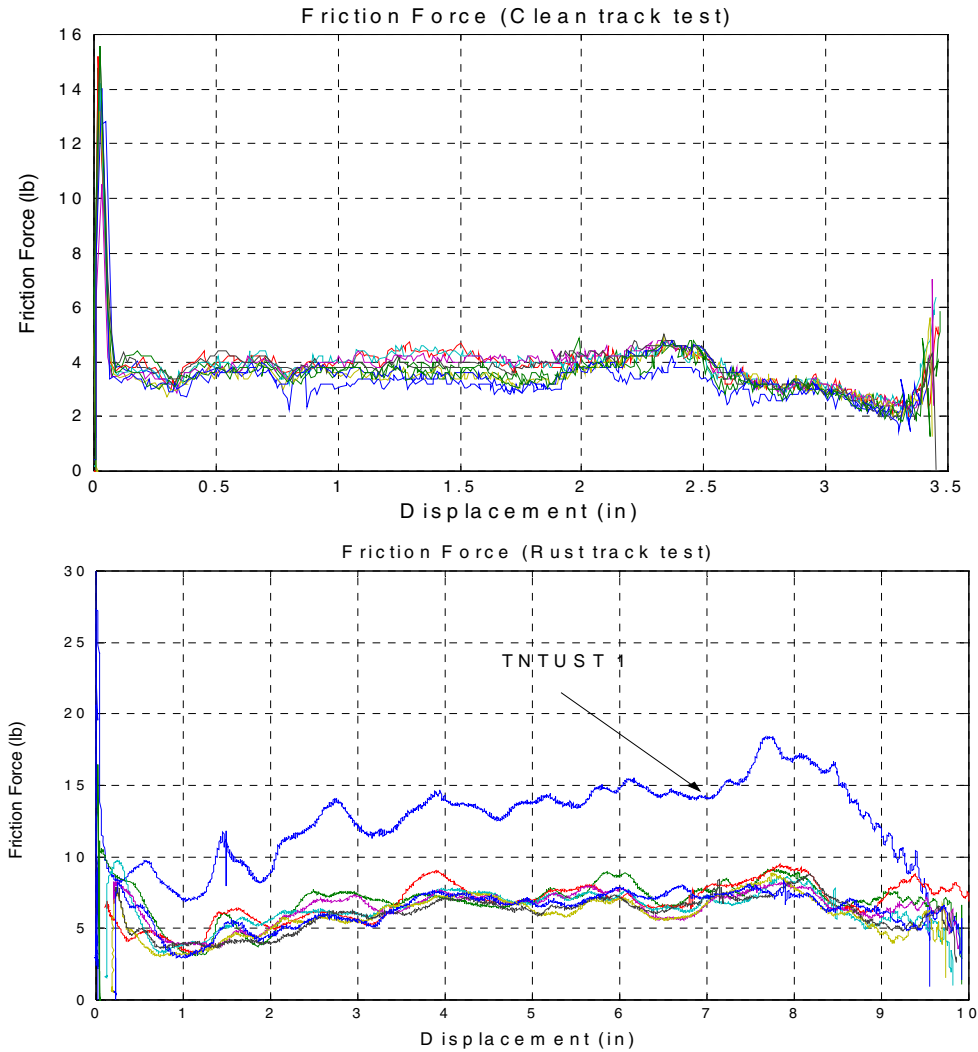


Figure 6-1 TNRUST results

The experiment results correlate closely to the theoretical predictions. From the experiment results the coefficient of roller friction was very small and it varies distinctly with respect to the unevenness of the surfaces but not the surface conditions of a given surface.

The Coefficient of roller friction reduces dramatically as more and more tests were repeated on the rust tests. As presented in TNRUST the coefficient of roller friction reduces as the number of test increases. This happens because the rust particle was initially the largest as more and more test been done; the roughness of the rust surface is reduced. The coefficients of roller friction increases again as the finer rust particles were accumulated. The friction force measure changes from pure roller surface friction to the equivalent force needed to overcome the humps.

Oily Track Test

The selected oily track test is presented as follows:

Experiment result: The resisting force data measured was collected and plotted against the displacement, shown in Figure 6-2.

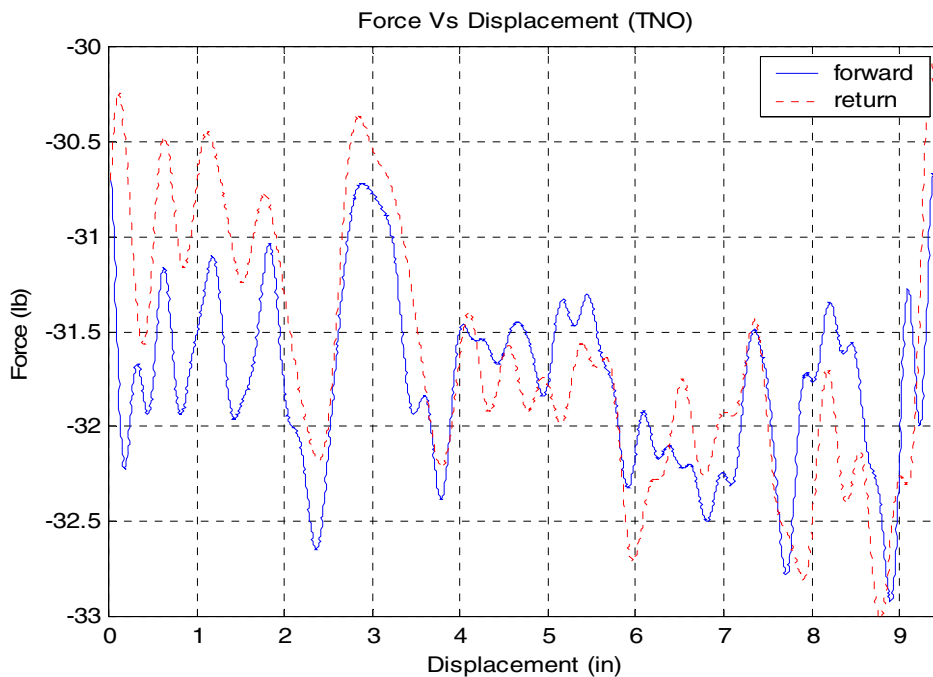


Figure 6-2 TNO results

Friction force = 0.64lb \ll $L \sin 6 = 38.2$ lb (will restoring to center of gravity.)
 Calculation of the friction force was base on the difference of the average forward and return resisting force.)

Roller friction coefficient

$$L \cos 6 (\mu + \mu') = \text{friction force} \Rightarrow k = 0.00088$$

Theoretical value for Roller friction coefficient

$$0.0005 < \mu < 0.001 \text{ (Clean steel on Clean steel)}$$

Referring to “Mark’s Standard handbook for Mechanical Engineers, the 10th Editions by Eugene A. Avallone Theodore Barumeister”

Sand Track Test

Experiment result: The resisting force data measured was collected and plotted against the displacement, shown in Figure 6-3.

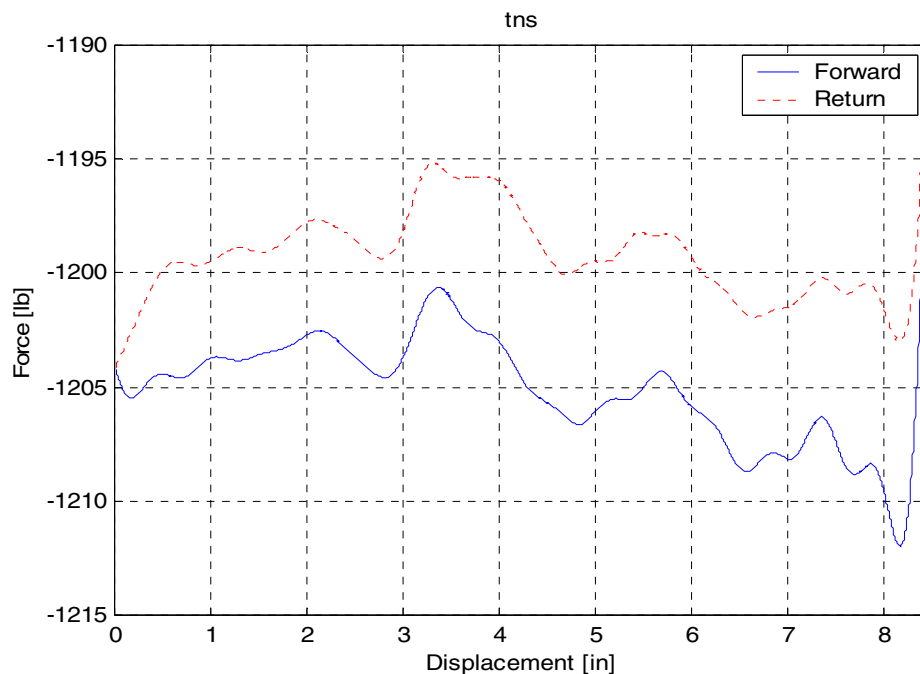


Figure 6-3 TNS results

Therefore, in order to guarantee the performance of the isolator system dirt and debris must be kept out of the rolling track.

Friction force = 8.85 lb \ll $L \sin 6 = 38.2$ lb (will restoring to center of gravity.)

Calculation of the friction force was base on the difference of the average forward and returning resisting force.

$$\text{Roller friction coefficient } (\mu k') = \text{friction force} \Rightarrow k = 0.012$$

Theoretical value for Roller friction coefficient

$$0.003 < \mu < 0.005 \text{ (Steel with surface of salt)}$$

Referring to “Mark’s Standard handbook for Mechanical Engineers, the 10th Editions by Eugene A. Avallone Theodore Barumeister”

Brief Summary

From all of these tests, it is found that under various track conditions, the rolling friction coefficient varies accordingly. However, even in the worst case of rusted conditions, the coefficient is still below 0.01. So, under extreme conditions, the roller bearing system can still function well. On the other hand, the sand track test exhibits the friction coefficient larger than 0.01 (which is 0.012).

APPENDIX B GROUND MOTIONS

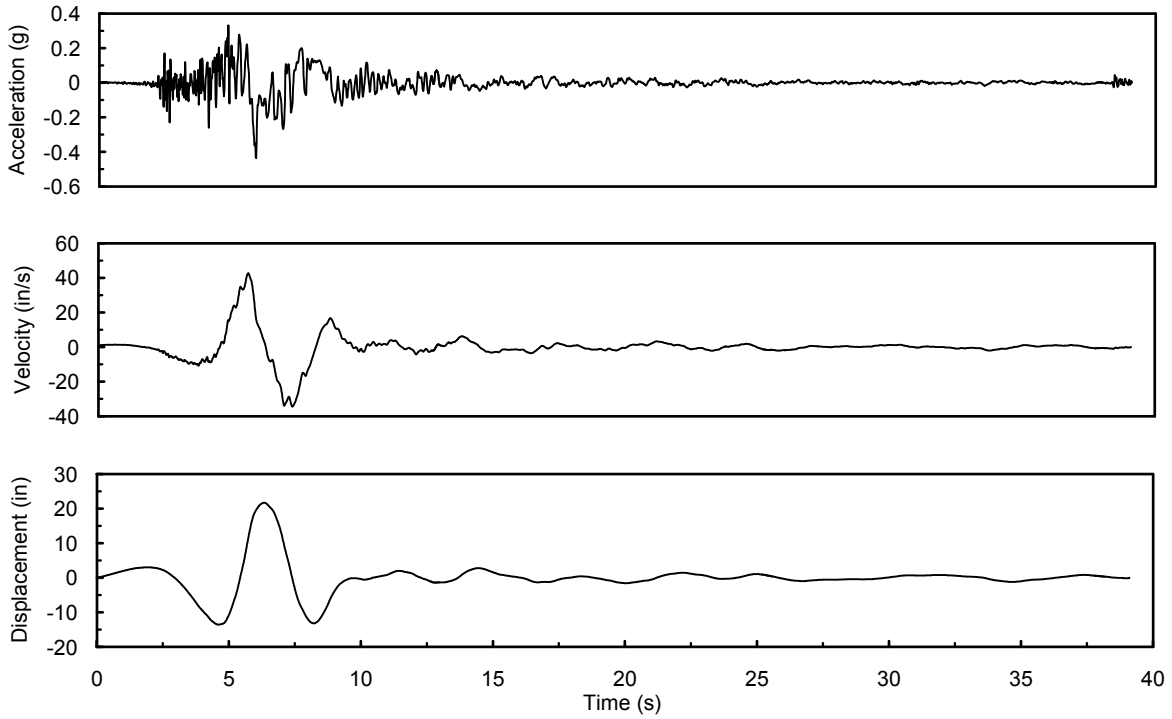


Figure B-1 El Centro Array #6, horizontal: 230 degrees

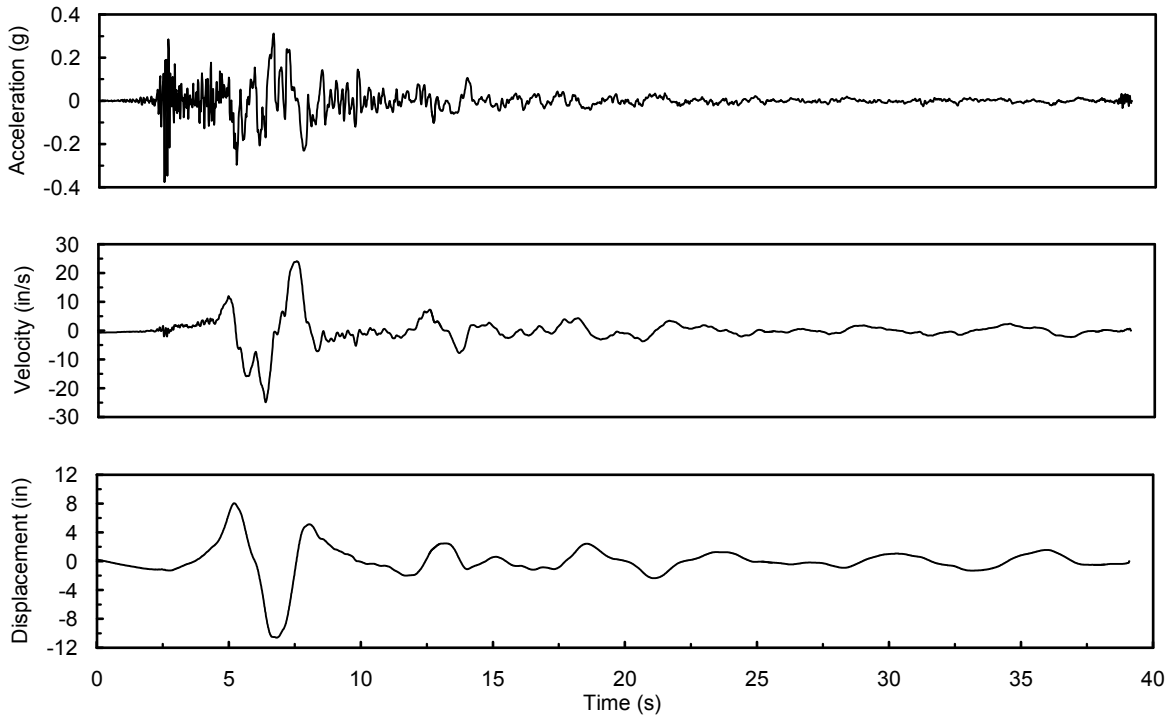


Figure B-2 El Centro Array #6, horizontal: 140 degrees

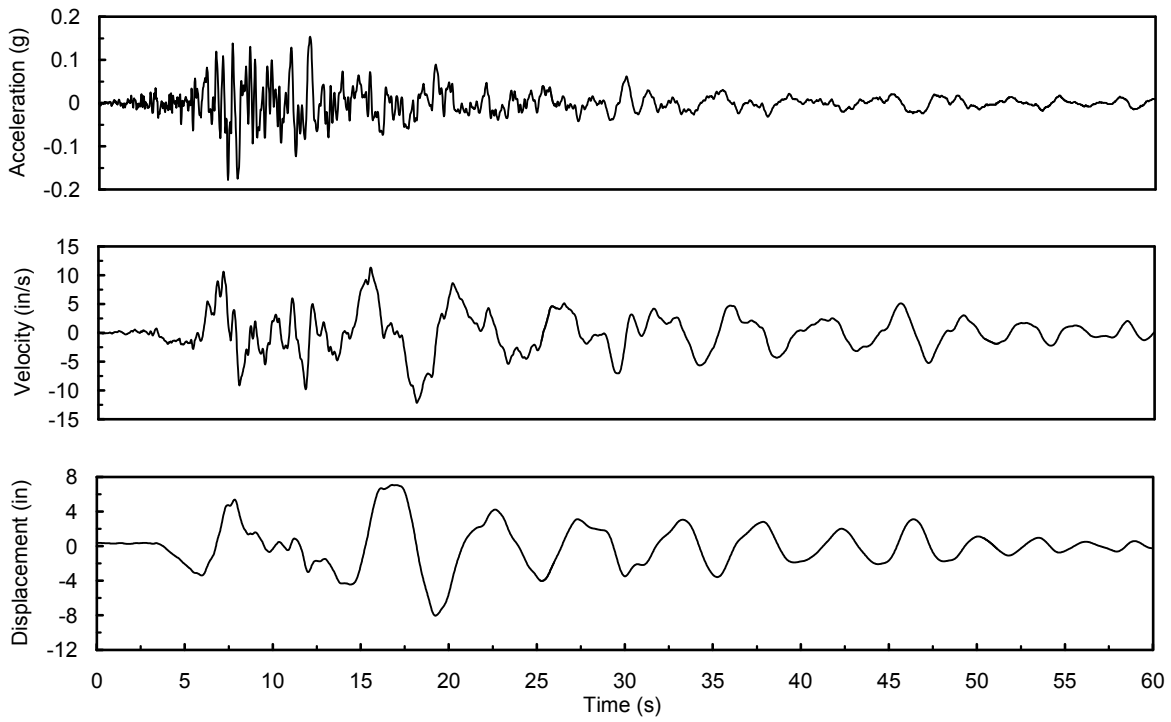


Figure B-3 Hollister, horizontal: 90 degrees

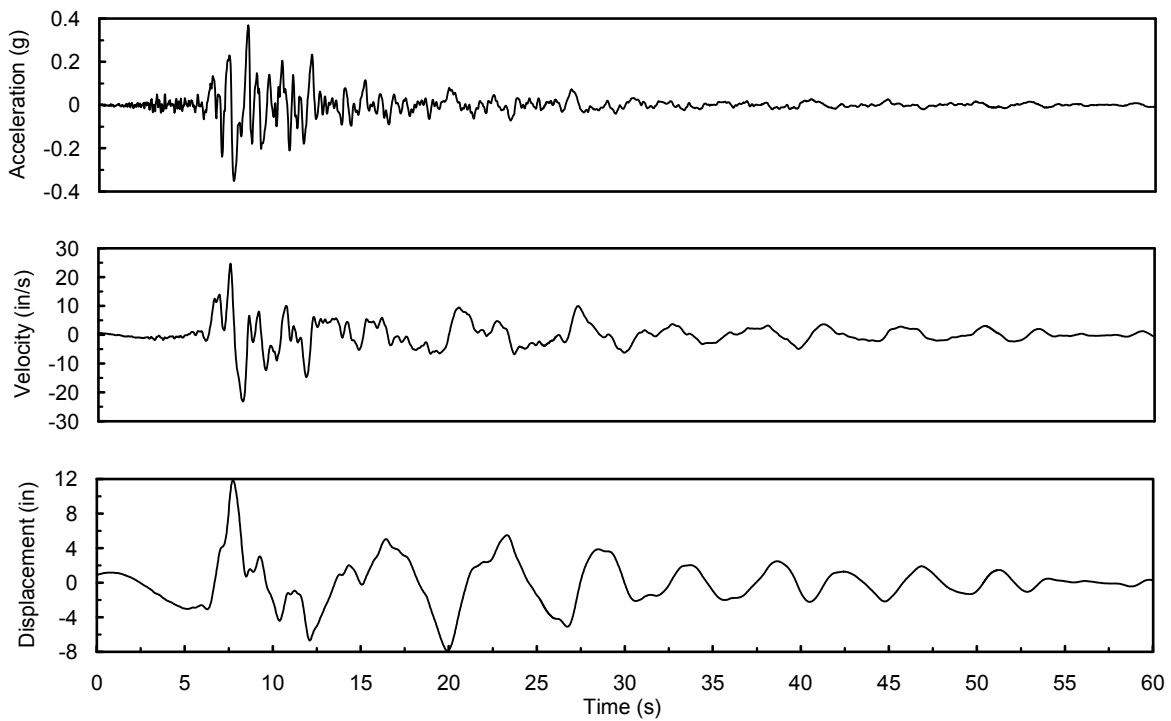


Figure B-4 Hollister, horizontal: 0 degrees

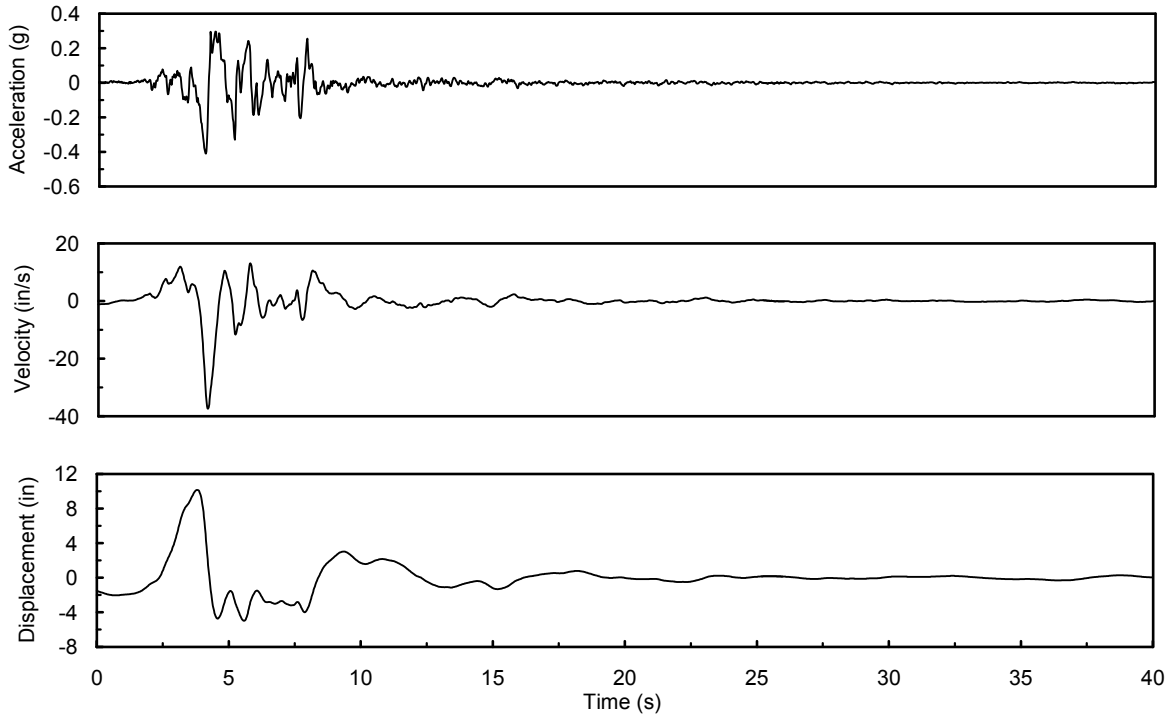


Figure B-5 Lexington Dam, horizontal: 90 degrees

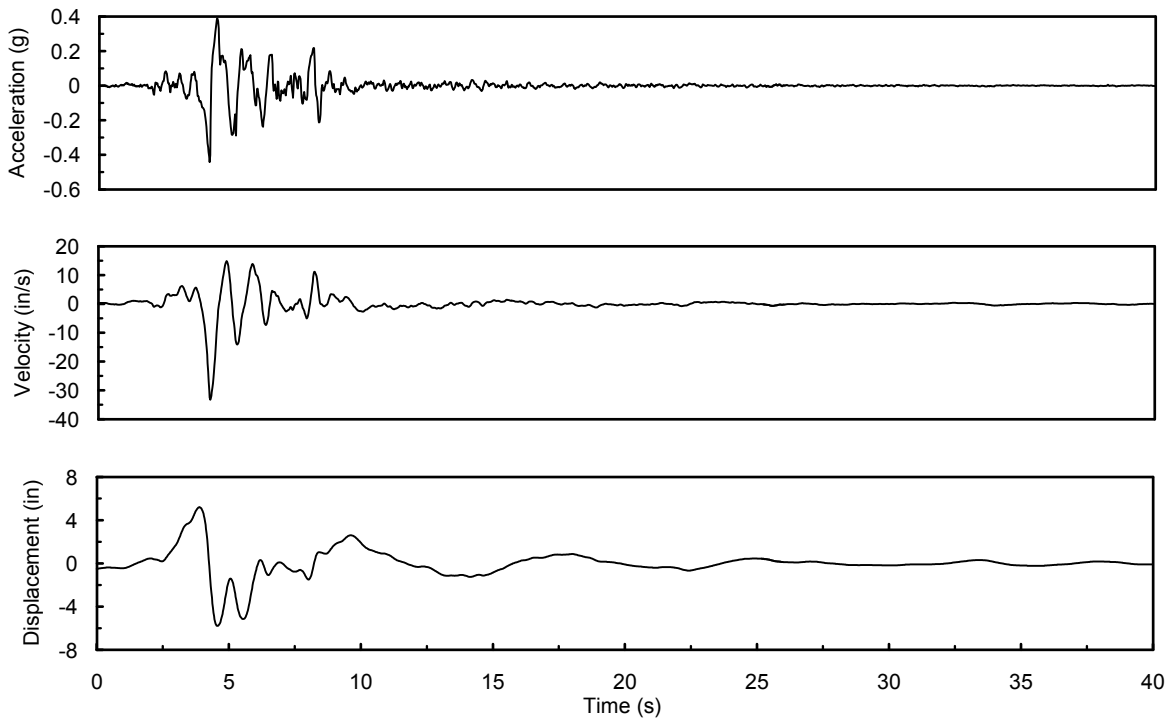


Figure B-6 Lexington Dam, horizontal: 0 degrees

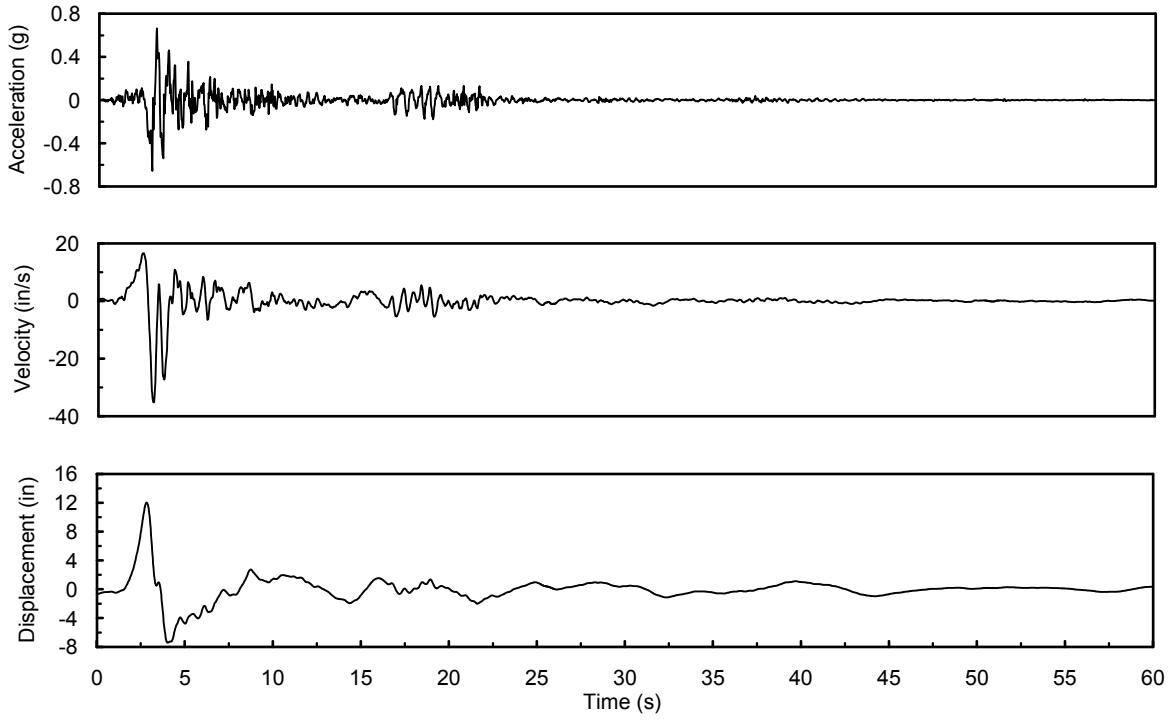


Figure B-7 Petrolia, horizontal: 90 degrees

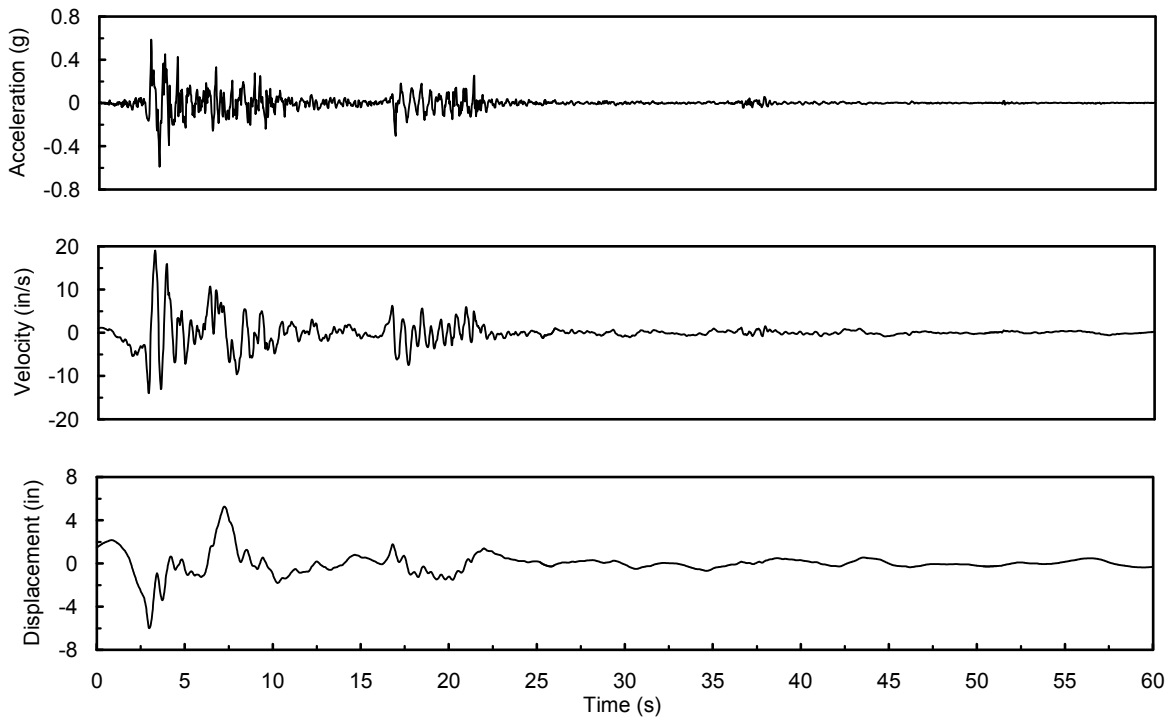


Figure B-8 Petrolia, horizontal: 0 degrees

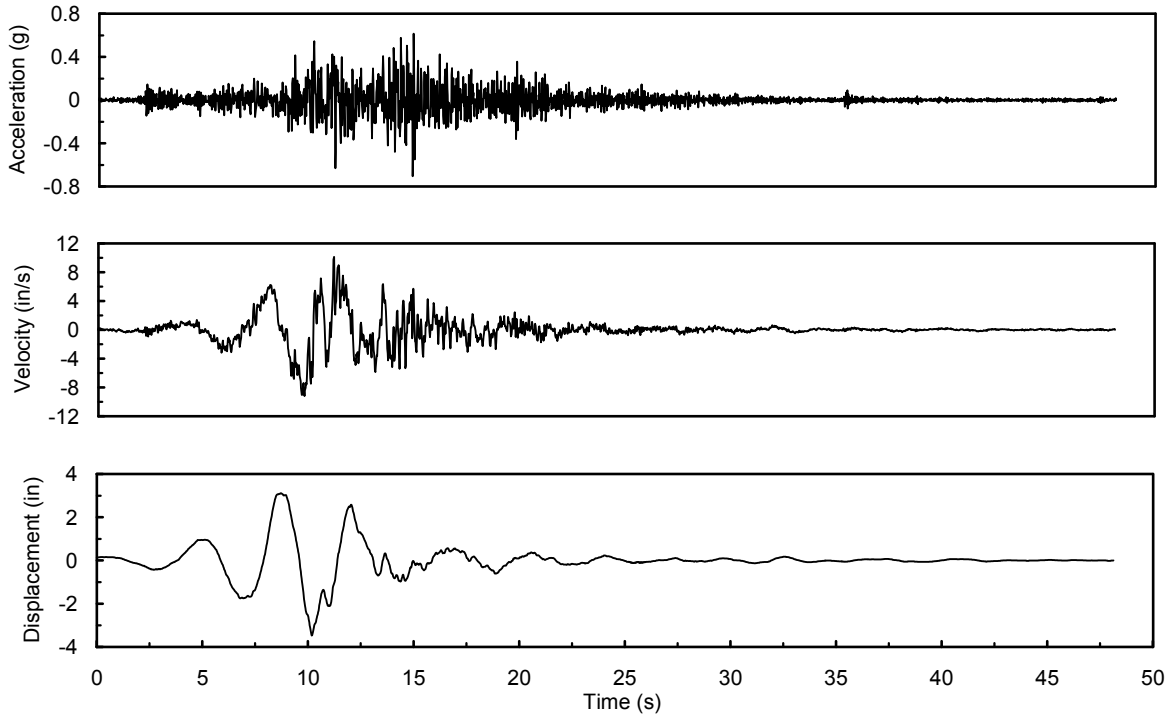


Figure B-9 Lucerne Valley, horizontal: L

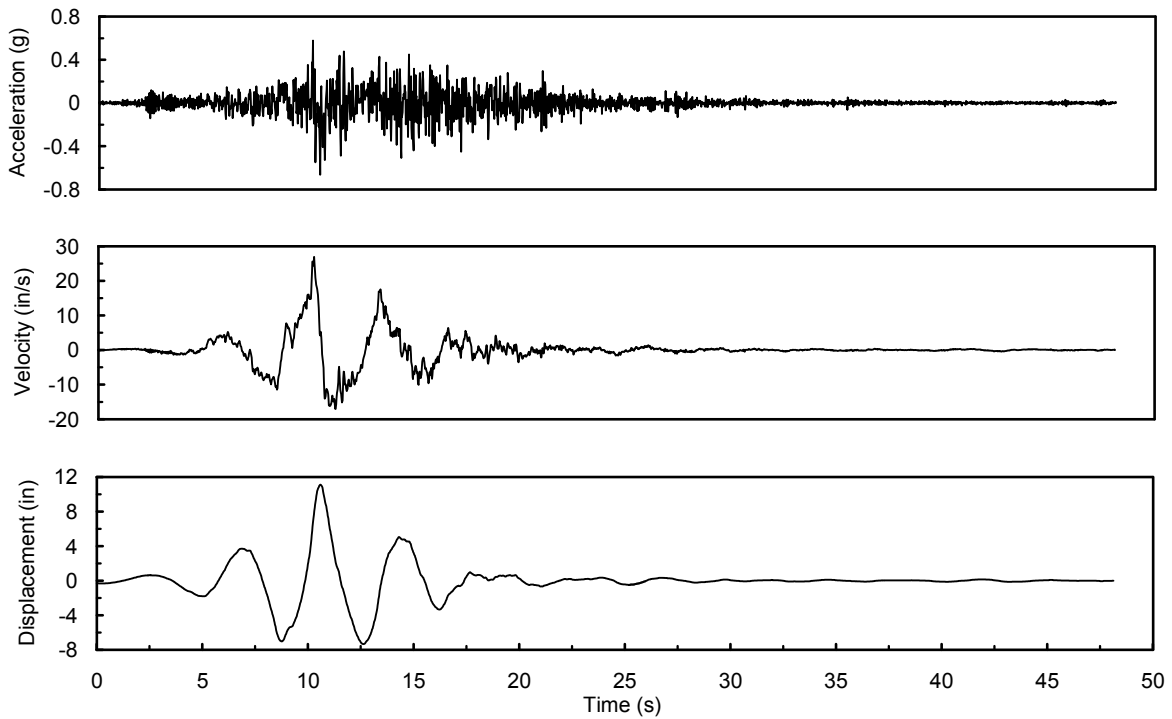


Figure B-10 Lucerne Valley, horizontal: T

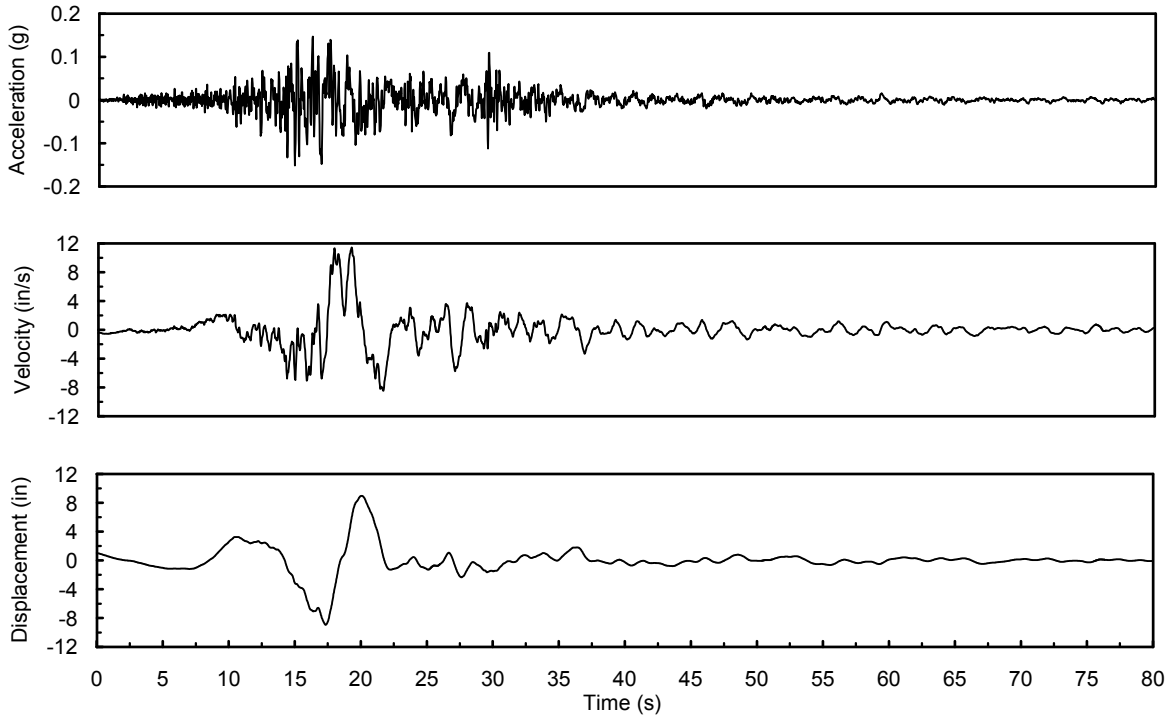


Figure B-11 Yermo, horizontal: 360 degrees

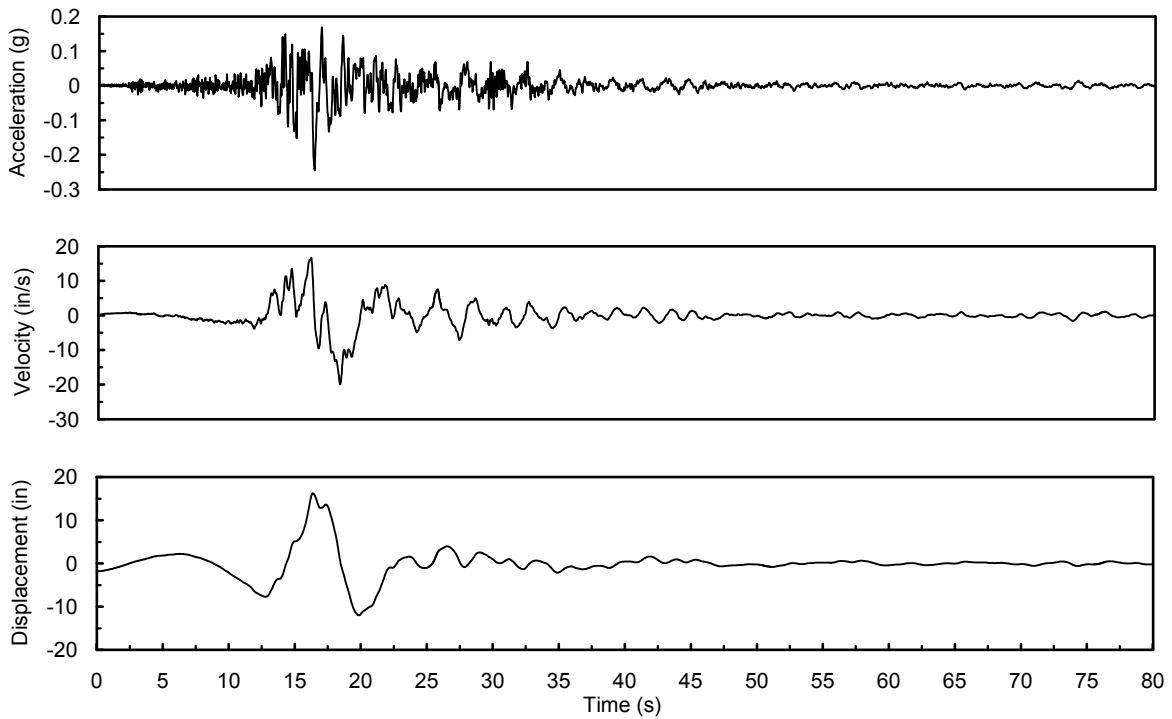


Figure B-12 Yermo, horizontal: 270 degrees

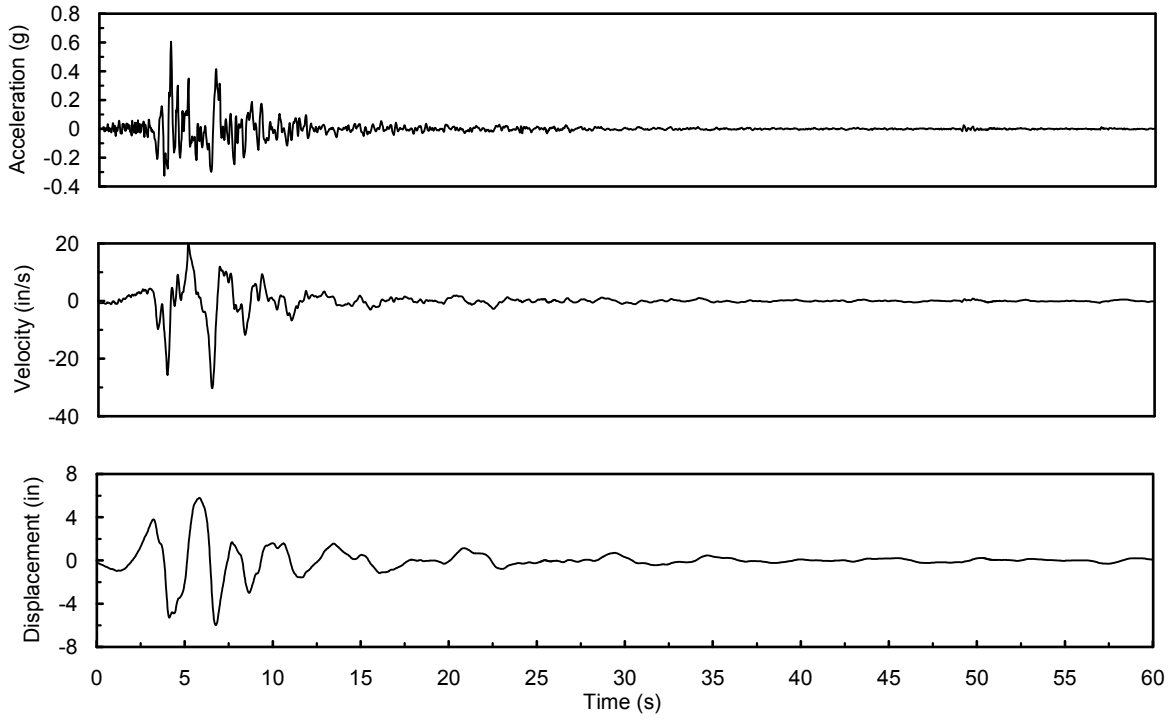


Figure B-13 Sylmar, horizontal: 90 degrees

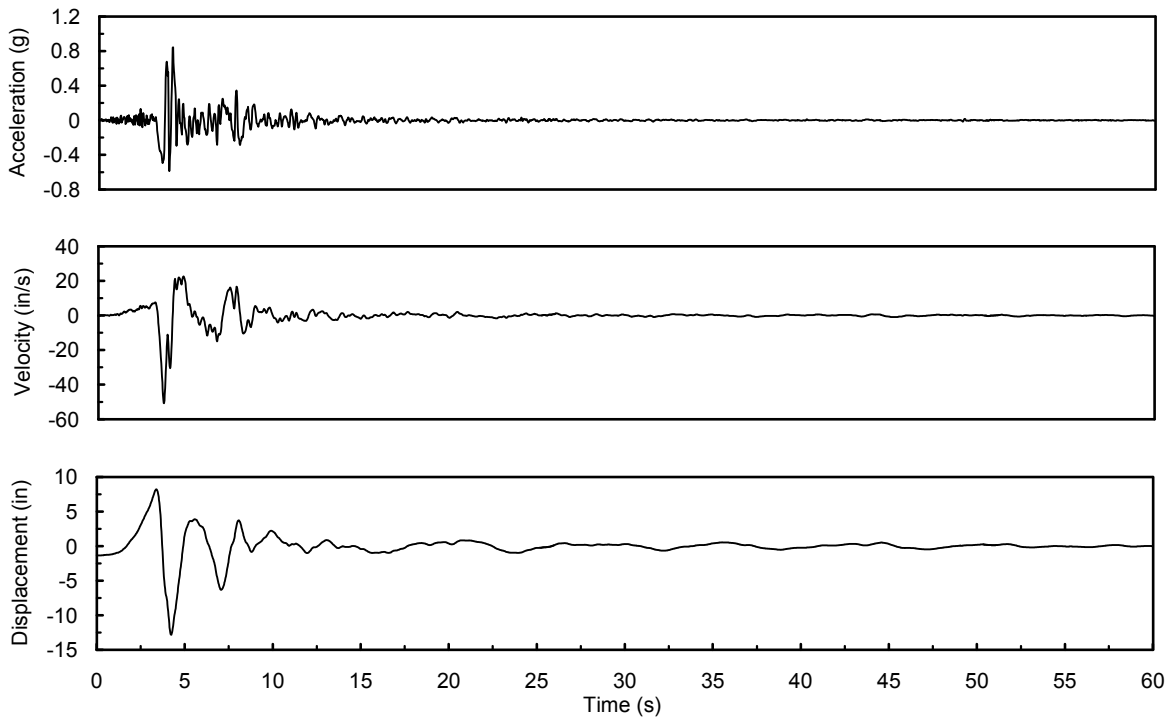


Figure B-14 Sylmar, horizontal: 360 degrees

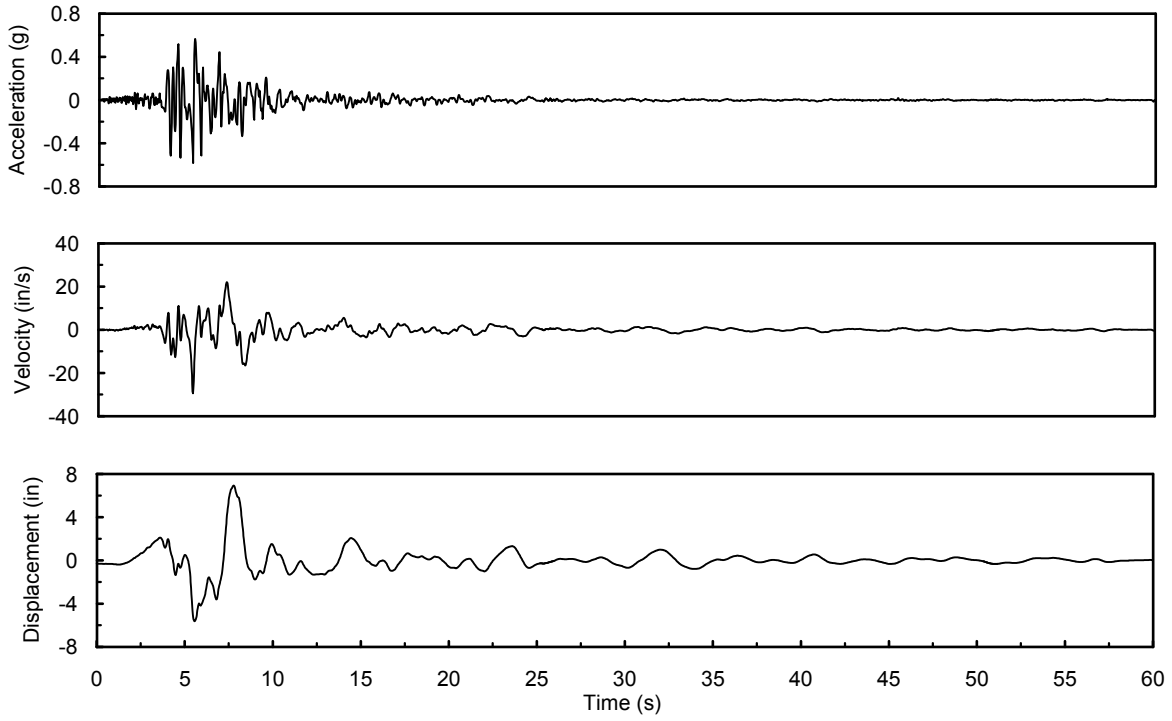


Figure B-15 Newhall Fire, horizontal: 90 degrees

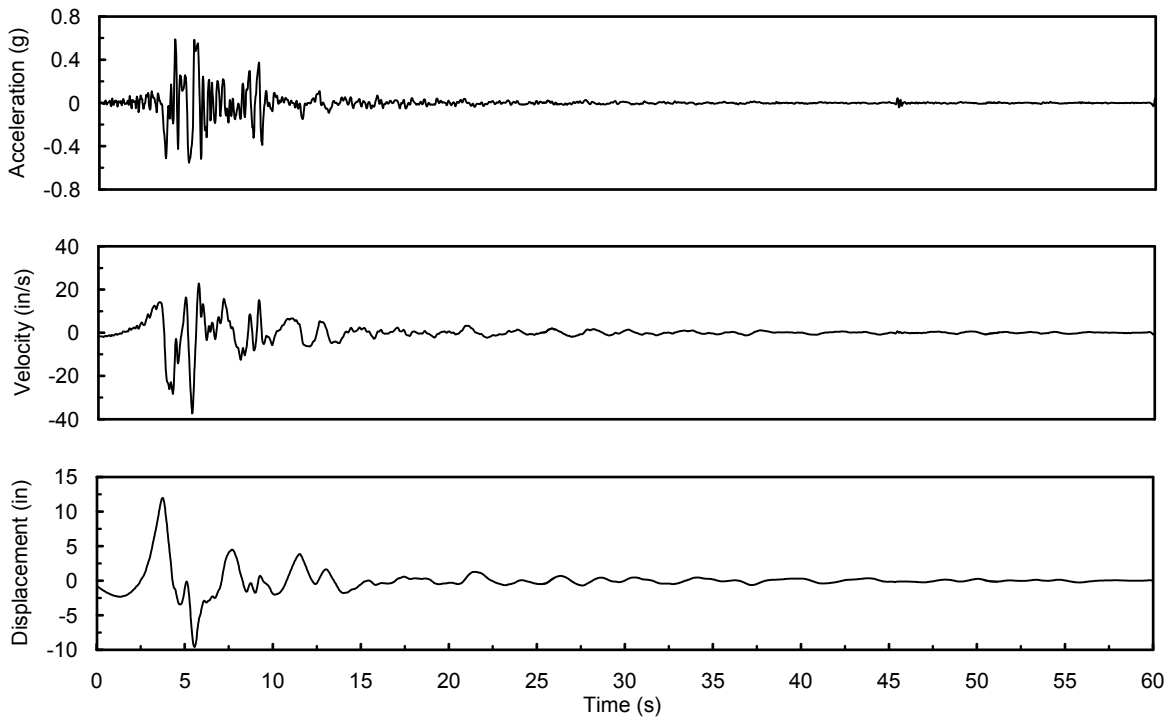


Figure B-16 Newhall Fire, horizontal: 360 degrees

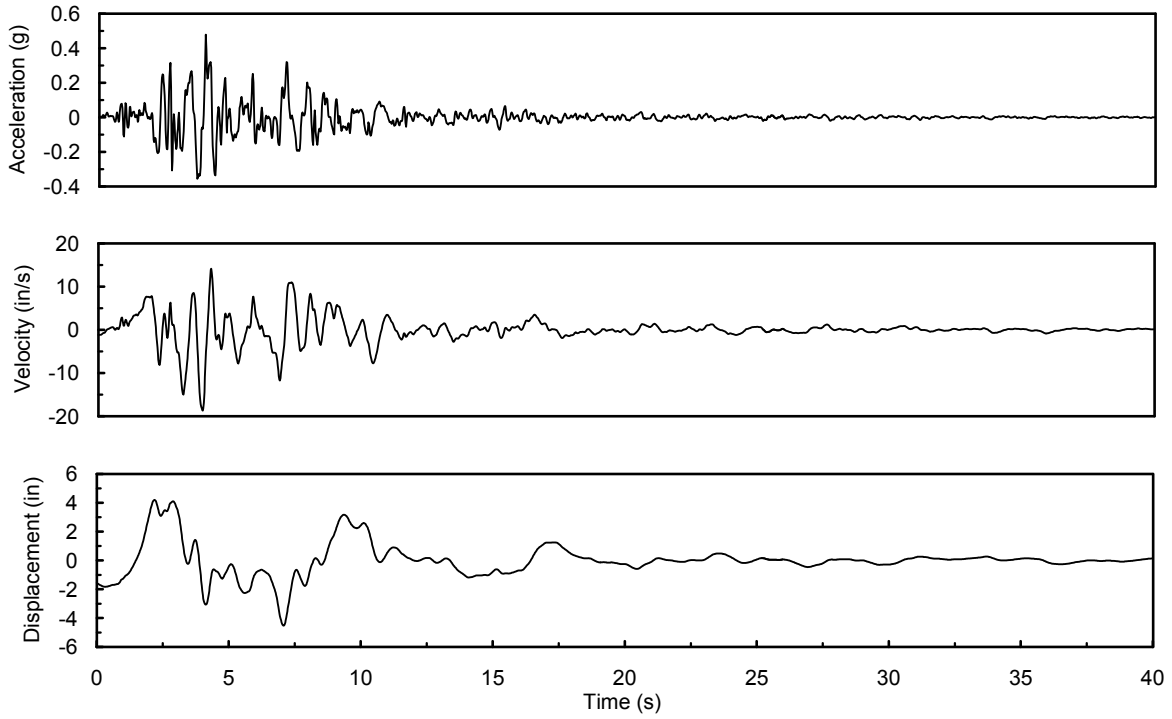


Figure B-17 Corralitos, horizontal: 90 degrees

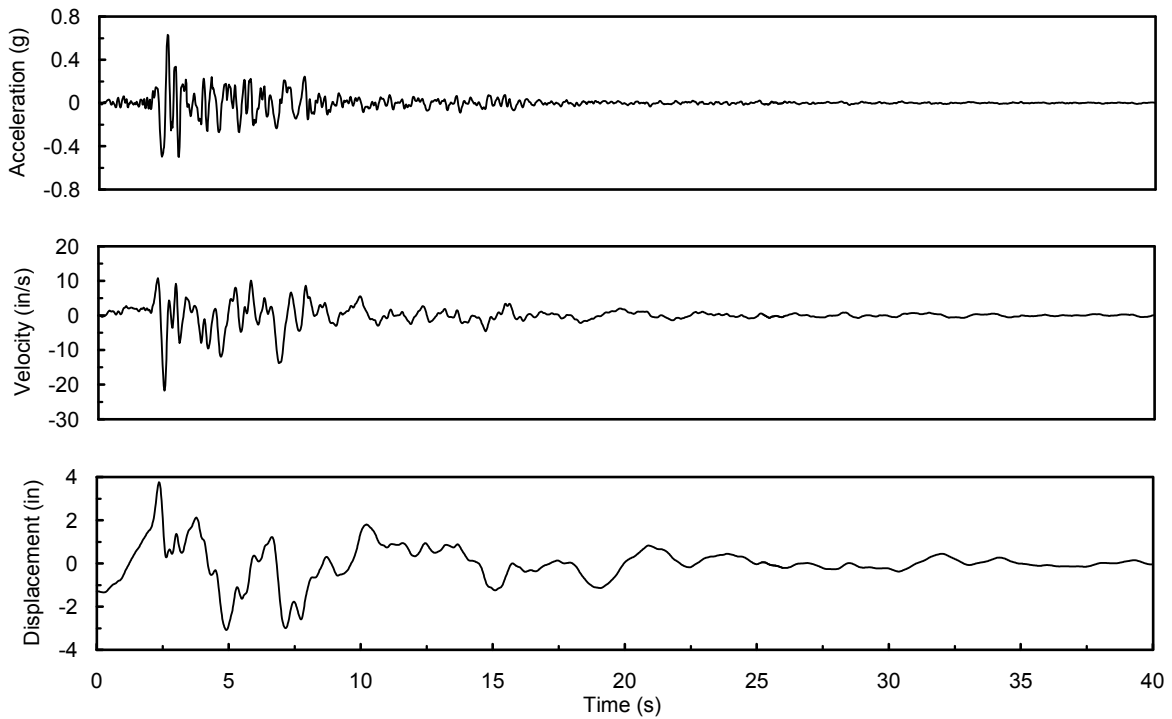


Figure B-18 Corralitos, horizontal: 0 degrees

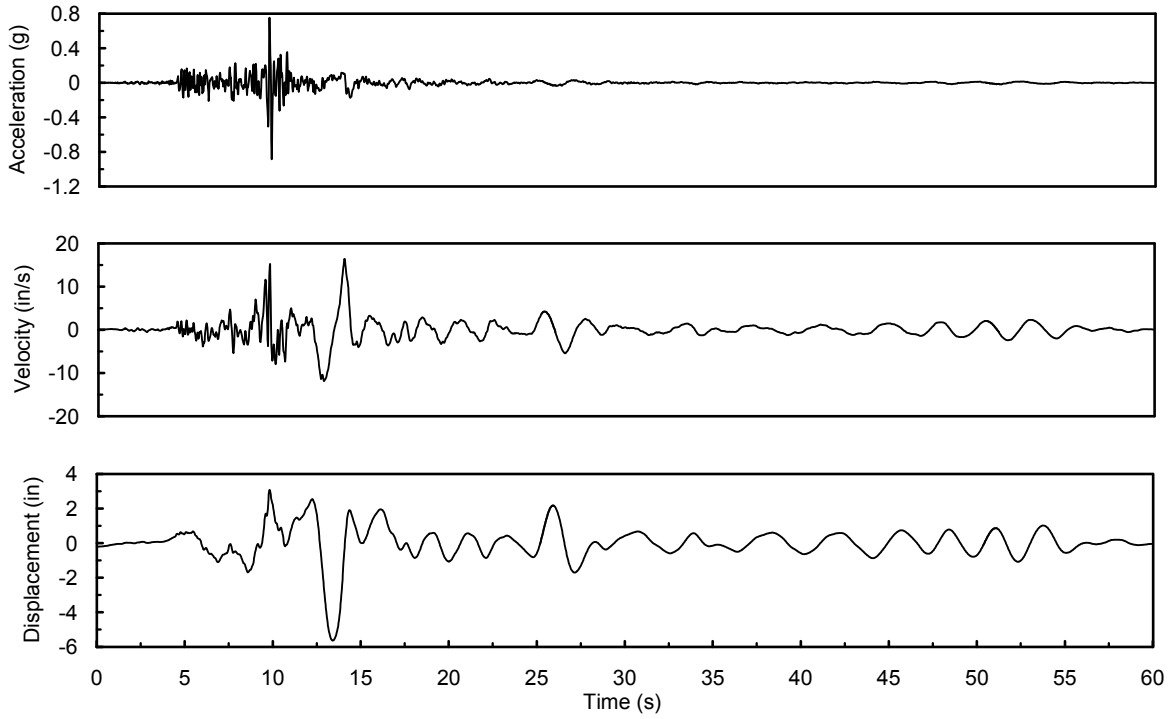


Figure B-19 Santa Monica City Hall Grounds, horizontal: 90 degrees

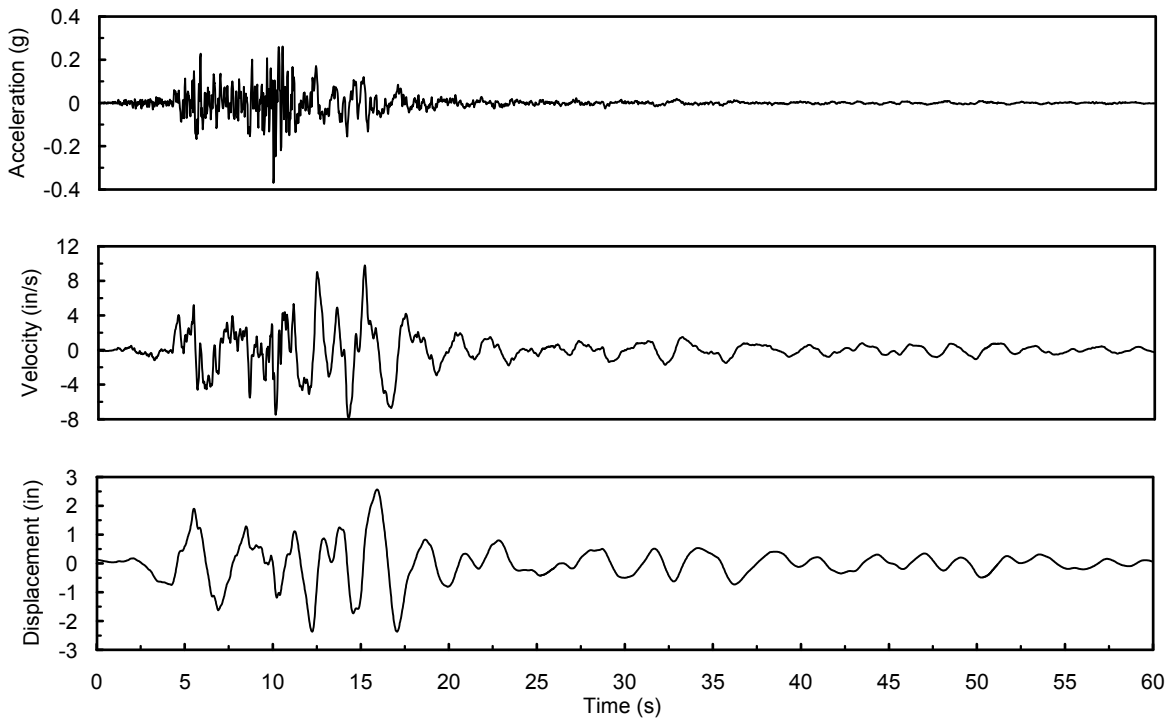


Figure B-20 Santa Monica City Hall Grounds, horizontal: 360 degrees

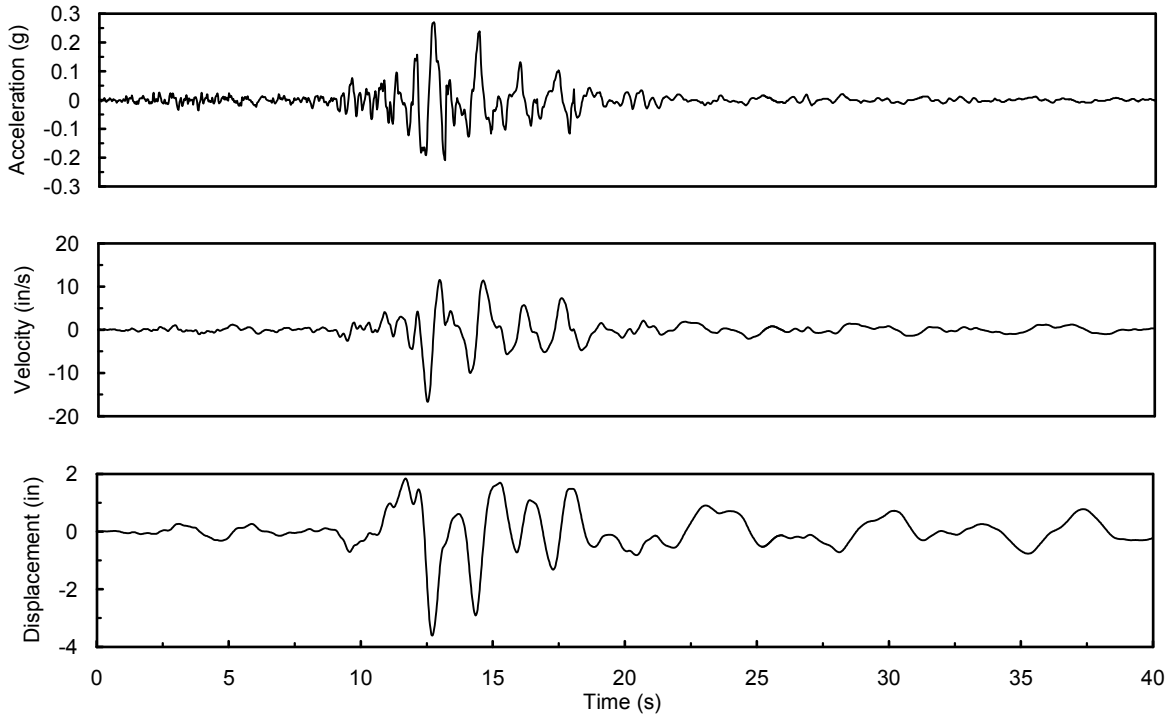


Figure B-21 Oakland Outer Harbor Wharf, horizontal: 305 degrees

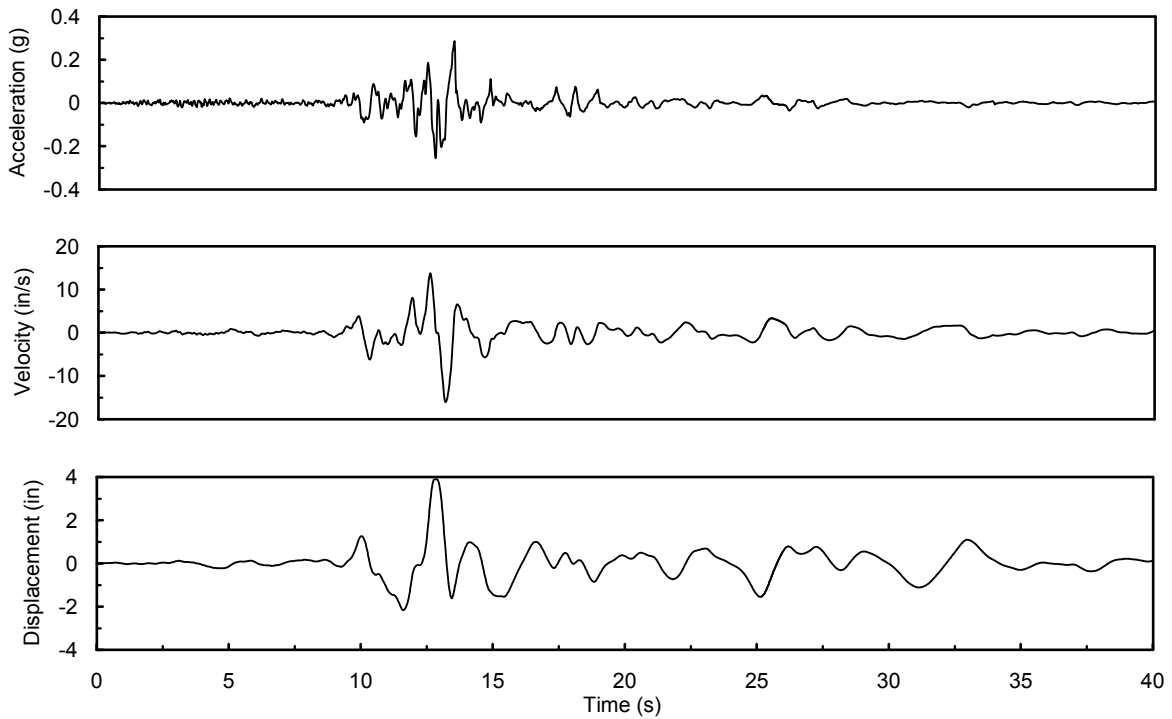


Figure B-22 Oakland Outer Harbor Wharf, horizontal: 35 degrees

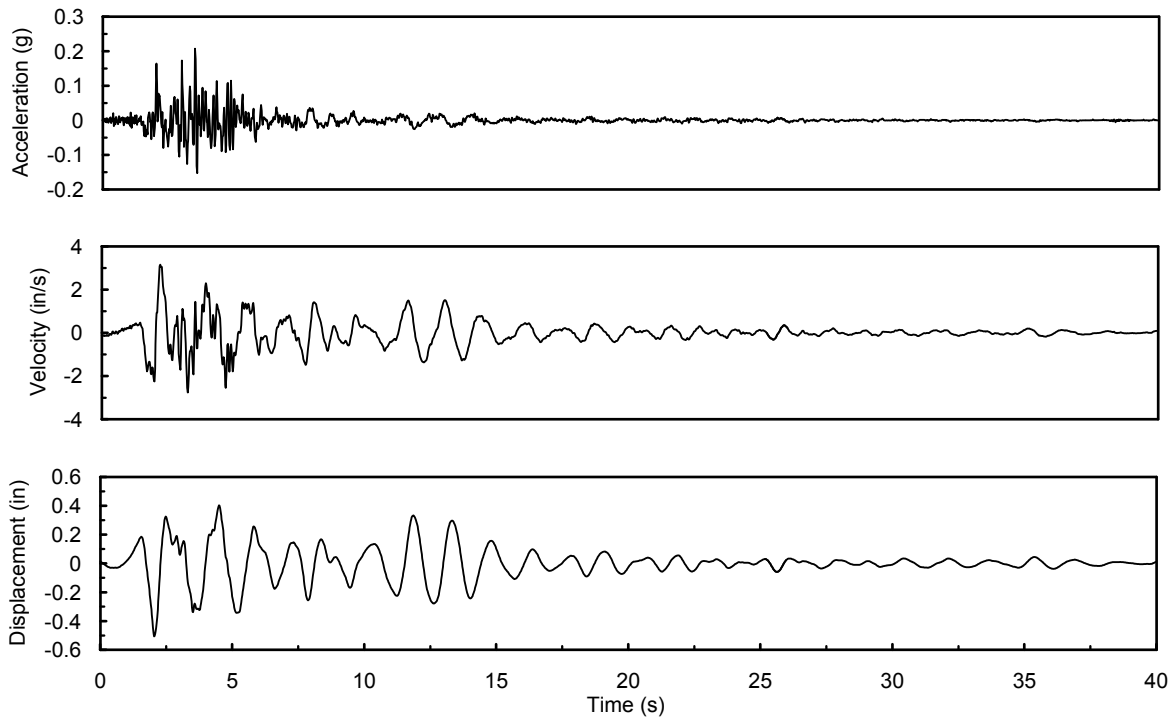


Figure B-23 Pomona, horizontal: 90 degrees

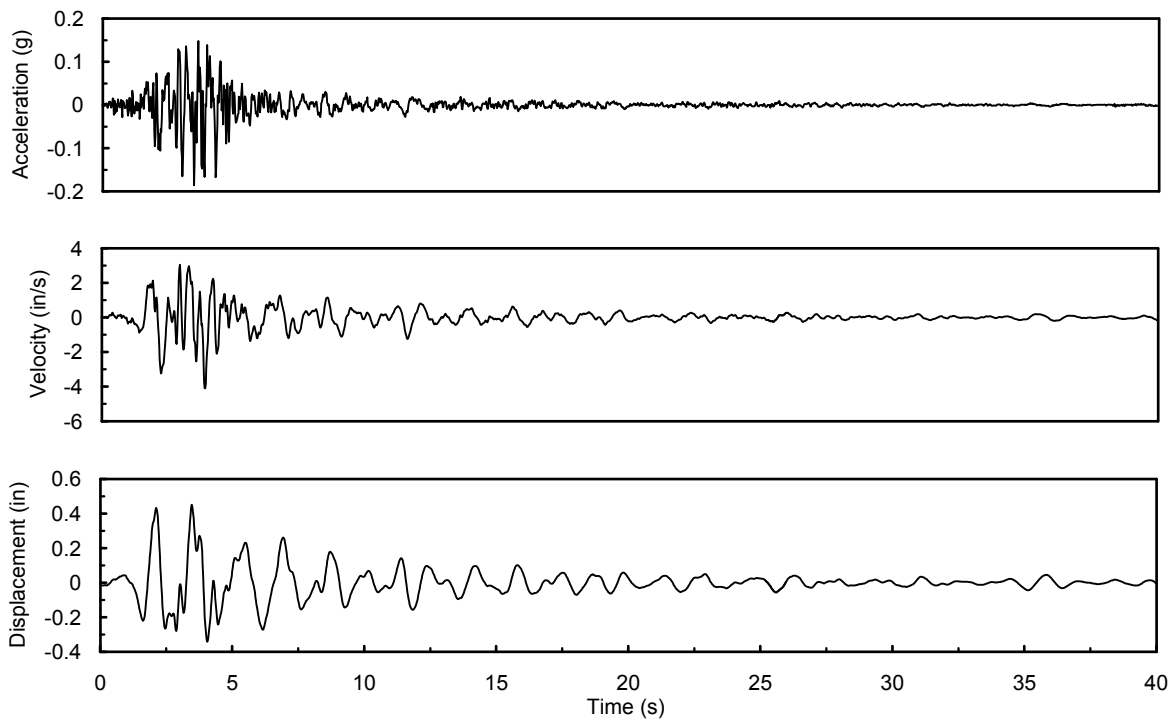


Figure B-24 Pomona, horizontal: 0 degrees

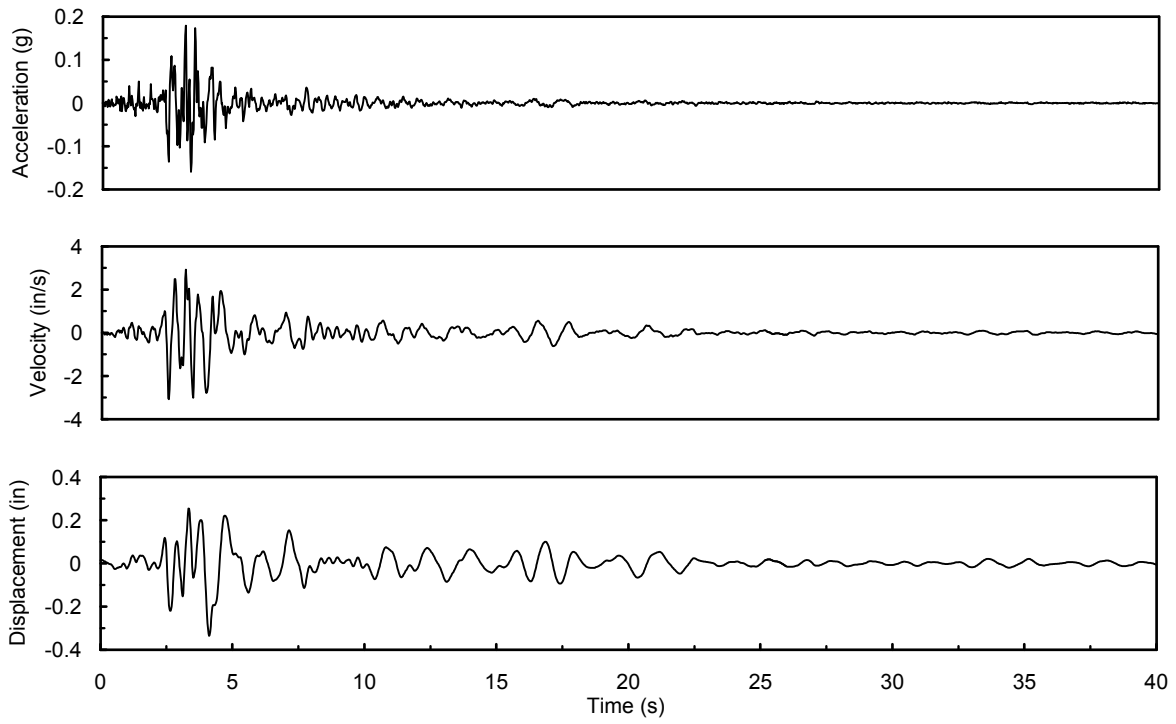


Figure B-25 Altadena, horizontal: 90 degrees

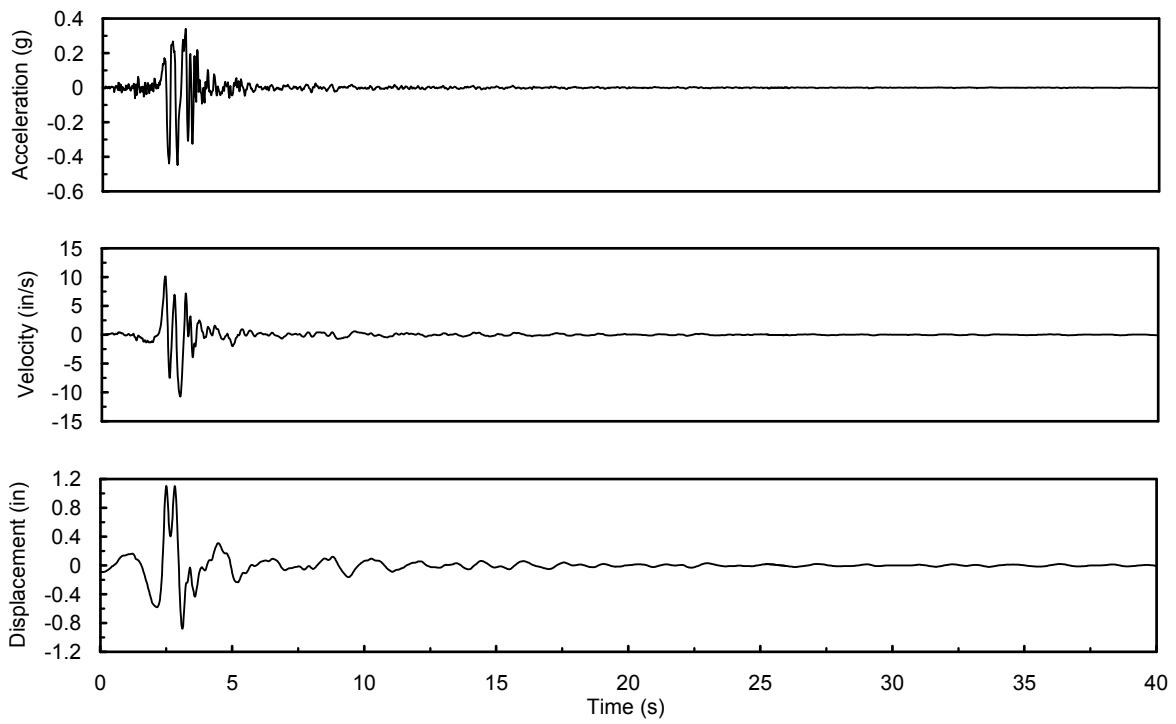


Figure B-26 Altadena, horizontal: 0 degrees

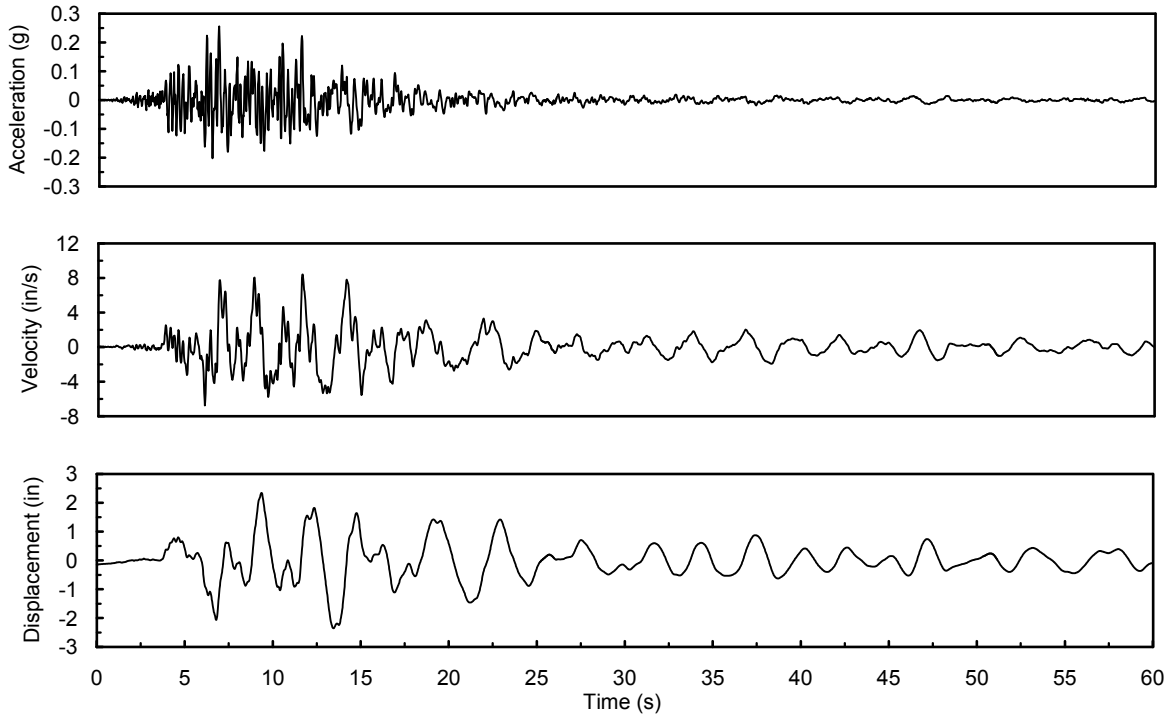


Figure B-27 Century City, horizontal: 90 degrees

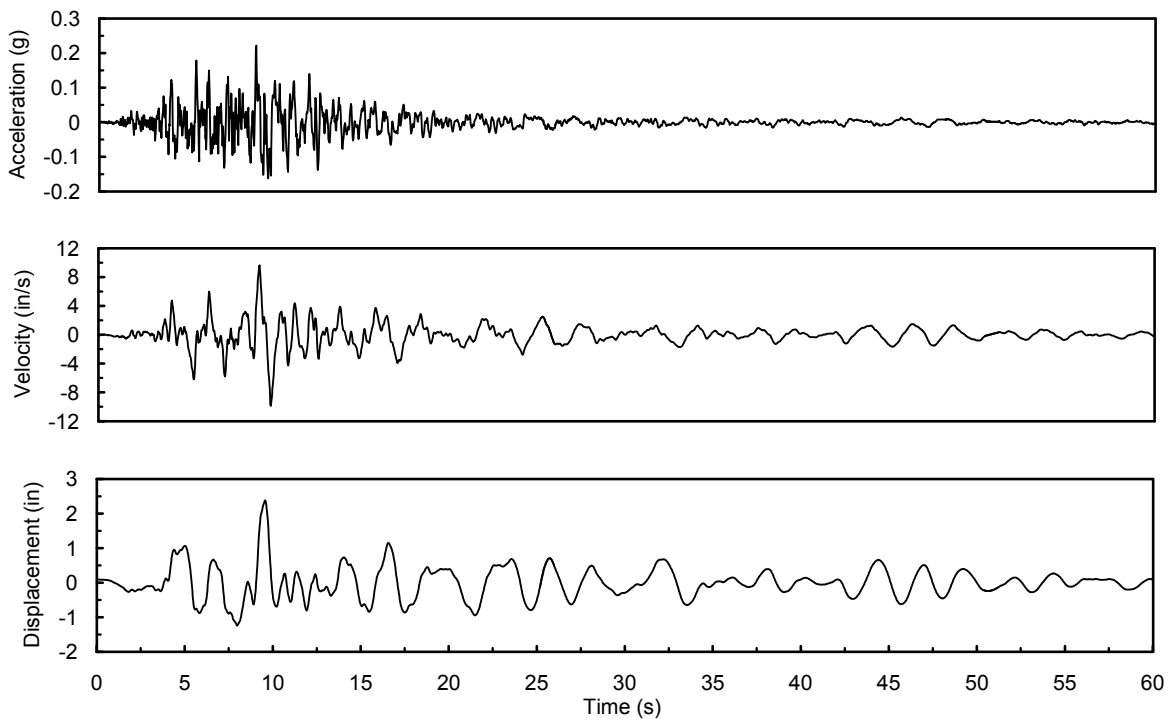


Figure B-28 Century City, horizontal: 360 degrees

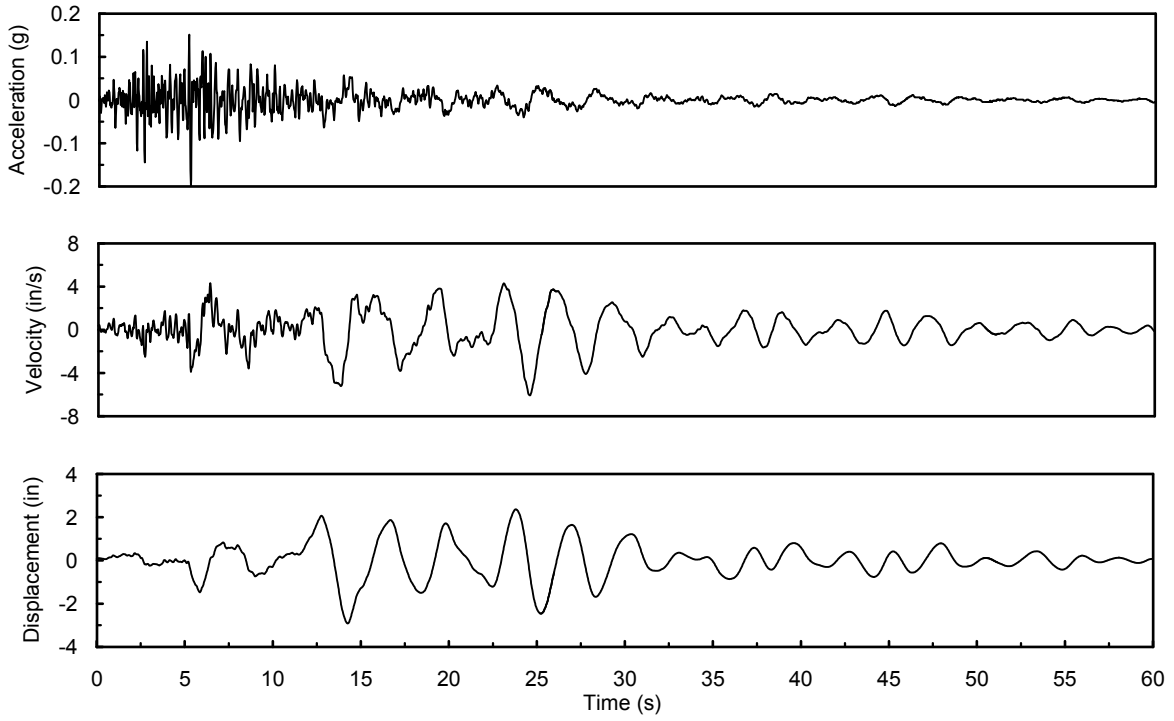


Figure B-29 Hollister, vertical

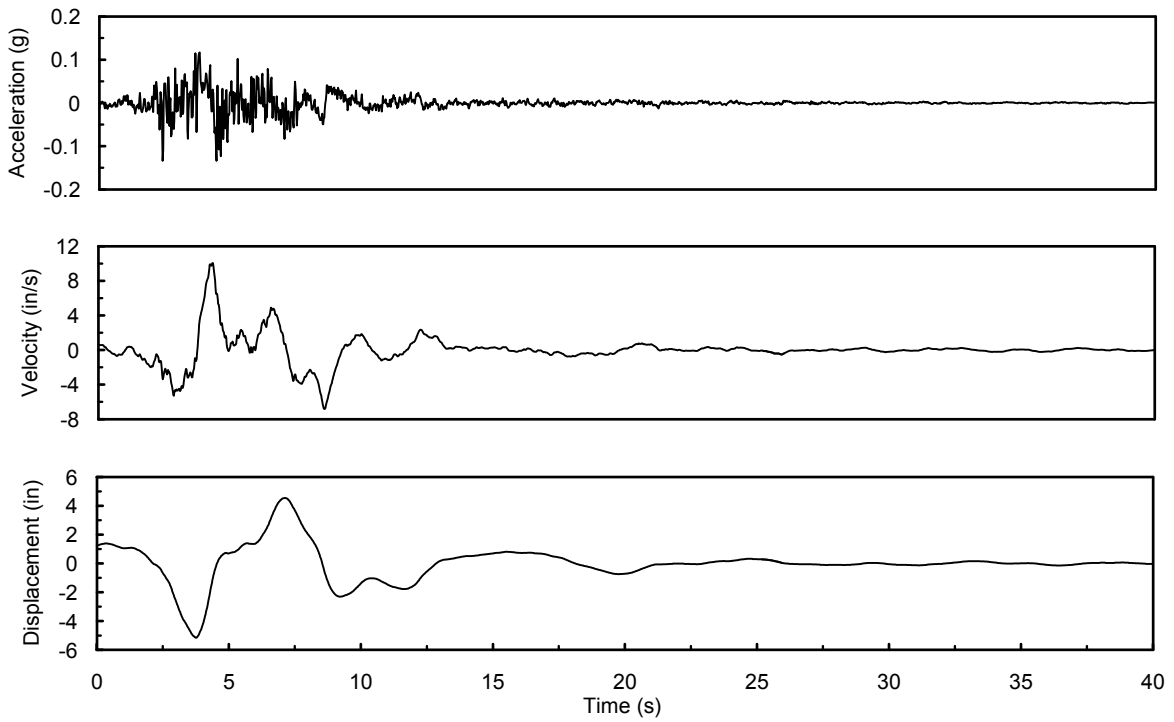


Figure B-30 Lexington Dam, vertical

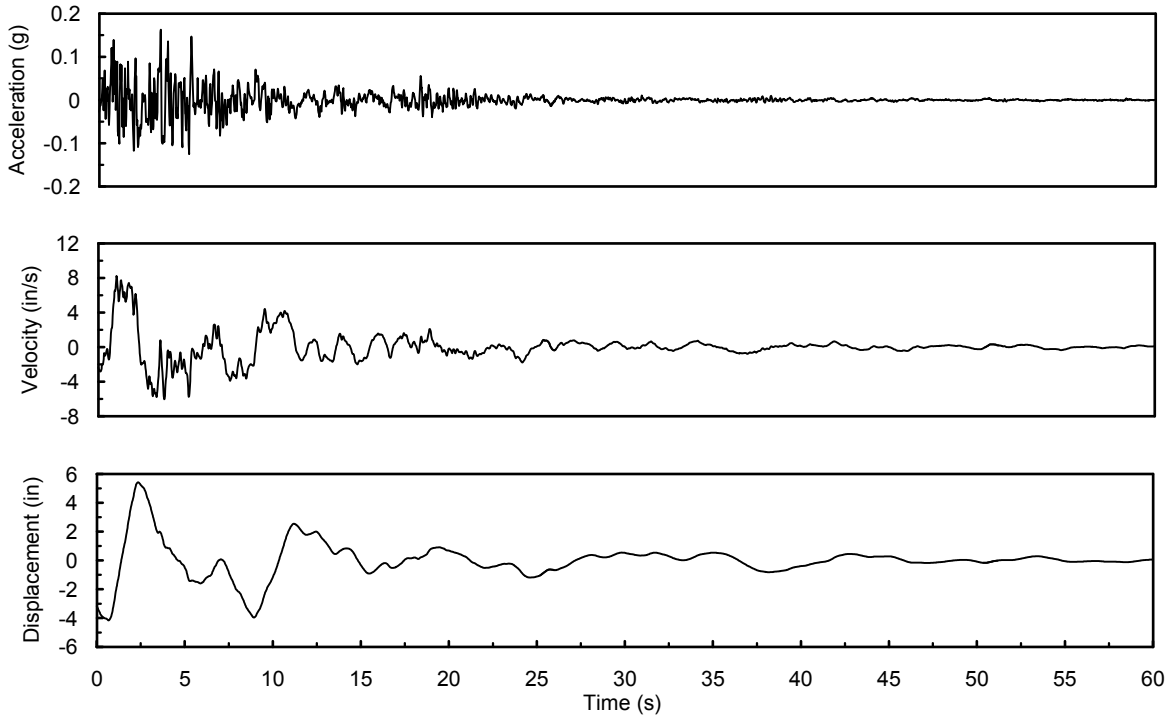


Figure B-31 Petrolia, vertical

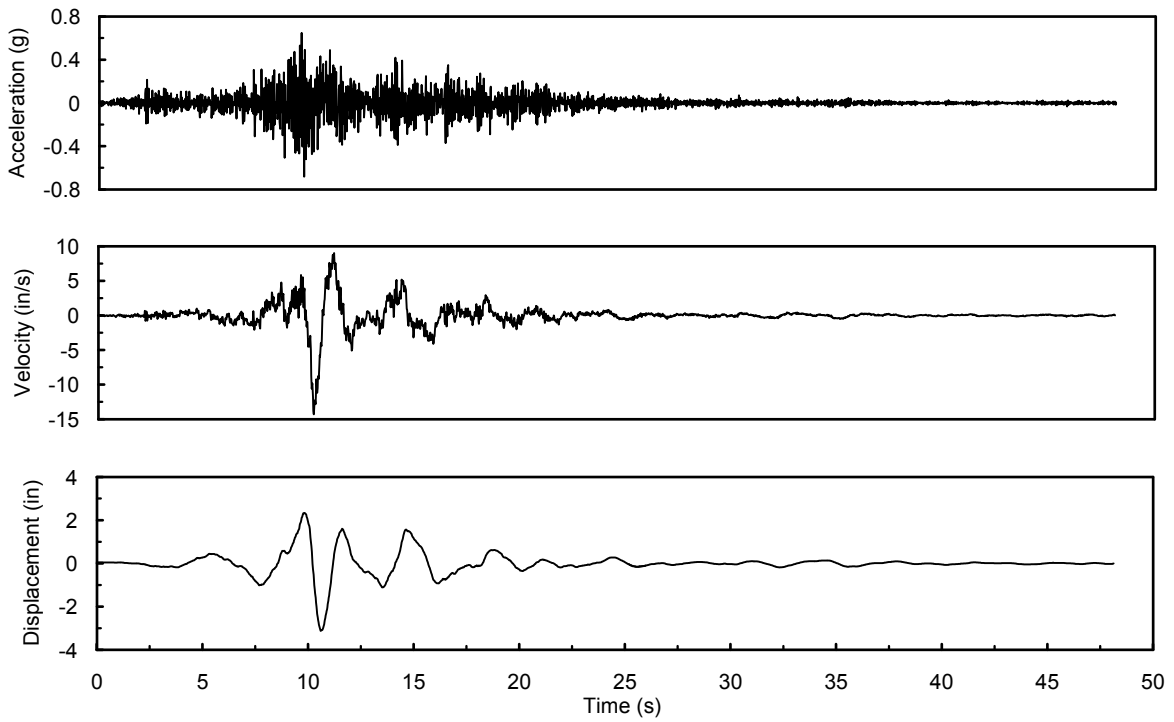


Figure B-32 Lucerne Valley, vertical

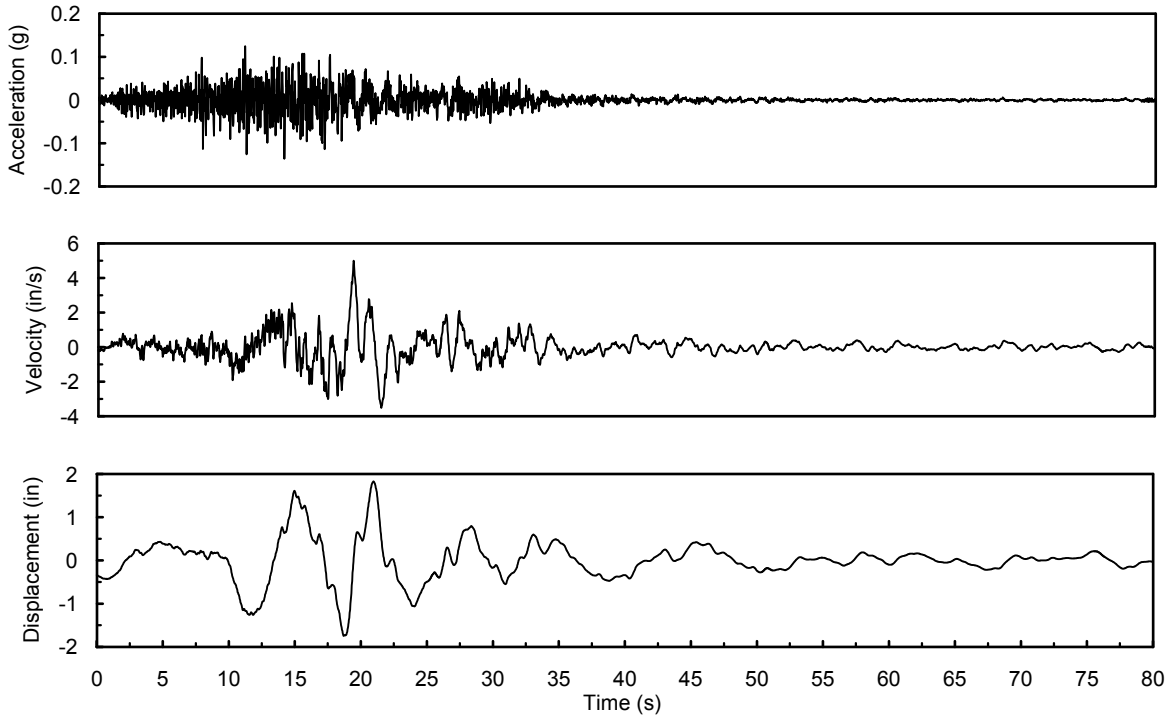


Figure B-33 Yermo, vertical

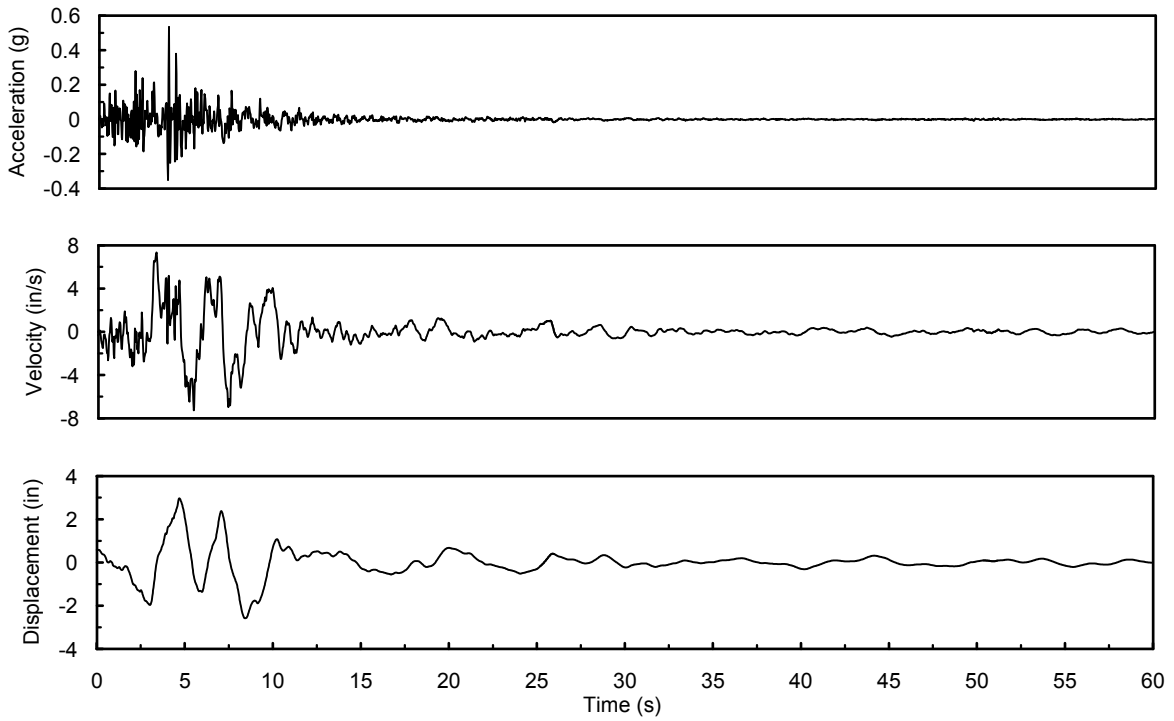


Figure B-34 Sylmar, vertical

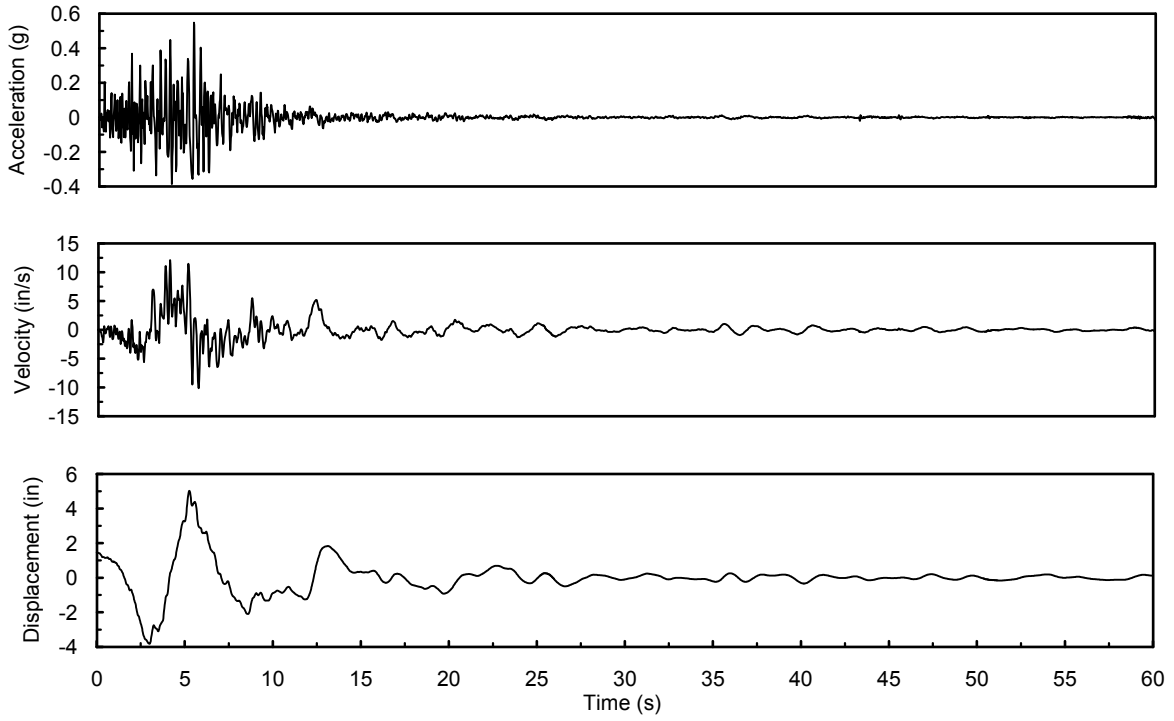


Figure B-35 Newhall Fire, vertical

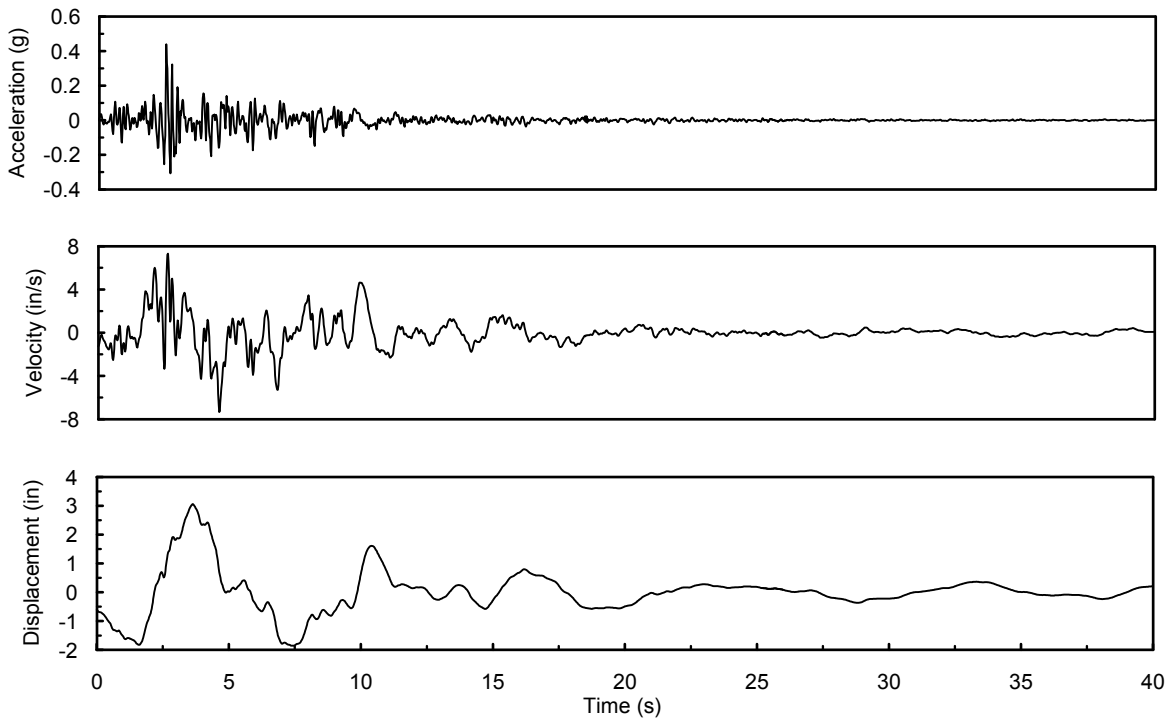


Figure B-36 Corralitos, vertical

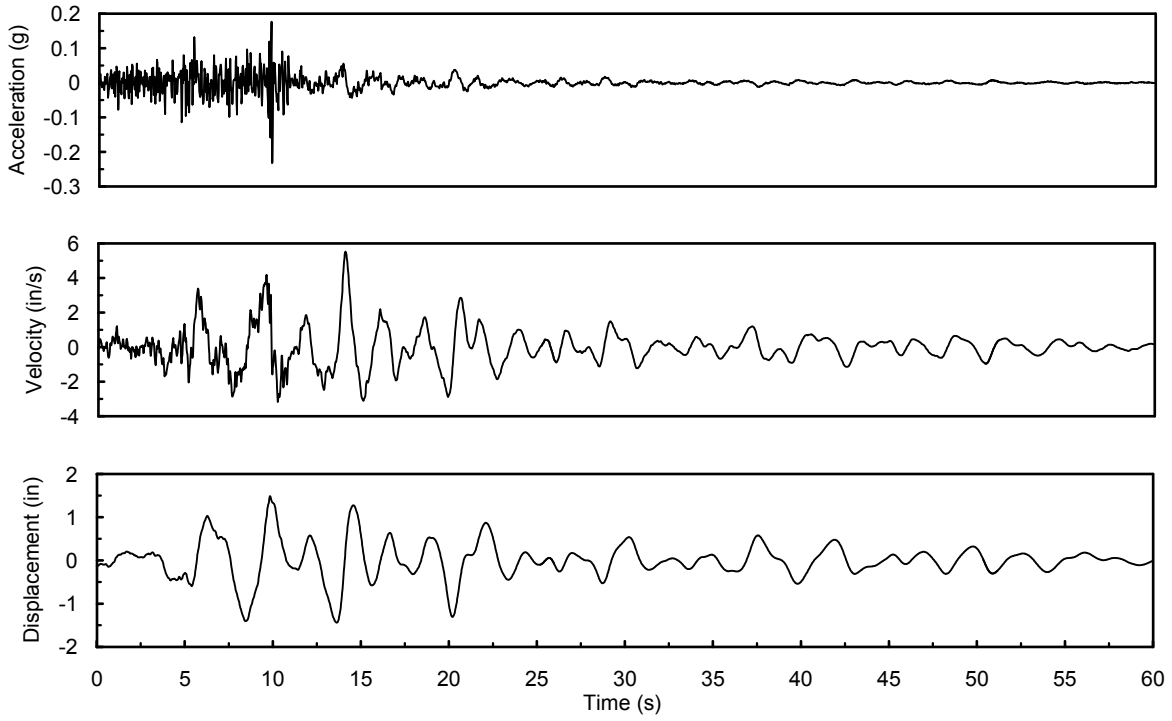


Figure B-37 Santa Monica City Hall Grounds, vertical

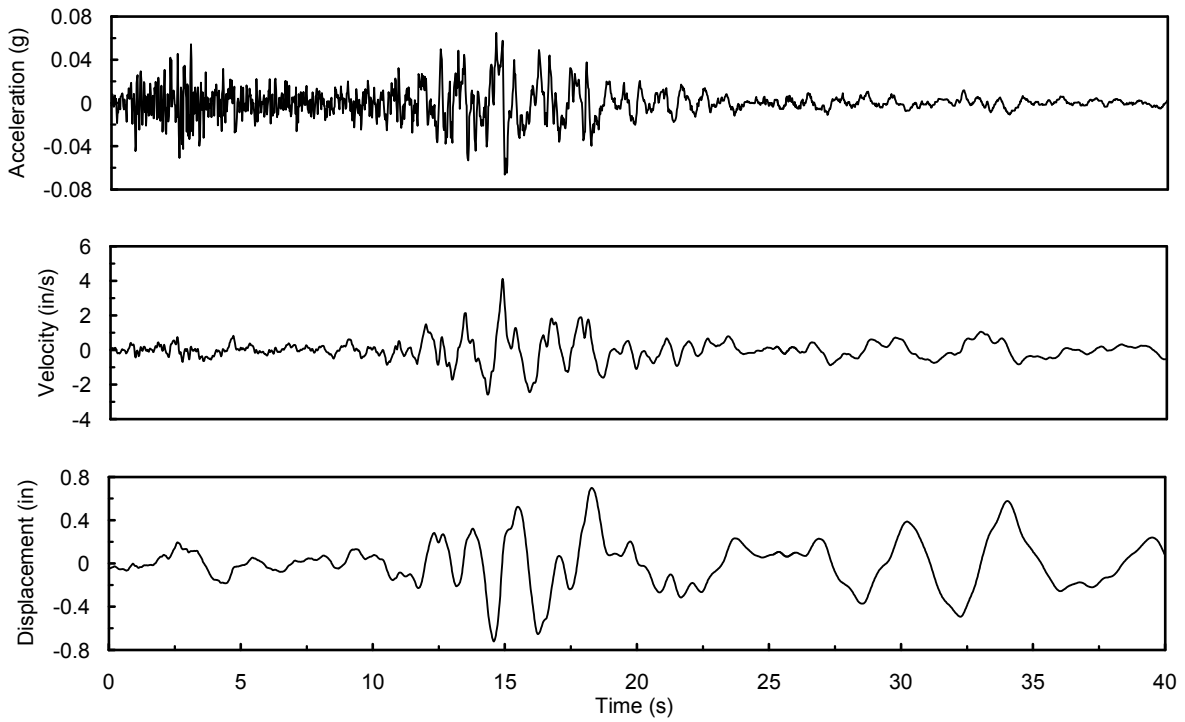


Figure B-38 Oakland Outer Harbor Wharf, vertical

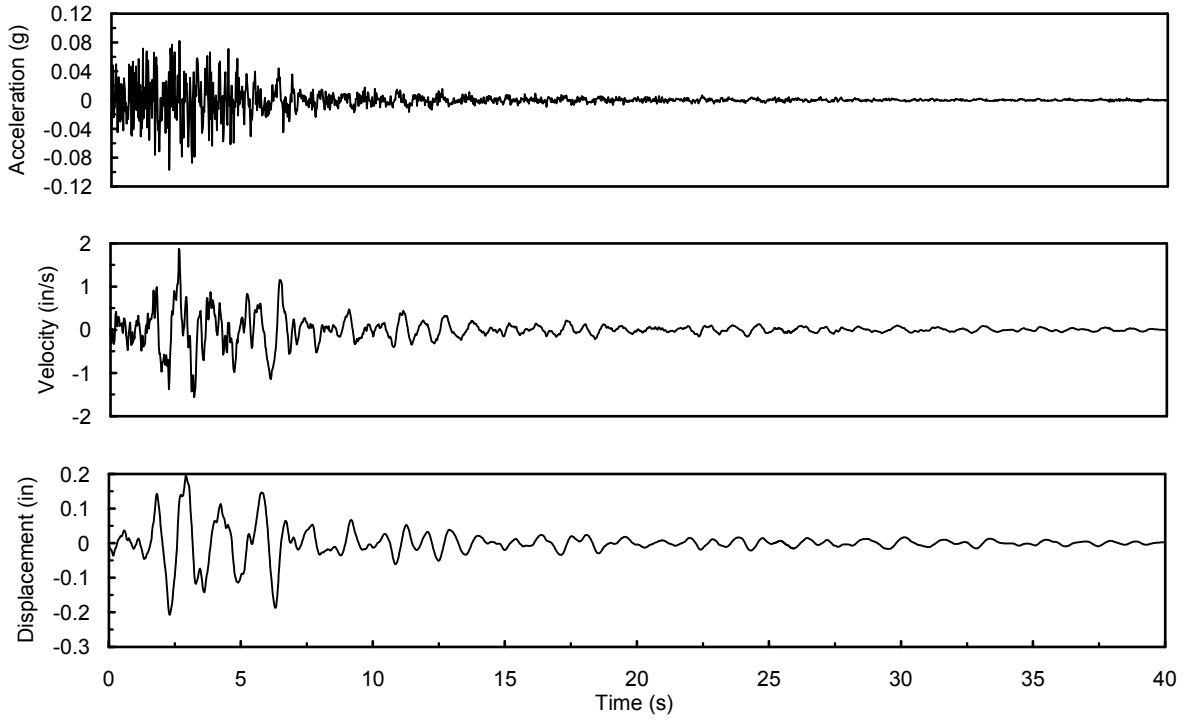


Figure B-39 Pomona, vertical

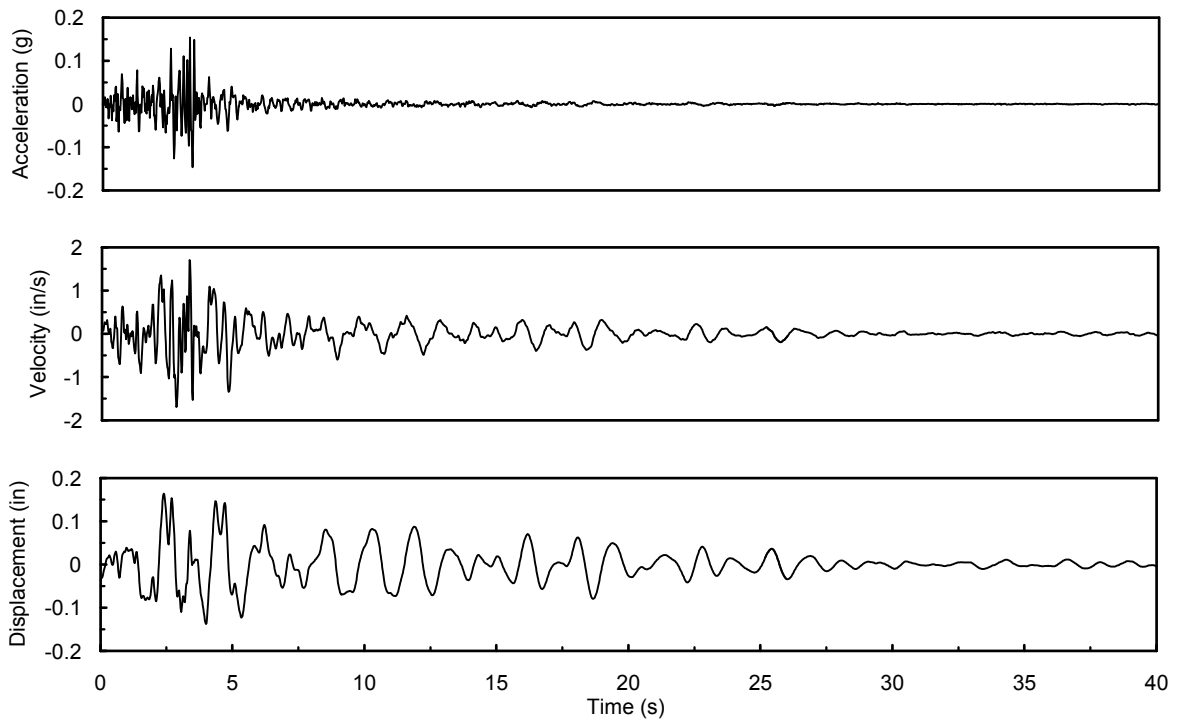


Figure B-40 Altadena, vertical

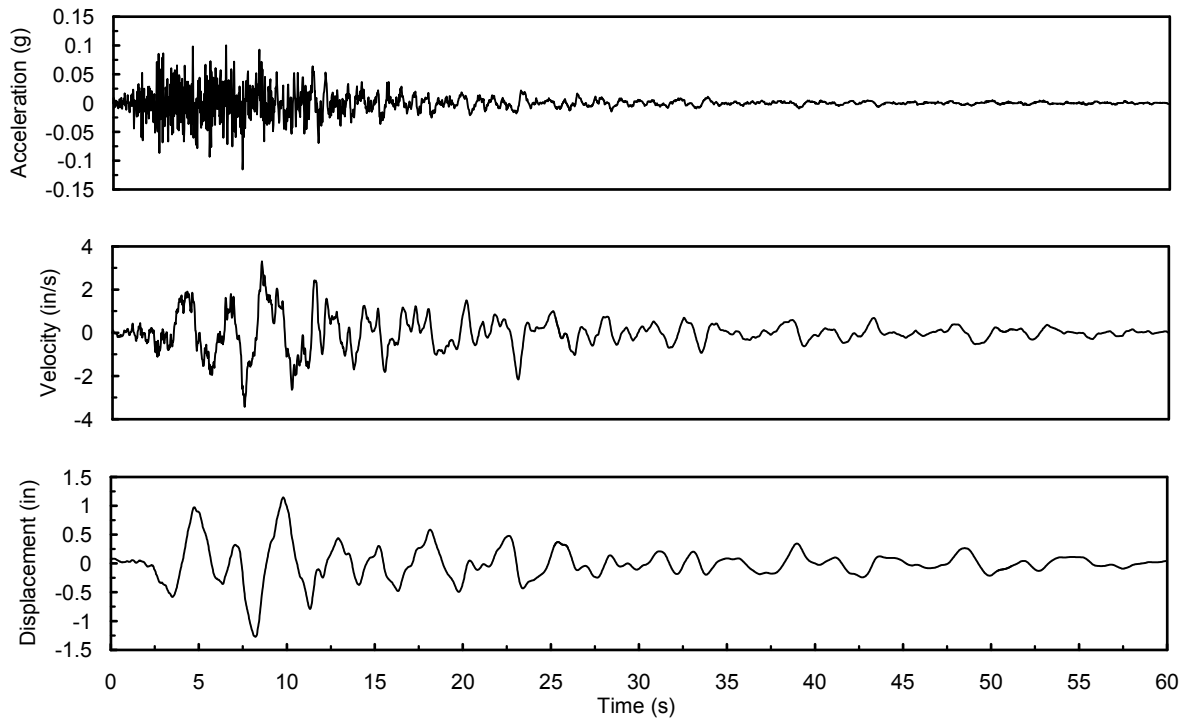


Figure B-41 Century City, vertical

MCEER Technical Reports

MCEER publishes technical reports on a variety of subjects written by authors funded through MCEER. These reports are available from both MCEER Publications and the National Technical Information Service (NTIS). Requests for reports should be directed to MCEER Publications, MCEER, University at Buffalo, State University of New York, Red Jacket Quadrangle, Buffalo, New York 14261. Reports can also be requested through NTIS, 5285 Port Royal Road, Springfield, Virginia 22161. NTIS accession numbers are shown in parenthesis, if available.

- NCEER-87-0001 "First-Year Program in Research, Education and Technology Transfer," 3/5/87, (PB88-134275, A04, MF-A01).
- NCEER-87-0002 "Experimental Evaluation of Instantaneous Optimal Algorithms for Structural Control," by R.C. Lin, T.T. Soong and A.M. Reinhorn, 4/20/87, (PB88-134341, A04, MF-A01).
- NCEER-87-0003 "Experimentation Using the Earthquake Simulation Facilities at University at Buffalo," by A.M. Reinhorn and R.L. Ketter, to be published.
- NCEER-87-0004 "The System Characteristics and Performance of a Shaking Table," by J.S. Hwang, K.C. Chang and G.C. Lee, 6/1/87, (PB88-134259, A03, MF-A01). This report is available only through NTIS (see address given above).
- NCEER-87-0005 "A Finite Element Formulation for Nonlinear Viscoplastic Material Using a Q Model," by O. Gyebe and G. Dasgupta, 11/2/87, (PB88-213764, A08, MF-A01).
- NCEER-87-0006 "Symbolic Manipulation Program (SMP) - Algebraic Codes for Two and Three Dimensional Finite Element Formulations," by X. Lee and G. Dasgupta, 11/9/87, (PB88-218522, A05, MF-A01).
- NCEER-87-0007 "Instantaneous Optimal Control Laws for Tall Buildings Under Seismic Excitations," by J.N. Yang, A. Akbarpour and P. Ghaemmaghami, 6/10/87, (PB88-134333, A06, MF-A01). This report is only available through NTIS (see address given above).
- NCEER-87-0008 "IDARC: Inelastic Damage Analysis of Reinforced Concrete Frame - Shear-Wall Structures," by Y.J. Park, A.M. Reinhorn and S.K. Kunnath, 7/20/87, (PB88-134325, A09, MF-A01). This report is only available through NTIS (see address given above).
- NCEER-87-0009 "Liquefaction Potential for New York State: A Preliminary Report on Sites in Manhattan and Buffalo," by M. Budhu, V. Vijayakumar, R.F. Giese and L. Baumgras, 8/31/87, (PB88-163704, A03, MF-A01). This report is available only through NTIS (see address given above).
- NCEER-87-0010 "Vertical and Torsional Vibration of Foundations in Inhomogeneous Media," by A.S. Veletsos and K.W. Dotson, 6/1/87, (PB88-134291, A03, MF-A01). This report is only available through NTIS (see address given above).
- NCEER-87-0011 "Seismic Probabilistic Risk Assessment and Seismic Margins Studies for Nuclear Power Plants," by Howard H.M. Hwang, 6/15/87, (PB88-134267, A03, MF-A01). This report is only available through NTIS (see address given above).
- NCEER-87-0012 "Parametric Studies of Frequency Response of Secondary Systems Under Ground-Acceleration Excitations," by Y. Yong and Y.K. Lin, 6/10/87, (PB88-134309, A03, MF-A01). This report is only available through NTIS (see address given above).
- NCEER-87-0013 "Frequency Response of Secondary Systems Under Seismic Excitation," by J.A. HoLung, J. Cai and Y.K. Lin, 7/31/87, (PB88-134317, A05, MF-A01). This report is only available through NTIS (see address given above).
- NCEER-87-0014 "Modelling Earthquake Ground Motions in Seismically Active Regions Using Parametric Time Series Methods," by G.W. Ellis and A.S. Cakmak, 8/25/87, (PB88-134283, A08, MF-A01). This report is only available through NTIS (see address given above).
- NCEER-87-0015 "Detection and Assessment of Seismic Structural Damage," by E. DiPasquale and A.S. Cakmak, 8/25/87, (PB88-163712, A05, MF-A01). This report is only available through NTIS (see address given above).

- NCEER-87-0016 "Pipeline Experiment at Parkfield, California," by J. Isenberg and E. Richardson, 9/15/87, (PB88-163720, A03, MF-A01). This report is available only through NTIS (see address given above).
- NCEER-87-0017 "Digital Simulation of Seismic Ground Motion," by M. Shinozuka, G. Deodatis and T. Harada, 8/31/87, (PB88-155197, A04, MF-A01). This report is available only through NTIS (see address given above).
- NCEER-87-0018 "Practical Considerations for Structural Control: System Uncertainty, System Time Delay and Truncation of Small Control Forces," J.N. Yang and A. Akbarpour, 8/10/87, (PB88-163738, A08, MF-A01). This report is only available through NTIS (see address given above).
- NCEER-87-0019 "Modal Analysis of Nonclassically Damped Structural Systems Using Canonical Transformation," by J.N. Yang, S. Sarkani and F.X. Long, 9/27/87, (PB88-187851, A04, MF-A01).
- NCEER-87-0020 "A Nonstationary Solution in Random Vibration Theory," by J.R. Red-Horse and P.D. Spanos, 11/3/87, (PB88-163746, A03, MF-A01).
- NCEER-87-0021 "Horizontal Impedances for Radially Inhomogeneous Viscoelastic Soil Layers," by A.S. Veletsos and K.W. Dotson, 10/15/87, (PB88-150859, A04, MF-A01).
- NCEER-87-0022 "Seismic Damage Assessment of Reinforced Concrete Members," by Y.S. Chung, C. Meyer and M. Shinozuka, 10/9/87, (PB88-150867, A05, MF-A01). This report is available only through NTIS (see address given above).
- NCEER-87-0023 "Active Structural Control in Civil Engineering," by T.T. Soong, 11/11/87, (PB88-187778, A03, MF-A01).
- NCEER-87-0024 "Vertical and Torsional Impedances for Radially Inhomogeneous Viscoelastic Soil Layers," by K.W. Dotson and A.S. Veletsos, 12/87, (PB88-187786, A03, MF-A01).
- NCEER-87-0025 "Proceedings from the Symposium on Seismic Hazards, Ground Motions, Soil-Liquefaction and Engineering Practice in Eastern North America," October 20-22, 1987, edited by K.H. Jacob, 12/87, (PB88-188115, A23, MF-A01). This report is available only through NTIS (see address given above).
- NCEER-87-0026 "Report on the Whittier-Narrows, California, Earthquake of October 1, 1987," by J. Pantelic and A. Reinhorn, 11/87, (PB88-187752, A03, MF-A01). This report is available only through NTIS (see address given above).
- NCEER-87-0027 "Design of a Modular Program for Transient Nonlinear Analysis of Large 3-D Building Structures," by S. Srivastav and J.F. Abel, 12/30/87, (PB88-187950, A05, MF-A01). This report is only available through NTIS (see address given above).
- NCEER-87-0028 "Second-Year Program in Research, Education and Technology Transfer," 3/8/88, (PB88-219480, A04, MF-A01).
- NCEER-88-0001 "Workshop on Seismic Computer Analysis and Design of Buildings With Interactive Graphics," by W. McGuire, J.F. Abel and C.H. Conley, 1/18/88, (PB88-187760, A03, MF-A01). This report is only available through NTIS (see address given above).
- NCEER-88-0002 "Optimal Control of Nonlinear Flexible Structures," by J.N. Yang, F.X. Long and D. Wong, 1/22/88, (PB88-213772, A06, MF-A01).
- NCEER-88-0003 "Substructuring Techniques in the Time Domain for Primary-Secondary Structural Systems," by G.D. Manolis and G. Juhn, 2/10/88, (PB88-213780, A04, MF-A01).
- NCEER-88-0004 "Iterative Seismic Analysis of Primary-Secondary Systems," by A. Singhal, L.D. Lutes and P.D. Spanos, 2/23/88, (PB88-213798, A04, MF-A01).
- NCEER-88-0005 "Stochastic Finite Element Expansion for Random Media," by P.D. Spanos and R. Ghanem, 3/14/88, (PB88-213806, A03, MF-A01).

- NCEER-88-0006 "Combining Structural Optimization and Structural Control," by F.Y. Cheng and C.P. Pantelides, 1/10/88, (PB88-213814, A05, MF-A01).
- NCEER-88-0007 "Seismic Performance Assessment of Code-Designed Structures," by H.H-M. Hwang, J-W. Jaw and H-J. Shau, 3/20/88, (PB88-219423, A04, MF-A01). This report is only available through NTIS (see address given above).
- NCEER-88-0008 "Reliability Analysis of Code-Designed Structures Under Natural Hazards," by H.H-M. Hwang, H. Ushiba and M. Shinozuka, 2/29/88, (PB88-229471, A07, MF-A01). This report is only available through NTIS (see address given above).
- NCEER-88-0009 "Seismic Fragility Analysis of Shear Wall Structures," by J-W Jaw and H.H-M. Hwang, 4/30/88, (PB89-102867, A04, MF-A01).
- NCEER-88-0010 "Base Isolation of a Multi-Story Building Under a Harmonic Ground Motion - A Comparison of Performances of Various Systems," by F-G Fan, G. Ahmadi and I.G. Tadjbakhsh, 5/18/88, (PB89-122238, A06, MF-A01). This report is only available through NTIS (see address given above).
- NCEER-88-0011 "Seismic Floor Response Spectra for a Combined System by Green's Functions," by F.M. Lavelle, L.A. Bergman and P.D. Spanos, 5/1/88, (PB89-102875, A03, MF-A01).
- NCEER-88-0012 "A New Solution Technique for Randomly Excited Hysteretic Structures," by G.Q. Cai and Y.K. Lin, 5/16/88, (PB89-102883, A03, MF-A01).
- NCEER-88-0013 "A Study of Radiation Damping and Soil-Structure Interaction Effects in the Centrifuge," by K. Weissman, supervised by J.H. Prevost, 5/24/88, (PB89-144703, A06, MF-A01).
- NCEER-88-0014 "Parameter Identification and Implementation of a Kinematic Plasticity Model for Frictional Soils," by J.H. Prevost and D.V. Griffiths, to be published.
- NCEER-88-0015 "Two- and Three- Dimensional Dynamic Finite Element Analyses of the Long Valley Dam," by D.V. Griffiths and J.H. Prevost, 6/17/88, (PB89-144711, A04, MF-A01).
- NCEER-88-0016 "Damage Assessment of Reinforced Concrete Structures in Eastern United States," by A.M. Reinhorn, M.J. Seidel, S.K. Kunnath and Y.J. Park, 6/15/88, (PB89-122220, A04, MF-A01). This report is only available through NTIS (see address given above).
- NCEER-88-0017 "Dynamic Compliance of Vertically Loaded Strip Foundations in Multilayered Viscoelastic Soils," by S. Ahmad and A.S.M. Israil, 6/17/88, (PB89-102891, A04, MF-A01).
- NCEER-88-0018 "An Experimental Study of Seismic Structural Response With Added Viscoelastic Dampers," by R.C. Lin, Z. Liang, T.T. Soong and R.H. Zhang, 6/30/88, (PB89-122212, A05, MF-A01). This report is available only through NTIS (see address given above).
- NCEER-88-0019 "Experimental Investigation of Primary - Secondary System Interaction," by G.D. Manolis, G. Juhn and A.M. Reinhorn, 5/27/88, (PB89-122204, A04, MF-A01).
- NCEER-88-0020 "A Response Spectrum Approach For Analysis of Nonclassically Damped Structures," by J.N. Yang, S. Sarkani and F.X. Long, 4/22/88, (PB89-102909, A04, MF-A01).
- NCEER-88-0021 "Seismic Interaction of Structures and Soils: Stochastic Approach," by A.S. Veletsos and A.M. Prasad, 7/21/88, (PB89-122196, A04, MF-A01). This report is only available through NTIS (see address given above).
- NCEER-88-0022 "Identification of the Serviceability Limit State and Detection of Seismic Structural Damage," by E. DiPasquale and A.S. Cakmak, 6/15/88, (PB89-122188, A05, MF-A01). This report is available only through NTIS (see address given above).
- NCEER-88-0023 "Multi-Hazard Risk Analysis: Case of a Simple Offshore Structure," by B.K. Bhartia and E.H. Vanmarcke, 7/21/88, (PB89-145213, A05, MF-A01).

- NCEER-88-0024 "Automated Seismic Design of Reinforced Concrete Buildings," by Y.S. Chung, C. Meyer and M. Shinozuka, 7/5/88, (PB89-122170, A06, MF-A01). This report is available only through NTIS (see address given above).
- NCEER-88-0025 "Experimental Study of Active Control of MDOF Structures Under Seismic Excitations," by L.L. Chung, R.C. Lin, T.T. Soong and A.M. Reinhorn, 7/10/88, (PB89-122600, A04, MF-A01).
- NCEER-88-0026 "Earthquake Simulation Tests of a Low-Rise Metal Structure," by J.S. Hwang, K.C. Chang, G.C. Lee and R.L. Ketter, 8/1/88, (PB89-102917, A04, MF-A01).
- NCEER-88-0027 "Systems Study of Urban Response and Reconstruction Due to Catastrophic Earthquakes," by F. Kozin and H.K. Zhou, 9/22/88, (PB90-162348, A04, MF-A01).
- NCEER-88-0028 "Seismic Fragility Analysis of Plane Frame Structures," by H.H-M. Hwang and Y.K. Low, 7/31/88, (PB89-131445, A06, MF-A01).
- NCEER-88-0029 "Response Analysis of Stochastic Structures," by A. Kardara, C. Bucher and M. Shinozuka, 9/22/88, (PB89-174429, A04, MF-A01).
- NCEER-88-0030 "Nonnormal Accelerations Due to Yielding in a Primary Structure," by D.C.K. Chen and L.D. Lutes, 9/19/88, (PB89-131437, A04, MF-A01).
- NCEER-88-0031 "Design Approaches for Soil-Structure Interaction," by A.S. Veletsos, A.M. Prasad and Y. Tang, 12/30/88, (PB89-174437, A03, MF-A01). This report is available only through NTIS (see address given above).
- NCEER-88-0032 "A Re-evaluation of Design Spectra for Seismic Damage Control," by C.J. Turkstra and A.G. Tallin, 11/7/88, (PB89-145221, A05, MF-A01).
- NCEER-88-0033 "The Behavior and Design of Noncontact Lap Splices Subjected to Repeated Inelastic Tensile Loading," by V.E. Sagan, P. Gergely and R.N. White, 12/8/88, (PB89-163737, A08, MF-A01).
- NCEER-88-0034 "Seismic Response of Pile Foundations," by S.M. Mamoon, P.K. Banerjee and S. Ahmad, 11/1/88, (PB89-145239, A04, MF-A01).
- NCEER-88-0035 "Modeling of R/C Building Structures With Flexible Floor Diaphragms (IDARC2)," by A.M. Reinhorn, S.K. Kunnath and N. Panahshahi, 9/7/88, (PB89-207153, A07, MF-A01).
- NCEER-88-0036 "Solution of the Dam-Reservoir Interaction Problem Using a Combination of FEM, BEM with Particular Integrals, Modal Analysis, and Substructuring," by C-S. Tsai, G.C. Lee and R.L. Ketter, 12/31/88, (PB89-207146, A04, MF-A01).
- NCEER-88-0037 "Optimal Placement of Actuators for Structural Control," by F.Y. Cheng and C.P. Pantelides, 8/15/88, (PB89-162846, A05, MF-A01).
- NCEER-88-0038 "Teflon Bearings in Aseismic Base Isolation: Experimental Studies and Mathematical Modeling," by A. Mokha, M.C. Constantinou and A.M. Reinhorn, 12/5/88, (PB89-218457, A10, MF-A01). This report is available only through NTIS (see address given above).
- NCEER-88-0039 "Seismic Behavior of Flat Slab High-Rise Buildings in the New York City Area," by P. Weidlinger and M. Ettouney, 10/15/88, (PB90-145681, A04, MF-A01).
- NCEER-88-0040 "Evaluation of the Earthquake Resistance of Existing Buildings in New York City," by P. Weidlinger and M. Ettouney, 10/15/88, to be published.
- NCEER-88-0041 "Small-Scale Modeling Techniques for Reinforced Concrete Structures Subjected to Seismic Loads," by W. Kim, A. El-Attar and R.N. White, 11/22/88, (PB89-189625, A05, MF-A01).
- NCEER-88-0042 "Modeling Strong Ground Motion from Multiple Event Earthquakes," by G.W. Ellis and A.S. Cakmak, 10/15/88, (PB89-174445, A03, MF-A01).

- NCEER-88-0043 "Nonstationary Models of Seismic Ground Acceleration," by M. Grigoriu, S.E. Ruiz and E. Rosenblueth, 7/15/88, (PB89-189617, A04, MF-A01).
- NCEER-88-0044 "SARCF User's Guide: Seismic Analysis of Reinforced Concrete Frames," by Y.S. Chung, C. Meyer and M. Shinozuka, 11/9/88, (PB89-174452, A08, MF-A01).
- NCEER-88-0045 "First Expert Panel Meeting on Disaster Research and Planning," edited by J. Pantelic and J. Stoyke, 9/15/88, (PB89-174460, A05, MF-A01).
- NCEER-88-0046 "Preliminary Studies of the Effect of Degrading Infill Walls on the Nonlinear Seismic Response of Steel Frames," by C.Z. Chrysostomou, P. Gergely and J.F. Abel, 12/19/88, (PB89-208383, A05, MF-A01).
- NCEER-88-0047 "Reinforced Concrete Frame Component Testing Facility - Design, Construction, Instrumentation and Operation," by S.P. Pessiki, C. Conley, T. Bond, P. Gergely and R.N. White, 12/16/88, (PB89-174478, A04, MF-A01).
- NCEER-89-0001 "Effects of Protective Cushion and Soil Compliancy on the Response of Equipment Within a Seismically Excited Building," by J.A. HoLung, 2/16/89, (PB89-207179, A04, MF-A01).
- NCEER-89-0002 "Statistical Evaluation of Response Modification Factors for Reinforced Concrete Structures," by H.H-M. Hwang and J-W. Jaw, 2/17/89, (PB89-207187, A05, MF-A01).
- NCEER-89-0003 "Hysteretic Columns Under Random Excitation," by G-Q. Cai and Y.K. Lin, 1/9/89, (PB89-196513, A03, MF-A01).
- NCEER-89-0004 "Experimental Study of 'Elephant Foot Bulge' Instability of Thin-Walled Metal Tanks," by Z-H. Jia and R.L. Ketter, 2/22/89, (PB89-207195, A03, MF-A01).
- NCEER-89-0005 "Experiment on Performance of Buried Pipelines Across San Andreas Fault," by J. Isenberg, E. Richardson and T.D. O'Rourke, 3/10/89, (PB89-218440, A04, MF-A01). This report is available only through NTIS (see address given above).
- NCEER-89-0006 "A Knowledge-Based Approach to Structural Design of Earthquake-Resistant Buildings," by M. Subramani, P. Gergely, C.H. Conley, J.F. Abel and A.H. Zaghaw, 1/15/89, (PB89-218465, A06, MF-A01).
- NCEER-89-0007 "Liquefaction Hazards and Their Effects on Buried Pipelines," by T.D. O'Rourke and P.A. Lane, 2/1/89, (PB89-218481, A09, MF-A01).
- NCEER-89-0008 "Fundamentals of System Identification in Structural Dynamics," by H. Imai, C-B. Yun, O. Maruyama and M. Shinozuka, 1/26/89, (PB89-207211, A04, MF-A01).
- NCEER-89-0009 "Effects of the 1985 Michoacan Earthquake on Water Systems and Other Buried Lifelines in Mexico," by A.G. Ayala and M.J. O'Rourke, 3/8/89, (PB89-207229, A06, MF-A01).
- NCEER-89-R010 "NCEER Bibliography of Earthquake Education Materials," by K.E.K. Ross, Second Revision, 9/1/89, (PB90-125352, A05, MF-A01). This report is replaced by NCEER-92-0018.
- NCEER-89-0011 "Inelastic Three-Dimensional Response Analysis of Reinforced Concrete Building Structures (IDARC-3D), Part I - Modeling," by S.K. Kunnath and A.M. Reinhorn, 4/17/89, (PB90-114612, A07, MF-A01). This report is available only through NTIS (see address given above).
- NCEER-89-0012 "Recommended Modifications to ATC-14," by C.D. Poland and J.O. Malley, 4/12/89, (PB90-108648, A15, MF-A01).
- NCEER-89-0013 "Repair and Strengthening of Beam-to-Column Connections Subjected to Earthquake Loading," by M. Corazao and A.J. Durrani, 2/28/89, (PB90-109885, A06, MF-A01).
- NCEER-89-0014 "Program EXKAL2 for Identification of Structural Dynamic Systems," by O. Maruyama, C-B. Yun, M. Hoshiya and M. Shinozuka, 5/19/89, (PB90-109877, A09, MF-A01).

- NCEER-89-0015 "Response of Frames With Bolted Semi-Rigid Connections, Part I - Experimental Study and Analytical Predictions," by P.J. DiCorso, A.M. Reinhorn, J.R. Dickerson, J.B. Radzinski and W.L. Harper, 6/1/89, to be published.
- NCEER-89-0016 "ARMA Monte Carlo Simulation in Probabilistic Structural Analysis," by P.D. Spanos and M.P. Mignolet, 7/10/89, (PB90-109893, A03, MF-A01).
- NCEER-89-P017 "Preliminary Proceedings from the Conference on Disaster Preparedness - The Place of Earthquake Education in Our Schools," Edited by K.E.K. Ross, 6/23/89, (PB90-108606, A03, MF-A01).
- NCEER-89-0017 "Proceedings from the Conference on Disaster Preparedness - The Place of Earthquake Education in Our Schools," Edited by K.E.K. Ross, 12/31/89, (PB90-207895, A012, MF-A02). This report is available only through NTIS (see address given above).
- NCEER-89-0018 "Multidimensional Models of Hysteretic Material Behavior for Vibration Analysis of Shape Memory Energy Absorbing Devices, by E.J. Graesser and F.A. Cozzarelli, 6/7/89, (PB90-164146, A04, MF-A01).
- NCEER-89-0019 "Nonlinear Dynamic Analysis of Three-Dimensional Base Isolated Structures (3D-BASIS)," by S. Nagarajaiah, A.M. Reinhorn and M.C. Constantinou, 8/3/89, (PB90-161936, A06, MF-A01). This report has been replaced by NCEER-93-0011.
- NCEER-89-0020 "Structural Control Considering Time-Rate of Control Forces and Control Rate Constraints," by F.Y. Cheng and C.P. Pantelides, 8/3/89, (PB90-120445, A04, MF-A01).
- NCEER-89-0021 "Subsurface Conditions of Memphis and Shelby County," by K.W. Ng, T-S. Chang and H-H.M. Hwang, 7/26/89, (PB90-120437, A03, MF-A01).
- NCEER-89-0022 "Seismic Wave Propagation Effects on Straight Jointed Buried Pipelines," by K. Elhadi and M.J. O'Rourke, 8/24/89, (PB90-162322, A10, MF-A02).
- NCEER-89-0023 "Workshop on Serviceability Analysis of Water Delivery Systems," edited by M. Grigoriu, 3/6/89, (PB90-127424, A03, MF-A01).
- NCEER-89-0024 "Shaking Table Study of a 1/5 Scale Steel Frame Composed of Tapered Members," by K.C. Chang, J.S. Hwang and G.C. Lee, 9/18/89, (PB90-160169, A04, MF-A01).
- NCEER-89-0025 "DYNA1D: A Computer Program for Nonlinear Seismic Site Response Analysis - Technical Documentation," by Jean H. Prevost, 9/14/89, (PB90-161944, A07, MF-A01). This report is available only through NTIS (see address given above).
- NCEER-89-0026 "1:4 Scale Model Studies of Active Tendon Systems and Active Mass Dampers for Aseismic Protection," by A.M. Reinhorn, T.T. Soong, R.C. Lin, Y.P. Yang, Y. Fukao, H. Abe and M. Nakai, 9/15/89, (PB90-173246, A10, MF-A02). This report is available only through NTIS (see address given above).
- NCEER-89-0027 "Scattering of Waves by Inclusions in a Nonhomogeneous Elastic Half Space Solved by Boundary Element Methods," by P.K. Hadley, A. Askar and A.S. Cakmak, 6/15/89, (PB90-145699, A07, MF-A01).
- NCEER-89-0028 "Statistical Evaluation of Deflection Amplification Factors for Reinforced Concrete Structures," by H.H.M. Hwang, J-W. Jaw and A.L. Ch'ng, 8/31/89, (PB90-164633, A05, MF-A01).
- NCEER-89-0029 "Bedrock Accelerations in Memphis Area Due to Large New Madrid Earthquakes," by H.H.M. Hwang, C.H.S. Chen and G. Yu, 11/7/89, (PB90-162330, A04, MF-A01).
- NCEER-89-0030 "Seismic Behavior and Response Sensitivity of Secondary Structural Systems," by Y.Q. Chen and T.T. Soong, 10/23/89, (PB90-164658, A08, MF-A01).
- NCEER-89-0031 "Random Vibration and Reliability Analysis of Primary-Secondary Structural Systems," by Y. Ibrahim, M. Grigoriu and T.T. Soong, 11/10/89, (PB90-161951, A04, MF-A01).

- NCEER-89-0032 "Proceedings from the Second U.S. - Japan Workshop on Liquefaction, Large Ground Deformation and Their Effects on Lifelines, September 26-29, 1989," Edited by T.D. O'Rourke and M. Hamada, 12/1/89, (PB90-209388, A22, MF-A03).
- NCEER-89-0033 "Deterministic Model for Seismic Damage Evaluation of Reinforced Concrete Structures," by J.M. Bracci, A.M. Reinhorn, J.B. Mander and S.K. Kunnath, 9/27/89, (PB91-108803, A06, MF-A01).
- NCEER-89-0034 "On the Relation Between Local and Global Damage Indices," by E. DiPasquale and A.S. Cakmak, 8/15/89, (PB90-173865, A05, MF-A01).
- NCEER-89-0035 "Cyclic Undrained Behavior of Nonplastic and Low Plasticity Silts," by A.J. Walker and H.E. Stewart, 7/26/89, (PB90-183518, A10, MF-A01).
- NCEER-89-0036 "Liquefaction Potential of Surficial Deposits in the City of Buffalo, New York," by M. Budhu, R. Giese and L. Baumgrass, 1/17/89, (PB90-208455, A04, MF-A01).
- NCEER-89-0037 "A Deterministic Assessment of Effects of Ground Motion Incoherence," by A.S. Veletsos and Y. Tang, 7/15/89, (PB90-164294, A03, MF-A01).
- NCEER-89-0038 "Workshop on Ground Motion Parameters for Seismic Hazard Mapping," July 17-18, 1989, edited by R.V. Whitman, 12/1/89, (PB90-173923, A04, MF-A01).
- NCEER-89-0039 "Seismic Effects on Elevated Transit Lines of the New York City Transit Authority," by C.J. Costantino, C.A. Miller and E. Heymsfield, 12/26/89, (PB90-207887, A06, MF-A01).
- NCEER-89-0040 "Centrifugal Modeling of Dynamic Soil-Structure Interaction," by K. Weissman, Supervised by J.H. Prevost, 5/10/89, (PB90-207879, A07, MF-A01).
- NCEER-89-0041 "Linearized Identification of Buildings With Cores for Seismic Vulnerability Assessment," by I-K. Ho and A.E. Aktan, 11/1/89, (PB90-251943, A07, MF-A01).
- NCEER-90-0001 "Geotechnical and Lifeline Aspects of the October 17, 1989 Loma Prieta Earthquake in San Francisco," by T.D. O'Rourke, H.E. Stewart, F.T. Blackburn and T.S. Dickerman, 1/90, (PB90-208596, A05, MF-A01).
- NCEER-90-0002 "Nonnormal Secondary Response Due to Yielding in a Primary Structure," by D.C.K. Chen and L.D. Lutes, 2/28/90, (PB90-251976, A07, MF-A01).
- NCEER-90-0003 "Earthquake Education Materials for Grades K-12," by K.E.K. Ross, 4/16/90, (PB91-251984, A05, MF-A05). This report has been replaced by NCEER-92-0018.
- NCEER-90-0004 "Catalog of Strong Motion Stations in Eastern North America," by R.W. Busby, 4/3/90, (PB90-251984, A05, MF-A01).
- NCEER-90-0005 "NCEER Strong-Motion Data Base: A User Manual for the GeoBase Release (Version 1.0 for the Sun3)," by P. Friberg and K. Jacob, 3/31/90 (PB90-258062, A04, MF-A01).
- NCEER-90-0006 "Seismic Hazard Along a Crude Oil Pipeline in the Event of an 1811-1812 Type New Madrid Earthquake," by H.H.M. Hwang and C-H.S. Chen, 4/16/90, (PB90-258054, A04, MF-A01).
- NCEER-90-0007 "Site-Specific Response Spectra for Memphis Sheahan Pumping Station," by H.H.M. Hwang and C.S. Lee, 5/15/90, (PB91-108811, A05, MF-A01).
- NCEER-90-0008 "Pilot Study on Seismic Vulnerability of Crude Oil Transmission Systems," by T. Ariman, R. Dobry, M. Grigoriu, F. Kozin, M. O'Rourke, T. O'Rourke and M. Shinozuka, 5/25/90, (PB91-108837, A06, MF-A01).
- NCEER-90-0009 "A Program to Generate Site Dependent Time Histories: EQGEN," by G.W. Ellis, M. Srinivasan and A.S. Cakmak, 1/30/90, (PB91-108829, A04, MF-A01).
- NCEER-90-0010 "Active Isolation for Seismic Protection of Operating Rooms," by M.E. Talbott, Supervised by M. Shinozuka, 6/8/9, (PB91-110205, A05, MF-A01).

- NCEER-90-0011 "Program LINEARID for Identification of Linear Structural Dynamic Systems," by C-B. Yun and M. Shinozuka, 6/25/90, (PB91-110312, A08, MF-A01).
- NCEER-90-0012 "Two-Dimensional Two-Phase Elasto-Plastic Seismic Response of Earth Dams," by A.N. Yiagos, Supervised by J.H. Prevost, 6/20/90, (PB91-110197, A13, MF-A02).
- NCEER-90-0013 "Secondary Systems in Base-Isolated Structures: Experimental Investigation, Stochastic Response and Stochastic Sensitivity," by G.D. Manolis, G. Juhn, M.C. Constantinou and A.M. Reinhorn, 7/1/90, (PB91-110320, A08, MF-A01).
- NCEER-90-0014 "Seismic Behavior of Lightly-Reinforced Concrete Column and Beam-Column Joint Details," by S.P. Pessiki, C.H. Conley, P. Gergely and R.N. White, 8/22/90, (PB91-108795, A11, MF-A02).
- NCEER-90-0015 "Two Hybrid Control Systems for Building Structures Under Strong Earthquakes," by J.N. Yang and A. Daniellians, 6/29/90, (PB91-125393, A04, MF-A01).
- NCEER-90-0016 "Instantaneous Optimal Control with Acceleration and Velocity Feedback," by J.N. Yang and Z. Li, 6/29/90, (PB91-125401, A03, MF-A01).
- NCEER-90-0017 "Reconnaissance Report on the Northern Iran Earthquake of June 21, 1990," by M. Mehrain, 10/4/90, (PB91-125377, A03, MF-A01).
- NCEER-90-0018 "Evaluation of Liquefaction Potential in Memphis and Shelby County," by T.S. Chang, P.S. Tang, C.S. Lee and H. Hwang, 8/10/90, (PB91-125427, A09, MF-A01).
- NCEER-90-0019 "Experimental and Analytical Study of a Combined Sliding Disc Bearing and Helical Steel Spring Isolation System," by M.C. Constantinou, A.S. Mokha and A.M. Reinhorn, 10/4/90, (PB91-125385, A06, MF-A01). This report is available only through NTIS (see address given above).
- NCEER-90-0020 "Experimental Study and Analytical Prediction of Earthquake Response of a Sliding Isolation System with a Spherical Surface," by A.S. Mokha, M.C. Constantinou and A.M. Reinhorn, 10/11/90, (PB91-125419, A05, MF-A01).
- NCEER-90-0021 "Dynamic Interaction Factors for Floating Pile Groups," by G. Gazetas, K. Fan, A. Kaynia and E. Kausel, 9/10/90, (PB91-170381, A05, MF-A01).
- NCEER-90-0022 "Evaluation of Seismic Damage Indices for Reinforced Concrete Structures," by S. Rodriguez-Gomez and A.S. Cakmak, 9/30/90, PB91-171322, A06, MF-A01).
- NCEER-90-0023 "Study of Site Response at a Selected Memphis Site," by H. Desai, S. Ahmad, E.S. Gazetas and M.R. Oh, 10/11/90, (PB91-196857, A03, MF-A01).
- NCEER-90-0024 "A User's Guide to Strongmo: Version 1.0 of NCEER's Strong-Motion Data Access Tool for PCs and Terminals," by P.A. Friberg and C.A.T. Susch, 11/15/90, (PB91-171272, A03, MF-A01).
- NCEER-90-0025 "A Three-Dimensional Analytical Study of Spatial Variability of Seismic Ground Motions," by L-L. Hong and A.H.-S. Ang, 10/30/90, (PB91-170399, A09, MF-A01).
- NCEER-90-0026 "MUMOID User's Guide - A Program for the Identification of Modal Parameters," by S. Rodriguez-Gomez and E. DiPasquale, 9/30/90, (PB91-171298, A04, MF-A01).
- NCEER-90-0027 "SARCF-II User's Guide - Seismic Analysis of Reinforced Concrete Frames," by S. Rodriguez-Gomez, Y.S. Chung and C. Meyer, 9/30/90, (PB91-171280, A05, MF-A01).
- NCEER-90-0028 "Viscous Dampers: Testing, Modeling and Application in Vibration and Seismic Isolation," by N. Makris and M.C. Constantinou, 12/20/90 (PB91-190561, A06, MF-A01).
- NCEER-90-0029 "Soil Effects on Earthquake Ground Motions in the Memphis Area," by H. Hwang, C.S. Lee, K.W. Ng and T.S. Chang, 8/2/90, (PB91-190751, A05, MF-A01).

- NCEER-91-0001 "Proceedings from the Third Japan-U.S. Workshop on Earthquake Resistant Design of Lifeline Facilities and Countermeasures for Soil Liquefaction, December 17-19, 1990," edited by T.D. O'Rourke and M. Hamada, 2/1/91, (PB91-179259, A99, MF-A04).
- NCEER-91-0002 "Physical Space Solutions of Non-Proportionally Damped Systems," by M. Tong, Z. Liang and G.C. Lee, 1/15/91, (PB91-179242, A04, MF-A01).
- NCEER-91-0003 "Seismic Response of Single Piles and Pile Groups," by K. Fan and G. Gazetas, 1/10/91, (PB92-174994, A04, MF-A01).
- NCEER-91-0004 "Damping of Structures: Part 1 - Theory of Complex Damping," by Z. Liang and G. Lee, 10/10/91, (PB92-197235, A12, MF-A03).
- NCEER-91-0005 "3D-BASIS - Nonlinear Dynamic Analysis of Three Dimensional Base Isolated Structures: Part II," by S. Nagarajaiah, A.M. Reinhorn and M.C. Constantinou, 2/28/91, (PB91-190553, A07, MF-A01). This report has been replaced by NCEER-93-0011.
- NCEER-91-0006 "A Multidimensional Hysteretic Model for Plasticity Deforming Metals in Energy Absorbing Devices," by E.J. Graesser and F.A. Cozzarelli, 4/9/91, (PB92-108364, A04, MF-A01).
- NCEER-91-0007 "A Framework for Customizable Knowledge-Based Expert Systems with an Application to a KBES for Evaluating the Seismic Resistance of Existing Buildings," by E.G. Ibarra-Anaya and S.J. Fennes, 4/9/91, (PB91-210930, A08, MF-A01).
- NCEER-91-0008 "Nonlinear Analysis of Steel Frames with Semi-Rigid Connections Using the Capacity Spectrum Method," by G.G. Deierlein, S-H. Hsieh, Y-J. Shen and J.F. Abel, 7/2/91, (PB92-113828, A05, MF-A01).
- NCEER-91-0009 "Earthquake Education Materials for Grades K-12," by K.E.K. Ross, 4/30/91, (PB91-212142, A06, MF-A01). This report has been replaced by NCEER-92-0018.
- NCEER-91-0010 "Phase Wave Velocities and Displacement Phase Differences in a Harmonically Oscillating Pile," by N. Makris and G. Gazetas, 7/8/91, (PB92-108356, A04, MF-A01).
- NCEER-91-0011 "Dynamic Characteristics of a Full-Size Five-Story Steel Structure and a 2/5 Scale Model," by K.C. Chang, G.C. Yao, G.C. Lee, D.S. Hao and Y.C. Yeh," 7/2/91, (PB93-116648, A06, MF-A02).
- NCEER-91-0012 "Seismic Response of a 2/5 Scale Steel Structure with Added Viscoelastic Dampers," by K.C. Chang, T.T. Soong, S-T. Oh and M.L. Lai, 5/17/91, (PB92-110816, A05, MF-A01).
- NCEER-91-0013 "Earthquake Response of Retaining Walls; Full-Scale Testing and Computational Modeling," by S. Alampalli and A-W.M. Elgamal, 6/20/91, to be published.
- NCEER-91-0014 "3D-BASIS-M: Nonlinear Dynamic Analysis of Multiple Building Base Isolated Structures," by P.C. Tsopelas, S. Nagarajaiah, M.C. Constantinou and A.M. Reinhorn, 5/28/91, (PB92-113885, A09, MF-A02).
- NCEER-91-0015 "Evaluation of SEAOC Design Requirements for Sliding Isolated Structures," by D. Theodossiou and M.C. Constantinou, 6/10/91, (PB92-114602, A11, MF-A03).
- NCEER-91-0016 "Closed-Loop Modal Testing of a 27-Story Reinforced Concrete Flat Plate-Core Building," by H.R. Somaprasad, T. Toksoy, H. Yoshiyuki and A.E. Aktan, 7/15/91, (PB92-129980, A07, MF-A02).
- NCEER-91-0017 "Shake Table Test of a 1/6 Scale Two-Story Lightly Reinforced Concrete Building," by A.G. El-Attar, R.N. White and P. Gergely, 2/28/91, (PB92-222447, A06, MF-A02).
- NCEER-91-0018 "Shake Table Test of a 1/8 Scale Three-Story Lightly Reinforced Concrete Building," by A.G. El-Attar, R.N. White and P. Gergely, 2/28/91, (PB93-116630, A08, MF-A02).
- NCEER-91-0019 "Transfer Functions for Rigid Rectangular Foundations," by A.S. Veletsos, A.M. Prasad and W.H. Wu, 7/31/91, to be published.

- NCEER-91-0020 "Hybrid Control of Seismic-Excited Nonlinear and Inelastic Structural Systems," by J.N. Yang, Z. Li and A. Daniellians, 8/1/91, (PB92-143171, A06, MF-A02).
- NCEER-91-0021 "The NCEER-91 Earthquake Catalog: Improved Intensity-Based Magnitudes and Recurrence Relations for U.S. Earthquakes East of New Madrid," by L. Seeber and J.G. Armbruster, 8/28/91, (PB92-176742, A06, MF-A02).
- NCEER-91-0022 "Proceedings from the Implementation of Earthquake Planning and Education in Schools: The Need for Change - The Roles of the Changemakers," by K.E.K. Ross and F. Winslow, 7/23/91, (PB92-129998, A12, MF-A03).
- NCEER-91-0023 "A Study of Reliability-Based Criteria for Seismic Design of Reinforced Concrete Frame Buildings," by H.H.M. Hwang and H-M. Hsu, 8/10/91, (PB92-140235, A09, MF-A02).
- NCEER-91-0024 "Experimental Verification of a Number of Structural System Identification Algorithms," by R.G. Ghanem, H. Gavin and M. Shinozuka, 9/18/91, (PB92-176577, A18, MF-A04).
- NCEER-91-0025 "Probabilistic Evaluation of Liquefaction Potential," by H.H.M. Hwang and C.S. Lee," 11/25/91, (PB92-143429, A05, MF-A01).
- NCEER-91-0026 "Instantaneous Optimal Control for Linear, Nonlinear and Hysteretic Structures - Stable Controllers," by J.N. Yang and Z. Li, 11/15/91, (PB92-163807, A04, MF-A01).
- NCEER-91-0027 "Experimental and Theoretical Study of a Sliding Isolation System for Bridges," by M.C. Constantinou, A. Kartoum, A.M. Reinhorn and P. Bradford, 11/15/91, (PB92-176973, A10, MF-A03).
- NCEER-92-0001 "Case Studies of Liquefaction and Lifeline Performance During Past Earthquakes, Volume 1: Japanese Case Studies," Edited by M. Hamada and T. O'Rourke, 2/17/92, (PB92-197243, A18, MF-A04).
- NCEER-92-0002 "Case Studies of Liquefaction and Lifeline Performance During Past Earthquakes, Volume 2: United States Case Studies," Edited by T. O'Rourke and M. Hamada, 2/17/92, (PB92-197250, A20, MF-A04).
- NCEER-92-0003 "Issues in Earthquake Education," Edited by K. Ross, 2/3/92, (PB92-222389, A07, MF-A02).
- NCEER-92-0004 "Proceedings from the First U.S. - Japan Workshop on Earthquake Protective Systems for Bridges," Edited by I.G. Buckle, 2/4/92, (PB94-142239, A99, MF-A06).
- NCEER-92-0005 "Seismic Ground Motion from a Haskell-Type Source in a Multiple-Layered Half-Space," A.P. Theoharis, G. Deodatis and M. Shinozuka, 1/2/92, to be published.
- NCEER-92-0006 "Proceedings from the Site Effects Workshop," Edited by R. Whitman, 2/29/92, (PB92-197201, A04, MF-A01).
- NCEER-92-0007 "Engineering Evaluation of Permanent Ground Deformations Due to Seismically-Induced Liquefaction," by M.H. Baziar, R. Dobry and A-W.M. Elgamal, 3/24/92, (PB92-222421, A13, MF-A03).
- NCEER-92-0008 "A Procedure for the Seismic Evaluation of Buildings in the Central and Eastern United States," by C.D. Poland and J.O. Malley, 4/2/92, (PB92-222439, A20, MF-A04).
- NCEER-92-0009 "Experimental and Analytical Study of a Hybrid Isolation System Using Friction Controllable Sliding Bearings," by M.Q. Feng, S. Fujii and M. Shinozuka, 5/15/92, (PB93-150282, A06, MF-A02).
- NCEER-92-0010 "Seismic Resistance of Slab-Column Connections in Existing Non-Ductile Flat-Plate Buildings," by A.J. Durrani and Y. Du, 5/18/92, (PB93-116812, A06, MF-A02).
- NCEER-92-0011 "The Hysteretic and Dynamic Behavior of Brick Masonry Walls Upgraded by Ferrocement Coatings Under Cyclic Loading and Strong Simulated Ground Motion," by H. Lee and S.P. Prawl, 5/11/92, to be published.
- NCEER-92-0012 "Study of Wire Rope Systems for Seismic Protection of Equipment in Buildings," by G.F. Demetriades, M.C. Constantinou and A.M. Reinhorn, 5/20/92, (PB93-116655, A08, MF-A02).

- NCEER-92-0013 "Shape Memory Structural Dampers: Material Properties, Design and Seismic Testing," by P.R. Witting and F.A. Cozzarelli, 5/26/92, (PB93-116663, A05, MF-A01).
- NCEER-92-0014 "Longitudinal Permanent Ground Deformation Effects on Buried Continuous Pipelines," by M.J. O'Rourke, and C. Nordberg, 6/15/92, (PB93-116671, A08, MF-A02).
- NCEER-92-0015 "A Simulation Method for Stationary Gaussian Random Functions Based on the Sampling Theorem," by M. Grigoriu and S. Balopoulou, 6/11/92, (PB93-127496, A05, MF-A01).
- NCEER-92-0016 "Gravity-Load-Designed Reinforced Concrete Buildings: Seismic Evaluation of Existing Construction and Detailing Strategies for Improved Seismic Resistance," by G.W. Hoffmann, S.K. Kunnath, A.M. Reinhorn and J.B. Mander, 7/15/92, (PB94-142007, A08, MF-A02).
- NCEER-92-0017 "Observations on Water System and Pipeline Performance in the Limón Area of Costa Rica Due to the April 22, 1991 Earthquake," by M. O'Rourke and D. Ballantyne, 6/30/92, (PB93-126811, A06, MF-A02).
- NCEER-92-0018 "Fourth Edition of Earthquake Education Materials for Grades K-12," Edited by K.E.K. Ross, 8/10/92, (PB93-114023, A07, MF-A02).
- NCEER-92-0019 "Proceedings from the Fourth Japan-U.S. Workshop on Earthquake Resistant Design of Lifeline Facilities and Countermeasures for Soil Liquefaction," Edited by M. Hamada and T.D. O'Rourke, 8/12/92, (PB93-163939, A99, MF-E11).
- NCEER-92-0020 "Active Bracing System: A Full Scale Implementation of Active Control," by A.M. Reinhorn, T.T. Soong, R.C. Lin, M.A. Riley, Y.P. Wang, S. Aizawa and M. Higashino, 8/14/92, (PB93-127512, A06, MF-A02).
- NCEER-92-0021 "Empirical Analysis of Horizontal Ground Displacement Generated by Liquefaction-Induced Lateral Spreads," by S.F. Bartlett and T.L. Youd, 8/17/92, (PB93-188241, A06, MF-A02).
- NCEER-92-0022 "IDARC Version 3.0: Inelastic Damage Analysis of Reinforced Concrete Structures," by S.K. Kunnath, A.M. Reinhorn and R.F. Lobo, 8/31/92, (PB93-227502, A07, MF-A02).
- NCEER-92-0023 "A Semi-Empirical Analysis of Strong-Motion Peaks in Terms of Seismic Source, Propagation Path and Local Site Conditions, by M. Kamiyama, M.J. O'Rourke and R. Flores-Berrones, 9/9/92, (PB93-150266, A08, MF-A02).
- NCEER-92-0024 "Seismic Behavior of Reinforced Concrete Frame Structures with Nonductile Details, Part I: Summary of Experimental Findings of Full Scale Beam-Column Joint Tests," by A. Beres, R.N. White and P. Gergely, 9/30/92, (PB93-227783, A05, MF-A01).
- NCEER-92-0025 "Experimental Results of Repaired and Retrofitted Beam-Column Joint Tests in Lightly Reinforced Concrete Frame Buildings," by A. Beres, S. El-Borgi, R.N. White and P. Gergely, 10/29/92, (PB93-227791, A05, MF-A01).
- NCEER-92-0026 "A Generalization of Optimal Control Theory: Linear and Nonlinear Structures," by J.N. Yang, Z. Li and S. Vongchavalitkul, 11/2/92, (PB93-188621, A05, MF-A01).
- NCEER-92-0027 "Seismic Resistance of Reinforced Concrete Frame Structures Designed Only for Gravity Loads: Part I - Design and Properties of a One-Third Scale Model Structure," by J.M. Bracci, A.M. Reinhorn and J.B. Mander, 12/1/92, (PB94-104502, A08, MF-A02).
- NCEER-92-0028 "Seismic Resistance of Reinforced Concrete Frame Structures Designed Only for Gravity Loads: Part II - Experimental Performance of Subassemblages," by L.E. Aycaardi, J.B. Mander and A.M. Reinhorn, 12/1/92, (PB94-104510, A08, MF-A02).
- NCEER-92-0029 "Seismic Resistance of Reinforced Concrete Frame Structures Designed Only for Gravity Loads: Part III - Experimental Performance and Analytical Study of a Structural Model," by J.M. Bracci, A.M. Reinhorn and J.B. Mander, 12/1/92, (PB93-227528, A09, MF-A01).

- NCEER-92-0030 "Evaluation of Seismic Retrofit of Reinforced Concrete Frame Structures: Part I - Experimental Performance of Retrofitted Subassemblages," by D. Choudhuri, J.B. Mander and A.M. Reinhorn, 12/8/92, (PB93-198307, A07, MF-A02).
- NCEER-92-0031 "Evaluation of Seismic Retrofit of Reinforced Concrete Frame Structures: Part II - Experimental Performance and Analytical Study of a Retrofitted Structural Model," by J.M. Bracci, A.M. Reinhorn and J.B. Mander, 12/8/92, (PB93-198315, A09, MF-A03).
- NCEER-92-0032 "Experimental and Analytical Investigation of Seismic Response of Structures with Supplemental Fluid Viscous Dampers," by M.C. Constantinou and M.D. Symans, 12/21/92, (PB93-191435, A10, MF-A03). This report is available only through NTIS (see address given above).
- NCEER-92-0033 "Reconnaissance Report on the Cairo, Egypt Earthquake of October 12, 1992," by M. Khater, 12/23/92, (PB93-188621, A03, MF-A01).
- NCEER-92-0034 "Low-Level Dynamic Characteristics of Four Tall Flat-Plate Buildings in New York City," by H. Gavin, S. Yuan, J. Grossman, E. Pekelis and K. Jacob, 12/28/92, (PB93-188217, A07, MF-A02).
- NCEER-93-0001 "An Experimental Study on the Seismic Performance of Brick-Infilled Steel Frames With and Without Retrofit," by J.B. Mander, B. Nair, K. Wojtkowski and J. Ma, 1/29/93, (PB93-227510, A07, MF-A02).
- NCEER-93-0002 "Social Accounting for Disaster Preparedness and Recovery Planning," by S. Cole, E. Pantoja and V. Razak, 2/22/93, (PB94-142114, A12, MF-A03).
- NCEER-93-0003 "Assessment of 1991 NEHRP Provisions for Nonstructural Components and Recommended Revisions," by T.T. Soong, G. Chen, Z. Wu, R-H. Zhang and M. Grigoriu, 3/1/93, (PB93-188639, A06, MF-A02).
- NCEER-93-0004 "Evaluation of Static and Response Spectrum Analysis Procedures of SEAOC/UBC for Seismic Isolated Structures," by C.W. Winters and M.C. Constantinou, 3/23/93, (PB93-198299, A10, MF-A03).
- NCEER-93-0005 "Earthquakes in the Northeast - Are We Ignoring the Hazard? A Workshop on Earthquake Science and Safety for Educators," edited by K.E.K. Ross, 4/2/93, (PB94-103066, A09, MF-A02).
- NCEER-93-0006 "Inelastic Response of Reinforced Concrete Structures with Viscoelastic Braces," by R.F. Lobo, J.M. Bracci, K.L. Shen, A.M. Reinhorn and T.T. Soong, 4/5/93, (PB93-227486, A05, MF-A02).
- NCEER-93-0007 "Seismic Testing of Installation Methods for Computers and Data Processing Equipment," by K. Kosar, T.T. Soong, K.L. Shen, J.A. HoLung and Y.K. Lin, 4/12/93, (PB93-198299, A07, MF-A02).
- NCEER-93-0008 "Retrofit of Reinforced Concrete Frames Using Added Dampers," by A. Reinhorn, M. Constantinou and C. Li, to be published.
- NCEER-93-0009 "Seismic Behavior and Design Guidelines for Steel Frame Structures with Added Viscoelastic Dampers," by K.C. Chang, M.L. Lai, T.T. Soong, D.S. Hao and Y.C. Yeh, 5/1/93, (PB94-141959, A07, MF-A02).
- NCEER-93-0010 "Seismic Performance of Shear-Critical Reinforced Concrete Bridge Piers," by J.B. Mander, S.M. Waheed, M.T.A. Chaudhary and S.S. Chen, 5/12/93, (PB93-227494, A08, MF-A02).
- NCEER-93-0011 "3D-BASIS-TABS: Computer Program for Nonlinear Dynamic Analysis of Three Dimensional Base Isolated Structures," by S. Nagarajaiah, C. Li, A.M. Reinhorn and M.C. Constantinou, 8/2/93, (PB94-141819, A09, MF-A02).
- NCEER-93-0012 "Effects of Hydrocarbon Spills from an Oil Pipeline Break on Ground Water," by O.J. Helweg and H.H.M. Hwang, 8/3/93, (PB94-141942, A06, MF-A02).
- NCEER-93-0013 "Simplified Procedures for Seismic Design of Nonstructural Components and Assessment of Current Code Provisions," by M.P. Singh, L.E. Suarez, E.E. Matheu and G.O. Maldonado, 8/4/93, (PB94-141827, A09, MF-A02).
- NCEER-93-0014 "An Energy Approach to Seismic Analysis and Design of Secondary Systems," by G. Chen and T.T. Soong, 8/6/93, (PB94-142767, A11, MF-A03).

- NCEER-93-0015 "Proceedings from School Sites: Becoming Prepared for Earthquakes - Commemorating the Third Anniversary of the Loma Prieta Earthquake," Edited by F.E. Winslow and K.E.K. Ross, 8/16/93, (PB94-154275, A16, MF-A02).
- NCEER-93-0016 "Reconnaissance Report of Damage to Historic Monuments in Cairo, Egypt Following the October 12, 1992 Dahshur Earthquake," by D. Sykora, D. Look, G. Croci, E. Karaesmen and E. Karaesmen, 8/19/93, (PB94-142221, A08, MF-A02).
- NCEER-93-0017 "The Island of Guam Earthquake of August 8, 1993," by S.W. Swan and S.K. Harris, 9/30/93, (PB94-141843, A04, MF-A01).
- NCEER-93-0018 "Engineering Aspects of the October 12, 1992 Egyptian Earthquake," by A.W. Elgamal, M. Amer, K. Adalier and A. Abul-Fadl, 10/7/93, (PB94-141983, A05, MF-A01).
- NCEER-93-0019 "Development of an Earthquake Motion Simulator and its Application in Dynamic Centrifuge Testing," by I. Krstelj, Supervised by J.H. Prevost, 10/23/93, (PB94-181773, A-10, MF-A03).
- NCEER-93-0020 "NCEER-Taisei Corporation Research Program on Sliding Seismic Isolation Systems for Bridges: Experimental and Analytical Study of a Friction Pendulum System (FPS)," by M.C. Constantinou, P. Tsopelas, Y-S. Kim and S. Okamoto, 11/1/93, (PB94-142775, A08, MF-A02).
- NCEER-93-0021 "Finite Element Modeling of Elastomeric Seismic Isolation Bearings," by L.J. Billings, Supervised by R. Shepherd, 11/8/93, to be published.
- NCEER-93-0022 "Seismic Vulnerability of Equipment in Critical Facilities: Life-Safety and Operational Consequences," by K. Porter, G.S. Johnson, M.M. Zadeh, C. Scawthorn and S. Eder, 11/24/93, (PB94-181765, A16, MF-A03).
- NCEER-93-0023 "Hokkaido Nansei-oki, Japan Earthquake of July 12, 1993, by P.I. Yanev and C.R. Scawthorn, 12/23/93, (PB94-181500, A07, MF-A01).
- NCEER-94-0001 "An Evaluation of Seismic Serviceability of Water Supply Networks with Application to the San Francisco Auxiliary Water Supply System," by I. Markov, Supervised by M. Grigoriu and T. O'Rourke, 1/21/94, (PB94-204013, A07, MF-A02).
- NCEER-94-0002 "NCEER-Taisei Corporation Research Program on Sliding Seismic Isolation Systems for Bridges: Experimental and Analytical Study of Systems Consisting of Sliding Bearings, Rubber Restoring Force Devices and Fluid Dampers," Volumes I and II, by P. Tsopelas, S. Okamoto, M.C. Constantinou, D. Ozaki and S. Fujii, 2/4/94, (PB94-181740, A09, MF-A02 and PB94-181757, A12, MF-A03).
- NCEER-94-0003 "A Markov Model for Local and Global Damage Indices in Seismic Analysis," by S. Rahman and M. Grigoriu, 2/18/94, (PB94-206000, A12, MF-A03).
- NCEER-94-0004 "Proceedings from the NCEER Workshop on Seismic Response of Masonry Infills," edited by D.P. Abrams, 3/1/94, (PB94-180783, A07, MF-A02).
- NCEER-94-0005 "The Northridge, California Earthquake of January 17, 1994: General Reconnaissance Report," edited by J.D. Goltz, 3/11/94, (PB94-193943, A10, MF-A03).
- NCEER-94-0006 "Seismic Energy Based Fatigue Damage Analysis of Bridge Columns: Part I - Evaluation of Seismic Capacity," by G.A. Chang and J.B. Mander, 3/14/94, (PB94-219185, A11, MF-A03).
- NCEER-94-0007 "Seismic Isolation of Multi-Story Frame Structures Using Spherical Sliding Isolation Systems," by T.M. Al-Hussaini, V.A. Zayas and M.C. Constantinou, 3/17/94, (PB94-193745, A09, MF-A02).
- NCEER-94-0008 "The Northridge, California Earthquake of January 17, 1994: Performance of Highway Bridges," edited by I.G. Buckle, 3/24/94, (PB94-193851, A06, MF-A02).
- NCEER-94-0009 "Proceedings of the Third U.S.-Japan Workshop on Earthquake Protective Systems for Bridges," edited by I.G. Buckle and I. Friedland, 3/31/94, (PB94-195815, A99, MF-A06).

- NCEER-94-0010 "3D-BASIS-ME: Computer Program for Nonlinear Dynamic Analysis of Seismically Isolated Single and Multiple Structures and Liquid Storage Tanks," by P.C. Tsopelas, M.C. Constantinou and A.M. Reinhorn, 4/12/94, (PB94-204922, A09, MF-A02).
- NCEER-94-0011 "The Northridge, California Earthquake of January 17, 1994: Performance of Gas Transmission Pipelines," by T.D. O'Rourke and M.C. Palmer, 5/16/94, (PB94-204989, A05, MF-A01).
- NCEER-94-0012 "Feasibility Study of Replacement Procedures and Earthquake Performance Related to Gas Transmission Pipelines," by T.D. O'Rourke and M.C. Palmer, 5/25/94, (PB94-206638, A09, MF-A02).
- NCEER-94-0013 "Seismic Energy Based Fatigue Damage Analysis of Bridge Columns: Part II - Evaluation of Seismic Demand," by G.A. Chang and J.B. Mander, 6/1/94, (PB95-18106, A08, MF-A02).
- NCEER-94-0014 "NCEER-Taisei Corporation Research Program on Sliding Seismic Isolation Systems for Bridges: Experimental and Analytical Study of a System Consisting of Sliding Bearings and Fluid Restoring Force/Damping Devices," by P. Tsopelas and M.C. Constantinou, 6/13/94, (PB94-219144, A10, MF-A03).
- NCEER-94-0015 "Generation of Hazard-Consistent Fragility Curves for Seismic Loss Estimation Studies," by H. Hwang and J-R. Huo, 6/14/94, (PB95-181996, A09, MF-A02).
- NCEER-94-0016 "Seismic Study of Building Frames with Added Energy-Absorbing Devices," by W.S. Pong, C.S. Tsai and G.C. Lee, 6/20/94, (PB94-219136, A10, A03).
- NCEER-94-0017 "Sliding Mode Control for Seismic-Excited Linear and Nonlinear Civil Engineering Structures," by J. Yang, J. Wu, A. Agrawal and Z. Li, 6/21/94, (PB95-138483, A06, MF-A02).
- NCEER-94-0018 "3D-BASIS-TABS Version 2.0: Computer Program for Nonlinear Dynamic Analysis of Three Dimensional Base Isolated Structures," by A.M. Reinhorn, S. Nagarajaiah, M.C. Constantinou, P. Tsopelas and R. Li, 6/22/94, (PB95-182176, A08, MF-A02).
- NCEER-94-0019 "Proceedings of the International Workshop on Civil Infrastructure Systems: Application of Intelligent Systems and Advanced Materials on Bridge Systems," Edited by G.C. Lee and K.C. Chang, 7/18/94, (PB95-252474, A20, MF-A04).
- NCEER-94-0020 "Study of Seismic Isolation Systems for Computer Floors," by V. Lambrou and M.C. Constantinou, 7/19/94, (PB95-138533, A10, MF-A03).
- NCEER-94-0021 "Proceedings of the U.S.-Italian Workshop on Guidelines for Seismic Evaluation and Rehabilitation of Unreinforced Masonry Buildings," Edited by D.P. Abrams and G.M. Calvi, 7/20/94, (PB95-138749, A13, MF-A03).
- NCEER-94-0022 "NCEER-Taisei Corporation Research Program on Sliding Seismic Isolation Systems for Bridges: Experimental and Analytical Study of a System Consisting of Lubricated PTFE Sliding Bearings and Mild Steel Dampers," by P. Tsopelas and M.C. Constantinou, 7/22/94, (PB95-182184, A08, MF-A02).
- NCEER-94-0023 "Development of Reliability-Based Design Criteria for Buildings Under Seismic Load," by Y.K. Wen, H. Hwang and M. Shinozuka, 8/1/94, (PB95-211934, A08, MF-A02).
- NCEER-94-0024 "Experimental Verification of Acceleration Feedback Control Strategies for an Active Tendon System," by S.J. Dyke, B.F. Spencer, Jr., P. Quast, M.K. Sain, D.C. Kaspari, Jr. and T.T. Soong, 8/29/94, (PB95-212320, A05, MF-A01).
- NCEER-94-0025 "Seismic Retrofitting Manual for Highway Bridges," Edited by I.G. Buckle and I.F. Friedland, published by the Federal Highway Administration (PB95-212676, A15, MF-A03).
- NCEER-94-0026 "Proceedings from the Fifth U.S.-Japan Workshop on Earthquake Resistant Design of Lifeline Facilities and Countermeasures Against Soil Liquefaction," Edited by T.D. O'Rourke and M. Hamada, 11/7/94, (PB95-220802, A99, MF-E08).

- NCEER-95-0001 “Experimental and Analytical Investigation of Seismic Retrofit of Structures with Supplemental Damping: Part 1 - Fluid Viscous Damping Devices,” by A.M. Reinhorn, C. Li and M.C. Constantinou, 1/3/95, (PB95-266599, A09, MF-A02).
- NCEER-95-0002 “Experimental and Analytical Study of Low-Cycle Fatigue Behavior of Semi-Rigid Top-And-Seat Angle Connections,” by G. Pekcan, J.B. Mander and S.S. Chen, 1/5/95, (PB95-220042, A07, MF-A02).
- NCEER-95-0003 “NCEER-ATC Joint Study on Fragility of Buildings,” by T. Anagnos, C. Rojahn and A.S. Kiremidjian, 1/20/95, (PB95-220026, A06, MF-A02).
- NCEER-95-0004 “Nonlinear Control Algorithms for Peak Response Reduction,” by Z. Wu, T.T. Soong, V. Gattulli and R.C. Lin, 2/16/95, (PB95-220349, A05, MF-A01).
- NCEER-95-0005 “Pipeline Replacement Feasibility Study: A Methodology for Minimizing Seismic and Corrosion Risks to Underground Natural Gas Pipelines,” by R.T. Eguchi, H.A. Seligson and D.G. Honegger, 3/2/95, (PB95-252326, A06, MF-A02).
- NCEER-95-0006 “Evaluation of Seismic Performance of an 11-Story Frame Building During the 1994 Northridge Earthquake,” by F. Naeim, R. DiSulio, K. Benuska, A. Reinhorn and C. Li, to be published.
- NCEER-95-0007 “Prioritization of Bridges for Seismic Retrofitting,” by N. Basöz and A.S. Kiremidjian, 4/24/95, (PB95-252300, A08, MF-A02).
- NCEER-95-0008 “Method for Developing Motion Damage Relationships for Reinforced Concrete Frames,” by A. Singhal and A.S. Kiremidjian, 5/11/95, (PB95-266607, A06, MF-A02).
- NCEER-95-0009 “Experimental and Analytical Investigation of Seismic Retrofit of Structures with Supplemental Damping: Part II - Friction Devices,” by C. Li and A.M. Reinhorn, 7/6/95, (PB96-128087, A11, MF-A03).
- NCEER-95-0010 “Experimental Performance and Analytical Study of a Non-Ductile Reinforced Concrete Frame Structure Retrofitted with Elastomeric Spring Dampers,” by G. Pekcan, J.B. Mander and S.S. Chen, 7/14/95, (PB96-137161, A08, MF-A02).
- NCEER-95-0011 “Development and Experimental Study of Semi-Active Fluid Damping Devices for Seismic Protection of Structures,” by M.D. Symans and M.C. Constantinou, 8/3/95, (PB96-136940, A23, MF-A04).
- NCEER-95-0012 “Real-Time Structural Parameter Modification (RSPM): Development of Innervated Structures,” by Z. Liang, M. Tong and G.C. Lee, 4/11/95, (PB96-137153, A06, MF-A01).
- NCEER-95-0013 “Experimental and Analytical Investigation of Seismic Retrofit of Structures with Supplemental Damping: Part III - Viscous Damping Walls,” by A.M. Reinhorn and C. Li, 10/1/95, (PB96-176409, A11, MF-A03).
- NCEER-95-0014 “Seismic Fragility Analysis of Equipment and Structures in a Memphis Electric Substation,” by J-R. Huo and H.H.M. Hwang, 8/10/95, (PB96-128087, A09, MF-A02).
- NCEER-95-0015 “The Hanshin-Awaji Earthquake of January 17, 1995: Performance of Lifelines,” Edited by M. Shinozuka, 11/3/95, (PB96-176383, A15, MF-A03).
- NCEER-95-0016 “Highway Culvert Performance During Earthquakes,” by T.L. Youd and C.J. Beckman, available as NCEER-96-0015.
- NCEER-95-0017 “The Hanshin-Awaji Earthquake of January 17, 1995: Performance of Highway Bridges,” Edited by I.G. Buckle, 12/1/95, to be published.
- NCEER-95-0018 “Modeling of Masonry Infill Panels for Structural Analysis,” by A.M. Reinhorn, A. Madan, R.E. Valles, Y. Reichmann and J.B. Mander, 12/8/95, (PB97-110886, MF-A01, A06).
- NCEER-95-0019 “Optimal Polynomial Control for Linear and Nonlinear Structures,” by A.K. Agrawal and J.N. Yang, 12/11/95, (PB96-168737, A07, MF-A02).

- NCEER-95-0020 "Retrofit of Non-Ductile Reinforced Concrete Frames Using Friction Dampers," by R.S. Rao, P. Gergely and R.N. White, 12/22/95, (PB97-133508, A10, MF-A02).
- NCEER-95-0021 "Parametric Results for Seismic Response of Pile-Supported Bridge Bents," by G. Mylonakis, A. Nikolaou and G. Gazetas, 12/22/95, (PB97-100242, A12, MF-A03).
- NCEER-95-0022 "Kinematic Bending Moments in Seismically Stressed Piles," by A. Nikolaou, G. Mylonakis and G. Gazetas, 12/23/95, (PB97-113914, MF-A03, A13).
- NCEER-96-0001 "Dynamic Response of Unreinforced Masonry Buildings with Flexible Diaphragms," by A.C. Costley and D.P. Abrams, 10/10/96, (PB97-133573, MF-A03, A15).
- NCEER-96-0002 "State of the Art Review: Foundations and Retaining Structures," by I. Po Lam, to be published.
- NCEER-96-0003 "Ductility of Rectangular Reinforced Concrete Bridge Columns with Moderate Confinement," by N. Wehbe, M. Saiidi, D. Sanders and B. Douglas, 11/7/96, (PB97-133557, A06, MF-A02).
- NCEER-96-0004 "Proceedings of the Long-Span Bridge Seismic Research Workshop," edited by I.G. Buckle and I.M. Friedland, to be published.
- NCEER-96-0005 "Establish Representative Pier Types for Comprehensive Study: Eastern United States," by J. Kulicki and Z. Prucz, 5/28/96, (PB98-119217, A07, MF-A02).
- NCEER-96-0006 "Establish Representative Pier Types for Comprehensive Study: Western United States," by R. Imbsen, R.A. Schamber and T.A. Osterkamp, 5/28/96, (PB98-118607, A07, MF-A02).
- NCEER-96-0007 "Nonlinear Control Techniques for Dynamical Systems with Uncertain Parameters," by R.G. Ghanem and M.I. Bujakov, 5/27/96, (PB97-100259, A17, MF-A03).
- NCEER-96-0008 "Seismic Evaluation of a 30-Year Old Non-Ductile Highway Bridge Pier and Its Retrofit," by J.B. Mander, B. Mahmoodzadegan, S. Bhadra and S.S. Chen, 5/31/96, (PB97-110902, MF-A03, A10).
- NCEER-96-0009 "Seismic Performance of a Model Reinforced Concrete Bridge Pier Before and After Retrofit," by J.B. Mander, J.H. Kim and C.A. Ligozio, 5/31/96, (PB97-110910, MF-A02, A10).
- NCEER-96-0010 "IDARC2D Version 4.0: A Computer Program for the Inelastic Damage Analysis of Buildings," by R.E. Valles, A.M. Reinhorn, S.K. Kunnath, C. Li and A. Madan, 6/3/96, (PB97-100234, A17, MF-A03).
- NCEER-96-0011 "Estimation of the Economic Impact of Multiple Lifeline Disruption: Memphis Light, Gas and Water Division Case Study," by S.E. Chang, H.A. Seligson and R.T. Eguchi, 8/16/96, (PB97-133490, A11, MF-A03).
- NCEER-96-0012 "Proceedings from the Sixth Japan-U.S. Workshop on Earthquake Resistant Design of Lifeline Facilities and Countermeasures Against Soil Liquefaction, Edited by M. Hamada and T. O'Rourke, 9/11/96, (PB97-133581, A99, MF-A06).
- NCEER-96-0013 "Chemical Hazards, Mitigation and Preparedness in Areas of High Seismic Risk: A Methodology for Estimating the Risk of Post-Earthquake Hazardous Materials Release," by H.A. Seligson, R.T. Eguchi, K.J. Tierney and K. Richmond, 11/7/96, (PB97-133565, MF-A02, A08).
- NCEER-96-0014 "Response of Steel Bridge Bearings to Reversed Cyclic Loading," by J.B. Mander, D-K. Kim, S.S. Chen and G.J. Premus, 11/13/96, (PB97-140735, A12, MF-A03).
- NCEER-96-0015 "Highway Culvert Performance During Past Earthquakes," by T.L. Youd and C.J. Beckman, 11/25/96, (PB97-133532, A06, MF-A01).
- NCEER-97-0001 "Evaluation, Prevention and Mitigation of Pounding Effects in Building Structures," by R.E. Valles and A.M. Reinhorn, 2/20/97, (PB97-159552, A14, MF-A03).
- NCEER-97-0002 "Seismic Design Criteria for Bridges and Other Highway Structures," by C. Rojahn, R. Mayes, D.G. Anderson, J. Clark, J.H. Hom, R.V. Nutt and M.J. O'Rourke, 4/30/97, (PB97-194658, A06, MF-A03).

- NCEER-97-0003 "Proceedings of the U.S.-Italian Workshop on Seismic Evaluation and Retrofit," Edited by D.P. Abrams and G.M. Calvi, 3/19/97, (PB97-194666, A13, MF-A03).
- NCEER-97-0004 "Investigation of Seismic Response of Buildings with Linear and Nonlinear Fluid Viscous Dampers," by A.A. Seleemah and M.C. Constantinou, 5/21/97, (PB98-109002, A15, MF-A03).
- NCEER-97-0005 "Proceedings of the Workshop on Earthquake Engineering Frontiers in Transportation Facilities," edited by G.C. Lee and I.M. Friedland, 8/29/97, (PB98-128911, A25, MR-A04).
- NCEER-97-0006 "Cumulative Seismic Damage of Reinforced Concrete Bridge Piers," by S.K. Kunnath, A. El-Bahy, A. Taylor and W. Stone, 9/2/97, (PB98-108814, A11, MF-A03).
- NCEER-97-0007 "Structural Details to Accommodate Seismic Movements of Highway Bridges and Retaining Walls," by R.A. Imbsen, R.A. Schamber, E. Thorkildsen, A. Kartoum, B.T. Martin, T.N. Rosser and J.M. Kulicki, 9/3/97, (PB98-108996, A09, MF-A02).
- NCEER-97-0008 "A Method for Earthquake Motion-Damage Relationships with Application to Reinforced Concrete Frames," by A. Singhal and A.S. Kiremidjian, 9/10/97, (PB98-108988, A13, MF-A03).
- NCEER-97-0009 "Seismic Analysis and Design of Bridge Abutments Considering Sliding and Rotation," by K. Fishman and R. Richards, Jr., 9/15/97, (PB98-108897, A06, MF-A02).
- NCEER-97-0010 "Proceedings of the FHWA/NCEER Workshop on the National Representation of Seismic Ground Motion for New and Existing Highway Facilities," edited by I.M. Friedland, M.S. Power and R.L. Mayes, 9/22/97, (PB98-128903, A21, MF-A04).
- NCEER-97-0011 "Seismic Analysis for Design or Retrofit of Gravity Bridge Abutments," by K.L. Fishman, R. Richards, Jr. and R.C. Divito, 10/2/97, (PB98-128937, A08, MF-A02).
- NCEER-97-0012 "Evaluation of Simplified Methods of Analysis for Yielding Structures," by P. Tsopelas, M.C. Constantinou, C.A. Kircher and A.S. Whittaker, 10/31/97, (PB98-128929, A10, MF-A03).
- NCEER-97-0013 "Seismic Design of Bridge Columns Based on Control and Repairability of Damage," by C-T. Cheng and J.B. Mander, 12/8/97, (PB98-144249, A11, MF-A03).
- NCEER-97-0014 "Seismic Resistance of Bridge Piers Based on Damage Avoidance Design," by J.B. Mander and C-T. Cheng, 12/10/97, (PB98-144223, A09, MF-A02).
- NCEER-97-0015 "Seismic Response of Nominally Symmetric Systems with Strength Uncertainty," by S. Balopoulou and M. Grigoriu, 12/23/97, (PB98-153422, A11, MF-A03).
- NCEER-97-0016 "Evaluation of Seismic Retrofit Methods for Reinforced Concrete Bridge Columns," by T.J. Wipf, F.W. Klaiber and F.M. Russo, 12/28/97, (PB98-144215, A12, MF-A03).
- NCEER-97-0017 "Seismic Fragility of Existing Conventional Reinforced Concrete Highway Bridges," by C.L. Mullen and A.S. Cakmak, 12/30/97, (PB98-153406, A08, MF-A02).
- NCEER-97-0018 "Loss Assessment of Memphis Buildings," edited by D.P. Abrams and M. Shinozuka, 12/31/97, (PB98-144231, A13, MF-A03).
- NCEER-97-0019 "Seismic Evaluation of Frames with Infill Walls Using Quasi-static Experiments," by K.M. Mosalam, R.N. White and P. Gergely, 12/31/97, (PB98-153455, A07, MF-A02).
- NCEER-97-0020 "Seismic Evaluation of Frames with Infill Walls Using Pseudo-dynamic Experiments," by K.M. Mosalam, R.N. White and P. Gergely, 12/31/97, (PB98-153430, A07, MF-A02).
- NCEER-97-0021 "Computational Strategies for Frames with Infill Walls: Discrete and Smeared Crack Analyses and Seismic Fragility," by K.M. Mosalam, R.N. White and P. Gergely, 12/31/97, (PB98-153414, A10, MF-A02).

- NCEER-97-0022 "Proceedings of the NCEER Workshop on Evaluation of Liquefaction Resistance of Soils," edited by T.L. Youd and I.M. Idriss, 12/31/97, (PB98-155617, A15, MF-A03).
- MCEER-98-0001 "Extraction of Nonlinear Hysteretic Properties of Seismically Isolated Bridges from Quick-Release Field Tests," by Q. Chen, B.M. Douglas, E.M. Maragakis and I.G. Buckle, 5/26/98, (PB99-118838, A06, MF-A01).
- MCEER-98-0002 "Methodologies for Evaluating the Importance of Highway Bridges," by A. Thomas, S. Eshenaur and J. Kulicki, 5/29/98, (PB99-118846, A10, MF-A02).
- MCEER-98-0003 "Capacity Design of Bridge Piers and the Analysis of Overstrength," by J.B. Mander, A. Dutta and P. Goel, 6/1/98, (PB99-118853, A09, MF-A02).
- MCEER-98-0004 "Evaluation of Bridge Damage Data from the Loma Prieta and Northridge, California Earthquakes," by N. Basoz and A. Kiremidjian, 6/2/98, (PB99-118861, A15, MF-A03).
- MCEER-98-0005 "Screening Guide for Rapid Assessment of Liquefaction Hazard at Highway Bridge Sites," by T. L. Youd, 6/16/98, (PB99-118879, A06, not available on microfiche).
- MCEER-98-0006 "Structural Steel and Steel/Concrete Interface Details for Bridges," by P. Ritchie, N. Kaulh and J. Kulicki, 7/13/98, (PB99-118945, A06, MF-A01).
- MCEER-98-0007 "Capacity Design and Fatigue Analysis of Confined Concrete Columns," by A. Dutta and J.B. Mander, 7/14/98, (PB99-118960, A14, MF-A03).
- MCEER-98-0008 "Proceedings of the Workshop on Performance Criteria for Telecommunication Services Under Earthquake Conditions," edited by A.J. Schiff, 7/15/98, (PB99-118952, A08, MF-A02).
- MCEER-98-0009 "Fatigue Analysis of Unconfined Concrete Columns," by J.B. Mander, A. Dutta and J.H. Kim, 9/12/98, (PB99-123655, A10, MF-A02).
- MCEER-98-0010 "Centrifuge Modeling of Cyclic Lateral Response of Pile-Cap Systems and Seat-Type Abutments in Dry Sands," by A.D. Gadre and R. Dobry, 10/2/98, (PB99-123606, A13, MF-A03).
- MCEER-98-0011 "IDARC-BRIDGE: A Computational Platform for Seismic Damage Assessment of Bridge Structures," by A.M. Reinhorn, V. Simeonov, G. Mylonakis and Y. Reichman, 10/2/98, (PB99-162919, A15, MF-A03).
- MCEER-98-0012 "Experimental Investigation of the Dynamic Response of Two Bridges Before and After Retrofitting with Elastomeric Bearings," by D.A. Wendichansky, S.S. Chen and J.B. Mander, 10/2/98, (PB99-162927, A15, MF-A03).
- MCEER-98-0013 "Design Procedures for Hinge Restrainers and Hinge Sear Width for Multiple-Frame Bridges," by R. Des Roches and G.L. Fenves, 11/3/98, (PB99-140477, A13, MF-A03).
- MCEER-98-0014 "Response Modification Factors for Seismically Isolated Bridges," by M.C. Constantinou and J.K. Quarshie, 11/3/98, (PB99-140485, A14, MF-A03).
- MCEER-98-0015 "Proceedings of the U.S.-Italy Workshop on Seismic Protective Systems for Bridges," edited by I.M. Friedland and M.C. Constantinou, 11/3/98, (PB2000-101711, A22, MF-A04).
- MCEER-98-0016 "Appropriate Seismic Reliability for Critical Equipment Systems: Recommendations Based on Regional Analysis of Financial and Life Loss," by K. Porter, C. Scawthorn, C. Taylor and N. Blais, 11/10/98, (PB99-157265, A08, MF-A02).
- MCEER-98-0017 "Proceedings of the U.S. Japan Joint Seminar on Civil Infrastructure Systems Research," edited by M. Shinozuka and A. Rose, 11/12/98, (PB99-156713, A16, MF-A03).
- MCEER-98-0018 "Modeling of Pile Footings and Drilled Shafts for Seismic Design," by I. PoLam, M. Kapuskar and D. Chaudhuri, 12/21/98, (PB99-157257, A09, MF-A02).

- MCEER-99-0001 "Seismic Evaluation of a Masonry Infilled Reinforced Concrete Frame by Pseudodynamic Testing," by S.G. Buonopane and R.N. White, 2/16/99, (PB99-162851, A09, MF-A02).
- MCEER-99-0002 "Response History Analysis of Structures with Seismic Isolation and Energy Dissipation Systems: Verification Examples for Program SAP2000," by J. Scheller and M.C. Constantinou, 2/22/99, (PB99-162869, A08, MF-A02).
- MCEER-99-0003 "Experimental Study on the Seismic Design and Retrofit of Bridge Columns Including Axial Load Effects," by A. Dutta, T. Kokorina and J.B. Mander, 2/22/99, (PB99-162877, A09, MF-A02).
- MCEER-99-0004 "Experimental Study of Bridge Elastomeric and Other Isolation and Energy Dissipation Systems with Emphasis on Uplift Prevention and High Velocity Near-source Seismic Excitation," by A. Kasalanati and M. C. Constantinou, 2/26/99, (PB99-162885, A12, MF-A03).
- MCEER-99-0005 "Truss Modeling of Reinforced Concrete Shear-flexure Behavior," by J.H. Kim and J.B. Mander, 3/8/99, (PB99-163693, A12, MF-A03).
- MCEER-99-0006 "Experimental Investigation and Computational Modeling of Seismic Response of a 1:4 Scale Model Steel Structure with a Load Balancing Supplemental Damping System," by G. Pekcan, J.B. Mander and S.S. Chen, 4/2/99, (PB99-162893, A11, MF-A03).
- MCEER-99-0007 "Effect of Vertical Ground Motions on the Structural Response of Highway Bridges," by M.R. Button, C.J. Cronin and R.L. Mayes, 4/10/99, (PB2000-101411, A10, MF-A03).
- MCEER-99-0008 "Seismic Reliability Assessment of Critical Facilities: A Handbook, Supporting Documentation, and Model Code Provisions," by G.S. Johnson, R.E. Sheppard, M.D. Quilici, S.J. Eder and C.R. Scawthorn, 4/12/99, (PB2000-101701, A18, MF-A04).
- MCEER-99-0009 "Impact Assessment of Selected MCEER Highway Project Research on the Seismic Design of Highway Structures," by C. Rojahn, R. Mayes, D.G. Anderson, J.H. Clark, D'Appolonia Engineering, S. Gloyd and R.V. Nutt, 4/14/99, (PB99-162901, A10, MF-A02).
- MCEER-99-0010 "Site Factors and Site Categories in Seismic Codes," by R. Dobry, R. Ramos and M.S. Power, 7/19/99, (PB2000-101705, A08, MF-A02).
- MCEER-99-0011 "Restrainer Design Procedures for Multi-Span Simply-Supported Bridges," by M.J. Randall, M. Saiidi, E. Maragakis and T. Isakovic, 7/20/99, (PB2000-101702, A10, MF-A02).
- MCEER-99-0012 "Property Modification Factors for Seismic Isolation Bearings," by M.C. Constantinou, P. Tsopelas, A. Kasalanati and E. Wolff, 7/20/99, (PB2000-103387, A11, MF-A03).
- MCEER-99-0013 "Critical Seismic Issues for Existing Steel Bridges," by P. Ritchie, N. Kauh and J. Kulicki, 7/20/99, (PB2000-101697, A09, MF-A02).
- MCEER-99-0014 "Nonstructural Damage Database," by A. Kao, T.T. Soong and A. Vender, 7/24/99, (PB2000-101407, A06, MF-A01).
- MCEER-99-0015 "Guide to Remedial Measures for Liquefaction Mitigation at Existing Highway Bridge Sites," by H.G. Cooke and J. K. Mitchell, 7/26/99, (PB2000-101703, A11, MF-A03).
- MCEER-99-0016 "Proceedings of the MCEER Workshop on Ground Motion Methodologies for the Eastern United States," edited by N. Abrahamson and A. Becker, 8/11/99, (PB2000-103385, A07, MF-A02).
- MCEER-99-0017 "Quindío, Colombia Earthquake of January 25, 1999: Reconnaissance Report," by A.P. Asfura and P.J. Flores, 10/4/99, (PB2000-106893, A06, MF-A01).
- MCEER-99-0018 "Hysteretic Models for Cyclic Behavior of Deteriorating Inelastic Structures," by M.V. Sivaselvan and A.M. Reinhorn, 11/5/99, (PB2000-103386, A08, MF-A02).


- MCEER-99-0019 "Proceedings of the 7th U.S.- Japan Workshop on Earthquake Resistant Design of Lifeline Facilities and Countermeasures Against Soil Liquefaction," edited by T.D. O'Rourke, J.P. Bardet and M. Hamada, 11/19/99, (PB2000-103354, A99, MF-A06).
- MCEER-99-0020 "Development of Measurement Capability for Micro-Vibration Evaluations with Application to Chip Fabrication Facilities," by G.C. Lee, Z. Liang, J.W. Song, J.D. Shen and W.C. Liu, 12/1/99, (PB2000-105993, A08, MF-A02).
- MCEER-99-0021 "Design and Retrofit Methodology for Building Structures with Supplemental Energy Dissipating Systems," by G. Pekcan, J.B. Mander and S.S. Chen, 12/31/99, (PB2000-105994, A11, MF-A03).
- MCEER-00-0001 "The Marmara, Turkey Earthquake of August 17, 1999: Reconnaissance Report," edited by C. Scawthorn; with major contributions by M. Bruneau, R. Eguchi, T. Holzer, G. Johnson, J. Mander, J. Mitchell, W. Mitchell, A. Papageorgiou, C. Scaethorn, and G. Webb, 3/23/00, (PB2000-106200, A11, MF-A03).
- MCEER-00-0002 "Proceedings of the MCEER Workshop for Seismic Hazard Mitigation of Health Care Facilities," edited by G.C. Lee, M. Ettouney, M. Grigoriu, J. Hauer and J. Nigg, 3/29/00, (PB2000-106892, A08, MF-A02).
- MCEER-00-0003 "The Chi-Chi, Taiwan Earthquake of September 21, 1999: Reconnaissance Report," edited by G.C. Lee and C.H. Loh, with major contributions by G.C. Lee, M. Bruneau, I.G. Buckle, S.E. Chang, P.J. Flores, T.D. O'Rourke, M. Shinozuka, T.T. Soong, C-H. Loh, K-C. Chang, Z-J. Chen, J-S. Hwang, M-L. Lin, G-Y. Liu, K-C. Tsai, G.C. Yao and C-L. Yen, 4/30/00, (PB2001-100980, A10, MF-A02).
- MCEER-00-0004 "Seismic Retrofit of End-Sway Frames of Steel Deck-Truss Bridges with a Supplemental Tendon System: Experimental and Analytical Investigation," by G. Pekcan, J.B. Mander and S.S. Chen, 7/1/00, (PB2001-100982, A10, MF-A02).
- MCEER-00-0005 "Sliding Fragility of Unrestrained Equipment in Critical Facilities," by W.H. Chong and T.T. Soong, 7/5/00, (PB2001-100983, A08, MF-A02).
- MCEER-00-0006 "Seismic Response of Reinforced Concrete Bridge Pier Walls in the Weak Direction," by N. Abo-Shadi, M. Saiidi and D. Sanders, 7/17/00, (PB2001-100981, A17, MF-A03).
- MCEER-00-0007 "Low-Cycle Fatigue Behavior of Longitudinal Reinforcement in Reinforced Concrete Bridge Columns," by J. Brown and S.K. Kunnath, 7/23/00, (PB2001-104392, A08, MF-A02).
- MCEER-00-0008 "Soil Structure Interaction of Bridges for Seismic Analysis," I. PoLam and H. Law, 9/25/00, (PB2001-105397, A08, MF-A02).
- MCEER-00-0009 "Proceedings of the First MCEER Workshop on Mitigation of Earthquake Disaster by Advanced Technologies (MEDAT-1), edited by M. Shinozuka, D.J. Inman and T.D. O'Rourke, 11/10/00, (PB2001-105399, A14, MF-A03).
- MCEER-00-0010 "Development and Evaluation of Simplified Procedures for Analysis and Design of Buildings with Passive Energy Dissipation Systems, Revision 01," by O.M. Ramirez, M.C. Constantinou, C.A. Kircher, A.S. Whittaker, M.W. Johnson, J.D. Gomez and C. Chrysostomou, 11/16/01, (PB2001-105523, A23, MF-A04).
- MCEER-00-0011 "Dynamic Soil-Foundation-Structure Interaction Analyses of Large Caissons," by C-Y. Chang, C-M. Mok, Z-L. Wang, R. Settgast, F. Waggoner, M.A. Ketchum, H.M. Gonnermann and C-C. Chin, 12/30/00, (PB2001-104373, A07, MF-A02).
- MCEER-00-0012 "Experimental Evaluation of Seismic Performance of Bridge Restrainers," by A.G. Vlassis, E.M. Maragakis and M. Saiid Saiidi, 12/30/00, (PB2001-104354, A09, MF-A02).
- MCEER-00-0013 "Effect of Spatial Variation of Ground Motion on Highway Structures," by M. Shinozuka, V. Saxena and G. Deodatis, 12/31/00, (PB2001-108755, A13, MF-A03).
- MCEER-00-0014 "A Risk-Based Methodology for Assessing the Seismic Performance of Highway Systems," by S.D. Werner, C.E. Taylor, J.E. Moore, II, J.S. Walton and S. Cho, 12/31/00, (PB2001-108756, A14, MF-A03).

- MCEER-01-0001 “Experimental Investigation of P-Delta Effects to Collapse During Earthquakes,” by D. Vian and M. Bruneau, 6/25/01, (PB2002-100534, A17, MF-A03).
- MCEER-01-0002 “Proceedings of the Second MCEER Workshop on Mitigation of Earthquake Disaster by Advanced Technologies (MEDAT-2),” edited by M. Bruneau and D.J. Inman, 7/23/01, (PB2002-100434, A16, MF-A03).
- MCEER-01-0003 “Sensitivity Analysis of Dynamic Systems Subjected to Seismic Loads,” by C. Roth and M. Grigoriu, 9/18/01, (PB2003-100884, A12, MF-A03).
- MCEER-01-0004 “Overcoming Obstacles to Implementing Earthquake Hazard Mitigation Policies: Stage 1 Report,” by D.J. Alesch and W.J. Petak, 12/17/01, (PB2002-107949, A07, MF-A02).
- MCEER-01-0005 “Updating Real-Time Earthquake Loss Estimates: Methods, Problems and Insights,” by C.E. Taylor, S.E. Chang and R.T. Eguchi, 12/17/01, (PB2002-107948, A05, MF-A01).
- MCEER-01-0006 “Experimental Investigation and Retrofit of Steel Pile Foundations and Pile Bents Under Cyclic Lateral Loadings,” by A. Shama, J. Mander, B. Blabac and S. Chen, 12/31/01, (PB2002-107950, A13, MF-A03).
- MCEER-02-0001 “Assessment of Performance of Bolu Viaduct in the 1999 Duzce Earthquake in Turkey” by P.C. Roussis, M.C. Constantinou, M. Erdik, E. Durukal and M. Dicleli, 5/8/02, (PB2003-100883, A08, MF-A02).
- MCEER-02-0002 “Seismic Behavior of Rail Counterweight Systems of Elevators in Buildings,” by M.P. Singh, Rildova and L.E. Suarez, 5/27/02. (PB2003-100882, A11, MF-A03).
- MCEER-02-0003 “Development of Analysis and Design Procedures for Spread Footings,” by G. Mylonakis, G. Gazetas, S. Nikolaou and A. Chauncey, 10/02/02, (PB2004-101636, A13, MF-A03, CD-A13).
- MCEER-02-0004 “Bare-Earth Algorithms for Use with SAR and LIDAR Digital Elevation Models,” by C.K. Huyck, R.T. Eguchi and B. Houshmand, 10/16/02, (PB2004-101637, A07, CD-A07).
- MCEER-02-0005 “Review of Energy Dissipation of Compression Members in Concentrically Braced Frames,” by K.Lee and M. Bruneau, 10/18/02, (PB2004-101638, A10, CD-A10).
- MCEER-03-0001 “Experimental Investigation of Light-Gauge Steel Plate Shear Walls for the Seismic Retrofit of Buildings” by J. Berman and M. Bruneau, 5/2/03, (PB2004-101622, A10, MF-A03, CD-A10).
- MCEER-03-0002 “Statistical Analysis of Fragility Curves,” by M. Shinozuka, M.Q. Feng, H. Kim, T. Uzawa and T. Ueda, 6/16/03, (PB2004-101849, A09, CD-A09).
- MCEER-03-0003 “Proceedings of the Eighth U.S.-Japan Workshop on Earthquake Resistant Design of Lifeline Facilities and Countermeasures Against Liquefaction,” edited by M. Hamada, J.P. Bardet and T.D. O’Rourke, 6/30/03, (PB2004-104386, A99, CD-A99).
- MCEER-03-0004 “Proceedings of the PRC-US Workshop on Seismic Analysis and Design of Special Bridges,” edited by L.C. Fan and G.C. Lee, 7/15/03, (PB2004-104387, A14, CD-A14).
- MCEER-03-0005 “Urban Disaster Recovery: A Framework and Simulation Model,” by S.B. Miles and S.E. Chang, 7/25/03, (PB2004-104388, A07, CD-A07).
- MCEER-03-0006 “Behavior of Underground Piping Joints Due to Static and Dynamic Loading,” by R.D. Meis, M. Maragakis and R. Siddharthan, 11/17/03, (PB2005-102194, A13, MF-A03, CD-A00).
- MCEER-03-0007 “Seismic Vulnerability of Timber Bridges and Timber Substructures,” by A.A. Shama, J.B. Mander, I.M. Friedland and D.R. Allicock, 12/15/03.
- MCEER-04-0001 “Experimental Study of Seismic Isolation Systems with Emphasis on Secondary System Response and Verification of Accuracy of Dynamic Response History Analysis Methods,” by E. Wolff and M. Constantinou, 1/16/04 (PB2005-102195, A99, MF-E08, CD-A00).

- MCEER-04-0002 “Tension, Compression and Cyclic Testing of Engineered Cementitious Composite Materials,” by K. Kesner and S.L. Billington, 3/1/04, (PB2005-102196, A08, CD-A08).
- MCEER-04-0003 “Cyclic Testing of Braces Laterally Restrained by Steel Studs to Enhance Performance During Earthquakes,” by O.C. Celik, J.W. Berman and M. Bruneau, 3/16/04, (PB2005-102197, A13, MF-A03, CD-A00).
- MCEER-04-0004 “Methodologies for Post Earthquake Building Damage Detection Using SAR and Optical Remote Sensing: Application to the August 17, 1999 Marmara, Turkey Earthquake,” by C.K. Huyck, B.J. Adams, S. Cho, R.T. Eguchi, B. Mansouri and B. Houshmand, 6/15/04, (PB2005-104888, A10, CD-A00).
- MCEER-04-0005 “Nonlinear Structural Analysis Towards Collapse Simulation: A Dynamical Systems Approach,” by M.V. Sivaselvan and A.M. Reinhorn, 6/16/04, (PB2005-104889, A11, MF-A03, CD-A00).
- MCEER-04-0006 “Proceedings of the Second PRC-US Workshop on Seismic Analysis and Design of Special Bridges,” edited by G.C. Lee and L.C. Fan, 6/25/04, (PB2005-104890, A16, CD-A00).
- MCEER-04-0007 “Seismic Vulnerability Evaluation of Axially Loaded Steel Built-up Laced Members,” by K. Lee and M. Bruneau, 6/30/04, (PB2005-104891, A16, CD-A00).
- MCEER-04-0008 “Evaluation of Accuracy of Simplified Methods of Analysis and Design of Buildings with Damping Systems for Near-Fault and for Soft-Soil Seismic Motions,” by E.A. Pavlou and M.C. Constantinou, 8/16/04, (PB2005-104892, A08, MF-A02, CD-A00).
- MCEER-04-0009 “Assessment of Geotechnical Issues in Acute Care Facilities in California,” by M. Lew, T.D. O’Rourke, R. Dobry and M. Koch, 9/15/04, (PB2005-104893, A08, CD-A00).
- MCEER-04-0010 “Scissor-Jack-Damper Energy Dissipation System,” by A.N. Sigaher-Boyle and M.C. Constantinou, 12/1/04 (PB2005-108221).
- MCEER-04-0011 “Seismic Retrofit of Bridge Steel Truss Piers Using a Controlled Rocking Approach,” by M. Pollino and M. Bruneau, 12/20/04 (PB2006-105795).
- MCEER-05-0001 “Experimental and Analytical Studies of Structures Seismically Isolated with an Uplift-Restraint Isolation System,” by P.C. Roussis and M.C. Constantinou, 1/10/05 (PB2005-108222).
- MCEER-05-0002 “A Versatile Experimentation Model for Study of Structures Near Collapse Applied to Seismic Evaluation of Irregular Structures,” by D. Kusumastuti, A.M. Reinhorn and A. Rutenberg, 3/31/05 (PB2006-101523).
- MCEER-05-0003 “Proceedings of the Third PRC-US Workshop on Seismic Analysis and Design of Special Bridges,” edited by L.C. Fan and G.C. Lee, 4/20/05, (PB2006-105796).
- MCEER-05-0004 “Approaches for the Seismic Retrofit of Braced Steel Bridge Piers and Proof-of-Concept Testing of an Eccentrically Braced Frame with Tubular Link,” by J.W. Berman and M. Bruneau, 4/21/05 (PB2006-101524).
- MCEER-05-0005 “Simulation of Strong Ground Motions for Seismic Fragility Evaluation of Nonstructural Components in Hospitals,” by A. Wanitkorkul and A. Filiatrault, 5/26/05 (PB2006-500027).
- MCEER-05-0006 “Seismic Safety in California Hospitals: Assessing an Attempt to Accelerate the Replacement or Seismic Retrofit of Older Hospital Facilities,” by D.J. Alesch, L.A. Arendt and W.J. Petak, 6/6/05 (PB2006-105794).
- MCEER-05-0007 “Development of Seismic Strengthening and Retrofit Strategies for Critical Facilities Using Engineered Cementitious Composite Materials,” by K. Kesner and S.L. Billington, 8/29/05 (PB2006-111701).
- MCEER-05-0008 “Experimental and Analytical Studies of Base Isolation Systems for Seismic Protection of Power Transformers,” by N. Murota, M.Q. Feng and G-Y. Liu, 9/30/05 (PB2006-111702).
- MCEER-05-0009 “3D-BASIS-ME-MB: Computer Program for Nonlinear Dynamic Analysis of Seismically Isolated Structures,” by P.C. Tsopelas, P.C. Roussis, M.C. Constantinou, R. Buchanan and A.M. Reinhorn, 10/3/05 (PB2006-111703).


- MCEER-05-0010 “Steel Plate Shear Walls for Seismic Design and Retrofit of Building Structures,” by D. Vian and M. Bruneau, 12/15/05 (PB2006-111704).
- MCEER-05-0011 “The Performance-Based Design Paradigm,” by M.J. Astrella and A. Whittaker, 12/15/05 (PB2006-111705).
- MCEER-06-0001 “Seismic Fragility of Suspended Ceiling Systems,” H. Badillo-Almaraz, A.S. Whittaker, A.M. Reinhorn and G.P. Cimellaro, 2/4/06 (PB2006-111706).
- MCEER-06-0002 “Multi-Dimensional Fragility of Structures,” by G.P. Cimellaro, A.M. Reinhorn and M. Bruneau, 3/1/06 (PB2007-106974, A09, MF-A02, CD A00).
- MCEER-06-0003 “Built-Up Shear Links as Energy Dissipators for Seismic Protection of Bridges,” by P. Dusicka, A.M. Itani and I.G. Buckle, 3/15/06 (PB2006-111708).
- MCEER-06-0004 “Analytical Investigation of the Structural Fuse Concept,” by R.E. Vargas and M. Bruneau, 3/16/06 (PB2006-111709).
- MCEER-06-0005 “Experimental Investigation of the Structural Fuse Concept,” by R.E. Vargas and M. Bruneau, 3/17/06 (PB2006-111710).
- MCEER-06-0006 “Further Development of Tubular Eccentrically Braced Frame Links for the Seismic Retrofit of Braced Steel Truss Bridge Piers,” by J.W. Berman and M. Bruneau, 3/27/06 (PB2007-105147).
- MCEER-06-0007 “REDARS Validation Report,” by S. Cho, C.K. Huyck, S. Ghosh and R.T. Eguchi, 8/8/06 (PB2007-106983).
- MCEER-06-0008 “Review of Current NDE Technologies for Post-Earthquake Assessment of Retrofitted Bridge Columns,” by J.W. Song, Z. Liang and G.C. Lee, 8/21/06 06 (PB2007-106984).
- MCEER-06-0009 “Liquefaction Remediation in Silty Soils Using Dynamic Compaction and Stone Columns,” by S. Thevanayagam, G.R. Martin, R. Nashed, T. Shenthan, T. Kanagalingam and N. Ecemis, 8/28/06 06 (PB2007-106985).
- MCEER-06-0010 “Conceptual Design and Experimental Investigation of Polymer Matrix Composite Infill Panels for Seismic Retrofitting,” by W. Jung, M. Chiewanichakorn and A.J. Aref, 9/21/06 (PB2007-106986).
- MCEER-06-0011 “A Study of the Coupled Horizontal-Vertical Behavior of Elastomeric and Lead-Rubber Seismic Isolation Bearings,” by G.P. Warn and A.S. Whittaker, 9/22/06 (PB2007-108679).
- MCEER-06-0012 “Proceedings of the Fourth PRC-US Workshop on Seismic Analysis and Design of Special Bridges: Advancing Bridge Technologies in Research, Design, Construction and Preservation,” Edited by L.C. Fan, G.C. Lee and L. Ziang, 10/12/06 (PB2007-109042).
- MCEER-06-0013 “Cyclic Response and Low Cycle Fatigue Characteristics of Plate Steels,” by P. Dusicka, A.M. Itani and I.G. Buckle, 11/1/06 06 (PB2007-106987).
- MCEER-06-0014 “Proceedings of the Second US-Taiwan Bridge Engineering Workshop,” edited by W.P. Yen, J. Shen, J-Y. Chen and M. Wang, 11/15/06.
- MCEER-06-0015 “User Manual and Technical Documentation for the REDARS™ Import Wizard,” by S. Cho, S. Ghosh, C.K. Huyck and S.D. Werner, 11/30/06 (PB2007-114766).
- MCEER-06-0016 “Hazard Mitigation Strategy and Monitoring Technologies for Urban and Infrastructure Public Buildings: Proceedings of the China-US Workshops,” edited by X.Y. Zhou, A.L. Zhang, G.C. Lee and M. Tong, 12/12/06 (PB2008-500018).
- MCEER-07-0001 “Static and Kinetic Coefficients of Friction for Rigid Blocks,” by C. Kafali, S. Fathali, M. Grigoriu and A.S. Whittaker, 3/20/07 (PB2007-114767).
- MCEER-07-0002 “Hazard Mitigation Investment Decision Making: Organizational Response to Legislative Mandate,” by L.A. Arendt, D.J. Alesch and W.J. Petak, 4/9/07 (PB2007-114768).

- MCEER-07-0003 “Seismic Behavior of Bidirectional-Resistant Ductile End Diaphragms with Unbonded Braces in Straight or Skewed Steel Bridges,” by O. Celik and M. Bruneau, 4/11/07 (PB2008-105141).
- MCEER-07-0004 “Modeling Pile Behavior in Large Pile Groups Under Lateral Loading,” by A.M. Dodds and G.R. Martin, 4/16/07(PB2008-105142).
- MCEER-07-0005 “Experimental Investigation of Blast Performance of Seismically Resistant Concrete-Filled Steel Tube Bridge Piers,” by S. Fujikura, M. Bruneau and D. Lopez-Garcia, 4/20/07 (PB2008-105143).
- MCEER-07-0006 “Seismic Analysis of Conventional and Isolated Liquefied Natural Gas Tanks Using Mechanical Analogs,” by I.P. Christovasilis and A.S. Whittaker, 5/1/07.
- MCEER-07-0007 “Experimental Seismic Performance Evaluation of Isolation/Restraint Systems for Mechanical Equipment – Part 1: Heavy Equipment Study,” by S. Fathali and A. Filiatrault, 6/6/07 (PB2008-105144).
- MCEER-07-0008 “Seismic Vulnerability of Timber Bridges and Timber Substructures,” by A.A. Sharma, J.B. Mander, I.M. Friedland and D.R. Allicock, 6/7/07 (PB2008-105145).
- MCEER-07-0009 “Experimental and Analytical Study of the XY-Friction Pendulum (XY-FP) Bearing for Bridge Applications,” by C.C. Marin-Artieda, A.S. Whittaker and M.C. Constantinou, 6/7/07.
- MCEER-07-0010 “Proceedings of the PRC-US Earthquake Engineering Forum for Young Researchers,” Edited by G.C. Lee and X.Z. Qi, 6/8/07.
- MCEER-07-0011 “Design Recommendations for Perforated Steel Plate Shear Walls,” by R. Purba and M. Bruneau, 6/18/07.
- MCEER-07-0012 “Performance of Seismic Isolation Hardware Under Service and Seismic Loading,” by M.C. Constantinou, A.S. Whittaker, Y. Kalpakidis, D.M. Fenz and G.P. Warn, 8/27/07.
- MCEER-07-0013 “Experimental Evaluation of the Seismic Performance of Hospital Piping Subassemblies,” by E.R. Goodwin, E. Maragakis and A.M. Itani, 9/4/07.
- MCEER-07-0014 “A Simulation Model of Urban Disaster Recovery and Resilience: Implementation for the 1994 Northridge Earthquake,” by S. Miles and S.E. Chang, 9/7/07.
- MCEER-07-0015 “Statistical and Mechanistic Fragility Analysis of Concrete Bridges,” by M. Shinozuka, S. Banerjee and S-H. Kim, 9/10/07.
- MCEER-07-0016 “Three-Dimensional Modeling of Inelastic Buckling in Frame Structures,” by M. Schachter and AM. Reinhorn, 9/13/07.
- MCEER-07-0017 “Modeling of Seismic Wave Scattering on Pile Groups and Caissons,” by I. Po Lam, H. Law and C.T. Yang, 9/17/07.
- MCEER-07-0018 “Bridge Foundations: Modeling Large Pile Groups and Caissons for Seismic Design,” by I. Po Lam, H. Law and G.R. Martin (Coordinating Author), 12/1/07.
- MCEER-07-0019 “Principles and Performance of Roller Seismic Isolation Bearings for Highway Bridges,” by G.C. Lee, Y.C. Ou, Z. Liang, T.C. Niu and J. Song, 12/10/07.



EARTHQUAKE ENGINEERING TO EXTREME EVENTS

University at Buffalo, The State University of New York
Red Jacket Quadrangle ▪ Buffalo, New York 14261
Phone: (716) 645-3391 ▪ Fax: (716) 645-3399
E-mail: mceer@buffalo.edu ▪ WWW Site <http://mceer.buffalo.edu>



University at Buffalo *The State University of New York*

ISSN 1520-295X